NUMERICAL ANALYSIS OF EVAPOTRANSPIRATION AND ITS INFLUENCE ON EMBANKMENTS

Numerical Modelling of Evapotranspiration and it's Influence on Embankments.

by

VINCENT PANGANAI NYAMBAYO
BSc (Hons) MSc DIC CEng MICE

February ~~2003~~ 2004

A thesis submitted to the University of London
(Imperial College of Science, Technology and Medicine)
for the degree of
Doctor of Philosophy in the Faculty of Engineering

SYNOPSIS

Infrastructure embankments constructed of stiff clays in climatic regions epitomised by dry and wet seasons experience significant swelling and drying movements. The magnitude of movements are exacerbated where vegetation exists. During the dry seasons, high water demand during transpiration by vegetation results in increased water abstraction from the ground. This causes significant shrinkage movements in shrinkable soils. The pattern of movements is reversed during the wet seasons, primarily as a result of increased precipitation rates, coupled with low water demand by the vegetation.

Recent research on old UK railway embankments has shown that the seasonal cyclic shrink-swell movements induced by the pore water pressure changes can result in progressive failure, in the long term. The rate at which the progressive failure mechanism propagates is strongly influenced by the magnitude of pore water pressure changes during each seasonal cycle. The magnitude of the pore water pressure changes are governed by several factors. These include the complex process of water flow through the soil-vegetation-atmosphere continuum and the mass permeability of the ground.

Pore water pressure changes induced by vegetation through the process of transpiration are difficult to quantify because they depend on complex physiological, climatological and soil factors which affect water demand. The state-of-the-art in UK industry when analysing the influence of seasonal pore water pressure changes on infrastructure embankments involves prescribing winter and summer pore water pressure profiles that have been contrived to match field observations. There are no unified design pore water pressure profiles and predictions by designers vary widely. It is desirable that water abstraction by vegetation be more accurately quantified to enable accurate predictions of the behaviour of such structures.

In this thesis, a non-linear root water uptake model for transpiration has been developed and implemented in the Imperial College Finite Element Program (ICFEP). The model uses meteorological data as input and predicts the pore water pressure changes thereof, rather than for the user to prescribe them. The model has been validated against field monitoring data and is shown to give reasonable predictions of pore water pressures and ground movements. The predictions of pore water pressures on natural ground and within a typical old railway embankment are shown to match the monthly patterns of rainfall, evapotranspiration and soil moisture deficit.

It is also shown that in order to obtain realistic predictions of pore water pressure changes a permeability model which is capable of simulating the increase in permeability that occurs after desiccation cracking is required. The enhanced permeability resulting from desiccation cracking facilitates the recharge of water into desiccated ground during precipitation. A smeared crack permeability model has been developed and implemented in ICFEP to model such behaviour as part of this research.

Stability analyses using the root water uptake model confirm that seasonal pore water pressure changes induce strain softening and this process ultimately triggers a progressive failure mechanism as the number of seasonal cycles increases. The magnitude of seasonal movements and the rate at which the mechanism propagates is shown to increase with the mass permeability of the clay fill. The influence of the maximum root depth of the vegetation is investigated and reveals that for a given embankment geometry, stratigraphy and meteorological data, there is a magnitude of maximum root depth which induces the smallest seasonal movements. The latter would suggest that vegetation management can be a useful method of controlling seasonal movements in infrastructure embankments. The influence of the stiffness of the clay fill is also investigated and the results indicate that this parameter does not have a significant influence on the rate at which the progressive failure mechanism propagates.

ACKNOWLEDGEMENTS

I would like to thank my supervisors, Dr Trevor Addenbrooke and Professor David Potts for their guidance, enthusiasm, encouragement and motivation over the four years this research has taken to complete. Their technical input has been as invaluable as their friendship and support, during the difficult periods.

I also benefited greatly from the many prolonged discussions with friends and colleagues at Imperial College. In particular, I wish to acknowledge the importance of the discussions with the late Professor Alec Skempton on the history of old railway embankments whilst Professor Peter Vaughan's generosity in giving both his time and suggestions is also greatly appreciated. I am also indebted to Dr Lidija Zdravkovic who assisted me to understand some of the technical aspects of ICFEP.

The list must include Dr Malcolm Hough of the Meteorological Office (Bracknell) who provided the meteorological data used in this research and Dr Brian McGinnity of London Underground Ltd (LUL) who gave me access to a number of technical reports on previous research undertaken on embankments on the LUL network. In a similar way, Mr Mike Crilly of the Geotechnical Consulting Group availed me with the digitised field monitoring data on ground movements at Chattenden, for which I am grateful.

Special thanks are also due to Dr Nebosha Kovacecic, of the Geotechnical Consulting Group for giving me several opportunities to engage in discussions on "numerical modelling of progressive failure in embankments". I also had the privilege to interact on a frequent basis with Dr Andrew Ridley and Dr Kieran Dineen of Geotechnical Observations Ltd. Through this interaction, cross fertilisation of my ideas and their experience in field monitoring of pore water pressures and ground movements in old UK railway embankments benefited my research.

I would also like to extend my thanks to other academic staff and research students at Imperial College who contributed to this thesis through comments, questions, constructive criticism, suggestions at colloquia and in many others ways. As usual, a list of this type often misses a few "forgotten names" for which I apologise, nevertheless, I will give it a go (in alphabetical order): Abbas Qadimi, Adam Pellew, Akihiro Takahashi, Angeliki Grammatikopoulou, Dave Edwards, Prof. Dick Chandler, Emilio Saldivar, Felix Schroder, Graham Taylor, Dr Jamie Standing, Jian

Vhou, Prof John Burland, Juliet Bird, Julio Colmenares, Kirsty Boydell, Kostis Georgiadis, Liana Gasparre, Maria Mavralidou, Dr Matthew Coop, Monica Melgarejo, Nguyen Minh, Ni Jotisankasa, Niki Franzius, Peter Bourne-Webb, Phil Smith, Rafael Monroy, Reinaldo Rolo, Prof. Richard Jardine, Satoshi Nishimura, Stavroula Kontoe, Stuart Hardy, Tizi Rossetto and Dr Zejlko Cabarkapa. Phew! What a gigantic agglomeration of geotechnical brains!

During the period of my research I was funded by the Engineering and Physical Research Council, for which I am grateful.

Finally, my deepest gratitude goes to my wife Juliet, my children Vhenekayi, Joyce and Lily, my mum (Violet), my siblings (Joyce, Rebecca, Julius, Andrew and Marian) and many friends, who gave me the strength, encouragement and determination throughout the difficult periods of this research. I shall be eternally grateful.

TABLE OF CONTENTS

CHAPTER 3: THE FINITE ELEMENT METHOD

CHAPTER 4: THE INFLUENCE OF PERMEABILITY ON PROGRESSIVE FAILURE

List of figures

List of tables

Chapter 1

INTRODUCTION

1.1 General

The use of vegetation to stabilise slopes is widely practised in civil engineering (Coppin and Richards, 1990; Barker, 1995; Gray, 1995; MacNeil *et al*, 2001 and Marriot *et al*, 2001; among many others). In general, vegetation enhances slope stability through two primary mechanisms ie. pore water pressure reduction during transpiration and root reinforcement. This thesis focuses on the geotechnical aspects related to pore water pressure changes in embankments and does not include studies concerning root reinforcement. Most of the current knowledge regarding pore water pressure changes induced by vegetation only comprises a qualitative description of the process. Little research has been carried out in geotechnical engineering to develop models which quantify water abstracted by roots in conventional slope stability models.

In the UK, one of the issues of major interest to geotechnical engineers relates to the serviceability and stability of old vegetated railway embankments. These embankments comprise a large part of the railway infrastructure. A number of the embankments experience significant movements associated with seasonal pore water pressure changes (McGinnity *et al*, 1998 and McGinnity & Russell, 1996). The majority of the railway embankments were built in the mid to late 19th century and are therefore more than a century old. The embankments were constructed by trial and error using end and/or side tipping, with little or no compaction. A large proportion of the embankments were constructed using stiff clay and ash ballast. The clay fill was sourced from borrow areas and tunnel excavations. In the UK, ash was used as ballast until 1945 and was primarily sourced from power stations or steam locomotives. Excavation for the fill materials was largely carried out by hand, using picks and shovels.

The excavated clay would have comprised clay clods of 50-300mm nominal diameter, resulting in a highly voided clay fill (Skempton, 2000). As water from precipitation permeated the formation, the initial voids probably rapidly disappeared as the clay clods collapsed and swelled. The fill material probably retained a significant but variable degree of structure (fabric and bonding) due to the original geological history of the parent material. The clay fill can be idealised as relatively stiff lumps of stiff clay in a matrix of softened material, heavily contaminated with foreign granular

material. The matrix is likely to be weaker, less stiff and more permeable. Ground investigations have indicated that the composition and structure of the clay fill is highly variable over short distances.

Skempton (1996) reviewed historical records of the construction of the UK's old earthworks and established that a number of the higher embankments suffered slip failures during or soon after construction. The majority of repairs took the form of loose dumping ash to restore the track alignment and levels. Other repair methods also used, albeit to a lesser extent include toe walls, drainage and bored pile walls (McGinnity, *et al*, 1998).

Significant research and investigations into the stability of old railway embankments has been carried out in recent years by the Soil Mechanics Group at Imperial College. The research has largely focussed on embankments on the London Underground network; which are typical of the UK's old railway embankments. The research has involved field measurements of pore water pressures and numerical modelling (eg. Kovacevic *et al*, 2002). The studies have revealed that two main modes of movement are operational. The first occurs within the ash mantle; mostly during the summer season when the ash loses its shear strength on drying, into a loose granular structure. This movement primarily occurs where there is no lateral support at the crest of an embankment and is believed to be exacerbated by train-induced dynamic loading. The second type of movement is more dominant and occurs within the clay fill. This movement is caused by vegetation and is cyclic in nature. During summer, the high water demand required for transpiration leads to large shrinkage. This is followed by swelling during winter, when transpiration demand by vegetation is low and is coupled with large precipitation rates. The shrink-swell cycles have been observed to induce vertical movements of up to 50mm in some embankments as well as continued lateral spreading (McGinnity *et al*, 1998). The latter mode of movement has been shown to mirror the pattern of soil moisture balance as quantified by soil moisture deficit (ICON, 2001).

The results of numerical studies at Imperial College revealed that the alternate shrinkage and swelling cycles induce a progressive failure mechanism in the clay fill embankments (Kovacevic *et al*, 2001). The results also indicated that the magnitude of seasonal movements was such that the progressive failure mechanism being propagated would take several years before slip failure could occur. The seasonal cyclic movements are therefore more critical during service as these attract huge refettling and other maintenance costs.

To correctly predict the ground movements associated with transpiration by vegetation requires knowledge of the root water uptake process. However, this aspect has received very little attention by researchers in civil/geotechnical engineering; notwithstanding that research has been carried out in soil science for agronomical plants to model root water eg. Nour el Din *et al* (1987), McCarthy *et al* (1992) and Karajeh & Tanji (1994).

In the UK geotechnical industry, the current methodology to model pore water pressure changes induced by vegetation in numerical analyses of old railway embankments involves a simplification procedure whereby the governing pore water pressure profiles for winter and summer are contrived to match desiccated profiles observed in the field eg. Kovacevic *et al* (2001) and Russell *et al* (2000). The main drawback associated with this approach is the fact that by prescribing the governing summer and winter pore water pressure profiles, the numerical program must generate water flow to achieve the prescribed specified pore water pressure profiles. The water flow required to attain these pore water pressure profiles may be of a magnitude not achieved by vegetation in the field. Moreover, the pore water pressure regime is quasi-stable ie. it continuously changes throughout the year, hence the categorisation of the pore water pressure regime into two seasons annually is an oversimplification of the process.

Pore water pressures in vegetated ground are mainly governed by the species of the vegetation, the root depth, permeability of the soil and the climatic conditions. In effect, the pore water pressures existing in vegetated ground reflect the net water balance arising from water flow through the soil-plant-atmosphere continuum.

The author believes that an ideal way forward in geotechnical engineering would be to model the soil-plant-atmosphere continuum using rainfall and evapotranspiration as input data in coupled analyses which incorporate a root water uptake model. Such an approach allows the pore water profile to be predicted, rather than prescribed.

The application of root water uptake models is still in its infancy in geotechnical engineering and the majority of this work has largely involved one dimensional numerical modelling of soil columns eg. Tratch *et al* (1995) and Mathur (1999). A variety of root water uptake formulations abound in soil science and the type of formulations that are applicable to vegetation such as that encountered in civil/geotechnical engineering are those which define the plant water uptake characteristics as a function of the soil pore water pressure. Such a model was adopted and coded in the finite element program used in this thesis. The model uses potential evapotranspiration as input data to compute

the actual evapotranspiration rates. The program also takes account of precipitation during the process to compute the overall water balance in the ground.

In the UK, the Meteorological Office routinely computes the values of potential evapotranspiration for a number of plant types (mostly agricultural crops) and different rainfalls, using the Meteorological Office Rainfall and Evaporation Calculation System (MORECS) on a 40km x 40km grid basis across the whole country (Hough *et al*, 1997). The vegetation types within MORECS include pasture grasslands and deciduous fruit trees and these two can be considered to be representative of grass and deciduous trees encountered in civil engineering, respectively (Biddle, 1998).

In this thesis, the potential evapotranspiration and precipitation data computed by MORECS for a site in the SE of England were used as input data into a root water uptake numerical model, to predict pore water pressure changes and ground movements. In theory, the availability of meteorological data country-wide would constitute another major advantage of using root water models since the appropriate site-specific data would be used. This contrasts to the current approach used in industry where assumed winter and summer pore water profiles deemed to apply across a large part of the country are prescribed in embankment analyses.

1.2 Objectives and scope

The key objective of this research was to investigate the applicability of modelling evapotranspiration using a root water uptake model in numerical analysis of vegetated old railway embankments. The following specific objectives were spawned from this central theme.

- To determine, via a literature review, the construction history of old railway embankments and the research undertaken to date to understand the mechanisms of movement and instability.

- To establish, via a literature review, the physics of root water uptake and models that have been developed within soil science and agronomy to numerically model evapotranspiration. This would enable the most appropriate root water uptake model amenable to vegetation encountered in UK infrastructure embankments to be identified.

- To code the root water uptake model identified in the preceding section into the Imperial College Finite Element Program.

- To predict pore water pressure changes and ground movements in level ground and in embankments using the root water uptake model.

- To determine whether progressive failure in old railway embankments can be reproduced by a numerical model using the root water uptake model.

1.3 Thesis layout

The research undertaken in this thesis is divided into the following chapters:

Chapter 2 presents a review of the relevant literature with regard to numerical modelling of progressive failure in embankments constructed in stiff clays, the soil physics of root water uptake and its influence on soil volume changes. A brief review of the root water uptake models used in soil science and agronomy is given. The seasonal movements in old railway embankments induced by pore water pressure changes and the research that has been undertaken to understand their behaviour are reviewed. From this review, the limitations of the current methodologies used in geotechnical engineering to model pore water pressure changes induced by vegetation are identified. It is proposed that in order to more accurately predict the behaviour of old railway embankments, pore water pressure changes induced by vegetation should be modelled using root water uptake models.

Chapter 3 gives an overview of the finite element method used in this thesis. It presents the formulation and solution of the governing equations, constitutive models, boundary conditions relevant to this thesis, and the output and post-processing facilities.

Chapter 4 gives the results of numerical analyses on a typical UK old railway embankment that were carried out to investigate the influence of the mass permeability of the clay fill. The analyses were carried out in cognisance of the fact that the mass permeability of the clay fill in UK's old railway embankments is likely to vary by large magnitudes. This is due to the influence of granular inclusions (identified during ground investigations) which are known to vary widely in grading and spatial distribution. The analyses for this chapter were executed using the current industry approach of modelling pore water pressure changes induced by vegetation. Similar analyses using the root water uptake model were also carried out and are discussed in Chapter 7.

Chapter 5 describes the mathematical derivation of a nonlinear root water uptake model (RWUM) that has been coded in the Imperial College Finite Element Program (ICFEP) as part of the development work undertaken in this thesis. The RWUM constitutes a new flow boundary condition to model evapotranspiration in ICFEP. The main facets of the RWUM are described including data input and computation of flows in the numerical algorithm, to model evapotranspiration. The predictions of pore water pressure changes and movements using the RWUM are presented, incorporating sensitivity and parametric studies that were executed as part of the validation exercise. They comprise sensitivity to mesh density, maximum root depth, permeability, soil suctions and meteorological data. The chapter concludes with a description of a smeared crack model that has been developed and implemented in ICFEP to model the increase in permeability arising from the opening of desiccation cracks.

Chapter 6 presents the results of ground movements and pore water pressures predicted for a Building Research Establishment (BRE) test bed site at Chattenden (Kent). A brief outline of the site and field measurements of ground movements carried out by BRE over a 10 year period to assess the influence of vegetation are described. The predictions using the coded RWUM in ICFEP are then presented and comparisons made with BRE's field measurements.

Chapter 7 examines the behaviour of a typical UK vegetated railway embankment. In contrast to Chapter 4 where the current industry methodology was used to model pore water pressure changes induced by vegetation, the numerical analysis in this chapter were executed using the RWUM to model evapotranspiration. The focus of this chapter is to demonstrate the efficacy of the RWUM in reproducing the seasonal pattern of pore water pressure changes and movements, and the development of a progressive failure mechanism. Four main areas are investigated to assess the effects of the RWUM on embankment behaviour: the influence of maximum root depth; stiffness of the clay fill; permeability increase due to desiccation cracking; and mass permeability of the clay fill.

Chapter 8 presents the main conclusions to this thesis and draws together the results of the numerical studies undertaken in Chapters 4 to 7. This chapter also presents suggestions for further research.

Chapter 2

A REVIEW OF PROGRESSIVE FAILURE IN VEGETATED STIFF CLAY EMBANKMENTS

2.1 Introduction

The cyclic pattern of shrinkage and swelling clays and the geotechnical problems associated with this behaviour have been known for a long time. Numerous studies have been carried out worldwide to quantify the movements, pore water pressure changes and damage associated with such soils. The majority of the studies have been carried out in order to understand the damage to foundations and pavements caused by shrinkable soils eg. Ward (1953), Croney (1977), Driscoll (1983), Biddle (1983, 1998) and Crilly and Driscoll (2000), among many others.

In the UK, research has shown that the magnitude of seasonal movements are accentuated by vegetation, especially trees. During a UK summer, the large transpiration rates by trees accompanied by relatively low precipitation rates cause significant moisture depletion; which results in desiccation. During winter, the low transpiration rates by deciduous trees coupled with relatively large precipitation rates results in moisture recovery within the ground and is accompanied by swelling. The latter process also occurs when trees are removed.

More recently, the seasonal cyclic movements associated with vegetation have been shown to contribute to progressive failure of embankment slopes in old railway embankments constructed in stiff clays (ICON (1999), McGinnity *et al* (1999), Russell *et al* and Kovacevic *et al* (2000)).

This chapter presents a literature review on the geotechnical aspects concerning progressive failure in stiff clay embankments induced by seasonal cyclic pore water pressure changes. The mechanical behaviour and permeability of stiff clays are discussed first. This is followed by a discussion on progressive failure, including the numerical modelling of it. Relevant aspects of root morphology and root water uptake (transpiration) are reviewed, including models that have been developed in soil science and agronomy to model root water uptake. A brief review of the influence of desiccation on the mechanical behaviour and permeability of soils is then given. This is followed by a description of the research that has been carried out in the UK on progressive failure in vegetated old railway embankments.

2.2 Mechanical behaviour of stiff clays

2.2.1 Peak strength

Cohesive soils primarily derive their strength from inter-particle bonding and friction. The behaviour of cohesive soils under general shear was elegantly described by Bishop (1971a). He established that cohesion has a component which is related to inter-particle bonding which develops in nature and another component which is a function of void ratio. Under general shear, the stress-strain curve reaches a peak beyond which it rapidly falls to a plateau. Peak strength for most stiff overconsolidated clays are attained at less than 5% strains. Beyond peak strength, the reduction in strength associated with brittle behaviour involves destruction of the cohesive bonds and structure of the intact material. The latter processes are is irreversible. Bishop (1971a) noted that in undisturbed soils both components of cohesion are present but for remoulded soils only that which varies as a function of voids ratio is present.

The peak strength envelope of intact overconsolidated soils lies above that of the same soil when remoulded (Burland (1990), Burland *et al* (1996), Leroueil & Vaughan (1990) and Cotecchia & Chandler (1997) and Georgiannou & Burland, (2001)). The peak strength is also influenced by anisotropy and stress rotation (Hight, 1998), the size of the test specimen and strain rate (Bishop, 1971a) and fatigue, weathering and suction (Leroueil, 2001).

The influence of pore water pressure variation on soil strength was investigated indirectly by Lacerda (1989) who carried out drained cyclic tests in which the effective stress was varied at constant deviatoric stress. Similar tests were carried out by Santos (1997) on a residual soil and in both situations, it was concluded that the peak strength was lowered with increased cyclic wetting and drying cycles.

Leroueil & Vaughan (1990) considered the effects of destructuration of a micro-structured clay when subjected to alternating evaporation and swelling regimes. They postulated that if such a soil element is subjected to evaporation, its effective stresses increase isotropically and if it reaches the yield limit state curve (see Figure 2.1), begins to destructure due to compression. It also progressively dries out as suction and effective stresses increase. For the swelling situation, they postulated that the progressively unloaded soil element destructures when the effective stresses decrease and reach the limit state curve.

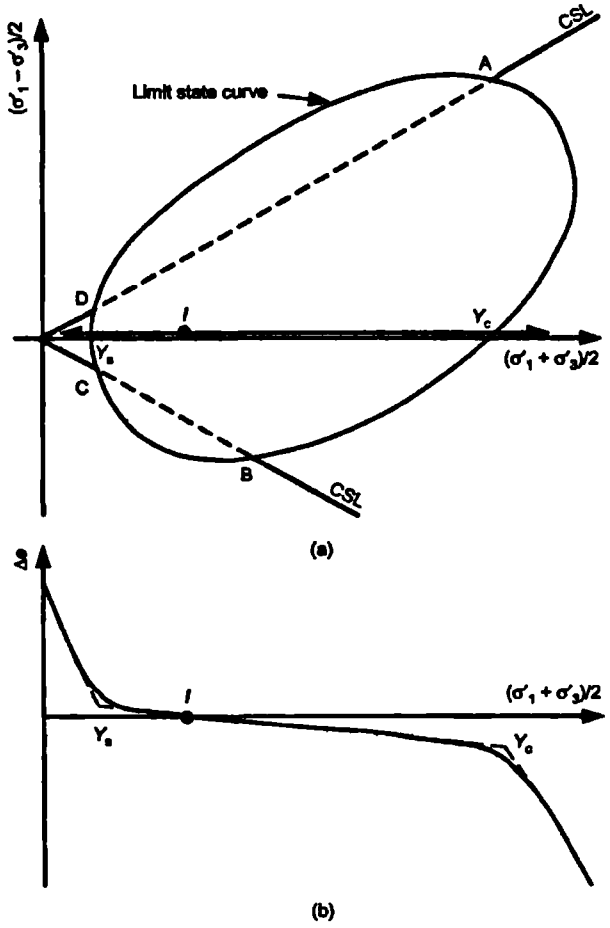

Figure 2.1 Schematised yielding by compression and by swelling (after Leroueil ,2000)

Burland (1990) reported tests on Todi clay in which he showed that the strength envelope of the undisturbed soil was well above that obtained after the clay had been allowed to undergo free swelling for a period of 3 months; hence affirming the concept of destructuration. The strength envelope of the reconstituted clay was lower than that of tests on the clay that had been destructured by free swelling.

Leroueil (2001) stated "More generally, for clays close to the surface and in contact with water, there can be primary and secondary swelling, destructuration by swelling or drying-wetting, chemical weathering, and, in marine clays, a progressive decrease in salinity, all factors that contribute to a decrease in strength and stability."

2.2.2 Post-rupture strength

The concept of post-rupture was first introduced by Burland (1990) in his Rankine Lecture. Burland (1990) reassessed the results of consolidated undrained and consolidated drained triaxial tests on London Clay samples and noted that the strength of intact samples at low to intermediate confining pressures fall rapidly from peak to a well defined plateau. The behaviour at peak strength is characterised by the formation of rupture planes and the deformation to post rupture strength involves only a few millimetres of movement.

Tests on Vallerica Clay from Italy (Burland *et al* (1996) and Georgiannou & Burland (2001)) showed that the post rupture strength lies close to the intrinsic line (critical state line for the reconstituted material). Figure 2.2 shows idealised failure envelopes for stiff clays. However, more recent studies (Georgiannou & Burland (2001) suggest that at low confining stresses, the post rupture strength line lies a little above the intrinsic line and at high confining stresses it lies a little below the intrinsic line

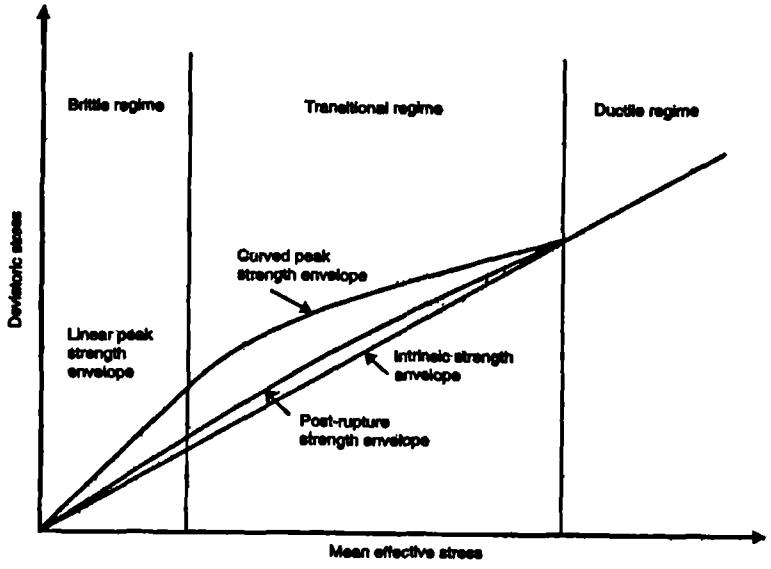

Figure 2.2 Idealised failure envelopes for stiff clays (after Burland *et al*, 1996)

2.2.3 Residual strength

In stiff clays the strength drops to residual after very large displacements, concentrated in thin shear zones (Skempton (1964), Skempton & Petley (1967), Skempton (1985a) and Lupini *et al* 1981)). Residual strength is the minimum drained strength attained at slow rates of shearing and after large shearing displacements (Figure 2.3). The large displacements are accompanied by reorientation of the clay particles along a thin shear zone. The soil either side of the shear zone will still have higher strength. The strength reduction from post rupture to residual takes place gradually as the clay particles become aligned during sliding. Residual strength is usually determined in the laboratory from shear box tests or using a ring shear apparatus.

Residual strength is governed by several factors including mineralogy, plasticity, applied stress, type of shearing, shearing rate and pore water chemistry. The residual angle decreases as the clay

fraction or plasticity increases (Figure 2.4). It is also assumed that in soils with a low plasticity index and a high granular content, shearing takes place by rolling or rotation of particles, referred to as turbulent shear (Lupini *et al*, 1981). For soils with a high plasticity index, the shearing will not be dominated by rolling or rotation but by sliding at residual strength. In the latter case, a well defined slicken-sided slip surface is formed but this type of behaviour might not be observed in clays that do not have platey particles.

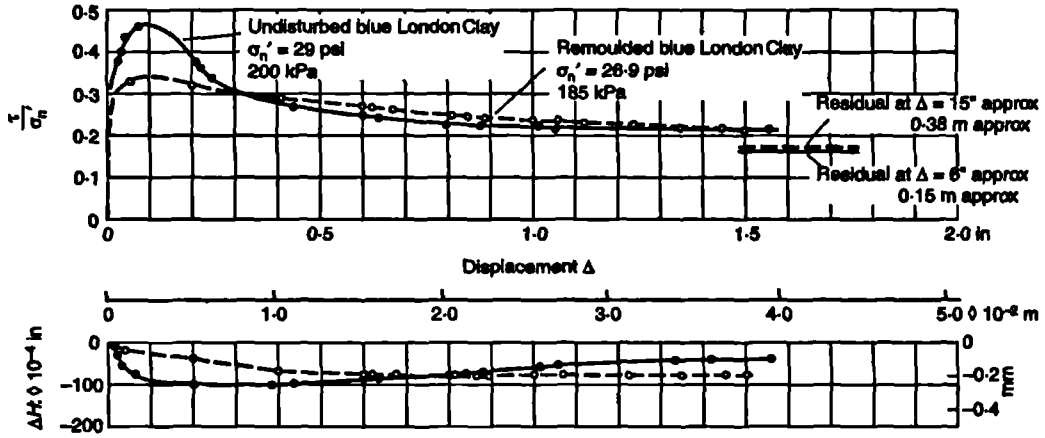

Figure 2.3 Stress ratio-displacement relationships from drained ring shear tests for undisturbed and remoulded blue London Clay from Wraysbury (after Bishop *et al*, 1971)

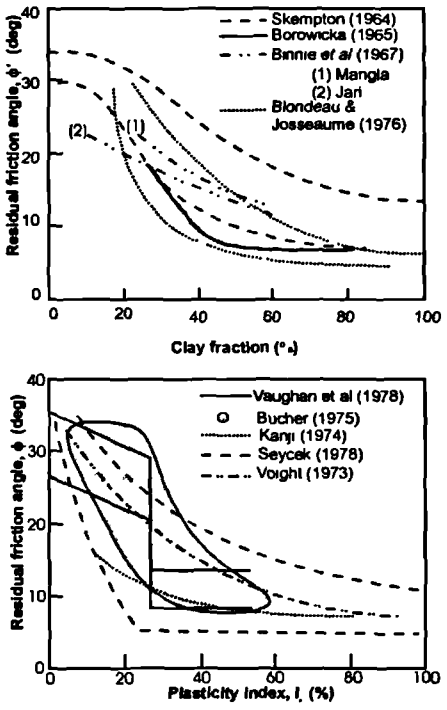

Figure 2.4 Effect of clay fraction and plasticity index on residual angle of shearing resistance (after Lupini *et al*, 1981)

Tests by Lupini (1980), Lemos (1986) and Tika *et al* (1996) showed that residual strength increases by a small percentage when the rate of displacement increases by one order of magnitude. It has been observed that at faster shearing rates the residual strength may increase, decrease or remain constant depending on the soil and testing conditions. Tika *et al* (1996) concluded that a decrease in residual strength at fast rates resulted from an increase in void ratio in the shear zone and would exist if free water were available.

Post peak behaviour in general is difficult to quantify. In general, the residual strength determined in the laboratory is dependent on the type of test performed

eg. the conditions in triaxial samples post-peak become non-uniform when shear zones form, which casts some doubt on the validity of measurements in the triaxial apparatus. In the ring shear apparatus, continuous displacements are allowed as the sample shears along well defined shear surface and this yields the lowest value of residual strength.

Skempton (1985a) and Bromhead (1992) reported that tests on specimens including natural slip surfaces gave residual strengths very similar to those deduced from back-analyses. The laboratory value is usually less than the value predicted from back analyses by about 1-3° for London clay (Chandler, 1984 and Skempton, 1985a) as a result of uneven shear surface which exist in the field (Figure 2.5). It is noteworthy however, that back-analyses of landslides is particularly difficult because the geometry and pore water pressures are usually not fully known and the effects of the three dimensional nature of the slip surface is usually ignored, and yet they can be significant. Back-calculated strengths therefore reflect the assumptions made in the analyses.

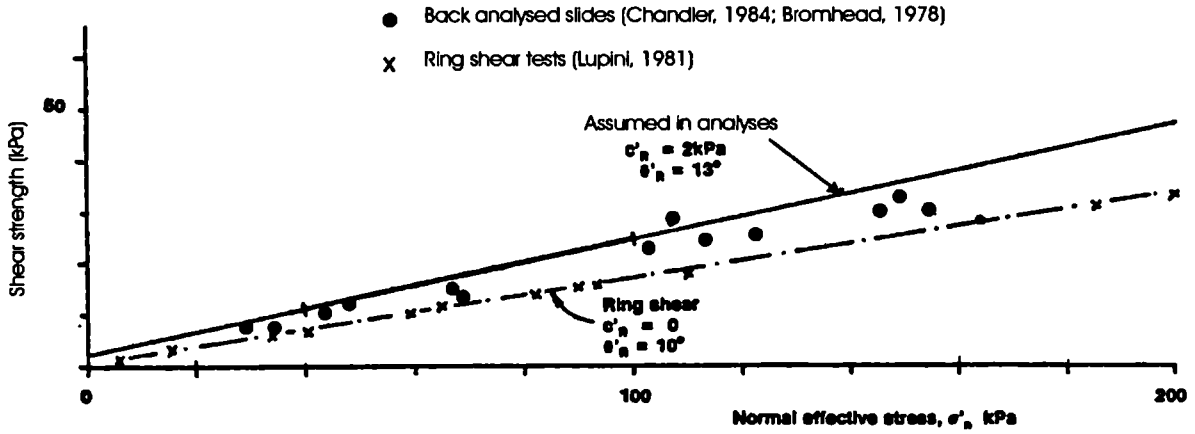

Figure 2.5 Residual strength of London Clay as measured in the ring shear apparatus (Lupini, 1981) and back-calculated from slides and as assumed in the analyses (after Kovacevic ,1994)

2.2.4 Brittleness indices and coefficients

Most clay soils exhibit strain softening behaviour. The strength reaches a peak value and then reduces with further straining towards an ultimate value ie. brittleness. The rate and magnitude of progressive movements that occur within a soil mass at failure are largely dependent on its brittleness. When analysing a geotechnical problem involving progressive failure, it is necessary

that the rate and amount of brittleness of the soil be quantified. This can be achieved by defining the stress-strain relationship. Brittleness indices and coefficients give an indication of the degradation of shear strength with strain and enable comparisons to be made between different soils.

The indices are usually expressed in terms of peak, τ_p, residual τ_r, and the mobilised shear strength, τ_{mob}. A coefficient which gives an indication of the ratio between τ_p, and τ_r is one given by Haefeli (1965) called the Residual Coefficient, I_R :

$$I_R = \frac{\tau_r}{\tau_p} \qquad \text{Equation 2.1}$$

An alternative coefficient proposed by Bishop (1967) is the brittleness index, I_B given as:

$$I_B = \frac{(\tau_p - \tau_r)}{\tau_p} \qquad \text{Equation 2.2}$$

where τ_p and τ_r are the peak and residual shear strengths, respectively. Equations 2.1 and 2.2 only describe the stress-strain behaviour of the soil. In boundary value problems, it is also useful to describe the ratio of shear strength mobilised along the slip surface. The most commonly used is the one given by Skempton (1964), called the residual factor:

$$R = \frac{(\tau_p - \tau_{mob})}{(\tau_p - \tau_r)} \qquad \text{Equation 2.3}$$

where τ_{mob} is the average strength mobilised along the shear surface. From this definition, it can be seen that if R = 0; there is no progressive failure whereas if R = 1, the average strength has reached residual. More recently, D'Elia et al (1998) proposed a brittleness index defined as follows:

$$I_{GB} = \frac{(\tau_p - \tau_{mob})}{\tau_p} \qquad \text{Equation 2.4}$$

The value of I_{GB} varies from 0 at the peak and equals Bishop's brittleness index at residual strength. It is also important to point out the fact that brittleness is not a soil parameter but only an indication of its behaviour.

The mechanism of progressive failure is an incremental process which involves the gradual increase of plastic deviatoric strains. The process can take many years before complete collapse of a slope

can occur. Dounias (1987), Kovacevic (1994), Potts *et al* (1997) and Potts & Zdravkovic (2001) reported numerical analyses of embankments and cut slopes in London clay and highlight the limitations and inability of conventional limit equilibrium methods to model progressive failure. By definition, limit equilibrium analyses assume full mobilisation of shear strength along assumed shear surfaces whereas in a progressive failure mechanism, the soil along a potential slip surface is at different strengths.

The propagation of a shear failure along a potential slip plane in a non-brittle soil results in small post-failure movements since limit conditions represent more or less a state of equilibrium (Vaughan & Hamza, 1977 and Vaughan *et al*, 1978). In a brittle soil, the local loss of strength results in energy release from the surrounding soil mass leading to further propagation of failure until general failure occurs when the strength reduction in post-peak regions exceeds the increase in mobilised strength in the pre-peak regions (Bishop, 1971a). This results in relatively large post-failure deformations.

2.3 Permeability models

2.3.1 Introduction

The anisotropic behaviour of soils is now well known and this behaviour is also reflected in permeability eg. Lambe & Whitman (1969), de Mello (1977), Bromhead & Vaughan (1980), Vaughan & Walbancke (1975), Vaughan (1989) and Vaughan (1994). During an analysis, it is necessary to input permeability values for the soils undergoing seepage (whether steady or coupled).

The type of permeability model selected is governed by the requirements to match field behaviour and also consideration of the nature of the analysis eg. whether it's at the preliminary or detailed design stage. Several models exist eg. isotropic, anisotropic, isotropic but spatially varying and nonlinear varying with mean effective stress or void ratio. The following gives a brief outline of the models.

2.3.2 Isotropic permeability

This is the simplest model and involves an assumption that the permeability is constant and isotropic at any point, whence a single value of the coefficient of permeability, k, can be specified in the analysis. This basic assumption can be improved upon to reproduce observed field behaviour

eg. permeability reducing with increasing mean effective stress. The latter involves spatially varying k in the horizontal and /or vertical direction to reproduce field behaviour. This model was used in the analyses reported in Chapter 4 .

2.3.3 Anisotropic permeability

An improvement to the previous model is to take account of anisotropy by making the permeability direction dependent. Values of the coefficients of permeability are specified using a set of 3 permeability coordinates which may or may not coincide with the global mesh coordinate system. If the permeability coordinate system is different to the global system, the matrix of the coefficients of permeability have to be transformed into the global system, first. This model can be enhanced further through an option to make the permeability spatially varying.

2.3.4 Permeability dependent on void ratio

Lambe and Whitman (1969) presented experimental relationships between coefficient of permeability, k, and void ratio, e, for numerous soils. These showed that, to a close approximation:

$$\log \mathrm{k} = A + B\mathrm{e} \text{ or } k = e^{(A+Be)} \qquad \text{Equation 2.5}$$

where A and B are constants (material parameters) and e is the voids ratio (see Figure 2.6). It is necessary that the voids ratio be known throughout the analysis. In most situations the material parameters, A and B are difficult to determine and this limits the applicability of this model.

2.3.5 Nonlinear Permeability dependent on mean effective stress

Vaughan (1989) presented nonlinear permeability models which relate permeability to mean effective stress and are presented below.

2.3.5.1 Logarithm law

By assuming that the coefficient of volume compressibility, m_v, to be constant, Vaughan (1989) derived the following equations for permeability:

$$\ln\left(\frac{k}{k_0}\right) = -ap' \text{ or } k = k_0 e^{(-ap')} \qquad \text{Equation 2.6}$$

where k_0 is the coefficient of permeability at zero mean effective stress and a is a constant equal to $-Bm_v(1+e_0)$. e_0 is the initial void ratio at zero mean effective stress. This law was used in the majority of the analyses reported in this thesis (Chapters 5-7).

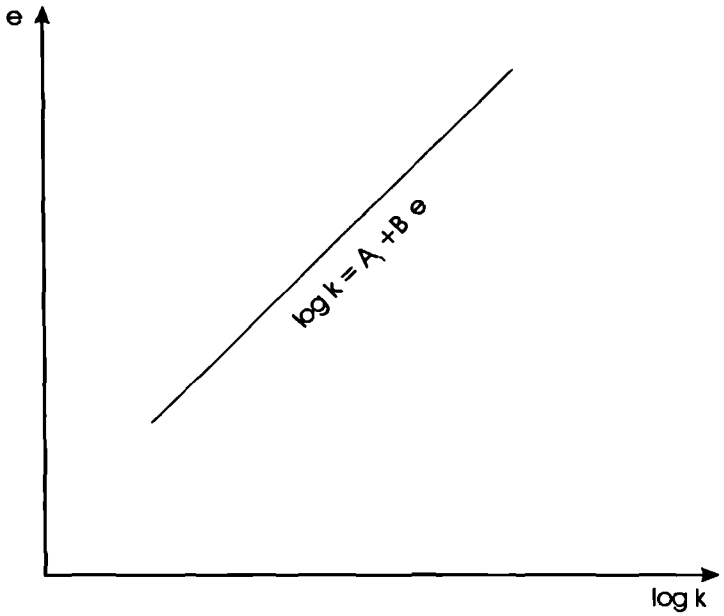

Figure 2.6 Theoretical relationship between permeability and voids ratio

2.3.5.2 Power law

Vaughan (1989) also derived an equation for the coefficient of permeability by assuming that the compression index, C_c is constant, as for one dimensional consolidation; which yields:

$$k = k_0(p')^{-a} \qquad \text{Equation 2.7}$$

where a is a material parameter.

The relationships between permeability and mean effective stress are not valid for cases where local failure occurs or high stress ratios are involved. Vaughan (1989) investigated and compared the rate of decrease in permeability with depth given by the power law and the logarithmic law. He showed that with the power law (Equation 2.7) the decrease mainly occurs at the top of the profile where the void ratio and the permeability change most rapidly with depth whereas for the logarithmic law (Equation 2.6), the decrease in permeability occurs mainly at the bottom of the profile. From this work he concluded that the power law would apply to a profile of clay, normally consolidated one dimensionally, whereas the logarithmic law would be more relevant to a fill.

Vaughan (1989) also investigated the maximum difference in predictions of pore water pressure changes between the two laws on level ground over the depth of greatest engineering interest (ie. 0.3D where D is the overall depth of the profile). His investigations revealed that although the maximum pore water pressures in the lower part of the profile were significantly different, the pore water pressure distribution in the upper part of the profile was similar for the two laws.

The effect of permeability has ramifications for cyclic movements in slopes where progressive failure may occur. The rate of softening of a soil undergoing seasonal cyclic movements not only depends on the brittleness of the soil but is also a function of the magnitude of straining occurring during each cycle. Large magnitudes of cyclic strains result in shorter times to yield, and subsequent failure. Permeability plays a key role in this process because it governs the rate of pore water pressure changes, which in turn determine the magnitude of volume changes in the soil.

2.4 Progressive failure of slopes in stiff clays

2.4.1 Introduction

The mechanisms of progressive failure in stiff-fissured clay slopes were identified in the 1930's by Terzaghi. From their studies, Terzaghi & Peck (1948) and Taylor (1948) concluded that progressive failure is largely caused by softening. The classical definition of progressive failure was given by Terzaghi and Peck (1948) as: "..... the total shearing force that acts on a surface of sliding at the instance of complete failure is considerably smaller than the shearing resistance on the basis of the peak values."

A lot of research has been carried out worldwide on progressive failure since Terzaghi's definition; among them Skempton (1964, 1985b), Bjerrum (1967), Bishop (1967, 1971b), Vaughan and Hamza (1977), Vaughan *et al* (1978), Dounias (1987), Kovacevic (1994), Potts *et al* (1997), Cooper *et al* (1998), Russell *et al* (2000), Leroueil (2001) and Kovacevic *et al* (2001). The majority of the studies have been on natural slopes, with relatively few studies on embankments constructed from brittle materials.

Leroueil (2001) noted that "... owing to the complexity of the processes involved, a complete understanding of progressive failure will come only from representative numerical modelling". Significant advances have been made by the Soil Mechanics Group at Imperial College in the application of the finite element method to analyse geotechnical boundary value problems involving

progressive failure. These include analysis of the Carsington Dam failure by Dounias (1987), Potts *et al* (1990), analysis of embankment dams and cut slopes in London Clay by Kovacevic (1994), Potts *et al* (1997) and more recently, analysis of old railway embankments ICON (1999a and 1999b) and Kovacevic *et al* (2001).

2.4.2 Mechanism of progressive failure

Bishop (1967) identified the main conditions for progressive failure to occur as (i) readjustments of pore water pressures resulting from unloading during excavations or due to modification of ground water level, (ii) delayed release of strain energy and (iii) reduction in the rheological components of shear strength. As a result of progressive failure, the average strength mobilised in a slope at failure will be intermediate between the peak and the ultimate strengths (Skempton (1964), Duncan (1992) and Vaughan (1994)). Based on their wide experience in the application of the finite element method to geotechnical boundary value problems involving progressive failure, Potts *et al* (1997) and Potts & Zdravkovic (2001) noted that the amount of progressive failure is influenced by (i) the relative stiffness of the materials involved, (ii) the nature of the loading, and (iii) the scale of the shearing surface.

Non-uniformities in strains frequently occur in slopes. These can be accentuated by the presence of interbedded layers of different materials, local weaknesses, high pore water pressures, weathered materials, swelling layers, rigid boundaries or irregular boundaries. Unrealistic stress concentrations need careful assessment and consideration in numerical analyses as these can easily dominate the overall mechanism; which may not be a true representation of the actual slope behaviour (Kovacevic, 1994).

2.4.3 Numerical modelling of progressive failure

Traditional methods for slope stability analysis use the limit equilibrium method to assess safety factors while deformations are computed using elastic analyses combined with consolidation theory. Advances to this simplified approach have involved use of continuum analyses which can yield information on stability and deformations. Although limit equilibrium methods are simple and fast to use and may yield relatively accurate results for non-brittle soils, they are inaccurate when brittle soils are involved. This is because the mobilised strength is an input to the analysis and at limiting conditions, the strain and therefore strength distribution is unknown. Another disadvantage is that

they yield no information on the distribution of stresses and displacements. But their greatest drawback is that the engineer has to assume the position of the slip surface.

Skempton (1964) recognised the need to incorporate progressive failure effects in limit equilibrium analyses, as an expedient. This was achieved by carrying out conventional limit equilibrium analyses using a cohesion value of zero. Other methods proposed included use of critical state values (Schofield and Wroth, 1968), empirical reduction factors (Bishop, 1971b) or to reduce the friction angle and cohesion to residual values over parts of the assumed slip surface based on field and laboratory evidence (James, 1971). These techniques only consider brittleness and do not address the issues of stress distributions and magnitude of movements.

In his review of methods used to model progressive failure, Dounias (1987) identified a number of methods which he referred to as "purpose built methods". In the methods, the exact failure mechanism is postulated and the stress-strain curves, stiffnesses and volume change characteristics determined. The analyses are carried out assuming the soil to be linear-elastic perfectly plastic or linear elastic with strain softening.

In general, although numerical methods are powerful and ideal for analysing geotechnical problems, their use and development has been hindered by the large computer resources that are required. However, this scenario changed during the 1990s, as developments in computer technology made it possible for powerful computers to be readily available in research centres and industry. As a result, significant breakthroughs were achieved in the application of FEM to model progressive failure.

The application of the finite element method to analyse slopes was outlined by Naylor (1999). The work reported by Potts and Zdravkovic (2001) using the computer code ICFEP (Imperial College Finite Element Program) considered the stability of cut slopes and embankments experiencing progressive failure using a model of the Mohr-Coulomb type in which the strength parameters c' and ϕ' varied with deviatoric plastic strain.

In real plastic clays one or more shear surfaces are likely to develop when peak strength is mobilised and the ensuing loss of strength as sliding occurs along the shear surface. Such thin zones are not reproduced in finite element meshes. Kovacevic (1994) investigated the influence of element thickness on the rate of softening and established that when varied over a realistic range, it does not have a major influence on the results. Kovacevic (1994) also observed that in order to

accurately model progressive failure, it is essential to monitor the convergence norms of the iterative nodal displacements, loads, flows and pore water pressures and keep them very low (typically less than 1%) as well as monitor and maintain the residual stresses at integration points to low values (typically less than 0.1kPa when approaching collapse).

2.4.4 Numerical analysis of embankments involving seasonal pore water pressure changes

To the author's knowledge, the only published work involving numerical modelling of progressive failure induced by seasonal cyclic movements has been carried out in the UK. The majority of the research was undertaken in the late 1990's by the Soil Mechanics Group at Imperial College using ICFEP; (Kovacevic *et al*, 2001). Some research was also carried out in industry using FLAC (Fast Lagrangian Analysis of Continua) and reported by Russell *et al* (2000), however, the analyses were of limited scope. Most of the embankments that were analysed related to railway embankments constructed from London Clay fill.

The work by Kovacevic *et al* (2001) and Russell *et al* (2000) reflects the state-of-the-art in the UK, to model the surface flow boundary involving root water extraction. The surface flow boundary was modelled by assuming pore water pressure distribution patterns for winter and summer which were believed to prevail in the field. The winter and summer pore water pressures were applied cyclically, until progressive failure was achieved. Although their analyses involved coupled consolidation/swelling, they allowed full equalisation of pore water pressures at the end of each winter and summer cycle. In prototype embankments, the pore water pressure regime is continually changing in response to evapotranspiration, rainfall and ground water flow such that at the end of each season only a transient pore water regime exists. The main drawback with this approach is that the pore water pressure distributions are assumed and may not necessarily prevail in the field.

The complexities involved in modelling the surface pore water pressure boundary mainly arise from the fact that it involves the interaction of the atmosphere, plants and the ground; where the flow of water depends on several variables. Geotechnical researchers have attempted to model this flow boundary situation eg. (Blight (1997), Fredlund (2000), Wilson *et al* (1994 & 1997), Fourie *et al* (1999) and Ng *et al* (2001).

Whilst the climatic variables govern the amount of rainfall and evapotranspiration, within the ground, the rate of water flow is primarily governed by the permeability of the soil. In addition,

transpiration occurs at depth through root water uptake. Therefore it is necessary to develop models which reproduce this phenomenon more realistically. This latter aspect has received nominal attention in soil mechanics because the long-held view is that it's the domain of soil physicists and agronomists. However, geotechnical engineers need to carry out research in this area because in certain conditions, vegetation can play a dominant role in boundary value problems.

2.5 Influence of vegetation on pore water pressures and ground movements

2.5.1 Introduction

As previously mentioned, a lot of research has been carried out in Civil Engineering to assess the influence of trees on foundations in clays eg. Ward (1953), Driscoll (1983), Coppin and Richards (1990), Crilly *et al* (1992) and Biddle (1998) from which it has been shown that significant shrinkage movements can occur as a result of desiccation induced by the evapotranspiration effects of vegetation. Chandler *et al* (1992) studied the results of laboratory filter paper tests on intact samples of stiff clay retrieved from boreholes and concluded that desiccation caused by trees in south-east England can be as deep as 8m.

In the last decade, there has been a surge in interest within the geotechnical community to understand the influence of vegetation on soil behaviour, particularly in relation to slope stability. There is now increased awareness among geotechnical engineers for the need to link the constitutive behaviour of soils to plant water-uptake models in geotechnical numerical algorithms eg. Greenway (1987) and Mathur (1999). In order to develop realistic algorithms, some knowledge of root morphology and plant physiology is required. The following sections describe the pertinent aspects of root morphology and plant physiology for developing plant water uptake models.

2.5.2 Growth and function of root systems

The four main functions of a root system are (i) to support and anchor the tree in the soil, (ii) to absorb and conduct nutrients required for growth, (iii) to absorb and conduct water and (iv) to act as a storage organ for starch.

The requirements for prolific growth are an adequate supply of water and oxygen, suitable soil temperature and absence of mechanical impedance. The level of minimum oxygen concentrations

required varies with species, root temperature and with the aerial environment. In their growth roots tend to follow moisture gradients; always tracking zones of maximum water potential. Optimum root growth requires oxygen levels of at least 15%; which is rarely existent under field conditions in clayey soils. The level of oxygen supply largely depends on diffusion. This process is facilitated in clays when it cracks on shrinkage. Where soil is saturated root growth is inhibited because the rate of diffusion in water is much lower.

Absorption of water largely takes place through the unsuberised portion of the fine roots, which lie immediately behind the root tip. The majority of these fine roots are 1mm in diameter. The surface area of this water uptake zone is greatly increased by root hairs, which are unicellular outgrowths from the outer cells of the fine roots. Root hairs are typically less than 1000μm long and 10-15μm in diameter and therefore invisible to the naked eye (Russell, 1977). There is much variation in both their size and longevity.

The amount of water taken up by the roots depends on a number of factors including (i) the availability of water in the soil, (ii) the species, size and vigour of the tree and (iv) the rate of evaporation under prevailing weather conditions.

Climate, the distribution of roots and soil characteristics all interact in determining the magnitude of pore water pressure gradients in the soil under growing plants. Under field conditions, variation in water supply is frequently the major cause of differences in the distribution of roots, particularly the depth they attain in the soil. Roots also have a capacity for compensating growth; a restriction of growth in part of the root system may lead to increased growth of more favourably placed roots.

The most important characteristic of the root systems of many plants which contributes to their survival in dry conditions is the ability to extend sufficiently rapidly to continue maintaining contact with water. If there is an adequate supply of water throughout the rooting zone, the size of root systems may be more than ample to supply the needs of the plant. When water stress occurs for only a limited period, a further characteristic of the root system can be of considerable importance; namely the rapidity with which new roots develop after the water potential in the soil becomes favourable; especially in the upper layers.

The response of root systems to variations in water supply under natural conditions is perhaps the most difficult aspect of the behaviour of plants to predict or to describe in quantitative terms. Uncertainty is caused both by the rapid and largely unpredictable changes in water supply which

seasonal weather can bring about and the equally rapid response of plants to these changed conditions. Moreover, it is possible that the closeness of contact between roots and the soil, and hence the resistance to the transfer in water can be affected.

Mechanical impedance of the ground also plays a significant role in root growth. The axial pressure exerted by the root tip is related to the osmotic pressure and the turgor of the cells. For a root to elongate, mechanical impedance of the soil acting against the cross-section of the root tip must be less than the pressure exerted by the root tip. In fine grained soils the soil particles must be moved aside if the root is to penetrate. The embankments in the current research were constructed of loose dumped clayfill whose initial void ratio was high with a maximum diameter of the clay clods estimated to be up to 300mm (Skempton, 2000). It is therefore generally believed that root growth would have been prolific, under minimal mechanical impedance.

In practice, many natural clay soils such as London Clay have a bulk density in excess of 1.8g/cm^2 and their resistance increases as the soil dries. In high strength soils it is considered unlikely that roots would be able to penetrate the soil to great depths (Materechera *et al*, 1991). The roots will tend to exploit the fissures induced by shrinkage cracking and other macro-pores created by invertebrates or previous roots. Favourable conditions for root growth in these soils are therefore primarily in the shallow horizons of the ground, however, it is the search for water which is by far the dominant factor in determining the morphology of a root system.

The root plate is that zone comprising the roots and the surrounding soil. In observations by Kew Gardens on uprooted trees following a major storm in October 1987 in England (UK), it was noted that root plates are much shallower than was originally thought. Observations on over 4500 trees and 40 genera revealed that in 50% of cases the root plate was less than 1m in depth and the root plate depth exceeded 2m in less than 4% of the cases, (Cutler *et al* (1990) and Gasson & Cutler (1990)).

The majority of uprooted trees in the Kew survey were on level ground therefore caution needs to be exercised when extrapolating this data to trees on steep slopes, such as those on embankments. On steep slopes the depth of roots is likely to be significantly influenced by the requirements for anchorage and also the fact that drainage on slopes tends to lower the piezometric profile to deeper strata. This is corroborated by occasional root sightings at depth during ground investigations for remedial works, although their preponderance has never been investigated. Their significance in terms of water uptake is also open to conjecture.

2.5.3 The soil-root interface

The resistance of the soil to the movement of water to roots is often regarded as consisting of two components - the pararhizal and the rhizosphere resistances. The former is the resistance to the movement of water through the bulk soil to the rooting zone, the rhizosphere resistance being that in the soil immediately adjacent to each single root. If the rhizosphere resistance were sufficiently high, the roots of a rapidly transpiring plant would, in theory, increase suctions in the neighbouring soil to near the wilting point, even though the water potential a short distance away were close to field capacity. Roots would thus have access only to water in their immediate vicinity and the quantity of water they would extract would be closely related to the total root density.

If on the other hand the rhizosphere resistance were relatively low, pore water pressures would change only slowly with the distance from roots and the zone from which they could draw water would be considerably larger. In this latter case, root density would be less important in determining water uptake. In field conditions the real behaviour lies between these two extreme scenarios.

2.5.4 Transpiration

Transpiration accounts for 99% of a plant's water uptake, with the balance being incorporated into sugar or cell contents through the process of photosynthesis (Marsland *et al*, 1998 and Biddle, 1998). As water evaporates from the leaves of a plant, forces are set up in the water transmitting regions of the plant tissue (xylem) that move water from the roots to the leaves. The forces set up in the xylem tissue cause the pressure head of groundwater at the root-soil interface to decrease. A hydraulic gradient develops within the soil in such a way that water flows towards the root. The flux and pressure head at the root-soil interface is the resultant of the interaction between the evaporative demand and the water supplying ability of the soil. This interaction is modified and affected by the resistance to flow in the soil, the plant and the atmosphere adjacent to the leaves.

The flow of water to the root is a dynamic unsteady state phenomenon. The whole process is primarily controlled by special leaf cells called stomata. Whenever there is an adequate supply of water, the stomata are open and carbon dioxide can diffuse in while water vapour diffuses out, but if there is insufficient water, the stomata close to prevent further water loss. Differences in stomata number, size, location and overall control account for some of the differences in water demand between species (Biddle, 1998).

Biddle (1998) states that "In practice, even if water is freely available and conditions are conducive to high transpiration rates (ie. high temperature, low vapour pressure and sufficient air movement), the absorption of water usually cannot keep pace with transpiration loss and a deficit within the plant occurs; which may be sufficient to lead to loss of turgidity and temporary closure of the stomata". In practice, water uptake by a plant is heavily dependent on water availability; which makes it extremely difficult to try and predict or calculate the quantity of water that might be lost in transpiration by a tree.

During summer, the amount of water absorbed by the roots is usually greater than that supplied by rainfall, causing the soil to progressively dry out from the top downwards. In winter, deciduous trees lose their leaves and transpiration rates drastically reduce. This allows the soil to recover its water deficit. In most situations the soil recovers fully each winter, so that the influence of the tree is entirely seasonal (Shaw, 1994). However, in some situations full recovery cannot occur during the winter, leaving some of the soil strata permanently desiccated. The maximum suctions tolerated by plants are species dependent but are thought to typically lie between 1200kPa and 2000kPa (Kozlowski, 1971).

2.5.5 Modelling root water uptake

2.5.5.1 Microscopic models

In dealing with water uptake by plant roots, it has been customary to adopt one of two distinctly different approaches. In the first approach, water flow to a single root is considered (microscopic models) while in the other approach (macroscopic models), the integrated properties of the entire root system over a representative volume of the soil are considered.

In microscopic models the root is considered to be a hollow cylinder of uniform radius and infinite length having uniform water absorbing properties (eg. Gardner (1960) and Hillel *et al* (1975 & 1976)). In order to solve the equation of water flow, it is assumed that the water flux through the rooted zone and the plant is proportional to the total water head difference and inversely proportional to the total resistance met in the system. The equation is then solved by using the analogy of Ohm's Law for the relation between voltage and current flow.

Alternatively, an analogy of Biot's Law for heat flow to a linear sink of infinite length is used to calculate the rate of water flow as a function of the coefficient of permeability and matrix suction.

In the latter approach, Darcy's flow equation is written in radial coordinates which can then be integrated to derive the flow. The applicability of microscopic models to solving boundary value problems is very limited since the detailed geometry of the rooting system is difficult to determine, is time dependent and any finite element mesh would need to be very fine.

2.5.5.2 Macroscopic models

Macroscopic models constitute the majority of root water uptake models used to simulate root water uptake for hydrological use. The earliest attempt to describe root water uptake by considering the whole rooted zone as one unit rather than individual roots was made by Danielson (1967) who developed an empirical rule which assumes that 40%, 30%, 20% and 10%, respectively, of the total transpiration requirements come from each successively deeper quarter of the root zone. Over the years, advances in soil physics have made it possible to describe root water uptake using mathematical equations based on semi-empirical rules. It is now possible to represent water uptake by roots using a volumetric sink term which is simply added to the water flow continuity equation.

The sink term is the volume of water extracted per unit time per unit bulk volume of soil. It is a function of the soil suction as well as the depth. Various forms of the sink term exist in the literature depending on the assumptions made on parameters such as transpiration rate, root density, root distribution and root length. These include Gardner (1964), Molz and Remson (1970), Feddes & Rijtema (1972), Feddes *et al* (1978), Hoogland *et al* (1981), Prasad (1988), Green and Clothier (1999), Li *et al* (1999 & 2001) and Vrugt *et al* (2001a & 2001b). The numerical implementation of a generalised sink term in the continuity equation is discussed in more detail in Section 3.3.3 of Chapter 3.

The majority of the mathematical functions assume a linear distribution of the transpiration rate with depth of one form or another which is directly proportional to the potential evapotranspiration. Other models assume an exponential distribution function to describe the rate of water uptake with depth. Potential evapotranspiration is the evapotranspiration that occurs when the water supply to roots is unlimited. This takes place when the volumetric water content is at least equal to the field capacity. The advantage of such an approach is that it allows direct combination of the root water uptake with transient soil water flow.

Root water uptake is generally considered to be simply a function of the vertical dimension only, even in models where two or three dimensions are being modelled. Such an assumption may be valid where uniform vegetation cover exists but for isolated trees, water uptake is complex.

Modelling of complex scenarios are presently hampered by lack of data to support spatial variation of root water uptake in three dimensions. The majority of the models currently available are one dimensional (eg. Feddes *et al* (1976), Hoogland *et al* (1988), Prasad (1988) and Jarvis (1989), with a few two dimensional models (eg. Neuman *et al* (1975), Coelho and Or (1996). More recently, Vrugt *et al* (2001) presented a model which can be extended to two and three dimensions. Although the model by Vrugt *et al* (2001) allows for maximum root water uptake at any depth, it still incorporates empirical parameters which cannot be readily derived for various types of vegetation and climate.

A comparison of the moisture content profile predictions around a single almond tree was made for the one, two and three dimension sink terms of Vrugt *et al* (2001) using the HYDRUS software package. The variation of permeability with suction was defined using the method proposed by Van Genuchten (1980) and Mualem (1976). The three dimension model was able to predict the spatial variation in root water uptake. However, there were some differences between the measured and simulated water content values and these were mainly attributed to model errors arising from the assumptions made regarding the geometry of the rooting system and inhomogeneity of hydraulic properties of the soil.

In reality, more regions within the rooted zone may show local maximum uptake because as water demand increases, the roots source water from zones of readily available water (Nyamah and Black, 1977 and Green & Clothier, 1999) whereas in the model only a single region of maximum water uptake is assumed. Li *et al* (2000) noted that although some attempt has been made by some researchers to account for the enhanced root water uptake from deeper horizons when under water stress conditions eg. Jarvis (1989), the models had not yet been tested as an integral part of the continuity equation for water flow.

A number of numerical implementation of root water uptake models abound in soil science and other related agronomical sciences but will not be cited here because they do not incorporate constitutive models of soil behaviour; which are essential for geotechnical analyses. The majority of the models have been developed and validated on agricultural crops; either in the laboratory or field conditions. In general, the models incorporate parameters which have been derived from statistical analysis of data from crops.

2.5.6 The shrinkage and swelling cycle

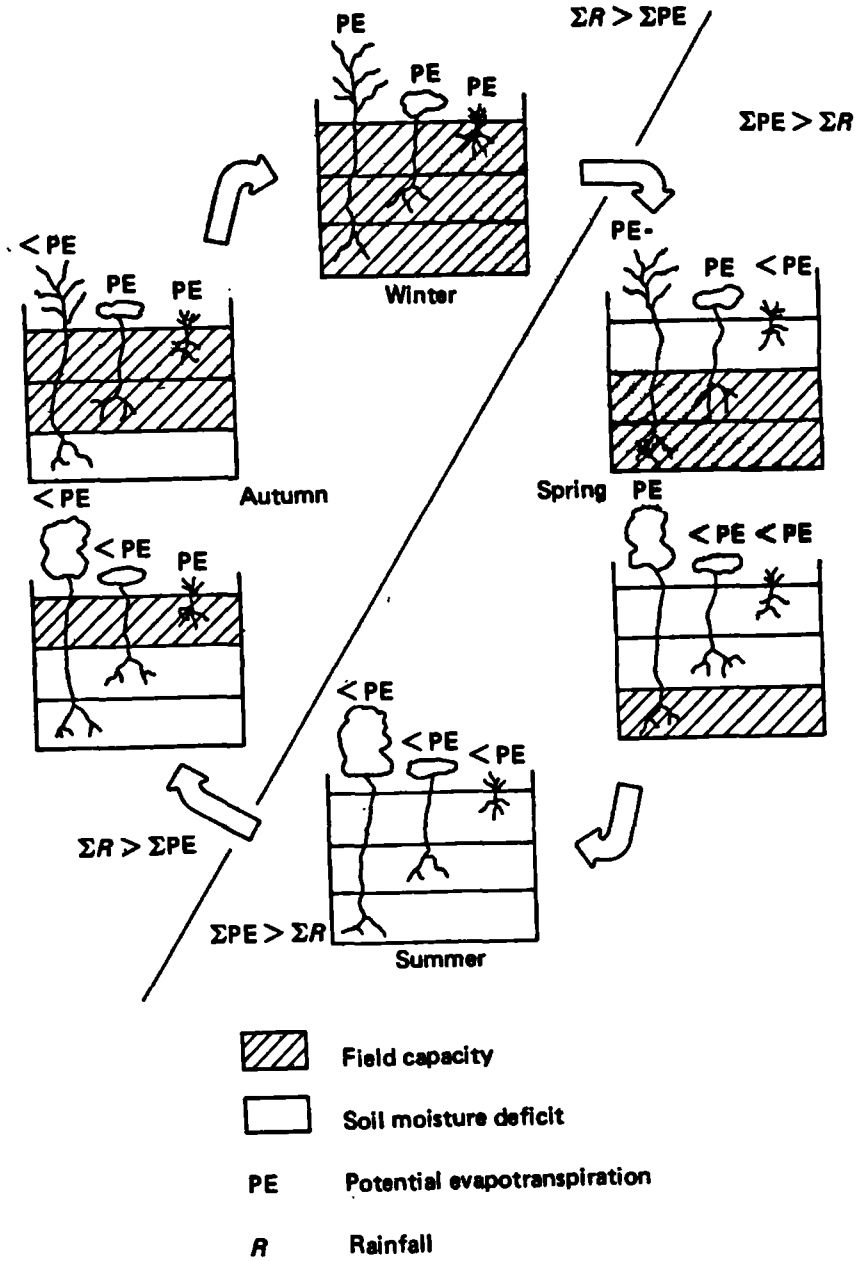

Figure 2.7 Idealised annual soil moisture cycle for 3 vegetation types. (after Shaw ,1994)

Knowledge of the seasonal pattern of magnitude and distribution of suctions within vegetated ground is essential in order to assess the validity and performance of new models. Figure 2.7 shows an idealised annual soil moisture cycle for three vegetation types in a typical UK climate (Shaw, 1994). As can be seen from the figure, at the end of winter the upper most horizon of the soil profile is at field capacity. Field capacity is the stage at which a soil profile can no longer retain any more water in the voids. At field capacity, any further infiltration or ingress of water from

ground flow simply flows through the soil profile but is not necessarily equivalent to conditions at full saturation.

With the onset of spring, the metabolic activity of deciduous trees increases, which results in a higher uptake of water in line with increasing evapotranspiration rates. Although precipitation still occurs, its intensity is relatively less than that during winter. The net effect is moisture depletion coupled with the development of a desiccated profile which gradually deepens during the summer. Conditions during summer are typified by high evapotranspiration rates.

During autumn, deciduous trees lose their leaves and overall evapotranspiration rates decrease. Precipitation also increases and the combined effect results in excess inflow of water into the soil profile, commencing in the upper most horizon. Recharge of water continues at an accelerated rate during winter and this results in the upper horizons reaching field capacity. The overall depth of the desiccated profile significantly reduces and may even disappear by the end of winter, depending on the intensities of precipitation, actual evapotranspiration and antecedent ground water regime.

Results of field monitoring (eg. Biddle (1998) and Crilly and Driscoll (2000)) on natural ground have shown that under trees, a permanent desiccated profile exists whereas in grass covered areas full recharge of groundwater occurs at the end of winter. Crilly and Driscoll (2000) reported suctions of up to 300kPa at 5.5m depth on filter paper tests carried out on borehole samples from a gently sloping Building Research Establishment testing site at Chattenden (Kent) in UK. Parry (1992) reported results of filter paper tests on London Clay samples from a housing development in Essex (UK) which indicated a desiccated profile to 7m depth.

Suctions of up to 500kPa were recorded at 2.5 m depth. In both cases (Crilly & Driscoll, 2000 and Parry, 1992), the filter paper tests results had not been corrected for the in situ mean effective stress. Walbancke (1976) reported the results of pore water pressures typically found in grass covered embankments and cut slopes. It was observed that pore water pressures in these types of earthworks fully recovered at the end of winter with a zero pore water pressure profile at 1m below ground level, on average (Figure 2.8).

Anderson and Kneale (1980a, and 1980b) reported pore water pressures on a grass covered section of an embankment along the M4 motorway west of Swindon constructed from Oxford and Kimmeridge clay that had suffered several shallow slips since the early 1970's. The results indicated higher suctions (up to 40kPa) at 0.25m depth compared to the tensiometer located at 1m

depth which recorded a maximum suction of 25kPa. There was evidence to suggest that the pore water pressures fully recovered at the end of winter during the monitoring period (February 1978 to March 1979).

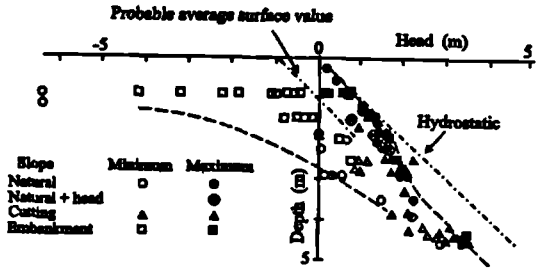

Figure 2.8 Measurements of maximum winter and minimum summer pore water pressures below grass cover in clay slopes in south east and central England. (Walbancke, 1976; Vaughan, 1994)

More recent field based research on pore water pressures in UK's old railway and highway embankments is described in Section 2.6 below. In general, the limitations of state-of-the-art field testing equipment for measuring suctions make assessment of the in situ desiccated profile difficult. Because of these limitations, the field desiccated profile prevailing during summer has never been fully understood. This in turn makes it difficult to validate root water uptake models.

2.5.7 Desiccation and swelling cracking

The relationship between crack depth and spacing is not fully understood, although a general trend of large spacing for deeper cracks seems to exist. A number of researchers have carried out field and laboratory investigations on desiccation from which mathematical equations have been developed to represent the initiation, patterns and propagation of cracks. The field evidence suggests wide variations in maximum crack widths and depths being reported by researchers eg. Reeve *et al* (1980), Morris *et al* (1992), Blight (1997) and Kodikara *et al* (2000).

It is commonly considered that desiccating clayey soils crack when the tensile stress developed in the soil due to the matrix suction exceeds the tensile strength of the soil. Subsequent wetting causes swelling and closure of the cracks. If loose material enters the cracks before swelling can occur, restrained swelling stresses will be generated. Skempton *et al* (1969) concluded that these stresses can be large enough so as to cause the soil to fail passively, creating swelling fissures.

The original work by Lachenbruch (1961) involved the use of elastic theory and fracture mechanics to explain the magnitudes of depth and spacing of thermal contraction cracks in permafrost regions. Morris *et al* (1992) made use of the partially saturated soil mechanics theory and developed equations for predicting crack depths. Konrad and Ayad (1997) presented an idealised model for the analysis of clayey soils undergoing desiccation, utilising fracture mechanical principles.

Bishop and Blight (1963), Blight (1967, 1971 & 1997) invoked the theories of partially saturated soils and earth pressures and assumed that cracking occurs at the surface when the relationship between the effective vertical stresses and the horizontal stress is such that the soil fails or fractures. Blight (1997) suggested that a Griffith or Mohr-Coulomb failure criterion is applicable both at the surface and at depth. He used the Griffith failure criterion to derive solutions for the crack inclinations.

Blight (1997) also considered the strain energy released during crack propagation to determine the crack geometry. He concluded that a minimum of crack surface area will relieve a given strain energy per unit volume of soil ie. the ratio of the area to the perimeter for the crack pattern will be a minimum. Patterns of squares and/or regular hexagons fit this postulation and are therefore the most likely to form in the field. Kodikara *et al* (1999 & 2000) noted that observed field aerial cracking patterns can be divided into orthogonal and non-orthogonal. The process usually involves formation of primary blocks and further drying out sub-divides the primary blocks, sequentially. The non-orthogonal patterns tend to appear simultaneously.

Anderson *et al* (1982) monitored shrinkage cracks during the period August 1979 to February 1980 on a 7m high motorway embankment located west of Swindon along the M4 motorway, discussed in the preceding sub-section. The study area was 12m by 9m on a south facing slope. The embankment was constructed from Oxford and Kimmeridge Clay. They noted visible indications of crack formation in June after which the crack widths and depths closely correlated with the magnitude of precipitation. Subsequent closure was apparent in all locations by February 1980. In addition, a number of 5cm dia. core samples were subjected to radiographical analysis and it was noted that although the cracks had closed at the surface, they remained open at depth. Nevertheless, under field condition the cracks would be expected to close fully with time during periods of prolonged precipitation.

Field measurements of saturated permeability using a constant head method were carried out following crack closure in February 1980. The results indicated a permeability of $4\times10^{-5}\,cm/\sec$ at the surface and $1\times10^{-7}\,cm/\sec$ at 1m depth. Vaughan *et al* (1978) and Symons (1978) also referred to the increased pore water pressure at shallow depths resulting from the ingress of water into the cracks during subsequent wet weather.

The influence of cracks on permeability is of paramount importance since pore water pressures govern the overall stability of a slope. Desiccation cracks significantly increases the mass

permeability of the ground and this results in accelerated recharge of ground water during periods of precipitation. Table 2.1 is an exerpt from BS8004 (1986) and shows typical permeabilities of fissured and unfissured clays. From the table, it can be seen that the permeability of an unfissured clay can increase by up to 8 orders of magnitude when cracked.

Table 2.1 Permeability characteristics of soils: from BS 8004 (1986) with permeability descriptions from Carter and Bentley (1991) (after Fig 4.27 of Biddle, 1998).

Coefficient of permeability k (m/s)	1	10^{-1}	10^{-2}	10^{-3}	10^{-4}	10^{-5}	10^{-6}	10^{-7}	10^{-8}	10^{-9}	10^{-10}
Permeability	High			Medium		Low			Very low		Practically impermeable
Type of soil	Clean gravels		Clean sands and sand-gravel mixtures			Very fine sands, silts and clay-silt laminates			Unfissured clays and well-mixed clay silts containing more than 20% clay		
			Desiccated and fissured clays								

The development of cracks poses one of the greatest challenges in the analysis of boundary value problems involving seasonal cyclic pore water pressure changes in clayey soils. In the field, cracking physically involves separation of the material. This results in significant changes not only in constitutive behaviour, but also permeability of the soil. Most numerical algorithms can account for large displacements but cannot cope with a discontinuous domain; which in turn renders it difficult to model permeability changes arising from crack initiation.

Where permeability changes induced by cracks is deemed to dominate an analysis, simplistic assumptions are usually made. An example of such an approach is that adopted by Kovacevic (1994), using ICFEP to investigate the influence of permeability increase on the stability of a typical UK road embankment. To simulate desiccation cracks, he increased the coefficient of permeability of the assumed cracked layer at the surface by 1 order of magnitude. His investigations were only diagnostic, not predictive.

Developments in constitutive modelling for expansive soils and application of numerical methods in geotechnical engineering during the last decade have also been applied to crack and block models by researchers; all geared to illuminate the effects of cracks on field behaviour eg. Wallace and Lytton (1992) and Prat *et al* (2002).

A long established procedure used to predict ground movements associated with desiccation in clayey soils involves the use of a water shrinkage factor ie. an empirical factor that relates changes in soil moisture contents to volume changes. The factor is variable with depth for a given soil and

typically ranges from 1 to 3 for London Clay. Crilly *et al* (1992) used such an approach to calculate vertical movements at a field testing site in SE England by assuming that the soil was saturated and that there was no lateral component of movement. A similar methodology is widely used in soil science/agronomy (Bronswijk 1988, 1989 and 1991). His numerical procedure models the water balance, cracking and vertical ground movements. The water balance components of the model are computed by considering rainfall and evapotranspiration (through a sink term in the continuity equation of water). Cracking and ground movements are taken account of through invokation of the shrinkage characteristics, soil water characteristics and permeability of the soil. Assumptions are then made of the crack geometry to convert volume changes into crack widths and vertical movements.

The computations are carried out for sub-layers and the crack volume of the entire soil profile is obtained by summation. The model was successfully tested to predict settlement arising from tile drains installed at 1m depth at an experimental site in the Netherlands (Bronswijk, 1989). Climatic input data comprised daily actual precipitation and daily potential evapotranspiration.

In their numerical analyses of LUL embankments, ICON (1999c) developed a formula to estimate the depth of desiccation cracks on vegetated ground. The main assumption made in the derivation of the formula is that cracks form when the total minor principal stress, σ_3, is equal to zero. To facilitate derivation, level ground was also assumed. ICON (1999c) proposed that the suction when cracking occurs, u_c, can be given as:

$$u_c = \sigma_v - (\sigma'_v)_{crack} = \sigma_v \left(1 - \frac{1}{\sin\phi'}\right) \qquad \text{Equation 2.18}$$

where σ_v is the total vertical stress, $(\sigma'_v)_{crack}$ is the effective vertical stress when cracking occurs and ϕ' is the friction angle of the soil.

The depth to which tension cracks form can be found by comparing the actual pore water pressure profile with that given by Equation 2.18. This equation can also be used to estimate the magnitude of suctions if the depth to which cracks occurs is known. ICON (1999c) reviewed field data and estimated that roots induce pore water pressure changes to maximum depths of 5m, which gives u_c values of 200-300kPa, on average. Analyses using this assumption are presented in Chapter 4.

2.5.8 Influence of suction on shear strength and permeability

The development of partially saturated soil mechanics started in the early 1960's when it was recognised that the fundamental theories of effective stress as developed by Terzaghi were only applicable to fully saturated soil, which is essentially a special case since most soils are partially saturated. Early research eg. Jennings (1961) and Burland (1961) Bishop and Blight (1963) and Blight (1965), showed that the controlling factor on shear strength is matrix suction, defined as (u_a-u_w), in which u_a and u_w are the pore air and pore water, u_w, respectively.

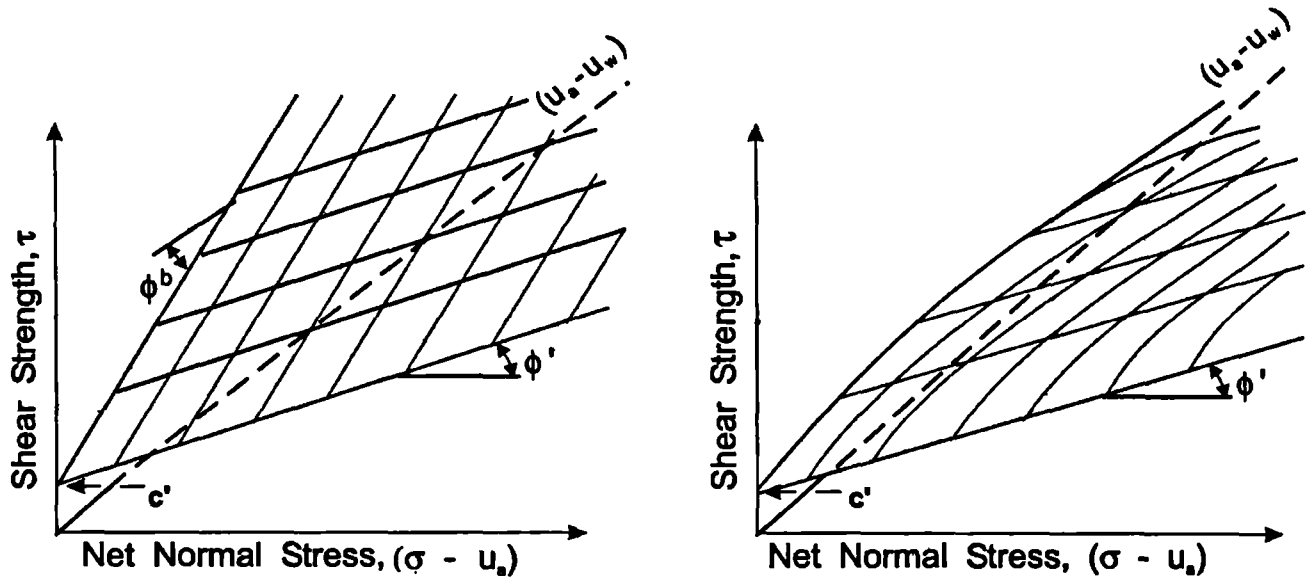

(a) Linear strength envelope *(b) Non-linear strength envelope*

Figure 2.9 Extended shear strength envelope showing the strength parameters for a saturated-unsaturated soil (after Fredlund, 2000)

Shear strength constitutive relationship

More recently, Fredlund (2000) proposed a form for the shear strength , τ, for a saturated-unsaturated soil defined as:

$$\tau = c' + (\sigma_n - u_a)\tan\phi' + (u_a - u_w)\Theta^p \tan\phi^b \qquad \text{Equation 2.19}$$

where c' is the effective cohesion intercept , σ_n is the total normal stress on the failure plane at failure, u_a is the pore air pressure, ϕ' is the effective angle of shearing restance, u_w is the pore water pressure and ϕ^b is the angle defining the rate of increase in shear strength with respect to soil suction. Θ is the normalised water content, $\frac{w(u_a - u_w)}{w_s}$ and w_s is the water content at full saturation. $w(u_a - u_w)$ is the gravimetric water content at any suction and can be represented by

the soil-water characteristic curve, and p, is a fitting parameter. The shear strength surface is curvilinear in shape because the increase in strength changes nonlinearly with respect to suction (Figure 2.9).

Seepage constitutive relationship

The flow through a soil can be described by Darcy's law (Equation 3.4). A number of mathematical relationships have been proposed to establish the relationship between the unsaturated coefficient of permeability and the soil water characteristic curve (eg. Van Genuchten (1980), Fredlund and Xing (1994) and Leong and Rahardjo (1997). Most of the formulations involve normalisation by the saturated permeability, k_s.

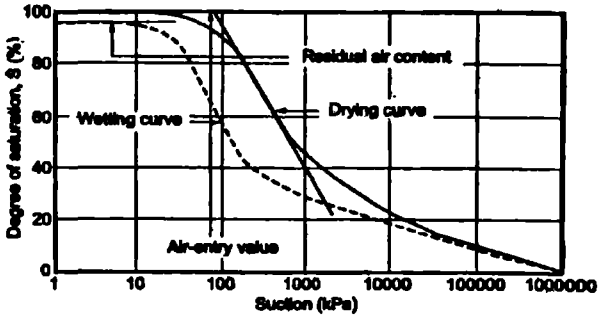

Figure 2.10a Typical soil-water characteristic curve features for the drying and wetting of a soil (after Vanapalli *et al*, 1996)

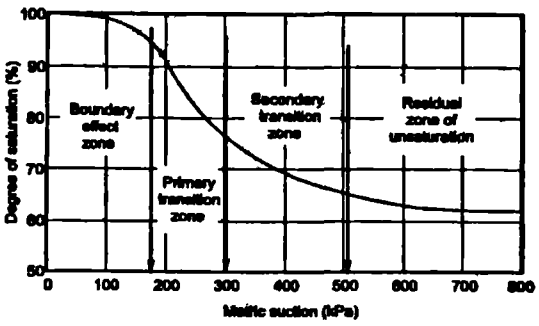

Figure 2.10b Degree of saturation - soil suction curve for a hypothetical porous medium (after Vanapalli *et al*, 1996)

The majority of constitutive models that have been developed are based on the soil water characteristic curve which relates degree of saturation or water content to the applied soil suction under conditions where net normal stress, $(\sigma - u_a)$, is zero or very small (Figure 2.10a). The ordinate in Figure 2.10a. can be specified in terms of gravimetric water content w, degree of saturation, S, or volumetric water content, θ. There are three identifiable stages of desaturation (Figure 2.10b), viz. the boundary effects stage, the transition stage (with primary and secondary transition stages), and the residual stage. The wetting and drying branches form the extreme bounds for the soil-water characteristic curve; while an infinite number of intermediate scanning curves (drying and wetting) pertaining to in situ/field conditions exist between these two bounds. There is no unique curve for all soils, and in general the currently proposed models fit better experimental data for coarse grained soils than clayey soils.

Croney (1977) investigated the relationship between suction and water content for the major clay types found in SE England. He observed that the suction/moisture content relationship for heavy clays exhibits hysteresis, even when the soil is saturated. He also observed that for London clay

samples, the air entry value was in excess of 1000kPa. Marinho (1994) performed suction controlled oedometer tests and filter paper suction measurements on London clay samples from BRE's test site at Chattenden and obtained air entry values in excess of 4000kPa.

The development of suctions in the ground as a result of evapotranspiration has profound effects on the shear strength and permeability of a soil. It is desirable that these additional facets of partly saturated soil behaviour be taken account of in constitutive models, in order to correctly predict soil volume changes and stresses thereof. The development of numerical algorithms that are able to model partly saturated soils of expansive soils is still in its infancy eg. Alonso and Gens (1994). In the framework, it is assumed that as matrix suction increases, the entire limit state curve expands, which implies that peak strength and the critical state strength increase with suction. Conversely, wetting up of the soil results in shrinkage of the failure envelope and soil strength.

2.6 UK old railway embankments

2.6.1 Introduction

The United Kingdom has some of the world's oldest railway embankments dating back to the 1790s, a majority of which are still in service today. Historical records on the construction of the embankments are scarce and current theories and knowledge on their formation is largely derived from ground investigations undertaken in recent years to understand the nature of instability and design of remedial measures. It is generally believed that the embankments were constructed by trial and error, in line with the then current embankment construction techniques. The construction procedure involved end or side tipping material with little or no compaction (Skempton, 1996). Engineering application of compaction techniques only started after the publication of Proctor's theories on compaction in 1933.

Evidence from recent research suggests that most old railway embankments over 6-7m high exhibit some evidence of failure (Vaughan 1994). This has been confirmed by a few available contemporary construction records which reveal that failures commonly occurred during or soon after construction of the higher embankments. A variety of remedial measures were implemented to stabilise the slips and mostly comprised of placing additional fill to attain a stable profile and in some cases augmented with counterfort drains, toe walls, toe drains or grouting. Occasionally, deep seated slips occur, usually following heavy rainfall preceded by a prolonged dry period eg. the wet winter of 2001 which triggered several landslips on motorway and railway earthworks (Geotechnical Observations, 2001).

The instability of embankments is now known to involve progressive failure. On railway embankments the process is exacerbated by vegetation which accentuates seasonal shrinkage and swelling, in line with dry summer and wet winter seasons (McGinnity *et al*, 1996; Perry *et al*, 1999; CIRIA, 2000; and Kovacevic *et al*, 2001). Figure 2.11 shows the main geotechnical problems associated with instability of these embankments.

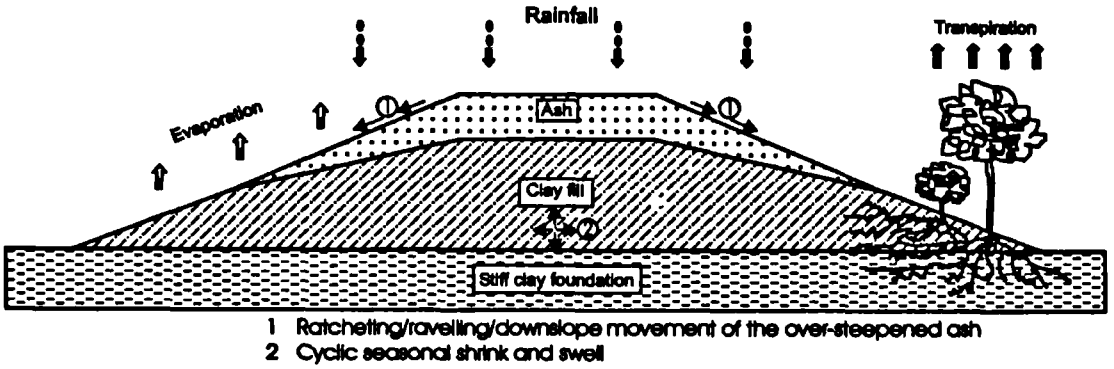

Figure 2.11 Typical geotechnical problems associated with UK old railway embankments

The frequent maintenance undertaken on these embankments constitutes a significant financial drain on resources. Moreover for railway embankments, the poor track quality necessitates the imposition of speed limits on a number of sections of the railway lines. The occasional deep seated slips usually result in severe disruption to train services.

Our understanding of the influence of vegetation on the geotechnical behaviour of old railway embankments in UK has largely come about through ground breaking research that has been carried out during the past 10 years by the Soil Mechanics Group at Imperial College. Through this research, remedial works were spawned and implemented on old railway embankments. Other noteworthy research was carried out by Mott MacDonald (old railway embankments) and the Transport Research Laboratory (motorway embankments). This research builds upon previous research carried out at Imperial College. The relevant previous research carried out in the past 10 years will now be described to put the current research into context.

2.6.2 Research at Imperial College

2.6.2.1 Background

Substantial research commissioned by London Underground Limited (LUL) was carried out at Imperial College in the 1990's. The work encompassed field instrumentation, laboratory testing and numerical analyses. The findings from LUL embankments are also applicable to Network Rail

embankments because they were constructed at the same time, using the same techniques. The Transport and Road Research Laboratory recently undertook studies on the influence of vegetation on pore water pressure changes in motorway embankments. Their studies are relevant to the current research and are discussed in section 2.6.5.

2.6.2.2 Field based research

Research into the stability of old railway embankments at Imperial College dates back to the early 1990's when LUL embarked on a 10 year asset renewal programme to stem the ever-increasing maintenance costs. The majority of the LUL embankments were constructed in London Clay fill and ash ballast. Remedial works during the 19th century primarily involved the addition of ash at crest level to maintain running levels. Over the years the depth of ash gradually increased as "topping up" with ash continued and today, it is common to identify ash mantles ranging in depth between 1-3m, and in some cases up to 6m deep. Figure 2.12 shows typical seasonal movements along an embankment at Canons Park (Jubilee Line).

The first field based research involved instrumentation comprising inclinometers (to measure movements), tensiometers (to measure suctions) and Casagrande type piezometers (to measure compressive pore water pressures) on two LUL embankments; at High Barnet (Northern Line) and at Roding Valley (Central Line) and precise levelling at track level. The orientations of the inclinometers were vertical, raking (45°), and horizontal (inclined down at 5°) as shown in Figure 2.13. The results of the monitoring are shown in Figure 2.14, for the embankment at High Barnet. This latter figure reveals that the movements are cyclic in response to the winter and summer seasons; with more lateral movement occurring during winter when the embankment swells.

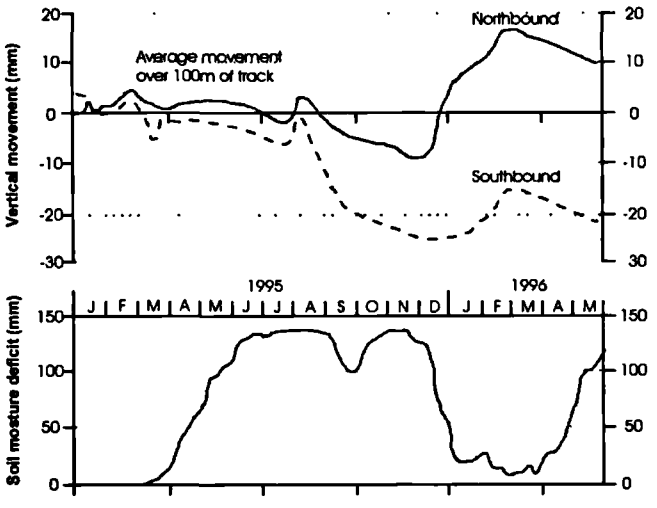

Figure 2.12 Settlement/heave of rails on embankment at Canons Park compared with Soil Moisture Deficit (grass) for London clay (after Kovacevic *et al*,2001)

From their investigations, ICON (1995) discovered that two types of movement could be identified. Within the ash, the movements were driven by the response of the material to seasonal pore water pressures changes. During winter, the material attains a more stable structure as a result of high suctions from the capillary meniscus surrounding the ash grains. With increasing evapotranspiration in the summer, the ash

gradually dries out and loses its shear strength contribution from suction.

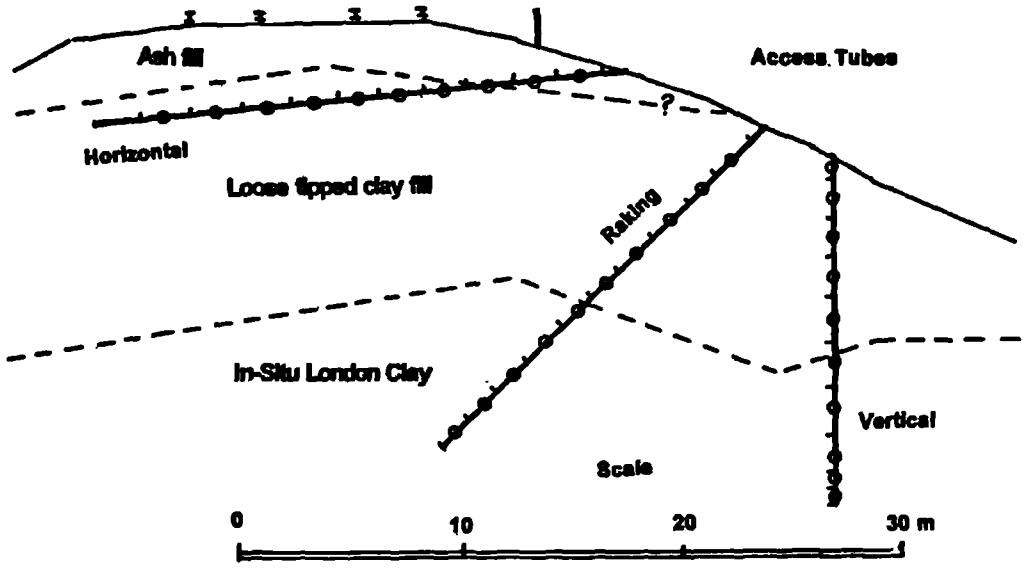

Figure 2.13 Location of access tubes and electro levels on an LUL embankment at High Barnet (after ICON ,1995)

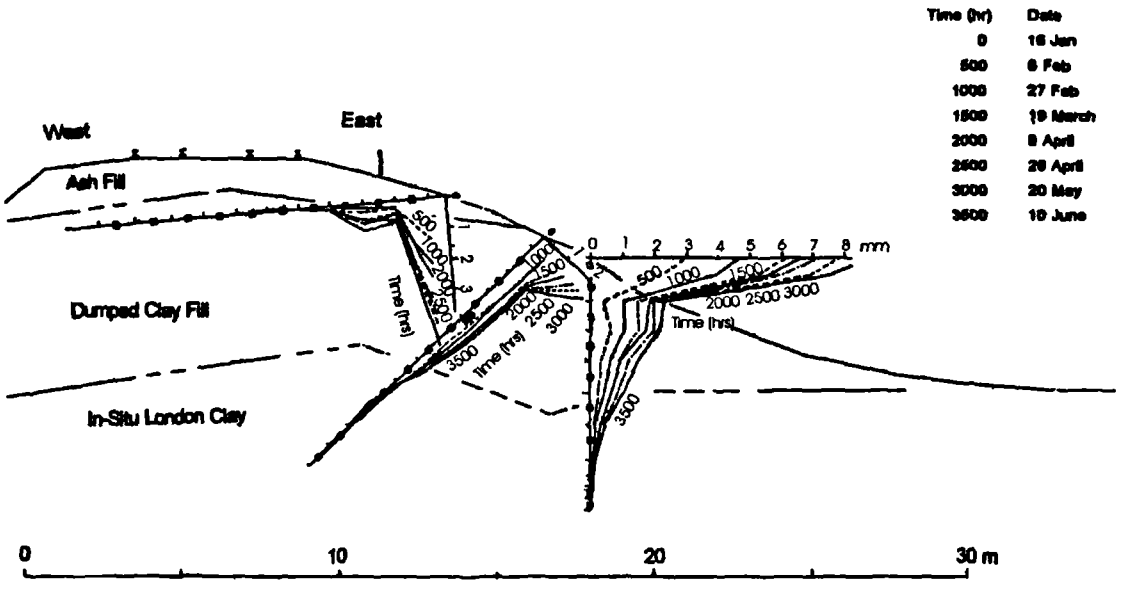

Figure 2.14 Displacements monitored at an LUL embankment at High Barnet in 1994 (after ICON ,1995)

Under dynamic loading resulting from the trains, the unstable dry and loose structure of the ash mantle collapses and fails in a mechanism similar to ratcheting. The latter behaviour is amplified

by the lack of lateral support of the ash on most old railway embankments. The studies also indicated that the magnitude of movement was greater where the ash was deeper.

In the clay fill, the results of field monitoring revealed that although seasonal and cyclic in nature, the behaviour is of a totally different mechanism. During winter, the large precipitation rates combined with nominal evapotranspiration rates by the deciduous vegetation results in pore water pressure increase and significant swelling of the stiff clay. During summer the process reverses and is epitomised by large evapotranspiration rates and little precipitation; all of which lead to significant shrinkage. Further studies and field monitoring identified the cyclic movements in the ash to be dominant.

The tensiometer data indicated that during winter, pore water pressures on the boundary of the clay fill return to zero in both cases where there was ash fill. During summer periods suctions develop in the clay fill in a random manner. This is probably due to evapotranspiration effects which are a function of root depth, root density and spatial distribution and tree type. Other field based research involved an innovative technique to bind the ash using a calcite cement injection and precipitation method (CIPS) (Kucharski *et al* 2000) and hence increase its strength and stiffness. A low viscosity silica based solution was sprinkled on a trial ash embankment. The solution physically binds the ash grains; similar to the natural processes that operate in karst geology. In the trial, different application rates were trialled following which dynamic probing tests were carried out to check the efficacy of the treatment. The trials indicated significant increases in strength and stiffness of the treated material. It is hoped that this technique could be used to stabilise the ash on railway embankments.

It is now known that there is a good correlation between embankment movements, embankment failure and soil moisture deficit (ICON, 1999c). Soil moisture deficit is the amount of water (mm) that is required to bring a soil to field capacity. At field capacity, a soil profile will cease retaining any more water in its structure ie. any further ingress resulting from precipitation or underground flow will runoff. Soil moisture deficit is routinely computed by the Meteorological Office for agricultural use (MORECS, 1995).

A noteworthy project carried out by ICON (2001) involved the monitoring of pore water pressures on an embankment along the Piccadilly Line between Rayners Lane and South Harrow stations. Remedial works undertaken on the embankment included a bored pile retaining wall, a reinforced earth retaining wall, slope regrading and vegetation management. The embankment was originally densely vegetated with semi-mature and mature deciduous trees. The vegetation was removed

during construction of the remedial works except for two trees; a 9m high semi-mature oak, with a trunk circumference of 160cm and a 15m high mature oak with a trunk circumference of 360cm. The two trees were about 40m apart.

Tracks levels recorded prior to the remediation works indicated track movements of up to 70mm on the westbound line. In the zone of dense vegetation, movements of up to 20mm on average were recorded whereas heave of nearly 10mm was recorded next to the semi-mature oak tree where vegetation had been cleared to facilitate construction of the remedial works. The section of the embankment between the two oak trees was instrumented with tensiometers located at various depths. The monitoring results revealed a cyclical pattern of pore water pressures closely correlating with the pattern of soil moisture deficit. Throughout the monitoring period, maximum winter pore water pressures did not reach hydrostatic conditions, except at very shallow depth. In general a suction of less than 10kPa was observed at the end of winter.

Pore water pressure measurements next to the semi-mature oak tree indicated suctions up to 1800kPa at the end of summer. The magnitude of suctions reduced at depth and with distance from the tree. Overall, the oak trees induced pore water pressure changes to a depth of about 3m and to a radial distance from the trees ranging between 1.0H and 1.5H, where H is the height of the tree. The maximum soil moisture deficit during the monitoring period was 230mm and no significant track deformations were observed. This may suggest that higher deficits are required before significant shrinkage movements can occur.

However, it is necessary to point out the fact that although the foregoing results are useful in revealing the influence of individual trees on the pore water pressures, the two oak trees were about 40m apart. In the field trees occur much closer to each other and the overall interactions and cumulative effects on moisture depletion are much more complex. The overall zone of influence and magnitude of maximum suctions will be larger.

Geotechnical Observations Ltd. (based at Imperial College) also undertook pore water pressure monitoring on the LUL network following the winter of 2000-2001 (Geotechnical Observations, 2001). This period (October 2000 to May 2001) proved to be the wettest winter in recent history eg. for grass the average wettest period using a zero soil moisture deficit as the indicator was 93 days (1987-1999) and 71 days for trees. This compares to 210 days (grass) and 128 days (trees) during the winter of 2001-2001. It was therefore considered prudent to monitor pore water pressures in the embankments and compare them with the currently used design standards by LUL.

The monitoring encompassed selected embankments across the whole LUL network where piezometers had been installed during earlier investigations.

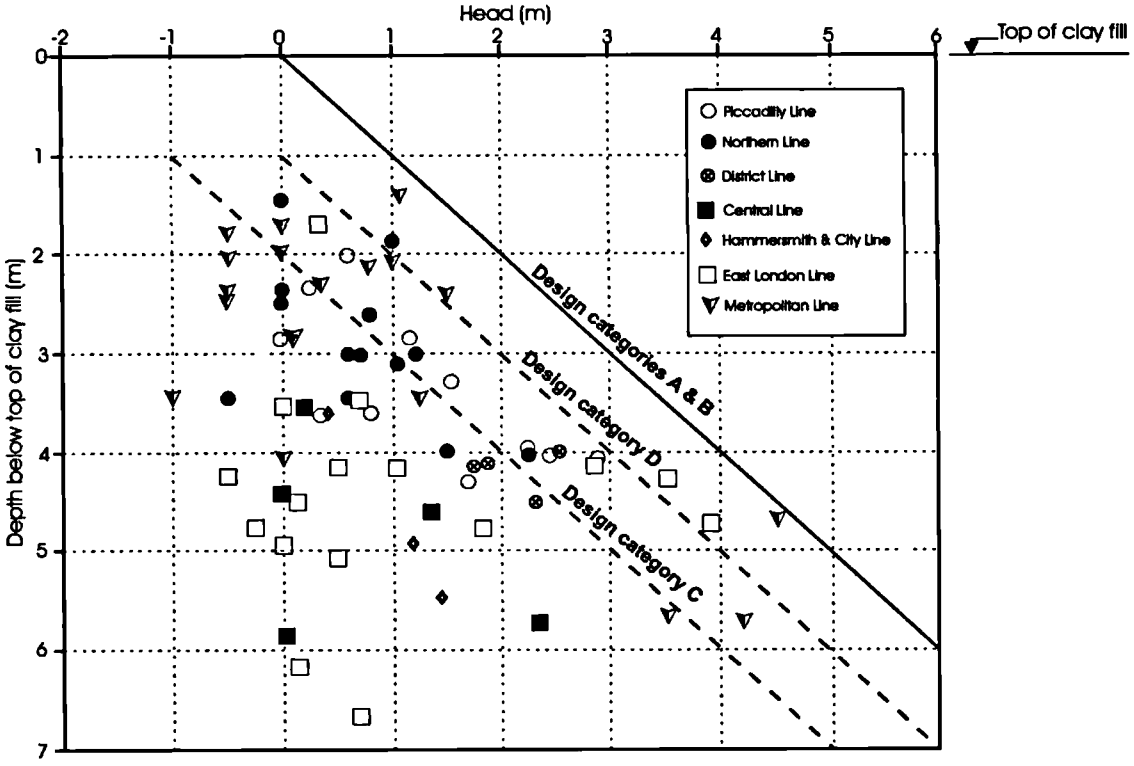

Design Category	Type of vegetation cover	Recommended design pore water pressure profile
A	Bare or grass covered slope with no ash	Hydrostatic below the zero pore water pressure line
B	Bare or grass covered slope and an ash surface layer	Hydrostatic below the zero pressure line which is assumed to be at the ash/clay interface
C	Mature tree covered slope where the desiccation effect is to be relied upon. No ash.	Hydrostatic below the zero pressure line which is assumed to be 2m below the slope surface
D	Mature tree covered slope, where the desiccation effect is to be relied upon. Ash surface layer present.	Hydrostatic below the zero pressure line which is assumed to be 1m below the ash/clay interface

Ref. The LUL Engineering Standard for the assessment of earth structures (E 3321 A4, October 2000)

Figure 2.15 Peak pore water pressures measured by ICON piezometers at the end of winter 2000/01 (after Geotechnical Observations, 2001)

The design guidance by LUL on pore water pressure profiles for clay embankments are given in E 3321 A4, October 2000. LUL categorises embankments in order to identify the design pore water

pressure profile. The categories are dependent on (i) the presence or otherwise of an ash mantle at the top of the embankment and (ii) the presence of vegetation (grass or trees). The categories are shown in Fig 2.15. In general terms, categories A and B represent a worst credible pore water pressure condition and categories C and D represent moderately conservative pore water pressure conditions.

The study confirmed that the maximum pore water pressures encountered in LUL embankments are extremely variable but overall positive or only slightly negative. Figure 2.15 shows a summary of the pore water pressure results. The results indicated that in some cases the pore water pressures exceeded conditions in design categories C and D, whence the desiccation influence from mature trees cannot always be relied upon for stability. Overall, the results confirmed the design guidelines.

The research into seasonal pore water pressure changes and their effect on infrastructure embankments is on-going at Imperial College by Geotechnical Observations Ltd (Geo). Their investigations encompass earthworks on both old railway embankments and motorways.

2.6.2.3 Numerical analyses of embankments

In order to further illuminate the mechanisms causing the movements of old railway embankments and identify suitable stabilisation measures, numerical studies were carried out on typical embankment profiles. The analyses were performed using an idealised embankment profile with simple soil models and estimates of in situ parameters, the intention being to obtain a general picture of conditions within the embankment.

The results indicated that the major causes of movements were not a direct result of train loading. They revealed that during winter, the slopes assume marginal stability as a result of increased pore water pressures in the London Clay fill. This may explain why a number of slip failures occurred during and soon after construction of these embankments. The analyses also indicated that collapse can occur as a result of progressive failure after many cycles of shrinkage and swelling. It was noted that the presence of vegetation accentuated seasonal movements, and this process was associated with permanent strain, albeit small per cycle. In the long term, the incremental build-up in strain level led to development of a progressive failure mechanism. Collapse was preceded by large deformations.

Numerical analyses were also carried to assess the performance of the strengthening works carried out on an embankment at Canons Park (Jubilee Line) using a twin contiguous pile wall with a horizontal tie bar (ICON, 1999a). The primary aim of the analysis was to study the progressive failure mechanism which occurs when a stabilised embankment which has not failed previously during construction or operation fails for the first time. A secondary aim was to examine the mechanism of failure and strain pattern preceding it and also to examine the effect of cycles of wetting and drying on deformation. The analyses did not include investigation into shear strength enhancement by tree roots. The study revealed that a stiff contiguous retaining wall attracts higher bending moments and shear forces compared to a softer wall; when subjected to the same regime of shrinkage and swelling cycles. It was also observed that in the long term after many seasonal cycles, the unsupported part of the slope on the passive side of the wall developed a progressive failure mechanism.

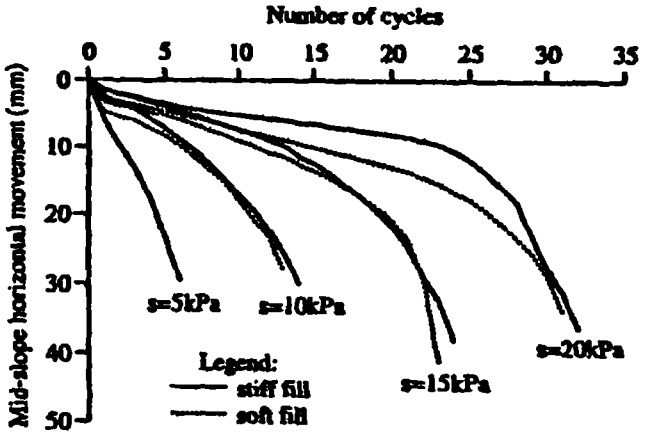

Figure 2.16 Variation of horizontal displacements at mid-slope with cycles - the influence of pore water pressure at the end of swell and of fill stiffness (Fig 9 of Kovacevic *et al*, 2001)

Other numerical studies involved sensitivity studies to investigate the effect of the magnitude of the surface pore water pressure boundary condition (ICON, 1999b and Kovacevic *et al*; 2001). The overall aim was to mimic various degrees of desiccation and winter pore water pressures and their influence on embankment stability. From the analyses, embankment collapse occurred through the fill during winter. The rate of development of progressive failure and hence the time to collapse was slower with increasing magnitude of the prescribed suctions at the surface boundary as shown in Figure 2.16. The parametric analyses involving reduction of stiffness of the London Clay fill suggested that this parameter has no significant effect on collapse.

2.6.3 Investigations by Mott MacDonald

2.6.3.1 Background

As part of its asset management strategy, LUL established the Earth Structures Project in 1992 to undertake the phased inspection, investigation, assessment, design and implementation of stabilisation works at high priority earth structures. Prior to this date remedial measures had generally been carried out on a reactive basis following disruption to train services or to reduce extensive maintenance at particular locations.

The investigations undertaken by Imperial College and discussed above in Section 2.6.2 primarily focused on research to develop an analytical framework within which the embankment behaviour could be assessed and quantified. Mott MacDonald's main thrust of work encompassed the phased inspection of the whole surface track system and implementation of ground investigations on selected representative embankments. From this work geotechnical characterisation of the embankments was made and enabled remedial measures to be designed effectively.

Although Mott MacDonald carried out some numerical analyses for the embankments (Russell *et al*, 2000), the analyses were of limited scope and were carried using simplistic methodologies. Their analyses will therefore not be discussed further in this thesis. The field and laboratory work by Mott MacDonald was presented as internal reports to LUL (eg. Mott MacDonald 1999a, 1999b and 1999c) and some of it was published (eg. McGinnity *et al*, 1998, and Russell *et al*, 2000).

2.6.3.2 Field based investigations

Mott MacDonald carried out systematic acquisition and interpretation of the field condition of LUL earth structures. This work was achieved through desk studies and a walkover survey of the entire surface railway to identify those factors and indicators most pertinent to earth structure stability eg. slope condition, vegetation, earth structure drainage and track condition. From this work, the earthworks were classified into either poor, marginal, serviceable or good condition.

2.6.3.3 Laboratory tests

Associated laboratory testing was carried out on selected samples and comprised index tests, grading, multiple-cycled oedometer tests and stress path triaxial testing on samples retrieved during the winter season of 1998 from sites along the Central and Metropolitan Lines. The sampling depths ranged between 1.2 and 4m on embankment slopes. The relevant soil parameters are presented in the sections dealing with numerical analyses (Chapters 4-7).

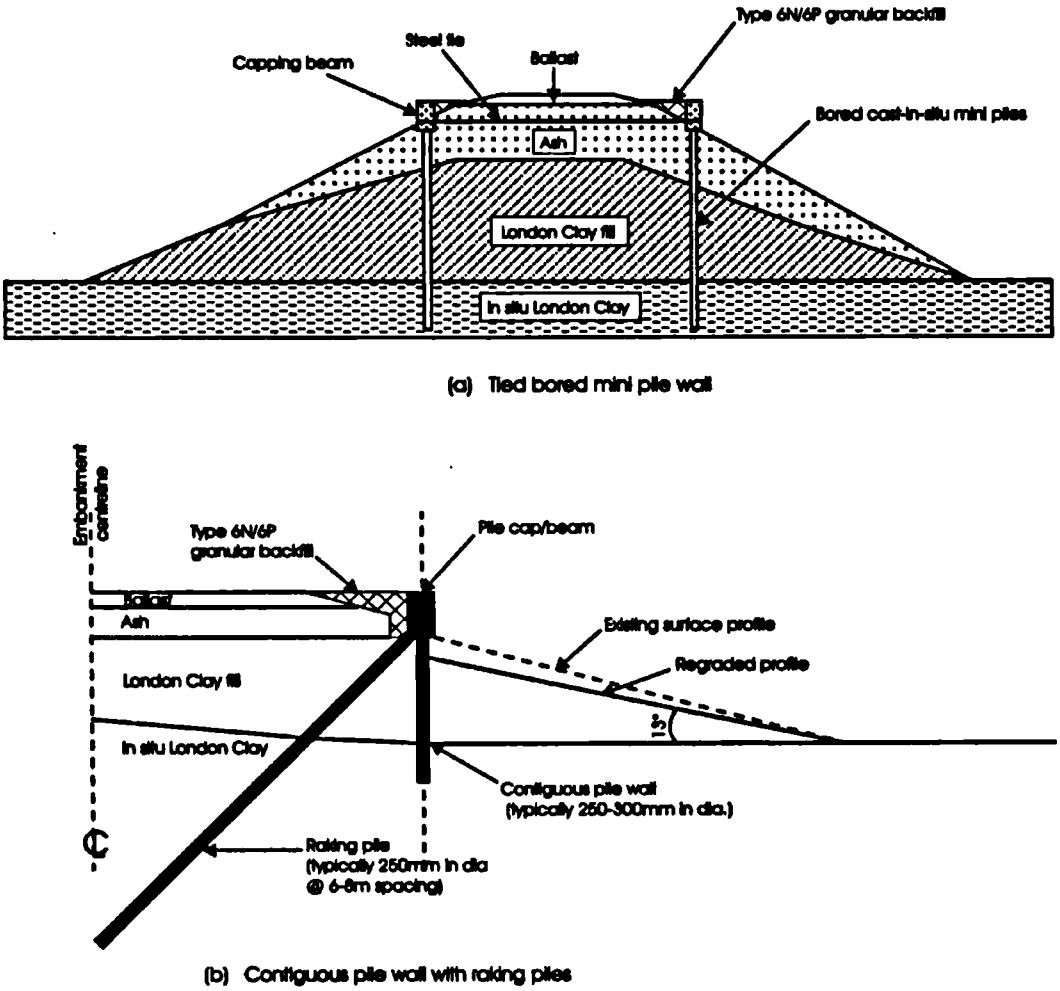

Figure 2.17 Typical remedial works using anchored bored pile walls

2.6.4 Remedial works implemented

2.6.4.1 Background

Conventional methods were adopted as stabilisation measures on the majority of LUL embankments. These typically involved bored mini-pile contiguous walls, anchored by raked mini-piles or a horizontal anchorage bar at the highest sections of the embankments (typically 6-12m), gabion walls and regrading. The contiguous mini-pile walls are anchored for shallower depths (typically 4-6m height). In general gabion retaining walls are installed for embankment sections 2-4m high. In all cases, the retrofitting measures are coupled with regrading to a shallower slope profile. Details of the different remedial measures adopted are discussed below.

2.6.4.2 Contiguous pile wall

By far the commonest techniques used as a remedial measure comprised contiguous bored mini pile walls, either anchored by a horizontal tie bar or raked mini piles (Figure 2.17a and Figure 2.17b, respectively). In general, mini piles of 300mm nominal diameter were installed at the top of the embankment. On the down slope regrading was carried out to an inclination matching the residual angle of London Clay. Where site conditions dictated the regraded profile was achieved by incorporating a gabion wall at the toe of the slope. The application of these methods on the LUL network and a discussion of their advantages and disadvantages are outlined by McGinnity *et al* (1996). Although conventional in design approach and construction, the technique is expensive. The tie bar also requires systematic inspection and maintenance throughout the design life of the wall.

2.6.4.3 Mixed-in-place logs and lime piles

This technique has been used to a limited scale in the UK because there is limited experience regarding its effectiveness and long-term performance for UK soils. A more detailed description of its application is given by McGinnity and Gellatley (1988). Figure 2.18 shows a typical cross section of an embankment where this method has been used.

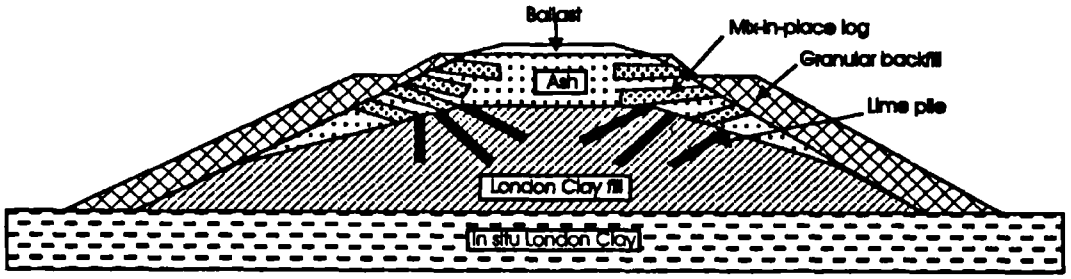

Figure 2.18 Remedial measures involving mixed-in-place logs and lime piles

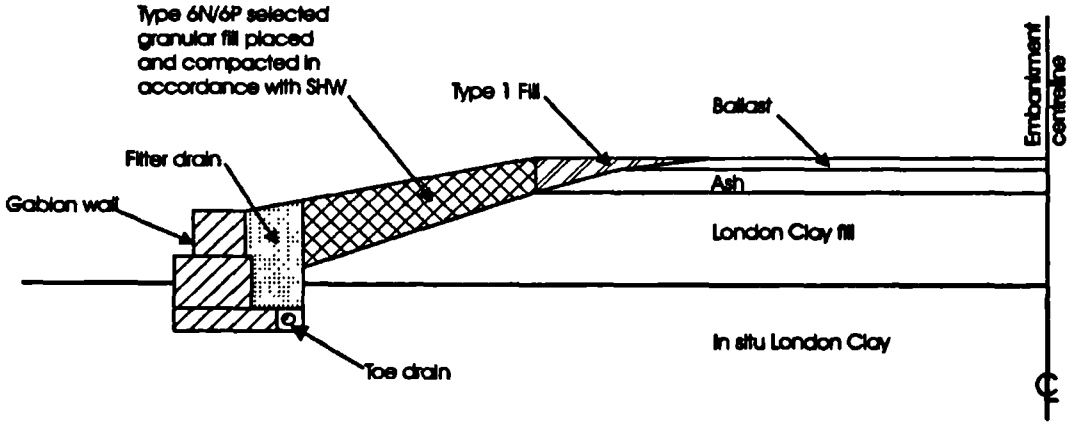

Figure 2.19 Remedial measures involving gabion walls

In the ash, a cement PFA grout is mixed with a low density ash to form a log of up to 600mm diameter, 3-4m long within the embankment ash shoulder. This improves the overall density and stiffness of the friable ash.In the clay fill small diameter holes, typically 300mm are bored and filled with quicklime which is restrained at both ends by steel plates held together by a connecting rod. The lime acts to stiffen the treated clay fill by a combination of moisture reduction, ion exchange and expansion. An additional benefit is that the pile acts as a stiffening element as the lime hydrates. The method is used in conjunction with regrading and/or gabion walls at the toe of the slope as necessary.The major advantages of this system are that it is relatively cheap, has reduced maintenance costs, is environmentally friendly and involves lower installation risk. However these advantages are offset by the lack of long-term performance records for these techniques in old railway embankments.

2.6.4.4 Gabion walls

Gabion walls are used as proprietary stabilisation measures to the two foregoing methods or on their own *per se* where the embankment height was relatively shallow; typically 2-4m. The gabions consist of hexagonal basket woven galvanised wire mesh (Figure 2.19). The baskets are filled with hard durable stone (Class 6G - Specification of Highway Works) of 200mm nominal diameter. Reno mattresses of similar configuration are usually used as foundations for the gabions.

2.6.4.5 Other methods

Over the years, other methods such as soil nails and reinforced earth have increasingly been used to stabilise embankments but will not be discussed in further detail in this research.

2.6.5 Investigations by TRL

The preponderance of shallow slips on motorway earthworks was researched and documented by Perry (1989). More recently, the TRL carried out a project to investigate pore water pressure changes in a trial embankment with vegetation; with a view to develop vegetation options to stabilize slopes. Their aim was to complement knowledge on the role of vegetation in slope reinforcement through the plant root system eg. Coppin and Richards (1990), Barker (1995) and Gray (1995).

Their initial research investigated tree species that can be effective in controlling pore water pressures in motorway slopes (Marriot *et al*, 2001; MacNeil *et al*, 2001 and Hiller and MacNeil, 2001). A variety of seedling species were planted in Gault Clay and Reading Clays under controlled conditions in greenhouses. Two temperature regimes were applied to simulate north and

south facing motorway slopes. Root morphology, soil porosity, moisture changes and soil mass shear strength were measured to assess the effects of various species. It was observed that in some cases roots grew by up to 75-110cm within a year; albeit in restricted containers.

Seedlings of the species which successfully grew during the greenhouse trials were selected for further research on a trial embankment. The trial embankment was constructed from Reading Beds and was 2m high, 34m long, with 1 in 1.94 side slopes. The crest width and overall base dimensions were 1.75m and 9.5m, respectively. A 150mm top soil layer was placed to aid vegetation establishment. Selected trees, shrubs and perennial plants were planted in bays on the embankment slopes. Tensiometers were installed to measure in situ pore water pressures at 0.25m, 0.5m, 0.75m and 1m depths below the topsoil/clay interface

Climatic data comprising rainfall, sunshine, maximum and minimum temperature were measured at a nearby meteorological station during the period February 1997 to June 2000. In addition, pore water pressure measurements and vegetation surveys were carried out at intervals during the field trial.

The suction measurements showed suction increases during summer, reaching their peak at the end of summer/early autumn. The results also indicated low suctions from the middle of autumn to the end of spring, during the period when plant metabolic activity is low. The overall conclusion from the suction monitoring was that during the most critical period for slope stability (end of winter and early spring), the root reinforcing action of vegetation is probably more important than its moisture depletion potential.

2.7 Summary

The foregoing review has outlined the state-of-knowledge regarding the mechanical behaviour of stiff clays and numerical modelling of progressive failure. The importance of permeability on pore water pressure and volume changes in shrinkable soils has been discussed as well as the type of models commonly used in geotechnical analyses. The influence of permeability on progressive failure in embankments is explored in more detail in Chapters 4 and 7.

The influence of vegetation on pore water pressures has been reviewed. The review has explored the physiological and morphological aspects governing root water uptake by vegetation. Root water uptake models developed in soil science/agronomy have been discussed and it has been shown that

macroscopic models are the most appropriate to model this process. The review has also shown that although the majority of root water uptake models have been developed and validated for agricultural crops, there is scope for adopting and developing those models which describe the root water uptake function without recourse to plant dependent parameters. Such a model has been implemented in ICFEP, as part of this research. The model adopted is based on Feddes *et al* (1976), Hoogland *et al* (1988) and Prasad (1999). Its implementation in ICFEP is discussed in Chapter 5. The model is validated on field data from BRE's testing site at Chattenden (Chapter 6) and applied to study the stability of a typical UK old railway embankment (Chapter 7).

The review has also established that although geotechnical engineers now understand the qualitative aspects of desiccation cracks and their influence on the mass permeability of a shrinkable soil, very little research has been carried out to mathematically describe the initiation and propagation of cracks and the change in permeability arising thereof. As part of this research, the author developed a permeability model for use in numerical analyses (Chapter 5). In the model, crack initiation is assumed to take place when the total minor principal stress, σ_3, exceeds the tensile strength of the soil (Section 5.5.5.5 of Chapter 5). The model automatically invokes an enhanced permeability in regions of the finite element mesh where cracking is predicted (NB. The model does not model propagation of individual cracks).

The state-of-knowledge regarding the influence of vegetation in the development of a partially saturated soil profile has been outlined. Geotechnical engineers now recognise the fact that in order to accurately predict soil strength, pore water pressure and volume changes in partially saturated soils requires a different framework to the well developed fully saturated soil mechanics theory. The development of appropriate constitutive models for partially saturated is still in its infancy. At the time this research was carried out, the development work to model partially saturated soils was still being implemented in ICFEP. All the analyses reported in this thesis were therefore carried out using fully saturated soil mechanics. Nevertheless, the majority of the studies are diagnostic and not predictive, hence the use of fully saturated soil mechanics principles does not invalidate the overall findings and conclusions of the research.

CHAPTER 3

THE FINITE ELEMENT METHOD

3.1 Introduction

Traditionally, geotechnical design has been carried out using simplified analyses or empirical methods and many design codes and manuals are based on such approaches. Whilst these methods may be simple to use, they do not satisfy all the requirements of a theoretical solution viz. equilibrium, compatibility, material constitutive behaviour and boundary conditions (both forces and displacements).

Solution methods which are capable of satisfying all the requirements of a theoretical solution are attractive to designers because they enable full analysis of a problem to be achieved, which results in a cost-effective design. Such solutions however, involve complex equations which can only be solved with the aid of computers. The finite element method (FEM) is a typical example of these latter sophisticated methods. It is a numerical technique which can provide approximate solutions to a wide variety of engineering problems. The theory of the FEM for geotechnical engineering is described in standard textbooks eg. Potts and Zdravkovic (1999).

In this thesis, the Imperial College Finite Element Program (ICFEP) has been used throughout. ICFEP was developed specifically to solve geotechnical problems. The program uses the displacement based FEM and is capable of analysing two dimensional (axi-symmetry, plane stress and strain) and three dimensional Fourier Series aided and full three dimensional problems involving geometric and material non-linearities. In this research, only plane strain problems have been considered.

The program is continually being developed and updated to keep abreast with recent developments in soil mechanics. In this research, a new flow boundary condition has been developed and coded in ICFEP. The boundary condition mimics transpiration by vegetation using a root extraction function. In association with the development of the vegetation boundary condition, an evaporation boundary condition was also coded. This latter boundary condition has not however been used to model the boundary value problems presented in this thesis.

This chapter outlines the general principles of the FEM, in particular the formulation and numerical solution of the governing non-linear equations. The boundary conditions and constitutive models

relevant to this thesis are also discussed and the chapter concludes with a brief overview of the pre- and post-processing facilities in ICFEP.

The material presented in this chapter, including most of the figures, is based on Potts and Zdravkovic (1999).

3.2 Theoretical considerations for coupled analysis

Real soil behaviour is often time related and pore pressure response is dependent on soil permeability, the rate of loading and the hydraulic boundary conditions. This behaviour is accounted for by combining the seepage equations and the equilibrium and constitutive equations; often referred to as the "coupled approach". In soil mechanics, the preferred method is to describe the material behaviour in terms of effective stress. This implies that in a coupled analysis, account must be taken of the time dependency of the change in pore fluid pressure and the effective stress.

Solution of the time dependent consolidation involves the solution of Biot's consolidation equations (Biot, 1941), coupled with the material constitutive model and the equilibrium equations. The governing equations for a saturated incompressible pore fluid are:

The equations of equilibrium:

$$\begin{aligned}
\frac{\partial \sigma'_x}{\partial x} + \frac{\partial p_f}{\partial x} + \frac{\partial \tau_{xy}}{\partial y} + \frac{\partial \tau_{xz}}{\partial z} + \gamma_x &= 0 \\
\frac{\partial \sigma'_y}{\partial y} + \frac{\partial p_f}{\partial y} + \frac{\partial \tau_{xy}}{\partial x} + \frac{\partial \tau_{yz}}{\partial z} + \gamma_y &= 0 \\
\frac{\partial \sigma'_z}{\partial z} + \frac{\partial p_f}{\partial z} + \frac{\partial \tau_{xz}}{\partial x} + \frac{\partial \tau_{yz}}{\partial y} + \gamma_z &= 0
\end{aligned} \qquad \text{Equation 3.1}$$

where σ'_i are direct effective stresses, p_f the pore pressures, τ_{ij} the shear stresses, and γ_i the components of the bulk unit weight in the x, y, and z global directions, respectively.

The constitutive behaviour expressed in terms of effective stress:

$$\{\Delta\boldsymbol{\sigma}'\} = [\mathbf{D}'][\Delta\boldsymbol{\varepsilon}] \qquad \text{Equation 3.2}$$

where $\{\Delta\boldsymbol{\sigma}'\}$ is the vector of incremental effective stresses, $[\mathbf{D}']$ is the constitutive matrix in terms of effective stresses and $\{\Delta\boldsymbol{\varepsilon}\}$ is the vector of incremental strains. In simple terms, the constitutive relationship is the stress-strain behaviour of the soil and therefore provides a link between equilibrium and compatibility. Since soil behaviour is non-linear, the constitutive relationship is usually given in terms of incremental stresses and strains as shown in Equation 3.2. The matrix $[\mathbf{D}']$ depends on the current stress state and past stress history.

The equation of continuity:

$$\frac{\partial v_x}{\partial x}+\frac{\partial v_y}{\partial y}+\frac{\partial v_z}{\partial z}-Q=\frac{\partial \varepsilon_v}{\partial t} \qquad \text{Equation 3.3}$$

where v_i are the components of the superficial velocity of the pore fluid in the coordinate directions, Q represents any sources and/or sinks, ε_v is the volumetric strain and t is time.

The generalised Darcy's law:

$$\begin{Bmatrix} v_x \\ v_y \\ v_z \end{Bmatrix} = -\begin{bmatrix} k_{xx} & k_{xy} & k_{xz} \\ k_{xy} & k_{yy} & k_{yz} \\ k_{xz} & k_{yz} & k_{zz} \end{bmatrix} \begin{Bmatrix} \frac{\partial h}{\partial x} \\ \frac{\partial h}{\partial y} \\ \frac{\partial h}{\partial z} \end{Bmatrix} \qquad \text{Equation 3.4}$$

where k_{ij} are the components of the coefficient of permeability and $\frac{\partial h}{\partial x}$, $\frac{\partial h}{\partial y}$ and $\frac{\partial h}{\partial z}$ the hydraulic gradients in the global x, y, and z directions, respectively. Equation 3.4 can also be written as:

$$\{\mathbf{v}\}=-[\mathbf{k}]\{\nabla\mathbf{h}\} \qquad \text{Equation 3.5}$$

the hydraulic head, h, is defined as:

$$h=\frac{p_f}{\gamma_f}+\left(xi_{Gx}+yi_{Gy}+zi_{Gz}\right) \qquad \text{Equation 3.6}$$

The unit vector $\{i_G\} = \{i_{Gx}, i_{Gy}, i_{Gz}\}^T$ is parallel but opposite in direction to gravity. If the soil is isotropic with a coefficient of permeability, k, then, $k = k_{xx} = k_{yy} = k_{zz}$ and $k_{xy} = k_{xz} = k_{yz} = 0$.

3.3 Formulation of the FEM

Formulation of the finite element method involves the following steps: (i) element discretisation, (ii) primary variable approximation, (iii) formulation of the element equations, (iv) assembly of the global equations, (v) specification of boundary conditions, (vi) solution of the global equations and (vii) determination of stresses and strains.

3.3.1 Element discretisation

This process involves the modelling of the geometry of the problem by an assemblage of small regions (finite elements). The elements have nodes defined on the element boundaries or within the element. The assemblage of the elements constitutes a mesh. Simple geometries comprising triangles or quadrilaterals are normally used to define the elements. Modelling of complex geometries eg. curves may require higher order elements such as 8-noded quadrilaterals which have mid-side nodes or their equivalent 6-noded triangular elements. In ICFEP, 4- and 8-noded elements are used to model soil and 2- and 3-noded line elements are used to model structural elements eg. anchors.

The equivalent element types in ICFEP for three dimensional analysis are 8-noded hexahedras, with nodes at the corners only. The corresponding elements incorporating mid-side nodes are 20-node hexahedras whilst 4- or 8-noded quadrilateral elements are available to model structural elements in three dimensions.

The construction of a mesh involves simplification of the geometry in some regions as necessary, as well as the use of a refined mesh in the zones where large gradients of stresses and strains are anticipated to occur, in order to achieve accuracy. In general, elements with regular shaped geometries give the best results.

3.3.2 Primary variable approximation

In the displacement based finite element method eg. ICFEP, the displacements are the primary variables. Stresses and strains are treated as secondary quantities which are computed from the displacement field; once it has been determined. In a three dimensional coordinate system x, y, and z, respectively, the displacement field has three corresponding displacement components (u, v, and w); termed displacement

degrees of freedom. A fundamental issue in the FEM is the method by which the displacement components are approximated in the domain under investigation. A simple polynomial form is usually used to define the variation of the displacement field across an element.

$$\mathbf{d}_E = \mathbf{N}.\mathbf{d}_{nE} \qquad \text{Equation 3.7}$$

where $\mathbf{d}_E$ is the vector defining the displacement field, $\mathbf{N}$ is the matrix of displacement interpolation functions (or shape functions) and $\mathbf{d}_{nE}$ is the vector of element nodal displacement components. The displacement components are thus expressed in terms of their values at the nodes.

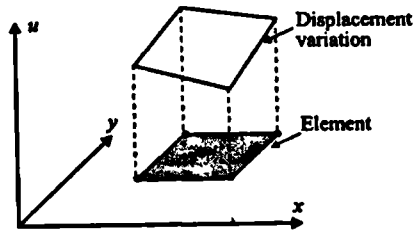

Figure 3.1 Linear variation of displacements across a 4 noded element (after Potts & Zdravkovic, 1999).

The order of the polynomial function essentially depends on the number of nodes in the element. For 4-noded quadrilaterals, this results in a linear variation of displacement across the element (Figure 3.1). For higher order 8-noded quadrilaterals, the displacement field varies quadratically.

In a coupled analysis, the pore pressure is also a primary variable and therefore a nodal degree of freedom, as with displacements. Assuming a pore water pressure field $\mathbf{p}_E$ across an element, a matrix of pore water pressure interpolation functions, $\mathbf{N}_p$, can be defined similar to that for displacements as follows:

$$\mathbf{p}_E = \mathbf{N}_p \cdot \mathbf{p}_{nE} \qquad \text{Equation 3.8}$$

where $\mathbf{p}_{nE}$ is the vector of element nodal water pressure.

Kovacevic (1994) explored the order of a polynomial function commonly used in Equation 3.8 and noted that if each node has a pore water pressure degree of freedom, the matrices of interpolation functions $\mathbf{N}_p$ (for pore water pressures) and $\mathbf{N}$ (for the displacement) would be the same. For two dimensional analyses using 8-noded quadrilateral elements, this implies that the pore water pressures and displacements vary quadratically. If the displacements vary quadratically, then the strains and (if the material behaviour is linear) the effective stresses vary linearly. If pore water pressures and effective stresses are to vary in the same manner, the pore water pressure should also vary linearly across the

element. This can be achieved by specifying pore water pressure degrees of freedom to only the corner nodes in 8-noded quadrilateral elements.

The accuracy of the displacement approximation depends on the element size and nature of the displacement approximation used. To achieve accuracy as the elements become smaller, the displacement approximation must be able to represent rigid body movement eg. translation and rotations, and ensure continuity of the displacement field to avoid gaps or overlaps and be able to represent constant strain rates. Simple polynomials satisfy these criteria. The process of defining the displacement field in terms of nodal displacements essentially reduces the problem of determining the displacement field over the whole mesh to determining the displacement components at a finite number of nodes only.

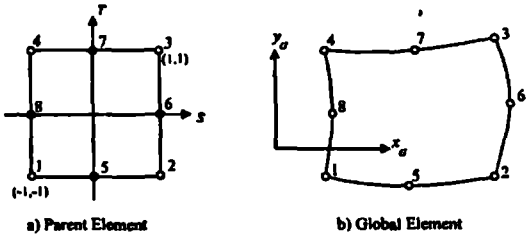

Figure 3.2 8-noded isoparametric element (after Potts & Zdravkovic, 1999)

In ICFEP, isoparametric elements are used ie. the displacement fields and element geometries are approximated using the same interpolation functions. A global element (in the finite element mesh) is derived from a parent element which has the same number of nodes but is defined with respect to a natural coordinate system (Figure 3.2). The natural coordinates (S, T and U) have values between -1 and 1. The global coordinates of a point in the element can be expressed as:

$$x = \sum_{i=1}^{N_n} N_i x_i$$

$$y = \sum_{i=1}^{N_n} N_i y_i \qquad \text{Equation 3.9}$$

$$z = \sum_{i=1}^{N_n} N_i z_i$$

where N_n is the number of nodes in the element, x_i, y_i and z_i are the global coordinates of the nodes in the element and N_i are the interpolation functions which constitute the matrix, $\mathbf{N}$, in Equation 3.7.

Stresses and strains are treated as secondary quantities and can be evaluated using the definition of strain (Equation 3.10) and by applying the material constitutive law (Equation 3.11):

$$\{\Delta\varepsilon\} = [\mathbf{B}]\{\Delta\mathbf{d}\}_{nE} \qquad \text{Equation 3.10}$$

$$\{\Delta\sigma\} = [\mathbf{D}']\{\Delta\varepsilon\} + \{\Delta\sigma_f\} \qquad \text{Equation 3.11}$$

where $[\mathbf{B}]$ is the matrix of the derivatives of the shape functions N_i as given below, $\{\Delta\sigma_f\}^T = \{\Delta p_f, \Delta p_f, \Delta p_f, 0, 0, 0\}$ and Δp_f is the increment pore fluid pressure. For an element with n nodes the matrix $[\mathbf{B}]$ is given by:

$$[\mathbf{B}] = \begin{bmatrix} \frac{\partial N_1}{\partial x} & 0 & \frac{\partial N_2}{\partial x} & 0 & \cdots & \cdots & \frac{\partial N_n}{\partial x} & 0 \\ 0 & \frac{\partial N_1}{\partial y} & 0 & \frac{\partial N_2}{\partial y} & \cdots & \cdots & 0 & \frac{\partial N_n}{\partial y} \\ \frac{\partial N_1}{\partial y} & \frac{\partial N_1}{\partial x} & \frac{\partial N_2}{\partial y} & \frac{\partial N_2}{\partial x} & \cdots & \cdots & \frac{\partial N_n}{\partial y} & \frac{\partial N_n}{\partial x} \\ 0 & 0 & 0 & 0 & \cdots & \cdots & 0 & 0 \end{bmatrix} \qquad \text{Equation 3.12}$$

3.3.3 Element equations

The equation of equilibrium (Equation 3.1) can be presented in a more convenient form by applying the principle of minimum potential energy which states:

$$\delta\Delta E = \delta\Delta W - \delta\Delta L = 0 \qquad \text{Equation 3.13}$$

where ΔE is the incremental total potential energy, ΔW is the incremental strain energy and ΔL is the incremental work done by applied loads. The work done by the incremental applied loads can be divided into contributions from body forces and surface tractions.

This yields the following finite element equations associated with equilibrium:

$$[\mathbf{K}_E]\{\Delta\mathbf{d}\}_{nE} + [\mathbf{L}_E]\{\Delta\mathbf{p}_f\}_{nE} = \{\Delta\mathbf{R}_E\} \qquad \text{Equation 3.14}$$

where:

$$\mathbf{K}_E = \int_{Vol} [\mathbf{B}]^T [\mathbf{D}'][\mathbf{B}] dVol \text{ (the element stiffness matrix)} \qquad \text{Equation 3.15}$$

$$\mathbf{L}_E = \int_{Vol} \{\mathbf{m}\}[\mathbf{B}]^T [\mathbf{N}_p] dVol \qquad \text{Equation 3.16}$$

$$\{\Delta \mathbf{R}_E\} = \int_{Vol} [\mathbf{N}]^T \{\Delta \mathbf{F}\} dVol + \int_{Srf} [\mathbf{N}]^T \{\Delta \mathbf{T}\} dSrf \text{ (the RHS load vector)} \qquad \text{Equation 3.17}$$

$$\{\mathbf{m}\}^T = \{1 \quad 1 \quad 1 \quad 0 \quad 0 \quad 0\} \qquad \text{Equation 3.18}$$

$\{\Delta \mathbf{F}\}$ and $\{\Delta \mathbf{T}\}$ are the vectors of the body forces and surface tractions, respectively.

The principle of virtual work is also applied to the continuity equation (Equation 3.3) and by making appropriate substitutions into Darcy's Law (Equation 3.4) the following finite element equation is obtained:

$$[\mathbf{L}_E]^T \left(\frac{\{\Delta \mathbf{d}\}_{nE}}{\Delta t} \right) - [\Phi_E] \{\mathbf{p}_f\}_{nE} = [n_E] + Q \qquad \text{Equation 3.19}$$

where:

$$[\Phi_E] = \int_{Vol} \frac{[\mathbf{E}]^T [\mathbf{k}][\mathbf{E}]}{\gamma_f} dVol \qquad \text{Equation 3.20}$$

$$n_E = \int_{Vol} [\mathbf{E}]^T [\mathbf{k}] \{\mathbf{i}_E\} dVol \qquad \text{Equation 3.21}$$

$$[\mathbf{E}] = \left[\frac{\partial N_p}{\partial x}, \frac{\partial N_p}{\partial y}, \frac{\partial N_p}{\partial z} \right]^T \qquad \text{Equation 3.22}$$

The element stiffness matrix and right hand side vector cannot be evaluated explicitly, except for special cases. Numerical integration is therefore invoked to solve the equations. In this procedure, the integral of a function is replaced by a weighted sum of the function evaluated at a number of integration points. The type of integration scheme determines the weights and location of the integration points. The number of integration points determine the integration order. In general, use of a high integration order yields higher accuracy.

The Gaussian integral function in three dimensions for an isoparametric element is:

$$\int_{-1}^{+1}\int_{-1}^{+1}\int_{-1}^{+1} f(S,T,U)\,dS\,dT\,dU \approx \sum_{i=1}^{n^3}\sum_{j=1}^{n^3}\sum_{k=1}^{n^3} w_i w_j w_k f(S_i,T_j,U_k) \qquad \text{Equation 3.23}$$

where (S_i,T_j,U_k) are the Gauss point coordinates and w_i, w_j and w_k are the corresponding weighting functions (for an integration order n there are n^3 Gauss points for 3D and n^2 for 2D). For the 8-noded regular quadrilateral elements used in this thesis, exact integration can be achieved using 9 (3x3) integration points, however, this requires large computer resources. Reduced integration (2x2) has been used throughout in the analyses for this thesis. In some cases reduced integration can lead to improved solutions (Naylor (1974) and Bathe (1982)).

Equations 3.14 and 3.19 can be solved using a time marching process in which it is assumed that the solution $(\{\Delta\mathbf{d}\}_{nE},\{\mathbf{p}_f\}_{nG})_1$ is known at time t_1 and the aim is to find the solution $(\{\Delta\mathbf{d}\}_{nE},\{\mathbf{p}_f\}_{nG})_2$ at time t_2. To achieve this requires the following assumption to be made:

$$\int_{t1}^{t2}[\Phi_E]\{\mathbf{p}_f\}_{nE}\,dt = [\Phi_E]\left[\beta(\{\mathbf{p}_f\}_{nE})_2 + (1-\beta)(\{\mathbf{p}_f\}_{nE})_1\right]\Delta t \qquad \text{Equation 3.24}$$

where β is a parameter. In order to ensure stability of the marching process, it is necessary to choose $\beta \geq \frac{1}{2}$ (Booker and Small, 1975). A value of $\beta = 0.8$ was used in this thesis.

Equations 3.24 can be substituted into Equation 3.19 and then combined with Equation 3.14 to yield the following set of element equations:

$$\begin{bmatrix}[\mathbf{K}_E] & [\mathbf{L}_E]\\ [\mathbf{L}_E]^T & -\beta\Delta t[\Phi_E]\end{bmatrix}\begin{Bmatrix}\{\Delta\mathbf{d}\}_{nE}\\ \{\Delta\mathbf{p}_f\}_{nE}\end{Bmatrix} = \begin{Bmatrix}\Delta\mathbf{R}_E\\ \left([\mathbf{n}_E]+Q+[\Phi_E](\{\mathbf{p}_f\}_{nE})_1\Delta t\right)\end{Bmatrix} \qquad \text{Equation 3.25}$$

Equation 3.25 provides a set of simultaneous equations in terms of the incremental nodal displacements $\{\Delta\mathbf{d}\}_{nE}$ and incremental nodal pore fluid pressures $\{\Delta p_f\}_{nE}$. The equation can be solved using a marching process.

3.3.4 Global equations

Once all the element equations have been determined, the next step in the FEM is to assemble them into a set of global equations. Equation 3.25 hence becomes:

$$\begin{bmatrix} [\mathbf{K}_G] & [\mathbf{L}_G] \\ [\mathbf{L}_G]^T & -\beta\Delta t[\Phi_G] \end{bmatrix} \begin{Bmatrix} \{\Delta \mathbf{d}\}_{nG} \\ \{\Delta \mathbf{p}_f\}_{nG} \end{Bmatrix} = \begin{Bmatrix} \Delta \mathbf{R}_G \\ \left([\mathbf{n}_G] + Q + [\Phi_G]\{\mathbf{p}_f\}_{nG}\right)\Delta t \end{Bmatrix} \quad \text{Equation 3.26}$$

where the subscript, **G**, refers to global. Assemblage of the global equations is usually done using the direct stiffness method and involves summation of the individual element contributions in the problem domain as follows:

$$\mathbf{K}_G = \sum_{i=1}^{n} (\mathbf{K}_E)_i \quad \text{Equation 3.27}$$

$$\mathbf{L}_G = \sum_{i=1}^{n} (\mathbf{L}_E)_i \quad \text{Equation 3.28}$$

$$\Phi_G = \sum_{i=1}^{n} (\Phi_E)_i \quad \text{Equation 3.29}$$

$$\mathbf{R}_G = \sum_{i=1}^{n} (\mathbf{R}_E)_i \quad \text{Equation 3.30}$$

$$\mathbf{n}_G = \sum_{i=1}^{n} (\mathbf{n}_E)_i \quad \text{Equation 3.31}$$

The size of the global stiffness matrix depends on the total number of degrees of freedom. For a 2D problem, there are 2 displacements and 1 pore pressure degrees of freedom at each node.

3.3.5 Boundary conditions

Prior to solving the simultaneous non-linear equations of the global stiffness matrix, the boundary conditions being applied to the domain need to be incorporated. These include any loads, displacements, fluid flows and pore fluid pressures. Loads eg. initial stresses, line loads, forces due to excavation or

construction and surcharges affect the right hand side of the global system of equations, as do any specified flows (ie. sources and sinks).

Displacement boundary conditions affect the global displacement vector, $\{\Delta \mathbf{d}\}_{nG}$, whereas prescribed pore pressures affect the global pore fluid pressure vector, $\{\Delta \mathbf{p_f}\}_{nG}$. During solution of a boundary value problem, it is necessary that sufficient displacement conditions are specified to maintain rigid body modes of deformation eg. rotations and translations; otherwise the equations become mathematically insoluble (singularity).

3.3.6 Solution of global equations

The assembled global stiffness matrix incorporating the boundary conditions fully mathematically defines the boundary value problem which can be solved. Since soil behaviour is often described using non-linear constitutive relationships, the global stiffness matrix, $\mathbf{K_G}$, depends on the previous and current stress and strain. The solution requires non-linear finite element techniques. The change in boundary conditions is applied in a series of increments, which results in an incremental form of the global equilibrium equation:

$$\left[\mathbf{K_G}^{i}\right]\{\Delta \mathbf{d}\}_{nG}^{i} = \{\Delta \mathbf{R}_G\}^{i} \qquad \text{Equation 3.32}$$

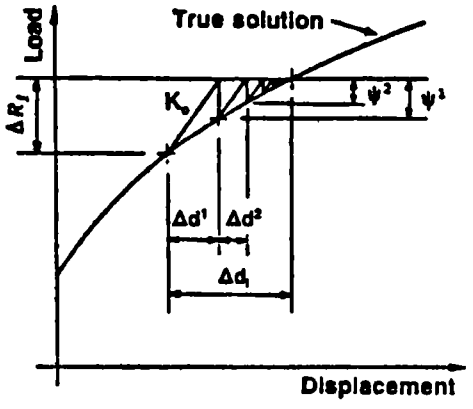

Figure 3.3 Modified Newton-Raphson method

Because of the non-linear constitutive behaviour the incremental stiffness matrix, $\left[\mathbf{K_G}^{i}\right]$ varies during an increment '**i**'; which makes determination of the nodal displacement vector, $\{\Delta \mathbf{d}\}_{nG}^{i}$, due to the applied incremental load vector, $\{\Delta \mathbf{R_G}\}^{i}$ more complicated. A number of solution strategies exist for solving these non-linear equations of which the visco-plastic, tangent stiffness, Newton-Raphson and modified Newton-Raphson (MNR) schemes are the commonest. Potts and Ganendra (1994) investigated the performance of these schemes and concluded that the MNR is the most efficient and reliable for a variety of geotechnical problems. In this thesis the MNR with a sub-stepping stress algorithm has been used.

In solving Equation 3.31, the MNR uses an iterative technique. In the first iteration, an approximate stiffness matrix, $\left[\mathbf{K_G}^0\right]$ and the incremental load vector $\{\Delta \mathbf{R_G}\}^i$ are used. The solution at the end of the iteration is likely to be in error therefore the predicted incremental displacements are used to calculate the out of balance or residual load, ψ^i; which is a measure of the error. Equation 3.31 is solved again using the error as the right hand side vector:

$$\left[\mathbf{K_G}^1\right]\left(\{\Delta \mathbf{d}\}^i_{nG}\right)^j = \{\psi\}^{j-1} \qquad \text{Equation 3.33}$$

In the above equation "*j*" refers to the iteration number and $\{\psi\}^0 = \{\Delta \mathbf{R_G}\}^i$. The process is repeated until convergence is achieved; according to the tolerances specified. Figure 3.3 gives an illustration of the scheme for a single degree of freedom problem; from which it can be seen that the incremental displacements are equal to the sum of the iterative displacements. In this thesis, the convergence of the solution was determined by checking the changes of both iterative applied loads (residual loads), iterative displacements and changes in iterative pore pressures. The convergence tolerance required the norm of the iterative values of the parameters to be less than 2% of the norm of the incremental and accumulated values. The norm, *n*, of both iterative and incremental values is defined as:

$$\|\eta\| = \sqrt{\mathbf{M}^{\mathrm{T}}\mathbf{M}} \qquad \text{Equation 3.34}$$

where $\mathbf{M}$ is either a nodal load, displacement or pore pressure vector. In the analyses involving strain softening, additional convergence criteria are necessary to achieve a solution and involve monitoring of residual stresses at all integration points to keep them small (Kovacevic, 1994).

The iterative scheme, in principle, ensures that for each solution increment the analysis satisfies all solution requirements. At the end of each iteration, the current estimate of the incremental displacements is calculated and used to evaluate the incremental strains at each integration point. The constitutive model is then integrated along the incremental strain paths to obtain an estimate of the stress changes. The incremental stress changes at the end of the increment are added to the accumulated stresses at the beginning of the increment, to evaluate consistent equivalent nodal forces. These forces are compared with the applied loads from the boundary conditions, to determine the residual load vector.

In the conventional MNR, the stiffness matrix is only calculated at the beginning of the increment (first iteration) and thereafter is kept constant throughout the increment for all subsequent iterations. Due to the nonlinear material behaviour, $\left[\mathbf{K_G}^i\right]$ is not constant but changes with the incremental stress and

strain changes. This deficiency can be overcome by updating the stiffness for any number of iterations during the increment.

In the analyses carried out in this research, the stiffness was updated during the first five iterations. The invokation of updating capabilities in a FEM algorithm might reduce the number of iterations needed for convergence, however, the assembly and inversion of the matrix is very time consuming and judicious judgement needs to be taken to determine the optimum number of stiffness updates. Another modification to the MNR available in ICFEP to reduce the number of iterations required for convergence is the acceleration procedure (Figure 3.4). In this technique, the iterative displacements, $\left(\{\Delta \mathbf{d}\}_{nG}^{i}\right)^{j}$ are increased before calculating the residual load, ψ^{i} using an accelerating parameter, α, (Thomas, 1984). An accelerated procedure was used in this thesis with a maximum of α =5.

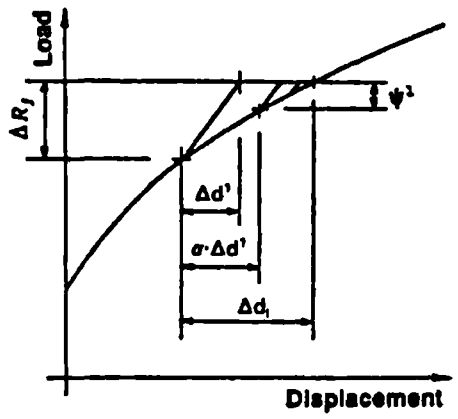

Figure 3.4 Accelerated Newton-Raphson method

Since the constitutive behaviour changes over the increment, care must be taken when integrating the constitutive equations to obtain the stress change. This procedure is carried out using stress point algorithms (either explicit or implicit). Two of the most widely used are the substepping algorithms (explicit) and return algorithms (implicit). The procedures enable the constitutive equations to be integrated along an incremental path.

A substepping algorithm (eg. Sloan, 1987) divides the strain path into a number of substeps or flow steps (Figure 3.5). The fundamental assumption made is that in each substep the strains $\{\Delta\varepsilon_{ss}\}$ are a proportion, ΔT, of the incremental strains $\{\Delta\varepsilon_{inc}\}$. This effectively implies that the strains vary proportionally over the increment. The constitutive equations are then integrated numerically over each substep using either an Euler, modified Euler or Runge Kutta scheme; all of which are available in ICFEP.

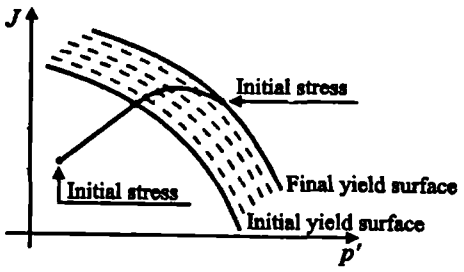

Figure 3.5 Substepping approach (after Potts & Zdravkovic, 1999)

The modified Euler scheme is the most widely used in ICFEP. The method uses the elasto-plastic matrix at the beginning of each sub-step to calculate the stress change over the sub-step, $\Delta\sigma_1$. This is

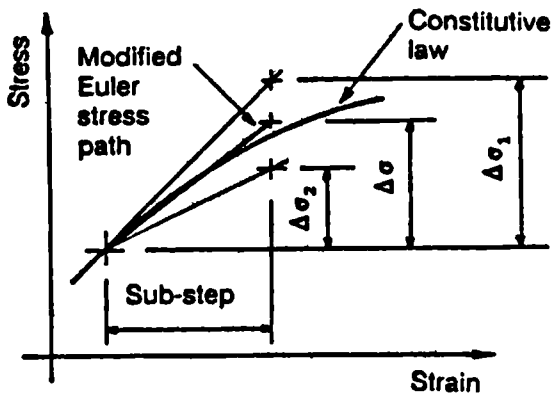

Figure 3.6 Modified Euler sub-stepping method

then added to the accumulated stress at the beginning of the sub-step and used to obtain a second estimate of the stress change using the elasto-plastic matrix at the end of the sub-step, $\Delta\sigma_2$. The average of $\Delta\sigma_1$ and $\Delta\sigma_2$ is taken as the stress change for the sub-step (Figure 3.6). The error in prediction is controlled by checking the difference between $\Delta\sigma_1$ and $\Delta\sigma_2$. In this thesis it was restricted to 0.01% of $\sigma + \frac{(\Delta\sigma_1 + \Delta\sigma_2)}{2}$. To achieve this tolerance, it was necessary to use several hundred flow steps in some of the analyses reported in this thesis.

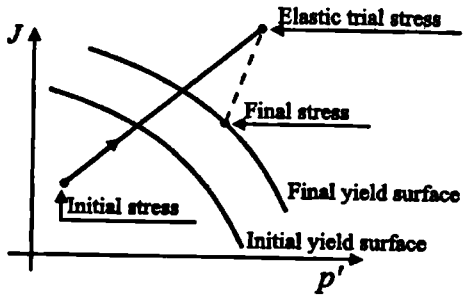

Figure 3.7 Return algorithm approach (after Potts & Zdravkovic, 1999)

In return algorithms eg. Borja and Lee (1990) and Borja (1991), the plastic strains over the increment are calculated from the stress conditions corresponding to the end of the increment (Figure 3.7). The latter have to be estimated since they are unknown at the beginning of the increment. An elastic predictor is usually made as a first approximation after which a complex sub-stepping procedure is carried out to transfer the stresses back to the yield surface. Care needs to be taken in this method to ensure that the stresses are computed within legal stress space.

Potts and Ganendra (1994) investigated the performance of explicit and implicit methods and concluded that although both give accurate results, the substepping procedure is more robust and can handle a wide variety of constitutive models eg. analyses where two yield surfaces are active simultaneously.

The substepping technique necessarily involves some approximations and this can easily result in drift of the yield surface. A correction is usually required at the end of the substep to return (project back) the stresses to the current yield surface as discussed by Potts and Gens (1985).

3.3.7 Calculation of stresses and strains

After solving the global equations from which nodal displacements will have been determined, the secondary quantities such as stresses and strains can be evaluated. Strains are calculated using Equation 3.10 and stresses are computed by using the constitutive relationship (Equation 3.11).

3.4 Geotechnical considerations

In order to be able to model geotechnical boundary problems more realistically, enhancements are required to the standard finite element theory. This section discusses the main aspects that are of relevance to the analyses carried out in this thesis.

3.4.1 Initial stresses

Knowledge of initial stresses is important for non-linear analyses because such analyses involve stress dependent material behaviour. In analyses involving unloading eg. excavation, it is necessary to know the initial stresses; regardless of whether the analysis is linear or non-linear. The commonest methods to specify initial stresses is by performing a gravity "turn-on" analysis or directly via a subroutine. The latter is useful where sloping ground and/or strata are involved.

3.4.2 Excavation

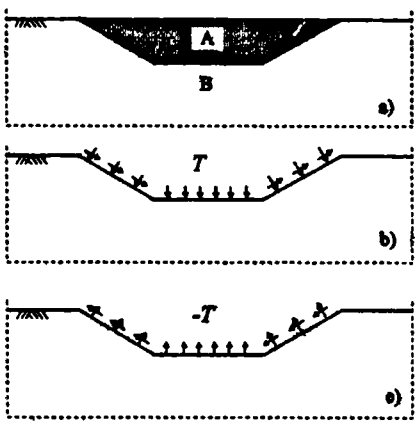

Figure 3.8 Simulation of excavation (after Potts & Zdravkovic, 1999)

Many geotechnical problems involve excavation and its simulation in a FEM is described here with reference to Figure 3.8. In Figure 3.8a, the material to be excavated (shaded area A) can be represented by surface traction forces at the interface with the material that will remain (material B). The effect of material A on material B is represented by the traction forces in Figure 3.8b. Under these conditions, the behaviour of material B is unchanged because the traction forces match the effects of material A. To model the removal of material A, the traction forces are reversed (Figure 3.8c). Under these conditions, the changes in stresses and strains as a result of the reversal in surface traction forces in material B will reflect the removal of material A.

During an analysis, excavation is therefore modelled by determining the tractions, T, at the new surface boundary. The new stiffness of the material B due to unloading is calculated and the tractions, -T, are applied at the new surface boundary. In a numerical algorithm the process essentially involves the

determination of nodal forces which are equivalent to the traction forces from the excavated elements adjacent to the excavated boundary using:

$$\{\mathbf{R}_E\} = \int_{Vol}[\mathbf{B}]^T\{\sigma\}dVol - \int_{Vol}[\mathbf{N}]^T\gamma dVol \qquad \text{Equation 3.35}$$

where $\{\sigma\}$ is the stress vector in the element, γ is the bulk unit weight and Vol is the volume of the excavated element. The calculation is undertaken for all nodes in elements adjacent to the excavated boundary (Brown and Booker, 1985). Since material behaviour is non-linear, it is necessary that the excavation process be carried out in increments. This is especially necessary where the excavation process involves installation of props. The following summarises the procedure:

- Elements to be excavated are specified.
- Nodal forces are computed using Equation 3.34. Excavated elements are deactivated and removed from the active mesh.
- The global stiffness matrix is reassemble using the remaining boundary conditions and is solved to give incremental changes in displacements, stresses and strains.
- incremental changes in displacements, stresses and strains are added to the accumulated values existing before the increment to give updated values.
- proceed to the next increment.

3.4.3 Construction

The construction boundary condition was extensively used in the present research to model construction of embankments. In ICFEP construction of material is achieved by adding a group of elements using a gravity "turn-on" analysis. The elements representing the material to be constructed must be present in the original mesh, but deactivated by prior excavation or at the outset of the analysis. During the construction process the elements are reactivated. The process has to be carried out incrementally to simulate layered construction. The addition of weight to the finite element mesh from the newly constructed elements is simulated by applying self weight body forces to the element. It is also essential that elements representing the new material should have a constitutive relationship which is consistent with its behaviour before and after placement.

In ICFEP, all elements to be constructed are assumed to behave linear elastically with a small stiffness. There are also options to modify the stresses to take account of suction in fills.

The use of elements with a small stiffness results in an overprediction of nodal displacements of nodes which are only connected to the constructed elements (ie. not connected to elements that were active at the previous increment). This is corrected by setting the displacements to zero at such nodes immediately after construction. Depending on the constitutive models used to represent the constructed material, it may be necessary to establish state parameters and/or adjust the stresses in the constructed elements. Any stress adjustments should be matched by equivalent adjustments to the accumulated right hand side vector to maintain equilibrium.

3.4.4 Structural elements

Structural elements such as retaining walls, props, anchors etc. are widely used in geotechnics and require special treatment in numerical modelling. In many boundary value problems, the size of structural elements compared to the overall geometry being modelled is such that if two dimensional continuum elements were to be used, it would result in a very larger number of elements or elements with ill-conditioned aspect ratios. In the majority of cases, it is the distribution of axial and shear forces and bending moments within the structural elements which is of interest to designers.

Special elements have been developed whereby one or more of the dimensions has been collapsed. The elements are formulated such that structural quantities such as bending moments, shear forces and their associated strains are calculated directly from the finite element analysis. A variety of formulations exists in the literature, most of which are based on the theory of a Mindlin beam eg. Day and Potts (1990). The input data usually comprises the moment of inertia, cross section area, Young's Modulus, Poisson's ratio and a shear correction factor. In ICFEP, beam elements transmits axial and shear forces and bending moments whereas bar elements transmit axial forces only.

3.4.5 Hydraulic boundary conditions

3.4.5.1 Introduction

The governing equation (Equation 3.26) includes nodes with pore pressure degrees of freedom, which can have either prescribed pore fluid pressure or prescribed nodal flows. Prescribed values of incremental nodal pore fluid pressure affect only the left hand side ie. $\{\Delta \mathbf{p}_f\}_{nG}$, of the system equations and are dealt with in the same way as prescribed displacements whereas prescribed nodal flows affect the right hand side vector (Q). Nodal flow boundary conditions can also be described in the form of precipitation, sinks, sources or infiltration. In this thesis, a new vegetation boundary condition which affects the right hand side vector, Q, has been coded (Chapter 5). The relevant boundary conditions used in this research are described below.

3.4.5.2 Prescribed pore fluid pressures

Pore fluid pressures can be specified in two ways. In the first method, the incremental change in nodal pore fluid pressure $\{\Delta \mathbf{p}_f\}_{nG}$ is specified. An alternative is to specify the accumulated (final) pore pressure values at the end of a particular increment and allow the program to calculate the incremental values. This boundary condition was used to model winter and summer pore pressure profiles using the current industry practice (the approach used by ICON was used in Chapter 4).

3.4.5.3 Precipitation

This boundary condition enables the user to specify a dual seepage boundary condition. Both an infiltration rate, q_n, and a threshold pore fluid pressure, p_{fb}, are specified simultaneously. At the beginning of an increment, the program compares the magnitude of the pore pressure of nodes along the boundary with p_{fb}. If the pore pressure is more compressive than p_{fb}, the boundary condition is taken as the prescribed incremental pore fluid pressure Δp_f, whose magnitude yields an accumulated value of p_{fb} at the end of the increment. However, if the flow rate at the node exceeds q_n or if the pore fluid is more tensile than p_{fb}, the boundary condition is taken as a prescribed infiltration with the nodal flow rate determined from q_n.

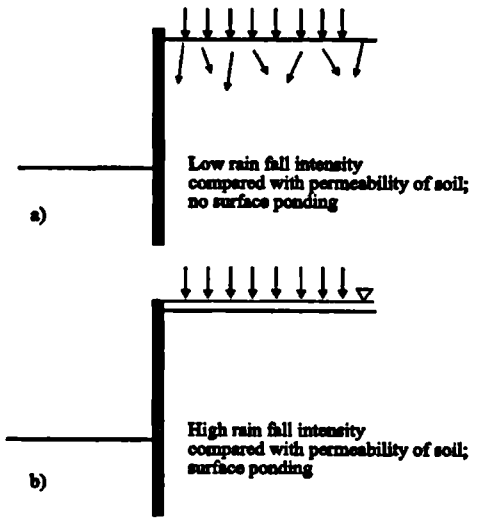

Figure 3.9 Rainfall infiltration boundary conditions (after Potts & Zdravkovic, 1999)

The boundary condition is useful in cases where the amount of precipitation may be limited by low permeability of the soil (Figure 3.9). Under these circumstances, high permeability and/or low intensity rainfall may allow infiltration of all the water into the soil (Figure 3.9a). A flow boundary condition is therefore relevant. However, should the rainfall intensity be high or the permeability too low, ponding or runoff will occur (Figure 3.9b), therefore a pore pressure boundary condition will be relevant in this case. The degree to which ponding is allowed is user defined. This boundary condition was used in conjunction with the newly developed vegetation boundary condition (Chapters 5-7).

As noted above, the program determines which boundary condition to use at the beginning of the increment of the analysis over which the precipitation boundary condition is active. This then applies for the complete increment. Should conditions change such that at a node a switch in boundary condition should occur, then at the end of the increment the boundary condition will be violated. The size of error depends on the size of the increment and at which stage the change should have occurred. The error is corrected in subsequent increments (if the precipitation boundary condition is still active) but the current increment will be in error.

Latest developments in ICFEP now allow the user to eliminate or significantly minimise this error by using an automatic incrementation option. When the option is active during an analysis, it divides each increment into smaller sub-steps and also tracks the precipitation boundary condition. If conditions change during an increment, thereby necessitating a switch in the boundary condition, the program automatically adjusts the size of the sub-increment and repeat the increment so that the precipitation boundary condition is accurately enforced.

Use of the automatic incrementation option involves longer computing times, especially where a non-linear analysis and many elements are involved in the analysis. The automatic incrementation option was used in the analyses reported in Chapter 6 (validation of the new vegetation boundary condition) but was not used in the embankment analyses reported in Chapter 7.

3.4.5.4 Sources and sinks

Sources (inflow) and sinks (outflow) are usually used to model extraction or injection of water at discrete nodes inside the mesh to model water injection and/or abstraction at localised points. This boundary condition is useful when modelling groundwater flow in wells as the prescribed nodal flow rate is determined from the pumping rates. In this thesis, the newly developed boundary condition presented in Chapter 5 models transpiration by vegetation as nodal flows within the rooted zone.

3.5 Constitutive Modelling

3.5.1 Introduction

The behaviour of soil under general shear is complex. Factors such as soil composition, direction of loading, rate effects, strain reversal etc. all result in anisotropy and non-linear behaviour of the soil. This behaviour presents major challenges to modellers since the numerous facets of real soil behaviour cannot be incorporated in one constitutive model. In general the simpler the constitutive model, the less

features of soil behaviour it is able to reproduce eg. linear elastic perfectly plastic models cannot reproduce strain hardening/softening.

The simple models can be improved by introducing further non-linearities. A common approach used in modelling is to consider the overall behaviour into two: pre-yield (elastic behaviour) and yield (plastic behaviour). Appropriate models are then used to simulate the behaviour of the soil at pre-peak, peak and post-peak strength. In this thesis, an isotropic non-linear elastic model was used to describe the pre-yield behaviour of the soil while a Mohr-Coulomb criterion with strain softening was used to describe behaviour at peak and post –peak strength.

During elastic behaviour, the principal directions of incremental stress and incremental strain coincide whereas during plastic behaviour, the principal directions of accumulated stress and incremental plastic strain are assumed to coincide. In general stress space, a yield function F, is defined. This is a scalar function of stress; expressed in terms of stress and state parameters, $\{\mathbf{k}\}$. The function separates purely elastic from elasto-plastic behaviour:

$$F(\{\boldsymbol{\sigma}\},\{\mathbf{k}\}) = 0 \qquad \text{Equation 3.36}$$

The value of F identifies the type of material behaviour. If $F(\{\boldsymbol{\sigma}\},\{\mathbf{k}\})$ is less than zero, behaviour is purely elastic, if $F(\{\boldsymbol{\sigma}\},\{\mathbf{k}\}) = 0$ behaviour is elasto-plastic. The yield function cannot be greater than 0. In stress space the function plots as a surface whose size changes as a function of the state parameters $\{\mathbf{k}\}$. The region enclosed by the yield surface is the elastic domain. Figure 3.10 shows simple representations of the yield function in two and three dimensional stress states. For perfect plasticity $\{\mathbf{k}\}$ is constant and represents the magnitude of the stresses at yield. For hardening and softening plasticity, $\{\mathbf{k}\}$ varies with plastic straining to represent how the magnitude of the stress state at yield changes.

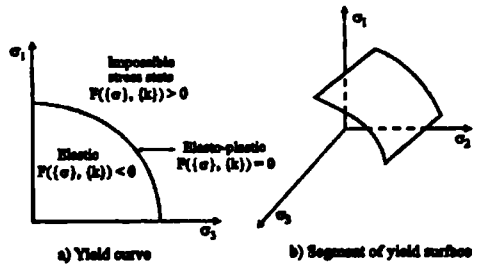

Figure 3.10 Yield function presentation (after Potts & Zdravkovic, 1999)

The direction of plastic strain increments at every plastic stress state are specified using a flow rule which is expressed as follows:

$$\Delta\varepsilon_i^P = \Lambda\frac{\partial P(\{\boldsymbol{\sigma}\}\{\mathbf{m}\})}{\partial\sigma_i} \qquad \text{Equation 3.37}$$

where $d\varepsilon_i^P$ represents the six components of incremental plastic strain, P is the plastic potential

function and Λ is a scalar multiplier. The value of Λ controls the magnitude of the strain components and depends on the hardening/softening rule. The flow rule governs dilatancy effects, which in turn govern volume changes and strength.

In its general form, the plastic potential function can be represented as:

$$P(\{\sigma\},\{m\}) = 0 \qquad \text{Equation 3.38}$$

where $\{m\}$ is a vector of state parameters. Figure 3.11 shows a graphical representation of Equation 3.37 where coincidence of principal directions of accumulated stress and incremental plastic strains has been assumed. As can be seen from Equation 3.37, only the differentials with respect to the stress components are of relevance in the flow rule. The values of $\{m\}$ are therefore immaterial.

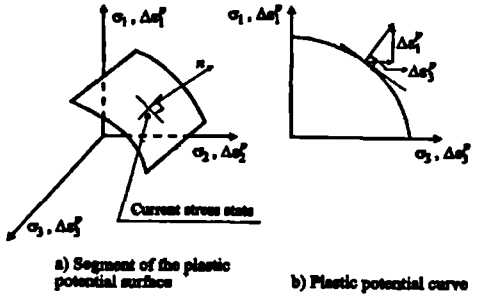

Figure 3.11 Plastic potential presentation (after Potts & Zdravkovic, 1999)

An assumption is sometimes made that the incremental plastic strain vector is normal to the yield surface (normality condition). In this situation $P(\{\sigma\},\{m\}) = F(\{\sigma\},\{k\}) = 0$ and the flow rule is said to be associated. When the flow rule is associated, the global stiffness matrix is symmetrical.

As previously discussed, the scalar parameters can be quantified through the hardening/softening rules which specify how the state parameters, $\{\mathbf{k}\}$, vary with plastic straining. Strain hardening occurs where the yield stress increases with increasing plastic strain whereas the opposite is true for strain softening conditions. The rules are commonly specified by relating the change in the size of the yield surface to the accumulated plastic strains, although occasionally the relationship is specified in terms of the plastic work (work hardening/softening). Where perfect plasticity is involved, there is no softening or hardening, whence Λ is undefined and the state parameters, $\{\mathbf{k}\}$, are constant.

3.5.2 Pre-yield behaviour

A number of models exist to describe the behaviour of elastic soils in the pre-peak region. The very simple models such as linear isotropic elastic and linear anisotropic are unable to reproduce most facets of soil behaviour, eg. nonlinearity behaviour where material parameters are dependent on stress and/or strain level. Early advances to incorporate nonlinear behaviour include power laws (eg. Skinner, 1975),

K-G models (eg. Naylor *et al*, 1991) and hyperbolic models (Kondner (1963) and Duncan and Chang (1970)).

Over the years, further developments have been made in modeling the pre-yield behaviour of soils. The main development involves modelling the observed behaviour of large stiffness at small strains (eg. Jardine *et al* (1986), Puzrin and Burland (1998), Al-Tabbaa and Wood (1989), Lade (1977) and Whittle (1993)). In general, the most sophisticated models require a plethora of soil parameters to fully specify them, some of which are not easily determinable from conventional laboratory tests. Moreover, some of the models have been developed using observed behaviour from laboratory tests on reconstituted materials; with no substantiating/corroborating evidence on laboratory tests on natural materials. These limitations reduce the applicability of some of the sophisticated models in boundary value problems.

In this thesis, a major part of the research involved the development of a new flow boundary condition and its application in prediction of ground movements and pore water pressures in embankments. It was therefore considered prudent to use a simple model that has been extensively used to model embankments in ICFEP.

The hyperbolic model is one such model that has been widely used in numerical analysis of embankments. This model is based on a hyperbolic function which approximates the stress-strain curve in a conventional triaxial compression tests. A non-linear elastic version of the model has been used at Imperial College (eg. Hamza (1976), Dounias (1987) and Kovacevic (1994)). The drained elastic parameters vary according to the following expressions:

$$E = E_i \frac{1 - ABS}{1 + BS} \qquad \text{Equation 3.39}$$

$$E_i = E_0 \left(\frac{p' + p_a}{p_a} \right)^c \qquad \text{Equation 3.40}$$

$$\mu = \left[I - L \log \left(\frac{p' + p_a}{p_a} \right) \right] (1 - S) + 0.49S \qquad \text{Equation 3.41}$$

$$E_u = HE_i \qquad \text{Equation 3.42}$$

where E_i and E_u are the drained Young's moduli on first loading and unloading/reloading respectively, μ is the Poisson's ratio, p_a is the atmospheric pressure, and E_0, A, B, C, I and L are model parameters. Figure 3.12 shows the prediction of an oedometer test from London clay fill retrieved on the LUL network. The predictions indicate that the appropriate value to use for H for the clayfill is 2.

The stress level, S, represents the proportion of the shear strength mobilized at the current mean effective stress, p'. It varies from zero, when the state of the stress is on the hydrostatic axis, to unity, when it is on the failure envelope given by cohesion, c', and angle of shearing resistance, ϕ' as shown in Figure 3.13.

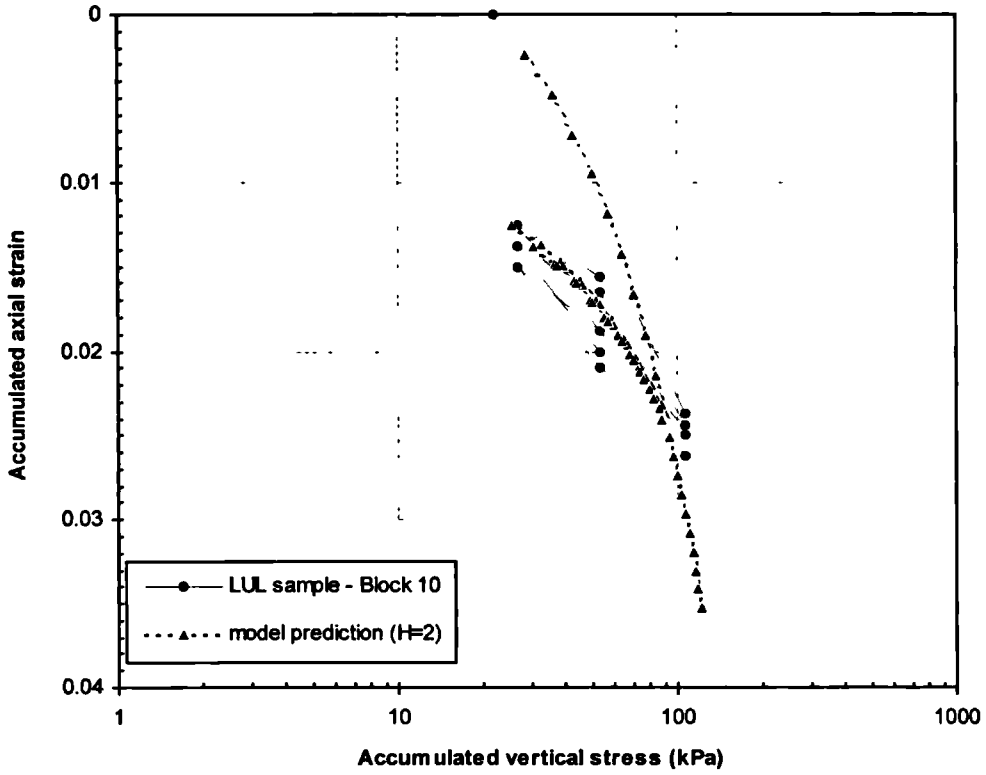

Figure 3.12 Prediction of oedometer tests by p' dependent model on a London clay sample from an LUL embankment.

In the present research, laboratory data for the clay fill was not available to derive the parameters A, B, C, H, I and L. The model was therefore further simplified to make it only dependent on p' by specifying a value of $C = 1$ whilst a value of zero was specified for the parameters A, B, H, I and L. This approach was also used in all the numerical analyses carried out for the LUL embankments by ICON (1999a and 1999b) and Kovacevic *et al* (2001).

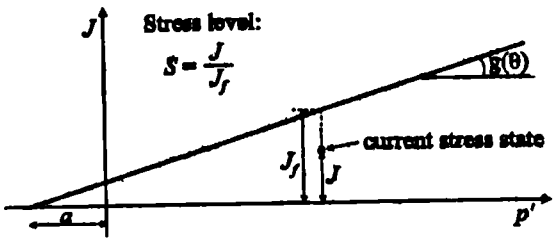

Figure 3.13 Definition of stress level, S (after Potts & Zdravkovic, 1999)

Use of this model by Kovacevic (1994) when analysing rockfill embankment dams indicates that while it is capable of accurately predicting vertical displacements, there are discrepancies between predicted and observed horizontal displacements.

3.5.3 Yield

As mentioned above in Section 3.4.1, the behaviour at yield was modelled using a non-associated Mohr-Coulomb model, with strain softening. The basic Coulomb failure criterion can be expressed as :

$$\tau_f = c' + \sigma'_{nf}\tan\phi' \qquad \text{Equation 3.43}$$

where τ_f and σ'_{nf} are the shear and normal effective stresses on the failure plane, c' is the cohesion and ϕ' is the angle of shearing resistance. When plotted in effective stress space using Mohr's circles, laboratory triaxial tests will plot as idealised in Figure 3.14. Equation 3.43 can also be presented as:

$$\sigma'_1 - \sigma'_3 = 2c'\cos\phi' + (\sigma'_1 + \sigma'_3)\sin\phi' \qquad \text{Equation 3.44}$$

where σ'_1 and σ'_3 are the major and minor principal stresses, respectively and the other parameters are as defined previously.

Equation 3.44 is often referred to as the generalised Mohr-Coulomb failure criterion:

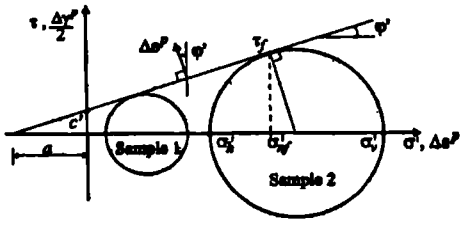

Figure 3.14 Mohr's circles of effective stress (after Potts & Zdravkovic, 1999)

$$F(\{\boldsymbol{\sigma}'\},\{\mathbf{k}\}) = \sigma'_1 - \sigma'_3 - 2c'\cos\phi' - (\sigma'_1 + \sigma'_3)\sin\phi' \qquad \text{Equation 3.45}$$

The yield function separates elastic from elasto-plastic behaviour and is a function of the stress state $\{\boldsymbol{\sigma}\}$ and its size changes as a function of the state parameters $\{\mathbf{k}\} = [c', \phi']$, which can be related to hardening/softening parameters. In hardening and

softening materials, c' and ϕ' vary with plastic straining to represent how the magnitude of the stress state at yield changes. For a perfectly plastic model, c' and ϕ' are constant.

Models in which hardening or softening is related to the magnitude of the plastic strains are known as strain hardening/softening models and those in which the hardening/softening is related to the magnitude of plastic work are called work hardening/softening models. The type of material behaviour is identified by the magnitude of the yield function. If $F(\{\sigma'\},\{k\})$ is less than zero, the behaviour is purely elastic whereas if $F(\{\sigma'\},\{k\})=0$ the behaviour is elasto-plastic. The yield surface equation can be rewritten in terms of stress invariants p', J and θ which are defined as follows:

$p' = \frac{1}{3}(\sigma_1' + \sigma_2' + \sigma_3')$ the mean effective stress Equation 3.46

$J = \frac{1}{\sqrt{6}}\sqrt{(\sigma_1' - \sigma_2')^2 + (\sigma_2' - \sigma_3')^2 + (\sigma_3' - \sigma_1')^2}$ the deviatoric stress Equation 3.47

$$\theta = \tan^{-1}\left[\frac{1}{\sqrt{3}}\left(2\frac{(\sigma_2' - \sigma_3')}{(\sigma_1' - \sigma_3')} - 1\right)\right] \quad \text{Equation 3.48}$$

In the foregoing equations, σ_2' is the intermediate principal stress and the others are as previously described. The relationship between the stress invariants is shown in Figure 3.15.

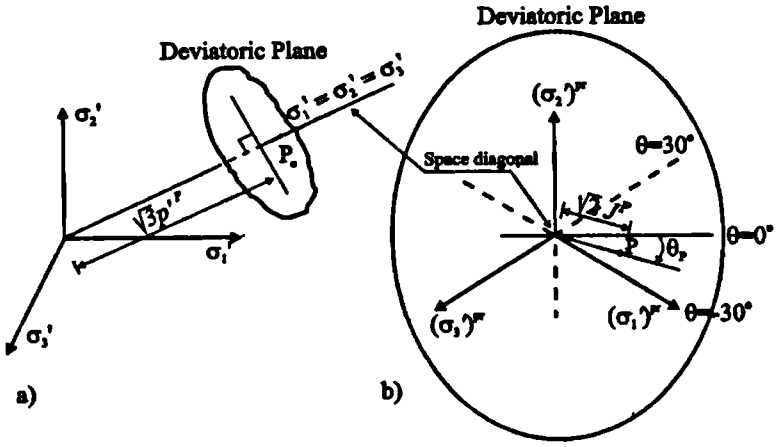

Figure 3.15 Invariants in principal stress space (after Potts & Zdravkovic, 1999)

In effective stress space p' is a measure of the distance along the space diagonal of the current deviatoric plane from the origin. J is a measure of the current stress state from the space diagonal while θ defines the orientation of the stress state in the deviatoric plane. An alternative way to express the invariants is given below:

$$\begin{Bmatrix}\sigma_1'\\ \sigma_2'\\ \sigma_3'\end{Bmatrix} = p'\begin{Bmatrix}1\\1\\1\end{Bmatrix} + \frac{2}{\sqrt{3}}J\begin{Bmatrix}\sin\left(\theta+\frac{2\pi}{3}\right)\\ \sin\theta\\ \sin\left(\theta-\frac{2\pi}{3}\right)\end{Bmatrix} \qquad \text{Equation 3.49}$$

Equation 3.49 can be substituted into Equation 3.45 to give the Mohr-Coulomb equation in the form of invariants as follows:

$$F(\{\sigma'\},\{k\}) = J - \left(\frac{c'}{\tan\theta'} + p'\right)g(\theta) = 0 \qquad \text{Equation 3.50}$$

where: $$g(\theta) = \frac{\sin\theta'}{\cos\theta + \frac{\sin\theta\sin\phi'}{\sqrt{3}}} \qquad \text{Equation 3.51}$$

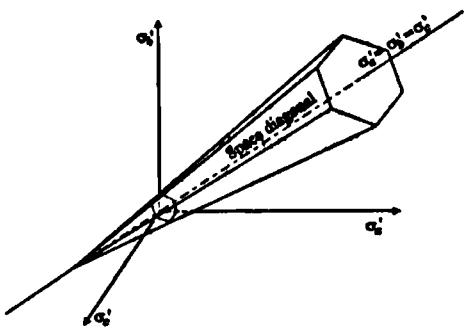

Figure 3.16 Mohr-Coulomb yield surface in principal stress space (after Potts & Zdravkovic, 1999)

Equation 3.50 is used in ICFEP as the yield surface. In principal effective stress, the Mohr-Coulomb yield function plots as an irregular hexagon as shown in Figure 3.16.

In the strain softening model coded in ICFEP, the strength parameters and angle of dilation, ν, as defined in Equation 3.52 and shown in Figure 3.17 are dependent on the accumulated deviatoric plastic strains E_d^p.

The angle of dilation is given by:

$$\nu = \sin^{-1}\left(-\frac{\Delta\varepsilon_1^p + \Delta\varepsilon_3^p}{\Delta\varepsilon_1^p - \Delta\varepsilon_3^p}\right) \qquad \text{Equation 3.52}$$

where $\Delta\varepsilon_1^p$ and $\Delta\varepsilon_3^p$ are the major and minor incremental plastic strain vectors.

If an associated flow rule is assumed then the plastic strain increment vector will be normal to the yield surface as indicated in Figure 3.14. In this situation it can be shown that $\nu = \phi'$. Such an assumption results in very large dilation greater than is observed in real soils and also, once the soil starts to dilate it will dilate forever. It is known that real soils may initially dilate after reaching the yield surface but will reach a constant volume condition at large strains. These problems can be overcome in numerical

algorithms by using non-associated rules. In the analyses carried out in this thesis, an angle of dilation equal to zero was used.

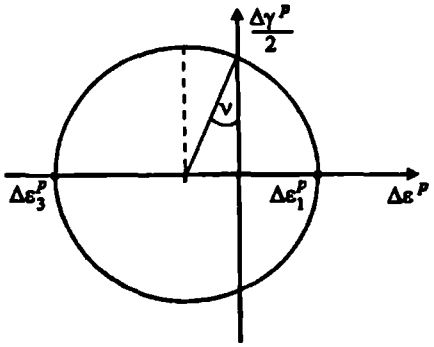

Figure 3.17 Mohr's circle of plastic strains (after Potts & Zdravkovic, 1999)

The basic Mohr-Coulomb model can be modified to enable brittleness to be modelled, eg. by making the strength parameters c' and ϕ', and the angle of dilation, ν, dependent on the accumulated plastic strains (Potts and Zdravkovic, 1999). Within ICFEP, c' and ϕ' depend on the accumulated deviatoric plastic strain E_d^p as shown in Figure 3.18. In this model, four zones can be identified:

Zone 1: the shear strength parameters c' and ϕ' are assumed to increase linearly from initial values (c_i' and ϕ_i') to peak values (c_p' and ϕ_p').

Zone 2: the shear strength parameters c' and ϕ' remain constant and are equal to the peak values (c_p' and ϕ_p').

Zone 3: the shear strength parameters c' and ϕ' are assumed to decrease linearly or exponentially from peak values (c_p' and ϕ_p') to residual values, (c_r' and ϕ_r').

Zone 4: the shear strength parameters c' and ϕ' remain constant and are equal to the residual values (c_r' and ϕ_r').

The model thus assumes strain hardening in zone 1, perfect plasticity in zone 2 and strain softening in zone 3. The angle of dilation, ν, is assumed to be proportional to the angle of shearing resistance, ϕ', ie. $\nu = \psi\phi'$. In zones 1 and 2 ψ is a constant. In zone 3, ν is assumed to decrease from its peak value in zone 2 to a residual value ν_r according to the same rule adopted for variation of strength parameters (ie. linearly or exponentially). To use the whole model requires specification of the following plastic parameters:

c_i', c_p', c_r', ϕ_i', ϕ_p', ϕ_r', $(E_d^p)_{c_i'}$, $(E_d^p)_{c_p'}$, $(E_d^p)_{\phi_i'}$, $(E_d^p)_{\phi_p'}$, ψ, ν_r and either $(E_d^p)_{c_r'}$ and $(E_d^p)_{\phi_r'}$, for linear softening or a_c and a_ϕ for exponential softening.

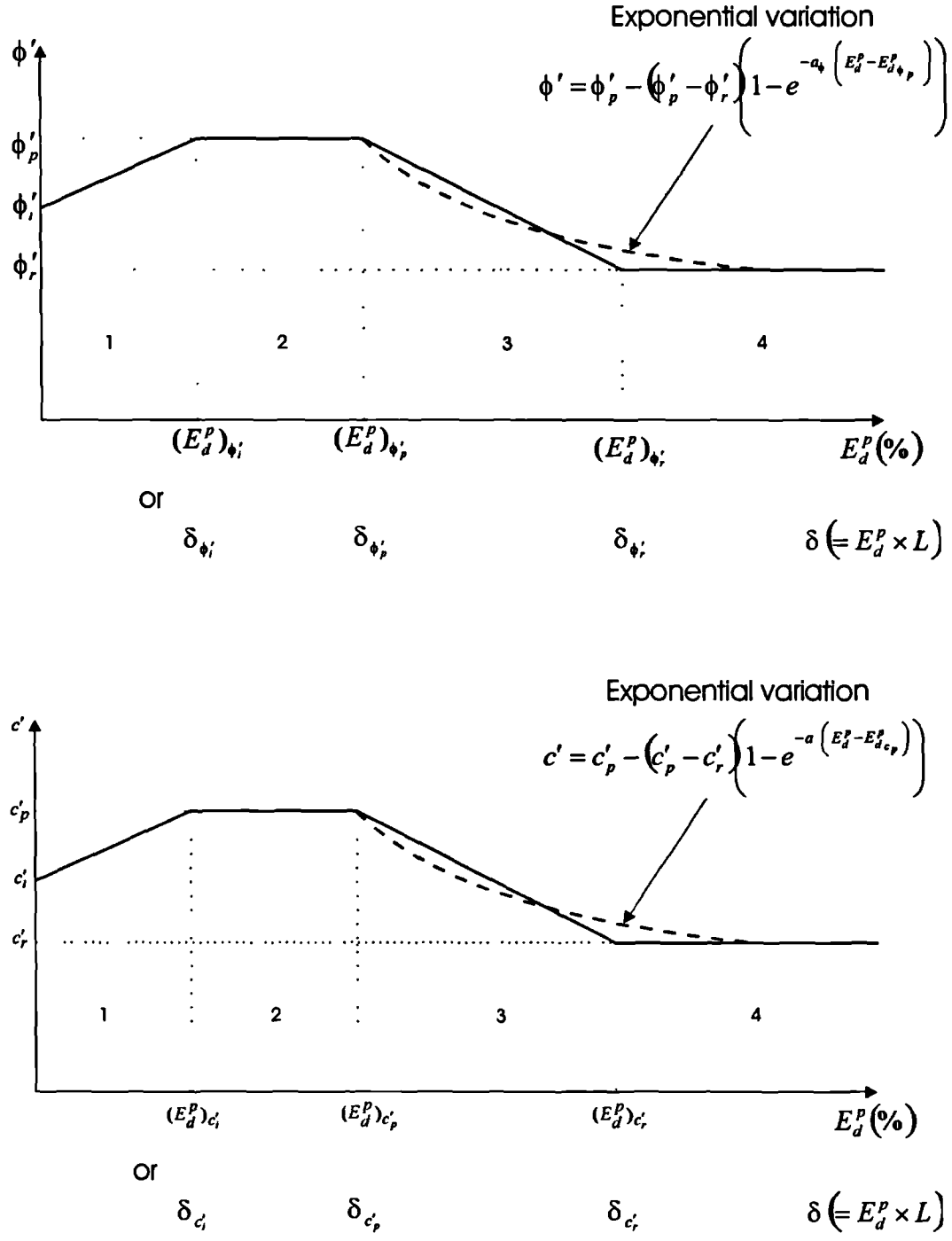

Figure 3.18 Definition of hardening/softening parameters in ICFEP (after Potts & Zdravkovic, 1999)

It is possible to select only part of the model deemed to be relevant to the problem being analysed, which reduces the amount of data input. This model was used in the embankment analyses in this research.

3.6 Processing of results

Data at various stages of the analysis can be stored on disc and used for a restart or post-processing analysis. Printed output (tabular or graphical format) can be requested during the analysis or at the end of the analysis from the saved disc. The graphical package in ICFEP allows incremental, accumulated and sub-accumulated values of stresses, strains, displacements etc. to be plotted as vectors, contours or as line graphs. Output can also be listed and exported into conventional graphics software.

Chapter 4

THE INFLUENCE OF PERMEABILITY ON PROGRESSIVE FAILURE

4.1 Introduction

This chapter focuses on the influence of permeability on the "predicted" stability of embankments constructed in stiff clay, which experience seasonal cyclic pore water pressure water changes. The investigation largely focuses on typical UK railway embankments as discussed in Section 2.6 of Chapter 2. Sensitivity analyses involving permeabilities of various orders of magnitude were carried out. The development of pore water pressures and movement from the end of construction until failure were studied to determine the influence of permeability.

The historical construction of the majority of UK railway embankments was discussed in Section 2.6.1 of Chapter 2. A key issue is the fact that the embankments were constructed prior to the discovery and application of compaction techniques during construction of fills. The embankments were constructed using end-tipping methods with very little or no compaction being carried out, which resulted in a highly voided structure. Results from ground investigations undertaken in recent times (Mott MacDonald, 1999a) also indicate that the clay fill is highly contaminated with granular material eg. sands and gravels of various grading. Therefore the clay fill would have swelled and collapsed upon ingress of water from precipitation; and is likely to have granular inclusions. The resultant mass permeability of the clay fill is therefore very variable, and strongly influenced by the presence and preponderance or otherwise of the granular inclusions.

Seasonal pore water pressure changes in embankments depend on the type of vegetation, root morphology, meteorological conditions and permeability of the soil; amongst others factors. The magnitude of seasonal pore water pressure changes determines the magnitude of strains induced in the soil. With time, the cumulative effect of pore water pressure changes results in increasing strains (since plastic strains are irreversible) and can ultimately lead to progressive failure. The influence of permeability and the magnitude of pore water pressure changes on the stability of stiff clay embankments has received very little attention from researchers.

4.2 Permeability models

A review of the permeability of soils was presented in detail in Section 2.3 of Chapter 2. In the analyses presented here, the main focus was to study the influence of mass permeability on progressive failure. The analyses involved a 7m high embankment experiencing large pore water pressure changes to simulate summer and winter pore water pressures hence the effect of permeability would be significant. Although a non-linear permeability model relating permeability to either void ratio or mean effective stress would be appropriate, its use would complicate both the analysis and the interpretation of the results. For these preliminary analyses, it was therefore decided to adopt homogeneous/uniform permeabilities. Non-linear permeabilities are introduced into the analyses in Chapters 5-7.

4.3 Governing winter and summer pore water pressure profiles

The process of root water uptake and development of pore water pressure profiles in the ground were discussed in more detail in Sections 2.5 of Chapter 2. It was noted that on grass covered slopes, field observations have shown that pore water pressures recover at the end of winter (Vaughan 1994) whereas in tree covered areas, results from field monitoring suggest the existence of a permanent desiccated profile (eg. Biddle, 1983 and 1998).

Maximum desiccation occurs towards the end of summer and coincides with maximum soil moisture deficit. This typically occurs towards the end of September for UK conditions. The corresponding least soil moisture deficit occurs towards the end of winter, at the end of February. Since the monthly distribution of rainfall and actual evapotranspiration is not uniform, the determination of the governing pore water pressures is highly complex.

The effect of roots on pore water pressure changes cannot be reproduced by conventional consolidation theory. Moreover, since roots also require air, it seems likely that a suction is applied sufficient to cause shrinkage cracking. Wetting up during winter is facilitated by cracks and may be quite rapid in the cracked zone. The state-of-the-art in UK industry in order to simulate the effect of tree roots involves major simplifications to model the zone of influence by the roots.

The method that has been used by Imperial College Consultants Ltd (ICON) and Mott MacDonald in numerical analyses of UK railway embankments involves imposition of an artificial pore water pressure which is estimated to be just sufficient to reduce the minor

principal total stress to zero and hence simulate cracking. For a typical railway embankment involving stiff clay fill with an ash mantle and constructed on a stiff clay foundation, this is achieved by imposing pore water pressure boundary conditions as indicated in Figure 4.1a which is deemed to be just sufficient to cause cracking. Note that due to the tension positive sign, conventional tensile pore water pressures are positive. The magnitude of suctions for level ground is presented in ICON (1999c) as follows:

$$u_c = \sigma_v\left(1 - \frac{1}{\sin\phi'}\right) \qquad \text{Equation 4.10}$$

where u_c is the pore water pressure which gives $\sigma_3 \rightarrow 0$, which should just cause cracking, and $\sigma_v = \gamma.z$. The philosophy behind the assumptions and derivation for the depth of cracks are discussed in ICON (1999c).

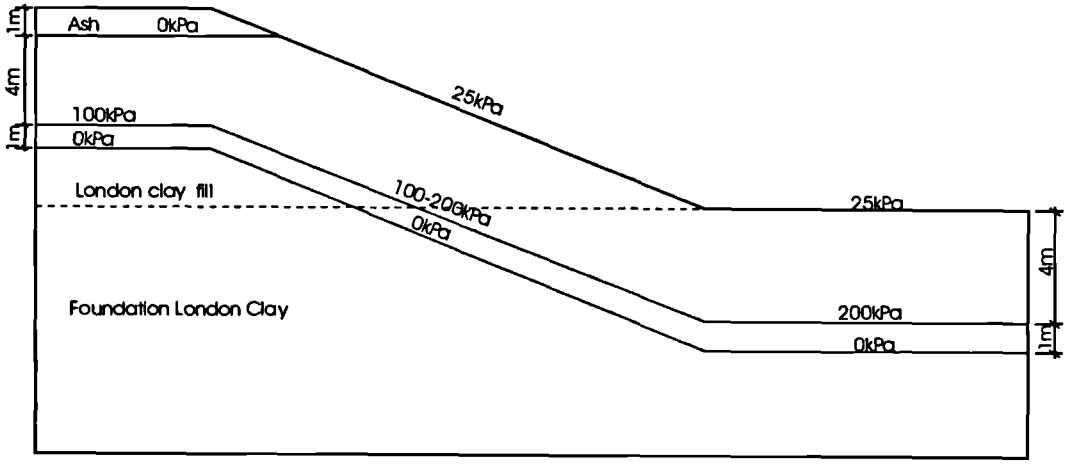

(a) Summer/shrinkage condition (suction = +ve)

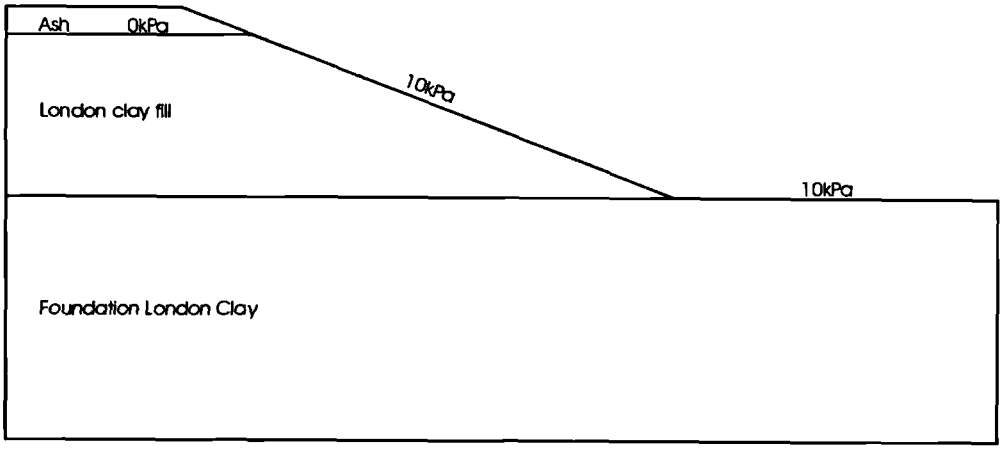

(b) Winter/swelling condition (suction = +ve)

Figure 4.1 ICON pore water pressure boundary conditions used to simulate summer & winter pore water pressure profiles for tree cover

For summer conditions, the layer of finite elements at 4-5m below ground level are modelled as a drainage layer and values of suction are set at 4 and 5m depths, at the top of the clay fill and at ground level of the foundation. The pore water pressures elsewhere in the clay fill and foundation are then allowed to consolidate/swell during a 6 month period to simulate a full summer season.

To simulate winter conditions, a surface suction is simulated at the top of the clay fill and foundation only (see Figure 4.1b). In this study, a suction of 10kPa was prescribed at the slope and top of foundation whilst a value of 0kPa was used throughout at the ash-clay fill interface. Consolidation was allowed to occur during a 6 month period to simulate a full winter season. The use of 0kPa in the latter location accords with results from field monitoring data which indicate that the ash acts as a capillary break and maintains higher positive pore water pressures in this part of the embankment (Vaughan, 1994). The ballast and ash are assumed to be always drained with zero pore water pressure.

The cycling process involves alternate imposition of summer and winter pore water pressure boundary conditions with each complete cycle comprising a summer and winter season simulating 1 year. It is noteworthy, however that in the analyses reported by Kovacevic *et al* (2001), consolidation during each season (summer or winter) was allowed to take place until full pore water pressure dissipation rather than prescribing 6 month long seasons. The results from Kovacevic *et al* (2001) are therefore not related to real time scales but to numbers of cycles and are therefore not so sensitive to the magnitudes of permeability used. The analyses in this thesis took account of real time behaviour since each season was modelled to last 6 months.

There are drawbacks associated with use of this approach to model governing winter and summer pore water pressures. By fixing the pore water pressure at some depth within the profile (equating to the maximum zone of influence), the numerical program must generate values of water flow in order to match the prescribed pore water pressure values. These flows may be of a magnitude not achievable on a vegetated slope.

It is also important to note that this methodology essentially imposes the same sequence of boundary condition year on year without monthly differentiation, which is a great simplification. The values of suctions can be quite variable as they depend on microclimatological and stratigraphical variations. Moreover, in prototype embankments the seasonal summer-winter-summer pore water pressure changes are much smoother, since they involve autumn and spring as well as monthly variations in rainfall and evapotranspiration.

The desiccated profile therefore varies greatly throughout the year and for more realistic predictions to be made, these variations need be taken into account. The latter can be achieved through use of root water uptake models which make use of meteorological data for rainfall and potential evapotranspiration as input data. The model then predicts the pore water pressures within the ground, rather than for the user to prescribe values which may never resemble in situ conditions for a particular embankment. The use of root extraction functions in such analyses is developed and demonstrated in Chapters 5 to 8.

4.4 The embankment analysed

4.4.1 The mesh

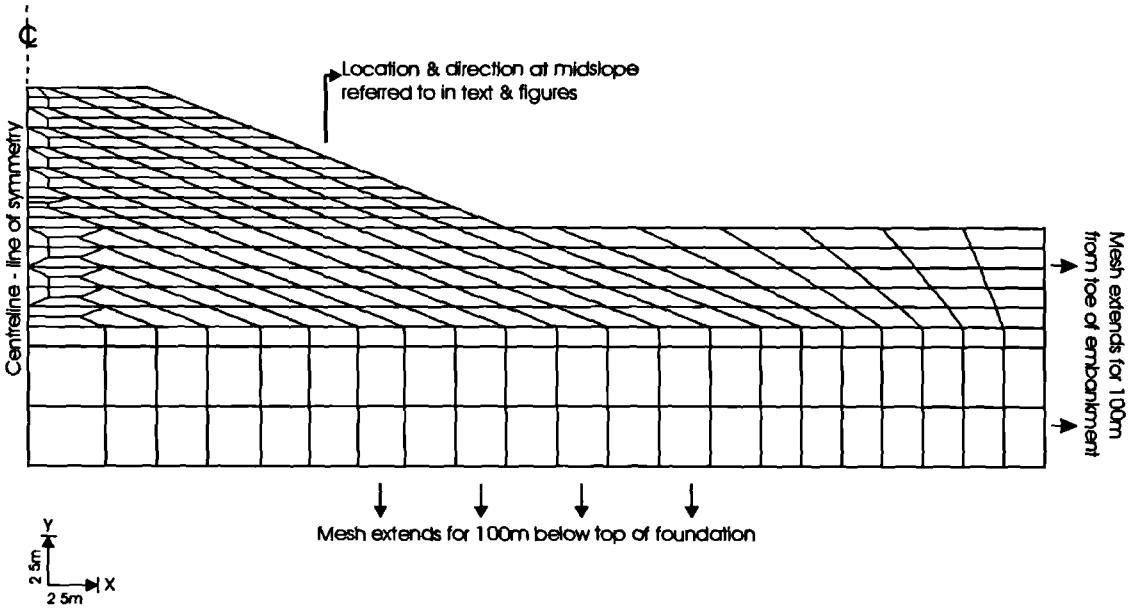

Figure 4.2 Finite element mesh used in embankment analyses for Chapters 4 & 7.

An idealised railway embankment shown in Figure 4.2 was analysed. The embankment was modelled as symmetrical and therefore in a plane strain analysis, a line of symmetry was assumed along the centreline of the embankment. The embankment was 7m high, 12m wide at the crest, with a 1 in 2.5 side slope angle. A 1m deep ash ballast layer was modelled at the crest. The effects of swelling are likely to be greatest when the ash fill is thin, because of the effects of a capillary break . The embankment was constructed from London Clay, resting on a 100m thick London Clay foundation. The depth of foundation was selected so as to eliminate any boundary effects in the numerical analyses.

4.4.2 Material properties

Table 4.1 Soil parameters used in analyses

Parameter	Ash fill	London Clay fill	In situ London Clay
Bulk unit weight (kN/m^3)	10.5	18.1	18.8
φ′ (peak)	36°	22.9° (@ 0-5% strain)	20° (@ 0-5% strain)
φ′ (residual)	N/A	13° (@ 50% strain)	13° (@ 20% strain)
c′ (peak)	2	3.4kPa (@ 0-5% strain)	7kPa (@ 0-5% strain)
c′ (residual)	N/A	2kPa (@ 50% strain)	2kPa (@ 20% strain)
Permeability (m/s)	Free draining	Case 1: $1x10^{-9}$ Case 2: $1x10^{-8}$ Case 3: $1x10^{-7}$	$2x10^{-10}$ for all three cases
Coefficient of earth pressure at rest, K_0	N/A	N/A	2.5 @ surface linearly reducing to 1.0 @ 15m depth
Stiffness (kPa)	1000 (linear elastic)	*See Equations 4.1 and 4.2* (minimum = 2500kPa)	*See Equations 4.1 and 4.2* (minimum = 4000kPa)
		See Equations 4.1 and 4.2 (minimum = 2500kPa)	*See Equations 4.1 and 4.2* (minimum = 4000kPa)
Poisson's ratio	0.3	0.3 (during construction) 0.2 (after construction)	0.2 (during and after construction)

$$E_l = E_0\left[\frac{p_a + p'}{p_a}\right]^c \qquad \text{Equation 4.1}$$

$$E_u = HE_l \qquad \text{Equation 4.2}$$

where E_l and E_u are the drained Young's moduli on first loading and unloading/reloading respectively, p_a is atmospheric pressure , p' is the mean effective stress and E_0 and c are model parameters.

The soil parameters used in the analyses are summarised in Table 4.1. These soil parameters

were used in previous investigations for LUL embankments and are based on laboratory tests and field experience. An elasto-plastic soil model in terms of effective stress, with a pre-failure stiffness (E') as a linear function of mean effective stress was used. During construction, the values of E_0, H, and c for both the clay fill and foundation London Clay were taken as 2500, 2 and unity, respectively. At the end of construction (inc. 8), the stiffness parameters of the clay fill remained unchanged but for the foundation, the values of E_0 and H were changed to 5000kPa and 1.

A strain-softening Mohr-Coulomb failure criterion was used (Figure 3.18) with an angle of dilation equal to zero. Once failure is reached, the strength remains constant for a fixed interval of deviatoric plastic strain, then the strength drops linearly proportional to further plastic strain until residual strength is reached. Once residual strength is reached, the strength remains constant with increasing strain.

Coupled consolidation was used throughout, with pore water pressures varying with time according to the specified permeabilities and drainage conditions. The soil properties adopted are very similar to the values used in previous analyses on similar old railway embankments (Vaughan, 1994; ICON, 1999b and Kovacevic *et al,* 2001). The strength and stiffness parameters were confirmed through laboratory tests carried out on samples from across the LUL network (Mott MacDonald, 1999a).

In the first set of analyses, the value of permeability for the clay fill was $1\times10^{-9}\,m/\sec$. The analysis was then repeated with the permeability increased by one order of magnitude ($1\times10^{-8}\,m/\sec$) and finally, by two orders of magnitude ($1\times10^{-7}\,m/\sec$), to investigate the influence of permeability on progressive failure. The permeability of the foundation was kept constant ($2\times10^{-10}\,m/\sec$).

4.4.3 Boundary conditions and analyses performed

The London Clay foundation was first established with $K_0 = 2.5$ at ground level, reducing to 1.0 at 15m depth, and then kept constant at 1.0 below 15m depth. A hydrostatic pore water pressure profile was assumed with a water table at 1m below ground level (and this yielded a suction of 9.81kPa at ground level). This profile was chosen primarily to avoid instability of the embankment at the end of construction. A rigid boundary was assumed at the base of the mesh at which zero vertical and horizontal movements were prescribed. Along the vertical left and right hand side boundaries, zero horizontal movements were prescribed but vertical

movement was allowed. The vertical boundaries and the bottom boundary were prescribed as no flow boundaries.

Table 4.2 summarises the key stages of construction and cycling modelled in the analyses. The embankment clay fill was constructed in 7 layers (increments 1-7) with an initial suction of 50kPa, prescribed during construction. The magnitude of suction is considered to be close to that which would have prevailed in the clay fill during construction, assuming stress relief in the fill material sourced from cuttings averaging 5m depth. It is also noteworthy that some of the fill material would have been sourced from tunnel excavations and the latter material is likely to have had higher suctions. However the magnitude of suctions would have reduced during transportation and handling as a result of frequent precipitation (typical of UK weather patterns) hence an overall value of 50kPa is considered to be reasonable (Skempton, 2000). During construction, the surface boundary was modelled as a no flow boundary.

Table 4.2 Modelled sequence of events

Stage	Inc. No.	Description of event	Time
0	0	Set initial stresses using assuming ground water level at 1m below ground level & surface suction of 9.81kPa	0 yrs
2	1-7	Construct loose London Clay fill quickly in 7 layers (each approx. 1m thick). Assume a 50kPa suction in clay fill during placement	0.08 yrs
3	8-20	Allow the fill and foundation to consolidate to a surface suction of 10kPa for 5 yrs. During this period, the effects of vegetation are assumed to be nominal	5 yrs
4	21-32	Extend stage 3 for 6 months to model the first winter. (NB. The pwp profile shown in Fig 4.3b is invoked)	0.5 yrs
5	33-44	Apply a pwp profile as shown in Figure 4.3a to model summer desiccation	0.5 yrs
6	45-56	Apply a pwp profile shown in Figure 4.3 b to model winter conditions	0.5 yrs
7	57-68	Ditto stage 5	0.5 yrs
8 onwards	69 onwards	Sequentially alternate stages 5 (summer) and 6 (winter) until the embankment fails	Each stage is 0.5 yrs long

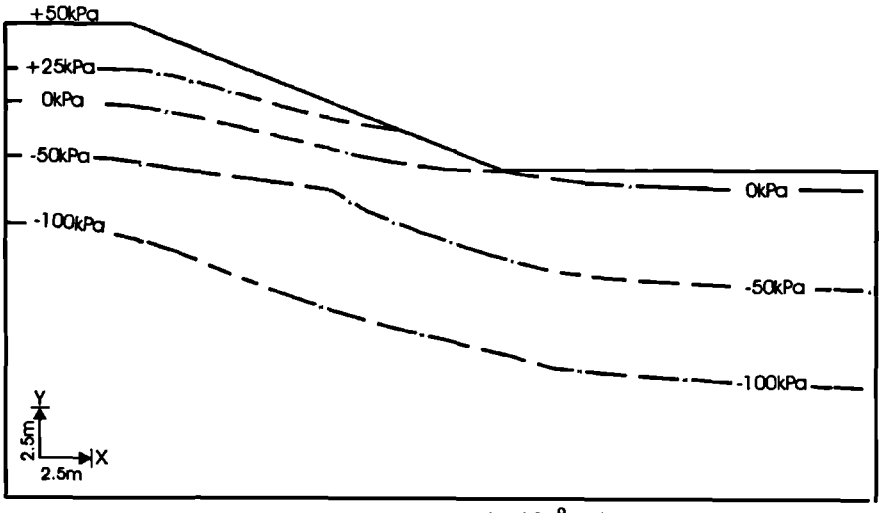

(a) Permeability = $1 \times 10^{-9} m/\sec$

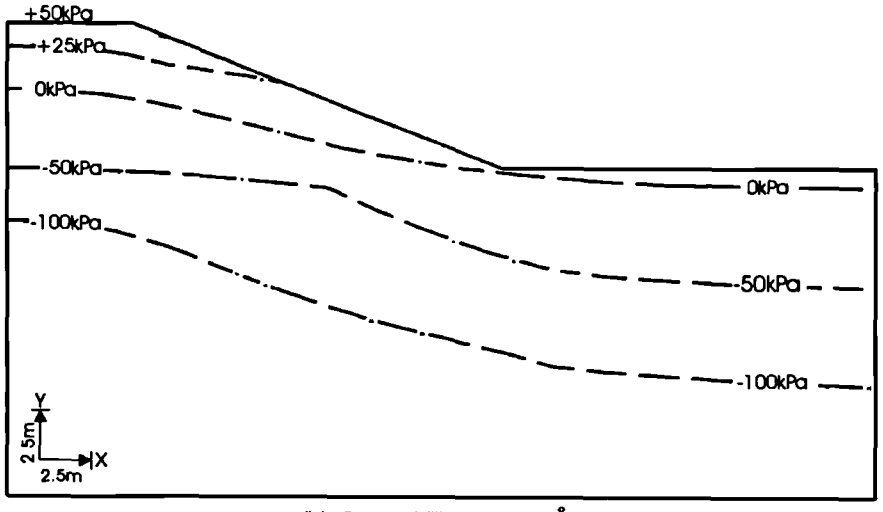

(b) Permeability = $1 \times 10^{-8} m/\sec$

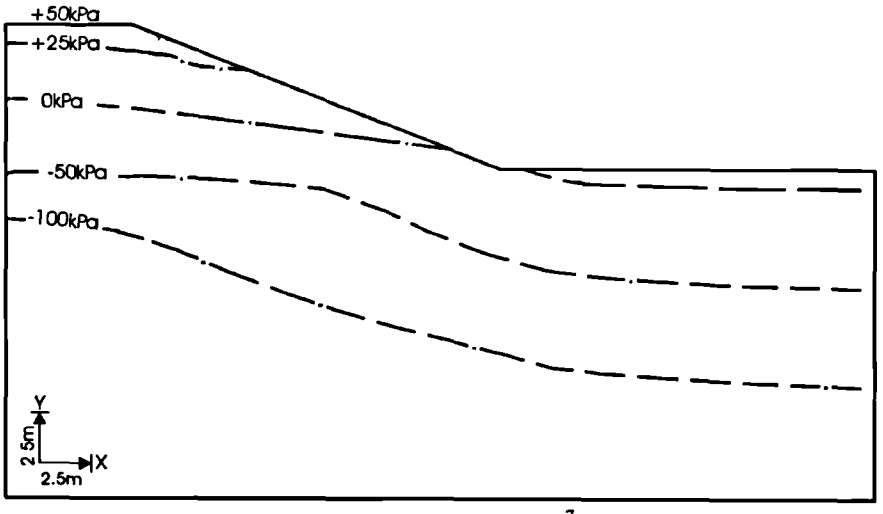

(c) Permeability = $1 \times 10^{-7} m/\sec$

Figure 4.3 Influence of permeability on contours of accumulated pore water pressure at the end of construction.

The ash ballast was constructed in two layers with no suction prescribed. The use of layered construction and the construction times (see Table 4.2) assumed are considered to be representative of end-tipping, and is characterised by negligible consolidation of the foundation at the end of construction.

An assumption was also made that vegetation would take up to 5 years to establish itself before it began to induce significant desiccation within the embankment. This was modelled by allowing the embankment to consolidate to a boundary pressure of 0kPa at the clay fill-ash interface and a 10kPa suction maintained on the slope of the embankment and top of the foundation beyond the toe of the embankment (inc. 9-20) ie. winter condition in Fig 4.1b. After the 5 year period, the embankment was then subjected to winter and summer cycles until failure. Each season was modelled in 12 increments (ie. inc 21-32: winter 1, inc 33-44: summer 1, inc 45-56: winter 2 etc.).

4.5 Effect of permeability

4.5.1 Embankment behaviour during construction

The convention used in the figures is as follows:

- suction and/or tensile pore water pressures (+ve)
- compressive mean effective stress, p' (+ve)
- compressive major (σ_1) and minor (σ_3) principal stresses (+ve)

The contours of pore water pressure distribution at the end of construction are shown in Figure 4.3, for the three permeabilities. During construction, the clay fill was assumed to have a suction of 50kPa during placement. It can be seen from the figure that for all three permeabilities, pore water pressure redistribution has occurred by the end of construction although residual suctions still exist in the material placed last. The degree of pore water pressure dissipation at the end of construction is dependent on the magnitude of permeability. Figure 4.3a reveals that the low permeability clay fill ($1\times10^{-9}\,m/\sec$) still retains high suctions over a significant section of the embankment unlike the higher permeability clay fill (Figs 4.3b and 4.3c) where significant pore water pressure dissipation is accompanied by build-up of compressive pore water pressures.

Figure 4.4 shows the distribution of pore water pressures along a vertical profile at mid-slope.

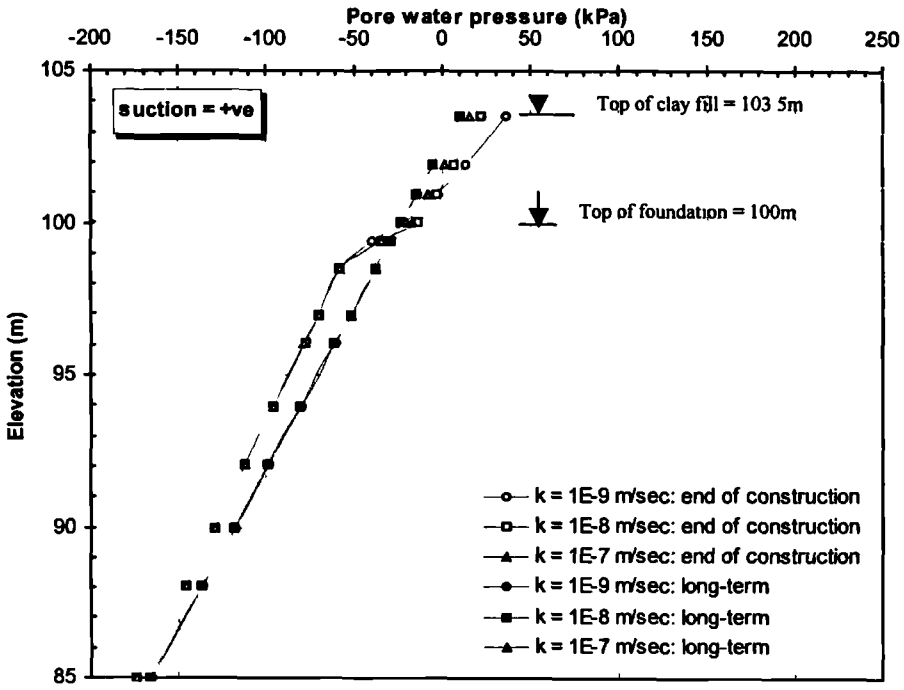

Figure 4.4 Influence of clay fill permeability on pore water pressure predictions at mid-slope at the end of construction and long-term situation

The location of this vertical profile is shown in Figure 4.2. The long term pore water pressure distribution is also shown in Figure 4.4, for comparison. The long term pore water pressures were established by carrying out a consolidation/swelling analysis at the end of construction during which pore water pressures were allowed to fully dissipate over many years. During the consolidation/swelling analysis, a 10kPa suction was prescribed at the surface boundary. Once again the influence of permeability on pore water pressure distribution within the clay fill is portrayed eg. at 2m above the base of the embankment (elevation 100m), the pore water pressures are approximately 15kPa (suction), 8kPa (suction) and 0kPa for clay fill permeabilities of $1\times10^{-9} m/\sec$, $1\times10^{-8} m/\sec$ and $1\times10^{-7} m/\sec$. In all three cases, the clay fill beneath the line of zero pore water pressure and uppermost sections of the foundation have pore water pressure profiles above hydrostatic. The latter is consistent with the assumption of "quick" construction that was assumed in the analyses to simulate end tipping.

Figure 4.5 shows the plots of the stress level S, (the proportion of the strength mobilised) at the end of construction. It can be seen that the foundation shear strength is fully mobilised at the clay fill/foundation interface. This suggests that further stressing of the foundation eg. increasing the embankment height, would lead to development of shear surfaces at the base of the embankment and could trigger a failure mechanism. This may explain why so many failures occurred during construction of these embankments.

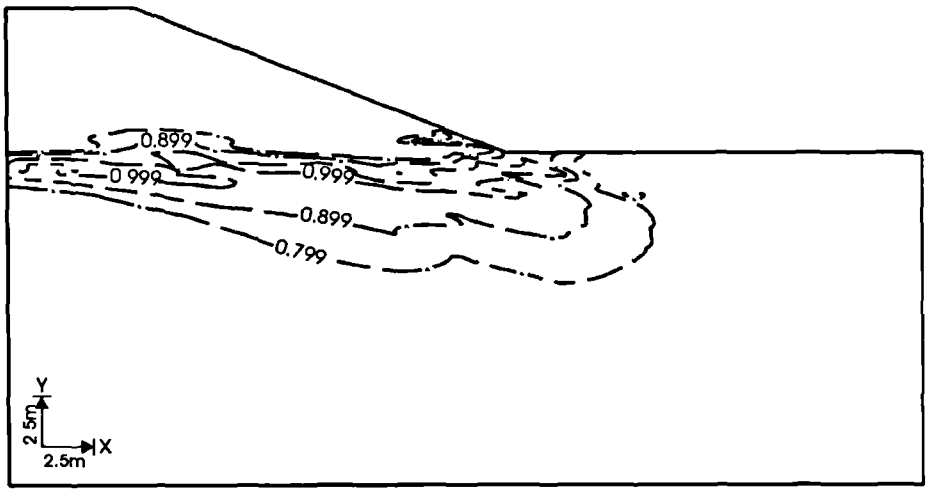

(a) Permeability = $1 \times 10^{-9}\ m/\text{sec}$

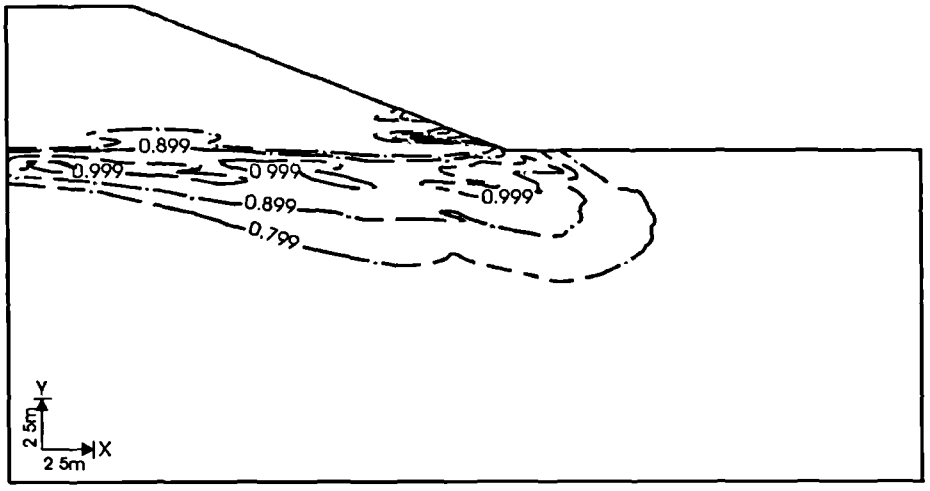

(a) Permeability = $1 \times 10^{-8}\ m/\text{sec}$

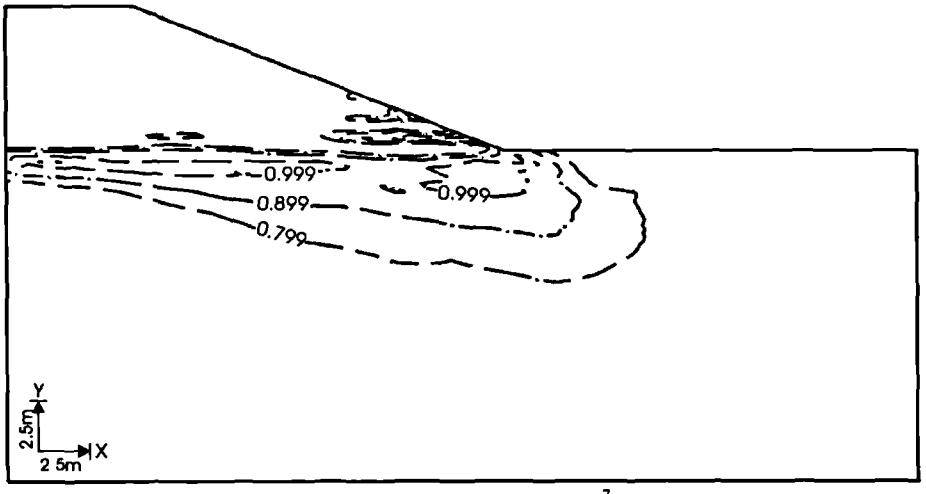

(a) Permeability = $1 \times 10^{-7}\ m/\text{sec}$

Figure 4.5 Contours of stress level at the end of construction predicted by 3 permeabilities

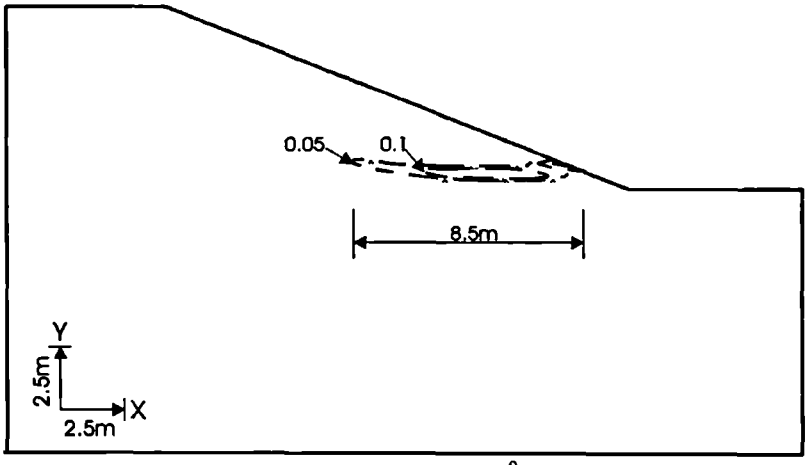

(a) Permeability = $1 \times 10^{-9} m / sec$

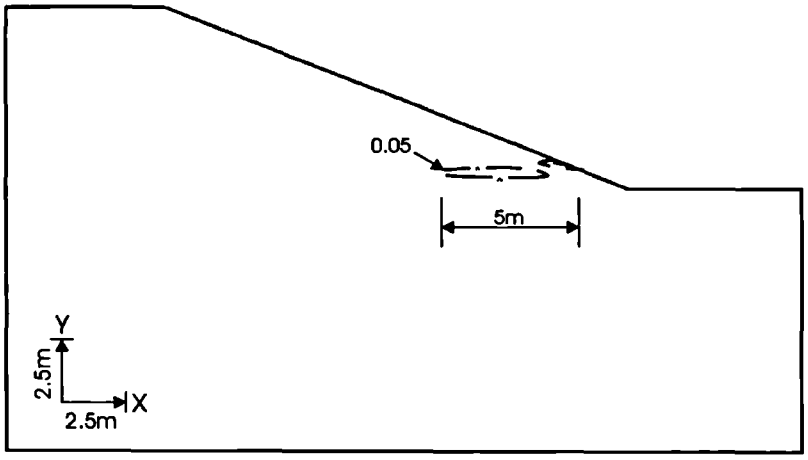

(b) Permeability = $1 \times 10^{-8} m / sec$

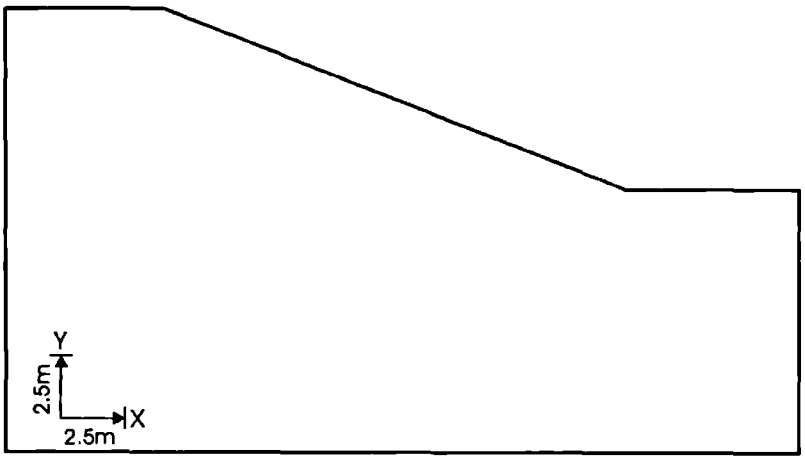

(c) Permeability = $1 \times 10^{-7} m / sec$

Figure 4.6 Contours of sub-accumulated deviatoric plastic strains predicted by 3 permeabilities during 5yr swelling/consolidation period.

4.5.2 Embankment behaviour during initial 5 years of swelling

As previously discussed, the embankment was allowed to swell/consolidate for a period of 5 years soon after construction to model the post-construction period during which vegetation established itself on the embankments. During this period, the influence of vegetation was assumed to be nominal hence consolidation was allowed to occur whilst a 10kPa suction was prescribed at ground level on the slope and the surface boundary away from the toe of the embankment (Figure 4.1b).

Figure 4.6 shows the contours of sub-accumulated deviatoric plastic strains during the 5 year swelling period. It can be seen that during this swelling period, significant plasticity occurs at the toe of the embankment in the clay fill of $1\times10^{-9} m/\sec$ permeability. Note that strain softening starts at $E_p = 0.05$ (5%) (ie. contour level "A").

It can be seen from Figure 4.6a that a significant portion of a potential slip surface experiences strain changes which exceed the peak strain level eg. the zone demarcated between $E_p = 0.05$ (5%) and $E_p = 0.1$ (10%) contours. The corresponding relatively lower pore water pressure changes during this swelling period in the clay fill of intermediate permeability ($1\times10^{-8} m/\sec$) result in less plasticity and are virtually nil in the clay fill of highest permeability ($1\times10^{-7} m/\sec$).

The onset of a potential slip surface is corroborated by the plots of velocity characteristics which are shown in Figure 4.7. The velocity characteristics represent the shear surfaces across which discontinuities in strain can occur. They make angles of $45^0 \pm \frac{\mu}{2}$ to the plane on which σ_3 operates, where μ is the angle of dilation. Within ICFEP, discontinuous shear zones can form with a minimum thickness of about half an element. In these analysis this is typically 0.5m. In the field, shear bands are likely to form in a much narrower zone than has been modelled here.

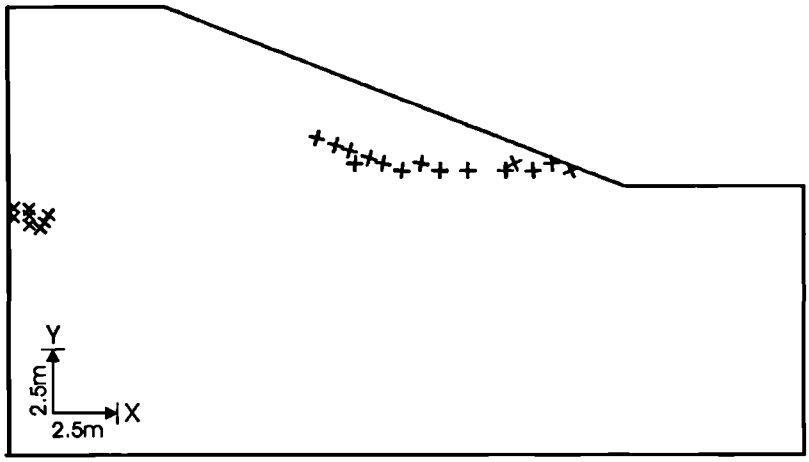

(a) Permeability = $1\times10^{-9}\,m/\text{sec}$

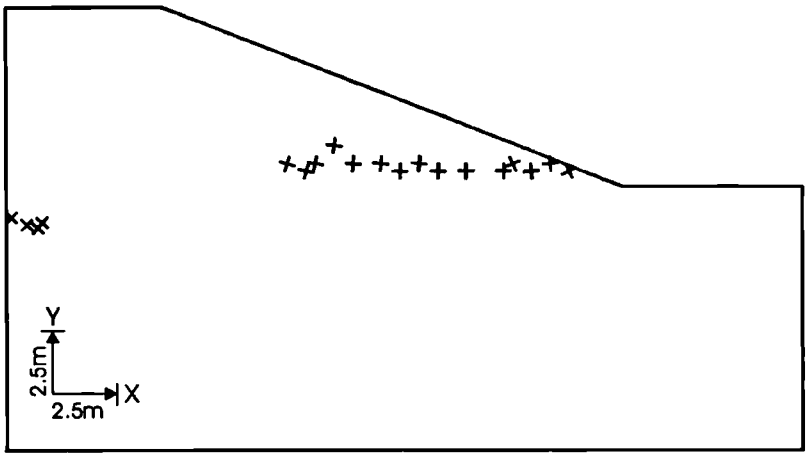

(b) Permeability = $1\times10^{-8}\,m/\text{sec}$

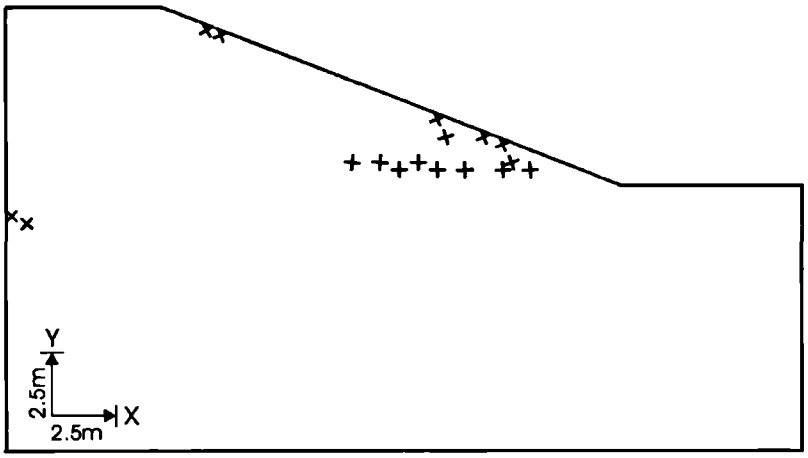

(c) Permeability = $1\times10^{-7}\,m/\text{sec}$

Figure 4.7 Velocity characteristics at the end of 5yrs swelling/consolidation period predicted by 3 permeabilities.

Potts *et al* (1992) showed that because of the rather wide shear zones which form (unless a very large number of elements is used in an analysis), the specification of an angle of dilation involves far more dilation than is observed in the field because the latter is concentrated in a very thin zone only. In order to overcome this problem, numerical analysts usually specify an angle of dilation equal to zero. This essentially eliminates dilation in an analysis and gives rupture surfaces at 45^0 to the direction of σ_1. Thus the rupture surfaces indicated by the crosses in the plots are at an angle which is slightly different to field conditions. The collapse load is unlikely to be too different but the location of the rupture surface is affected slightly.

The velocity characteristics indicate the planes of failure where the clay is behaving as a plastic material (failing). From Figure 4.7, it can be seen that plastic behaviour is occurring along a potential shear surfaces for all three permeabilities at the base of the clay fill near the toe.

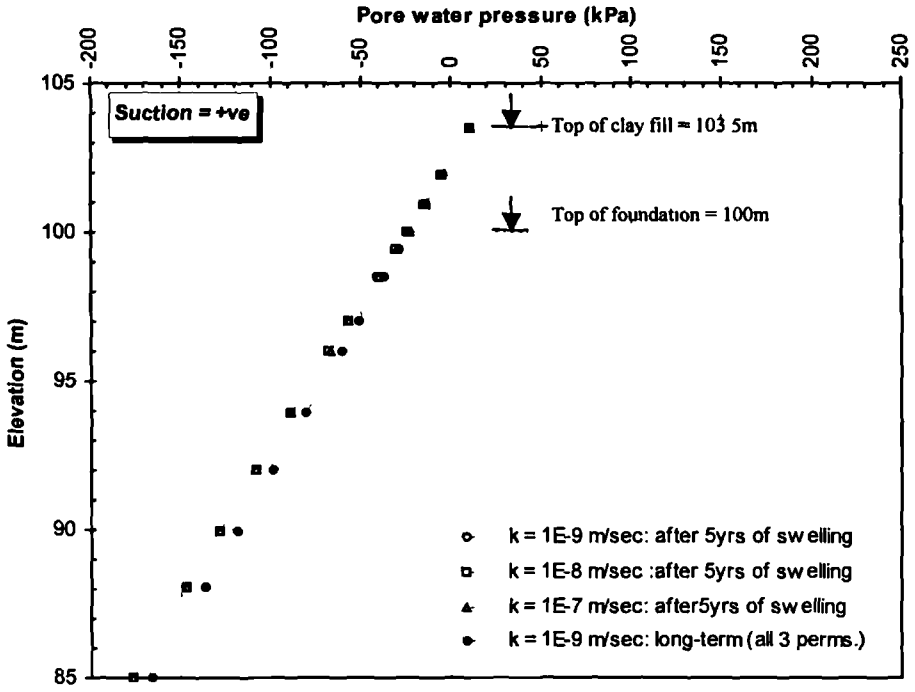

Figure 4.8 Influence of clay fill permeability on pore water pressures after 5yrs and long term situation.

The distribution of pore water pressures along a vertical profile at mid-slope is shown in Figure 4.8 together with the long term pore water pressure profile. It can be seen that pore water pressures within the embankment have effectively fully dissipated to their long term values. Within the foundation, some dissipation of pore water pressures also occurs in the upper horizons, but overall, the limited time scale of 5 years coupled with its low permeability (1×10^{-10} m/sec) and the long distances to drainage boundaries prevents significant dissipation.

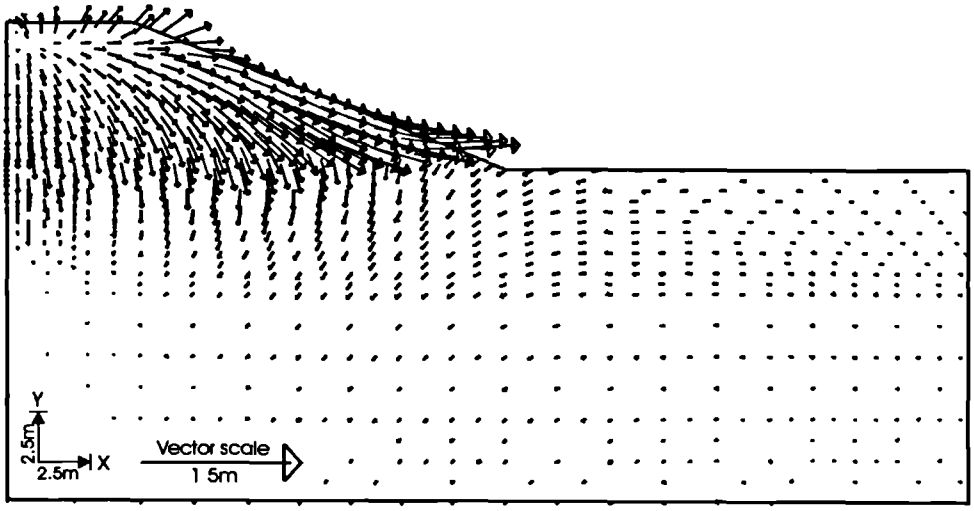

(a) Permeability = $1 \times 10^{-9} m / sec$

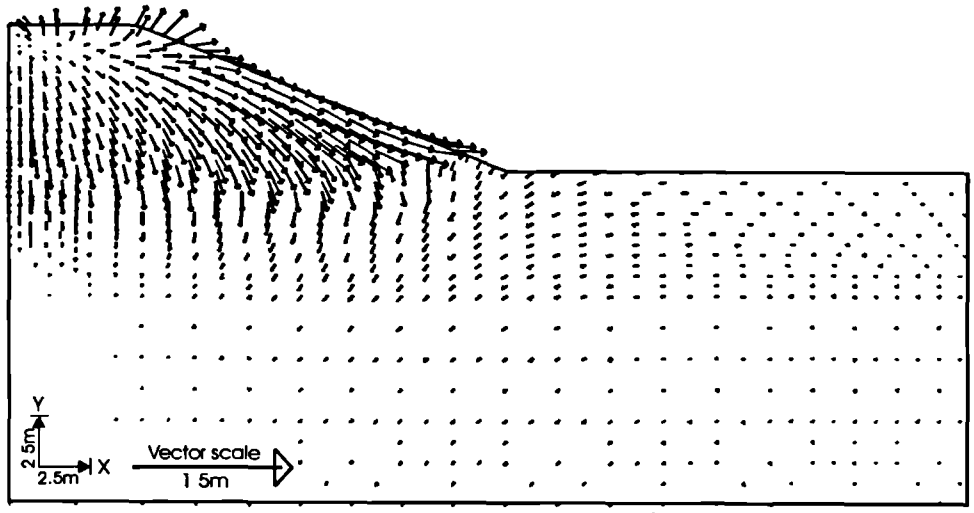

(b) Permeability = $1 \times 10^{-8} m / sec$

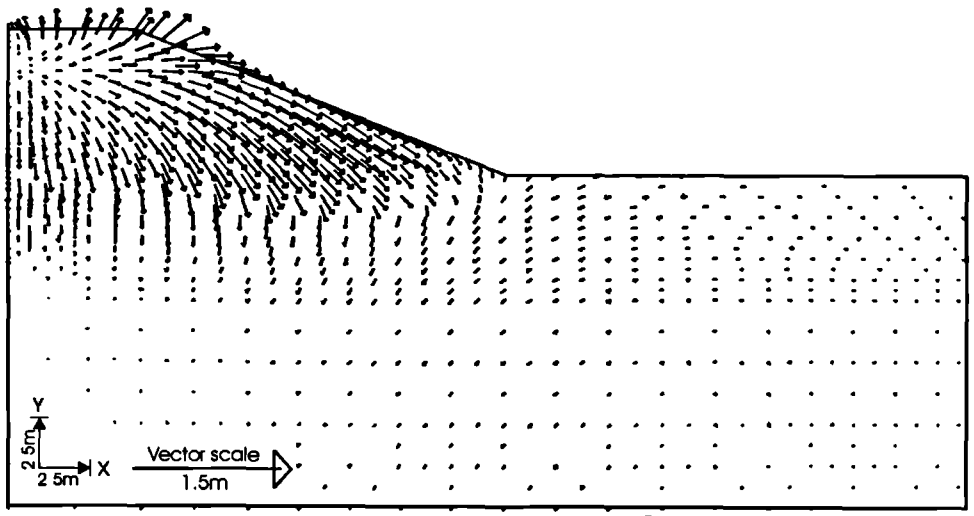

(b) Permeability = $1 \times 10^{-7} m / sec$

Figure 4.9 Vectors of sub-accumulated movements predicted by 3 permeabilities during 5 yrs of swelling/consolidation (inc. 8 - 20).

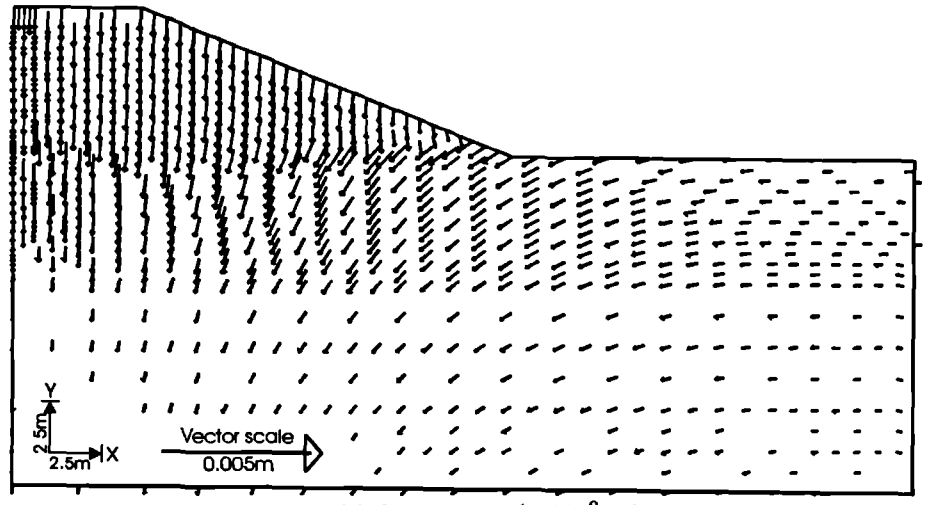

(a) Permeability = $1 \times 10^{-9}\, m/\text{sec}$

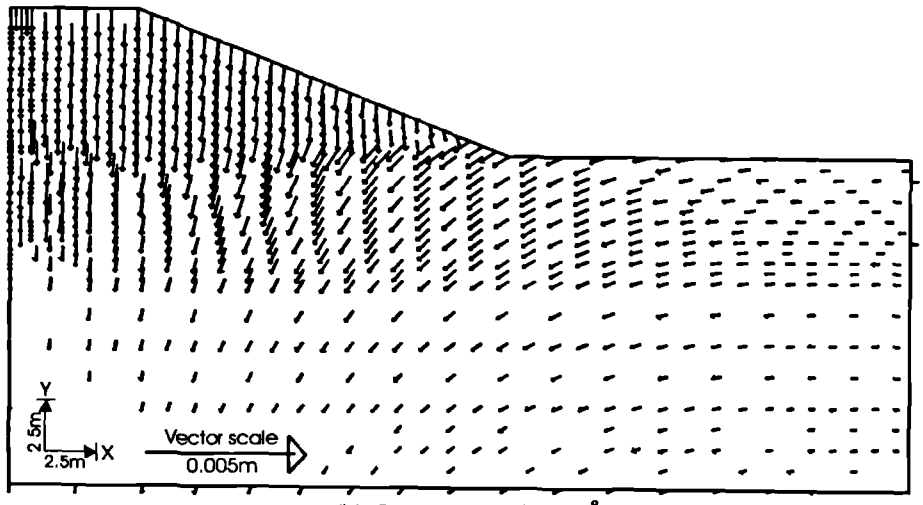

(b) Permeability = $1 \times 10^{-8}\, m/\text{sec}$

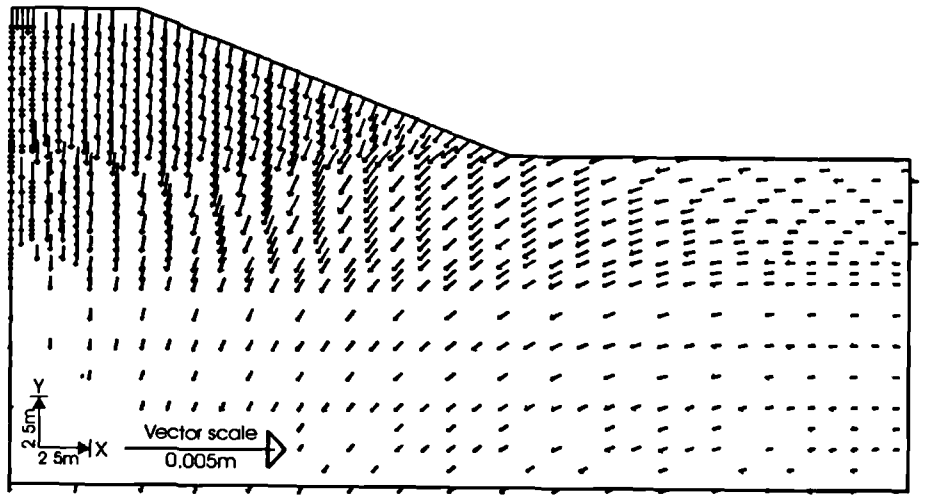

(b) Permeability = $1 \times 10^{-7}\, m/\text{sec}$

Figure 4.10 Vectors of incremental movements at the end of the 5yr swelling/consolidation period predicted by 3 permeabilities

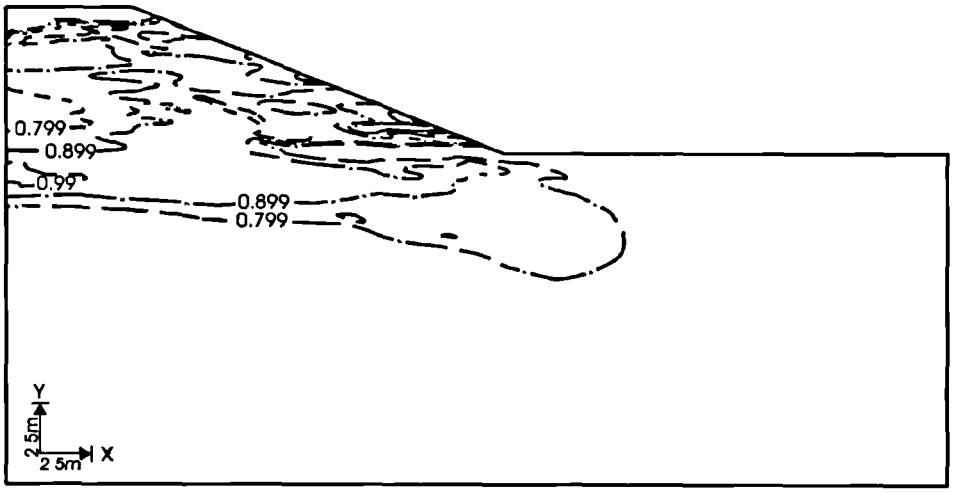

(a) Permeability = $1 \times 10^{-9}\, m/\text{sec}$

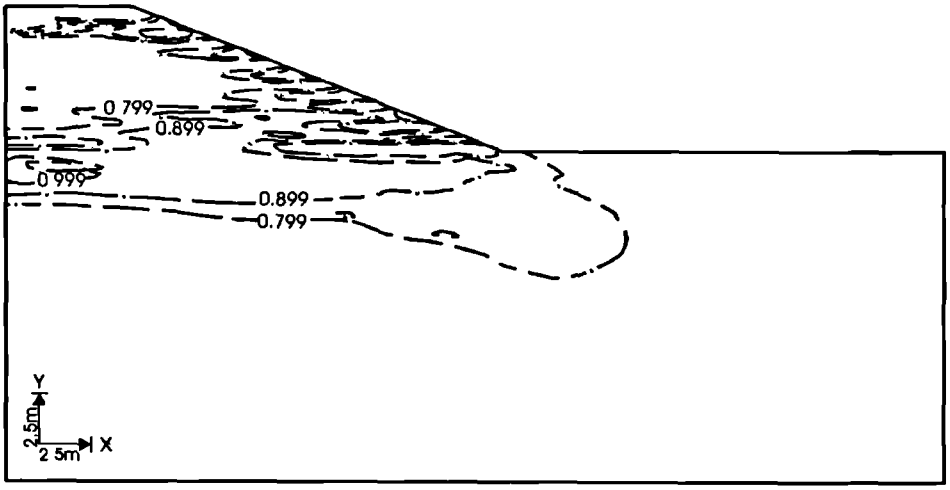

(b) Permeability = $1 \times 10^{-8}\, m/\text{sec}$

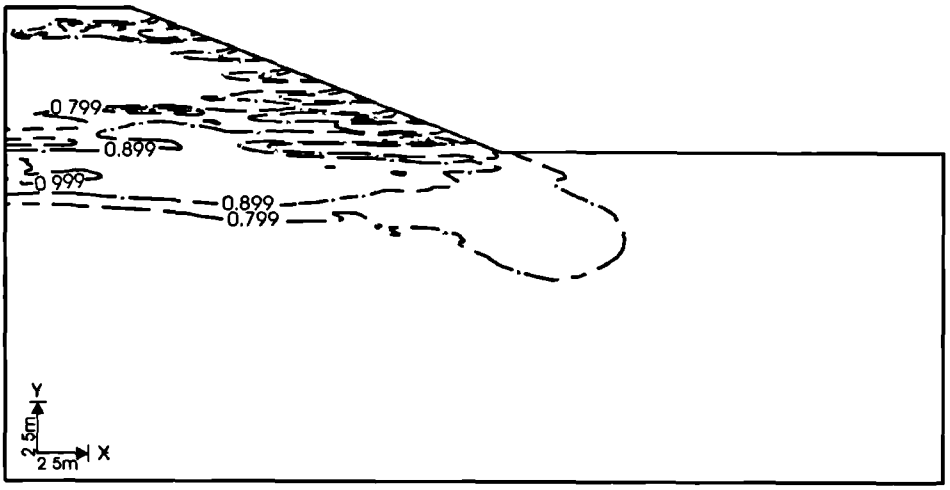

(c) Permeability = $1 \times 10^{-7}\, m/\text{sec}$

Figure 4.11 Contours of stress level, S, predicted by 3 permeabilities at the end of 5yrs of swelling/consolidation.

The movements that occur during the 5year swelling/consolidation period are shown in Figure 4.9. Although the pattern of movements is dominated by downward movement of the fill and foundation (which is indicative of consolidation) there is clear evidence of horizontal slope movements during this period. The overall pattern of movements is dependent on the permeability; with the largest magnitude occurring in the low permeability clay fill ($1\times10^{-9} m/\sec$). This corroborates the plasticity indicated in Figures 4.6 and 4.7.

It is also noteworthy that although the sub-accumulated movements suggest slope movements, the vectors of incremental movements at the end of the 5year swelling/consolidation period (Figure 4.10) do not indicate horizontal movements. This implies that the horizontal movements occurred at some earlier stage during swelling after which the embankment stabilised as a result of consolidation. The latter is borne testimony to by the contours of stress level, *S*, (Figure 4.11) which indicate a reduction in the zone of highly stressed material at the base of the embankment. However, although the latter is true for all the three permeabilities, the stress level contours in the clay fill of low permeability ($1\times10^{-9} m/\sec$)indicate an increase in stress level within the slope as a result of the horizontal slope movements that occur during swelling.

The influence of permeability during the swelling period revealed above has implications on some important historical aspects of UK old railway embankments. Where little contamination with gravel occurred in the stiff clay fill, the constructed embankments had overall low permeability. This resulted in relatively higher suctions at the end of construction compared to more permeable clay fills. The rate and amount of post-construction swelling that occurred would have been governed by the rate at which vegetation established itself on the embankments. Early and substantive transpiration by vegetation would have curtailed development of compressive pore water pressures, and on the basis of the foregoing results, would have assisted to reduce the magnitude of swelling and hence improve stability. The short term stability of these embankments would therefore have been highly dependent on the rate at which vegetation established itself on the embankments.

For the embankments in which the clay fill had been siginificantly contaminated by granular material during placement, their overall permeability may well have been high enough so as to cause significant dissipation of pore water pressures during and after construction, before vegetation established itself. Comparatively less movements would have occurred during swelling soon after construction and therefore the short term stability of these latter embankments would have been less dependent on the establishment of vegetation.

The foregoing comments are based on the assumption that the clay fill at the end of construction behaved as a continuum. Some researchers (eg. Vaughan, 2002) believe the clay fill at the end of construction was characterised by large clods (typically 300m in diameter) such that the clay fill behaved as a granular material. Permeability under these circumstances would have been very high, gradually reducing as the clay fill swelled with time.

Based on his discussion with Skempton (2000), the author believes that although the clay fill as placed comprised a large proportion of clods up to approximately 300mm in diameter, the overall grading achieved after handling would have comprised a large proportion of small diameter clods. Moreover, the bulk of the excavations were carried out by navvies using picks and shovels (Skempton, 2000) hence it is reasonable to assume that a significant proportion of small diameter material (approx. 50-100mm nominal diameter) resulted from such operations. The overall structure of the fill (as placed) would therefore have been voided but to a much lesser degree. With a wet climate such as that prevalent in the UK, the author believes the small diameter clods would have swelled quickly and filled up the voids in a relatively short time scale. The swelled fill would therefore behaved as a continuum, with a low permeability (unless some granular inclusions were present which would increase its mass permeability).

4.5.3 Embankment behaviour during cycling

At the end of the 5 year swelling period, the embankment was subjected to alternate winter and summer pore water pressure profiles until development of a failure mechanism using the pore water pressure profiles described in Section 4.3. In the analyses a winter profile was invoked first, with a suction of 10kPa prescribed on the slope and top of foundation. The summer and winter pore water pressures along a vertical profile at mid-slope are shown in Figure 4.12 a and b for the three permeabilities for the periods after 3 and 5 cycles, respectively. Figure 4.13 shows the corresponding plots after 5 and 10 cycles. As previously discussed, each cycle equates to 1 year and comprises winter (6 months) and summer (6 months).

Figure 4.12 shows that during winter, pore water pressures in the clay fill fully recover for permeabilites of $1\times10^{-8}m/\sec$ and 1×10^{-7}m/sec but not in the $1\times10^{-9}m/\sec$ clay fill. During summer, the latter clay fill attains slightly higher suctions. This is because the summer ICON pore water pressure profile is invoked at the end of winter during which relatively higher suctions are prevalent in the clay fill with a permeability of 1×10^{-9}m/sec compared to relatively lower suctions in the more permeable clay fills.

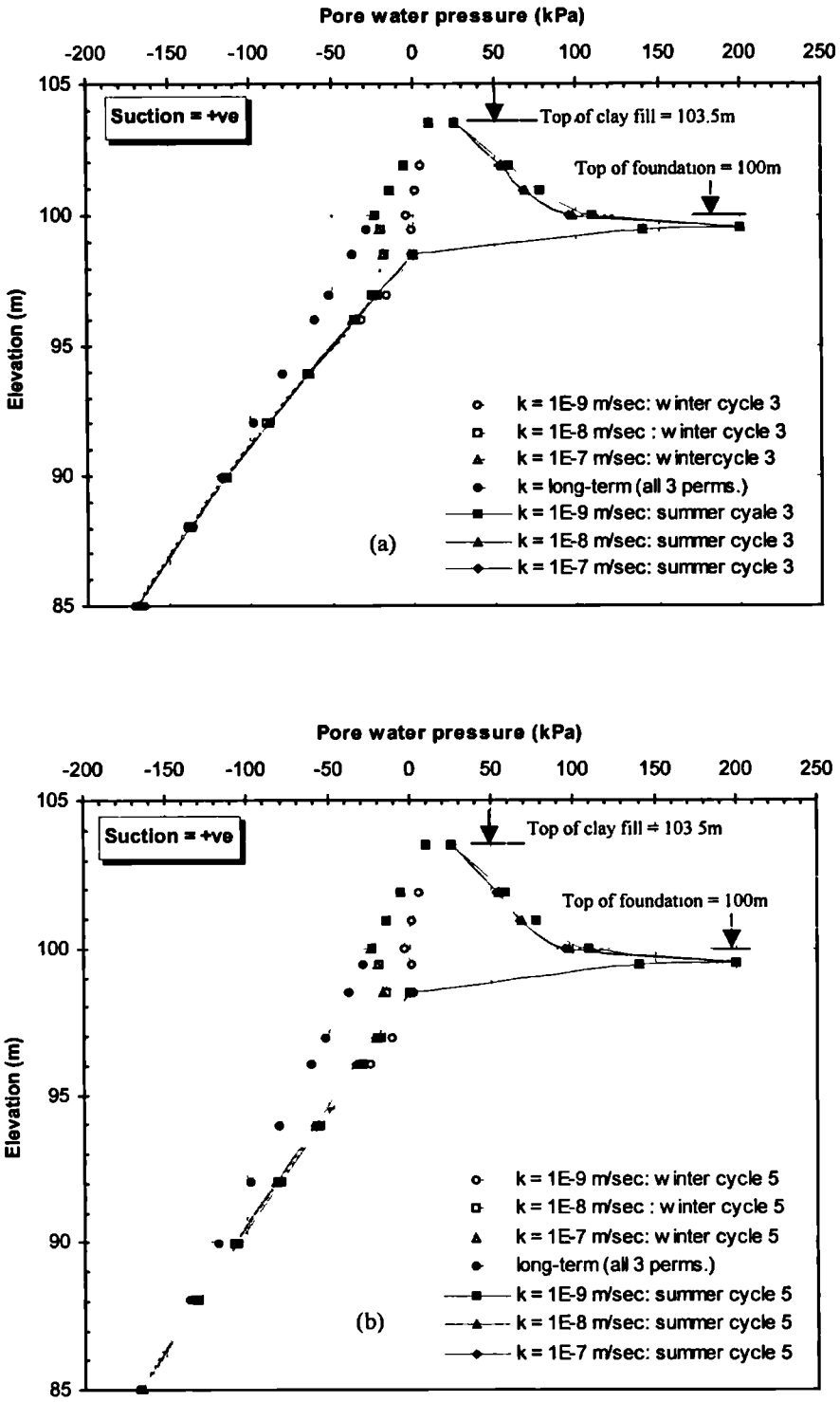

Figure 4.12 Influence of clay fill permeability on accumulated pore water pressure at mid-slope of the embankment after 5 cycles.

For winter and summer, the pore water pressure distributions for the $1\times10^{-7} m/\sec$ and $1\times10^{-8} m/\sec$ permeability clay fills are very similar. This suggests that the two permeabilities

are high enough for pore water pressure adjustments to the prescribed flow boundary conditions to be complete by the end of 6 months (duration of winter/summer season). The scenario is different for the lowest permeability ($1\times10^{-9}\,m/\sec$) where it can be seen that within the clay fill, suctions still exist at the end of the 6 month swelling period (winter). Overall, the least pore water pressure changes during each winter-summer cycle occur in the low permeability clay fill ($1\times10^{-9}\,m/\sec$). The magnitude of pore water pressure change in the intermediate and highest permeability clay fills is nearly the same.

The accumulated pore water pressure contours at the end of the first summer are shown in Figure 4.14 and indicate the pore water pressure distribution achieved by invoking the summer ICON pore water pressure profile for 6 months (to model a summer season). The corresponding end of summer contours of minor total principal stress, σ_3, are shown in Figure 4.15; for the three permeabilities. In all cases, a tension zone is predicted at the top of the clay fill and foundation. The depth of the tension zone is dependent on the permeability eg. in the area remote from the embankment, the depth of the tensile zone is 4m, 4.2m and 4.4m, for the low, intermediate and high permeabilities, respectively. The corresponding depths at the centreline of the embankment are 3.2m, 3.3m and 3.5m. The average depth of the tensile zone in the slope is 4.2m for the three permeabilities. Evidence of internal cracking up to 4m deep has been observed at an LUL embankment at Canons Park 9 (ICON, 1999a)

The vectors of sub-accumulated movements occurring during the first summer are shown in Figure 4.16. The direction of vectors in the clay fill is largely vertical and is indicative of shrinkage. Shrinkage essentially constitutes strain reversal to that which occurred during winter and hence the process can be associated with some plasticity. With increasing cycling, a progressive failure mechanism is developed in the most permeable clay fill ($1\times10^{-7}\,m/\sec$) where the largest pore water pressure changes occur. After 13 years of cycling very little change in plasticity has occurred in the clay fill of low and intermediate permeability ($1\times10^{-9}\,m/\sec$ and $1\times10^{-8}\,m/\sec$) as depicted in Figure 4.17 where contours of sub-accumulated strains from cycles 1 to 13 have been plotted.

Figure 4.18 shows the vectors of sub-accumulated movement between cycles 1 and 13. The direction of vectors bears testimony to the fact that during this period, movement in the clay fill with permeabilities of $1\times10^{-9}\,m/\sec$ and $1\times10^{-8}\,m/\sec$ is largely near vertical. In the clay fill with a permeability of $1\times10^{-7}\,m/\sec$, significant slope movements associated with development of a slip surface have occurred.

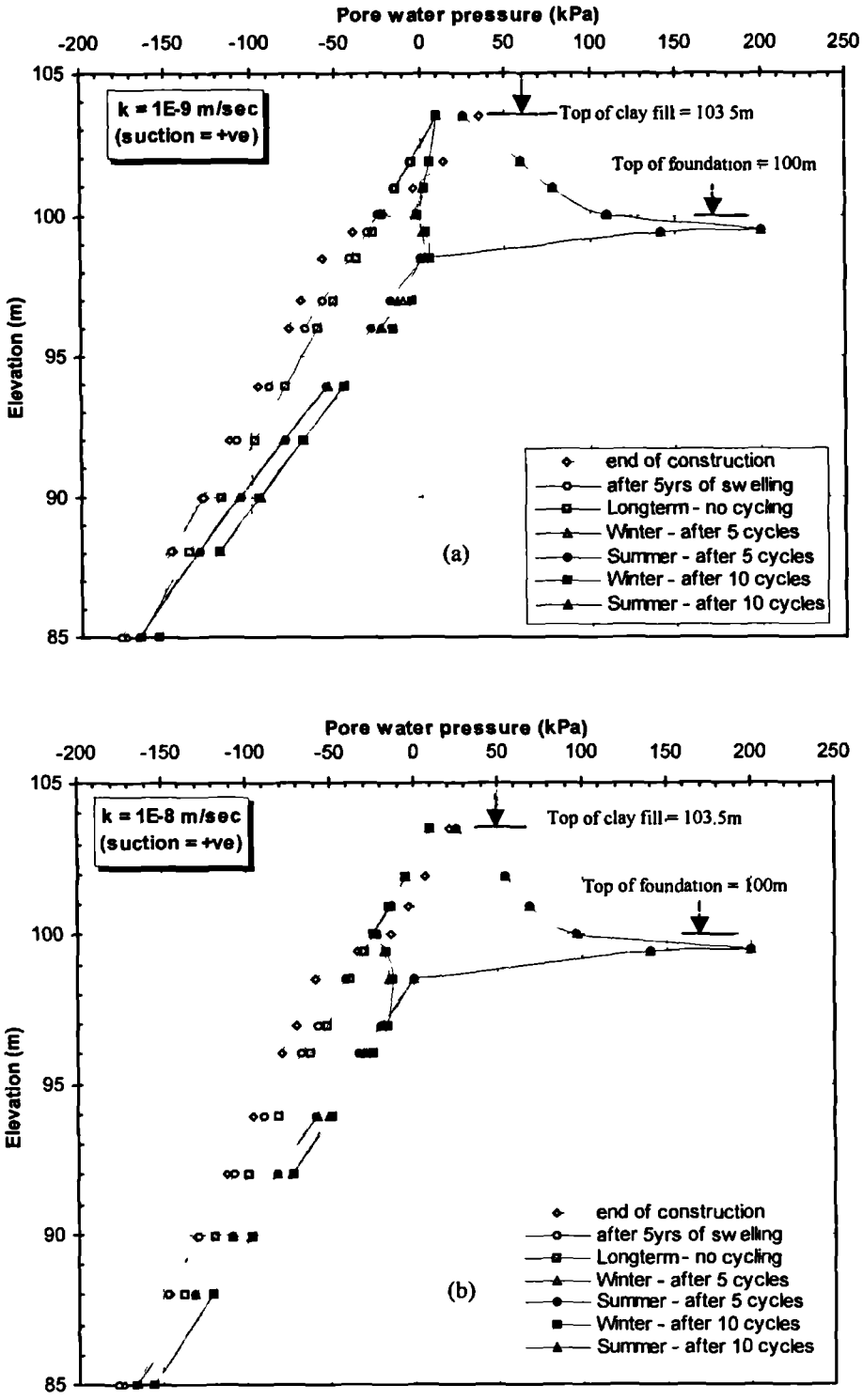

Figure 4.13 Influence of clay fill permeability on accumulated pore water pressure at mid-slope of the embankment after 5 & 10 cycles.

The vectors of incremental movements at this stage are shown in Figure 4.19. They indicate that in the clay fill with a permeability of $1\times10^{-7} m/\sec$, the failure mechanism has not yet

fully developed as revealed by the absence of significant horizontal components of the incremental vectors at the end of the 13th cycle. It is also noteworthy that the overall pattern of incremental movements among the three permeabilities is quite different, as indicated by a reduction in the magnitude of the vectors in the slope with increasing permeability. The existence of a potential rupture surface in the $1\times10^{-7} m/\sec$ permeability clay fill is further corroborated by the velocity characteristics which have lined up over a large distance from the toe (Figure 4.20a).

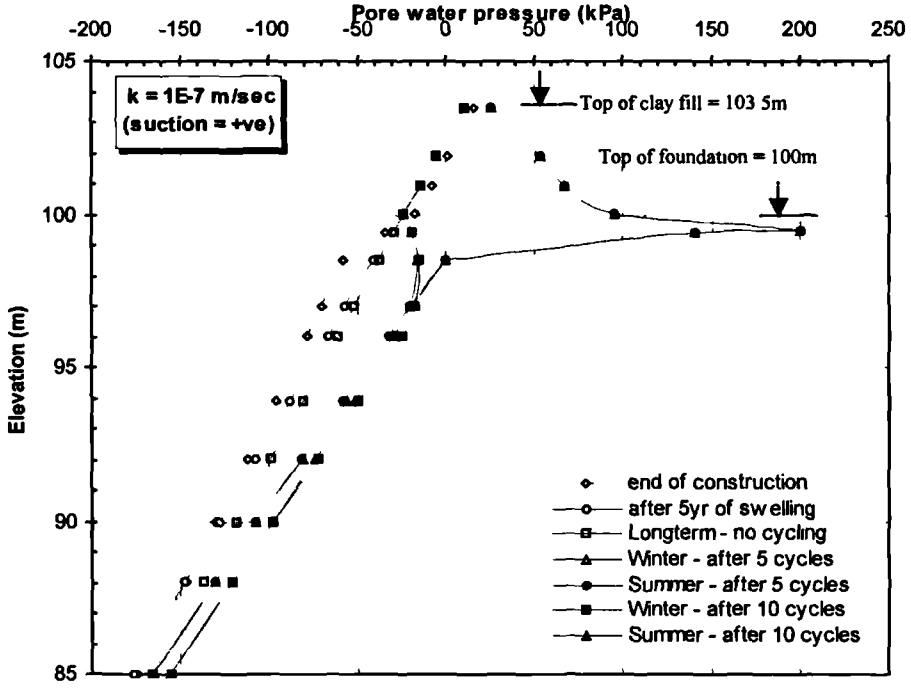

Figure 4.13c Influence of clay fill permeability on accumulated pore water pressure at mid-slope of the embankment after 5 & 10 cycles.

The accumulated horizontal movements at mid-slope (ground level) from construction up to the end of the 11th cycle are shown in Figure 4.21. From this figure, it can be seen that during the first 5 years of swelling, most of the movement occurs during the first 12 months in the clay fill of higher permeability ($1\times10^{-7} m/\sec$ and $1\times10^{-8} m/\sec$). Maximum movements of 30mm are attained, after which consolidation dominates behaviour and results in shrinkage of the embankment during the remaining 4 years of the 5 year swelling period. At the end of the swelling period the accumulated horizontal movements reduce to approximately 27mm.

In the clay fill with a permeability of $1\times10^{-9} m/\sec$, the behaviour during swelling is different and is characterised by continuous outward movement attaining a peak of approximately 42mm after 3.5 years. Beyond this period, consolidation dominates the behaviour and is marked by a small reduction in accumulated horizontal movements to 41mm.

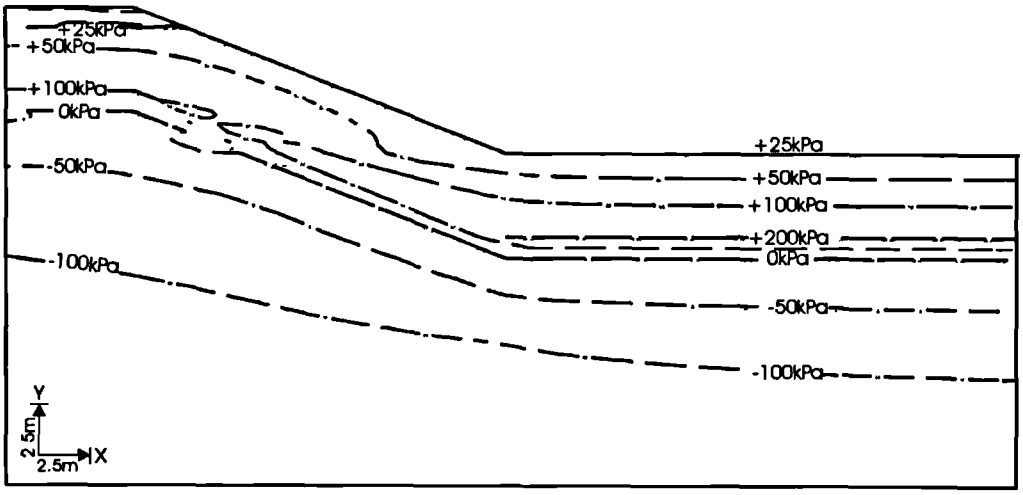

(a) Permeability = $1 \times 10^{-9} m/sec$

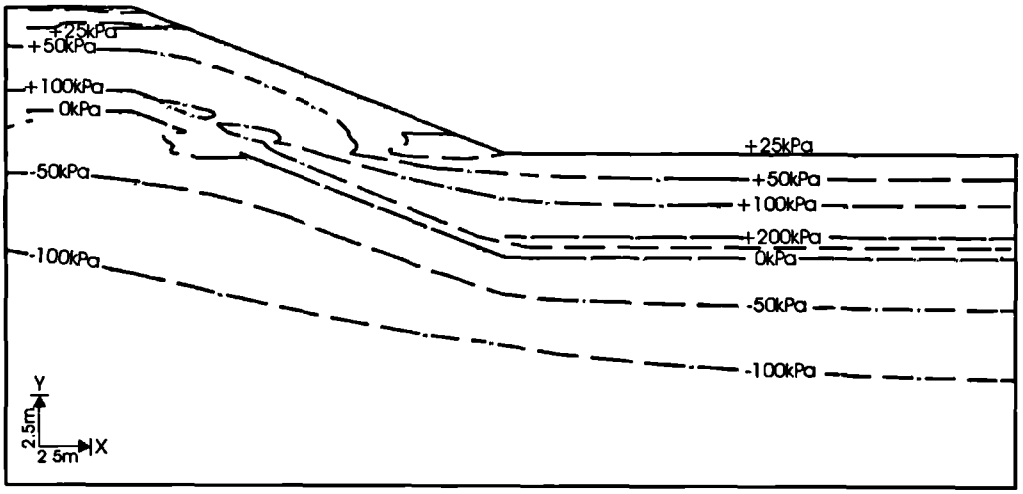

(b) Permeability = $1 \times 10^{-8} m/sec$

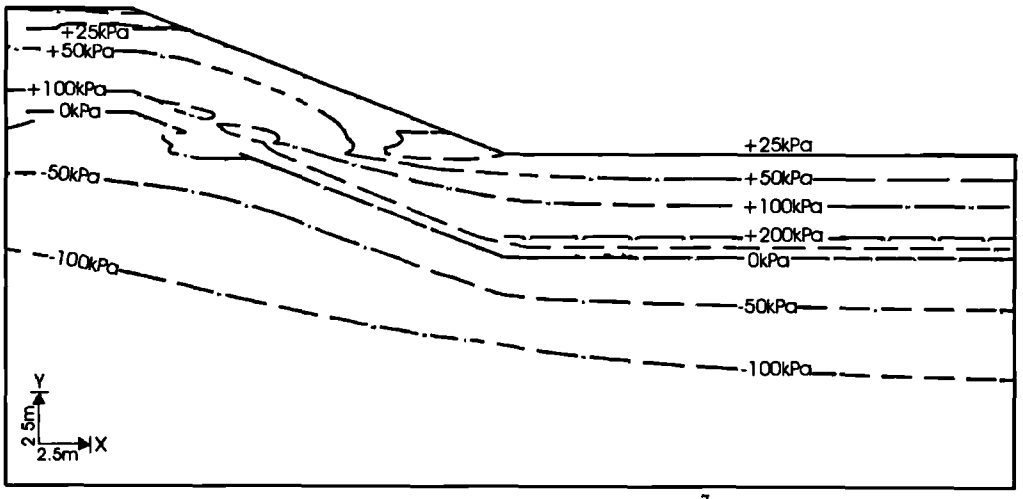

(b) Permeability = $1 \times 10^{-7} m/sec$

Figure 4.14 Contours of accumulated pore water pressures predicted by 3 permeabilities at the end of the first summer.

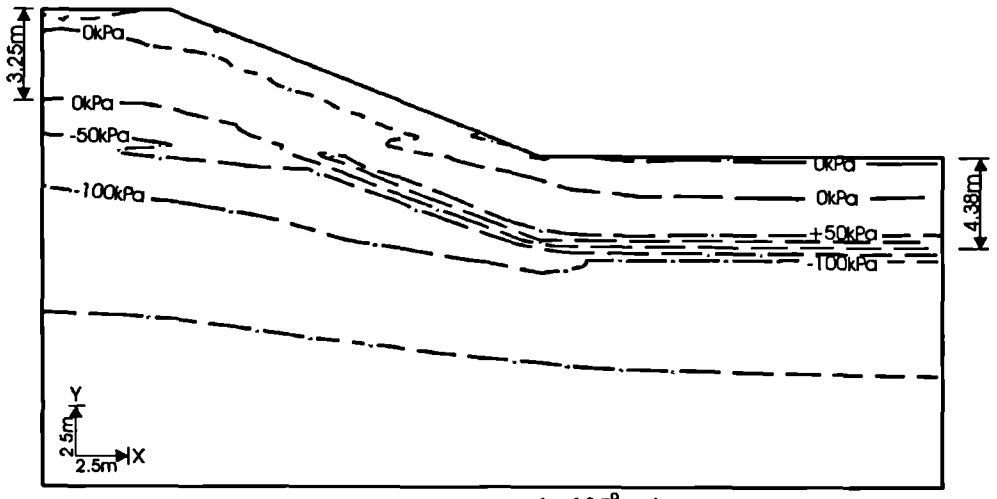

(a) Permeability = $1 \times 10^{-9}\, m/\text{sec}$

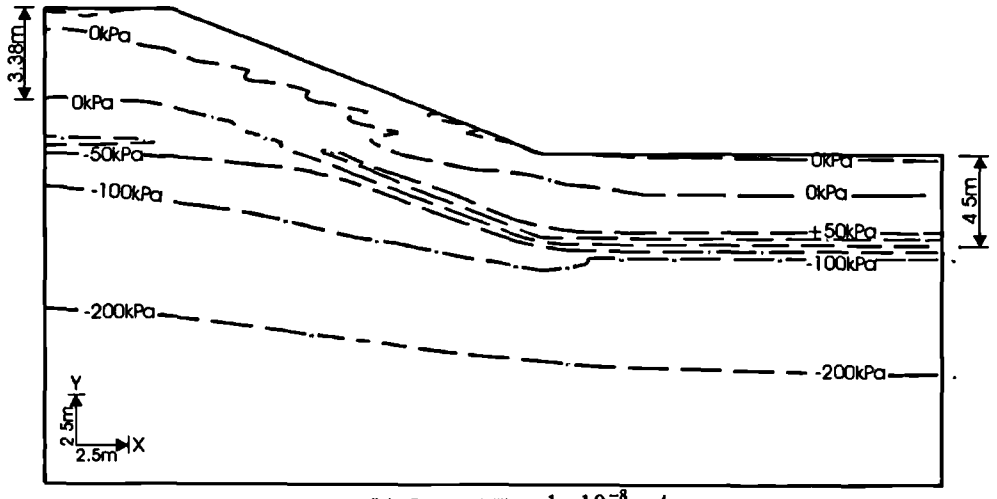

(b) Permeability = $1 \times 10^{-8}\, m/\text{sec}$

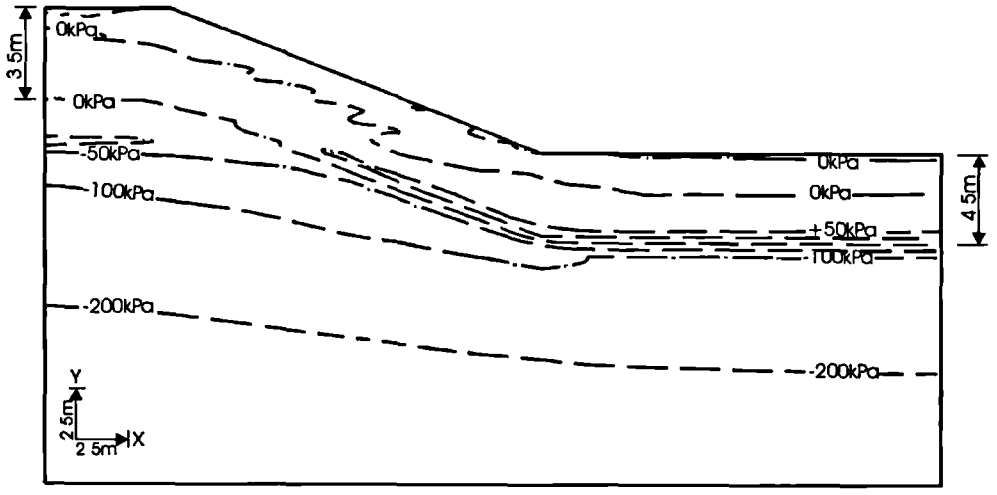

(c) Permeability = $1 \times 10^{-7}\, m/\text{sec}$

Figure 4.15 Contours of accumulated minimum principal total stress (sig3) predicted by 3 permeabilities at the end of the first summer.

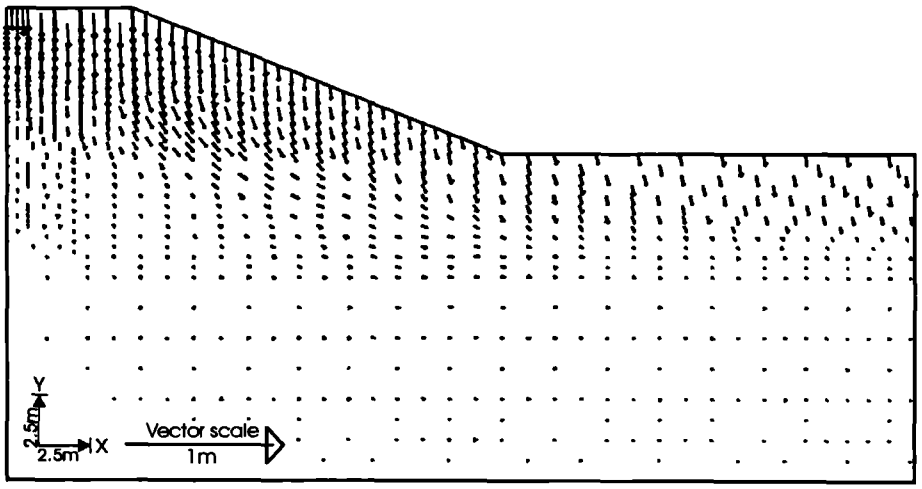

(a) Permeability = 1×10^{-9} *m* / sec

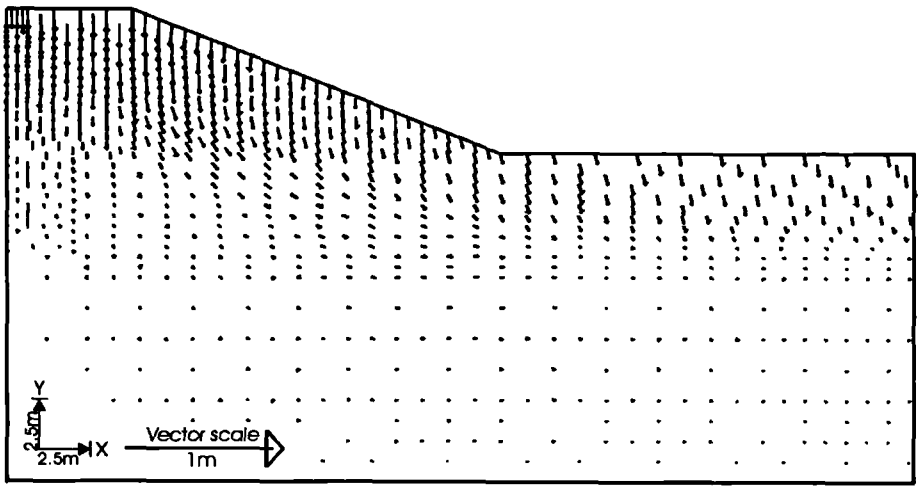

(b) Permeability = 1×10^{-8} *m* / sec

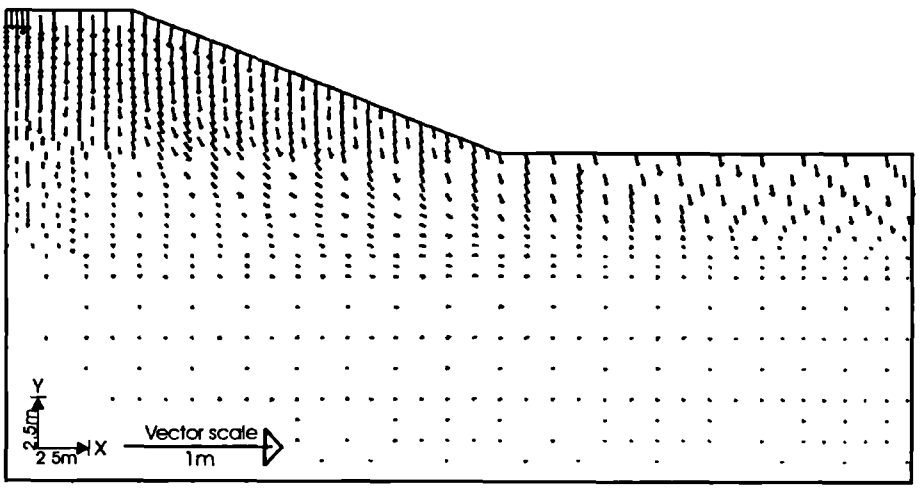

(c) Permeability = 1×10^{-7} *m* / sec

Figure 4.16 Vectors of sub-accumulated movements predicted by 3 permeabilities during summer of cycle 1.

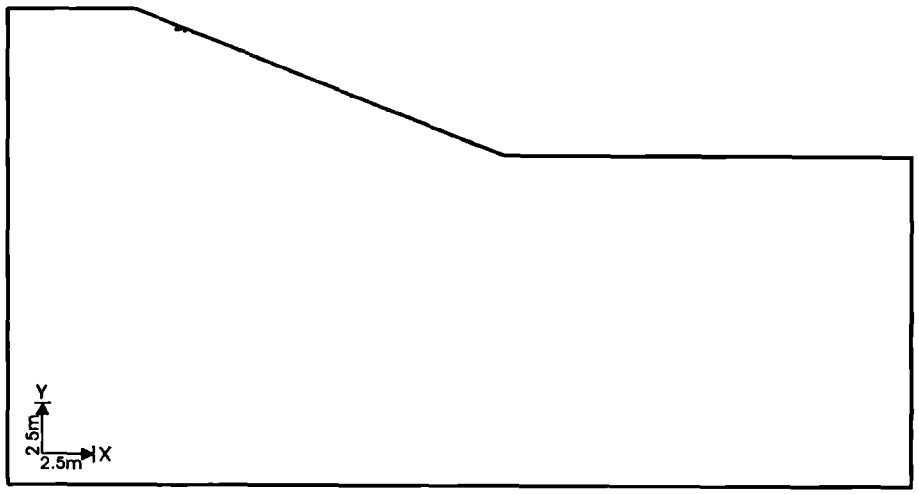

(a) Permeability = $1 \times 10^{-9} m / sec$

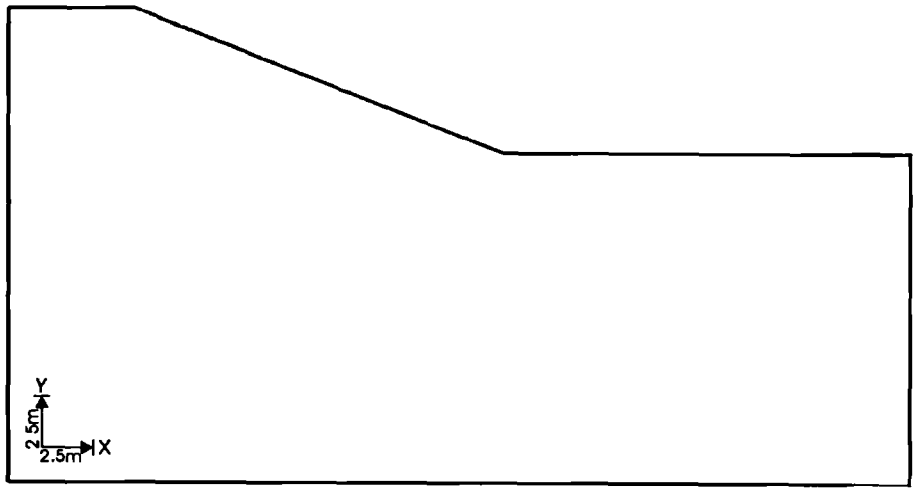

(b) Permeability = $1 \times 10^{-8} m / sec$

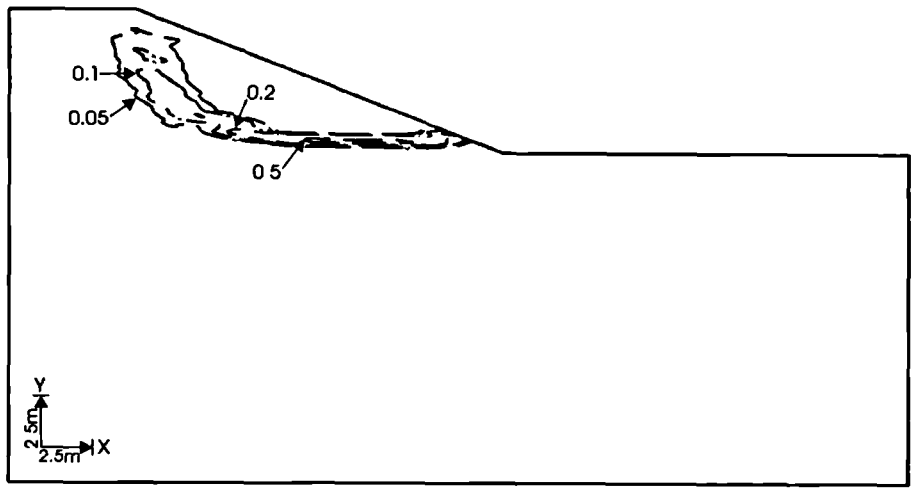

(c) Permeability = $1 \times 10^{-7} m / sec$

Figure 4.17 Contours of sub-accumulated deviatoric plastic strains predicted by 3 permeabilities during cycles 1-13.

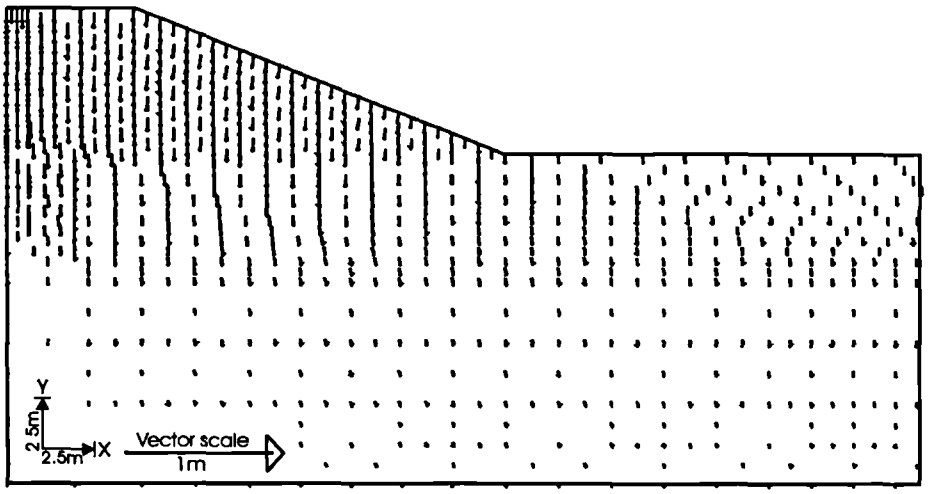

(a) Permeability = $1 \times 10^{-9}\, m / \text{sec}$

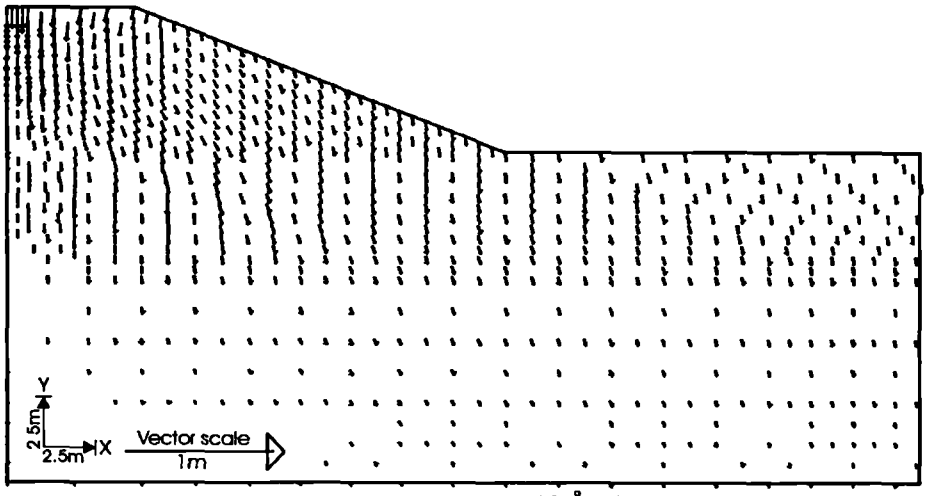

(b) Permeability = $1 \times 10^{-8}\, m / \text{sec}$

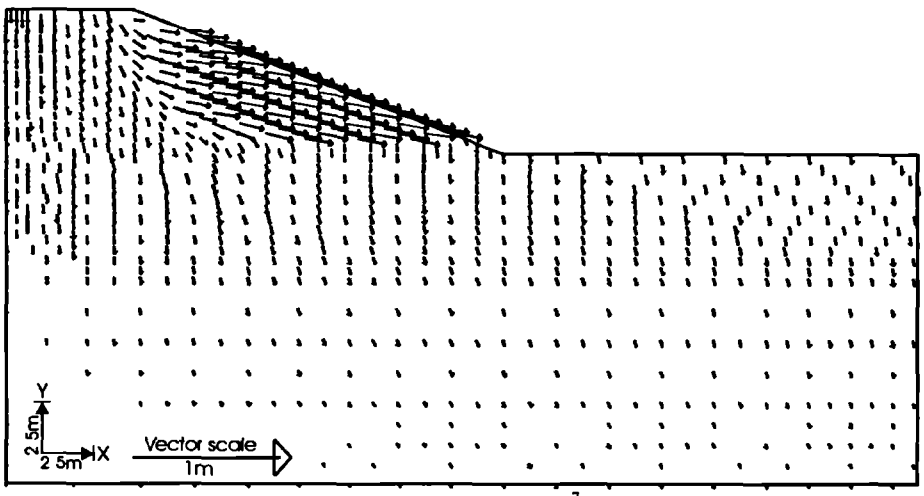

(c) Permeability = $1 \times 10^{-7}\, m / \text{sec}$

Figure 4.18 Vectors of sub-accumulated movements predicted by 3 permeabilities during cycles 1-13.

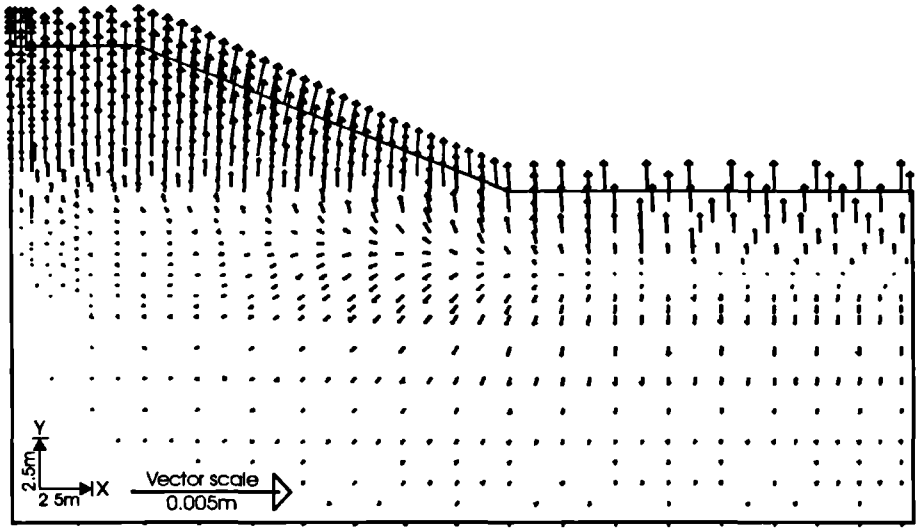

(a) Permeability = $1 \times 10^{-9} m / sec$

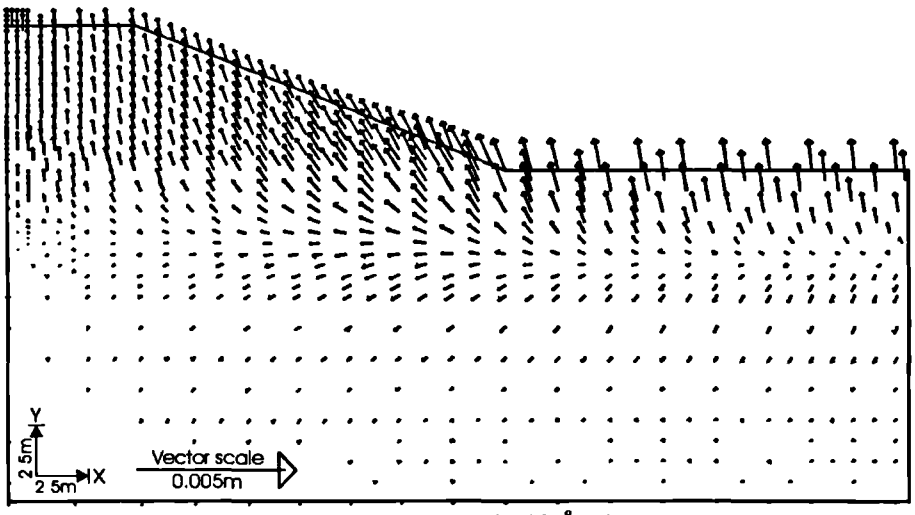

(b) Permeability = $1 \times 10^{-8} m / sec$

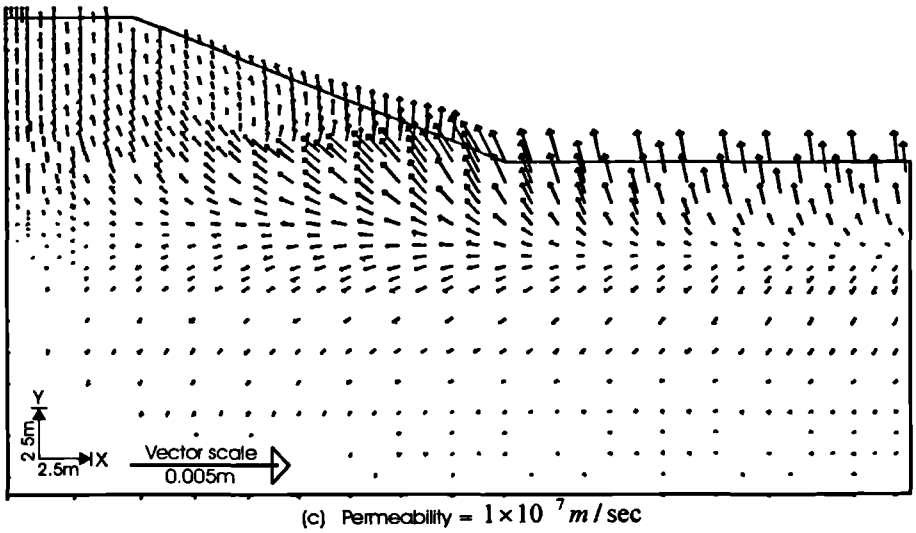

(c) Permeability = $1 \times 10^{-7} m / sec$

Figure 4.19 Vectors of incremental movements predicted by 3 permeabilities after 13 cycles.

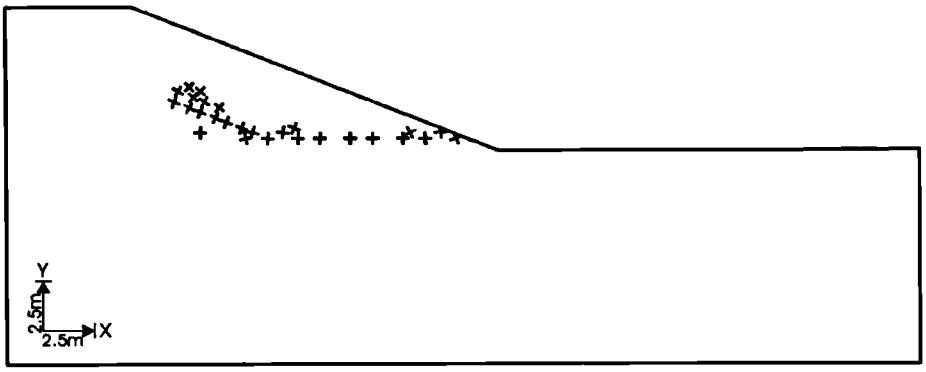

Figure 4.20 Velocity characteristics after 13 cycles.

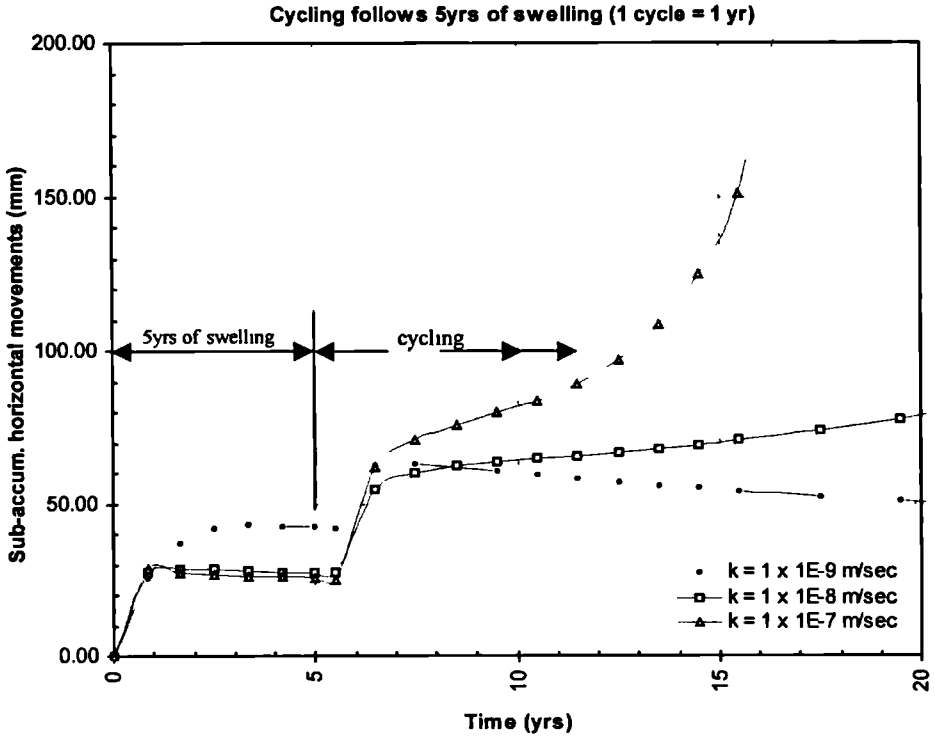

Figure 4.21 Influence of clay fill permeability on post-construction horizontal movements at mid-slope (short to medium term situation).

The amplitude of horizontal movements differs between the three permeabilities eg. after 5 cycles the seasonal amplitude during subsequent cycling (winter-summer) is 12.5mm, 29mm and 31mm for clay fill permeabilities of $1\times10^{-9}\,m/\sec$, $1\times10^{-8}\,m/\sec$ and $1\times10^{-7}\,m/\sec$, respectively. In the LUL embankments, seasonal cyclic movements of up to 50mm have been measured in some of the embankments (McGinnity *et al* 1998). With further cycling, the deviatoric plastic strains increased and the embankment with a permeability of $1\times10^{-7}\,m/\sec$ failed during the 15th year of cycling.

From the foregoing, it can be seen that all things being equal, an embankment which experiences small seasonal pore water pressure changes is likely to stand-up for a longer time before collapsing compared to an embankment that experiences large pore water pressure changes. This was confirmed when further cycling was carried out for another 24 cycles in the embankments with permeabilities of $1\times10^{-8}\,m/\text{sec}$ and $1\times10^{-9}\,m/\text{sec}$.

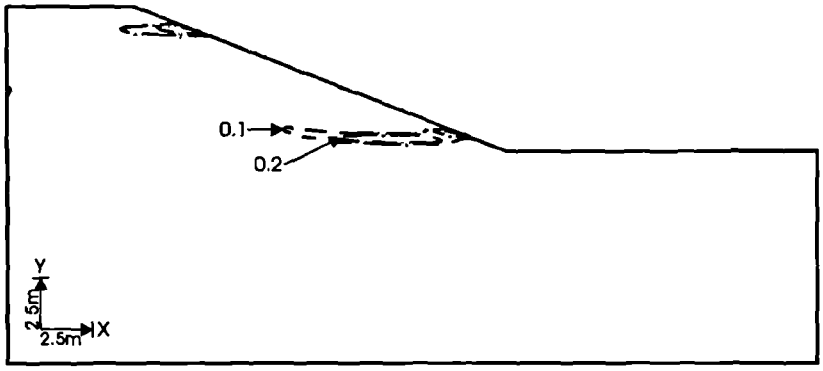

(a) Permeability = $1\times10^{-9}\,m/\text{sec}$

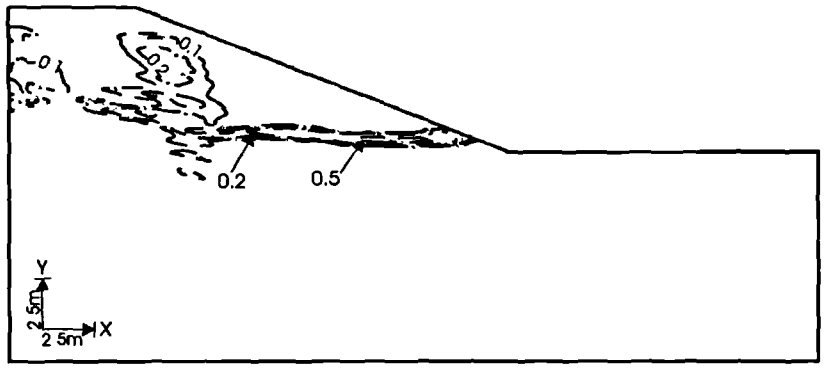

(a) Permeability = $1\times10^{-8}\,m/\text{sec}$

Figure 4.22 Contours of accumulated deviatoric plastic strains predicted after 37 cycles.

Figure 4.22 shows the accumulated plastic deviatoric strains at the end of 37 cycles. There is clearly a marked difference between the two permeabilities, with a potential slip surface defined by the contours in the $1\times10^{-8}\,m/\text{sec}$ permeability material. A significant proportion of the potential slip surface is already at residual strength (0.5 ie. 50% plastic strain contour). In contrast, there is virtually no discernible increase in plasticity between cycles 13 and 37 in the clay fill of low permeability ($1\times10^{-9}\,m/\text{sec}$). The latter is confirmed by the contours of sub-accumulated deviatoric plastic strains shown in Figure 4.23 which shows the results for both permeabilties.

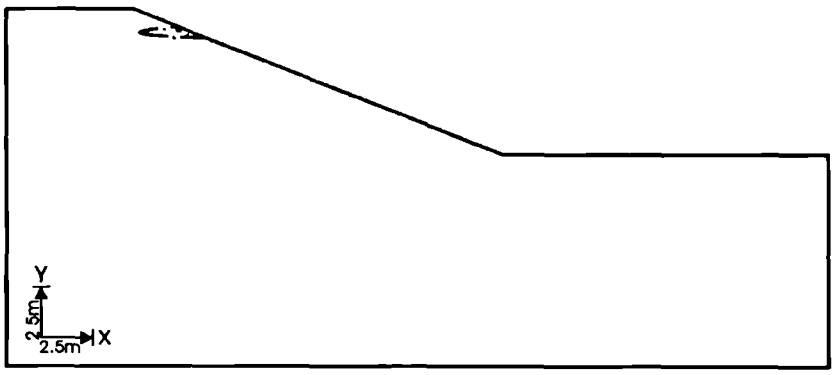

(a) Permeability = $1\times10^{-9}\,m/\sec$

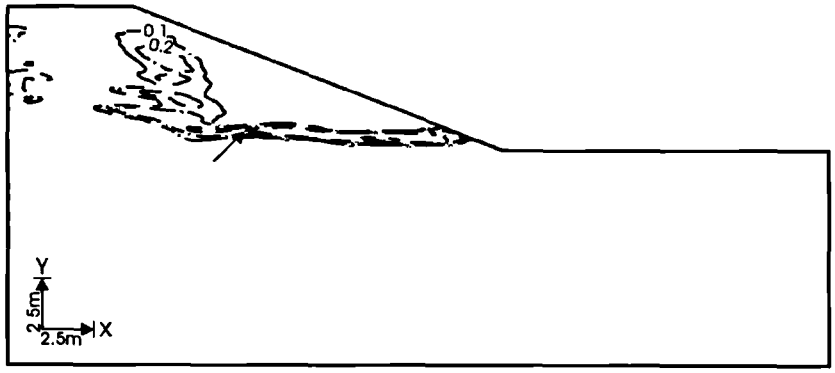

(b) Permeability = $1\times10^{-8}\,m/\sec$

Figure 4.23 Contours of sub-accumulated deviatoric plastic strains predicted between cycles 13 - 37.

The vectors of sub-accumulated movements from cycle 13 to cycle 37 for the two permeabilities are shown in Figure 4.24. They reveal that during this period, overall movement has been predominantly downward in the $1\times10^{-9}\,m/\sec$ permeability clay fill whereas in the $1\times10^{-8}\,m/\sec$ permeability clay fill, large horizontal movements have occurred. The existence of a failure mechanism in the latter embankment is depicted by the direction of incremental vectors in Figure 4.25 and by the velocity characteristics shown in Figure 4.26. This embankment failed after 40 cyles.

Figure 4.27a shows the pore water pressures along a vertical profile at mid-slope after 15, 20 and 40 years of cycling for a permeability of $1\times10^{-9}\,m/\sec$ while the corresponding plot for a permeability of $1\times10^{-8}\,m/\sec$ is shown in Figure 4.27b. Both figures indicate that as cycling continues, the winter pore water pressures in the clay fill and upper horizons of the foundation material do not change.

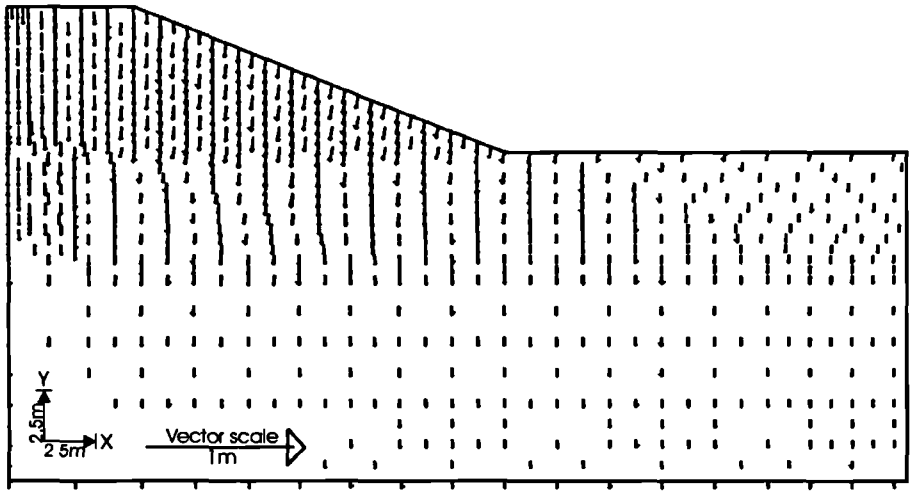

(a) Permeability = $1 \times 10^{-9} m / sec$

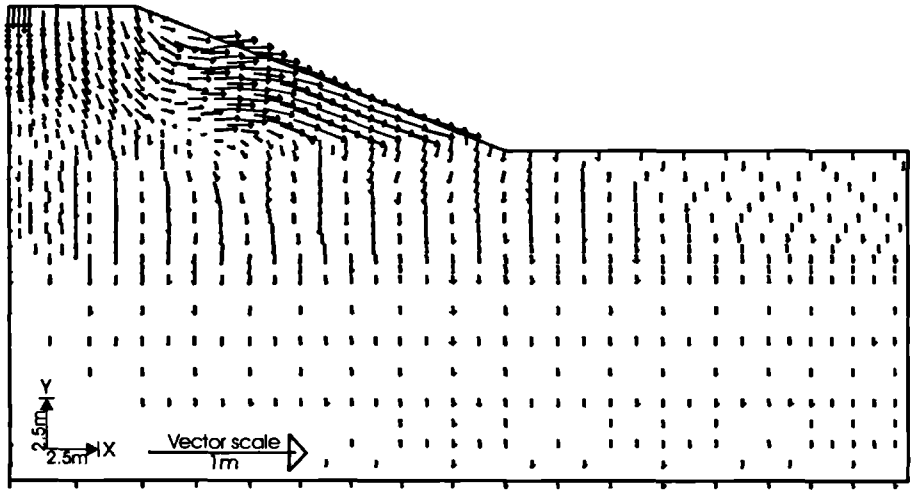

(b) Permeability = $1 \times 10^{-8} m / sec$

Figure 4.24 Vectors of sub-accumulated movements predicted between cycles 13-37.

The embankment with a clay fill permeability of $1 \times 10^{-9} m / sec$ was cycled for a total of 180 years but did not fail (although progressive movements were occurring); suggesting that if cycling had continued, the embankment would ultimately fail. Figure 4.28a shows the contours of sub-accumulated deviatoric plastic strains from cycles 37 and 180. There is some evidence of development of a potential slip surface which is likely to daylight at the mid-slope location. At the end of 180 cycles, the contours indicate maximum sub-accumulated deviatoric plastic strains of 10%, which indicates post-peak conditions (peak = 5%). The potential of a rupture daylighting at mid-slope is further highlighted by the pattern of vectors of sub-accumulated movements (Figure 4.29a).

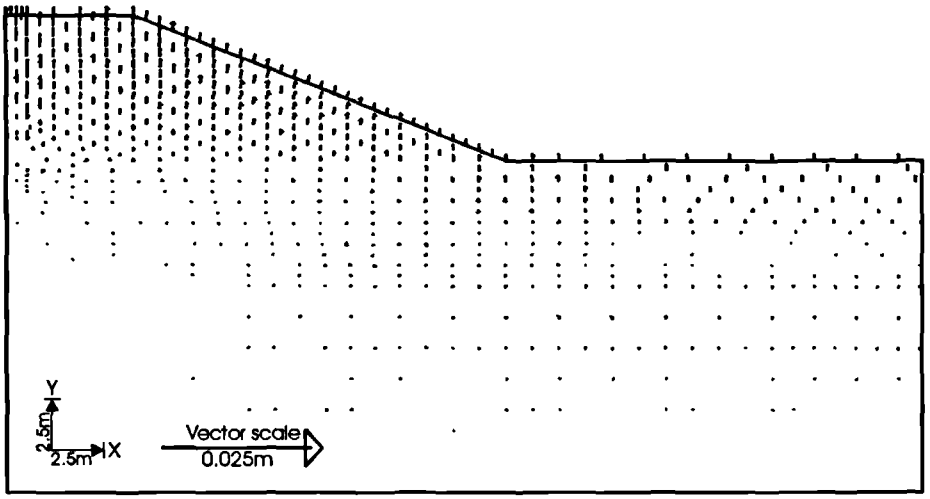

(a) Permeability = $1 \times 10^{-9} m / sec$

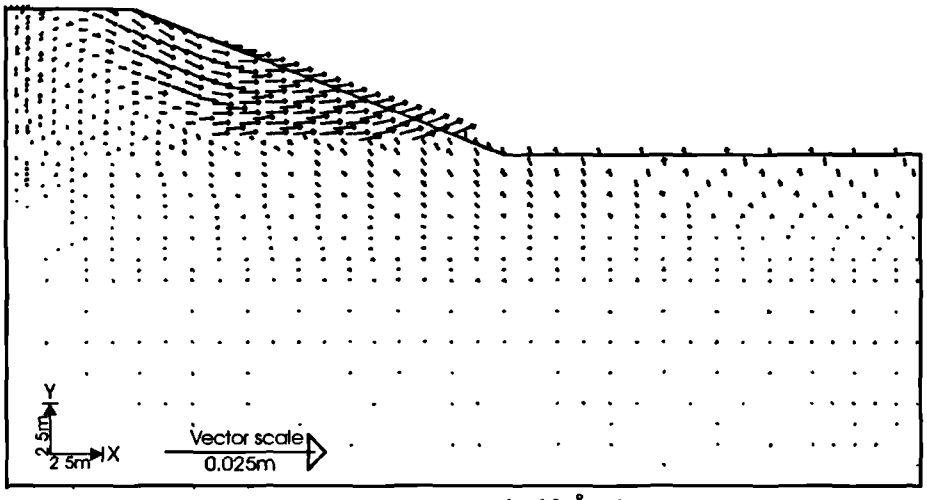

(b) Permeability = $1 \times 10^{-8} m / sec$

Figure 4.25 Vectors of incremental movements at the end of 37 cycles

The accumulated horizontal movements at ground level (mid-slope) from construction until failure had occurred are shown in Figure 4.30 for the three permeabilities. In the figure, values relating to the end of summer have been omitted for clarity. From the figure, it can be seen that the clay fill of low permeability ($1 \times 10^{9} m / sec$) initially consolidates and does not experience significant horizontal slope movements indicative of instability (horizontal outward movements) for approximately 70 cycles (75 years after construction). After this period, lateral slope movements suggestive of instability begin to show, albeit of a much reduced rate compared to permeabilities of $1 \times 10^{-8} m / sec$ and $1 \times 10^{-7} m / sec$. An analysis based on the

ICON pore water pressure profiles as used here and terminated prior to 70 years would classify the embankment to be stable - which is invalid when the post-70 cycles behaviour is put into consideration.

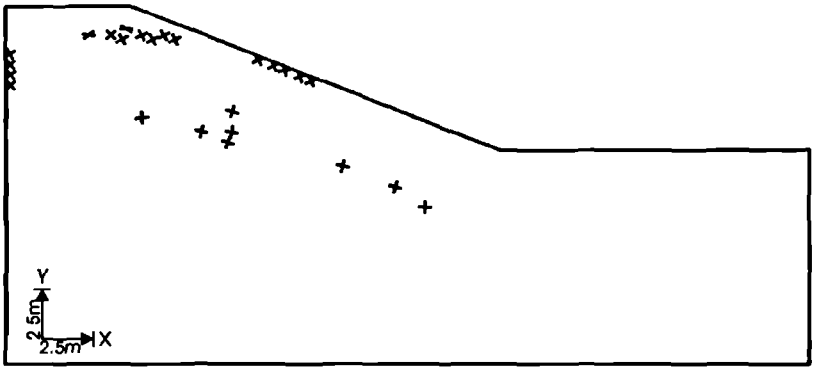

(a) Permeability = $1\times10^{-9}\,m/\sec$

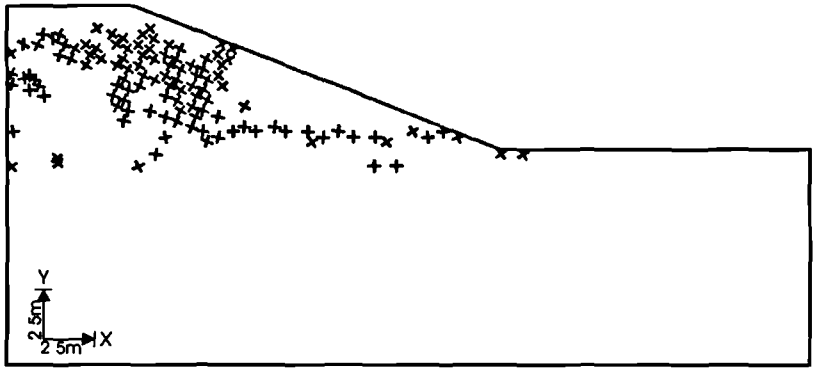

(b) Permeability = $1\times10^{-8}\,m/\sec$

Figure 4.26 Velocity characteristics at the end of the 37th cycle.

4.5.4 Stress paths

Figure 4.31 shows the stress path in $t'-s'$ space for a location in the zone of a potential slip surface beneath the mid-slope of the embankment. The stress paths show the period from end of construction until failure (**NB**. *In the figures, values corresponding to the desiccation (summer) part of the cycle have been omitted for clarity*).

From Figure 4.31 it can be seen that at the end of construction (point 1) the shear stress, t' is higher but average stress, s', is lower in the clay fill of highest pemeability ($1\times10^{-7}\,m/\sec$) compared to clay fills with permeabilities of $1\times10^{-8}\,m/\sec$ and $1\times10^{-9}\,m/\sec$. This is a

result of the relatively larger pore water pressure dissipation that occurs during construction in the clay fill with a permeability of $1 \times 10^{-7} m/\sec$, as earlier depicted in Figures 4.3 and 4.4.

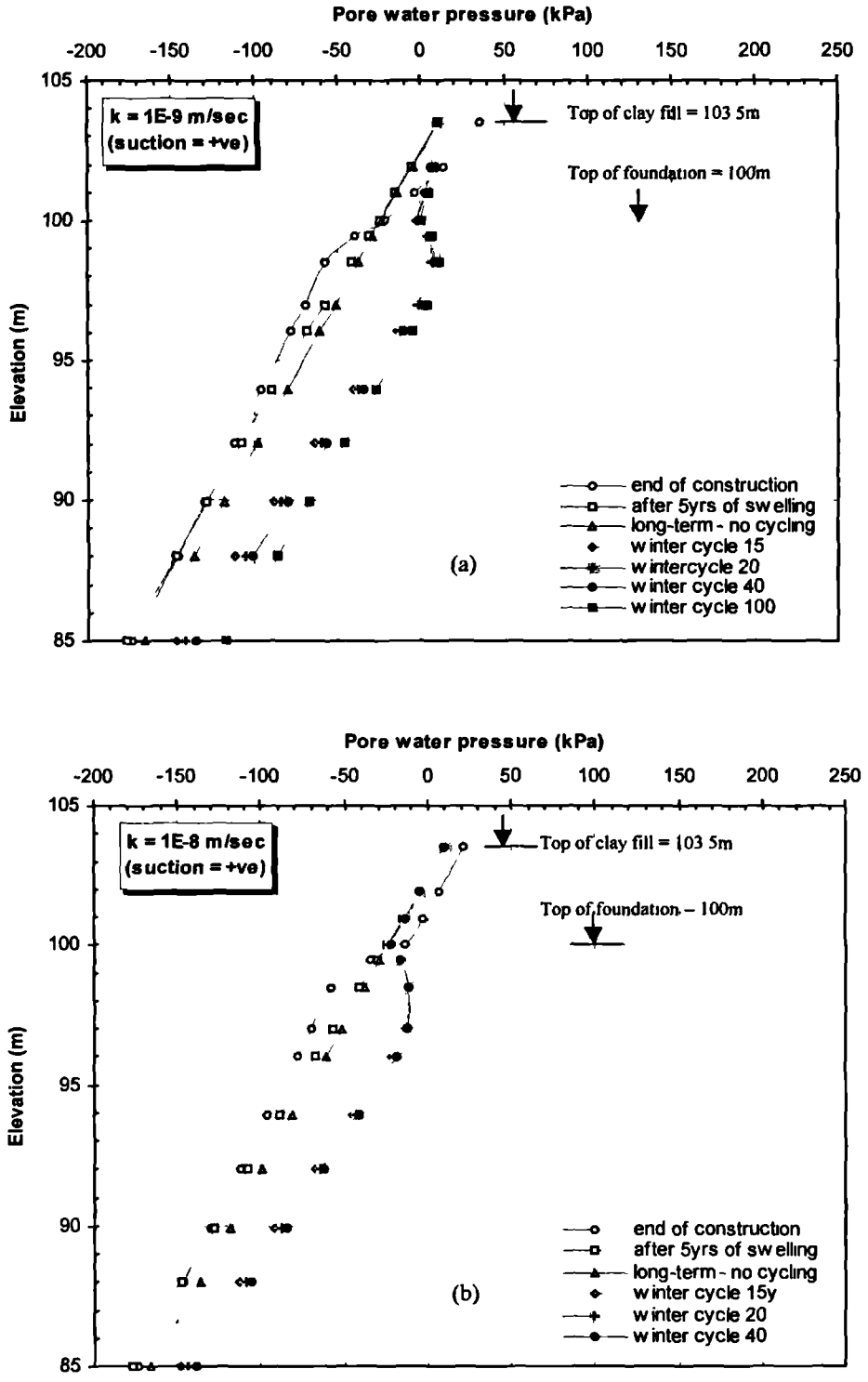

Figure 4.27 Influence of permeability on pore water pressure at mid-slope after 15, 20, 40 and 100 cycles.

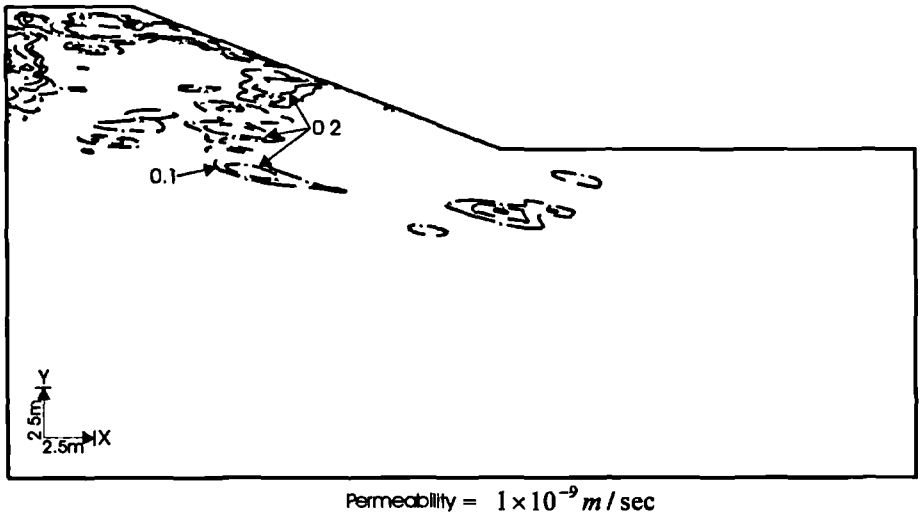

Figure 4.28 Contours of sub-accumulated deviatoric plastic strain between cycles 37-180.

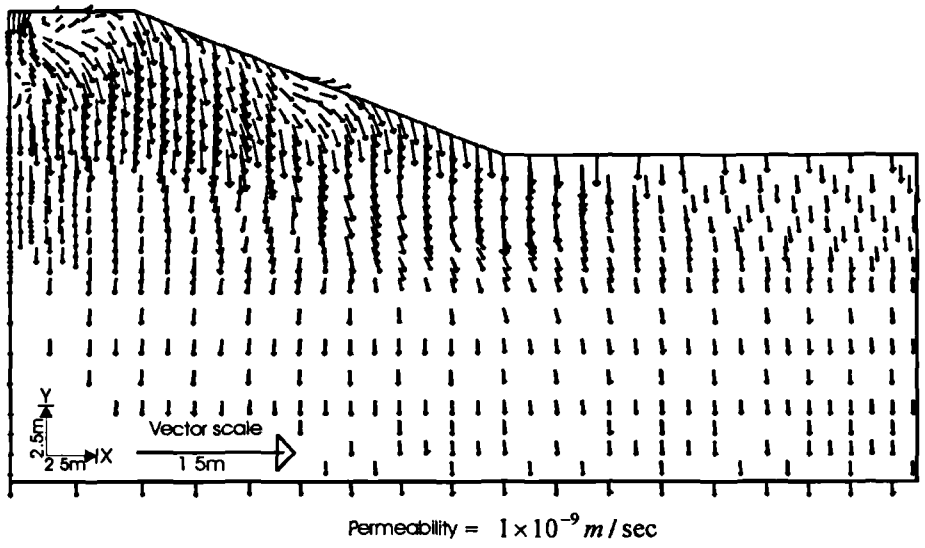

Figure 4.29 Vectors of sub-accumulated movements between cycles 37-180.

In the analyses, the end of construction was immediately followed by a 5 year period of swelling (path 1-2). The stress paths for the 3 permeabilities indicate a general increase in shear stress, t', coupled with a reduction in average stress, s'. At this location, peak shear stress is attained during swelling for all the 3 permeabilities. At the end of the 5 yr swelling period, the stress path is still at peak strength in the most permeable clay fill ($1\times10^{-7}m/sec$) whereas in the less permeable clay fills, it increases and is already at post-peak stage in the least permeable clay fill ($1\times10^{-9}m/sec$). The accumulated deviatoric plastic strains at this stage are 1.3%, 3.8% and 10.4% in the clay fill with permeabilities of $1\times10^{-7}m/sec$, $1\times10^{-8}m/sec$ and $1\times10^{-9}m/sec$, respectively.

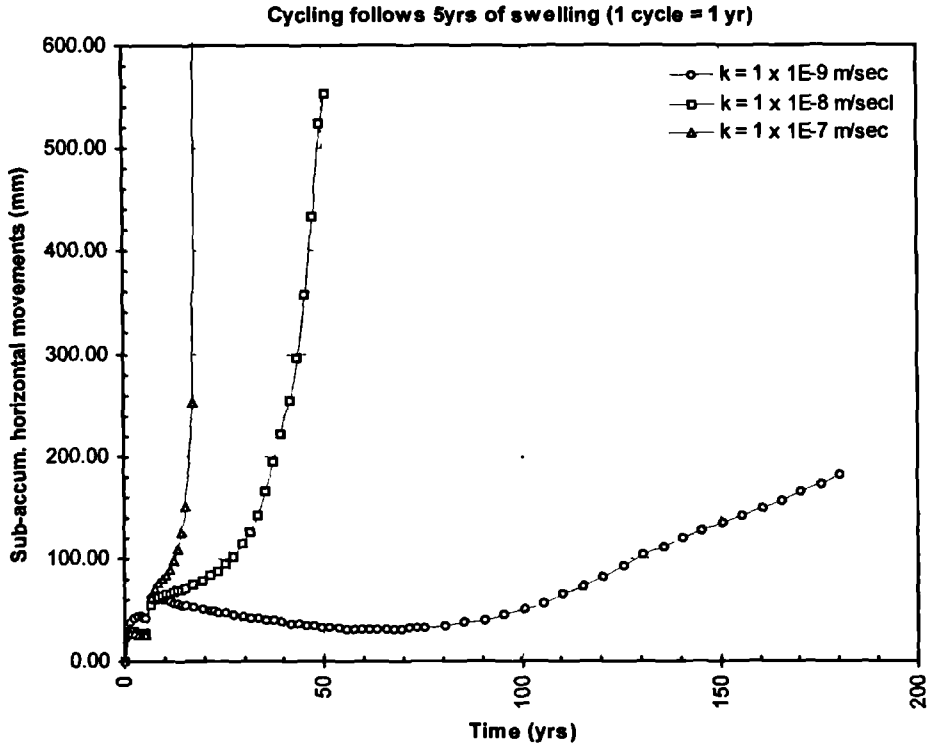

Figure 4.30 Influence of clay fill permeability on post-construction horizontal movements at mid-slope (medium to long term situation).

Upon invokation of the first few swelling-desiccation cycles (path 2-3), the stress paths indicate a reduction in shear stress, t' and an increase in average stress. This has a stabilising effect on the embankment as epitomised by a shift in the stress paths away from the failure line. The largest reduction occurs in the least permeable clay fill. This fact is confirmed by Figure 4.32 where the stress paths for the first two cycles only (winter1-summer1-winter2-summer2) have been plotted. The large shift from the failure line in the lowest permeable clay is clearly evident when the relative positions of W1 and W2 are considered in the stress path W1-S1-W2. The accumulated deviatoric plastic strains at this stage are still very similar to the end of stage 2 eg. after 3 cycles of swelling-desiccation the accumulated deviatoric plastic strains are 1.6%, 3.9% and 10.4% in the clay fill with permeabilities of $1\times10^{-7} m/\text{sec}$, $1\times10^{-8} m/\text{sec}$ and $1\times10^{-9} m/\text{sec}$, respectively.

The stabilising effects of desiccation following the first cycle gradually disappear and the overall behaviour begins to be dominated by an increase in deviatoric plastic strains, which ultimately leads to progressive failure. This is depicted by an initial increase in shear stress with cycling (path 3-4) tending towards the failure envelope but because the material is brittle, the stress path attains a second maximum and fails without reaching the failure envelope (path 4-5).

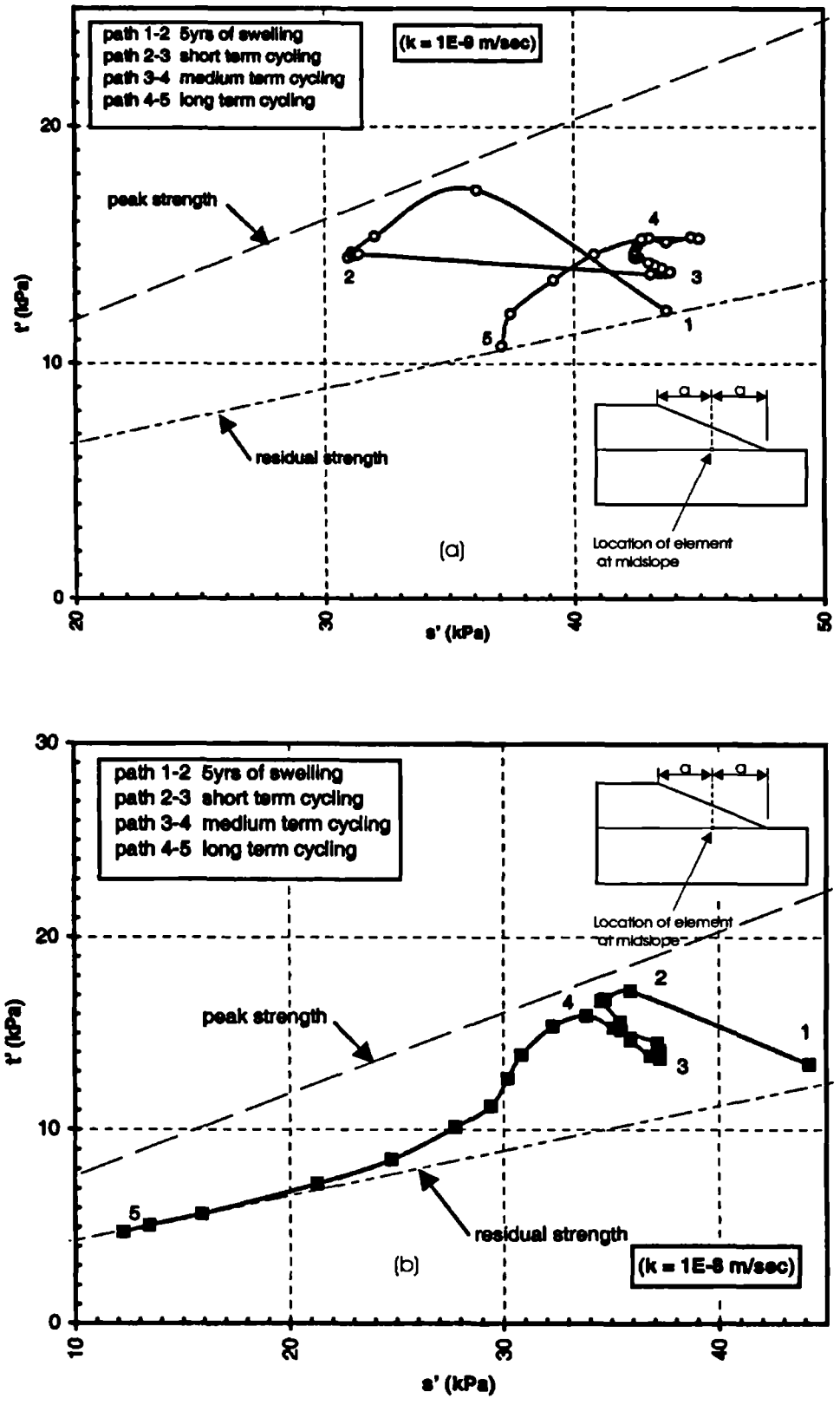

Figure 4.31 Stress path for an element at midslope along a potential slip surface.

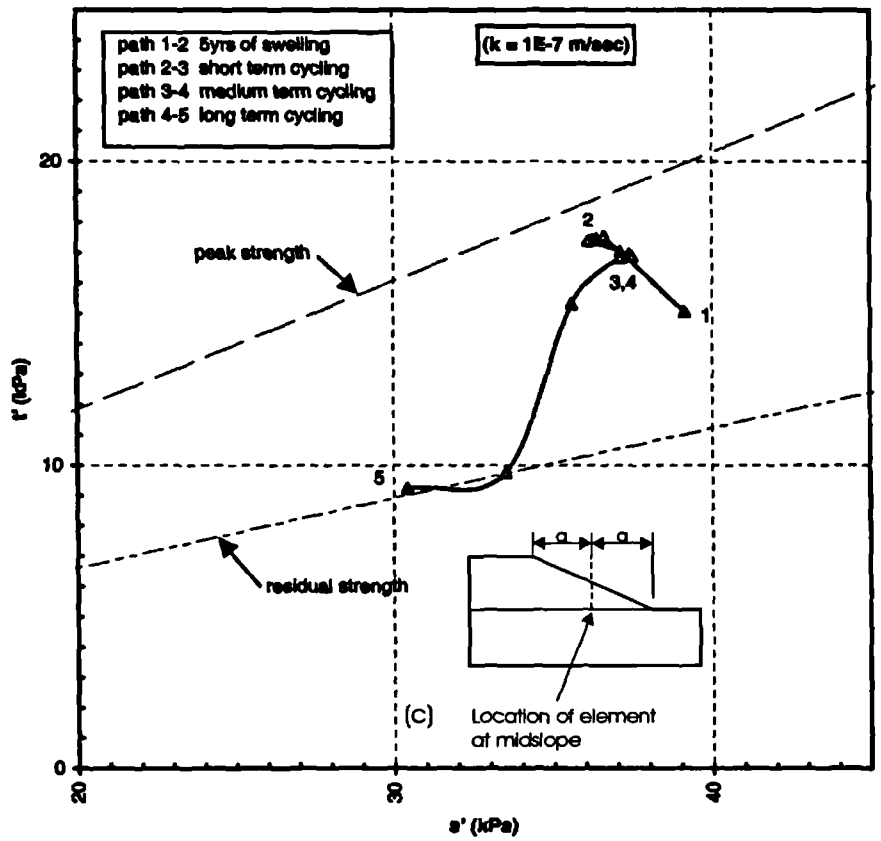

Figure 4.31 Stress path for an element at midslope along a potential slip surface.

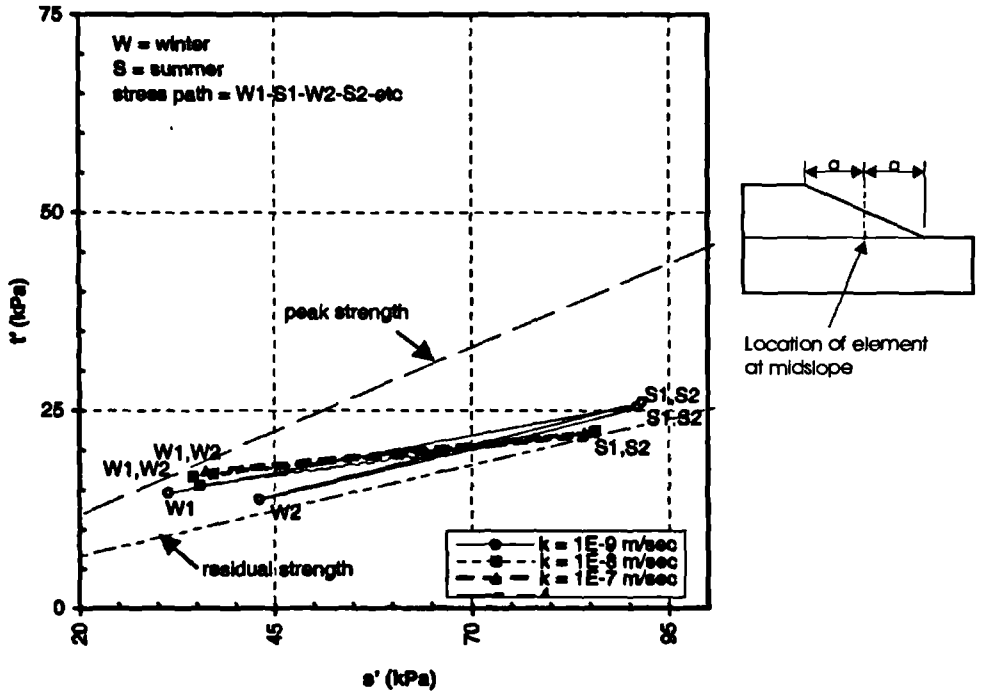

Figure 4.32 The influence of clay fill permeability on the stress path of an element along a potential slip surface at mid-slope during the first few cycles.

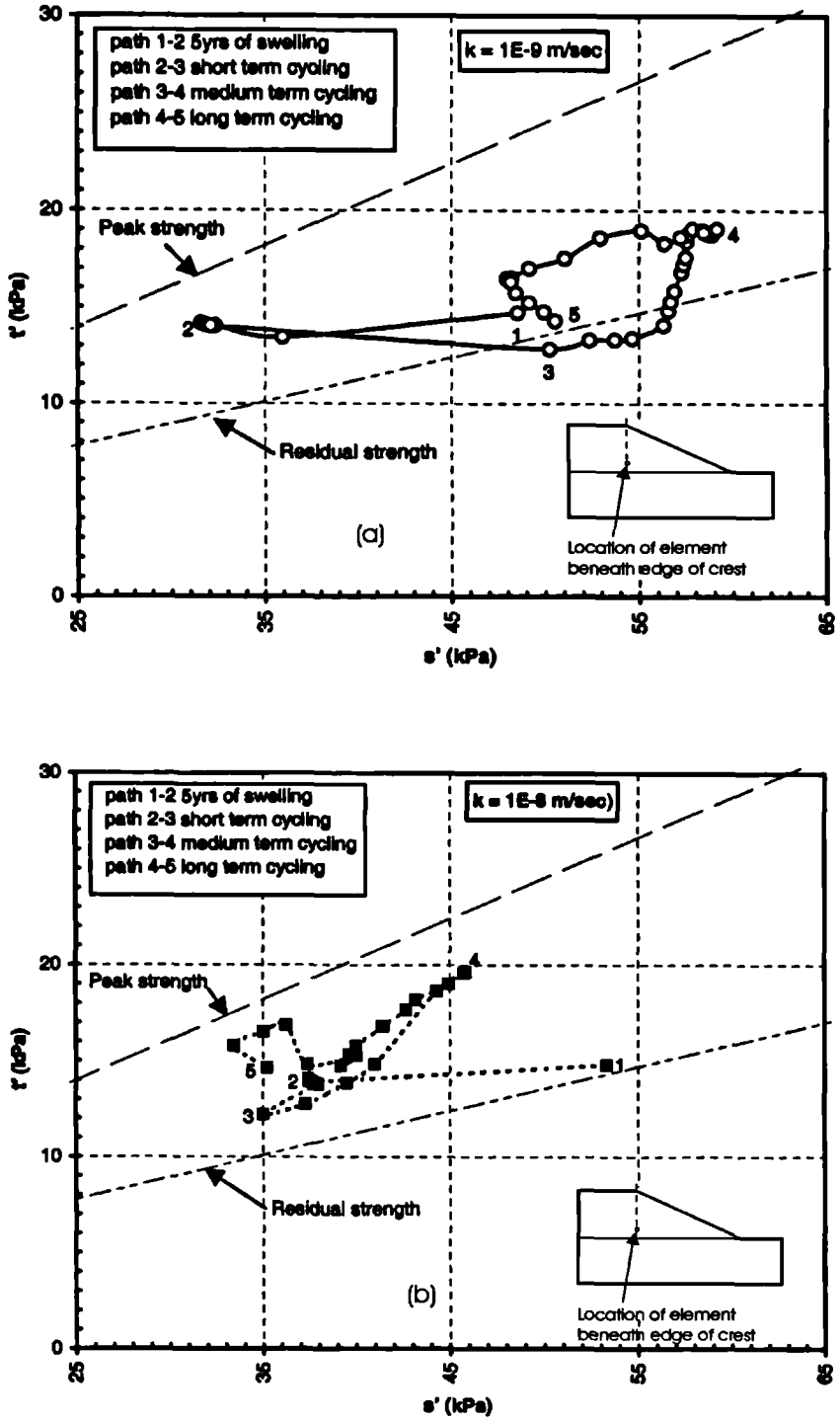

Figure 4.33 Stress path for an element located beneath the edge of the crest along a potential slip surface.

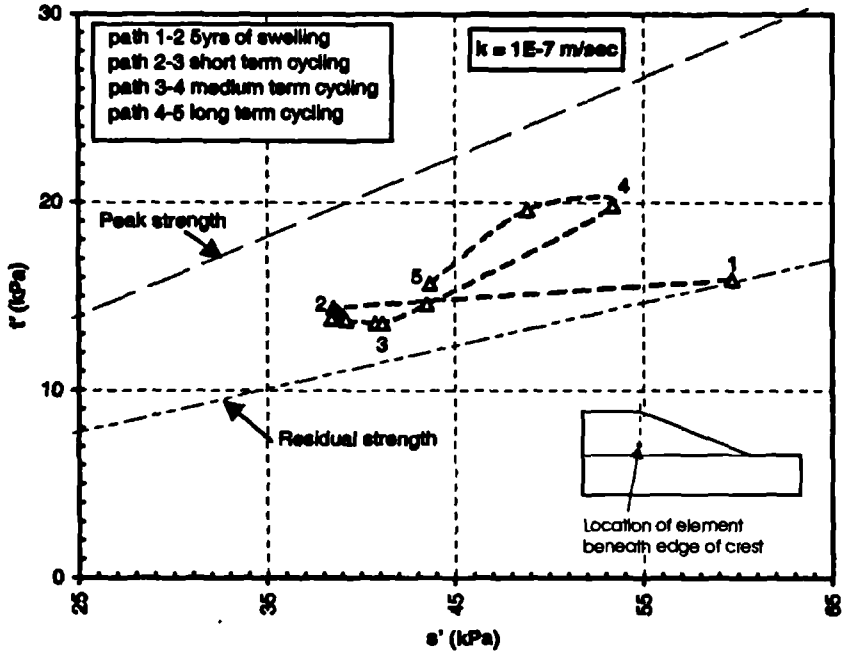

Figure 4.33c Stress path for an element located beneath the edge of the crest

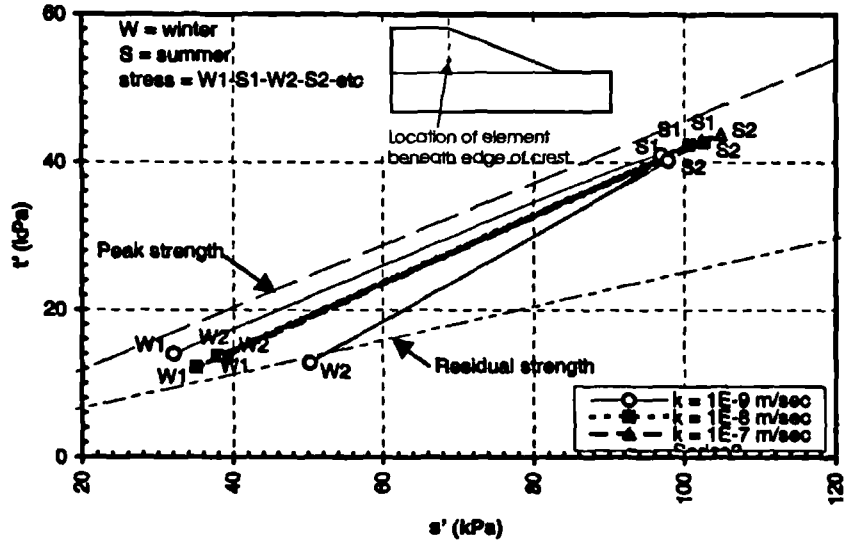

Figure 4.34 The influence of clay fill permeability on the stress path of an element beneath the edge of the crest, located on a potential slip surface.

The accumulated deviatoric plastic strains after 10 swelling-desiccation cyles are 7.4%, 3.9% and 10.4% in the clay fill with permeabilities of $1\times10^{-7}m/\sec$, $1\times10^{-8}m/\sec$ and $1\times10^{-9}m/\sec$, respectively.

A similar pattern in behaviour occurs further inside the embankment at a location beneath the edge of the crest, within a potential rupture surface (Figures 4.33 and 4.34). There is a delay in the time at which maximum shear stress is attained at this location. As expected, based on the discussion in Section 4.3.3, the largest swelling occurs in the clay fill of highest permeability, however peak strength is not reached during the 5 yr swelling period (path 1-2). In fact, the accumulated deviatoric strains after the swelling period are 0% for all the three permeabilities. Nevertheless, significant stress (and strain) reversal occurs during the first few desiccation cycles, which leads to the stress path moving away from the failure envelope (path 2-3) as previously observed for the previous element at mid-slope. The accumulated deviatoric plastic strains after 3 swelling-desiccation cycles are 1.6%, 1.5% and 1.6% in the clay fill with permeabilities of $1\times10^{-7}m/\sec$, $1\text{x}10^{-8}$m/sec and $1\times10^{-9}m/\sec$, respectively.

With continued cycling, the stress path moves towards the failure envelope (path 3-4). Eg. after 10 swelling-desiccation cycles, the accumulated deviatoric plastic strains are 2.7%, 1.6% and 1.6% in the clay fill with permeabilities of $1\times10^{-7}m/\sec$, $1\times10^{-8}m/\sec$ and $1\times10^{-9}m/\sec$, respectively. It is quite clear that at this location, collapse of the embankment occurs before peak strength is fully mobilised. This is consistent with a progressive failure mechanism where failure occurs when the average operational strength exceeds the shear strength along the rupture surface ie. the existence of non-uniform stresses along the rupture surface involves certain sections being at residual strength, some at peak strength and the remainder at pre-peak strength.

The pattern of stress paths indicates although desiccation enhances stability of the embankments in the initial stages of the desiccation-swelling cycles, the repetitive cycling ultimately results in progressive failure. The rate at which the progressive failure mechanism propagates is governed by the mass permeability of the clay fill.

4.6 Summary

The pattern of movement for the embankments with the relatively higher permeabilities of $1\times10^{-7}m/\sec$ and $1\times10^{-8}m/\sec$ in the long term is quite different to that with a permeability

of $1\times10^{-9}\,m/\sec$. There is no indication of instability during the initial stages of cycling in the latter clay embankment but instead, continual slope movements occur once cycling commences until progressive failure occurs.

Therefore in order to accurately model the behaviour of such types of embankment, it is necessary that the cycling history be correctly evaluated as this determines the magnitude of current plasticity within the embankment. Correct determination of current plasticity in turn leads to correct predictions of the medium and long term behaviour, otherwise there is a risk that an embankment is prematurely classified as stable, over the design period.

It is noteworthy that the majority of UK's railway embankments are approximately 100 years ie. they have stood up for nearly a century without collapsing. On the LUL network, most of the instability problems are associated with the post 1960s period when control of vegetation was suspended. This would have accentuated the seasonal cyclic movements, hence accelerating progressive slope movements. Another implication pertaining to old UK railway embankments is the fact that their current age (approx. 100 years) may now be approaching the post-quasi-stable phase, in which case instability problems are likely to get worse.

It is more likely that for old UK railway embankments, the mass permeability of the clay fill was initially high as a result of the voided nature of the clay clods during construction and the existence of granular inclusions. Of the embankments that stood up at the end of construction, behaviour during seasonal swelling and shrinkage cycles would have been strongly influenced by permeability. Embankments with high permeability are likely to have failed in the short to medium term (less than 20yrs) in response to cycling.

With time, the matrix of the clay fill would have collapsed and, coupled with the alternate shrinkage and swelling cycles, the mass permeability would have reduced. The true behaviour during the early history of these embankments is therefore more likely to have been characterised by initially larger progressive movements associated with a relatively higher permeability, followed by a reduction in the cyclic movement as overall permeability was altered to a lesser value. This aspect of permeability presents a major challenge when assessing the long-term stability of existing old railway embankments.

Nevertheless, it is necessary to reiterate that the ICON pore water pressure profile used here was contrived to model a desiccated profile in SE England (UK). There are significant limitations associated with this approach, as shall be discussed in Section 5 1 of Chapter 5.

Moreover the pore water pressure response in rooted soils of different permeabilities is not uniform as modelled using the ICON profiles. Therefore it is theoretically possible that the response of embankments whose permeabilities differ by various orders of magnitude could be different to the results of this sensitivity study if root water uptake is more accurately modelled. The application of a root water uptake model to embankment analysis is presented in Chapter 7.

Chapter 5

DEVELOPMENT OF A ROOT WATER UPTAKE MODEL

5.1 Introduction

The influence of vegetation on volume change in clayey soils involves the interfacing of dynamic factors of the atmosphere, vegetation and soil as discussed in greater detail in Chapter 2. Vegetation affects volume changes in soil primarily as a result of moisture reduction through the process of transpiration. In order to predict the water loss due to transpiration and hence accurately predict its impact on volume changes requires the development of models that are able to mimic root water uptake.

The state-of-the-art approach in UK civil engineering to model changes by vegetation was described in Chapter 4. It was noted that modelling the pore water pressure regime into two seasons (ie. summer and winter in Figure 4.1) as is current practice, is an oversimplification of the real situation because the pore water pressure regime is transient and continuously changes throughout the year. Another major drawback is the fact that by prescribing the governing summer and winter pore water pressure profiles contrived to match field observations, the numerical program must generate water flow to achieve the prescribed pore water pressures. These flows may be of a magnitude not achievable by vegetation during transpiration.

Moreover, the values of pore water pressures assumed are derived from engineering judgement, based on field and laboratory tests. The commonest field monitoring devices for measuring suction (suctions) used in Civil Engineering are tensiometers, (Ridley and Burland, 1995 and ICON, 2001). These devices are in general only reliable in measuring suctions whose magnitude is less than atmospheric pressure. For suctions greater than atmospheric pressure, the onset of cavitation and air entry reduces their accuracy. Laboratory suction tests such as the filter paper test (Chandler *et al*, 1992) are also prone to errors during interpretation because of the sensitive nature of the exponential relationship between suction and in situ moisture content at high magnitudes of suctions.

The author believes that an ideal way forward in geotechnical engineering would be to model the soil-plant-atmosphere continuum using rainfall and evapotranspiration values as input data in coupled analyses through the use of root water uptake models (RWUMs). Such an approach allows the pore water pressure profile to be predicted, rather than prescribed. As already discussed in Chapter 2, root water uptake models are used in other branches such as Agronomy, Soil Science and other Agro-forestry sciences eg. Nour el Din *et al* (1987), McCarthy *et al* (1992) and Karajeh & Tanji (1994).

To date, very little research has been carried out in geotechnical engineering regarding application of root water uptake models eg. Tratch *et al* (1995) described a one dimensional, transient, heat and mass transfer finite element model capable of evaluating evapotranspiration from unsaturated soil surfaces based after Prasad (1988). They also presented results of simulations of evapotranspiration in a soil column under laboratory conditions. Mathur (1999) presented results of settlement predictions on a 1.2m deep soil column induced by evapotranspiration. The soil was assumed to be homogeneous, isotropic and elastic. As yet, none of the published research and application pertains to real-time geotechnical boundary value problems incorporating non-linearity.

The various types of RWUMs were described in Section 2.5.5 (Chapter 2) from which it was noted that the more versatile RWUMs are those which do not involve plant-specific parameters in their algorithms as these can be applied to a wide variety of vegetation types. Such RWUMs define the plant water uptake (transpiration) to be dependent on the soil pore water pressure eg. Feddes *et al* (1978).

This chapter describes a nonlinear RWUM that has been coded into ICFEP. The RWUM has been applied to predict ground movements at a Building Research Establishment test bed site at Chattenden (Chapter 6) and to study the stability of a typical UK old railway embankment involving progressive failure (Chapters 7). The RWUM is based on Feddes *et al* (1978) and Prasad (1988).

The RWUM models a non-linear variation of water extraction rate decreasing with depth. The background and mathematical derivation of the function are described first. This is followed by a description of the UK meteorological system of calculation of evapotranspiration; which is used as input data into the coded function. The data input, numerical computations and output of the RWUM within ICFEP are then described. The chapter ends with a presentation of parametric studies carried out to investigate the performance of the RWUM.

5.2 Mathematical algorithm

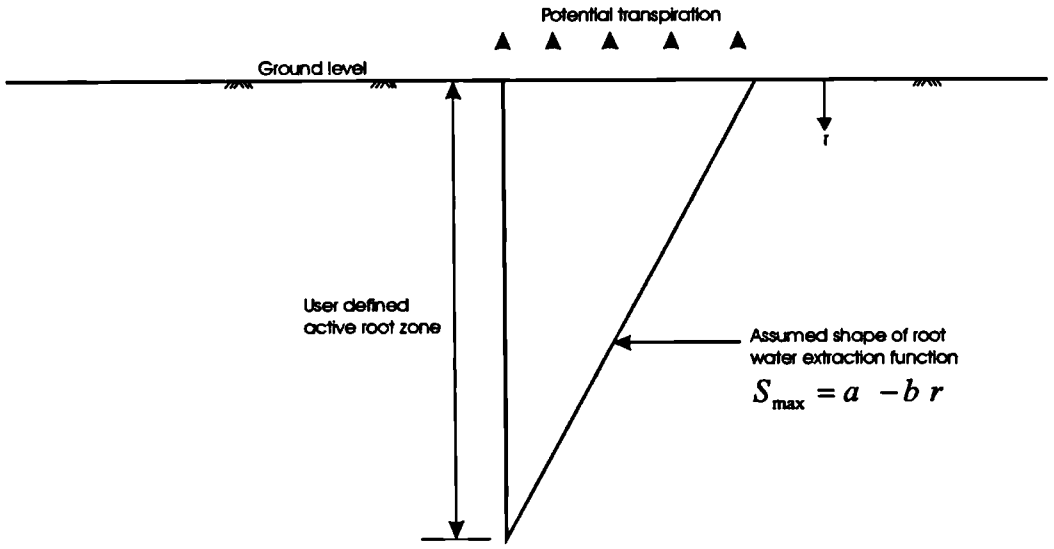

Figure 5.1 Assumed shape of root water extraction function in the rooted zone

Water uptake at various depths is primarily governed by the root density, conductivity of the soil-root system and the availability of water. In numerical algorithms, root-water uptake is taken account of by incorporating a sink term in the continuity equation of fluid flow (Equation 3.3). The sink term is the volume of water extracted per unit volume of soil, per unit time.

Prasad (1988) proposed a one dimensional linear RWUM as follows:

$$S_{max} = a - b\,r \qquad \text{Equation 5.1}$$

where S_{max} is the maximum water extraction rate and occurs when soil moisture is not limiting. a and b are the intercept and slope of the water uptake-depth relationship (Figure 5.1), respectively and r is the depth being considered. Conditions at maximum extraction rate correspond to potential evapotranspiration. Below the maximum root depth, water uptake is assumed to be zero, whence Equation 5.1 becomes:

$$S_{max} = a - b\,r = 0 \qquad \text{Equation 5.2}$$

The potential transpiration rate, T_p, is obtained by integrating Equation 5.1 over the whole rooted depth, r_{max}.

$$\int_0^{r_{max}} S_{max}\,dr = T_p \qquad \text{Equation 5.3}$$

Equations 5.1, 5.2 and 5.3 combined yield:

$$a = \frac{2T_p}{r_{max}} \qquad \text{Equation 5.4}$$

$$b = \frac{2T_p}{r_{max}^2} \qquad \text{Equation 5.5}$$

Equations 5.4 and 5.5 are substituted into Equation 5.1 to give the sink term when water supply is unlimited as:

$$S_{max} = \frac{2T_p}{r_{max}}\left(1 - \frac{r}{r_{max}}\right) \qquad \text{Equation 5.6}$$

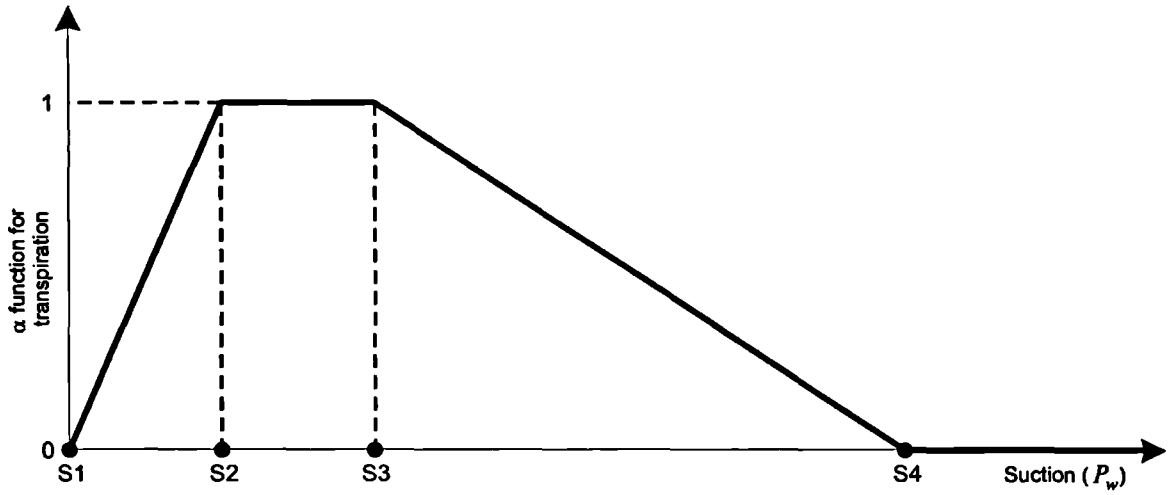

Figure 5.2 Linear variation of α function

Under field conditions, water supply is not unlimited. When the moisture content is low, actual transpiration is lower than the potential value. To simulate root water extraction under these more realistic limiting conditions Feddes *et al* (1978) proposed a modification parameter to the sink term, as follows:

$$S_{acc} = \alpha S_{max}$$ Equation 5.7

where S_{acc} is the actual transpiration rate under field conditions and α is a suction dependent function as shown in Figure 5.2. The α function describes the water uptake characteristics to be dependent on the soil suction. Root water uptake is assumed to be nil at suctions higher than the permanent wilting point, S4, and below the anaerobiosis point S1. The latter equates to water logged conditions when roots are unable to function. Root water extraction is assumed to be at its maximum and constant between points S2 and S3. A linear variation of α with soil suction is assumed between S1 and S2 and between S3 and S4.

The linear RWUM assumes the greatest potential root water extraction to occur in the shallower soil horizons with the extraction rate decreasing with depth. In a typical temperate climate such as that of the UK, the annual water balance is usually positive (total rainfall is greater than evapotranspiration). The weather pattern is also such that precipitation occurs throughout the year, constantly recharging the shallow horizons below ground level (albeit the overall annual pattern is characterised by wet winters and relatively dry summers). Moreover, evaporation occurs at the surface. Therefore the overall process of water abstraction through the combined process of transpiration and evaporation (evapotranspiration) in a temperate climate occurs in the uppermost horizons of a soil profile. The author therefore considers the proposed RWUM to be applicable in modelling evapotranspiration.

In the UK, the Meteorological Office routinely computes the values of potential evapotranspiration, for a number of plant types (mostly agricultural crops) using the Meteorological Office Rainfall and Evaporation Calculation System (MORECS). Among the vegetation types within MORECS include pasture grasslands and deciduous fruit trees and these can be considered to be representative of grass and deciduous trees encountered in civil engineering in the UK, respectively (Biddle, 1998).

In this thesis, the potential evapotranspiration data computed by MORECS was used in Equation 5.7 to calculate actual evapotranspiration from the soil profile. The associated rainfall data was input via the precipitation boundary condition, described in Section 3.4.5.3 (Chapter 3).

5.3 The Meteorological Office Rainfall & Evaporation Calculation System

5.3.1 Introduction

The Meteorological Office Rainfall and Evaporation Calculation System (MORECS) is used by the Meteorological Office to calculate estimated weekly and monthly rainfall, evaporation and soil moisture deficit in the United Kingdom (UK). The Hydrological Memorandum 45 (Hough *et al*, 1997) gives a detailed description of MORECS. Daily weather data from stations across the whole of the UK are used as input data and the results are output in the form of averages over 40 x 40 km grid squares. A single-site version of MORECS is also available whereby computations are based on site-specific or local climatic data.

5.3.2 Description of MORECS

Only the salient aspects of the system will be outlined here to facilitate an understanding of MORECS in the context of its implementation for a flow boundary condition to model root water extraction.

The first component of MORECS deals with the daily extraction of meteorological variables ie. sunshine, temperature, vapour pressure, wind speed and rainfall from the Synoptic Data Bank at Bracknell. The data is objectively interpolated on a 40 x 40 km grid basis to obtain average values. The errors involved in the interpolation process are considered to be small for temperature, humidity and wind speed. However, for sunshine values, the sparsity of both synoptic and climatological stations makes it difficult for representative long-term daily averages to be obtained. The preponderance of rainfall stations implies that errors associated with long-term values are small.

With the single-site MORECS version, the data are not averaged. Where data are missing for certain periods, values from nearby sites are used, wherever possible. In this research, analyses were carried out using single-site MORECS data for Chattenden, in Kent.

The next step in MORECS involves computation of the potential evapotranspiration for the various surfaces considered in the system. Evapotranspiration is inherently a very complex process which would require corresponding complex physically rigorous equations. Such equations would be analytically impossible to solve and the iterative methods required for a numerical solution would

be time-consuming for operational use. Simplification is therefore used in MORECS for these computations, and it is acknowledged that this may result in some loss of accuracy.

The Meteorological Office consider the main errors in MORECS to arise from interpolations involving missing data sets and in the incorrect specification of land use type. Calculation of evapotranspiration is based on a variant of the Penman-Monteith equation whereby water loss is assumed to be a function of the variables that affect the aerodynamic domain eg. air density, vapour pressure and latent heat of vaporization.

The crop models used in MORECS are idealized representations of crop growth which describe the main features which MORECS needs. The models describe the key development stages of the crops as well as physical parameters which are crucial in calculating transpiration eg. leaf area index and tree height. MORECS also computes actual evapotranspiration using a soil moisture extraction model based on the concept of available water content (AWC). However, the approach used by MORECS is less rigorous than the RWUM used in this thesis.

5.4 Coding of root water uptake model into ICFEP

5.4.1 Introduction

The RWUM developed for use in ICFEP is valid for one, two and three dimensional problems. The scope of this thesis covers one and two dimensional scenarios. For purposes of demonstrating the coding of the RWUM, a two dimensional case will be discussed. The description focuses on the three main aspects that are key to computation of transpiration from Equations 5.6 and 5.7 which are root depth, a suction dependent function and calculation of nodal flows. These are specified through a vegetation boundary condition over the relevant increments in an analysis.

The user is required to enter pieces of information under the following headings:

(i) Vegetation - this defines the extent of vegetation on the boundary of the mesh (Section 5.4.2).
(ii) Root depth - this defines the maximum root depth(s) (Section 5.4.2).
(iii) Actual transpiration properties - this defines the α function (Section 5.4.3).
(iv) Transpiration - this defines the magnitude of the potential transpiration rates (Section 5.4.4).

5.4.2 Extent of vegetation and maximum root depth

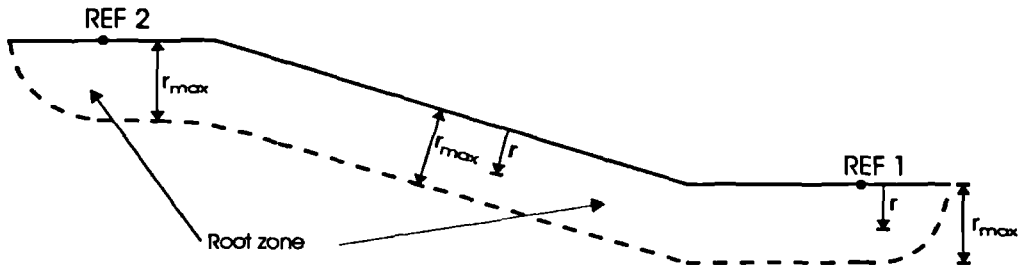

Figure 5.3 Definition of root zone and reference points in vegetation boundary condition

Figure 5.3 shows an idealised ground profile which includes horizontal and sloping ground, with the root zone annotated. Within ICFEP the surface boundary/boundaries over which vegetation exists is specified using reference points, positioned anticlockwise around the boundary ie. REF1 to REF2 in Figure 5.3. The reference points can either be nodes or coordinate points specifically input to define the vegetated boundary and must always be at the surface of the mesh. During excavation or construction, the program automatically transfers the vegetation boundary condition to the new mesh surface boundary between the reference points. Should excavation or construction result in a reference point being removed or incorporated inside the mesh, new reference points have to be defined at the surface boundary to specify the vegetation boundary condition.

Maximum root depths can be varied over specified increments during an analysis. The program is capable of analysing boundary value problems involving different maximum root depths in sections of the mesh during the same increment. eg. zones of different vegetation types in a mesh. The program also allows for only specific elements to invoke the vegetation boundary condition through a section card, as opposed to the default mode which assumes all elements within the maximum root depth to be active to the vegetation boundary condition.

The program is also capable of specifying a varying maximum root depth over a section of the mesh. In the event that more than one vegetation type is present within the same zone, the user has to make an engineering judgment to determine a representative maximum root depth that accounts for all vegetation types in the zone ie. the program can only compute flows using a single maximum root depth at each Gauss Point. Once the maximum root depth has been established, the program automatically identifies all the Gauss points within the rooted zone, as a precursor to computation of flows.

5.4.3 Suction dependent α function

The suction dependent function which defines the water uptake-soil suction relationship is input into ICFEP as a material property. Only material types that are directly affected by transpiration boundary conditions require specification of the α function. The materials also need to belong to elements which have pore water pressure degrees of freedom.

In ICFEP, the values of suction (S1, S2, S3, S4) defining the α values as shown on Figure 5.2 are input as material properties. The program can handle more than one material property in the same analysis and material properties can be altered at specified increments during an analysis. At the beginning of an increment the program assigns an α value to each Gauss point within the rooted zone from which the flow at the Gauss point is calculated using Equation 5.7. However, during the increment, the suctions in the rooted zone can change, which implies that α is also changing.

The dependency of the Gauss flow on the α value presents a complex scenario to analyse numerically. In ICFEP, the program first determines an α value at each Gauss point (beginning of increment n), based on the current pore water pressure (ie. end of increment n-1) using the material properties shown in Figure 5.2. The calculated α value is used to compute the flow during the first iteration of increment n. At the end of the iteration (iteration 1 of increment n) the pore water pressures would have changed during the iteration in response to the boundary conditions. The program then determines a more accurate estimate of the flow at each Gauss point by accounting for the predicted pore water pressure change and its effect on α. This is then compared to the initial estimate based on the α value at the beginning of the increment and the difference used to give an out of balance flow which is used in the next iteration. The process of determining the out of balance flow for each Gauss point is repeated for all subsequent iterations until convergence of that particular increment is achieved (ie. end of increment n). When this is complete, computations for the next increment (ie. increment $n+1$) then commence, again following the same procedure.

With reference to Figure 5.2, it can be seen that certain portions of the α function are characterised by sharp changes in gradient over relatively small suction changes. This must be accurately accounted for when estimating the flows during the iteration process. In ICFEP, the flows are calculated using a numerical integration scheme based on substepping, with error control. This is similar to that used in the stress point algorithm (see Potts and Zdravkovic, 1999). In order to

improve accuracy as well as avoid convergence problems, it may be necessary in certain situations to apply the vegetation boundary condition over several increments per given time step.

5.4.4 Calculation of nodal flow

Nodal flows are calculated from Gauss point values as described in detail in Section 3.3.2 of Chapter 3. This section more specifically describes the numerical implementation of Equations 5.6 and 5.7 to compute the flow at each Gauss point.

The program first establishes the Gauss points of any solid elements which are within the root zone (see Figure 5.3). The root zone is defined by the boundary range REF1-REF2 and by the maximum root depth, r_{max}. For each of these Gauss points, ICFEP computes the depth under consideration, r, perpendicularly to the surface boundary. The evapotranspiration flow rate is then calculated from Equations 5.6 and 5.7 as follows:

$$S_G = \frac{\alpha 2 T_p}{r_{max}}\left(1 - \frac{r}{r_{max}}\right) \qquad \text{Equation 5.8}$$

Where S_G is the Gauss point flow rate, α is the suction dependent function as defined in Figure 5.2 (dimensionless), T_p is the potential transpiration from MORECS, r is the perpendicular distance of the Gauss point to the surface boundary and r_{max} is the maximum root depth, also defined perpendicularly to the surface boundary. A volume integral is performed numerically using Gaussian Quadrature, over the solid elements whose integration points fall in the rooted zone, to determine the equivalent nodal flow rates.

As the values of r_{max} and T_p can vary along the boundary range REF1-REF2, the program has to assign values to each integration point within the root zone. It does this by calculating the coordinates where the line representing the shortest distance from the integration point to the boundary range REF1-REF2 intersects the boundary range. The relative position of this intersection point on the boundary range is then used to evaluate r_{max} and T_p.

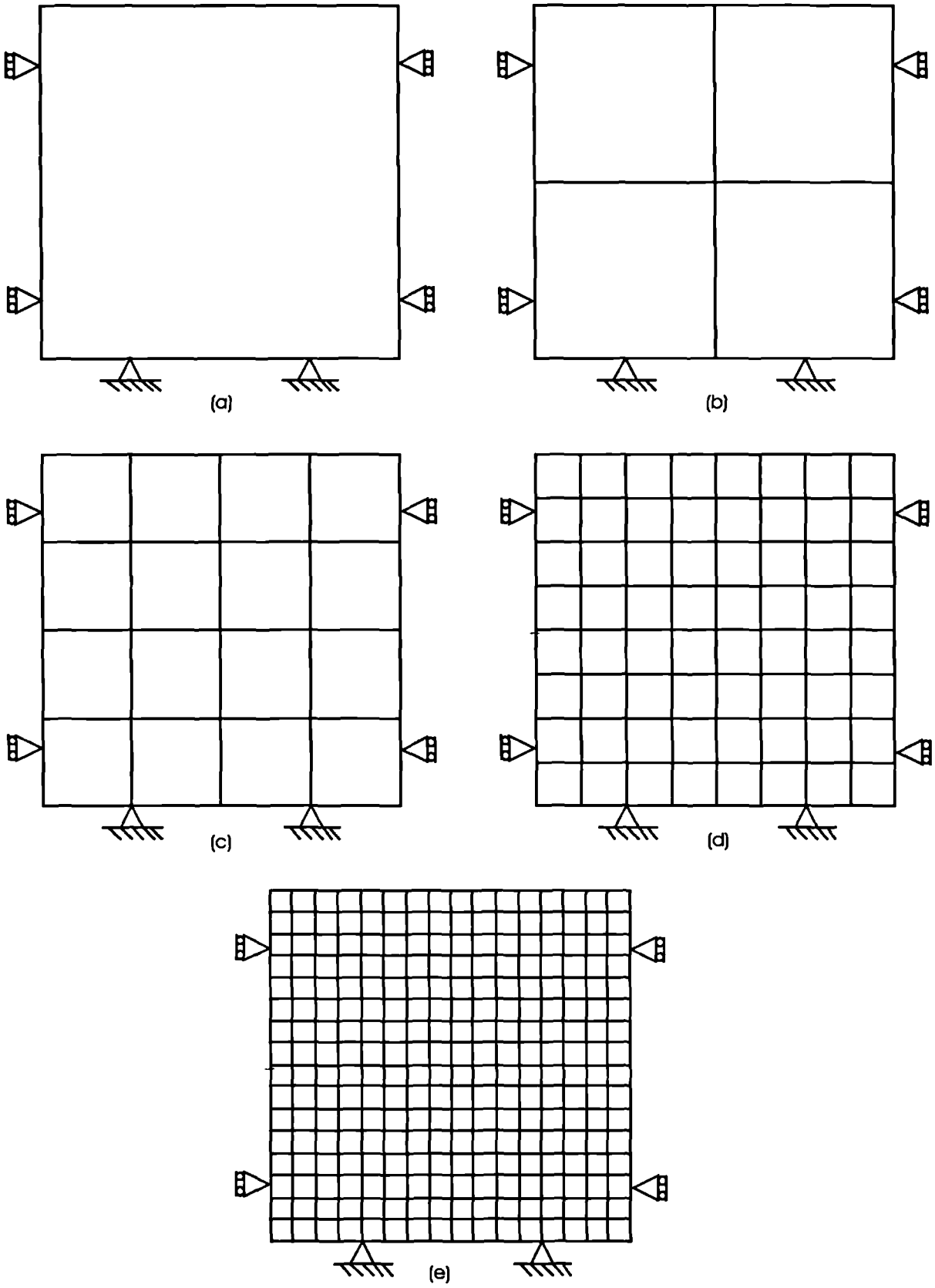

Figure 5.4 Finite element meshes used to investigate the influence of mesh density (all meshes 4m x 4m)

Vegetation boundary conditions in ICFEP can only be applied to elements with pore water pressure degrees of freedom. Integration points belonging to elements with no pore water pressure degrees of freedom in the rooted zone are ignored.

5.5 Testing of root water uptake model

A number of parametric studies were carried out in order to fully understand the behaviour of the coded RWUM. These were as follows:

(i) Influence of mesh density (Section 5.5.1).
(ii) Influence of initial meteorological data (Section 5.5.2).
(iii) Influence of maximum root depth (Section 5.5.3).
(iv) Influence of the S3 value of the α function (Section 5.5.4).
(v) Influence of permeability model (Section 5.5.5).

The convention used in the figures is as follows:

- suction and/or tensile pore water pressures (+ve)
- compressive mean effective stress, p' (+ve)
- compressive major (σ_1) and minor (σ_3) principal stresses (+ve)

5.5.1 Influence of mesh density

A study was carried to assess the sensitivity of the model to mesh density. The aim of this study was to identify the maximum element size to root depth ratio that can be used in boundary value problems involving a vegetation boundary condition; without compromising the accuracy of the results.

5.5.1.1 The mesh and boundary conditions

Two-dimensional analyses were carried out using the mesh configurations shown in Figure 5.4. These equated to element thickness to maximum root depth (r_{max}) ratios of 4, 2, 1, 0.5 and 0.25.

A 4m x 4m square was modelled in plane strain (the dimensions had no significance in this sensitivity study). A rigid boundary was assumed at the bottom of the mesh, thus restricting vertical

and horizontal movement at the base to zero. On the vertical boundaries horizontal movements were fixed to zero with no constraints on vertical movements; thereby allowing vertical deformations to occur in response to pore water pressure changes. No restrictions in movement were specified at the surface boundary.

The initial conditions assumed a hydrostatic suction profile of 39.24kPa at the top and 0kPa at the base of the mesh. The saturated bulk unit weight of the soil was assumed to be 20kN/m^3 and the coefficient of earth pressure at rest, K_0, equal to 1. Linear elastic material properties were assumed for the soil with a Poisson's ratio of 0.2 and a Young's modulus of 20 000kN/m^3. The soil was assumed to have a uniform permeability of 1x10^{-9}m/s.

A maximum root depth, r_{max}, equal to 1m was specified in all the analyses. A uniform potential transpiration rate of 0.05m/yr/m^2 was specified at the top boundary throughout the analyses. The analysis was carried out in 10 increments with each increment representing 1 month. For the α function, S1, S2, S3 and S4 values of 0kPa, 5kPa, 100kPa and 1500kPa, respectively were assumed.

5.5.1.2 Results and discussion

Figures 5.5 and 5.6 show vertical displacement and pore water pressure profiles, respectively along the centreline of the mesh after 1 month (inc. 1), 2 months (inc. 2), 5 months (inc. 5) and 10 months (inc. 10). As can be seen, the overall pattern of vertical movements in response to the vegetation boundary condition indicates maximum ground movements at ground level; with the magnitude of movement decreasing with depth; as expected.

A comparison of the magnitude of the movements at ground level indicates that for an element thickness to r_{max} ratio of 4, the vertical movements are under-predicted by approximately 60% compared to element thickness-root density ratios of 1, 0.5 and 0.25; the results for which are very similar to each other. The magnitude of under-prediction reduces with depth for all cases.

It can also be seen that for an element thickness to r_{max} ratio of 2, the vertical ground movements at ground level are over-predicted by approximately 15%. This may not be immediately obvious until the location of the integration points in the root zone contributing to nodal flows and the sink term (Equation 5.8) are considered.

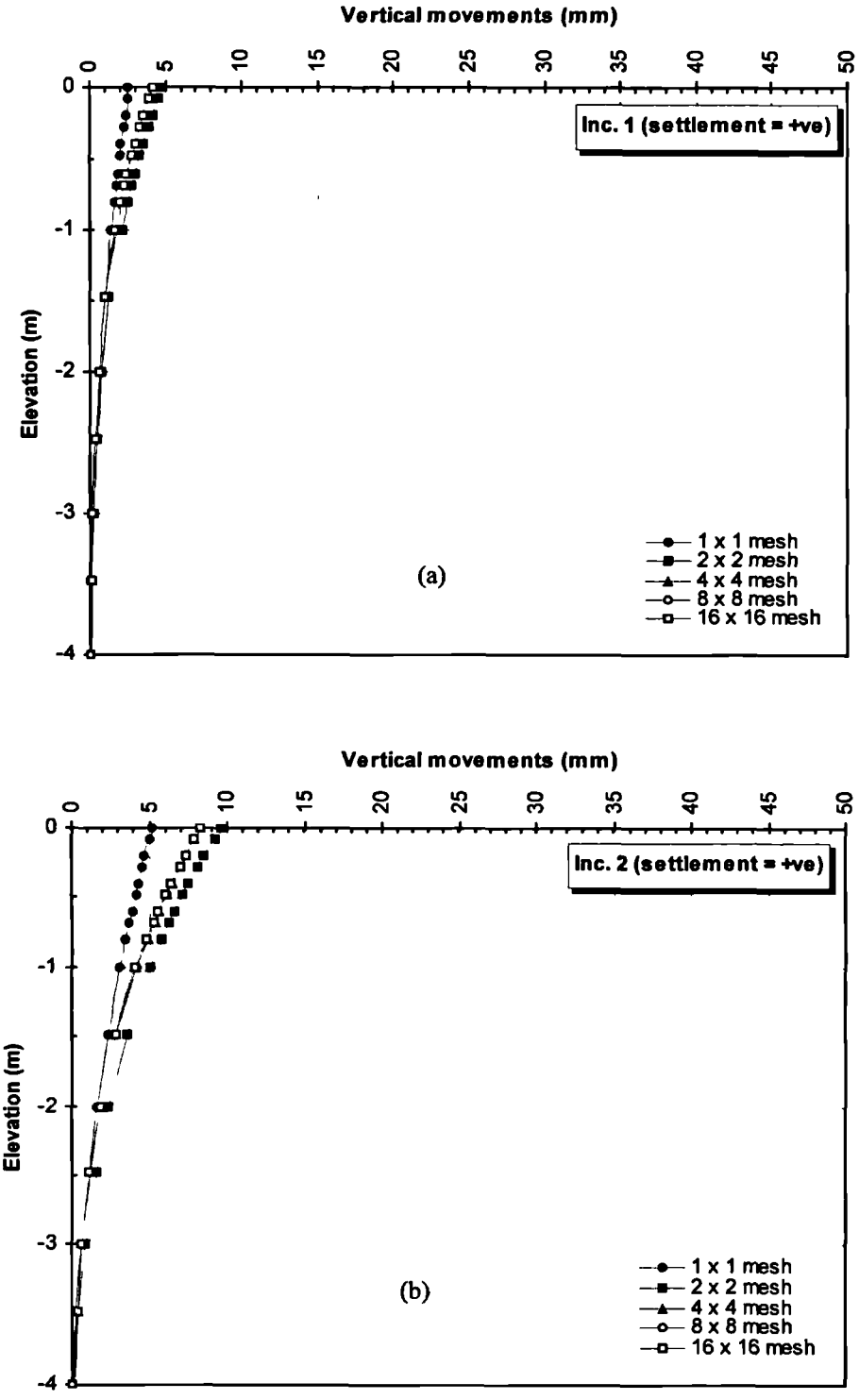

Figure 5.5 Prediction of vertical movements on an idealised 4m x 4m wall using the RWUM.

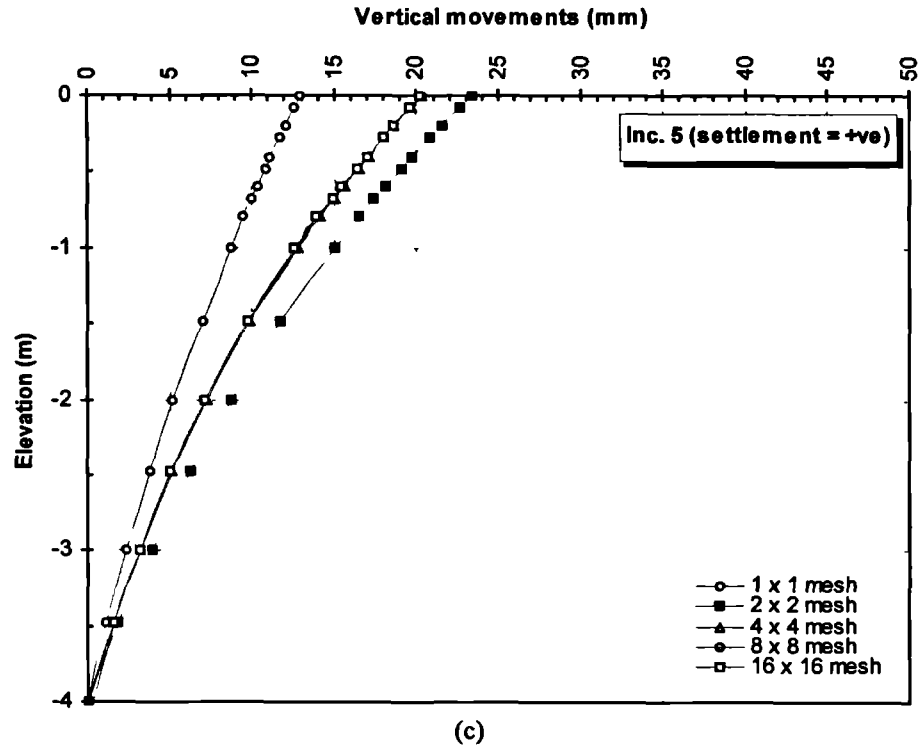

(c)

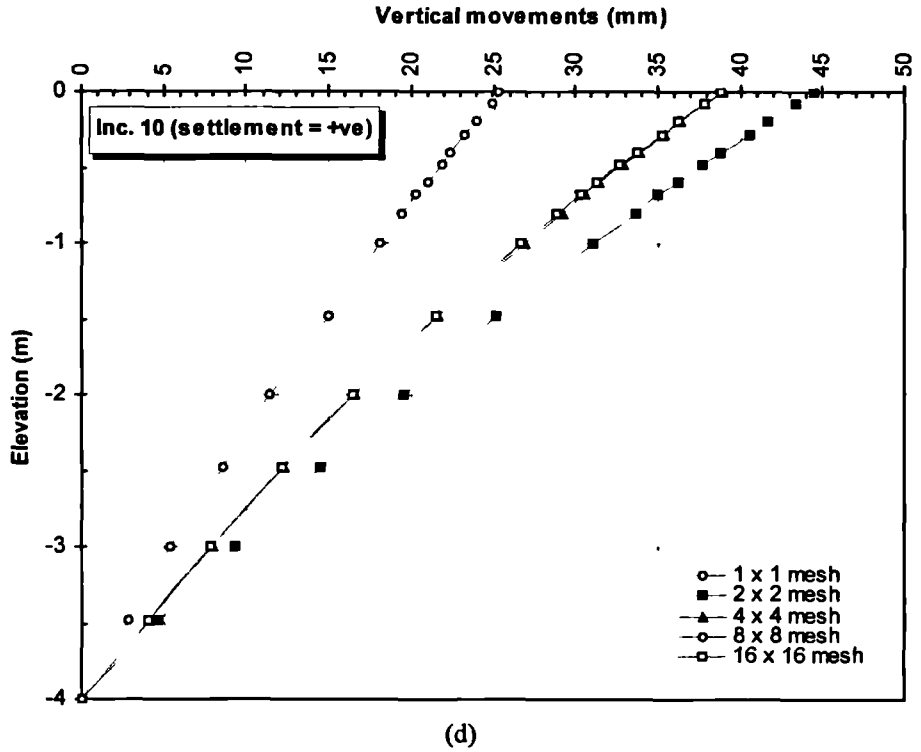

(d)

Figure 5.5 Prediction of vertical movements on an idealised 4m x 4m wall using the RWUM.

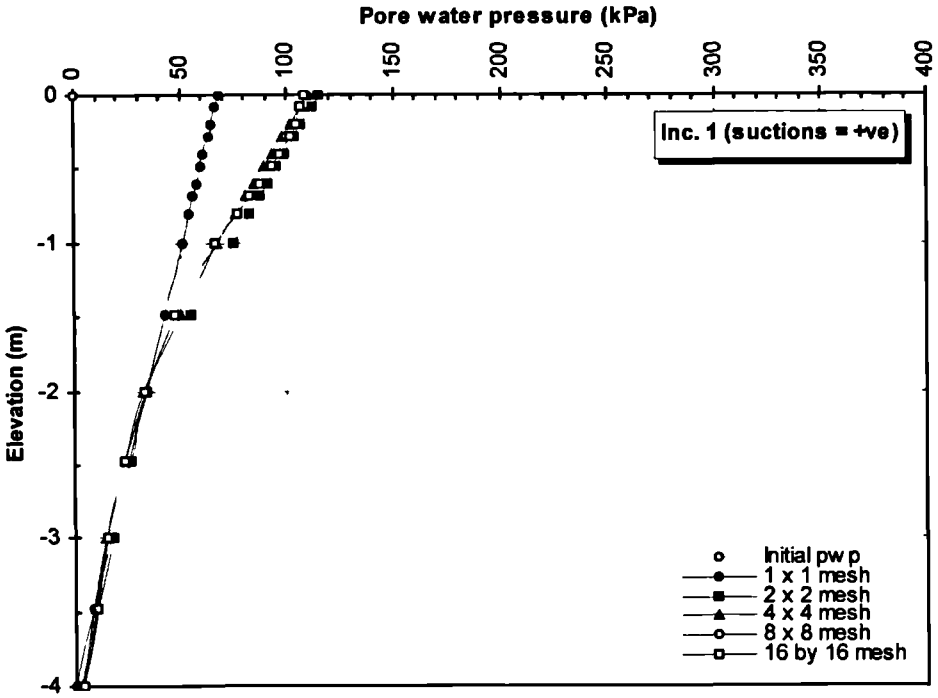

(a)

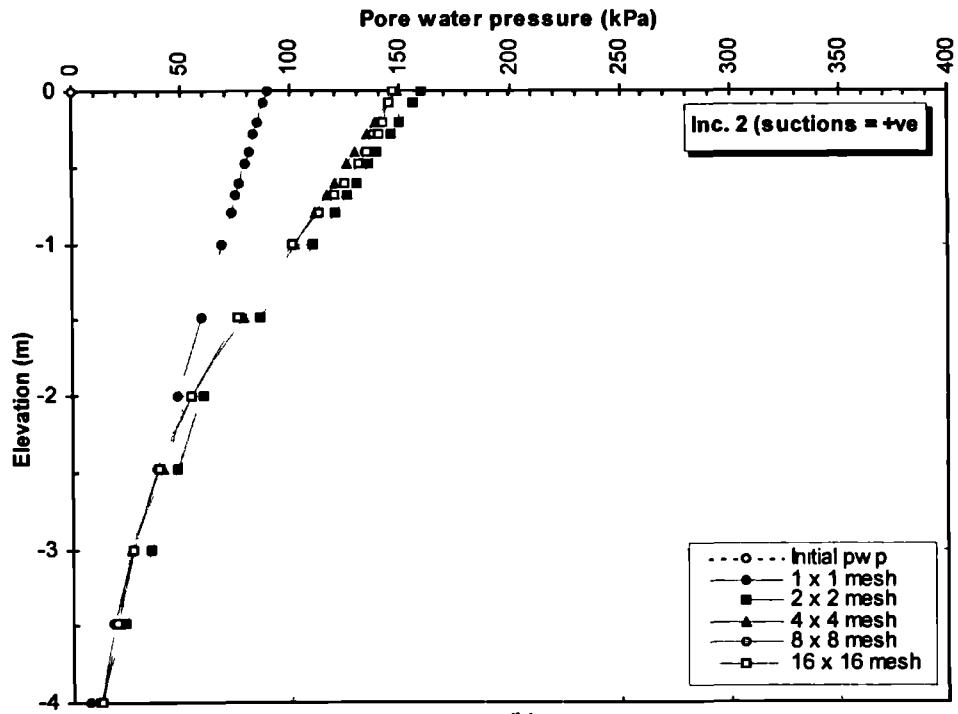

(b)

Figure 5.6 Prediction of pore water pressures on an idealised 4m x 4m wall using the RWUM.

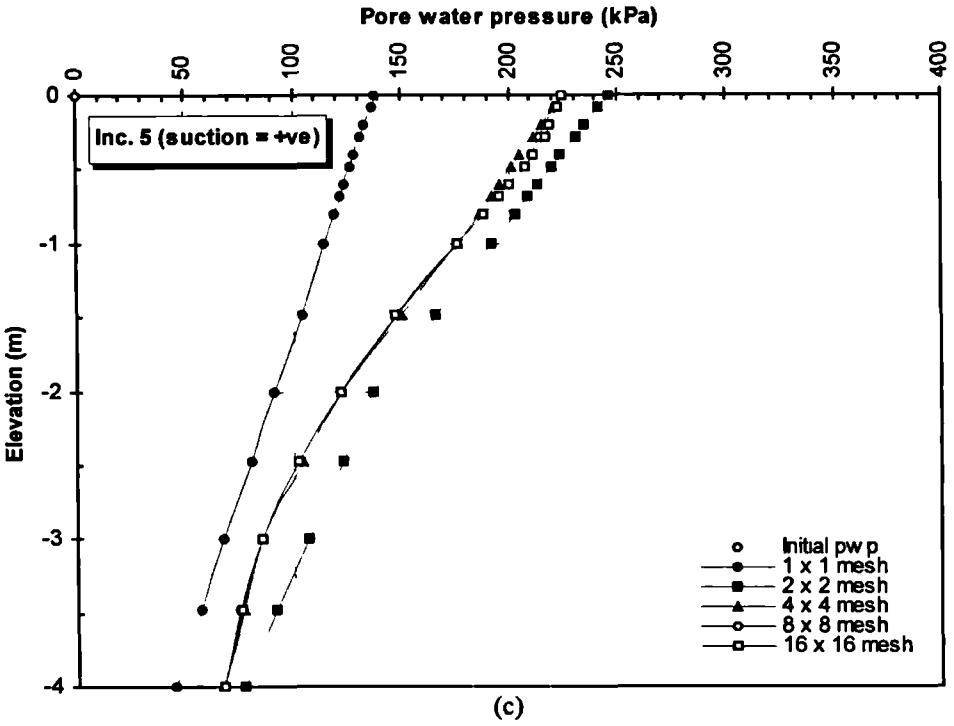

(c)

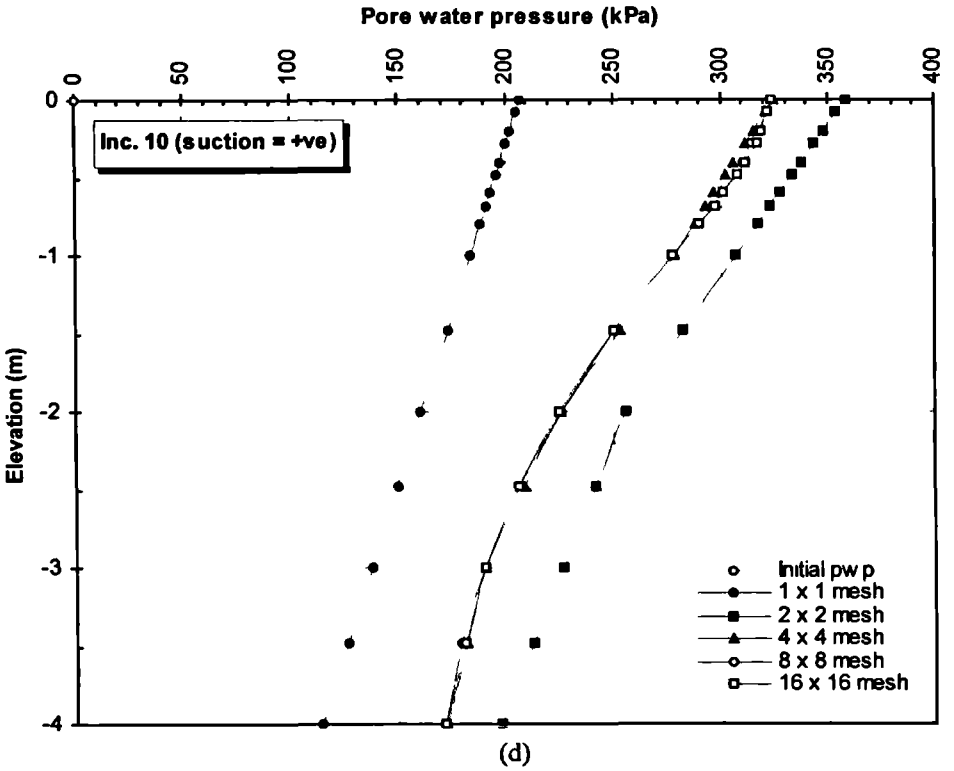

(d)

Figure 5.6 Prediction of pore water pressures on an idealised 4m x 4m wall using the RWUM.

For an element thickness to r_{max} ratio of 2, only the first row of Gauss points are contributing to flow. The location of these Gauss points is approximately at $0.57 \times \frac{1}{2}$ the element thickness = $0.57 \times \frac{1}{2} \times 2m = 0.57m$. This means that the location of the Gauss points is 0.43m below ground level ie. r in Equation 5.8 is 0.43m.

A similar calculation for the location of Gauss points for an element thickness to r_{max} ratio of 4 (element thickness = 4m) gives a value of 0.86m below ground level. All other things being equal, the flow at a Gauss point is primarily a function of the $\left(1 - \frac{r}{r_{max}}\right)$ ratio, from Equation 5.8. Therefore the predictions for actual transpiration, and hence movements for the element thickness to r_{max} of 2 will be approximately double that of an element thickness to r_{max} ratio of 4; notwitstanding that integration to get nodal flows depends on Gauss point values, their positions and the size of the element. A similar exercise for element thicknesses to r_{max} ratios of less than 2 yields values which lie between the two cases described above.

It can also be seen from Figure 5.5 that the predictions of vertical ground movements in the analyses with element thickness to r_{max} ratios of 1, 0.5 and 0.25 are all very similar in magnitude. This suggests that a maximum element thickness to r_{max} ratio of 1 (equal to the root depth) is accurate enough for prediction of ground movements when using this RWUM.

The predictions of pore water pressures after 1, 2, 5 and 10 months are shown in Figure 5.6. The results indicate progressive increase in suctions with time in response to the vegetation boundary condition, as expected. The overall pattern of pore water pressure profiles closely resembles that of vertical displacements. It can also be seen that pore water pressures at ground level are being under-predicted by approximately 60% in the analysis involving a mesh size-maximum root depth ratio of 4 compared to analyses involving mesh size-root depth ratios of 1, 0.5 and 0.25. The predictions for pore water pressures again indicate that a maximum mesh size to r_{max} ratio of 1 (equal to the root depth) is accurate enough for prediction of pore water pressures.

5.5.2 Influence of meteorological data

1

5.5.2.1 Introduction

It can be seen from Equations 5.7 and 5.8 that the computations for actual transpiration are strongly influenced by the value of the α function. Moreover, the α function itself is dependent on the current pore water pressure, hence there is a coupling effect. The pore water pressure regime is primarily governed by the net effects of water inflow (precipitation) and water loss through vegetation (transpiration) and directly from the ground (evaporation).

Another factor to consider is the pattern of rainfall and potential evapotranspiration (evaporation and transpiration). If long durations are considered, it is possible to have two periods (eg. weeks, months or years) with the same total quantities of rainfall and/or potential evapotranspiration. However, if short durations are considered, the distribution or pattern of rainfall and/or potential evapotranspiration over the periods under consideration may be quite different; eg. 2 months may have the same total rainfall but if the weekly distribution were considered, it may be found that in one month the intensity was uniform throughout whereas in the other month all the rainfall may have fallen in one week only.

The issue of rainfall and/or evapotranspiration pattern has implications on the predictions of actual evapotranspiration because values of the α function at any given time will be different, depending on current pore water pressures. It was therefore considered necessary to investigate the influence of the pattern of rainfall and potential evapotranspiration on predictions of pore water pressures and ground movements.

5.5.2.2 The stratigraphy and mesh

The stratigraphy and meteorological data for the Building Research Establishment (BRE) testing site at Chattenden, Kent (UK) were used in the analyses. This site was selected because the MORECS data required for the analyses was readily available.

The site comprises 45m of London Clay overlying 2m of Old Haven Beds, 18m of Lambeth Group deposits, 40m of Thanet sands and 205m of Chalk as shown in Figure 5.7. A one-dimensional situation was analysed using a 1m wide column in plane strain (Figure 5.8). A dense mesh was used in the upper stratum below ground level where most of the pore water pressure changes and ground movements were expected to occur. [1]A rigid boundary was assumed at the top of the

[1] Although pore water pressure changes were expected to occur in the upper horizon of the London clay only, the mesh was extended to deeper horizons in order to facilitate modelling of the underdrainage at the site.

chalk (105m below ground level) which effectively restricted horizontal and vertical movements at this elevation to zero. No horizontal movement was allowed along the vertical boundaries thus simulating symmetry along the vertical sides of the column. The top boundary was assumed to be free.

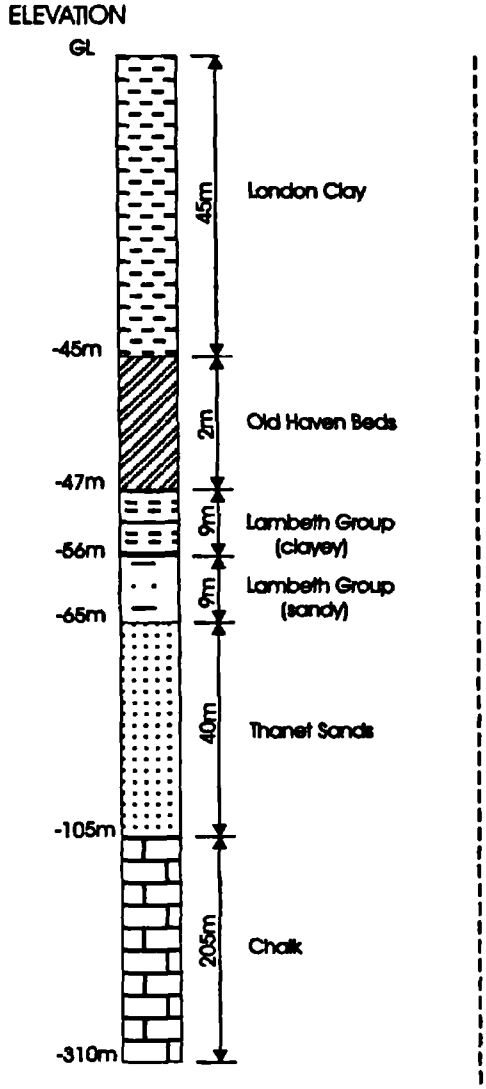

Figure 5.7 Chattenden BRE site - the stratigraphy (not to scale)

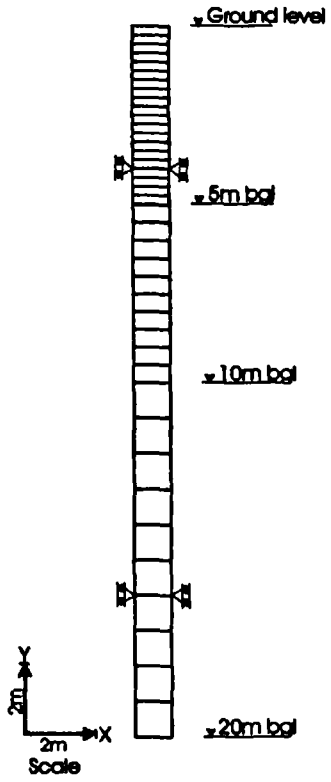

Figure 5.8 Chattenden BRE site - finite element mesh used in 1m wide single column analyses. (NB. mesh extends to 105m bgl)

The initial conditions assumed the phreatic surface to be at 1m below ground level (typical of winter pore water pressures in the UK) and hydrostatic below this surface. Above the phreatic surface a hydrostatic suction profile was assumed; with a suction of 9.81kPa at ground level. At the commencement of the analysis an initial pore water pressure stabilisation period of 5000 years was allowed, during which the ground water regime responded to specified values of pore water

pressure at the top of the old Haven Beds and Chalk, to match the under-drained pore water pressure profile observed in a well near the site.

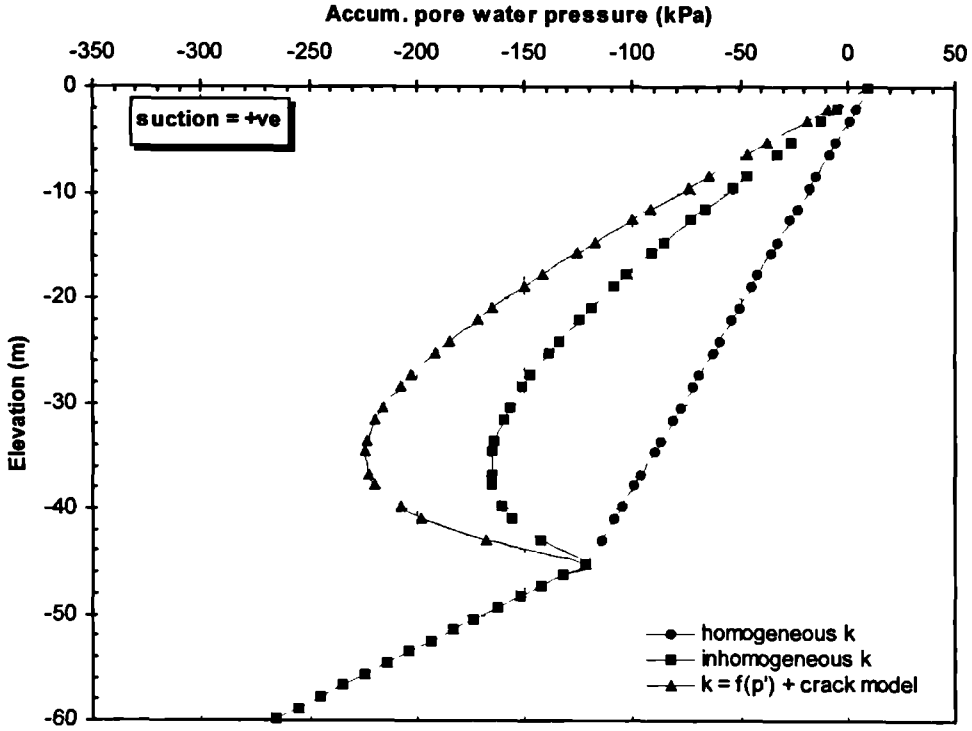

Figure 5.9 Accumulated pore water pressures at the commencement of the RWUM.

The stabilised pore water pressure profile (Figure 5.9) was then used as datum for the vegetation boundary condition. Note in Figure 5.9, the stabilised pore water pressure is shown for three different permeability assumptions for the London Clay. These will be discussed subsequently. K_0 in the London Clay was assumed to be 2 at ground level, reducing linearly to 1 at 10m depth. A uniform K_0 of 1 was assumed for all strata below 10m depth. After the 5000 years of pore water pressure equilibration, rainfall was modelled using the precipitation boundary condition. Ponding of rain water was not allowed at ground level and this was achieved in the analyses by limiting the maximum predicted compressive pore water pressures to 0kPa, using the precipitation boundary condition.

5.5.2.3 Soil parameters and constitutive modelling

The soil parameters used in the analysis are summarised in Table 5.1. To eliminate other variables, homogeneous permeability was used for all strata. Note that for this section (Section 5.5.2), only the homogeneous profile in Figure 5.9 is relevant in this discussion. A p' dependent stiffness

model described in Chapter 3 was used to model pre-peak behaviour of the London Clay. The model has been previously successfully used to model large strain reversals in London Clay eg. Kovacevic *et al* (2001). No movement was expected in the underlying strata and for these materials, a nonlinear model after Jardine *et al* (1986) was used.

Table 5.1a Soil parameters used in analyses

Parameter	In situ London Clay	Oldhaven Beds	Lambeth clays	Lambeth sands	Thanet Sand
Bulk unit weight	18.8 kN/m^3	18	20	20	20
φ′ (peak)	20° (at 0-5% strain)	34	27	34	40
φ′ (residual)	13° (at 20% strain)	N/A	N/A	N/A	N/A
c′ (peak)	2kPa (at 0-5% strain)	N/A	N/A	N/A	N/A
c′ (residual)	2kPa (at 20% strain)	N/A	N/A	N/A	N/A
Permeability	$k_0 = 2\times10^{-10}$ m/sec	1x10^{-7}	1x10^{-6}	1x10^{-6}	1x10^{-6}
Coefficient of earth pressure at rest, K_o	2.5 at ground level and reducing linearly to 1.0 at 15m depth	1.0	1.0	1.0	1.0
Non-linear elastic parameters	*See Equations 5.9 and 5.10*	*See Equations 5.11 and 5.12*			
Poisson's ratio ν	0.2	N/A	N/A	N/A	N/A

$$E_i = E_0\left[\frac{p_a + p'}{p_a}\right]^c \qquad \text{Equation 5.9}$$

$$E_u = HE_i \qquad \text{Equation 5.10}$$

where E_i and E_u are the drained Young's moduli on first loading and unloading/reloading respectively, p_a is atmospheric pressure , p' is the mean effective stress and E_0 and c are model parameters. The values of E_0, H, and c were taken as 2500, 2 and unity, respectively and a minimum value of 4000kPa was specified for E_i.

$$\frac{3G}{p'} = C_1 + C_2\cos\left[c_1 X^{c_2}\right] - C_2 c_1 c_2 \frac{X^{(c_2-1)}}{2.303}\sin\left[c_1 X^{c_2}\right] \qquad \text{Equation 5.11}$$

$$\frac{K}{p'} = C_4 + C_5\cos\left[c_3 X^{c_4}\right] - C_5 c_3 c_4 \frac{X^{(c_4-1)}}{2.303}\sin\left[c_3 X^{c_4}\right] \qquad \text{Equation 5.12}$$

where $X = \log_{10}\left(\frac{E_d}{1.732C_3}\right)$ and $Y = \log_{10}\left(\frac{\varepsilon_v}{C_6}\right)$

Table 5.1b Soil Parameters Used in Analyses

Stratum	C_1	C_2	C_3 (%)	c_1	c_2	$E_{d(\min)}$ (%)	$E_{d(\max)}$ (%)	$G_{\min}$ (kPa)
Lambeth clays	1000.0	1045.0	5.0×10^{-4}	1.344	0.591	13.8564×10^{-4}	0.38105	2667.0
Lambeth sands	1300.0	1380.0	1.0×10^{-4}	1.220	0.649	1.90526×10^{-4}	0.13	1000.0
Thanet Sand	930.0	1120.0	2.0×10^{-4}	1.100	0.700	13.64×10^{-4}	0.165	2000.0

Table 5.1c Soil Parameters Used in Analyses

Stratum	C_4	C_5	C_6 (%)	c_3	c_4	$\varepsilon_{v(\min)}$ (%)	$\varepsilon_{v(\max)}$ (%)	$K_{\min}$ (kPa)
Lambeth clays	530.0	460.0	5.0×10^{-4}	1.492	0.678	1.5×10^{-4}	0.16	5000.0
Lambeth sands	275.0	235.0	5.0×10^{-4}	1.658	0.535	5.1×10^{-4}	0.30	3000.0
Thanet Sand	190.0	110.0	1.0×10^{-4}	0.975	1.010	1.1×10^{-4}	0.20	5000.0

5.5.2.4 Evapotranspiration and rainfall boundary conditions

Only the London Clay was assumed to be active to the vegetation boundary condition. A maximum root depth of 2.5m was assumed in the analysis. The α function (Figure 5.2) was used with S1 = 0kPa, S2 = 5kPa, S3 = 50kPa and S4 = 1500kPa. The meteorological data used comprised MORECS median monthly data for evapotranspiration and rainfall for deciduous tree cover. Automatic incrementation was employed in the analysis to more accurately predict pore water pressure changes in the soil profile (Smith 2002).

Three main variants of the potential evapotranspiration data were used during the first 12 months, in order to investigate the influence of pattern/distribution of the data on predictions of pore water pressures and ground movements. These are:

Case 1: Potential evapotranspiration data was input sequentially from January (yr 1) to December (yr 1) corresponding to months 1 to 12 of the analysis, respectively.

Case 2: Potential evapotranspiration data was reversed and input such that data for December (yr 1) back to January (yr 1) was input corresponding to months 1 to 12 of the analysis, respectively.

Case 3: Potential evapotranspiration data was input sequentially but commencing in July (yr 1), August (yr 1) etc. up to June (yr 1) corresponding to months 1, 2, etc. up to month 12.

The three approaches are summarised in Table 5.2 below.

Table 5.2 Potential evapotranspiration used for the first 12 months

Month	1	2	3	4	5	6	7	8	9	10	11	12
Case1	Jan yr1	Feb yr1	Mar yr1	Apr yr1	May yr1	Jun yr1	Jul yr1	Aug yr1	Sep yr1	Oct yr1	Nov yr1	Dec yr1
Case2	Dec yr1	Nov yr1	Oct yr1	Sep yr1	Aug yr1	Jul yr1	Jun yr1	May yr1	Apr yr1	Mar yr1	Feb yr1	Jan yr1
Case3	Jul yr1	Aug yr1	Sep yr1	Oct yr1	Nov yr1	Dec yr1	Jan yr1	Feb yr1	Mar yr1	Apr yr1	May yr1	Jun yr1
Rainfall	Jan yr1	Feb yr1	Mar yr1	Apr yr1	May yr1	Jun yr1	Jul yr1	Aug yr1	Sep yr1	Oct yr1	Nov yr1	Dec yr1

Figure 5.10 shows plots of the potential evapotranspiration and rainfall data used for the three cases during the first 12 months. In all cases, potential evapotranspiration data for January of the second and all subsequent years was input sequentially without reversal (ie. January of the 2nd year = month 13 in the analysis, February of the 2nd year = month 14 in the analysis etc.). Rainfall data was not reversed but entered sequentially in all the analysis beginning with January of the first year (ie. January of the first year = month 1 in the analysis, February of the first year = month 2 in the analysis etc). It is essential to reiterate once again that although the potential evapotranspiration

data was reversed in the first 12 months, the total annual potential evapotranspiration values for all three cases was the same.

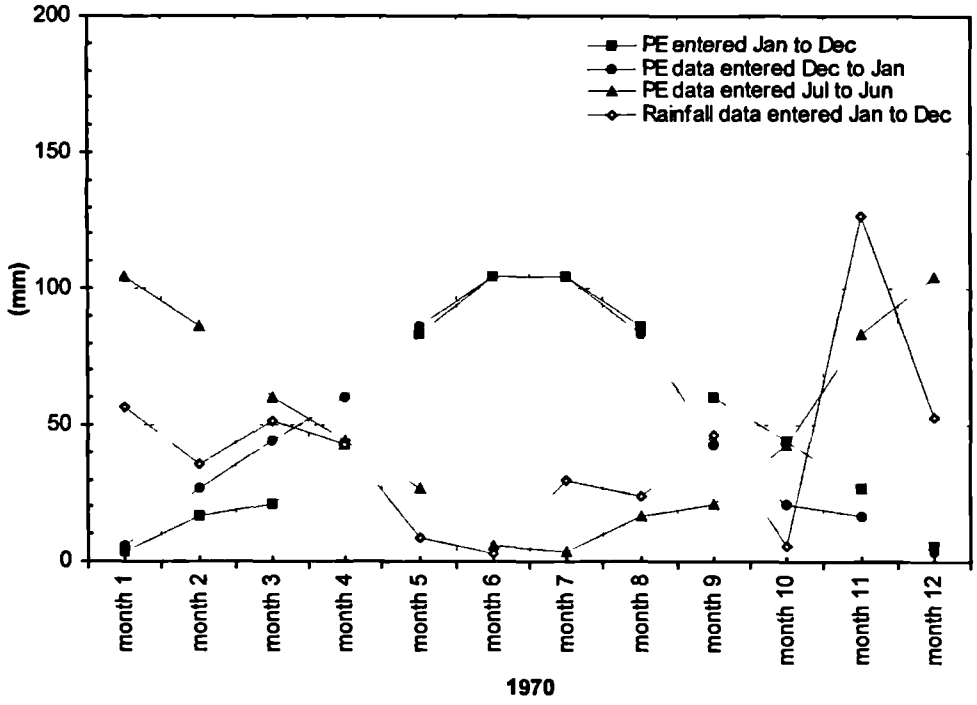

Figure 5.10 Meteorological data used in sensitivity analyses

5.5.2.5 Results and discussion

The results below are presented for the short term scenario (first 12 months) and for the medium to long-term scenarios (1 to 10 years).

Short term scenario (first 12 months):

The results for the accumulated pore water pressures along the centreline of the soil column after 6 and 12 months of application of the RWUM are shown in Figure 5.11a for the three cases. The pore water pressure profile after 5000 yrs of equilibration (prior to invokation of RWUM) is also shown (homogeneous permeability). It can be seen from this figure that the pattern of pore water pressure distribution closely mirrors the distribution of the potential evapotranspiration eg. during the first 6 months, there is a general downward trend in the magnitude of potential evapotranspiration for case 3 (data entered July to June); which results in relatively lower suctions at the end of 6 months. The scenario is different for case 1 (data entered January to December) and case 2 (data entered December to January) where an upward trend in potential evapotranspiration rates is matched by higher suctions at the end of 6 months.

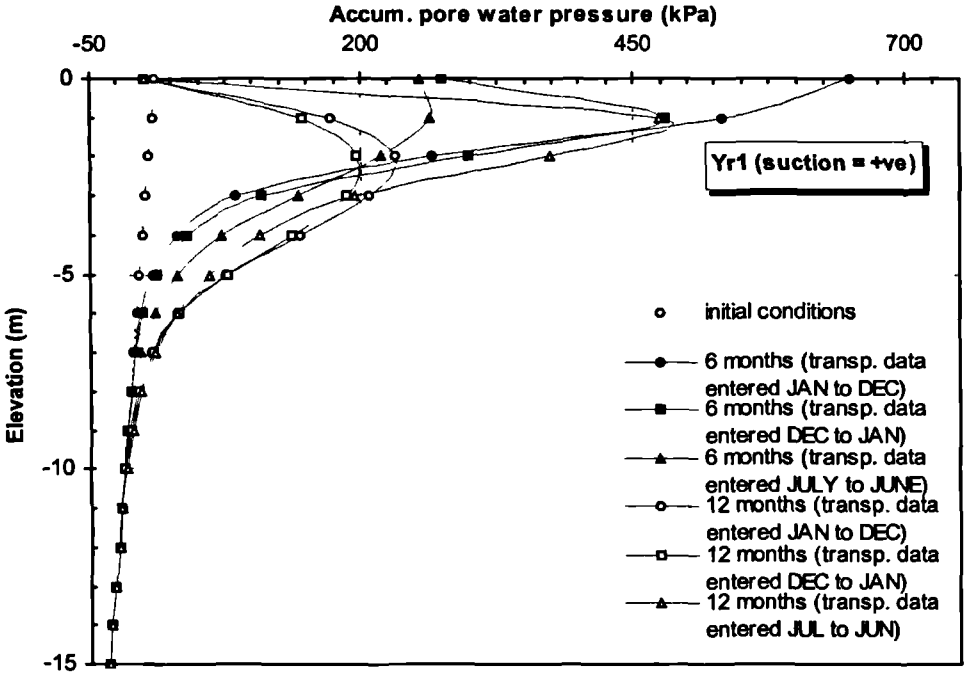

Figure 5.11a Influence of meteorological data on pore water pressure predictions during yr1.

During the second half of the year (months 7 to 12) the evapotranspiration trends for the three cases are opposite to the trends during the first half of the year discussed above. Again, the pore water pressure changes reflect this pattern; thus confirming the powerful ability of the RWUM to predict pore water pressures from meteorological data. It is also noteworthy that although the total annual potential evapotranspiration are the same, the differences in pore water pressure changes as influenced by the α function are significant as portrayed in Figure 5.11a.

It can also be seen that the depth to which pore water pressure changes have occurred is nearly 10m after 12 months. This depth is somewhat greater than was inferred from filter paper tests on undisturbed samples (Crilly and Driscoll, 2000).

Figure 5.11b shows the distribution of pore water pressures during the first 12 months at ground level and 1m depth. With reference to the meteorological data (Figure 5.10) for case 1 (potential evapotranspiration data entered Jan to Dec) it can be seen that during the first 6 months, the trend for potential evapotranspiration is upward and is accompanied by a gradual reduction in rainfall intensity. During this period, the magnitude of suctions at ground level (where there is continual infiltration) is overall lower than that at 1m depth. This reflects the development of a desiccation profile at depth, and reflects the capability of the RWUM to reproduce field behaviour.

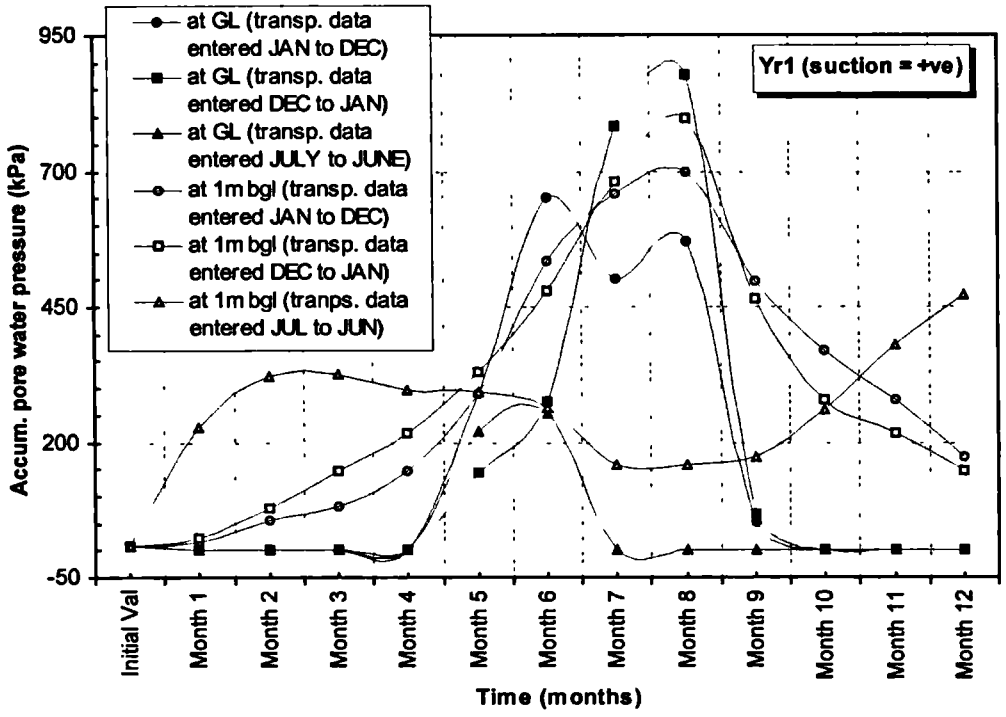

Figure 5.11b Influence of meteorological data on pore water pressure prediction at ground level and at 1m depth, during yr1.

The following 6 months (month 7-12) are characterized by increasing precipitation and a reduction in potential evapotranspiration rates. The ground response in this latter case is again shown in Figure 5.11b where it can be seen that full recharge in pore water pressures occurs at ground level occur during the 10th month (ie. suctions are eliminated). The magnitude of pore water pressures at 1m depth also reduces; albeit suctions of approximately 170kPa are predicted at the end of the 12th month. The differences in pore water pressure predictions among the three cases in Figure 5.11b further confirm the strong influence of the α function and its dependency on the current pore water pressures; which in turn depends on the intensity of precipitation and potential evapotranspiration.

The sub-accumulated vertical movements that occur along the centreline of the column after 6 months and 12 months of application of the RWUM are shown in Figure 5.12a. These movements are sub-accumulated from the end of the 5000yr pore water pressure equilibration at which the RWUM is initially applied. As expected, the pattern of movements closely mirrors that of the pore water pressure changes (Figure 5.11a). The overall pattern shows maximum ground movements at ground level whose magnitude reduces with depth. It can be seen from Figure 5.12a that after 12 months the magnitude of vertical movements are similar for case 1 (potential evapotranspiration

data entered Jan to Dec) and case 2 (potential evapotranspiration data entered Dec to Jan). Maximum movements of approximately 235mm are predicted at ground level.

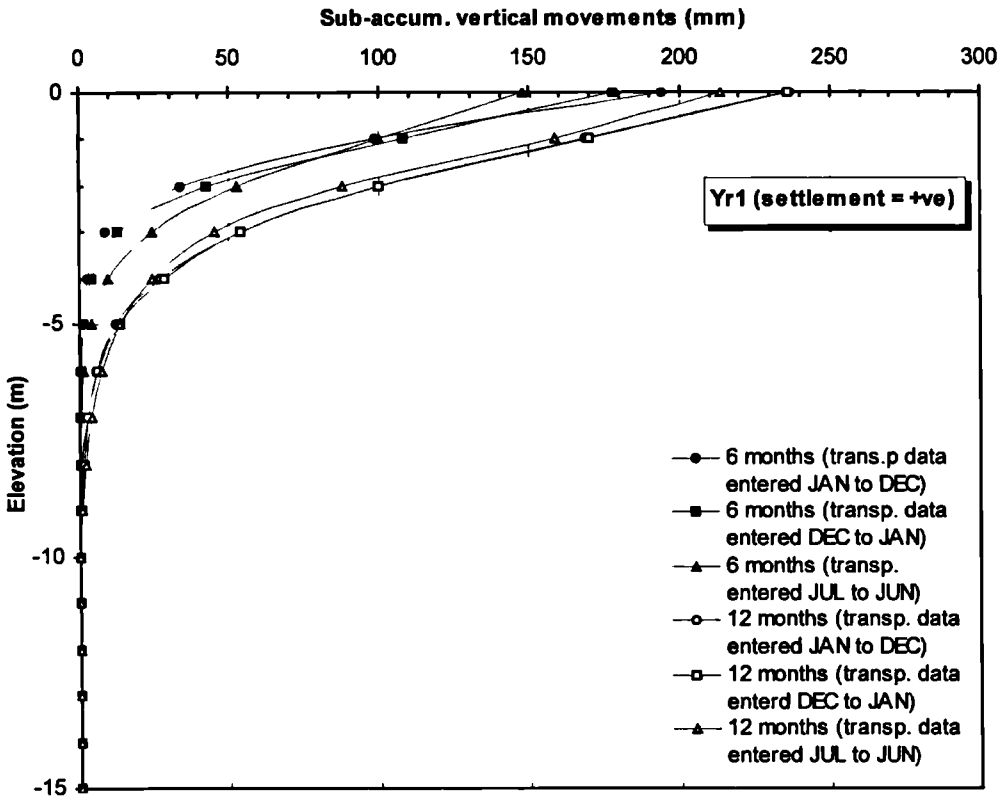

Figure 5.12a Influence of meteorological data on prediction of sub-accumulated vertical movements during year 1

The corresponding vertical movements for case 3 (potential evapotranspiration data entered Jul to Jun) are overall slightly less compared to cases 1 and 2 eg. maximum vertical movements of 215mm are predicted at ground level. This is likely to be a result of the low α values associated with the relatively high evapotranspiration rates when the RWUM is first applied (ie. very high transpiration rates in July compared to cases 1 and 2). The net effect results in a limited amount of water that can be removed in a given time, which in turn curtails the magnitude of volume changes. Although transpiration rates gradually reduce with time and attain their lowest values after 6 months for case 3 (see Figure 5.10), the recovery in α values does not occur fast enough in the given time to yield conditions which allow maximum transpiration can occur.

Figure 5.12b depicts the vertical movements at ground level and 1m depth for the three cases as a result of invokation of the RWUM during the first 12 months. It is clear from the figure that the magnitude of movements during the 12 months is dependent on the relative balance between

precipitation and potential evapotranspiration (which affects the α values). Nevertheless, the predictions largely become equal by the 10th month for cases 1 and 2 while for case 3, the difference (with those from cases 1 and 2) in predictions of movements gradually reduces from months 9-12.

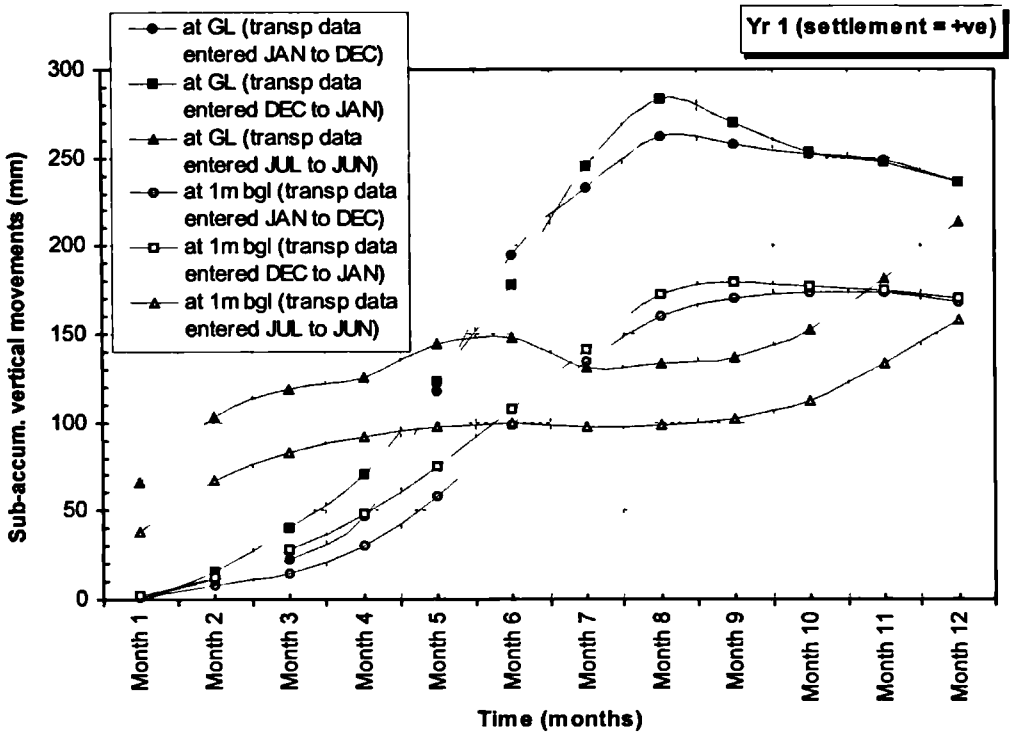

Figure 5.12b Influence of meteorological data on prediction of sub-accumulated vertical movements at ground level and 1m depth during yr 1 .

Medium to long-term scenario (yrs 1 to 10)

The analyses were continued for another 9 years to determine the medium to long term trend. The meteorological data used (yr 1 to 10) was identical in all three cases and is summarized in Figure 5.13.

Figure 5.14a shows accumulated pore water pressure distribution along the centreline of the soil column after 1 and 5 years. It is encouraging to note that the largest differences in pore water pressure predictions are exhibited at the end of the first year only, beyond that period, the predictions are similar. The convergence in pore water pressure predictions with time can be more clearly seen from the predictions at 1m depth in Figures 5.14b. The latter figure shows that that the pore water pressure predictions at this depth begin to converge by the end of the second year and by the end of the 5th year, all three cases have converged. It is likely that at depths greater than 1m, the pore water pressures take longer to converge.

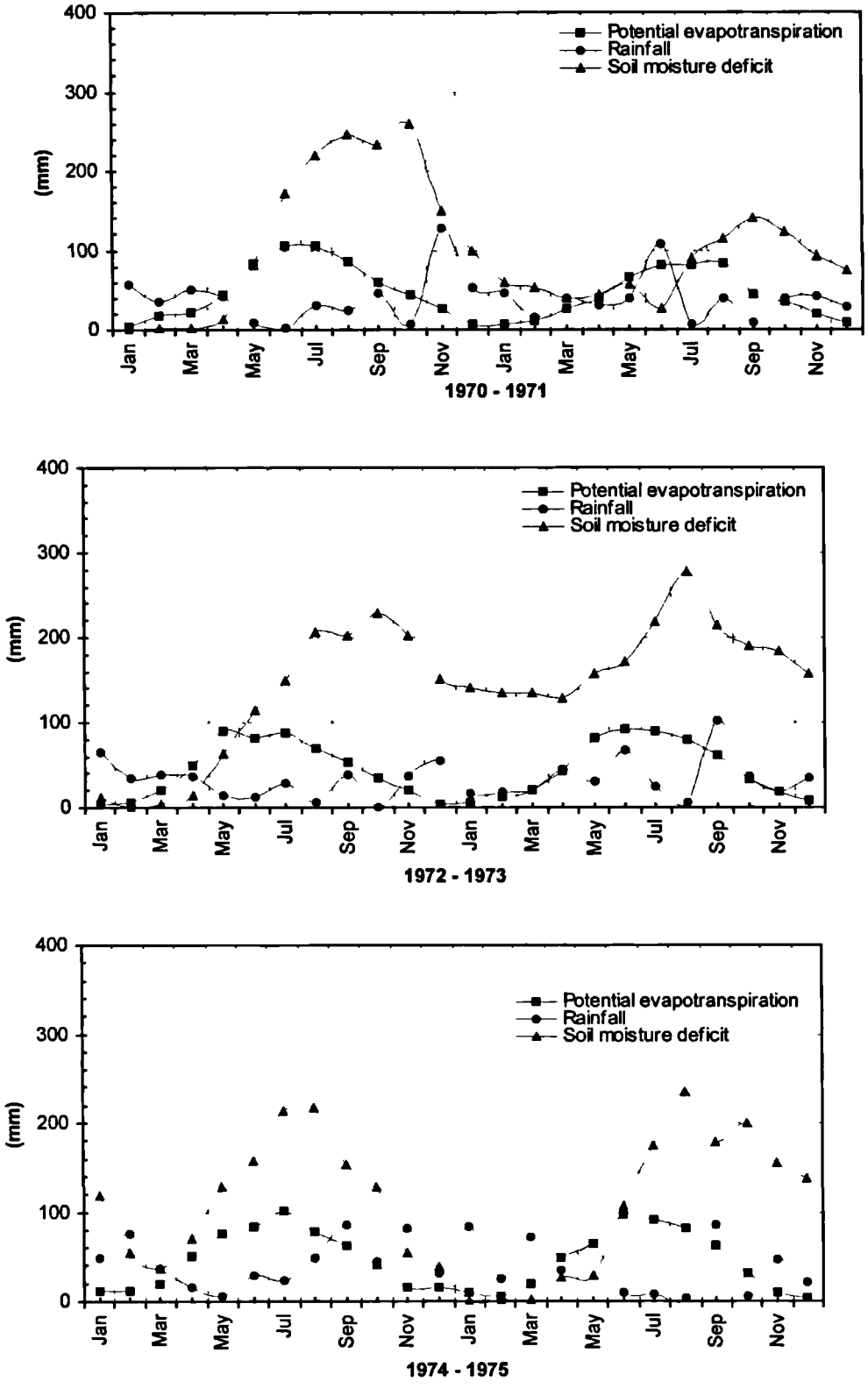

Figure 5.13a Meteorological data for Chattenden site

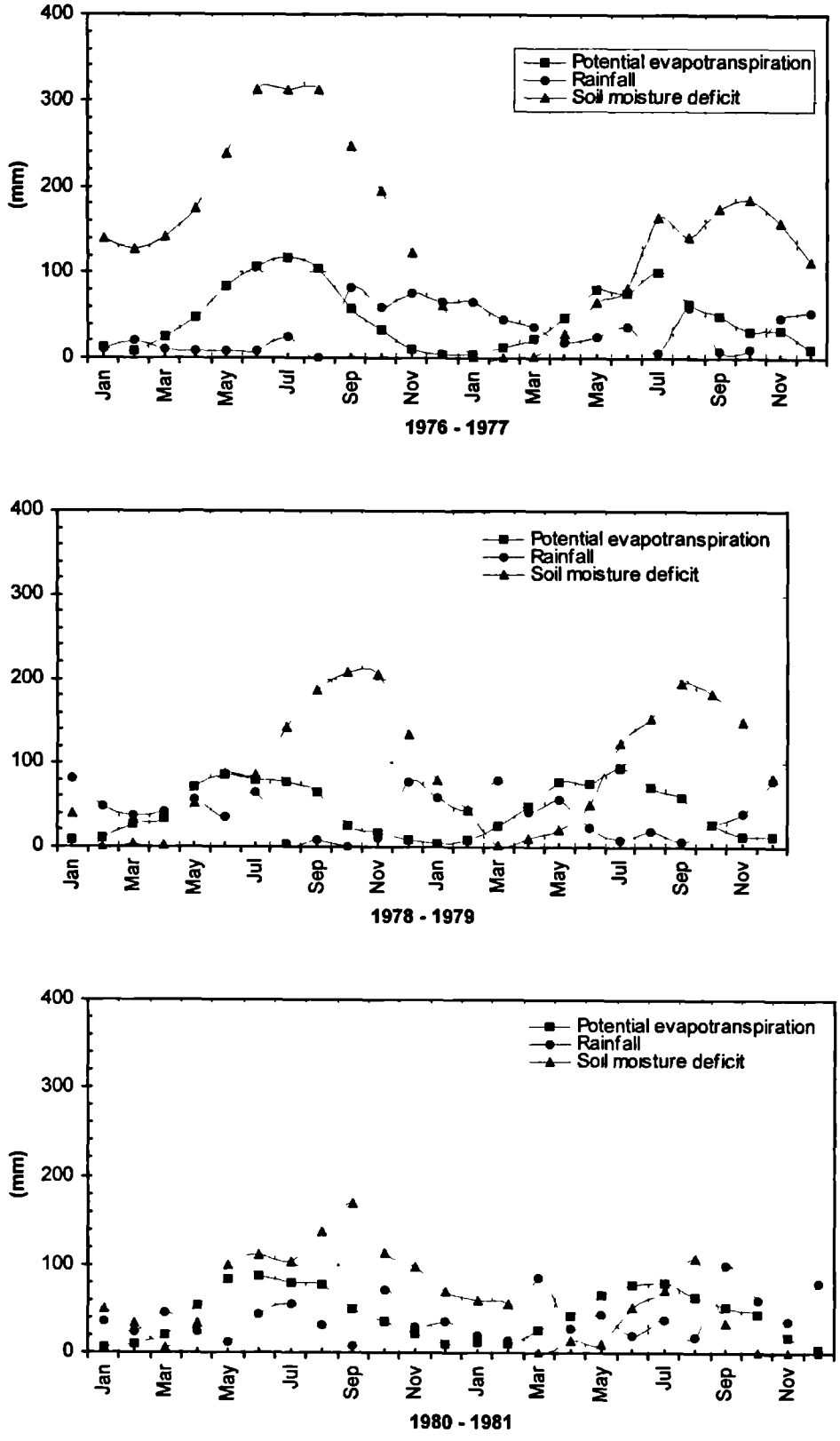

Figure 5.13b Meteorological data for Chattenden site

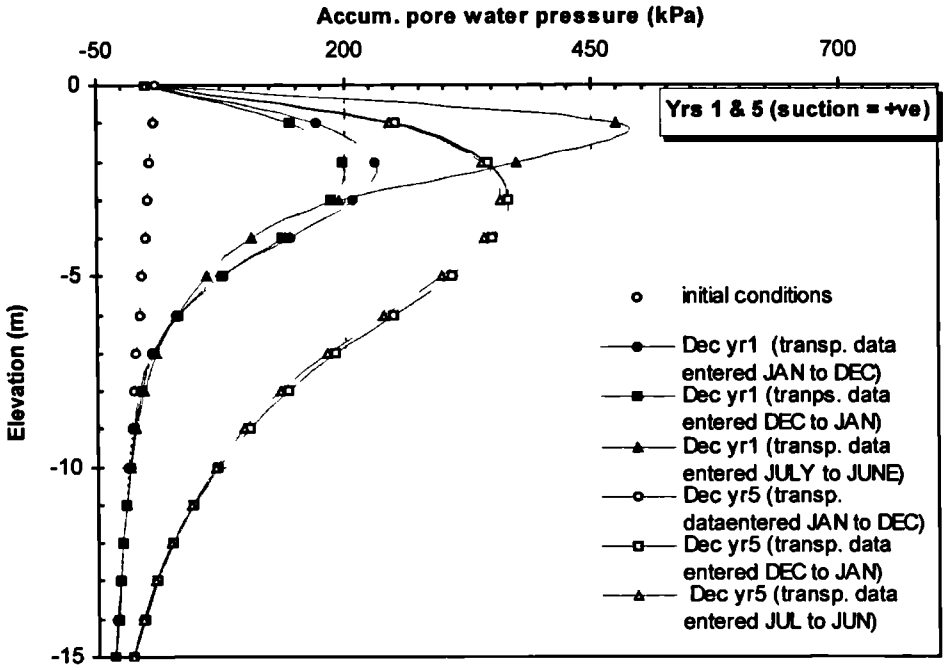

Figure 5.14a Influence of meteorological data on prediction of pore water pressures after 1 yr and 5 yrs.

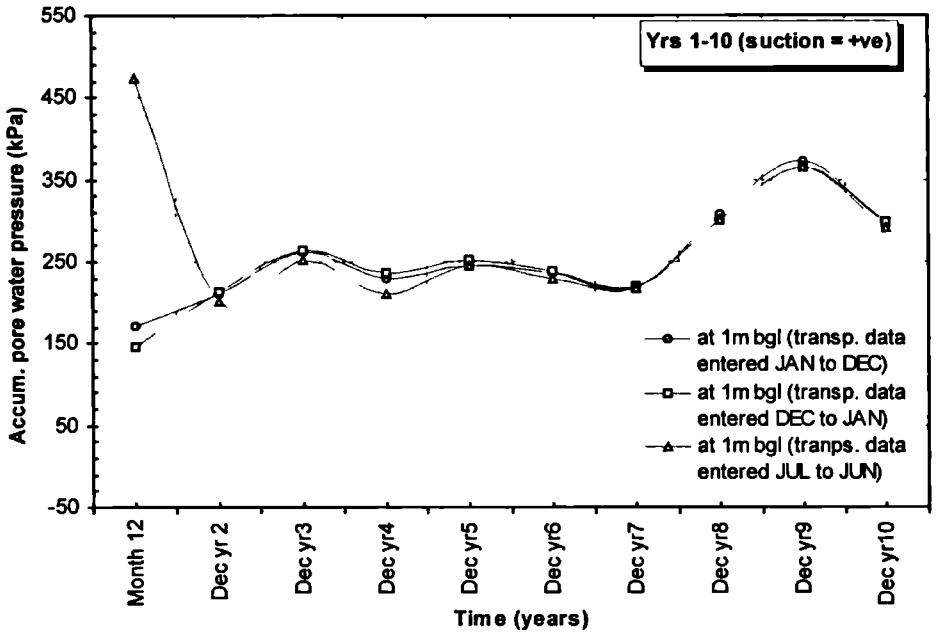

Figure 5.14b Influence of meteorological data on prediction of pore water pressures during the first 10yrs.

The predictions for sub-accumulated vertical ground movements along the centreline after 1 and 5 years are shown in Figure 5.15a. In general, the figure reveals that the difference in prediction which occurred in the first year in case 3 does not recover in the long term. Figure 5 15b shows the predictions for vertical movements at ground level and 1m depth throughout the 10 year period.

The latter figure shows that the difference in prediction becomes smaller at deeper horizons; which is consistent with the pattern of pore water pressure change in Figure 5.14b.

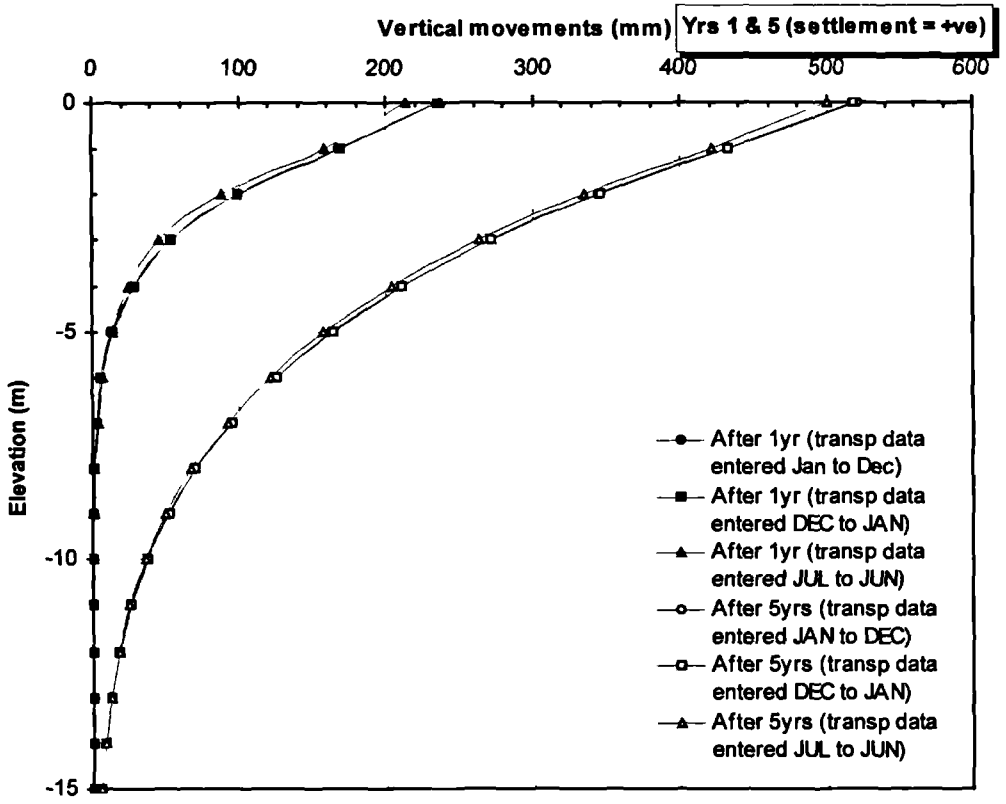

Figure 5.15a Influence of meteorological data on prediction of sub-accumulated vertical movements at ground level and 1m depth after 1yr and 5yrs.

The results of this study reveal the strong influence of the pattern of rainfall and potential evapotranspiration on prediction of pore water pressures and movements using the RWUM. It has been shown that during the first year when the distribution of potential evapotranspiration among the three cases are different, the predictions of pore water pressures and movements are also different. For case 1 (potential evapotranspiration data entered Jan to Dec) and case 2 (potential evapotranspiration data entered Dec to Jan), the distribution patterns are similar, ie. the data commences and ends during winter, with summer sandwiched in between. As a result, the resultant pore water pressures and movements at the end of 12 months are similar. For case 3, the data set commenced at peak summer (July) and ended at peak summer (June), with winter sandwiched in between. The resultant distribution of pore water pressures and movements are quite different.

The analyses have also shown that in the medium to long term when the potential evapotranspiration data was identical for all three cases (except for the first year), the predictions of pore water pressure changes and movements for each year were similar. With time, the predictions

of accumulated pore water pressures more or less became equal for all three cases whereas the predictions for movements revealed that the difference that occurred during the first year was never recovered as time progressed.

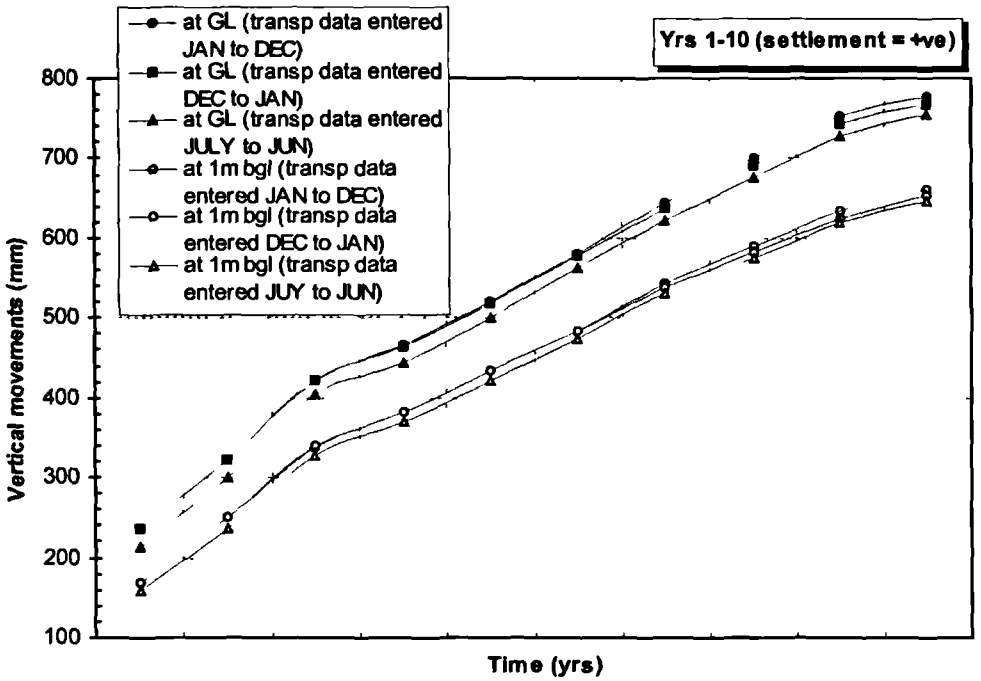

Figure 5.15b Influence of meteorological data on prediction of sub-accumulated vertical movements at ground level and 1m depth during the first 10 years.

These results suggest that the predictions of pore water pressures and movements are dependent on the magnitude of the meteorological input data. Therefore special care needs to be taken when assessing the frequency and distribution of meteorological input data in boundary value problems as this directly affects the predictions of accumulated values eg. pore water pressures and movements.

5.5.3 Influence of maximum root depth

5.5.3.1 Introduction

The root water uptake model coded in ICFEP assumes a linear distribution of potential transpiration over the whole root depth. The function becomes nonlinear when coupled with the α function. The maximum root depth defines the zone in which nodal flows are occurring, as computed from the integration points. Therefore, the maximum depth of the root zone assumed in the RWUM is likely to have an influence on the depth where the majority of pore water pressure changes occur. The

influence of the maximum root depth, r_{max}, on the predictions by the RWUM was investigated and the results are presented below.

5.5.3.2 Numerical model & assumptions

The stratigraphy, mesh, soil parameters, meteorological data and constitutive modelling were as described in Section 5.5.2. The meteorological data was input as per case 1 in Table 5.2. The vegetation boundary condition was input using the α function described in Section 5.5.2.4 with maximum root depths of 2m, 2.5m and 3m.

5.5.3.3 Results and discussion

The pertinent results were considered to comprise changes in pore water pressure, minimum total stress, σ_3 and vertical movements.

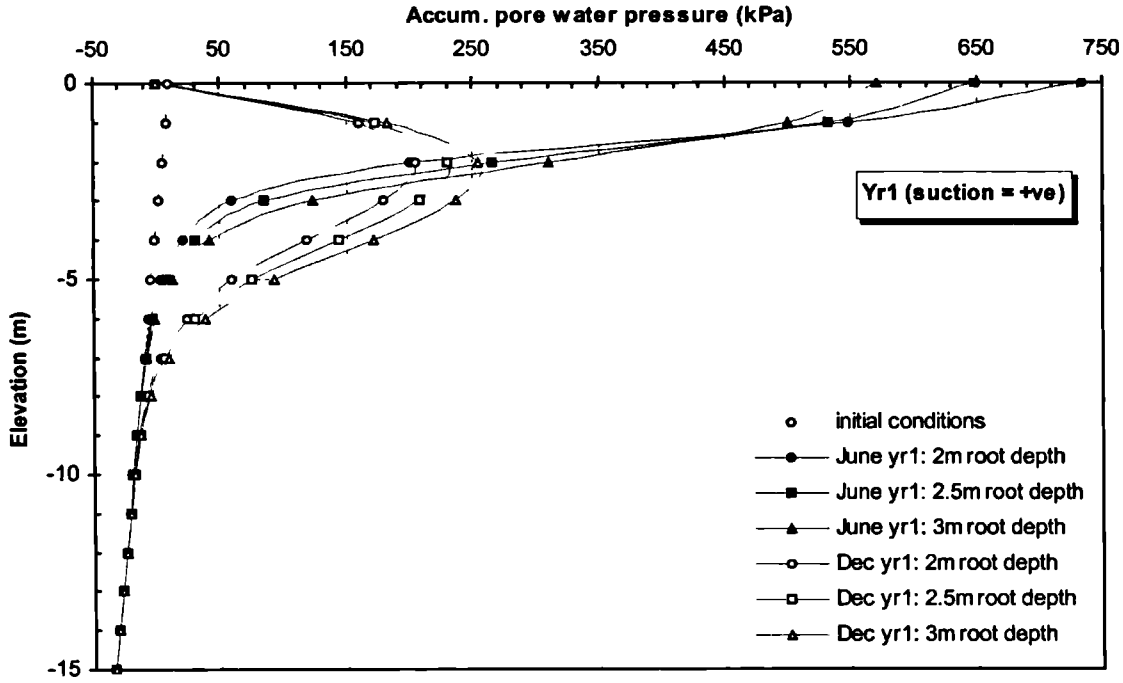

Figure 5.16a Influence of r_{max} on accumulated pore water pressures during yr 1.

Figure 5.16a shows the accumulated pore water pressures at the end of June and December of the first year. The figure reveals that during periods of peak evapotranspiration (eg. June) the highest suctions at very shallow depth (less than 1.3m) occur in the analysis involving a maximum root depth, r_{max}, of 2m. At ground level, the maximum suctions predicted during June are 730kPa, 650kPa and 570kPa for maximum root depths of 2m, 2.5m and 3m, respectively.

The pattern of pore water pressure predictions below 1.3m depth are however different. It can be seen that at this relatively deeper horizon, the maximum suctions are associated with the largest maximum root depth eg. at 2m depth, the maximum suctions predicted by maximum root depths of 2m, 2.5m and 3m are 200kPa, 265kPa and 310kPa, respectively.

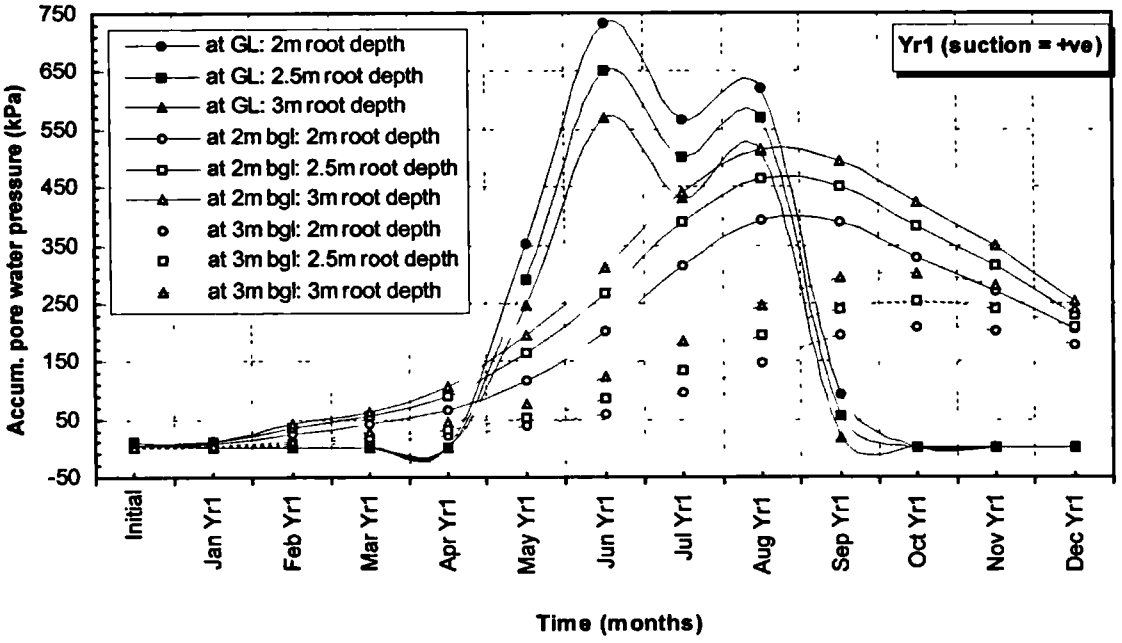

Figure 5.16b Influence of r_{max} on accumulated pore water pressures at ground level, 2m and 3m depths.

Figure 5.16b depicts the predicted monthly accumulated pore water pressures at ground level, 2m depth and 3m depths. The figure corroborates the trend identified in Figure 5.16a concerning the dependency of pore water pressure predictions on the magnitude of r_{max} assumed in the RWUM. Once again, it can be seen that at shallow depth throughout the 12 months (ground level plot in Figure 5.16b) the largest maximum suctions are associated with the smallest r_{max}. The reverse scenario occurs at deeper horizons (predictions at 2m and 3m depths in Figure 5.16b).

Figure 5.16c shows the pore water pressure changes occurring during the periods June-September and September-December. The figure further confirms the overall pore water pressure pattern identified in Figure 5.16a and the observation that the depth over which pore water pressure changes occur is approximately equal, for the 3 values of r_{max}. Since all other input data was

identical for the three analyses, the differences in pore water pressures are a reflection of the impact of the root zone on pore water pressure prediction.

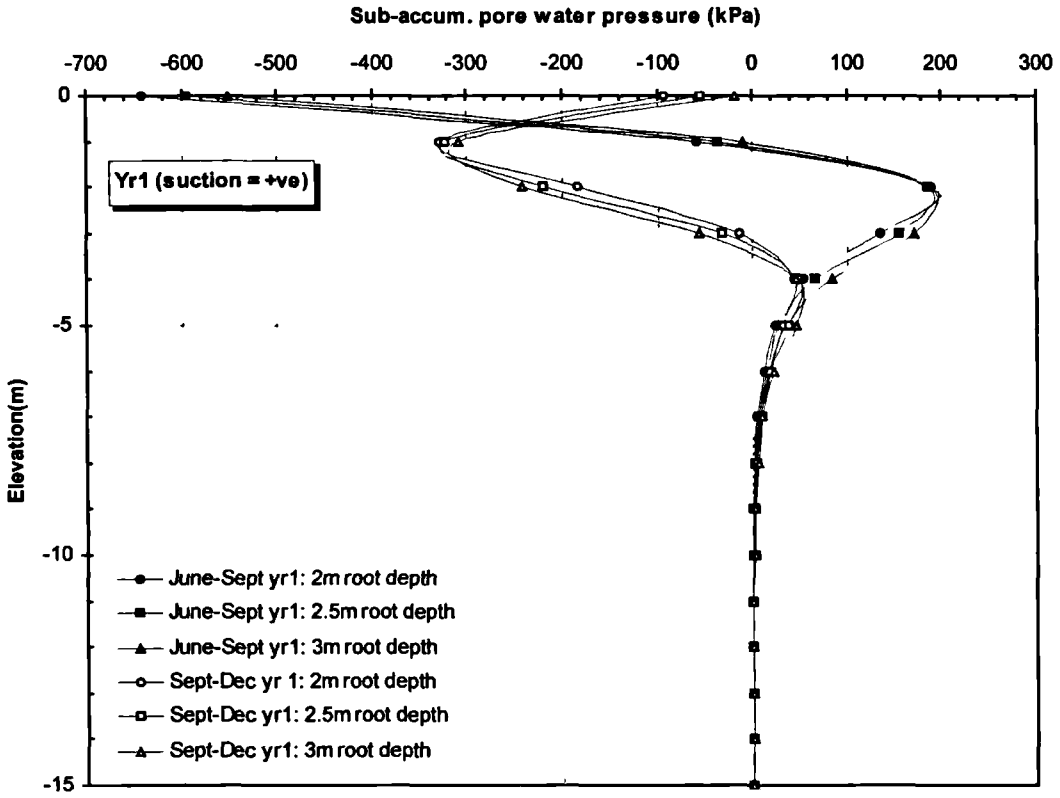

Figure 5.16c Prediction of pore water pressures changes in June & December of yr1 using the RWUM.

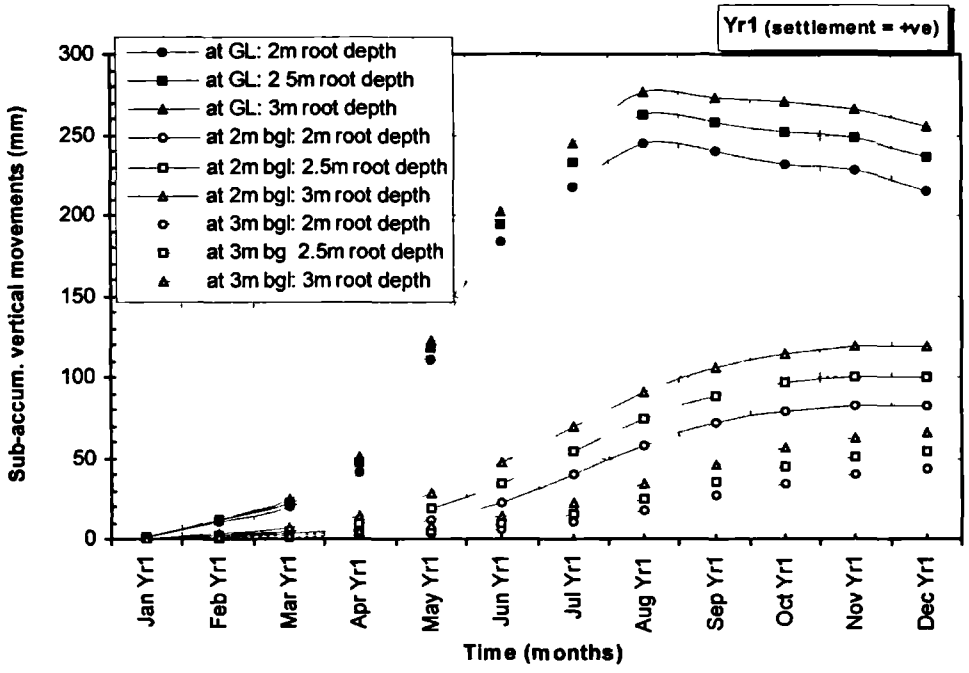

Figure 5.17a Influence of r_{max} on prediction of sub-accumulated vertical movements at ground level, 2m bgl and 3m bgl.

The vertical movements that occur during application of the RWUM (ie. sub-accumulated from, when the RWUM is first invoked) are shown in Figure 5.17a. The overall movements at the end of the 12 months comprise settlement, which is in line with the gradually development of a desiccated profile identified in Figure 5.16.

It can be seen from Figure 5.17a that the magnitude of movements are dependent on the magnitude of r_{max} eg. at the end of December, the predicted sub-accumulated vertical movements are 215mm, 235mm and 255mm for r_{max} values of 2m, 2.5m and 3m, respectively. The overall trend during the 12 months suggests that the larger the r_{max} value, the larger the sub-accumulated movements. This trend is in line with the observed global pattern of accumulated pore water pressures at depth identified earlier in Figure 5.16. There is therefore evidence that all other things being equal, large values of r_{max} yield higher values of actual transpiration. This is so because the nodes at deeper horizons for a large r_{max} are initially at relatively higher compressive pore water pressures, which in turn yields higher α values (N.B. initial conditions assumed the phreatic surface at 1m depth).

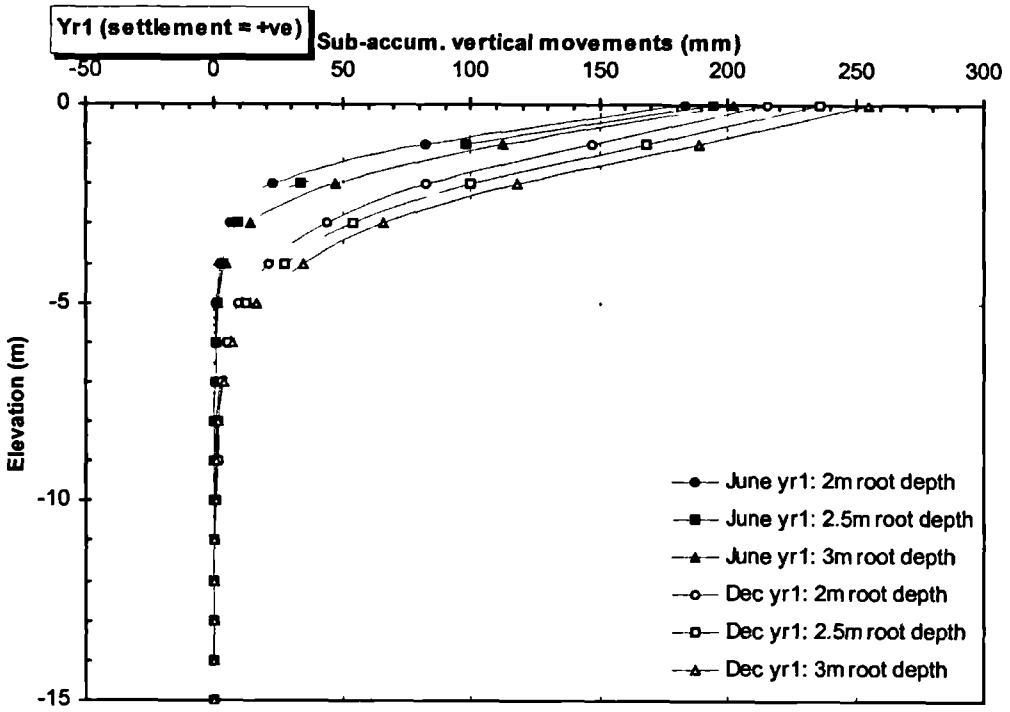

Figure 5.17b Influence of r_{max} on prediction of sub-accumulated vertical movements after 6 months and 12 months.

The sub-accumulated vertical movements (since inception of the WRUM) along a vertical profile through the soil are shown in Figure 5.17b at the end of June and December. The dependency of

the magnitude of movements on r_{max} is clearly obvious. It is also noteworthy that the overall depth over which movements occur by the end of December (7m) matches the depth over which pore water pressure changes occur (Figure 5.16a).

Another facet to consider is the magnitude of the minor principal total stress, σ_3, which in the desiccated zone governs the depth of potential desiccation cracks. In the field, desiccation cracks develop when the tensile strength of the soil is exceeded. Figure 5.18 shows the predictions of σ_3 in June and December for the three values of r_{max}. With reference to Figure 5.18, it is interesting to note that although the overall depth in which positive (tensile) values of σ_3 are predicted is dependent on the value of r_{max}, the difference among the 3 predictions is small eg. at the end of June, tensile values of σ_3 are predicted to 2.9m, 3m and 3.2m by r_{max} values of 2m, 2.5m and 3m, respectively. In the field, the depth over which the majority of roots play an active role in root water uptake is likely to average 2-3m. This would equate to the results of this sensitivity study involving r_{max} values of 2m, 2.5m and 3m. The predictions of σ_3 would therefore suggest that under field conditions, the depth of desiccation cracks is dependent more on the magnitude of the actual transpiration rather than r_{max}.

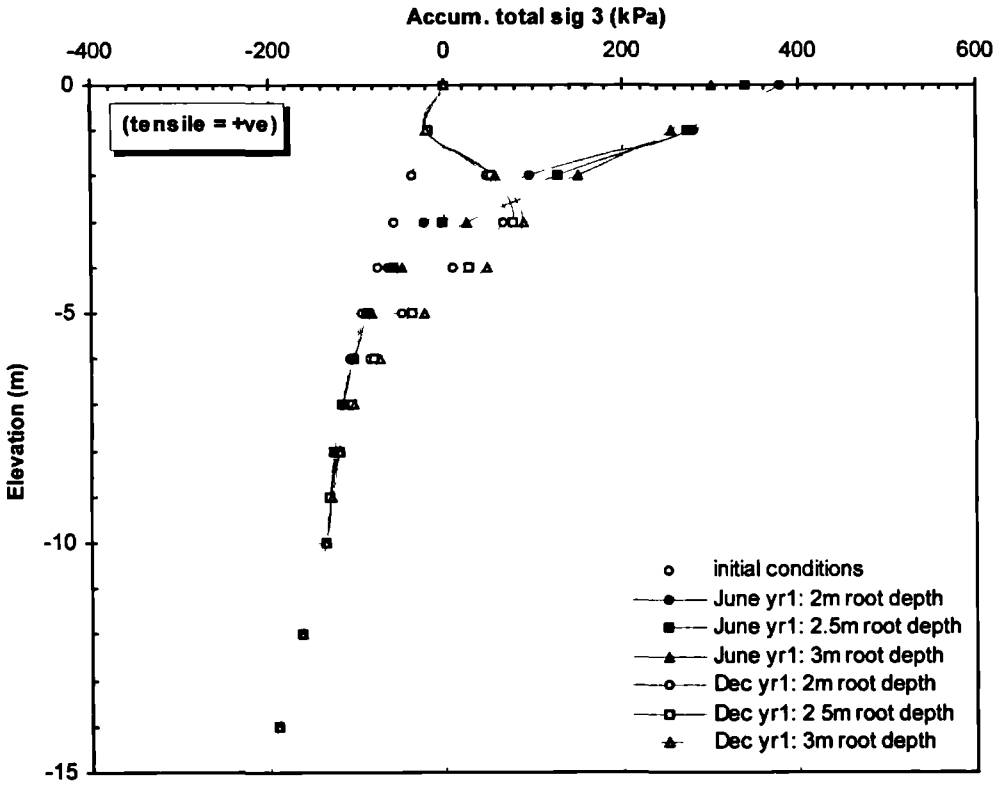

Figure 5.18 Influence of r_{max} prediction of total minor principal stress (σ_3) during yr1

5.5.4 Sensitivity of α function to S3 value

5.5.4.1 Introduction

The role played by the α function (see Figure 5.2) in the computation of actual transpiration from potential transpiration was described in detail in Section 5.4.3. With reference to Figure 5.2, the pore water pressures at which anaerobiosis conditions (S1), field capacity (S2) and permanent wilting point (S4) are generally accepted to be approximately 0kPa, 5kPa and 1500kPa, respectively. S3 marks the magnitude of soil suctions after which root water uptake significantly reduces ie. the magnitude of soil suctions significantly reduces the rate of water uptake by the roots, in response to the transpiration demand in the leaves.

The magnitude of soil suction at which plants begin to show signs of physiological stress as a result of their inability to extract water at a fast enough rate to match the transpiration demand (magnitude of S3 in this model) is thought to be species dependent. This view is corroborated by the existence of drought resistant plants, which are capable of tolerating very high soil suctions. Nevertheless, research by agro-scientists suggests a value of 50kPa to be applicable for most crops eg. Feddes *et al* (1976) and Hoogland *et al* (1978).

For deciduous trees under readily available moisture, data on root suctions by Moore *et al* (1995) suggests the value of S3 to be as high as 200kPa. The latter value is also used in MORECS for all vegetation types. In view of the uncertainty regarding the value of S3 to use in analyses, it was considered necessary to investigate the influence of S3 on the predictions by the coded RWUM.

5.5.4.2 Numerical model & assumptions

The stratigraphy, mesh, soil parameters, meteorological data and constitutive modelling were as described in Section 5.5.2. The meteorological data was input as per case 1 in Table 5.2. The vegetation boundary condition was input assuming a 2.5m root depth in all cases and an α function with S3 values of 50kPa, 100kPa, 200kPa and 400kPa.

5.5.4.3 Results and discussion

The pertinent results were considered to be comparisons of changes in pore water pressure, minimum total stress, σ_3 and vertical movements involving the 4 values of S3.

The prediction of the pore water pressure changes occurring during the periods June to September and September to December of the first 12 months are shown in Figure 5.19a. The figure reveals that the overall depth over which pore water pressure changes occur is approximately equal for all the values of S3 (8m depth). Nevertheless, the predictions of pore water pressures at intermediate depths significantly differs for high magnitudes of S3. The overall trend shows increasing suctions as the magnitude of S3 increases. The reason for this is that a large S3 value implies a wider range over which optimum actual transpiration occurs (ie. the suction range at which α is nearly unity, in Equation 5.8 eg. the predictions for pore water pressure changes at 2m depth during the period June to September of the first year (Figure 5.19a and Table 5.3).

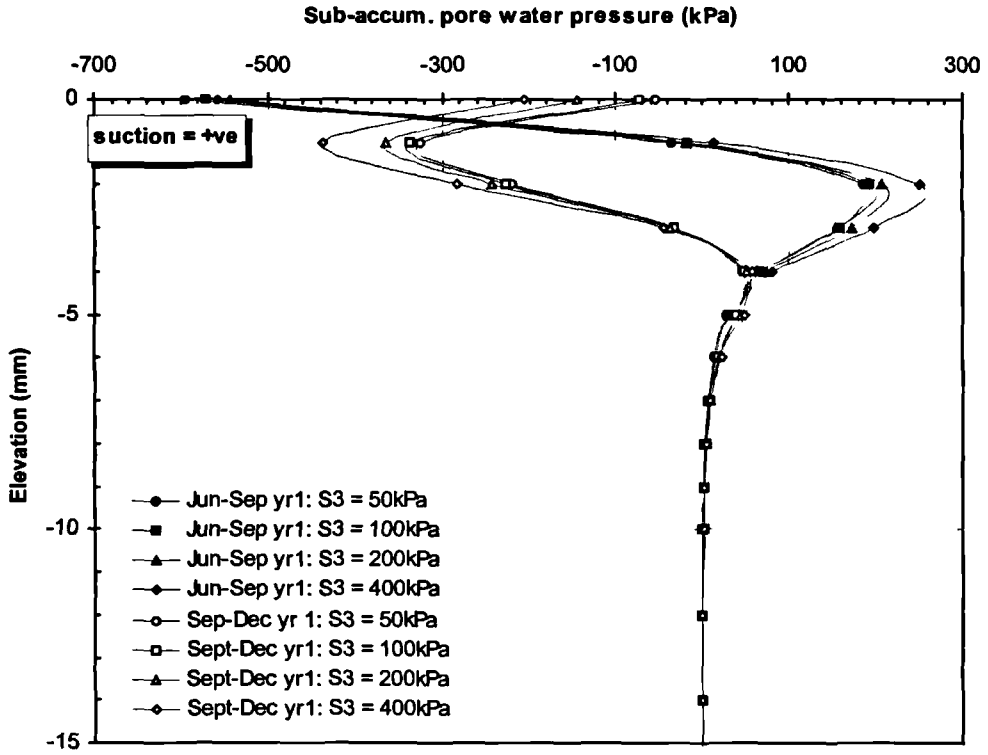

Figure 5.19a Influence of S3 on prediction of sub-accum. pore water pressures during yr1.

Table 5.3 Pore water pressure changes predicted at 2m depth

S3 value (kPa)	June - Sept of yr 1 (kPa)	% Increase
50	190	datum
100	200	5
200	215	13
400	260	37

In the table, the prediction involving an S3 of 50kPa has been taken as datum to compute the relative differences. It is evident that although the value of S3 is doubled in each case, the corresponding increase in the predictions of pore water pressure changes is initially small. This is not surprising when the gradient, $\frac{\partial \alpha}{\partial P_w}$, between points S3 and S4 (see Figure 5.2) is considered. It can be seen from Figure 5.2 that $\frac{\partial \alpha}{\partial P_w}$ increases as S3 increases; which is mirrored by the pattern in Table 5.3.

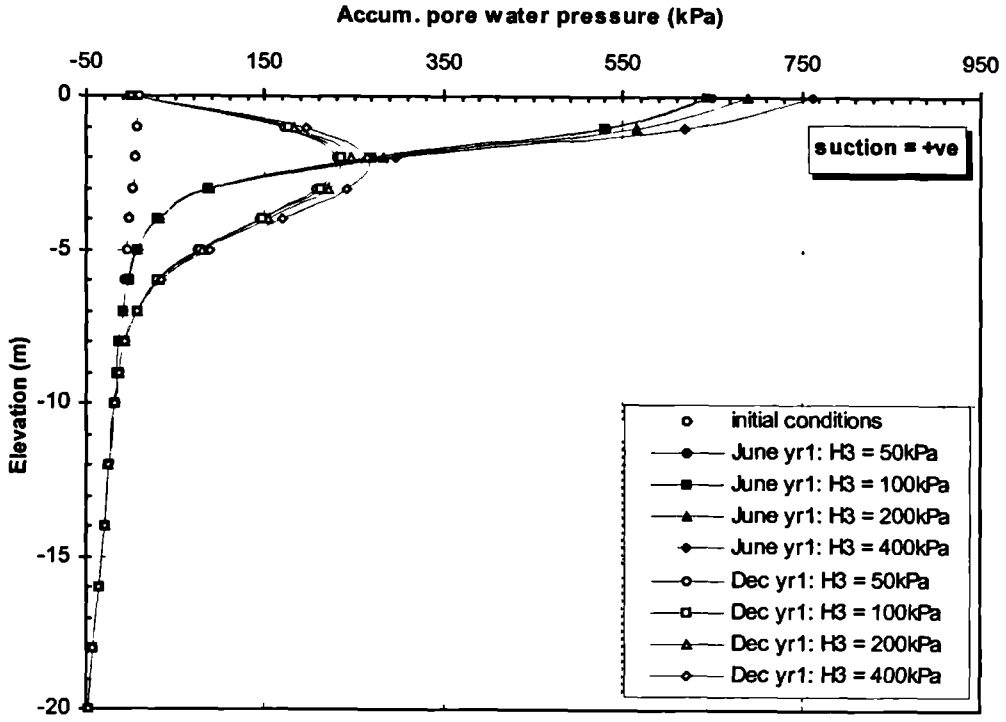

Figure 5.19b Influence of S3 on prediction of accumulated pore water pressures during yr1.

Figure 5.19b shows the accumulated pore water pressures at the end of June and December of the first year. The initial conditions are shown for comparison. It can be seen that there is only a minor difference in pore water pressure predictions between S3 values of 50kPa and 100kPa. However, as the value of S3 further increases beyond 100, differences in predictions of pore water pressures begin to emerge eg. the pore water pressure at ground level at the end of the 6 month for S3 values of 50kPa and 100kPa are 650kPa, compared to 690kPa (S3 = 200kPa) and 715kPa (S3 = 400kPa). This represents percentage increases of 6% and 10% for the latter two scenarios.

The predictions of vertical movements by the four α functions during application of the RWUM (sub-accumulated movements from increment 20 when the RWUM is invoked) are shown in Figure 5.19c. The overall pattern suggests decreasing magnitude of movements with depth, which is reasonable. The figure shows the sub-accumulated movements at the end of 6 months (June) and 12 months (December). There is evidence that in the long-term, the difference in predictions by the four α functions increases eg. it can be seen from the figure that at the end of the first 6 months, there are nominal differences in the predictions of vertical movements whereas at the end of 12 months, differences are discernible.

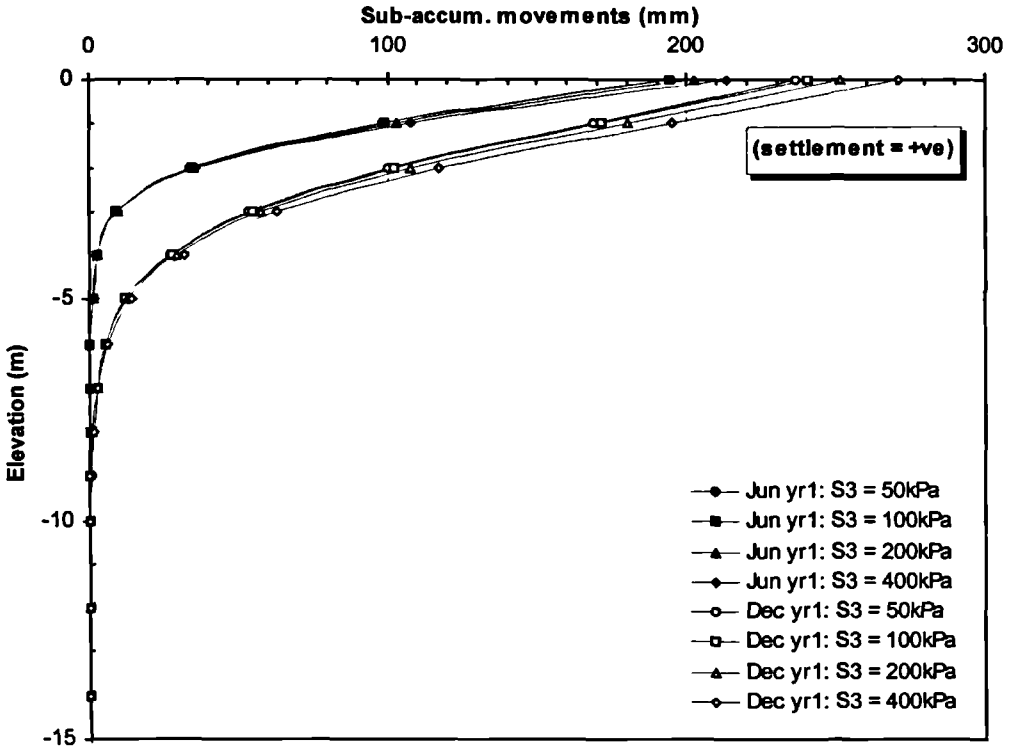

Figure 5.19c Influence of S3 on prediction of sub-accumulated vertical movements during yr1

Figure 5.20a shows the accumulated pore water pressures in December at the end of 10 and 20 years. The corresponding vertical movements for these periods are shown in Figure 5.20b. The figures confirm the divergence in predictions involving the various values of S3 values used in the α function, notwithstanding that the predictions involving S3 values of 50kPa and 100kPa are similar. This fact is mirrored by Table 5.4 which summarises the differences in pore water pressure predictions at 5m depth after 10 yrs and 20 yrs. In Table 5.4, the predictions involving an S3 value of 50kPa have been taken as datum to compute the relative differences in predictions. A similar pattern to that shown in Table 5.4 is depicted in the predictions for vertical movements (Figure 5.20b).

Table 5.4 Pore water pressure predictions at 5m depth

S3 value (kPa)	After 10 years (kPa)	% Increase	After 20 years (kPa)	% Increase
50	450	datum	545	datum
100	450	0	555	2
200	470	4	590	8
400	525	17	650	19

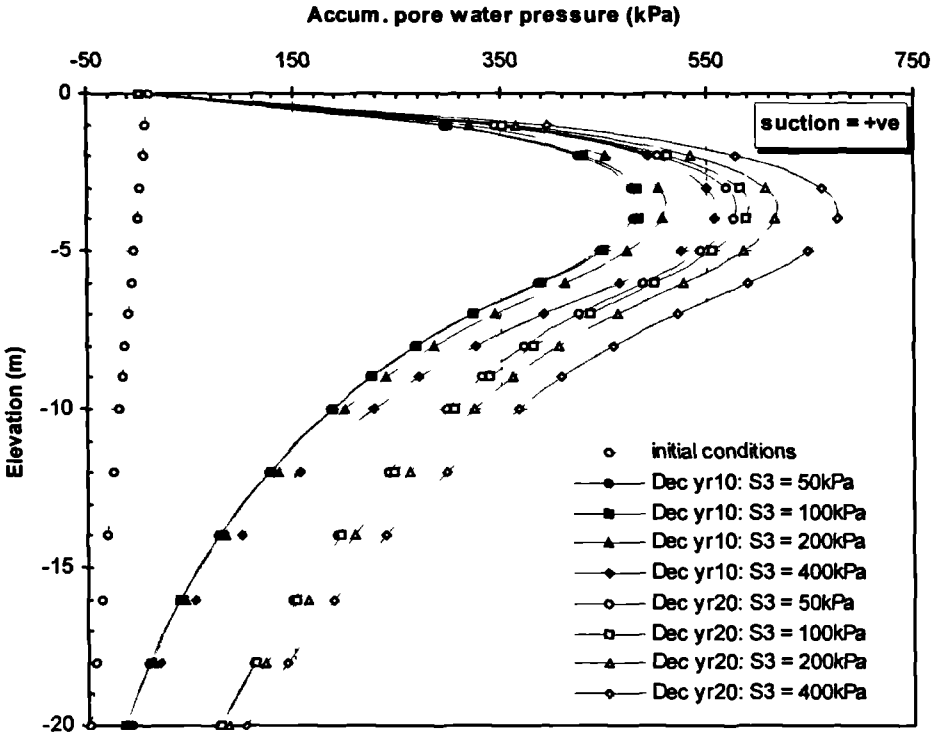

Figure 5.20a Influence of S3 on prediction of pore water pressures after 10yrs and 20yrs

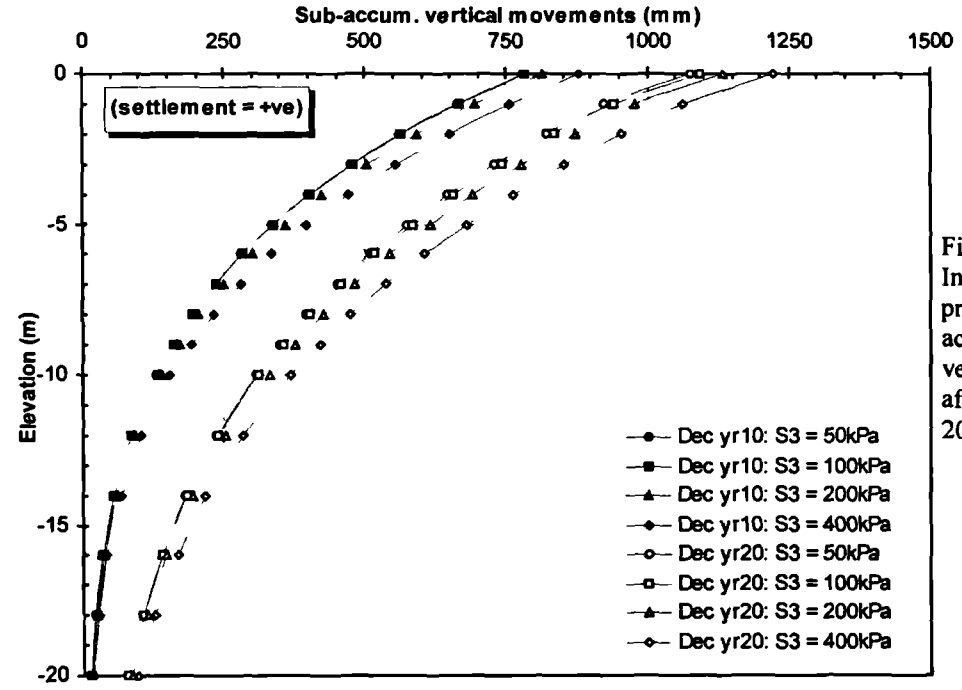

Figure 5.20b Influence of S3 on prediction of sub-accumulated vertical movements after 10yrs and 20yrs.

5.5.5 Influence of permeability model

5.5.5.1 Introduction

An important aspect of a new flow boundary condition in a geotechnical numerical algorithm is its interaction with routinely used permeability models. This is especially important for dissemination purposes, to enable geotechnical practitioners understand the pros and cons of using the new flow boundary condition. This section discusses the analyses that were carried out to investigate this issue.

In the first tranche of sensitivity analyses, the response of the RWUM to three permeability models was considered ie. homogeneous, inhomogeneous and a model in which permeability is a function of mean effective stress, p', using a power law relationship (Vaughan, 1994). The first two models prescribe the value(s) of the coefficient of permeability, k, which are maintained throughout the analysis. The latter model updates the k values during the analysis, using a non-linear algorithm to track the k value over an increment, as p' varies.

For most natural stiff clay deposits, it has been observed that field vertical permeability can be more accurately modelled using a permeability model dependent on p' (Vaughan, 1987). This reproduces the reduction in vertical permeability at depth that has been observed in the field; which is a step forward from using a homogeneous permeability model.

Although the reduction in permeability with depth can be simulated using an inhomogeneous model, its capabilities are limited. The major drawback is that the permeability profile is defined by the user at the beginning of an analysis and does not change during the analysis. When p' changes during the analysis, the permeability model does not update the permeability values accordingly.

In the UK, the homogeneous and inhomogeneous models are widely used in industry while the p' dependent model is more sophisticated and is mainly restricted to use by research institutions.

5.5.5.2 Numerical model & assumptions

The stratigraphy, mesh, initialisation of pore water pressures, constitutive modelling and vegetation boundary condition were as described in Section 5.5.2.2. The meteorological data was input sequentially from January to December throughout as per case 1 (Table 5.2). The permeability

values assumed for the London Clay are shown in Table 5.5. All the strata underlying the London Clay were assumed to have a homogeneous permeability with values shown in Table 5.1.

Table 5.5 Permeability values used in analyses

Permeability model	Value of k
homogeneous permeability	$k = 2\times10^{-10}$ m/sec
inhomogeneous permeability	$k = k_0 - mz$ m/sec where $m = 0.0063115$, z is the depth below top of the stratum and $k_0 = 2\times10^{-10}$ m/sec
Nonlinear permeability dependent on mean effective stress, p'	$k = k_0 e^{-ap'}$ m/sec where $k_0 = 2\times10^{-10}$ m/sec and $a = 0.0075$

5.5.5.3 Results and discussion

The results for pore water pressure changes and movements during application of the RWUM were considered in two parts - short and medium term (after 1 and 5 years) and in the long-term (after 10 and 20 years). In all cases, the results at the end of December were used to produce the plots, which corresponds to UK winter conditions.

The initial pore water pressure profiles for the three permeability models after 5000 years of pore water pressure stabilisation are shown in Figure 5.9 while Figure 5.21 shows plots of initial vertical permeability for the three models. As can be seen from the pore water pressure plots, the uniform permeability profile indicates the least compressive pressures over the depth shown; in response to the underdrainage in the chalk aquifer during the 5000 years. The actual field profile is believed to be close to the profile where permeability is a function of mean effective stress.

(i) <u>short and medium term</u>

Figure 5.22a shows the accumulated pore water pressures at the end of the 1st and 5th years during December (winter). From the figure, it can be seen that at shallow depth (less than 2.5m) the suctions predicted by the homogeneous and inhomogeneous permeability models are much lower (typically 370kPa) compared to those predicted by the model where permeability depends on p' (typically 1120kPa). The homogeneous and inhomogeneous models are therefore performing better

than the p' dependent model in predicting pore water pressure recovery during winter at shallow depth; notwithstanding that all the three models are predicting higher suctions than have been observed in the field during winter (Biddle, 1998). In general, the depth of maximum suction is greater for the uniform and inhomogeneous models (ie. 2-4m) compared to predictions using a permeability model dependent on p' (ie. 1m).

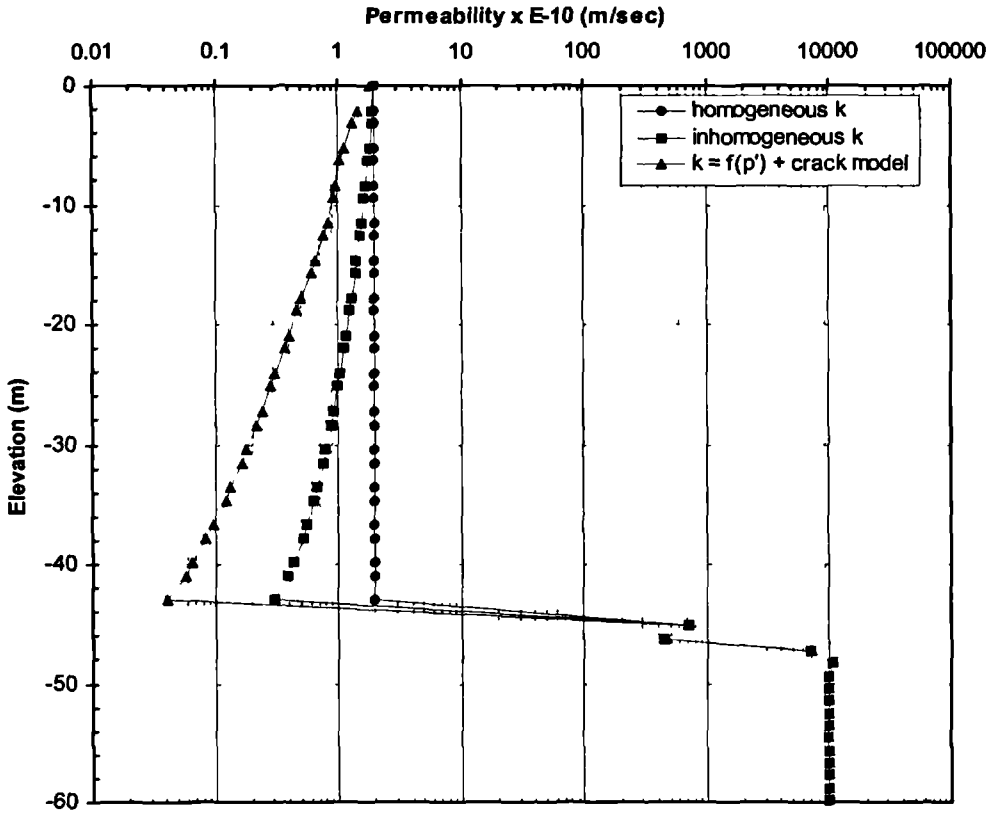

Figure 5.21 Permeability profiles at the commencement of the RWUM.

It can also be seen from Figure 5.22a that the depth and magnitude of the desiccated profile increases significantly during the 5 year period. There is no evidence from the meteorological data to suggest that this period was characterised by exceptionally dry periods (see meteorological data in Figure 5.13). The gradual increase in the desiccated profile with time is therefore considered not to be a true manifestation of field behaviour, but an inability of the permeability models to reproduce desiccation cracking. The phenomenon of cracking and its influence on permeability is discussed in more detail later in Section 5.5.5.4.

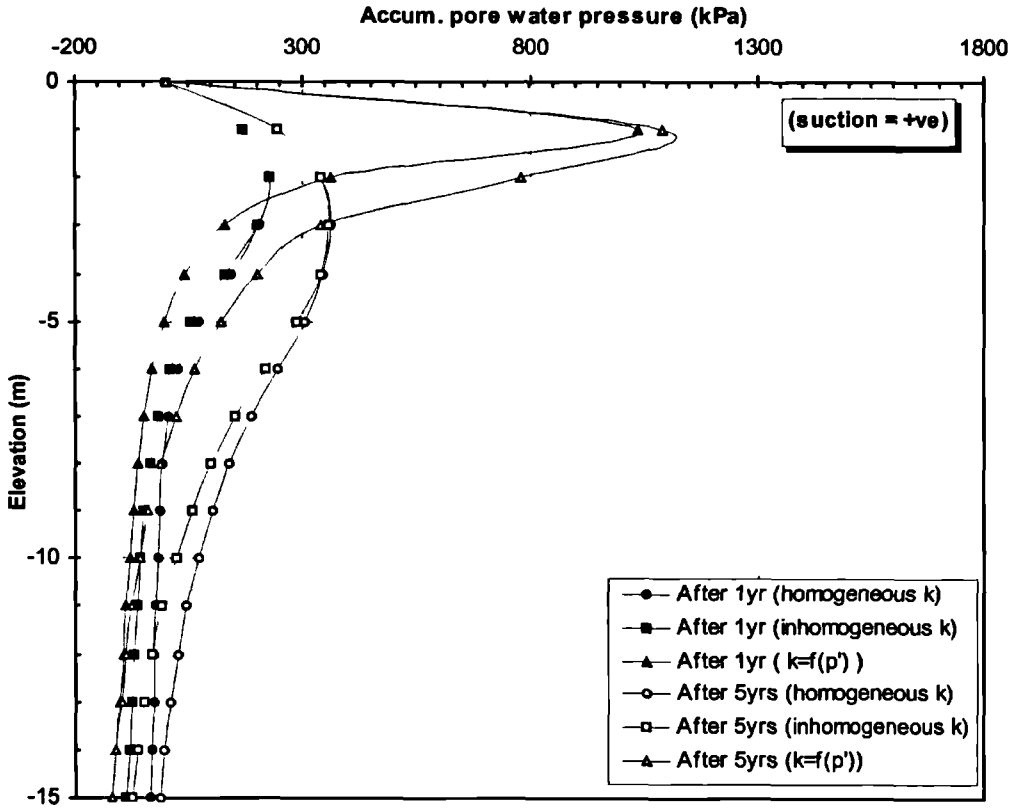

Figure 5.22a Influence of permeability on prediction of accumulated pore water pressures after 1yr and 5yrs.

Another feature discernible in Figure 5.22a is that the least changes in pore water pressure at deeper horizons occur where permeability is a function of p' eg. for the uniform and inhomogeneous permeability models, the accumulated pore water pressures increase by up to 120kPa at 10m depth compared to approximately 20kPa in the case where permeability is a function of p'. After 5 years, the uniform and inhomogeneous models predict desiccated profiles to 14m and 11m depths, respectively; which are much higher than have been observed in the field eg. Biddle (1998) and Crilly and Driscoll (2000). The corresponding predictions by the p' dependent permeability model is a desiccated profile to 8m depth. The latter model is therefore performing much better in limiting the depth of the desiccated profile at deeper horizons, which accords with field behaviour.

From Figure 5.22a it can also be seen that the maximum suctions after 1 year for the homogeneous and inhomogeneous models are of the same order of magnitude (approx. 230kPa). At the end of 5 years, the pore water pressure predictions are similar in the top 5m (max. suction of approx. 360kPa). This is not surprising because the values of vertical permeability are initially similar and only significantly differ at greater depths. Nevertheless, it is important to note that during the 4

year period from (December year 1 to December year 5) maximum suctions increase by 50% (ie. 230kPa to 360kPa). The position of maximum suctions also lowers by 1m. The equivalent scenario for the permeability model dependent on p' shows an increase in maximum suctions of less than 10% (1040kPa to 1120kPa); with no lowering of the depth of maximum suction (still at 1m below ground level).

The results indicate that where permeability is a function of p', the very low permeabilities associated with high suctions from desiccation get "locked-in". This phenomenon comes about because at high suctions, a very low α function is associated with the RWUM. The knock on effect is that relatively less water is abstracted by the RWUM while at the same time, the very low permeability (associated with the high p' arising from the high suctions) results in very little infiltration from precipitation. The net effect is that once high suctions are mobilised, very little changes in pore water pressures subsequently occur in those regions when a permeability model dependent on p' is being used.

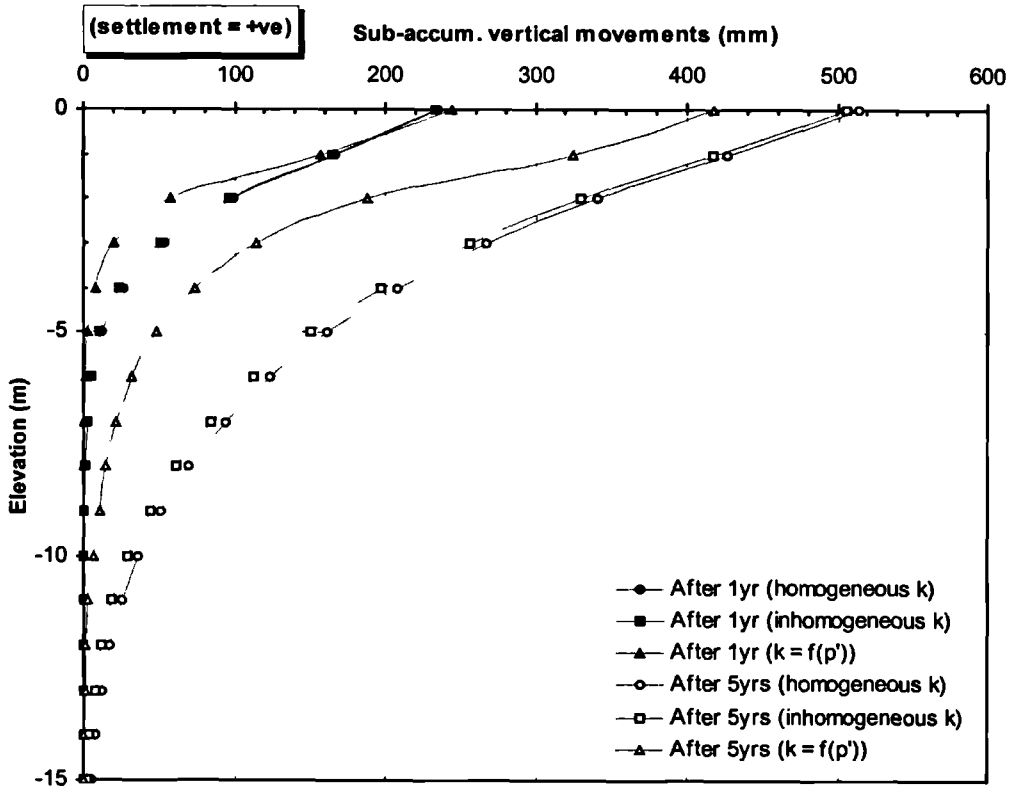

Figure 5.22b Influence of permeability on prediction of sub-accumulated vertical movements after 1yr and 5yrs.

It should also be reiterated that the plots in Figures 5.22a are December values; ie. towards end of winter when the degree of desiccation is greatly reduced. Recent tensiometer measurements at shallow depths (typically less than 2.5m) on London Clay fill embankments suggest end of winter suctions in treed areas of less than 50kPa (ICON, 2001). The magnitude of suctions on natural level ground, such as that modelled here, would be expected to be lower. The magnitude of suctions being predicted by the 3 models are therefore considered to be excessive.

Figure 5.22b depicts the vertical movements associated with the RWUM during the first 5 years. The magnitude of movements is initially similar at ground level at the end of the first year (240mm). However, the magnitude of the vertical movements significantly reduces with depth for the p' dependent permeability model compared to predictions using the homogeneous and inhomogeneous models. After 5 years, the difference is very large eg. at 3m depth, the homogeneous and inhomogeneous permeability models predict vertical movements of approx. 270mm compared to 120mm for a p' dependent permeability model.

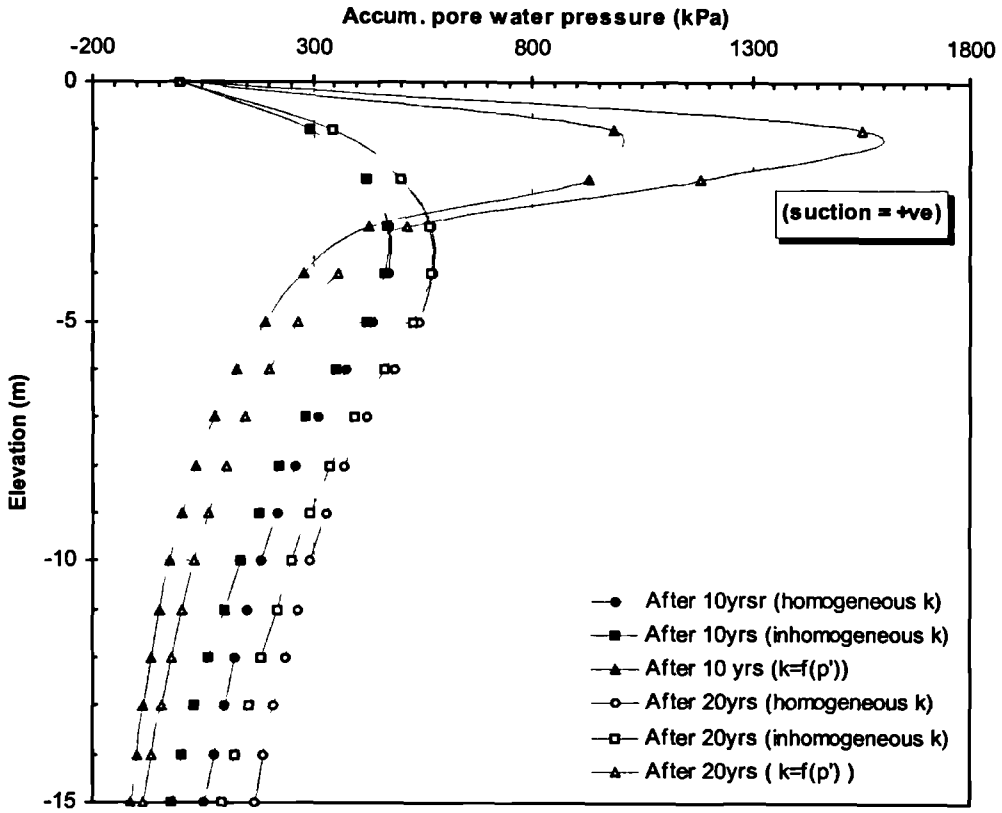

Figure 5.23a Influence of permeability on prediction of accumulated pore water pressures after 10yr and 20yrs.

(ii) Long-term

The predictions for accumulated pore water pressures since invokation of the RWUM after 10 and 20 years are shown in Figure 5.23a and reveal a trend similar to that identified for the short term scenario. A key observation is that after 20 years, the depth at which maximum suctions occur is still approximately the same as that observed after 5 years of application of the RWUM (Figure 5.22a). However, it is noteworthy that the pore water pressure distribution are epitomized by a gradually deepening of the phreatic surface as a result of redistribution of suctions to lower horizons eg. predictions by the p' dependent permeability model indicate that the overall depth of the desiccated zone increases from 9m depth at the end of 10 years to 11m after 20 years. The corresponding depths for the homogeneous and inhomogeneous models are deeper than 11m.

At shallow depth (less than 2m) although pore water pressures fully recover at ground level for all three permeability models, there has been a large build up of suctions below 0.25m depth. The pore water pressure predictions by the p' dependent permeability model suggest 1000kPa suctions at 1.0m depth after 10 years, which further increases to 1600kPa after 20 years ie. a 60% increase. The corresponding predictions at 1.0m depth by the homogeneous and inhomogeneous models are significantly less (ie. 290kPa after 10 years increasing to 350kPa, ie. a 20% increase).

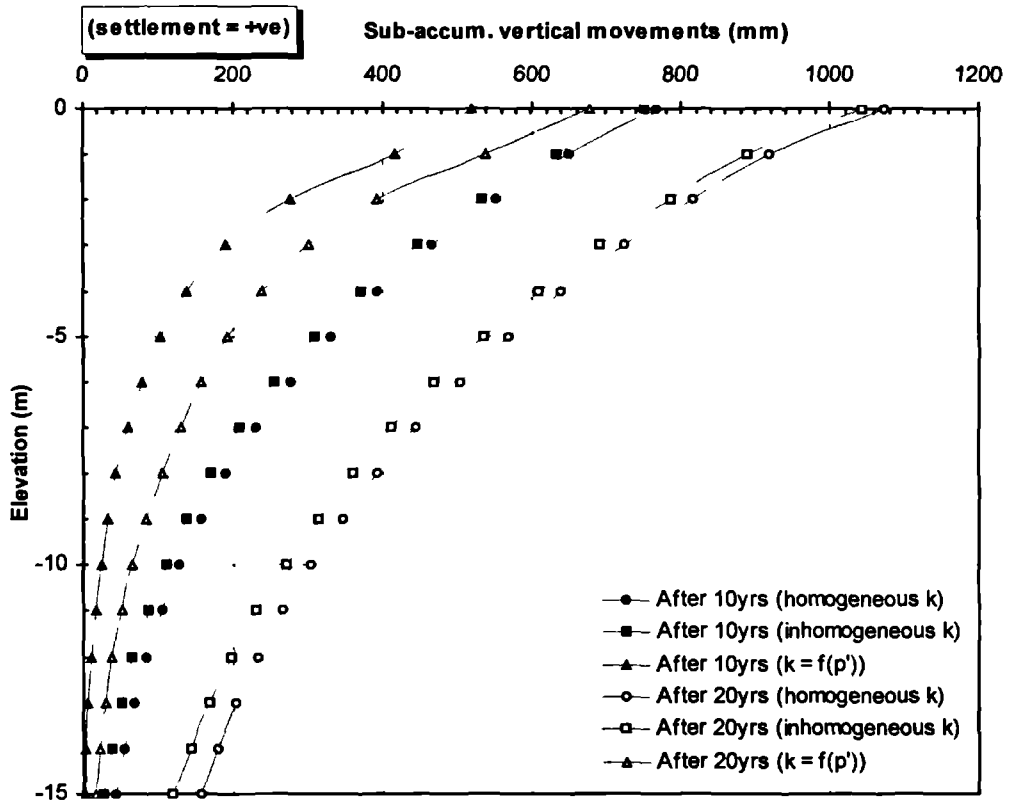

Figure 5.23b Influence of permeability on prediction of sub-accumulated vertical movements after 10yrs and 20yrs.

The corresponding sub-accumulated vertical movements since invokation of the RWUM are shown in Figure 5.23b. The large movements associated with the homogeneous and inhomogeneous permeability models are clearly depicted in this figure (eg. After 20 years they are 1070mm, 1040mm and 680mm for homogeneous, inhomogeneous and p' dependent permeability models, respectively).

5.5.5.4 Limitations of current permeability models

The foregoing results have revealed the deficiencies associated with the three permeability models to predict pore water pressure changes and ground movements using a RWUM. The homogeneous and inhomogeneous permeability models are incapable of tracking the change in permeability as p' changes seasonally. Compared to field measurements, all 3 models overpredict pore water pressure changes and ground movements at deeper horizons. Although the homogeneous and inhomogeneous models somewhat reproduce the observed behaviour of pore water pressure recovery at shallow depth during winter, the constant permeability associated with these models at greater depth limits their ability to fully reproduce the pore water pressure recovery that occurs in winter.

Overall, the results have reproduced the observed field pattern of pore water pressure changes on vegetated ground, ie. that the largest pore water pressure changes occur in the upper/shallow horizons. However, at shallow depth the p' dependent permeability model predicts high suctions during summer periods, which in turn yields very low permeability and inhibits the ingress of water, during precipitation. Therefore where desiccation plays a significant role in a boundary value problem, specification of permeability as a function of p', may result in erroneous predictions of pore water pressures in the vadose zone, whereas at deeper horizons, it performs satisfactorily.

Soils cannot sustain high tensile total stresses therefore desiccation cracks develop when the tensile strength of the soil is exceeded during drying. The presence of cracks significantly increases the mass permeability of the soil and this facilitates groundwater recharge in the cracked zone and strata just below this zone. This process is accompanied by relatively higher reductions in suctions compared to uncracked ground.

The influence of desiccation cracking on the mass permeability of a shrinkable soil has implications on the prediction of pore water pressure changes using a permeability model dependent on p'. The high mean effective stresses generated during drying will result in low permeabilities being

computed for elements within the desiccated zone and this in turn significantly reduces the amount of water that enters the soil during precipitation. Very large suctions in the desiccated zone are thus predicted by such type of permeability models; which is erroneous. Therefore although a p' dependent permeability model is efficacious in so far as tracking the permeability changes with mean effective stress is concerned, it cannot model the effects of desiccation cracking on permeability.

As discussed in Section 2.5.7 of Chapter 2, very little research has been carried out to understand crack initiation, propagation, its influence on permeability and numerical modelling thereof. As part of this research, some development work was carried to enhance the capabilities of a p' dependent permeability model for use in numerical analysis involving cracked ground. This development work is described in the following section.

5.5.5.5 Development of a smeared crack permeability model

In this thesis, a new smeared crack permeability model is used in conjunction with the p' dependent permeability model. The new model is only invoked in the zones where cracking is predicted to occur. The model does not model the initiation and propagation of individual cracks ie. a smeared approach is used in the zone where cracking is predicted. Isotropic conditions are assumed in the model, ie. the direction of cracking is not considered in the computation of the permeability. In the model, cracking is assumed to occur when the minimum total principal stress, σ_3, equals zero. For clarity, the description of the model shall be made with reference to Figure 5.24.

Figure 5.24 shows the relation between σ_3 (the most tensile principal stress in ICFEP) and coefficient of permeability, k, assumed in the model. The value of σ_{3_1} defines the magnitude of σ_3 at which crack initiation occurs while σ_{3_2} marks the magnitude of σ_3 at which full cracking is assumed to have occurred. The magnitude of permeability is assumed to increase from an initial k value, k_i (uncracked ground) to a final value, k_f, (fully cracked ground) according to a logarithmic relationship. The program identifies the integration points where tensile strength of the soil has been exceeded and appropriates a permeability value by intepolating along the curve shown in Figure 5.24.

The user inputs the values of σ_{3_1}, σ_{3_2}, and the ratio of the final to the initial permeabilities, $\frac{k_f}{k_i}$, at the beginning of the analysis. In the analyses reported in this thesis, the value of σ_{3_1} defining the onset of cracking was assumed to be zero while values of σ_{3_2} ranging from 100 to 350 were used.

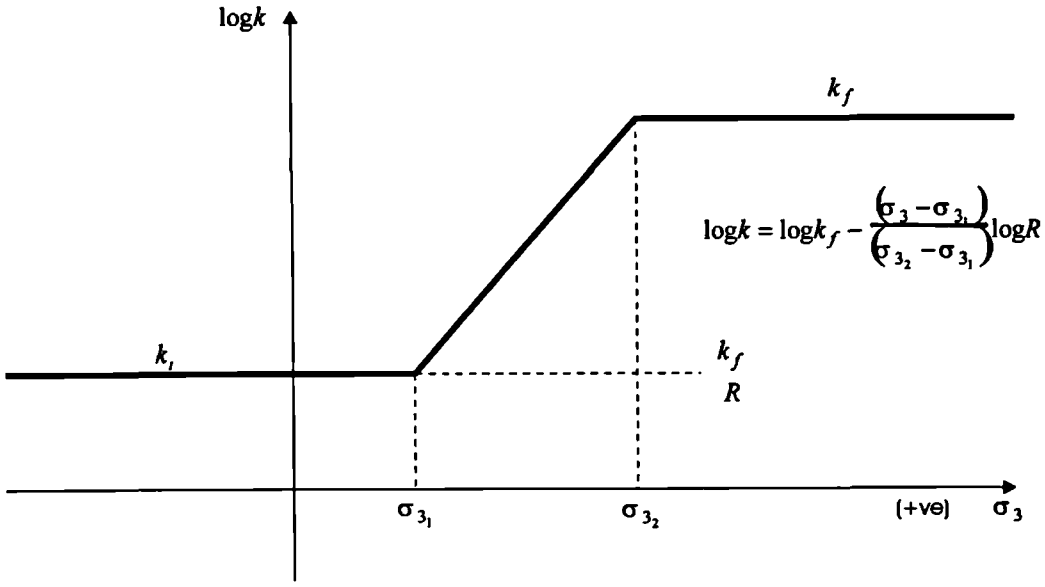

Figure 5.24 Variation of mass permeability with minimum principal total stress, σ_3, in smeared crack permeability model.

In the field, the rate at which the mass permeability changes from an initial value, k_i, to a final value k_f, depends on the rate at which the cracks propagate (gradient λ in Figure 5.24) and their spatial density. This aspect has received very little attention by researchers and is therefore not fully understood. The magnitude of the final permeability, k_f, is primarily a function of the crack widths and patterns, and again very little information has been published for specific soils. Table 2.1 shows typical permeability values of intact and cracked clays.

In the field, open cracks can get infilled with debris. The behaviour of infilled cracks is complex and primarily affects the rate at which the cracks close during wetting up and therefore the gradient λ in Figure 5.24. These aspects have not been addressed in the current model ie. the curve in Figure 5.24 has been assumed to be reversible along the same path.

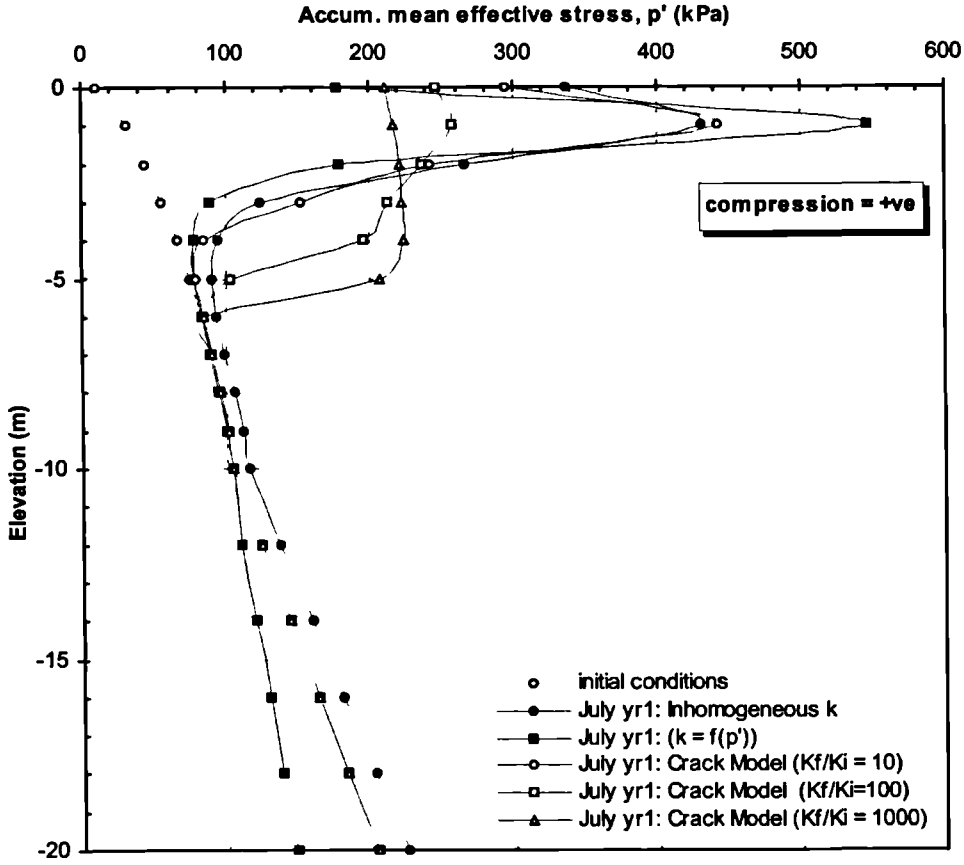

Figure 5.25a Influence of cracked permeability model on prediction of mean effective stress, p' (July yr1).

5.5.5.6 Predictions using the new crack permeability model

(i) short term

Analyses to test the new model were carried out using the methodology described in Section 5.5.5.2. In the analyses, the new crack model was used in tandem with a p' dependent permeability model with parameters shown Table 5.5. Predictions from the new crack model are compared with previously presented predictions from the inhomogeneous and p' dependent models. The influence of the $\frac{k_f}{k_i}$ ratio was investigated using values equal to 10, 100 and 1000.

Figure 5.25a shows the distribution of the accumulated mean effective stress, p', with depth 6 months after application of the RWUM (July year 1) as predicted by the crack model using $\frac{k_f}{k_i}$ ratios of 10, 100 and 1000. The predictions using an inhomogeneous permeability and

p' dependent permeability model are also shown for comparison. It can be seen from the figure that at shallow depth (less than 2m), p' has significantly reduced by invoking the crack model, with the magnitude in stress reduction increasing as the $\frac{k_f}{k_i}$ ratio increases. This is confirmed by Figure 5.25b where the maximum tensile stress σ_3 has been plotted and reveals the reduction in tensile stresses.

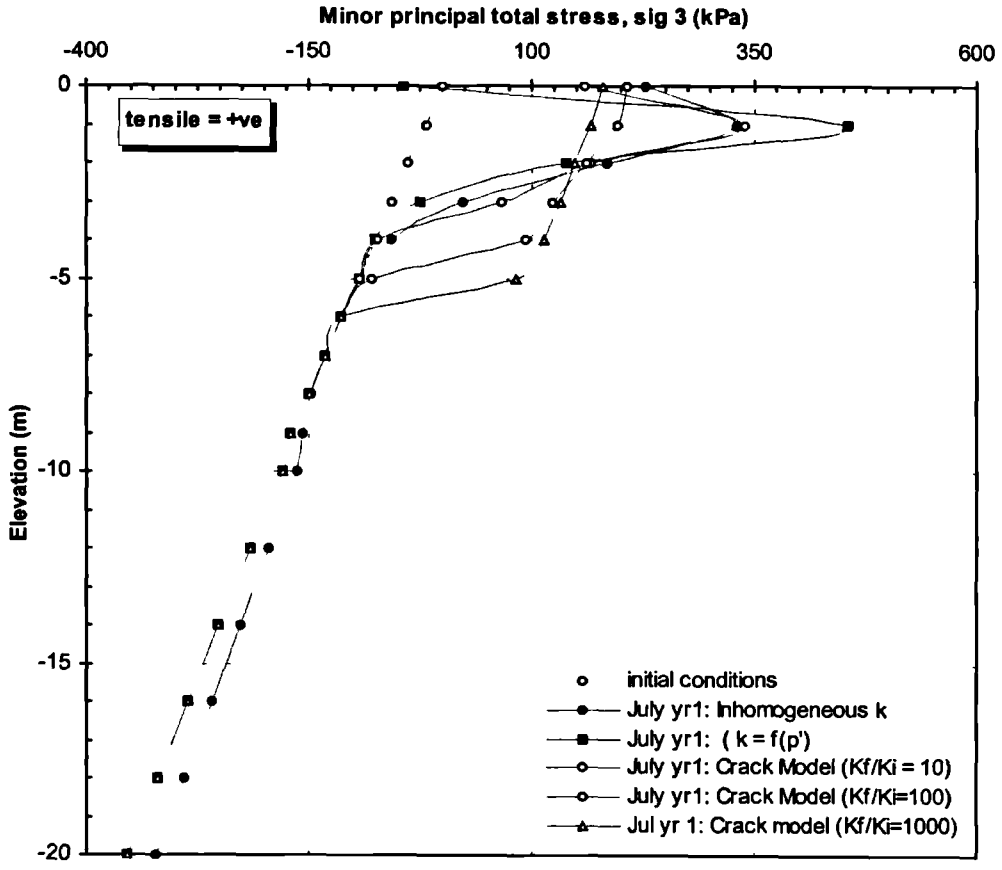

Figure 5.25b Influence of cracked permeability model on prediction of the minor principal total stress, σ_3 (July yr1).

There is also evidence that by using this model, the reduction in stress is not directly related to the magnitude of permeability increase. There appears to be a threshold value beyond which any further increase in the $\frac{k_f}{k_i}$ ratio does not yield a correspondingly large reduction in stresses eg. at 1m depth σ_3 reduces from 340kPa to 200kPa and 170kPa for $\frac{k_f}{k_i}$ ratios of 10, 100 and 1000, respectively. Figures 5.25a and b also reveal that invokation of the crack model leads to gradual

redistribution of p' and σ_3 to lower strata. The depth of redistribution increases as the $\frac{k_f}{k_i}$ ratio increases.

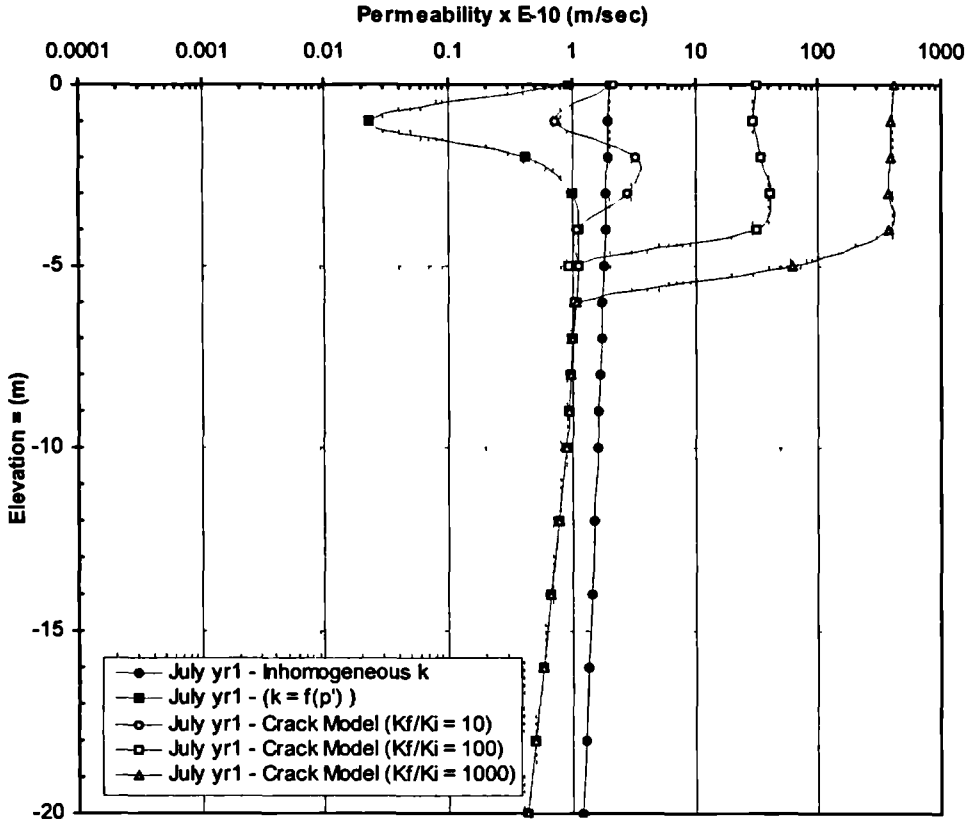

Figure 5.26a Influence of $\frac{k_f}{k_i}$ ratio on permeability in July yr1

Figure 5.26a shows the corresponding permeability profiles for that period (end of July year 1). The huge reduction in permeability for the p' dependent model is clearly portrayed in the top 2m of the strata. Similarly, the increase in permeability with increasing $\frac{k_f}{k_i}$ ratio is evident. When the crack model is invoked, the computed smeared crack permeability value is determined using the current value of permeability computed using the p' dependent permeability model.

Figure 5.26b shows the accumulated pore water pressure profiles at the end of July. Overall, the pattern closely matches the distribution of p' and σ_3. At 1m depth, maximum suctions of 890kPa predicted by the p' dependent permeability model have been reduced to 660kPa, 380kPa and 320kPa using $\frac{k_f}{k_i}$ ratios of 10, 100 and 1000, respectively. However, it can be seen from this figure

that the redistribution of suctions occurs to greater depths in the analysis involving crack permeability models, compared to the analysis involving a p' dependent permeability model.

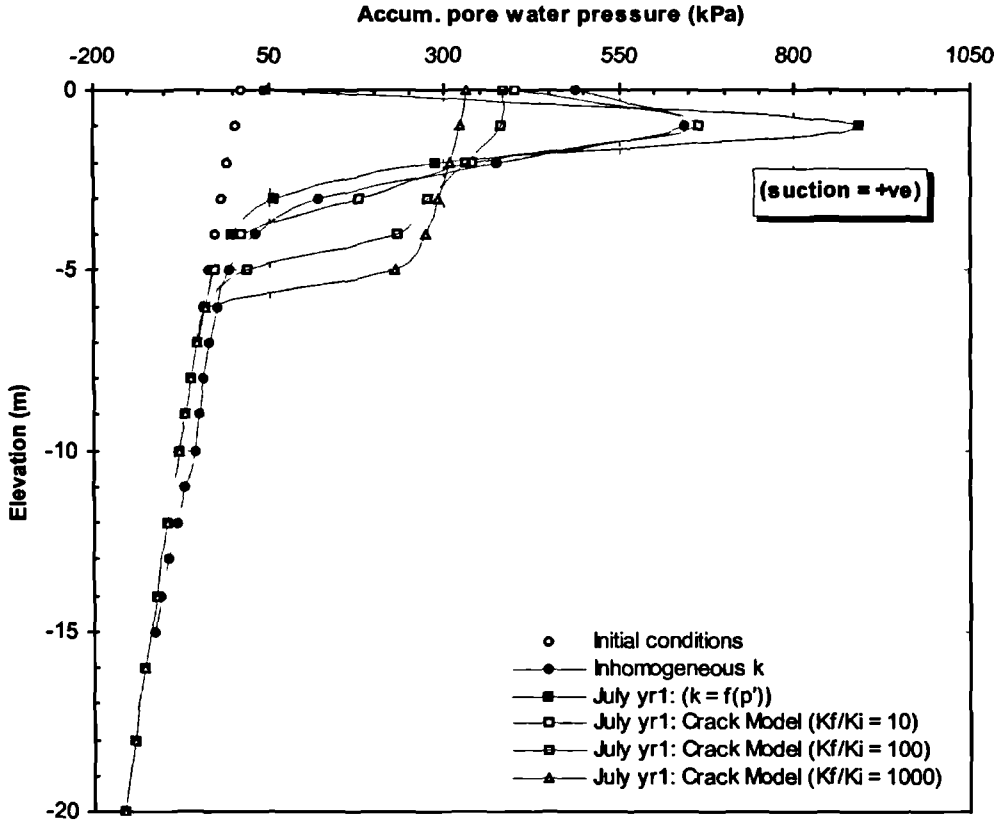

Figure 5.26b Influence of cracked permeability model on prediction of accumulated pore water pressure in July of yr1

The sub-accumulated movements since invokation of the RWUM are shown in Figure 5.26c. The movements at shallow depth are approximately of the same order eg. approximately 250mm at ground level. Movement at depth is primarily a function of the pore water pressure changes associated with the redistribution of suctions. The figure shows that significant movements have occurred to 5m depth in the crack models with $\frac{k_f}{k_i}$ ratios of 100 and 1000, whilst little difference exists in predictions by the p' dependent permeability model and a crack model with a $\frac{k_f}{k_i}$ ratio of 10.

Figure 5.27a shows the profiles of accumulated mean effective stress at the end of December yr1. It can be seen that p' has increased at shallow depth in the analysis involving a p' dependent

permeability model whereas the predictions by a crack model with a $\frac{k_f}{k_i}$ ratio of 10 yields a much lower p' eg. at 1m depth the value of p' increases from 540kPa (end of July) to 740kPa (end of December) for the analysis with a p' dependent permeability model compared to a reduction from 440kPa (end of July in Figure 5.25a) to 280kPa (end of December) in the analysis involving a crack model with a $\frac{k_f}{k_i}$ ratio of 10. The corresponding reductions in p' for higher $\frac{k_f}{k_i}$ ratios are 260kPa to 160kPa for a $\frac{k_f}{k_i}$ ratio of 100 and 220kPa to 150kPa for a $\frac{k_f}{k_i}$ ratio of 1000. The latter reduction in p' during winter associated with the crack models is in line with observed field behaviour ie. a reduction in potential transpiration coupled with increasing precipitation contributes to an overall reduction in mean effective stress.

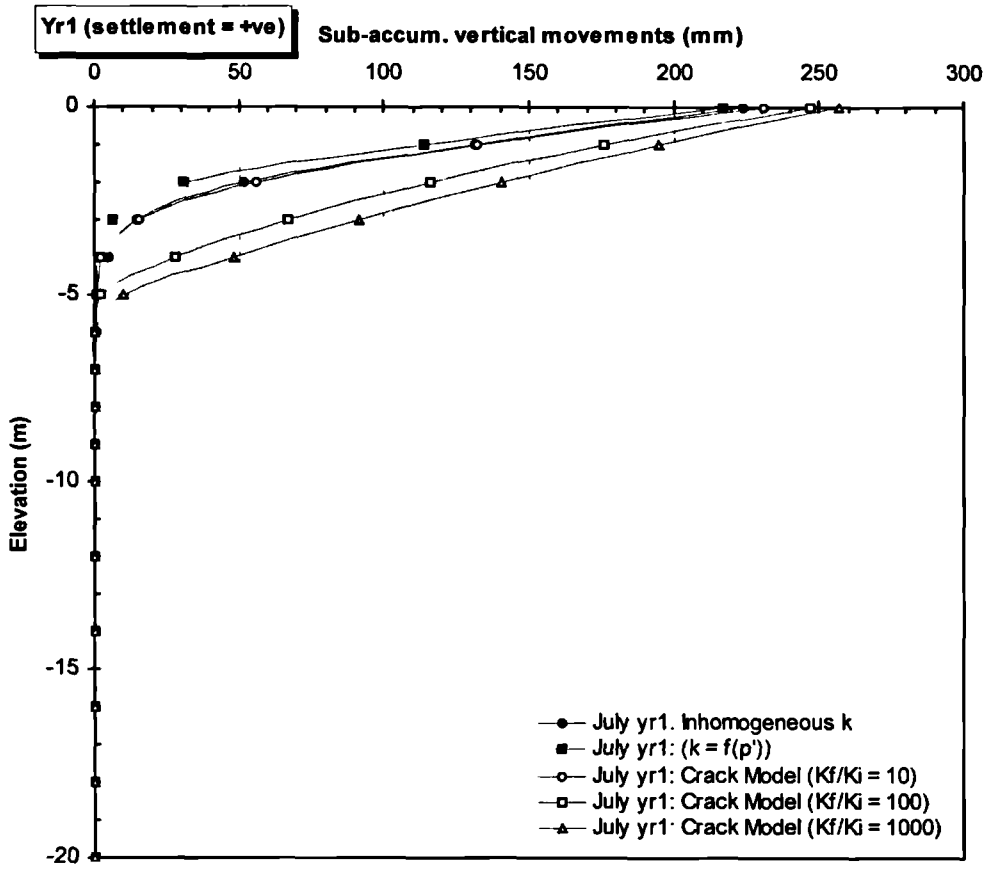

Figure 5.26c Influence of cracked permeability model on prediction of sub-accumulated vertical movements (July yr1)

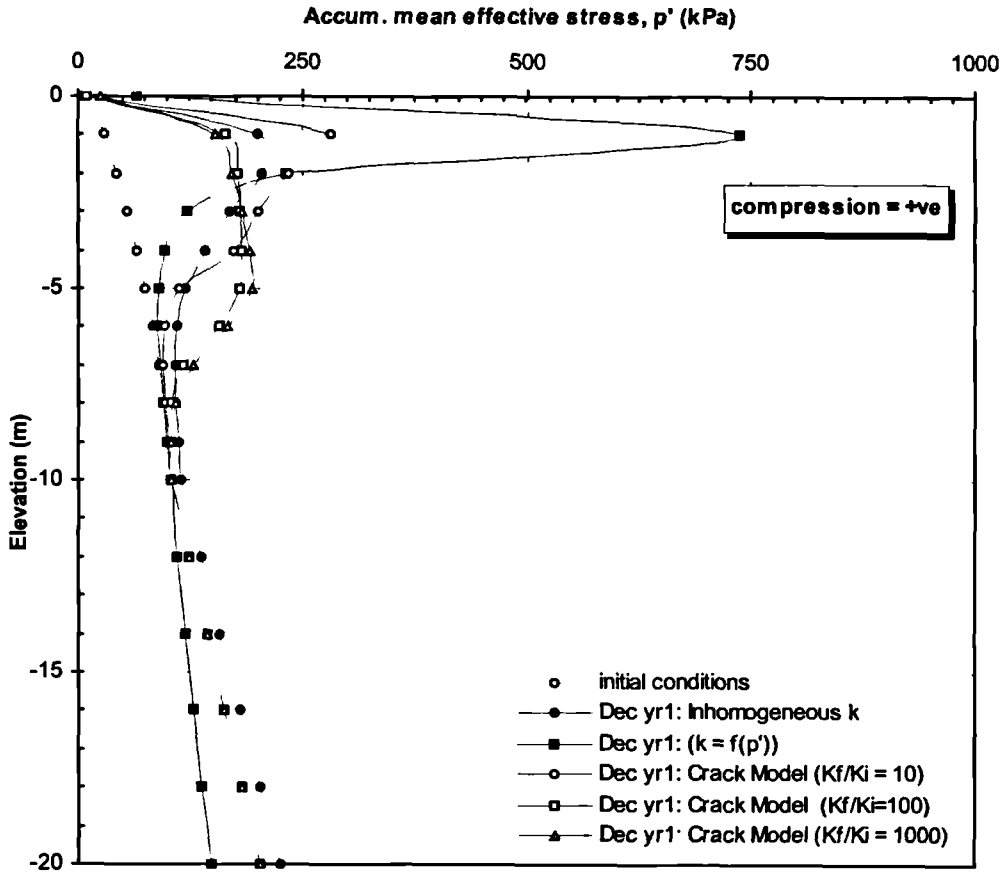

Figure 5.27a Influence of cracked permeability model on prediction of mean effective stress (Dec yr1).

Figure 5.27b shows profiles of σ_3 at the end of December, after 1 year of applying the RWUM. The profiles indicate an overall reduction in the magnitude of the stresses from the scenario at the end of July (Figure 5.25b). The permeability profiles corresponding to the end of December conditions are shown in Figure 5.28a. Overall, the magnitude of permeability reduces near ground level where the effects of precipitation are greatest; notwithstanding that the change in permeability for a crack model with a $\frac{k_f}{k_i}$ ratio of 10 are generally small.

The accumulated pore water pressures at the end of December yr1 are shown in Figure 5.28b. It is interesting to note that at this stage, the predictions by the crack models with $\frac{k_f}{k_i}$ ratios of 100 and 1000 are nearly of the same order of magnitude. This would suggest that any further increase in $\frac{k_f}{k_i}$ ratio is unlikely to yield significant differences in the pore water pressure predictions. It can

also be seen from Figure 5.28b that for crack models with $\frac{k_f}{k_i}$ ratios of 100 and 1000, the effect of redistribution of suctions at depth results in a larger spread of the zone of maximum suctions eg. it can be seen that maximum suctions of 200kPa are predicted between 1m and 5m below ground level. For the crack model with a $\frac{k_f}{k_i}$ ratio of 10, the maximum suctions (310kPa) are localized at 1m - 2m depth below ground level.

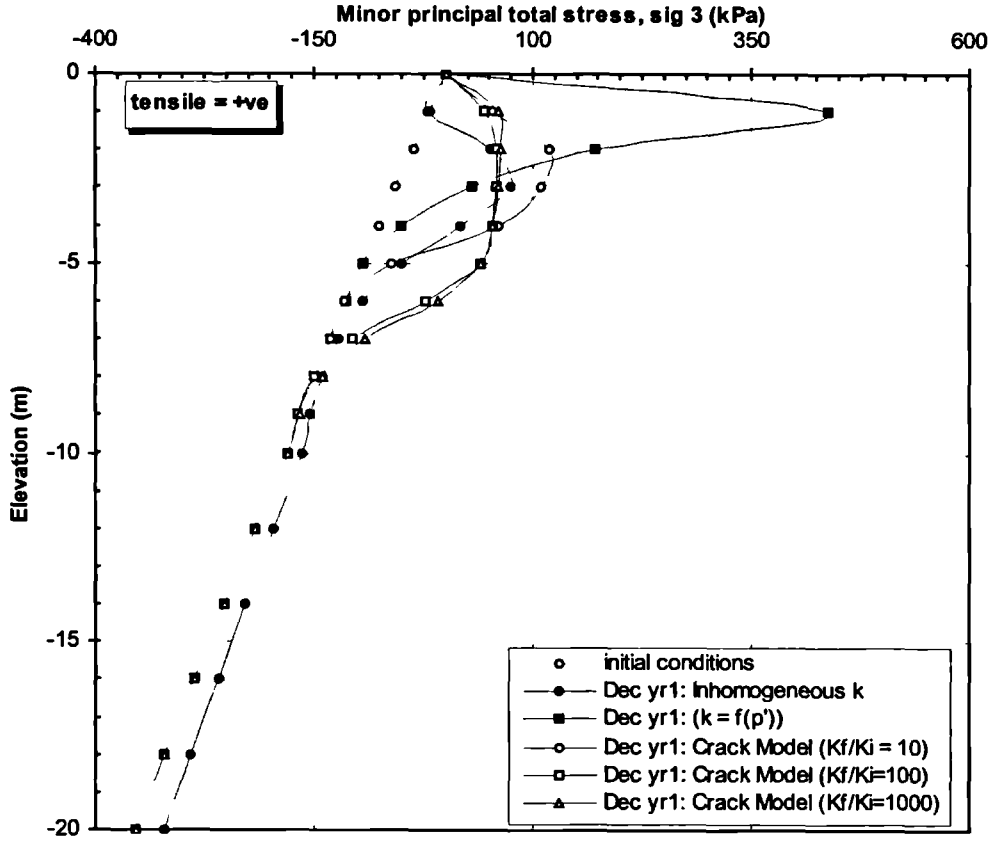

Figure 5.27b Influence of cracked permeability model on prediction of the minor principal total stress, σ_3 (Dec yr1).

The effects of redistribution of suctions to lower horizons have a significant impact on the predictions of vertical movements with time as can be seen in Figure 5.28c where the sub-accumulated movements at the end of December (after 1 year of application of the RWUM) are plotted. It is clear that although the vertical movements predicted by the crack model have only marginally increased at ground level, the movements at depth have significantly increased eg. at 2m depth, vertical movement of up to 100mm, 160mm and 180mm for $\frac{k_f}{k_i}$ ratios of 10, 100 and 1000, respectively are predicted. This contrasts with 50mm, 120mm and 140mm respectively, at the same

depth for end of July conditions (Figure 5.26c). In general, overall movements predicted by the crack model are greater than those predicted by the p' dependent and inhomogeneous permeability models.

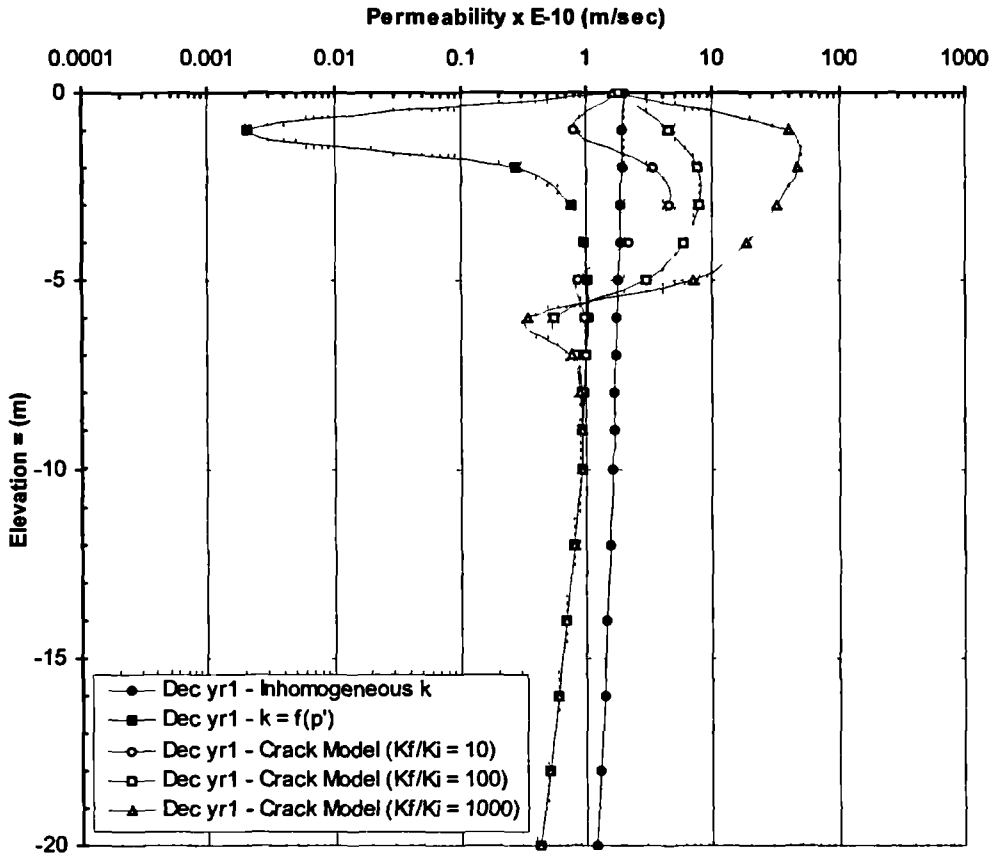

Figure 5.28a Influence of cracked permeability model on prediction of permeability in Dec yr1

Figures 5.29a and b show the variation of the accumulated p' at 1m and 4m depths, respectively, during the period January to December when the RWUM was in operation. The figures corroborate the observation that at shallow depth (Figure 5.29a), the p' dependent permeability model overpredicts the magnitude of p' because it cannot take account of permeability increase due to cracking. On the other hand, the predictions by the crack models at shallow depth further confirm the fact that the higher the $\frac{k_f}{k_i}$ ratio, the higher the permeability. This leads to more rainfall being absorbed, thus inducing larger reductions in mean effective stress.

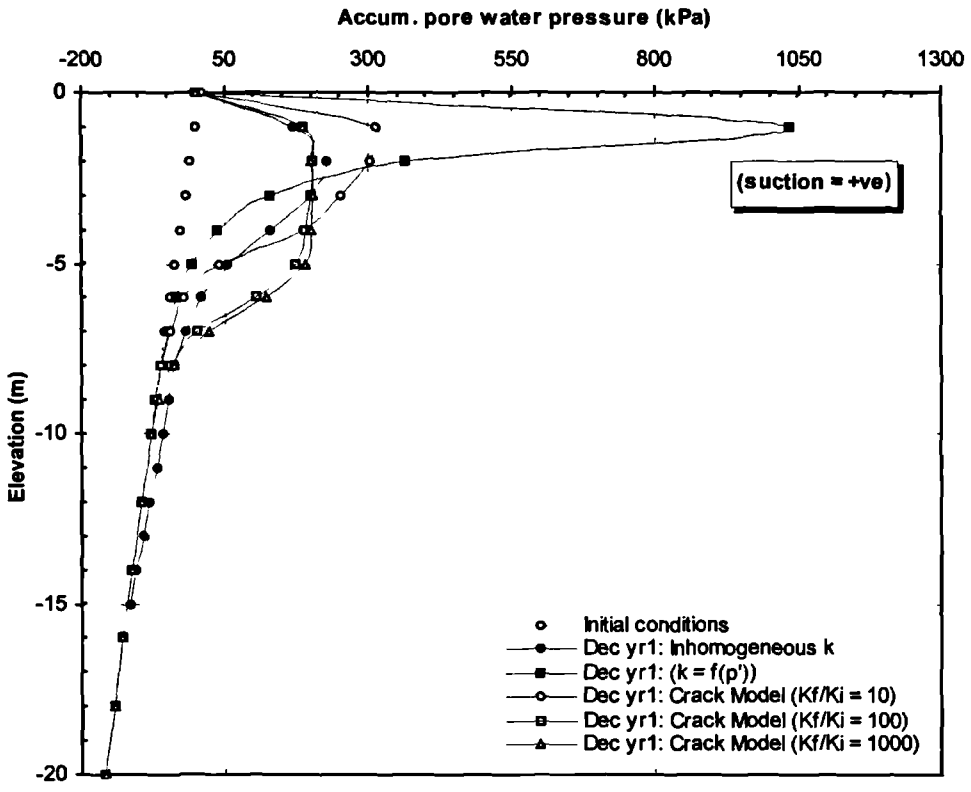

Figure 5.28b Influence of cracked permeability model on prediction of accumulated pore water pressure in Dec of yr1

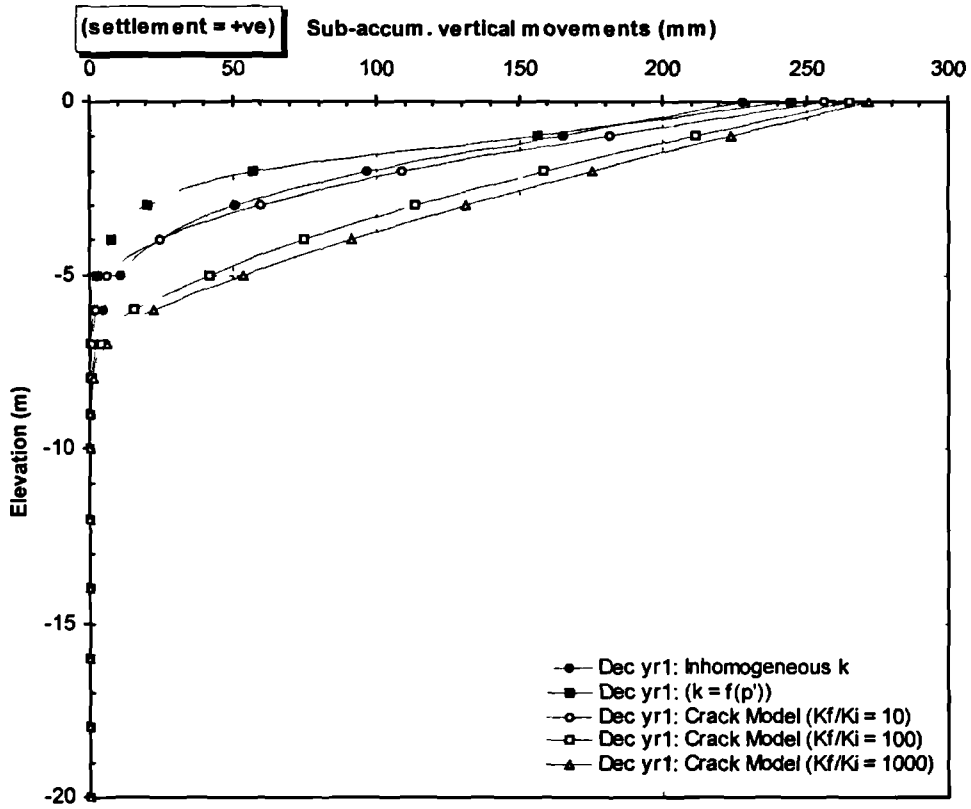

Figure 5.28c Influence of cracked permeability model on prediction of vertical movements (Dec yr1).

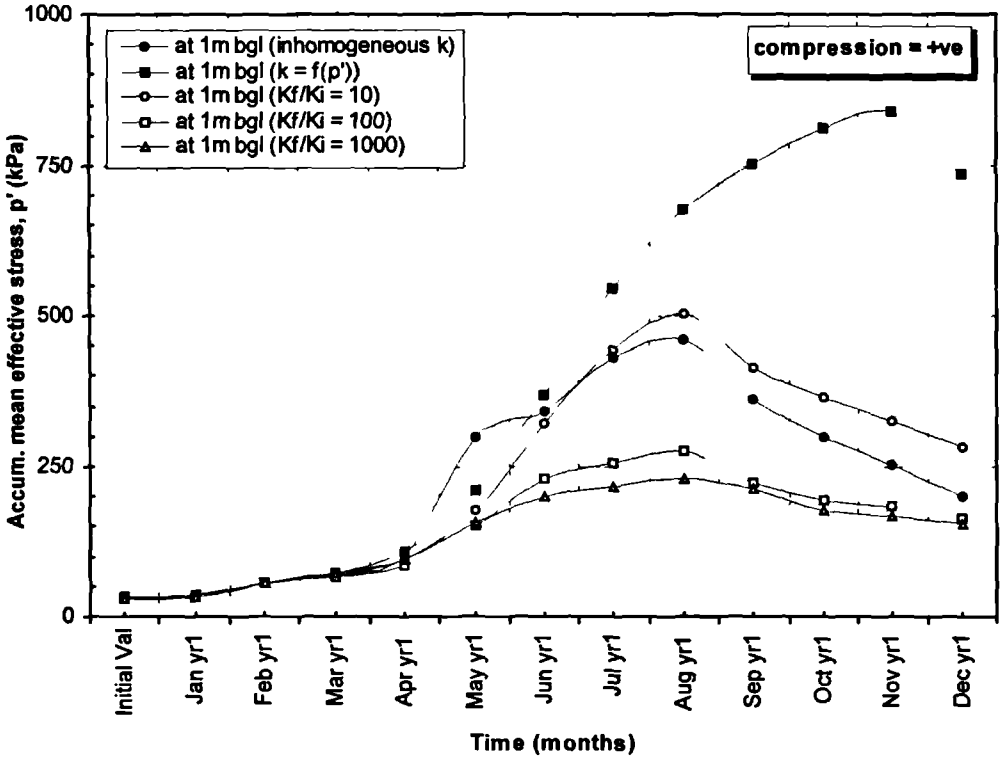

Figure 5.29a Influence of cracked permeability model on prediction of mean effective stress at 1m bgl during yr1

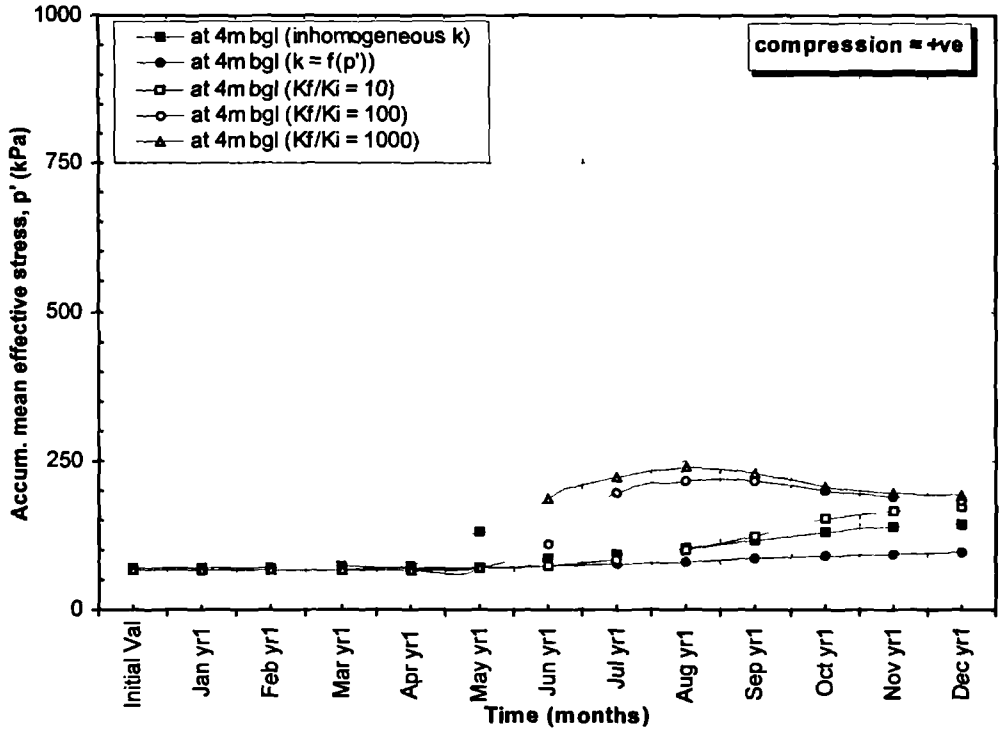

Figure 5.29b Influence of cracked permeability model on prediction of mean effective stress at 4m bgl during yr1

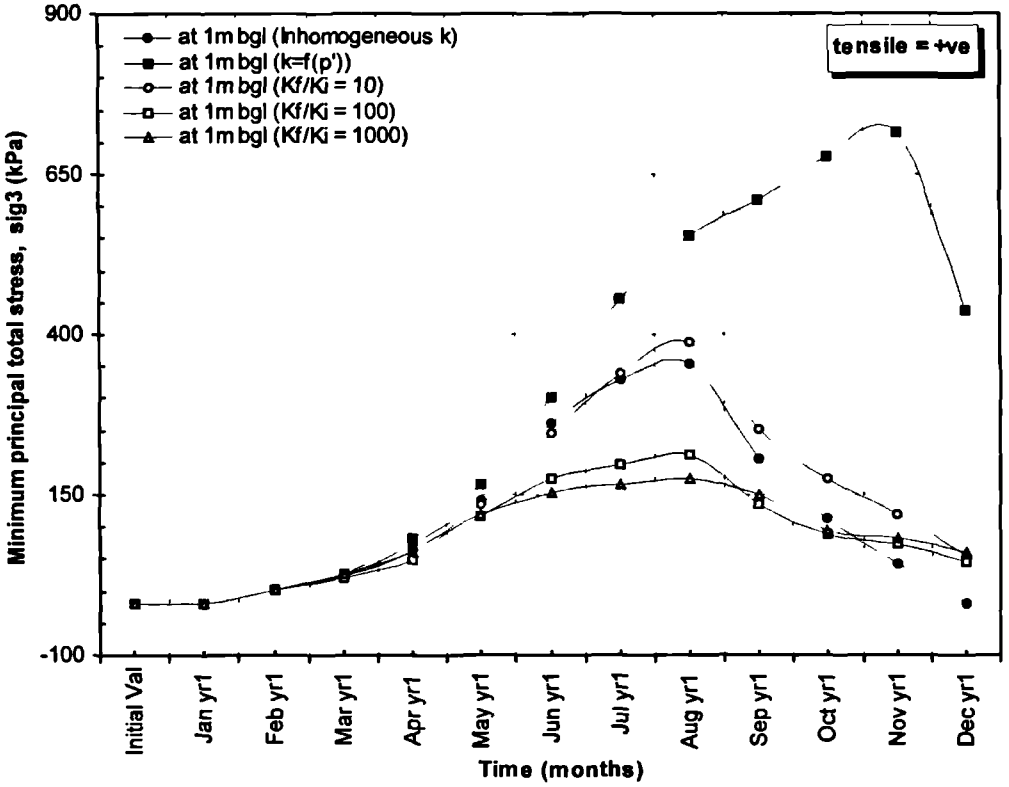

Figure 5.30a Influence of cracked permeability model on prediction of the minor principal total stress, σ_3, at 1m bgl during yr1.

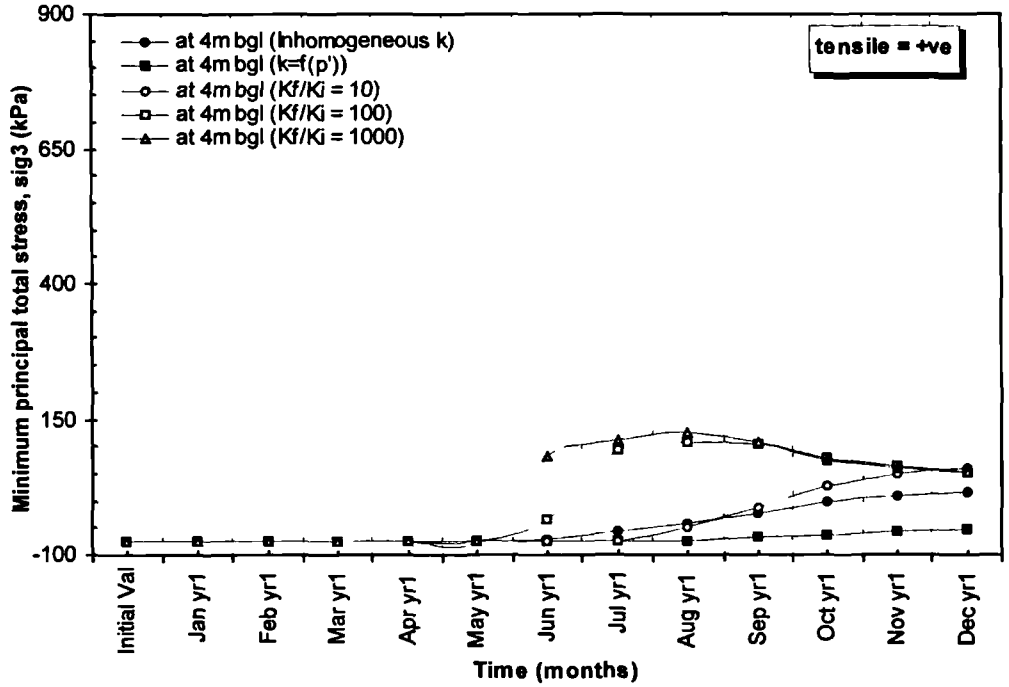

Figure 5.30b Influence of cracked permeability model on prediction of the minor principal total stress, σ_3, at 4m bgl during yr1.

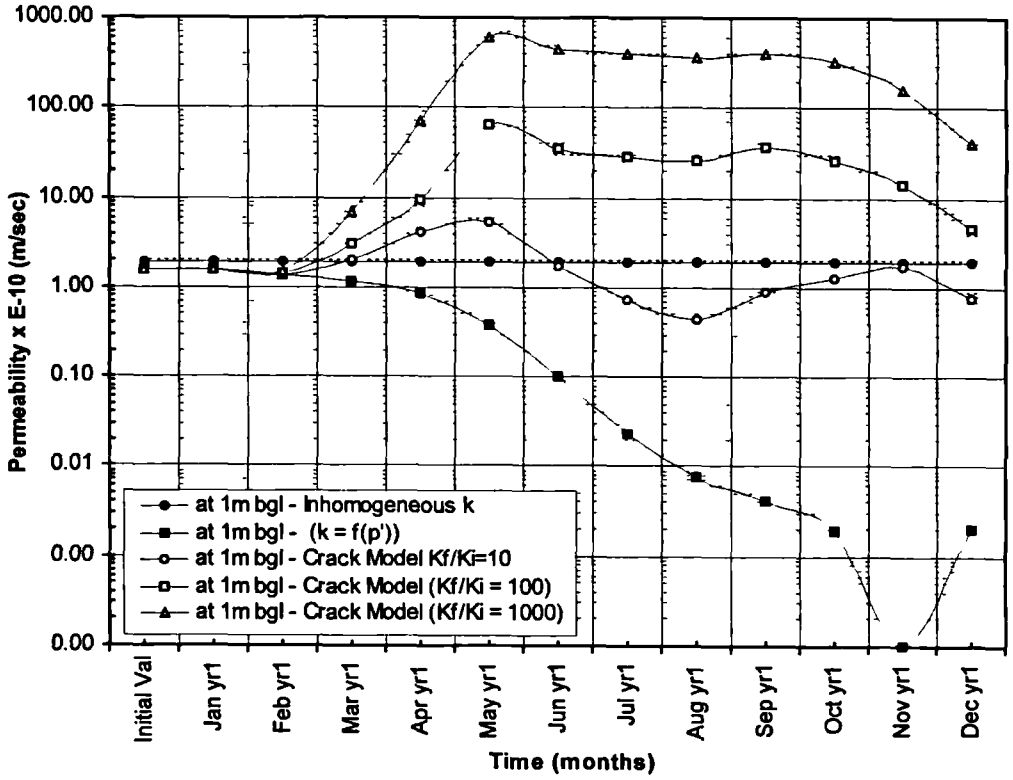

Figure 5.31a Influence of $\frac{k_f}{k_i}$ ratio on permeability at 1m bgl during yr1

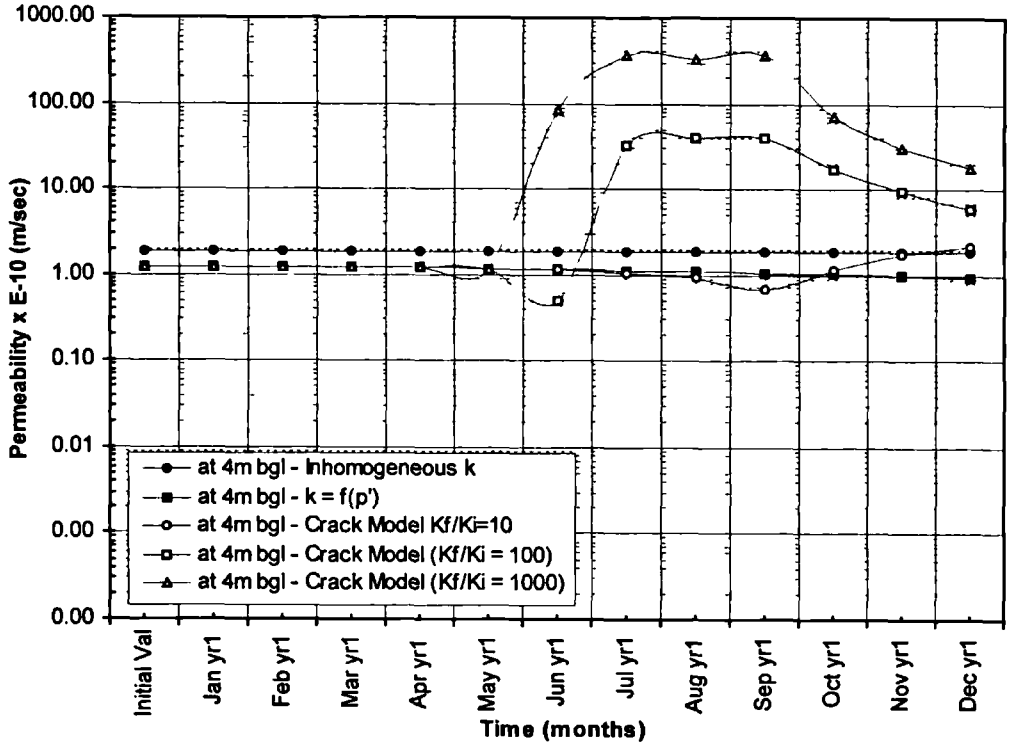

Figure 5.31b Influence of $\frac{k_f}{k_i}$ ratio on permeability at 4m bgl during yr1

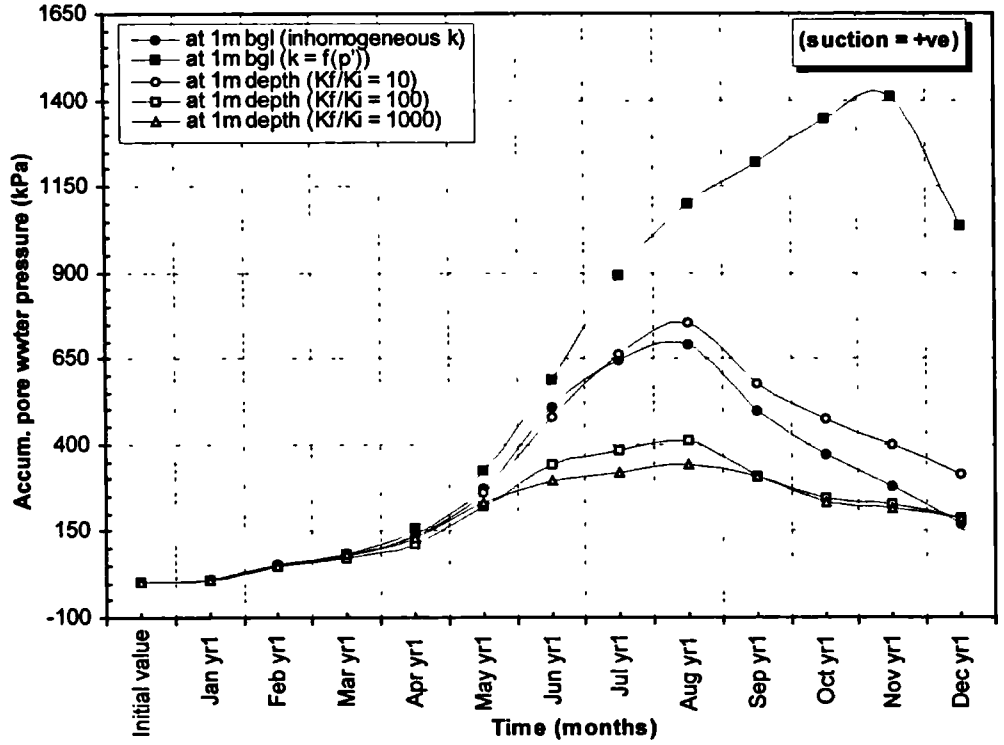

Figure 5.32a Influence of cracked permeability model on prediction of accumulated pore water pressure at 1m bgl during yr1

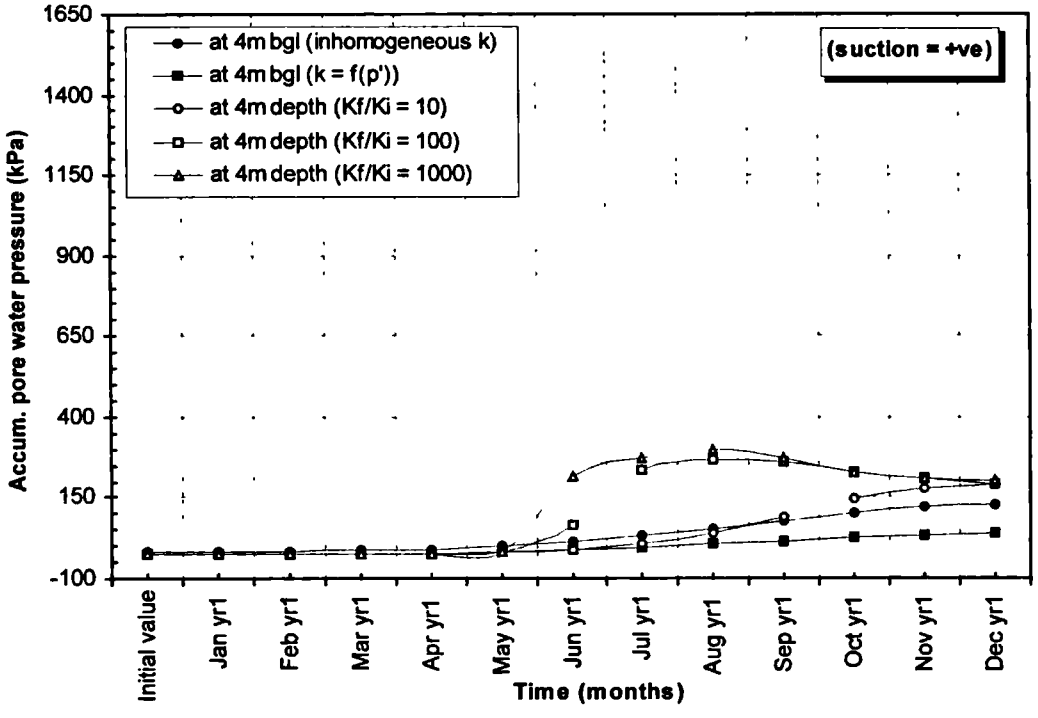

Figure 5.32a Influence of cracked permeability model on prediction of accumulated pore water pressure at 1m bgl during yr1

On the other hand, Figure 5.29b also corroborates the observation that although there is an overall reduction in stress changes at depth, the larger $\frac{k_f}{k_i}$ ratios are associated with larger magnitudes of redistributions in suction. This overall pattern is mirrored in the profiles of σ_3 (Figure 5.30), permeability (Figure 5.31) and accumulated pore water pressures (Figure 5.32). In general, the patterns display a strong correlation with the meteorological data (Figure 5.10) whereby the stress changes and corresponding increase in permeability (to simulate the influence of cracking) are dependent on the magnitude of potential evapotranspiration and rainfall.

(ii) Medium to long-term

In order to further illuminate the performance of the crack model, the analyses were continued for 20 years. This was particularly important to investigate the influence of redistribution of suctions in the long-term.

Figure 5.33a shows the accumulated p' at the end of December after 10 and 20 years of application of the RWUM. The figure reveals that there has been a large increase in p', with time. At shallow depth (less than 2m) the crack model performs reasonably well in reducing suctions whereas below this depth, the influence of redistribution of suctions significantly increases to an extent where stress changes predicted by the crack model become larger compared to predictions by the p' dependent permeability model eg. the crack model with a $\frac{k_f}{k_i}$ ratio of 10 predicts changes in p' to 20m depth after 20 years compared to 15m by the p' dependent permeability model. The predictions of the depth of cracking (depth where σ_3 is greater than 0kPa in Figure 5.33b) after 20 years are 11.5m and 7m as predicted by the crack and p' dependent models, respectively.

Figure 5.33c depicts the large reduction in permeability at the end of December after 20 years of application of the RWUM. The permeabilities predicted by the crack and p' dependent models are overall less than the inhomogeneous model, which is perturbing. It can also be seen that the prediction of permeability by the p' dependent model at 1m depth is nearly zero. The gradual reduction in permeability with time implies that the quantity of infiltration entering the ground also diminishes with time; which in turn leads to erroneous predictions in the long term.

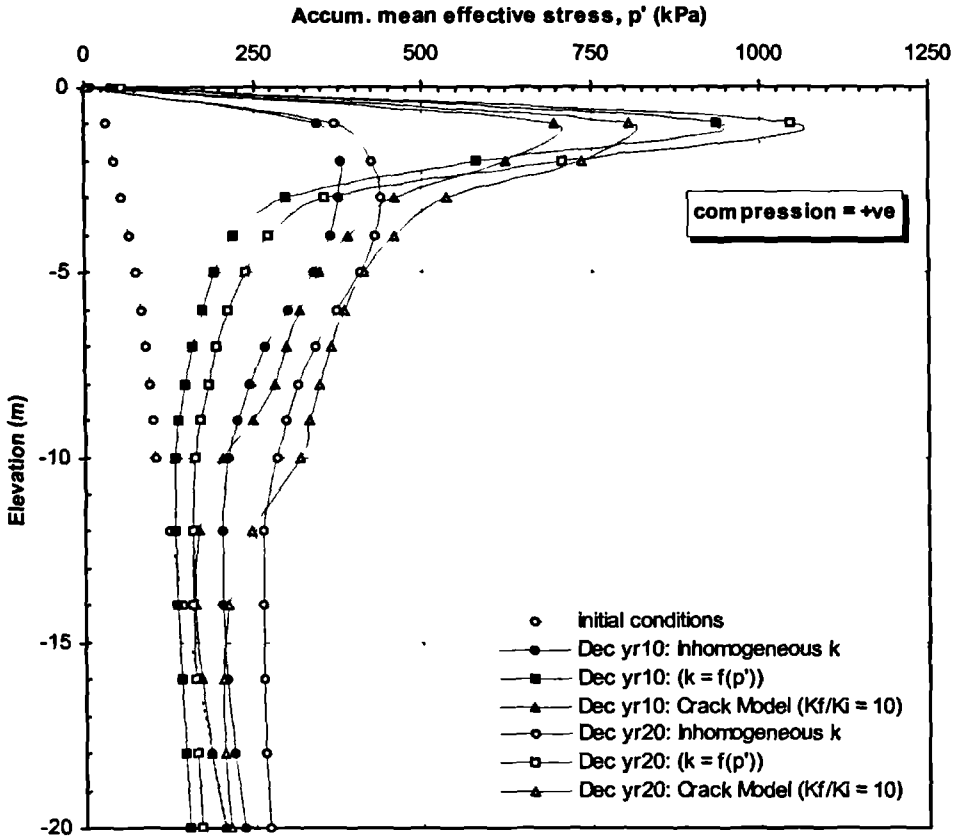

Figure 5.33a Influence of cracked permeability model on prediction of mean effective stress after 10 & 20yrs

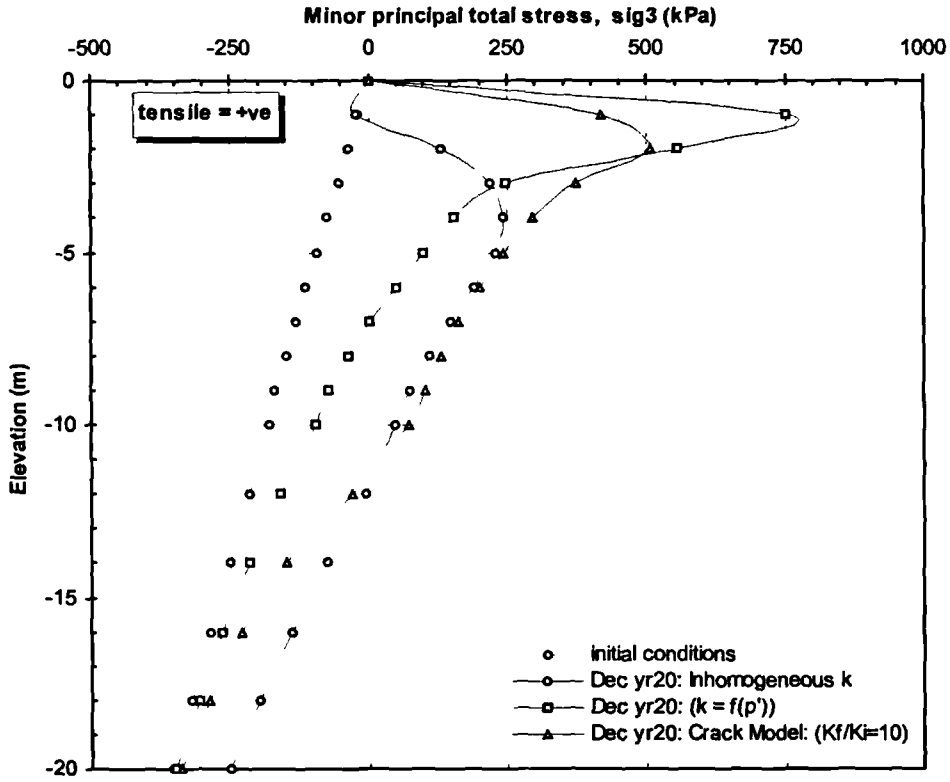

Figure 5.33b Influence of cracked permeability model on prediction of the minor principal total stress (σ_3) after 20yrs.

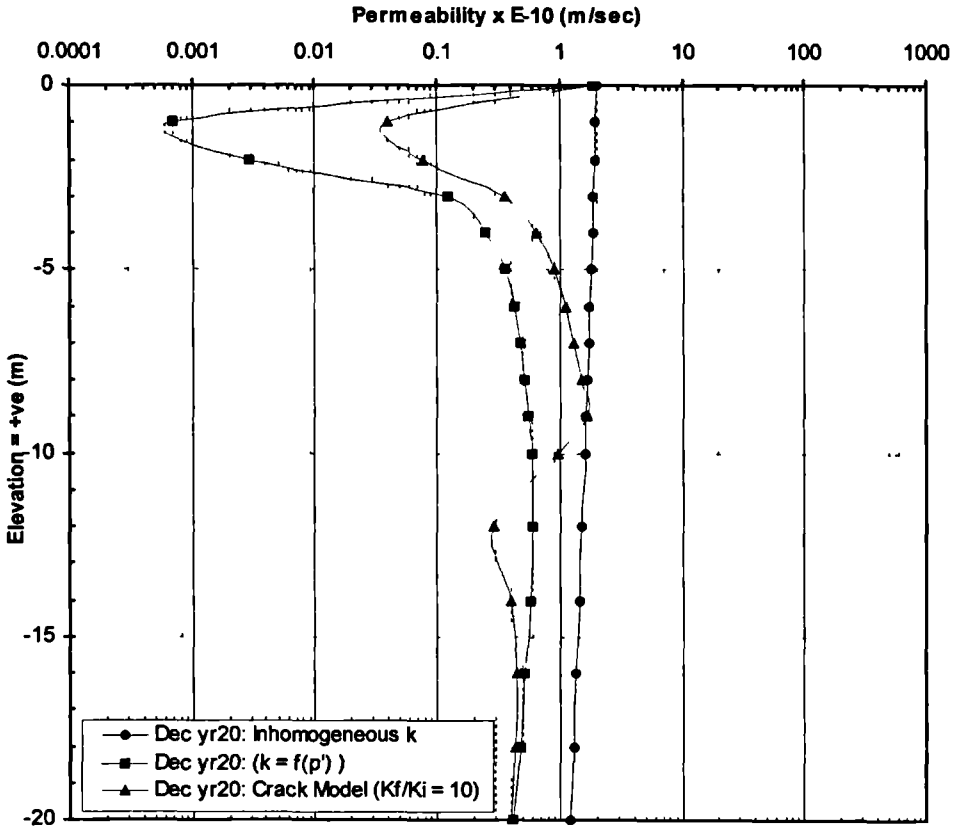

Figure 5.33c Influence of crack ratio on permeability after 20yrs.

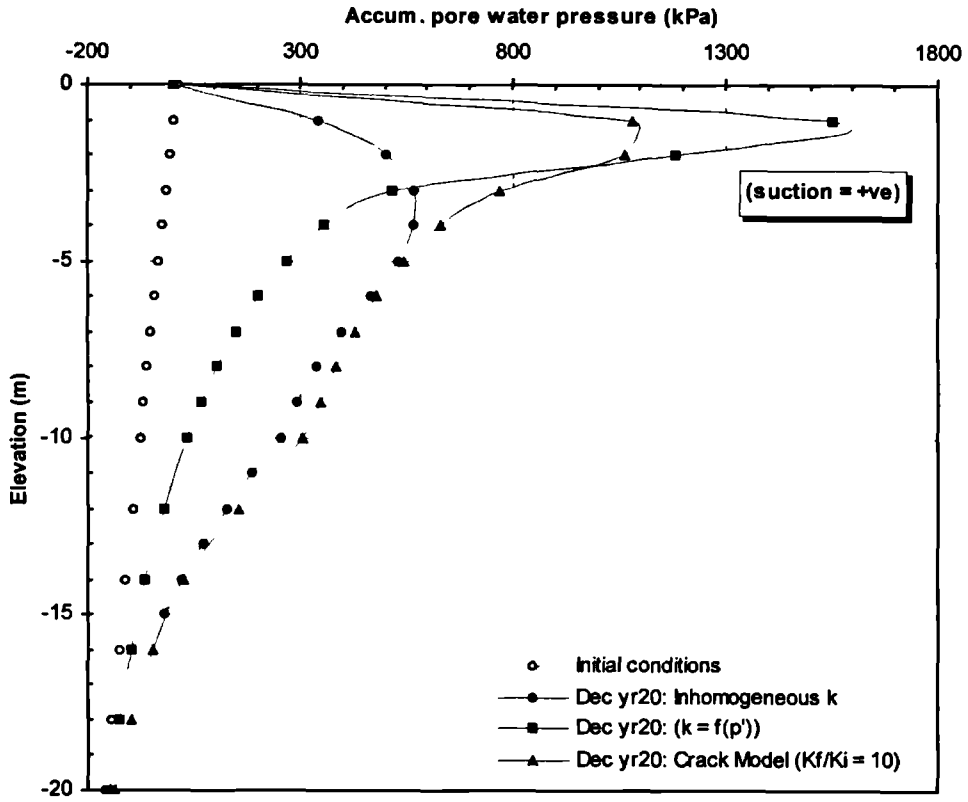

Figure 5.33d Influence of cracked permeability model on prediction of accumulated pore water pressure after 20yrs.

The accumulated pore water pressures at the end of 20 years of application of the RWUM are shown in Figure 5.33d. It is interesting to note that in general, there is a gradual increase in the size of the desiccated zone predicted by all 3 permeability models. The lowest suctions at shallow depth (less than 3m) are predicted by the inhomogeneous model while the largest suctions are predicted by the p' dependent model. Below 3m depth, the lowest suctions are predicted by the p' dependent model while predictions by the inhomogeneous and crack model are approximately similar, albeit the predictions by the latter are marginally higher. The pore water pressure predictions using crack models with higher $\frac{k_f}{k_i}$ ratios are likely to yield much higher suctions at depth.

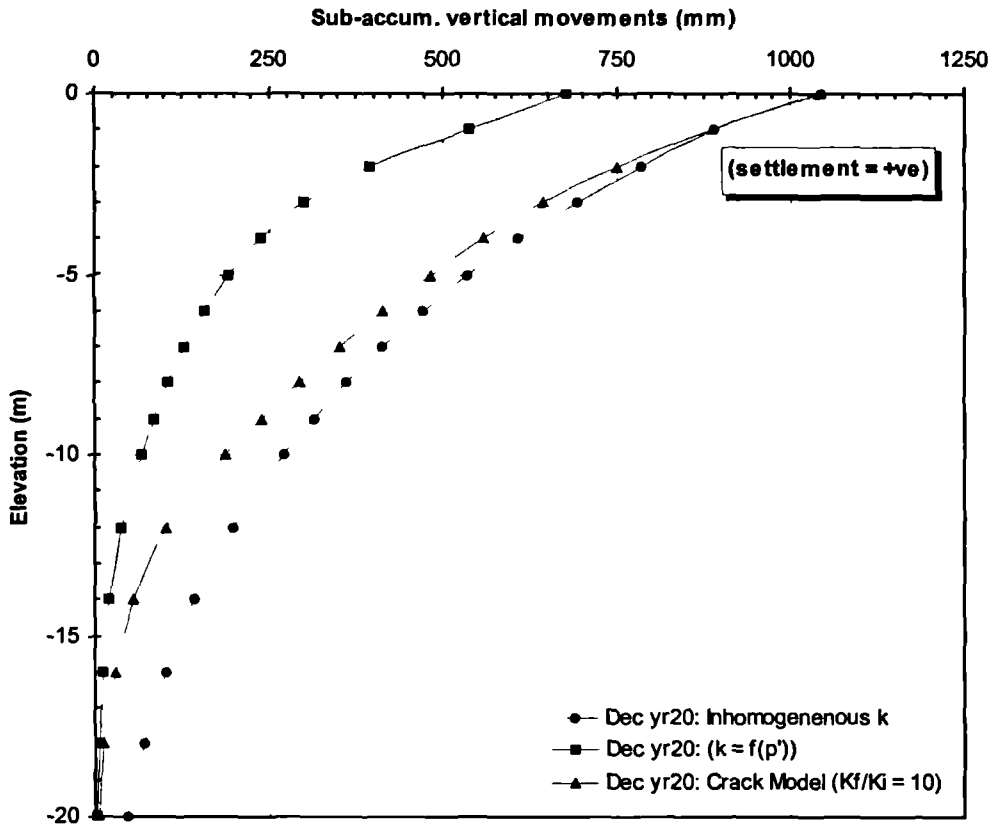

Figure 5.33e Influence of cracked permeability model on prediction of vertical movements after 20yrs.

Figure 5.33e shows the sub-accumulated vertical movements after 20 years. The figure shows that the predictions by the crack model lie in between the predictions by the inhomogeneous and p' dependent models. The comparatively high predictions by the former 2 models are a result of the large desiccations occurring at depth.

Summary

A nonlinear RWUM for modelling evapotranspiration has been presented. Studies carried out to investigate the maximum element size that can be used with the RWUM have shown that a maximum element thickness equal to the maximum root depth, r_{max}, is capable of producing satisfactory predictions.

The influence of the pattern of meteorological data was investigated. The results have indicated that predictions of changes in pore water pressures and associated vertical movements are sensitive to the pattern of the meteorological data, as this governs the magnitude of α. The influence of α on the response to the pore water pressure regime needs careful consideration when determining the time-step to use in a boundary value problem and the determination of initial conditions.

The results have demonstrated the capabilities of the RWUM to model seasonal variations in ground response to meteorological input data comprising rainfall and potential evapotranspiration. It has been shown that during summer, a desiccated profile develops within the ground and that the zone of desiccation reduces in size during winter when the rate of evapotranspiration reduces, coupled with an increase in precipitation rate.

The influence of root depth on the predictions by the RWUM have been studied. The study has revealed that the size and pattern of the desiccated profile is dependent on r_{max}. At shallow depths (typically less than 2m) the largest suctions are developed in analyses involving the smallest r_{max} whereas the converse is true at deeper horizons. The analyses have also shown that the overall depth to which pore water pressures and σ_3 changes occur is approximately the same for all the r_{max} values investigated (ie. 2m, 2.5m and 3m). The overall pattern suggests that the larger the r_{max} value, the greater the pore water pressure changes and vertical movements.

The study has investigated the performance of the RWUM under various magnitudes of S3 (the magnitude of soil suctions at which the ability of the roots to take up water begins to be restricted). S3 values of 50kPa, 100kPa, 200kPa and 400kPa have been investigated. The results have revealed that there is little difference in predictions over the range of S3 considered to be applicable to vegetation (50kPa - 200kPa). The overall trend suggests that the larger the S3 value, the larger the pore water pressure changes. The results also indicate that the difference among the predictions increases as the time span of the analysis increases.

Finally, an investigation was carried out to compare the predictions using homogeneous, inhomogeneous and p' dependent permeability models. The results have shown that at shallow depth (typically less than 2m) the least and maximum suctions are predicted by the homogeneous and p' dependent permeability models, respectively. At shallow depth the predictions by the inhomogeneous permeability model lie in between.

During development of suctions, the p' dependent permeability model yields very low permeability; which inhibits recharge of ground water during precipitation. This in turn leads to a further increase in soil suctions, and with time results in unsatisfactory predictions of pore water pressure changes.

The results have shown that at deeper horizons, the homogeneous and inhomogeneous models generate relatively large changes, with the former inducing the largest changes. The p' dependent permeability model generates the least pore water pressure changes at depth. Overall, there is a gradual increase in suctions with time predicted by all the models investigated. This is considered to be a result of the inability of the models to reproduce the field behaviour of cracking, which the author believes significantly increases the mass permeability of the soil. During precipitation, flow of water is facilitated by the cracks, which leads to greater recharge of water and results in reduction of suctions.

In order to model the effects of cracking on the mass permeability of the soil, a smeared crack permeability model was developed. The predictions by the new model have demonstrated its ability to simulate the recharge of water that occurs as a result of enhanced permeability when the ground cracks. The magnitude of the reductions increases as the $\frac{k_f}{k_i}$ ratio increases. However, the predictions have also suggested that there is a threshold/minimum value of the $\frac{k_f}{k_i}$ ratio beyond which the influence on pore water pressure changes in a given time step becomes negligible.

Overall, the predictions in the short term (less than 5-10 years) by the new crack model yield pore water pressure profiles which resemble observed field patterns compared to the inhomogeneous and p' dependent permeability models, which is encouraging. Nevertheless, the author acknowledges that the predictions in the medium to long term (10-20 yrs) have shown that the crack model redistributes suctions to greater depths compared to the p' dependent permeability model. The large suctions predicted at depth in turn result in larger vertical movements being predicted by the

crack model compared to the p' dependent permeability model. The large redistribution of suctions associated with the new crack model is believed to arise from the assumptions that cracks form when a threshold value of σ_3 is exceeded. The model is therefore predicting an increase in permeability in all the zones wherever the criterion for crack formation (as assumed) is satisfied. The author believes that crack formation (being a very complex process) is dependent on more than one parameter (σ_3), as currently modelled. Therefore further research is required to the new crack model; to improve its capabilities in predicting pore water pressures at depth. The formation of cracks in soils is currently not well researched and understood by geotechnical engineers.

The overall pattern of pore water pressures and ground movements suggests that in order to obtain predictions which reproduce field behaviour during both winter and summer, it is necessary to use a permeability model capable of simulating the reduction of permeability with increasing p' as well as reproduce the increase in mass permeability when desiccation cracks form. This can be achieved by combining a p' dependent model with a smeared crack model.

Chapter 6

PREDICTION OF GROUND MOVEMENTS USING THE ROOT WATER UPTAKE MODEL (CHATTENDEN SITE)

6.1 Introduction

A description of the Root Water Uptake Model (RWUM) coded in ICFEP to model evapotranspiration was given in Chapter 5. This chapter presents predictions of vertical ground movements using the RWUM, on natural London Clay at a gently sloping field test site in Kent (SE England). The predictions are compared with field monitoring data from rod extensometers, carried out by the Building Research Establishment (BRE) during the period 1988 - 1998.

Site specific meteorological data computed by the Meteorological Office, using MORECS, was used as input data to the RWUM. In the analyses, median values of rainfall and potential evapotranspiration were used (Figure 5.13 of Chapter 5). A number of analyses were carried out during which various combinations of maximum root depth (r_{max}), unload/reload stiffness ratio and S3 value of the α function were investigated using the RWUM, to compare their influence on ground movement predictions.

6.2 Description of the site

The BRE field test site at Chattenden lies in Kent, approximately 45 km east of central London as shown on the site plan (Figure 6.1). Freeman *et al* (1991), Crilly *et al* (1992) and Crilly & Driscoll (2000) give detailed descriptions of the site and the geotechnical investigations that were undertaken. The ground slopes gently at 1 in 10 and is covered by predominantly two types of vegetation. The first area is covered by grazing grass and the other by semi-mature trees. The trees are typically 20m high and mostly comprise Lombardy Poplars. Poplars are known to be high water demand tree species.

The stratigraphy comprises 45m of London Clay overlying 2m of Old Haven Beds, 18m of Lambeth Group deposits, 40m of Thanet sands and 205m of Chalk as shown in Figure 5.7. Reworked London Clay (typically less than 1.5m depth) was observed in some of the trial pit

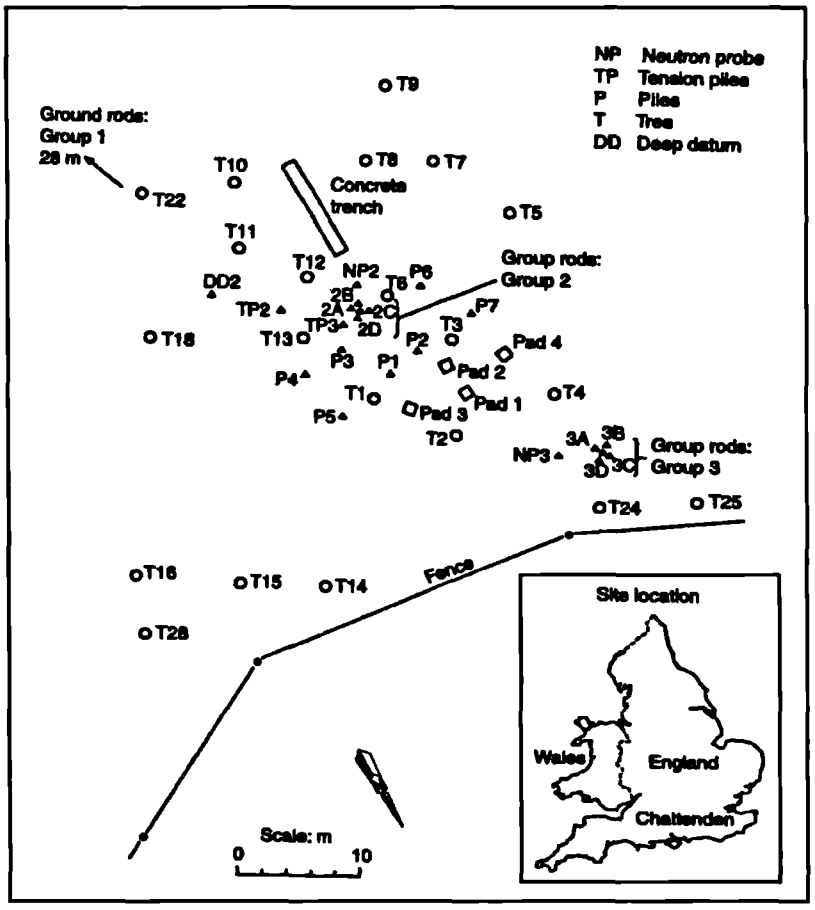

Figure 6.1 Chattenden BRE site: main experimental area (after Crilly & Driscoll, 2000)

exposures. The London Clay is classified as a silty clay of very high plasticity and is brecciated in the top 2m. The weathered London Clay was observed from borehole samples to extend to 12m depth.

Evidence of past down-slope movements to depths of 1.5m was observed in trial pits. During the ground investigation, desiccation cracks extending up to 1m depth were also observed in trial pits.

6.3 Investigations by BRE

A ground investigation involving boreholes, neutron probes to measure in situ moisture contents and associated laboratory tests were carried out. The latter included filter paper tests to measure suctions. The filter paper tests were carried out on samples trimmed from 100mm thin wall pushed samples. Sleeved ground rods were installed to measure ground movements at 1, 2, 3, and 4m depths at three locations as follows - in the tree-covered area, in the grass covered area and halfway between the two areas. Ground movements were also monitored on dummy foundations and instrumented piles, but are of no relevance to this thesis and will therefore not be discussed further. In this thesis, the RWUM has been used to predict movements in the tree covered area only.

Systematic measurement of ground movements commenced in June 1988 and continued at approximately monthly intervals for a decade. All the trees in the experiment area were felled on 19 and 20 September 1990, to initiate heave and study its effects on the foundations.

6.4 Numerical modelling

6.4.1 The mesh

An identical mesh to the one described in Chapter 5 (Figure 5.8) was used. For convenience, the salient features are repeated here. A one-dimensional analysis was executed using a 1m wide column as shown in Figure 5.8. The mesh was made dense in the upper strata where most of the pore water pressure and ground movements were expected to occur. A rigid boundary was assumed at the base of the mesh (top of the chalk ie. at 105m below ground level). At this lower boundary, zero horizontal and vertical movements were specified. No horizontal movement was allowed along the vertical boundaries of the mesh whilst the top boundary was assumed to be free.

6.4.2 Material properties

The soil parameters used in the analyses are summarised in Table 6.1. For the London Clay, a linear elasto-plastic soil model in terms of mean effective stress was used. A strain-softening Mohr-Coulomb failure criterion was specified as the yield function and an angle of dilation equal to zero was assumed. Very little or no movement was expected in the strata beneath the London Clay and for these, a small strain stiffness model after Jardine *et al* (1986) was used.

Coupled consolidation/swelling was used throughout the analyses. An inhomogeneous permeability model was used, as this had been shown to be still capable of reproducing pore water pressure recovery during winter at shallow depth, after several cycles. It should also be pointed out that at the time the analyses were executed, it was recognised that a smeared crack model with a realistic $\frac{k_f}{k_i}$ ratio (see Table 2.1) would yield better predictions, compared to the inhomogeneous, homogeneous or p' dependent models. However, the crack model was not used in this study because there were still unresolved numerical problems with the model when $\frac{k_f}{k_i}$ ratios greater than 100 were input. Nevertheless, runs in which $\frac{k_f}{k_i}$ ratios of 10 and 100; with a p' dependent

permeability model were carried as part of this study. The predictions of the latter analysis yielded very small movements compared to the field observations and have therefore been excluded from this discussion.

Table 6.1a Soil parameters used in analyses

Parameter	In situ London Clay	Oldhaven Beds	Lambeth clays	Lambeth sands	Thanet Sand
Bulk unit weight	18.8 kN/m^3	18	20	20	20
φ′ (peak)	20° (at 0-5% strain)	34	27	34	40
φ′ (residual)	13° (at 20% strain)	N/A	N/A	N/A	N/A
c′ (peak)	2kPa (at 0-5% strain)	N/A	N/A	N/A	N/A
c′ (residual)	2kPa (at 20% strain)	N/A	N/A	N/A	N/A
Permeability	$k = k_0 - mz$ m/sec where $m = 0.0063115$, z is the depth below top of the stratum and $k_0 = 2\times10^{-10}$ m/sec	1x10^{-7}	1x10^{-6}	1x10^{-6}	1x10^{-6}
Coefficient of earth pressure at rest, K_0	2.5 at ground level and reducing linearly to 1.0 at 15m depth	1.0	1.0	1.0	1.0
Non-linear elastic parameters	*See Equations 6.1 and 6.2*	*See Equations 6.3 and 6.4*			
Poisson's ratio ν	0.2	N/A	N/A	N/A	N/A

$$E_i = E_0\left[\frac{p_a + p'}{p_a}\right]^c \qquad \text{Equation 6.1}$$

$$E_u = HE_i \qquad \text{Equation 6.2}$$

where E_i and E_u are the drained Young's moduli on first loading and unloading/reloading respectively, p_a is atmospheric pressure, p' is the mean effective stress and E_0 and c are model parameters. The values of E_0, H and c were taken as 2500, 2 and unity, respectively.

$$\frac{3G}{p'} = C_1 + C_2\cos\left[c_1 X^{c_2}\right] - C_2 c_1 c_2 \frac{X^{(c_2-1)}}{2.303}\sin\left[c_1 X^{c_2}\right] \qquad \text{Equation 6.3}$$

$$\frac{K}{p'} = C_4 + C_5\cos\left[c_3 X^{c_4}\right] - C_5 c_3 c_4 \frac{X^{(c_4-1)}}{2.303}\sin\left[c_3 X^{c_4}\right] \qquad \text{Equation 6.4}$$

where $X = \log_{10}\left(\frac{E_d}{1.732C_3}\right)$ and $Y = \log_{10}\left(\frac{\varepsilon_v}{C_6}\right)$

Table 6.1b Soil parameters used in analyses

Stratum	C_1	C_2	C_3 (%)	c_1	c_2	$E_{d(\min)}$ (%)	$E_{d(\max)}$ (%)	$G_{\min}$ (kPa)
Lambeth clays	1000.0	1045.0	5.0×10^{-4}	1.344	0.591	13.8564×10^{-4}	0.38105	2667.0
Lambeth sands	1300.0	1380.0	1.0×10^{-4}	1.220	0.649	1.90526×10^{-4}	0.13	1000.0
Thanet Sand	930.0	1120.0	2.0×10^{-4}	1.100	0.700	13.64×10^{-4}	0.165	2000.0

Table 6.1c Soil parameters used in analyses

Stratum	C_4	C_5	C_6 (°o)	c_3	c_4	$\varepsilon_{v(\min)}$ (%)	$\varepsilon_{v(\max)}$ (°o)	$K_{\min}$ (kPa)
Lambeth clays	530.0	460.0	5.0×10^{-4}	1.492	0.678	1.5×10^{-4}	0.16	5000.0
Lambeth sands	275.0	235.0	5.0×10^{-4}	1.658	0.535	5.1×10^{-4}	0.30	3000.0
Thanet Sand	190.0	110.0	1.0×10^{-4}	0.975	1.010	1.1×10^{-4}	0.20	5000 0

6.4.3 Numerical modelling

The initial conditions assumed the phreatic surface to be at 1m below ground level. Above the phreatic surface, a hydrostatic suction profile was assumed with a suction of 9.81kPa at ground level. At the commencement of the analysis the pore water pressure distribution was allowed to stabilise over a 5000yr period to match the profile observed in a nearby well (Figure 5.9). The stabilised pore water pressure profile was then used as datum for the vegetation boundary condition (invokation of the RWUM).

In the analyses, rainfall was modelled using the precipitation boundary condition. Ponding of rain water was not allowed at ground level. This was achieved in the analyses by limiting the maximum

predicted compressive pore water pressures to 0kPa. The vertical boundaries were prescribed as no flow boundaries. MORECS monthly values of rainfall (using the precipitation boundary condition) and potential evapotranspiration (using the RWUM) were used.

The modelled sequence of events is summarised in Table 6.2 while Table 6.3 gives a summary of the suite of analyses that were executed. The results of the analyses were output at the dates which coincide with the published data by Crilly and Driscoll (2000), to compare predictions with field measurements. The discussion focuses on a comparison of the movements predicted before and after felling the trees.

Table 6.2 Modelled sequence of events

Inc. No.	Description of event	Time
0	Set initial stresses assuming ground water level at 1m below ground level & surface suction of 9.81kPa.	0yrs
1-20	Allow stabilisation of pore water pressures to match well records.	5000yrs
21-32	Apply vegetation boundary condition and rainfall for January 1970.	1month
33-44	Apply vegetation boundary condition and rainfall for February 1970.	1month
45-56	Apply vegetation boundary condition and rainfall for March 1970.	1month
57 onwards to inc. 4196	Sequentially apply vegetation boundary condition and rainfall on a month by month basis until December 1998.	12 inc. per month

NB. Potential evapotranspiration data for deciduous trees was used from January 1970 to September 1990, after which potential evapotranspiration for grass was then used, following tree removal. It was assumed in the analyses that prior to September 1990 the density of grass cover beneath the tree canopy was nominal but after the trees had been cut, grass was able to quickly establish itself as the main vegetation cover in the former tree covered area.

Table 6.3 Summary of analyses

Run No.	r_{max}	S3 value in α function	Unload/reload stiffness ratio (H)
1	2m	200kPa	2
2	2m	50kPa	2
3	2.5m	200kPa	2
4	2m	200kPa	4

The convention used in the figures is as follows:

- suction and/or tensile pore water pressures (+ve)
- compressive mean effective stress, p' (+ve)
- compressive major (σ_1) and minor (σ_3) principal stresses (+ve)

6.5 Pore water pressure predictions

Crilly and Driscoll (2000) presented the matrix suction profiles inferred from laboratory filter paper tests for the site. The profiles produced by Crilly and Driscoll (2000) were for summer 1991, 1993 and 1995 (Figure 3 of their paper). The actual months are however not stated in their paper. In this study, the finite element predictions for pore water pressures at the end of September will be compared with the field profiles reported by Crilly and Driscoll (2000). The predictions using the RWUM for September 1991 and 1995 are shown in Figures 6.2a and b, respectively. The filter paper test results by Crilly and Driscoll (2000) have also been included in the figures, for comparison.

The interpretation of filter paper test results requires knowledge of the in situ mean effective stress, p', the magnitude of which has to be deducted from the filter paper results , to take account of stress relief induced by unloading on sampling. The results by Crilly and Driscoll (2000) are the uncorrected filter paper tests results hence, it is necessary to superimpose the p' profile to facilitate interpretation of their results as shown in Figure 6.2. It is also worthwhile to point out the fact that direct comparison of the finite element predictions should only be made with laboratory filter test results which have been corrected for p' (ie. the net suction after subtracting p'). In the absence

of a detailed K_0 profile, this has been achieved by assuming K_0 values of 1.0 and 2.5 as shown in Figure 6, to enable comparison to be made with the finite element predictions.

It can be seen from Figure 6.2a that field evidence suggests a desiccated profile to approximately 5m depth at the end of summer 1991, as opposed to approximately 12m predicted by the RWUM. The prediction of large suctions by the RWUM at depths greater than 4m and the reasons for it have already been discussed at length in the previous chapter and will therefore not be repeated here. However, it is encouraging to note that over the depth of interest (0-4m bgl), the finite element predictions are approximately of the same order with field measurements; 20 years after application of the RWUM. It can also be seen that the depth at which maximum suctions are predicted by the RWUM is identical to the field value, which again portrays the ability of the RWUM in predicting pore water pressure changes. Maximum suctions of 430kPa are predicted by the RWUM compared to 460kPa measured in the field (after deducting the p' for a K_0 of 2.5), which is considered to be a good prediction in the light of the uncertainties regarding p' and time of sampling, discussed above.

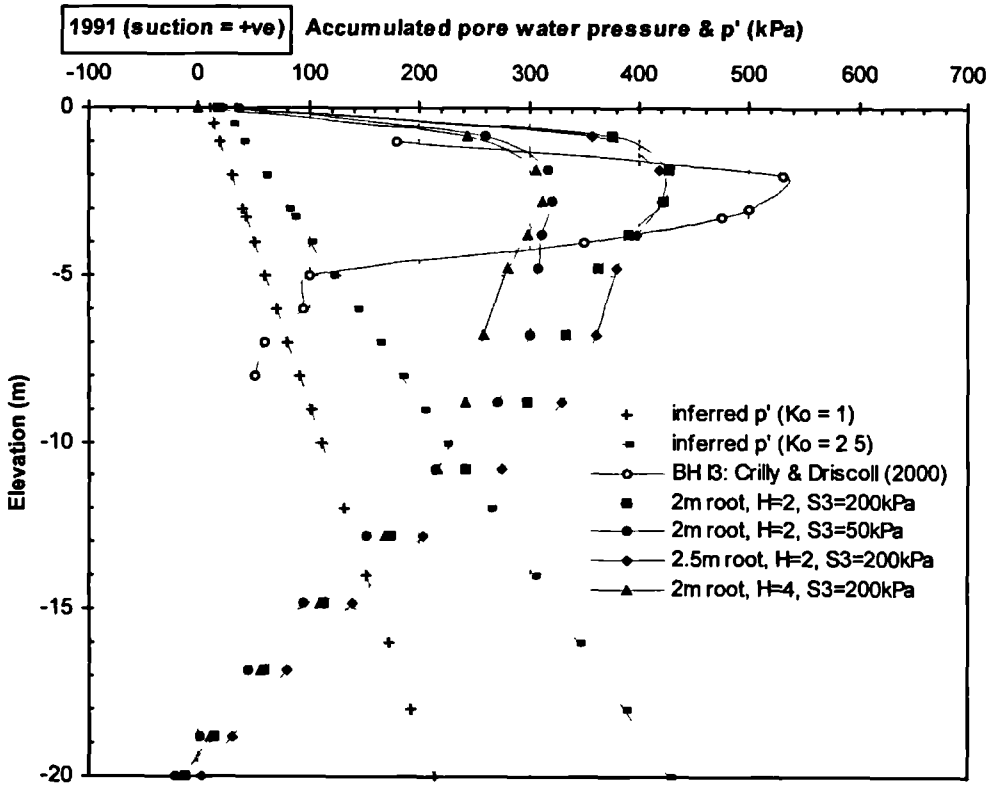

Figure 6.2a Comparison of pore water pressures predictions by the RWUM and filter paper tests by Crilly & Driscoll (2000) for summer 1991. (NB. RWUM predictions are for end of September).

Figure 6.2b shows the pore water pressure predictions for summer 1995. The field data indicates a marked reduction in the magnitude of suctions (180kPa) between 1 and 2m depth, however, this is not mirrored in the predictions by the RWUM. Another notable difference between field data and the RWUM predictions is the elevation at which maximum suctions occur. The RWUM still predicts the maximum suctions at 2m depth of 425-535kPa as opposed to the field data which shows maximum suctions at 3m depth of 700kPa; after deducting the p' for a K_0 of 2.5. Nevertheless, despite these differences, the overall pattern of pore water pressure distribution predicted by the RWUM in 1995 is similar to the field data. This is considered to be reasonable in the light of assumptions that have been made concerning the field data in addition to the limitations of the constitutive and permeability models.

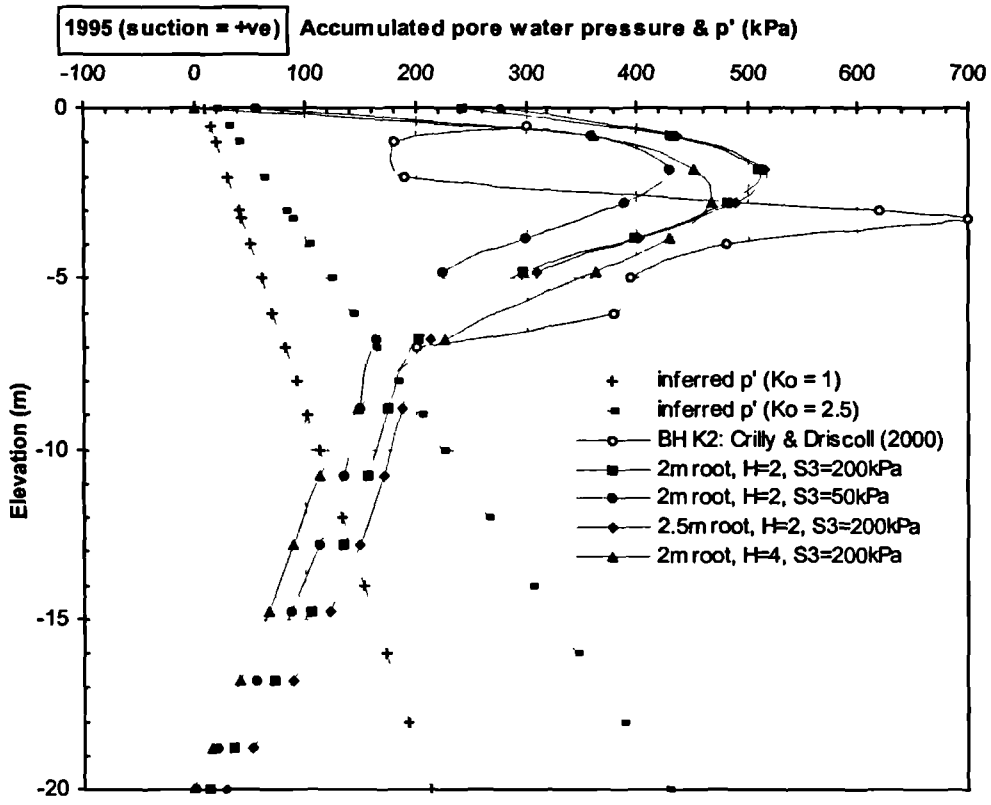

Figure 6.2b Comparison of pore water pressures predictions by the RWUM and filter paper tests by Crilly & Driscoll (2000) for summer 1995. (NB. RWUM predictions are for end of September).

6.6 Prediction of vertical ground movements

6.6.1 Period prior to cutting of trees

Freeman *et al* (1991), Crilly *et al* (1992) and Crilly & Driscoll (2000) give details of the vertical movements measured in the tree covered area at ground level, 1m, 2m 3m and 4m depth, respectively (June 1988 to September 1990), prior to felling of the trees. The corresponding predictions by the RWUM for the cases summarised in Table 6.3 are depicted in Figures 6.3 and 6.4. The results of BRE's monitoring (Figure 4 of Crilly and Driscoll (2000)) are also included in Figures 6.3 and 6.4, for comparison.

It is interesting to note that the prediction of vertical movements are not significantly affected by the magnitude of S3, r_{max}, or the unload/reload stiffness ratio, after 20 years of application of the RWUM. Overall, the predicted pattern of movements is similar to field observations and the following main points can be highlighted:

- The magnitude of S3, r_{max} and unload/reload stiffness does not have a significant influence on the predictions of vertical movements.

- The RWUM reproduces the seasonal cyclic movements identified at Chattenden ie. heave during winter and shrinkage during summer.

- Overall, the RWUM overpredicts the magnitude of the seasonal movements. The degree of overprediction varies with depth and the season. At shallow depth eg. ground level the greatest overprediction occurs in the magnitude of heave whereas at deeper horizons, eg. 4m depth the largest overpredictions occurs in the shrinkage movements.

- The RWUM reproduces the pattern of field measurements which indicates a net shrinkage of the ground of approximately 25mm at the end of the 3 year period (June 1998-June 1991).

- There is evidence that the RWUM redistributes suctions to deeper horizons. The redistribution results in overprediction of shrinkage movements at depth eg. the field data indicates a net settlement of 10mm at 4m depth at the end June 1991 whereas predictions by the RWUM indicate net settlements of 80mm, which is 8 times higher than the field measurement.

- Overall, the RWUM reproduces the observed field pattern of movements which indicates decreasing magnitude of movements with depth.

The differences between predicted and field measurements identified above are also portrayed in Figure 6.5 where predictions at 1m depth (Figure 6.5a) and at 4m depth (Figure 6.5b) are plotted. The similarities in the magnitude of predicted movements by the 4 analyses is evident at both elevations. Both confirm the large cyclic movements associated with the RWUM compared to the magnitude of movements that actually occurred in the field. It is considered that the predictions could be significantly improved if some facets of the constitutive model were improved; not least the ability to accurately reproduce the shrinkage characteristics of the soil at large strains such as those that prevail in the field. Figures 6.5a and b also reveal that the error in predictions increases with time. This is considered to be caused by the redistribution of suctions to deeper horizons predicted by the RWUM.

6.6.2 Period after cutting of trees

As previously mentioned, the trees in the test area were cut down towards the end of September 1990 to initiate heave. In the predictions carried out in this investigation, it has been assumed that after the trees were removed, grass established itself as the primary vegetation in the formerly treed area. Potential evapotranspiration rates for grazing grass were therefore used in the RWUM, with an r_{max} of 0.5m, during the post-September 1990 period. Unfortunately, the degree to which grass cover occurred at the site was not documented therefore the potential evapotranspiration rates for grazing grass may significantly differ from the field values.

The predictions of heave together with the monitoring data by BRE are shown in Figures 6.6 and 6.7. Movements for the first 5years only are shown. The overall pattern can be summarised as follows:

- The seasonal cyclic movements match field behaviour and are characterised by a gradually increasing magnitude of heave throughout the 5 year period.

- The magnitude of swell diminishes with depth, which is similar to the pattern of field measurements. However, it is noteworthy that whilst field measurements reveal very little heave (less than 5mm) at 4m depth, the RWUM predicts heave ranging from 20-40mm at the same depth.

- The RWUM predicts significantly larger cyclic movements at ground level (average winter/summer magnitudes of 50mm) compared to 10mm measured in the field. The amplitude

of the seasonal movements significantly reduces with depth. This is considered to be a result of larger evapotranspiration rates that have been modelled compared to field rates.

- Maximum heave of 140mm was measured at ground level in the field during the first 5 years of swelling compared to 140-150mm by the RWUM, which is considered to be a good prediction. However, it is also noteworthy that the analysis involving an unload/reload stiffness of 4 predicts maximum heave of 125mm during the same period as a result of the very high stiffness value on unloading.

- Overall, the field measurements reveal that the response to water recharge commences at ground level and gradually advances downward with time eg. significant heave at 2m depth in the field only starts 2 years after felling the trees compared to within less than 3 months at ground level and 1m depth. The corresponding response at 3m depth in the field takes even longer (3years). This behaviour reflects the gradual advance of the wetting front. In contrast, the predictions by the RWUM indicate very little lag in response over the 4m depth of interest. The prediction of ground response to water recharge is rapid and takes place within 3 months between 0-3m depth, with significant response being predicted at 4m depth by the end of the 6 month.

Figure 6.8 depicts a comparison of predicted and measured movements at 1m depth (Figure 6.8a) and at 4m depth (Figure 6.8b) during the same period. The figure confirms the good match in predictions at ground level identified earlier and the "quick" response to increasing compressive pore water pressures down to 4m depth during the first 6 months after cutting the trees. The significant heave occurring at 4m depth predicted by the RWUM is considered to be a result of the large strain reversals as pore water pressures recover following significant redistibution of suctions to deeper horizons, prior to the removal of the trees. In comparison, the degree of desiccation observed in the field was much smaller and this is also mirrored the comparatively small magnitude of heave observed in the field.

6.7 Summary

Predictions of pore water pressure profiles at the end of summer 1991 and 1995 using the RWUM have been compared with field measurements by BRE. The field measurements by BRE do not specify the exact month during which the samples were taken. In the absence of such information, the results for September have been selected for comparison with BRE's field measurements reported by Crilly and Driscoll (2000).

The predictions of pore water pressures by the RWUM at depths less than 5m are approximately of the same order of magnitude to the field measurements. The depth at which the maximum suctions are predicted also matches the field value. However, the RWUM overpredicts the depth of desiccation. The possible reasons for this were discussed in greater detail in Chapter 5.

A comparison of ground movements has been made with predictions by the RWUM. The predictions have indicated that the magnitude of S3 in the α function, maximum root depth, r_{max}, and unload/reload stiffness ratio, H, of the London Clay, have a small effect on the predictions of pore water pressures and ground movements after 20 years' application of the RWUM.

Overall, the predicted cyclic pattern of movements is similar to field observations. The predictions also reproduce the observed pattern which indicates the magnitude of movements reducing with depth. However, the magnitude of cyclic vertical movements predicted by the RWUM each season are larger than field measurements. Prior to removal of the trees (pre-September 1991), the predictions indicate overprediction of heave movements at shallow depth coupled with overprediction of settlements at deeper horizons. The latter is attributed to the greater degree of redistribution of suctions to deeper horizons and is considered to be caused by the inability of the constitutive and permeability models to reproduce volume changes and water flows consistent with field behaviour.

During heave (post September 1990 period), the pattern of movements predicted by the RWUM matches the field pattern. The magnitude of heave at ground level predicted by the RWUM closely matches the field values. However, at deeper horizons 3-4m depth the predictions of heave are significantly larger than the field measurements. This is expected because prior to tree removal, the RWUM had predicted a much deeper desiccated profile. The field measurements indicated that during swelling, the wetting front advanced slowly from shallow to deeper strata whereas the advance of the wetting front predicted by the RWUM was relatively "quick" over the 4m depth under consideration.

It is also noteworthy that Crilly *et al* (1992 & 2000) noted a discrepancy between the measured vertical displacements and those calculated using a water shrinkage factor approach (assuming fully saturated soil mechanics). This underscores the complexities and difficulties associated with developing a theoretical model which can reproduce the vertical strains associated with volumetric changes in cracked ground.

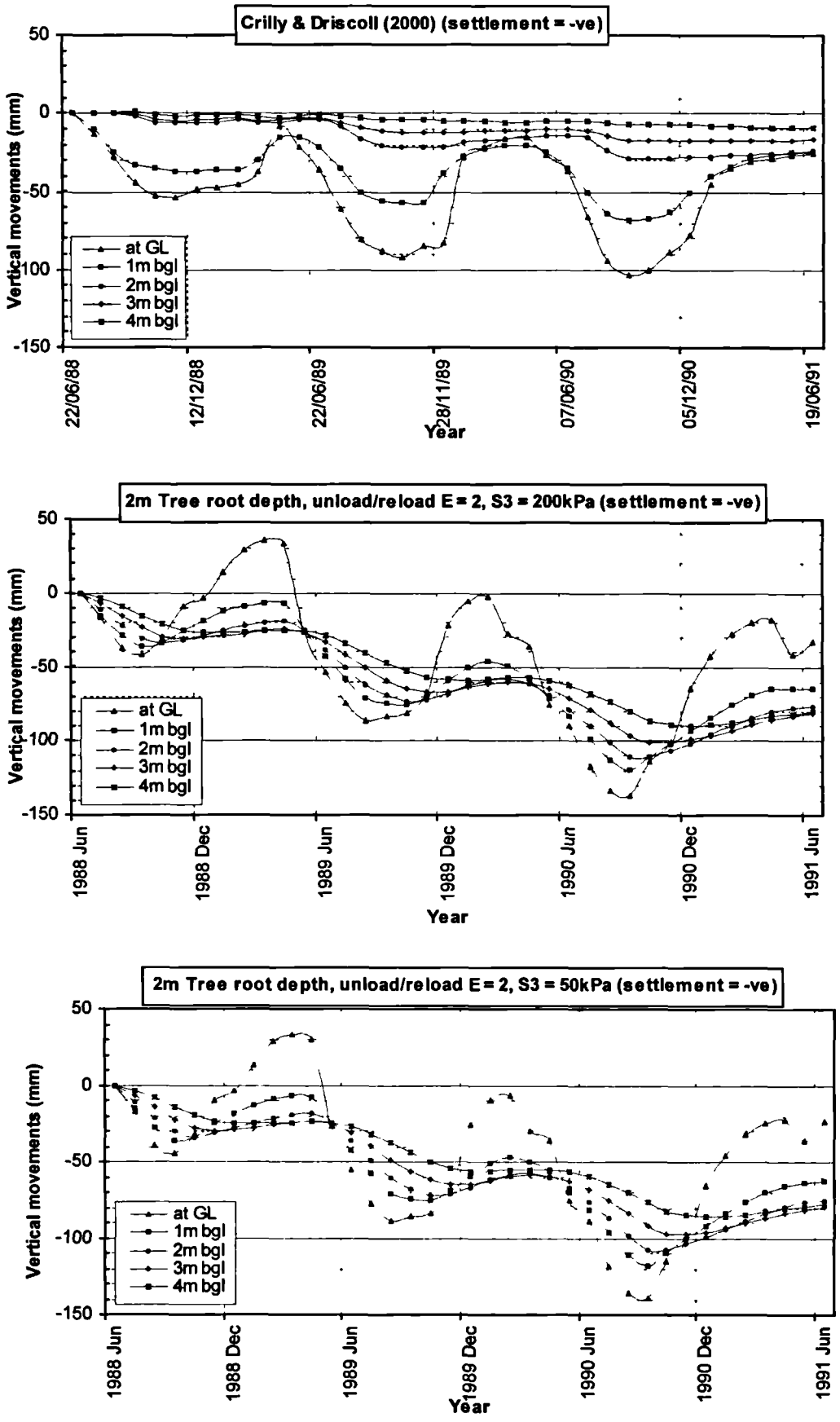

Figure 6.3 Predictions of vertical ground movements at Chattenden BRE site (Jun 1988-June 1991).

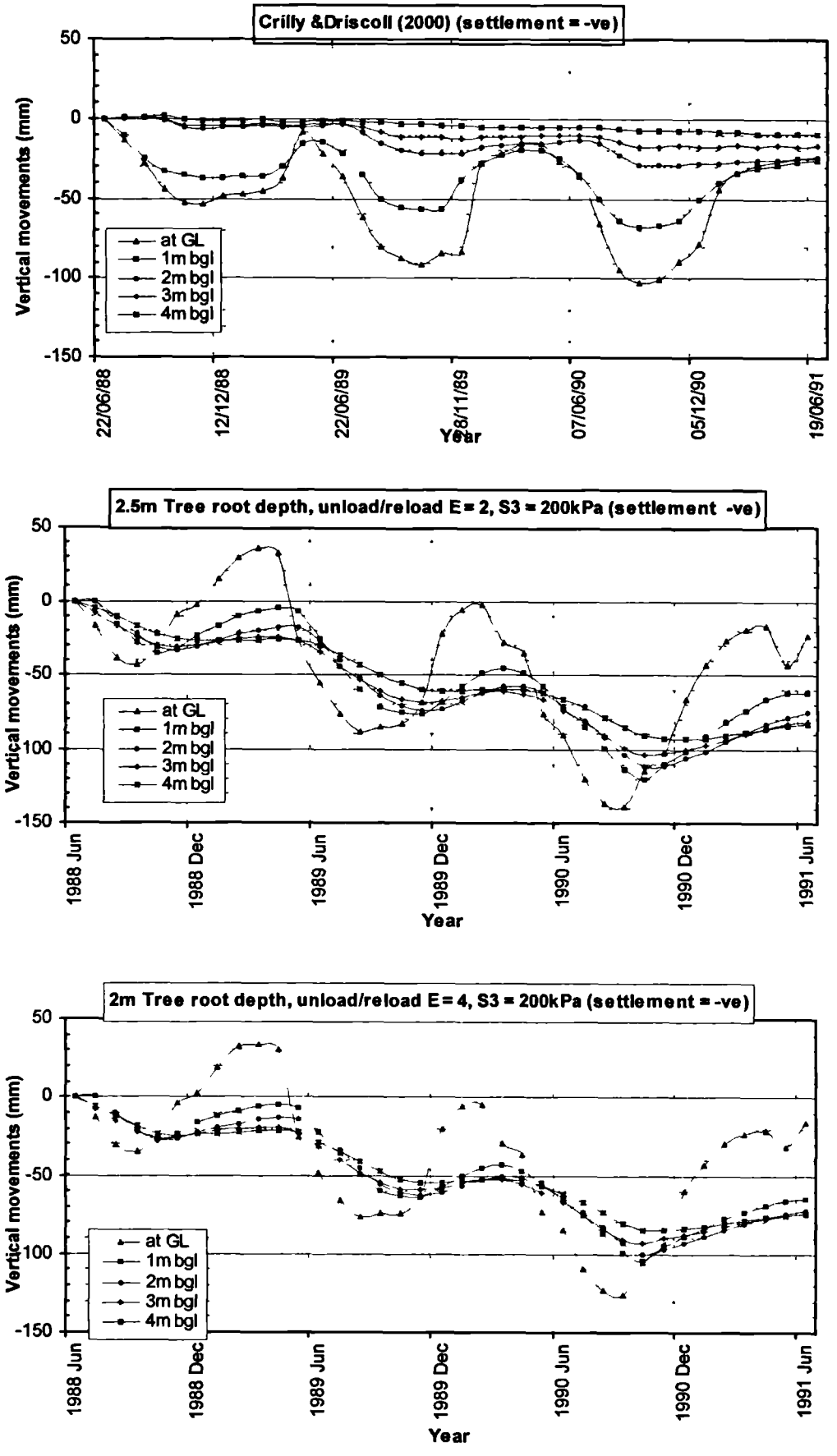

Figure 6.4 Predictions of vertical ground movements at Chattenden BRE site (Jun 1988-June 1991).

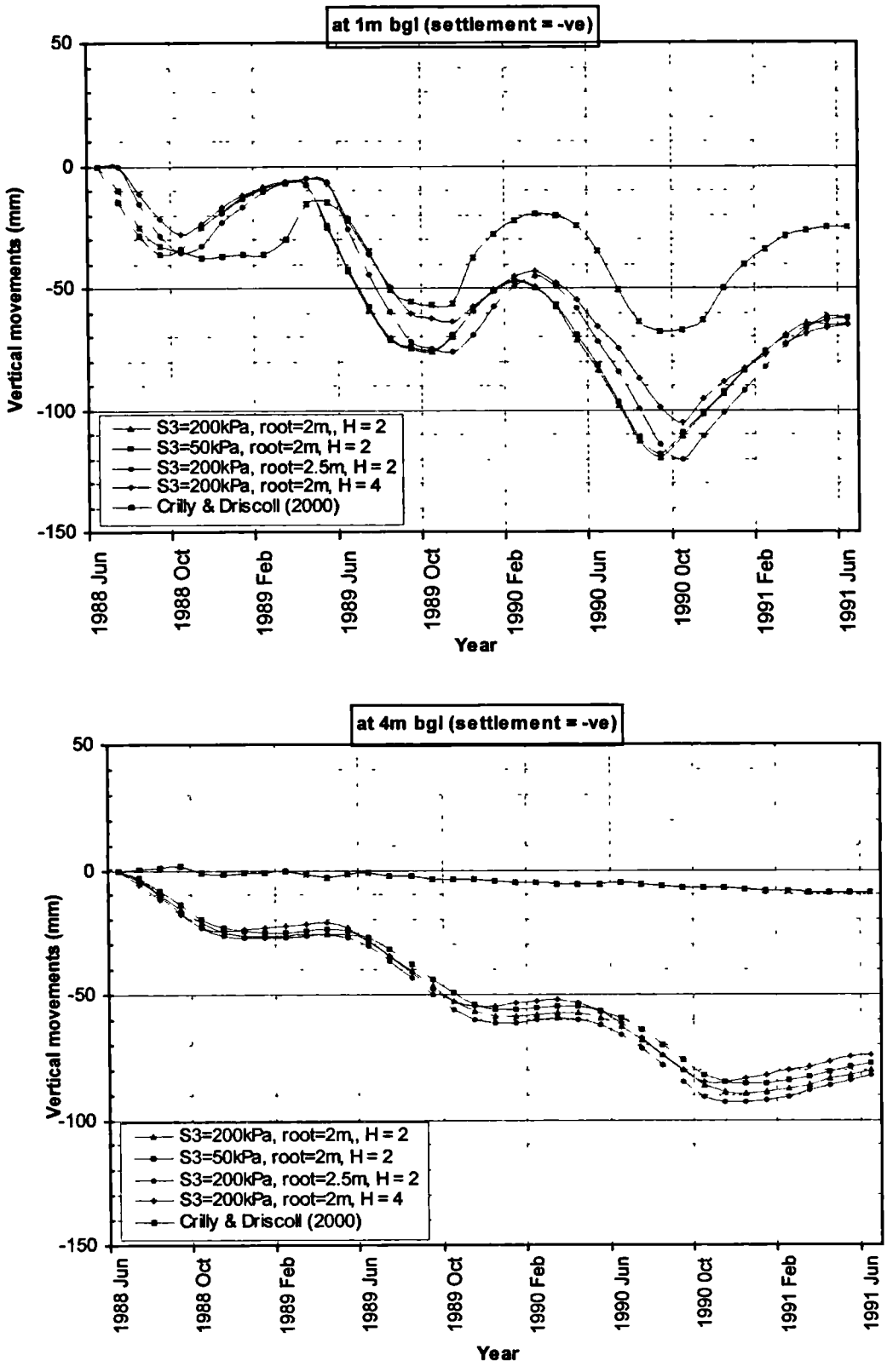

Figure 6.5 Comparison of vertical movements predictions for Chattenden using various combinations of maximum root depth, S3, and unload/reload E ratio (Jun 1988-Jun 1991).

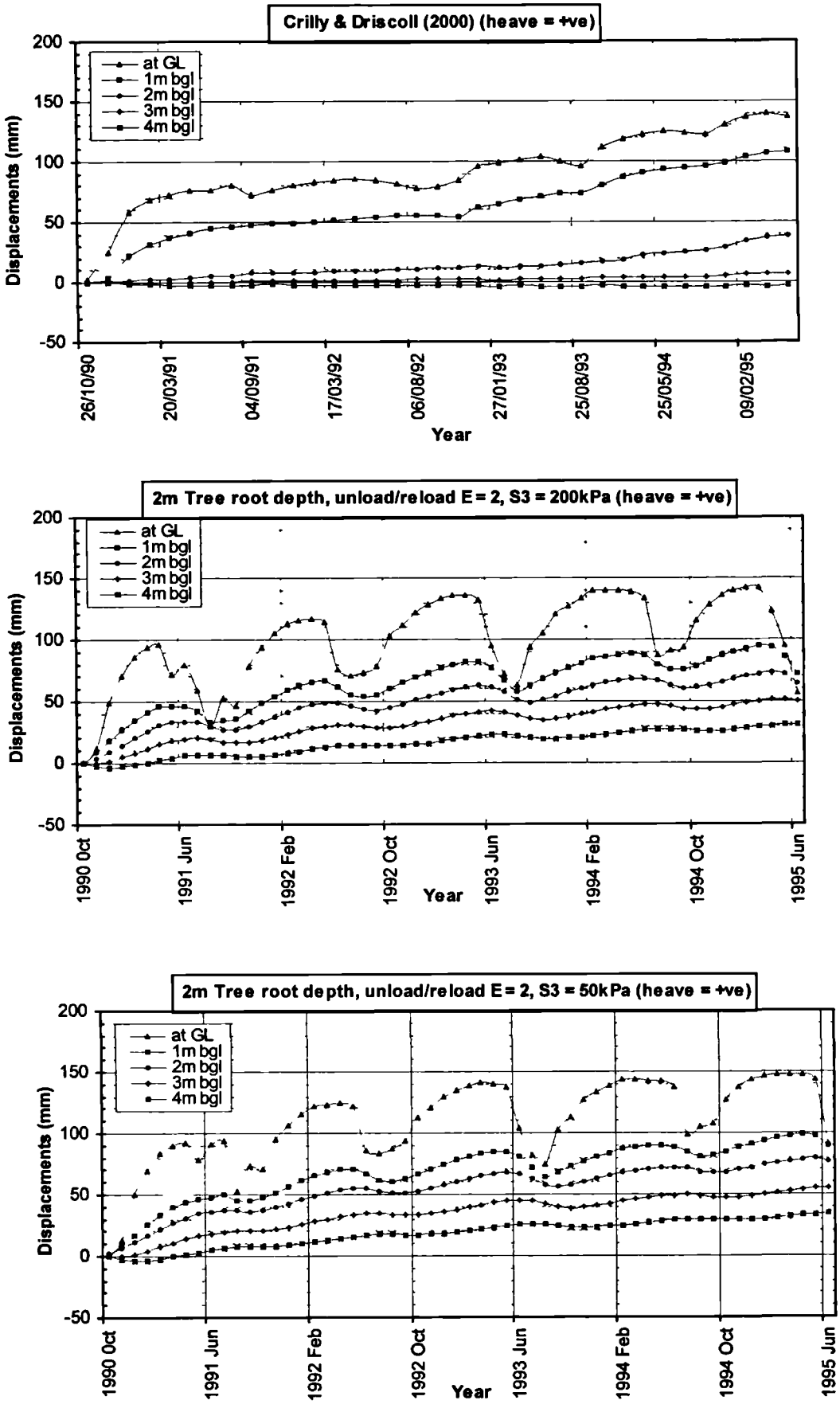

Figure 6.6 Predictions of heave at Chattenden BRE site after felling trees in September 1990 (Oct 1990-Jun 1995). During heave, grass with r_{max} of 0.5m is assumed.

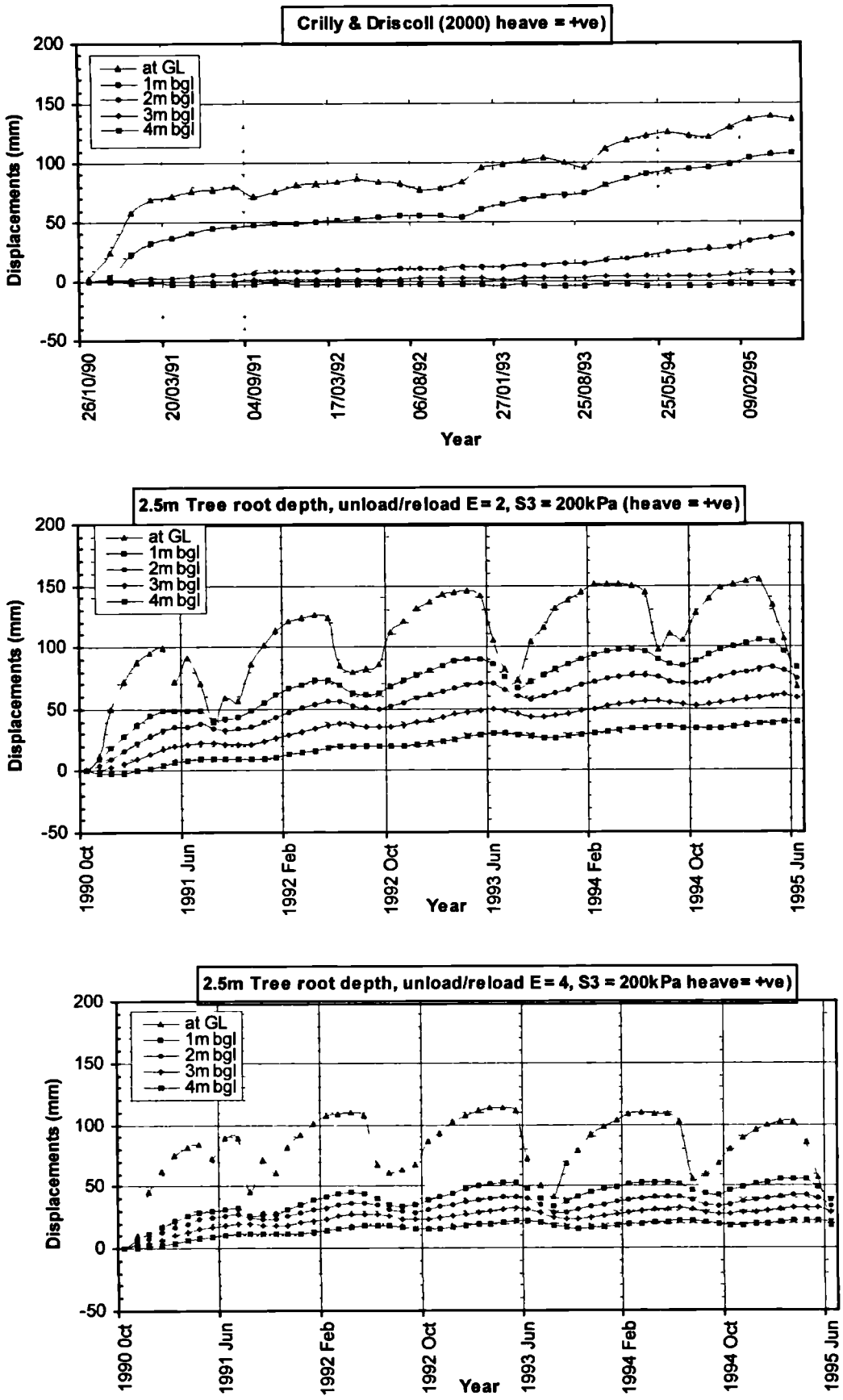

Figure 6.7 Predictions of heave at Chattenden BRE site after felling trees in September 1990 (Oct 1990-Jun 1995). During heave, grass with r_{max} of 0.5m is assumed.

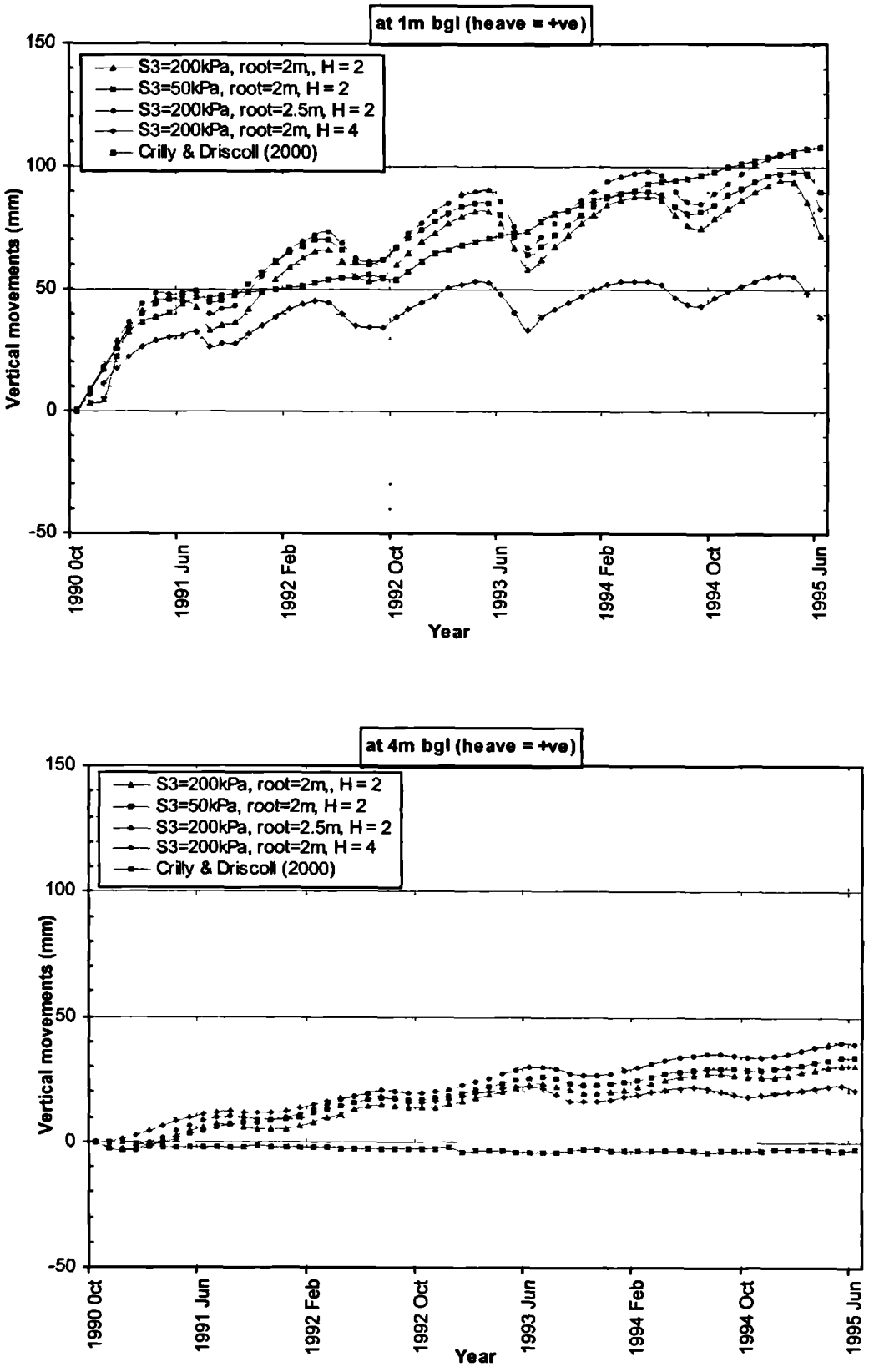

Figure 6.8 Comparison of heave predictions for Chattenden using various combinations of maximum root depth, S3, and unload/reload E ratio (Oct 1990-Jun 1991). During heave, grass with r_{max} of 0.5m is assumed.

Chapter 7

EMBANKMENT ANALYSIS USING A ROOT WATER UPTAKE MODEL

7.1 Introduction

The state-of-the-art approach in the UK industry to analyse the stability of embankments which experience seasonal pore water pressure changes induced by vegetation was described in Chapter 4. The shortcomings associated with the method were discussed, from which it was concluded that an efficaceous method would be to model the pore water pressure changes induced by vegetation using root water uptake models. The development of a typical root water uptake model amenable to geotechnical numerical analysis was presented in Chapter 5. The model was validated against field data from a Building Research Establishment testing site at Chattenden in Kent (SE England) and gave reasonable predictions (Chapter 6).

This chapter presents results from stability analyses carried out on a typical UK vegetated railway embankment using the root water uptake model. The geometry and stratigraphy of the embankment analysed is identical to that used in the analyses for Chapter 4. The focus of this chapter is to demonstrate the applicability of the root water uptake model in reproducing the seasonal pattern of pore water pressure changes, movements and the development of a progressive failure mechanism. Four main areas were investigated in the embankment analyses as follows:

(i) the influence of the maximum root depth, (Section 7.3)
(ii) the influence of the stiffness of the clay fill (Section 7.4)
(iii) the influence of permeability increases due to desiccation cracking (section 7.5)
(iv) the influence of the mass permeability of the clay fill (Section 7.6)

In all cases, the discussions focus on the pattern and magnitudes of movements, pore water pressure changes and the rate of propagation of the progressive failure mechanism. The shortcomings associated with the model (as currently coded) are also highlighted. The chapter ends with a summary of the key points drawn out of the sensitivity/parametric studies.

The convention used in the figures is as follows:

- suction and/or tensile pore water pressures (+ve)
- compressive mean effective stress, p' (+ve)
- compressive major (σ_1) and minor (σ_3) principal stresses (+ve)
- heave = +ve)

7.2 Embankment model and numerical modelling

7.2.1 The mesh

An identical mesh to the one described in Chapter 4 was used. For convenience, the salient features are outlined once more. Figure 4.2 shows the mesh used in the analyses. The embankment was assumed to be 7m high, 12m wide at the crest, with a 1 in 2.5 side slope angle and symmetrical. The embankment was assumed to be constructed from London clay fill (6m thick) with a 1m deep ash mantle at the top. The foundation was assumed to comprise London Clay up to 100m deep.

7.2.2 Material properties

The soil parameters used in the analyses are summarised in Table 7.1. An elasto-plastic soil model in terms of effective stress, with a pre-failure stiffness (E') as a linear function of mean effective stress was used. The strain-softening Mohr-Coulomb failure criterion described in Section 3.5 of Chapter 3 was used with an angle of dilation equal to zero.

Coupled consolidation/swelling was used throughout, with pore water pressures varying with time according to the specified permeabilities and drainage conditions. The soil properties adopted are very similar to the values used in previous analyses of these embankments (Vaughan, 1994; ICON, 1999b and Kovacevic *et al,* 2001). The strength parameters were confirmed through laboratory tests carried out on samples retrieved from a number of embankments across the LUL network (Mott MacDonald, 1999a).

The clay fill and foundation were assumed to have enhanced linear elastic unload-reload characteristics different from first loading. These assumptions take account of the increase in stiffness arising from the consolidation which occurs during and soon after construction. Permeability was assumed to be dependent on mean effective stress according to a power law (Vaughan, 1987). In the permeability sensitivity studies, three magnitudes of initial mass

permeability of the clay fill were used ie. $1\times10^{-9}e^{-0.003p'}m/\sec$, $1\times10^{-8}e^{-0.003p'}m/\sec$ and $1\times10^{-7}e^{-0.003p'}m/\sec$. The permeability of the foundation was kept the same ($2\times10^{-10}e^{-0.0075p'}m/\sec$). In the sensitivity analyses to investigate the influence of the magnitude of increase in permeability of cracked ground, ratios of cracked to uncracked permeability ($\frac{k_f}{k_i}$ ratio) of 10 and 100 were used. It is also noteworthy that in all other sensitivity analyses, a $\frac{k_f}{k_i}$ ratio of 10 was used for both the clay fill and foundation materials.

Table 7.1 Soil parameters used in analyses

Parameter	Ash fill	London Clay fill	In situ London Clay
Bulk unit weight	10.5kN/m^3	18.1 kN/m^3	18.8 kN/m^3
φ′ (peak)	36°	22.9° (at 0-5% strain)	20° (at 0-5% strain)
φ′ (residual)	N/A	13° (at 50% strain)	13° (at 20% strain)
c′ (peak)	2	5kPa (at 0-5% strain)	2kPa (at 0-5% strain)
c′ (residual)	N/A	3.4kPa (at 50% strain)	2kPa (at 20% strain)
Permeability	Free draining	Case 1: $1\times10^{-9}e^{-0.003p'}m/\sec$ Case 2: $1\times10^{-8}e^{-0.003p'}m/\sec$ Case 3: $1\times10^{-7}e^{-0.003p'}m/\sec$	$2\times10^{-10}e^{-0.0075p'}m/\sec$ for all three cases
Coefficient of earth pressure at rest, K_0	N/A	N/A	2.5 at ground level and reducing linearly to 1.0 at 15m depth
Stiffness (kPa)	1000 (linear elastic)	$E=2500\left[\frac{100+p'}{100}\right]$ (during construction - min=2500) $E=5000\left[\frac{100+p'}{100}\right]$ (after construction - min=5000)	$E=5000\left[\frac{100+p'}{100}\right]$ (during construction- min=5000) $E=10000\left[\frac{100+p'}{100}\right]$ (after construction - min=5000)
Poisson's ratio	0.3	0.3 (during construction) 0.2 (after construction)	0.2 (during and after construction)

7.2.3 Initial conditions, boundary conditions and sequence of analysis

The London Clay foundation was modelled with $K_0 = 2.0$ at ground level, reducing to 1.0 at 15m depth. A constant value of $K_0 = 1.0$ was used below 15m depth. A hydrostatic pore water pressure profile was assumed with a water table at 1m below ground level (ie. the hydrostatic profile gave a suction of 9.81kPa at ground level). This profile was chosen primarily to avoid instability of the embankment during construction. A rigid boundary was assumed at the base of the mesh at which zero vertical and horizontal movements were prescribed. Along the vertical left and right hand side boundaries, zero horizontal movements were prescribed but vertical movement was allowed. The vertical and bottom boundaries were prescribed as no flow boundaries.

The embankment clay fill was constructed in 7 layers (increment 1-7) with a suction of 50kPa prescribed during construction. The magnitude of suction is considered to be close to that which would have prevailed in the clay fill during construction, assuming stress relief in fill material sourced from cuttings averaging 5m depth. It is also noteworthy that some of the fill material used in embankments would have been sourced from tunnel excavations and the latter material is likely to have had higher suctions. However, the magnitude of suctions would have reduced during transportation and handling as a result of frequent precipitation (typical of UK "wet" climate) hence an overall value of 50kPa is considered to be reasonable (Skempton, 2000).

The ash ballast was constructed in two layers with zero pore water pressure prescribed. The use of layered construction and the construction assumed times (see Table 7.1) are considered to be representative of end-tipping, and is characterised by negligible consolidation of the foundation at the end of construction. The stiffness of the clay fill and foundation material were increased at the end of construction (inc. 8), to values shown in Table 7.1.

An assumption was made that vegetation would take up to 5 years to establish itself before it began to induce significant desiccation within the embankment. This was modelled by allowing the embankment to consolidate to a pore water pressure of 0kPa at the clayfill-ash interface and a 10kPa suction maintained on the slope of the embankment and top of the foundation beyond the toe of the embankment (inc. 9-20) (Figure 4.1b). After the 5 year consolidation/swelling period, the vegetation boundary condition was then applied. Each month was modelled in 12 increments ie. inc. 21-32 (January year1), inc. 33-44 (February year 1), inc. 45-56 (March year 1) etc.

In the sensitivity studies to determine the influence of maximum root depth (r_{max}), values of 2m, 2.5m and 3m were used. In all other parametric/sensitivity analyses, an r_{max} of 2.5m was used. Meteorological data from MORECS comprising potential evapotranspiration and rainfall for deciduous trees for the Chattenden site (Figure 5.13) were used. Median values were used for the MORECS data.

Vegetation was assumed to be growing over the whole surface boundary except across the crest width. Across the crest of the embankment, the contribution of evaporation on the bare surface was assumed to be 50% of the potential evapotranspiration values shown in Figure 5.13. The key stages of construction and application of the root extraction model are summarised in Table 7.2.

Table 7.2 Modelled sequence of events

Stage	Inc. No.	Description of event	Time
0	0	Set initial stresses using assuming ground water level at 1m below ground level & surface suction of 9.81kPa.	0 yrs
2	1-7	Construct loose London Clay fill quickly in 7 layers (each approx. 1m thick). Assume a suction of 50kPa in fill as placed.	0.08 yrs
3	8-20	Allow the fill and foundation to consolidate to a surface suction of 10kPa for 5 yrs. During this period, the effects of vegetation are assumed to be nominal.	5 yrs
4	21-32	Apply vegetation boundary condition and rainfall for January (year 1).	1 month
4	33-44	Apply vegetation boundary condition and rainfall for February (year 1).	1 month
4	45-56	Apply vegetation boundary condition and rainfall for March (year 1).	1 month
4 onwards	57 onwards	Sequentially apply vegetation boundary condition and rainfall on a month by month over period of interest or until failure, whichever is earlier.	12 inc. per month up to 5 yrs

The discussions in the following sections will focus on the period during which the RWUM was in operation (ie. from increment 20 onwards). For clarity, January year 1 is assumed to be datum for the time/periods quoted in the discussions.

7.3 Influence of maximum root depth

7.3.1 Introduction

The root water uptake model (RWUM) presented in Chapter 5 offers a major improvement to current methods of modelling pore water pressures induced by vegetation in that root water uptake is modelled using meteorological input data (rainfall and potential evapotranspiration). This enables pore water pressures to be predicted rather than prescribed. In the RWUM, the assumed maximum root depth (r_{max}) determines the overall depth over which water abstraction actively takes place. The rate at which water recharge occurs in the zone of abstraction is dependent on the permeability of the soil and this aspect is investigated in Sections 7.4 and 7.5. In this section, the results of studies executed to investigate the influence of r_{max} on the behaviour of a typical vegetated old railway embankment are presented.

7.3.2 Numerical modelling

The mesh, soil properties and modelling procedure used were as described in Section 7.2. The vegetation boundary condition was applied in three analysis assuming the following values of r_{max} (i) 2m (ii) 2.5m and (iii) 3m. As previously mentioned in Section 7.2, the vegetation boundary condition was not applied in the ash mantle/ballast as this area was assumed to be unvegetated. Where the vegetation boundary condition was applied (embankment slope and top of foundation remote from the embankment, r_{max} was assumed to be constant during each analysis.

7.3.3 Behaviour during summer (yr 1)

Invokation of the vegetation boundary condition (RWUM) commenced in January, which is a wet month. In UK, peak winter pressures (least suctions) usually occur towards the end of January/February. This is followed by spring, which marks the onset of vigorous vegetation growth, moisture depletion, and development of a moisture deficit in the ground. Spring and summer are characterised by relatively low rainfall as shown in the meteorological data in Figure 5.13.

Figure 7.1a shows the pore water pressure distribution at the beginning of January yr 1 for all the three r_{max}, prior to invokation of the RWUM. The distribution typically shows a zero pore water pressure line at approximately 1m below ground level on the slope and beneath ground level in the zone remote from the embankment in response to the applied pore water pressure

boundary condition during the 5 year swelling/consolidation period. The accumulated plastic strains at this stage are nil, as shown in Figure 7.1b.

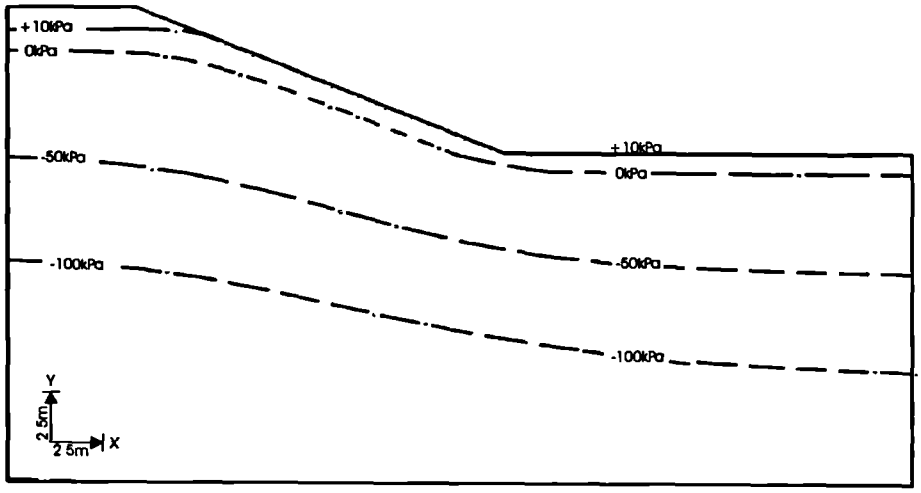

(a) Contours of accumulated pore water pressure at commencement of vegetation boundary condition (Jan yr1).

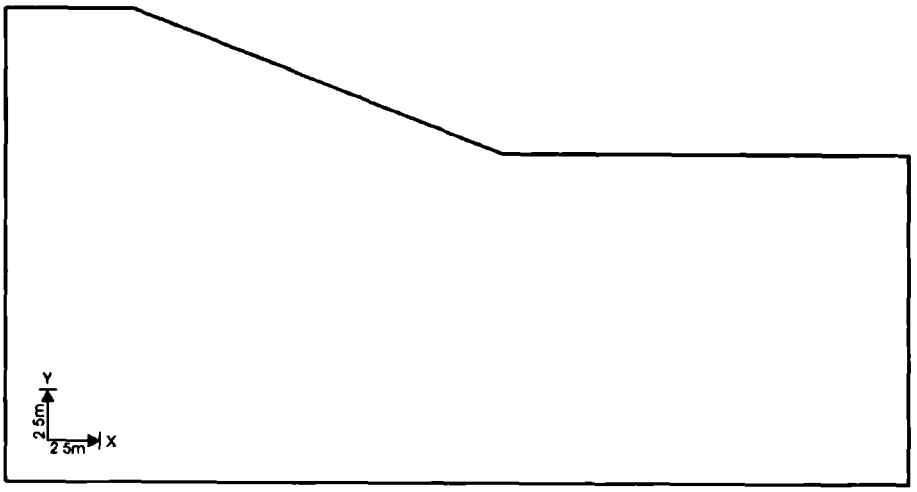

(b) Contours of accumulated plastic strains at commencement of vegetation boundary condition (Jan yr1).

Figure 7.1 Contours of accumulated pore water pressure and deviatoric plastic strains at the commencement of the vegetation boundary condition (Jan yr1).

The predicted accumulated pore water pressure contours in the embankment towards the end of the first summer (August yr 1) ie. after 8 months application of the RWUM are shown in Figure 7.2. It can be seen that a desiccated profile is predicted in the ground. In general, the maximum suctions in the embankment are predicted at the toe of the slope. Overall, the zone of maximum suctions increases as r_{max} reduces eg. zone demarcated by 700kPa contour. This difference, is expected when the pore water pressures prior to invokation of the RWUM are considered in the context of the α function.

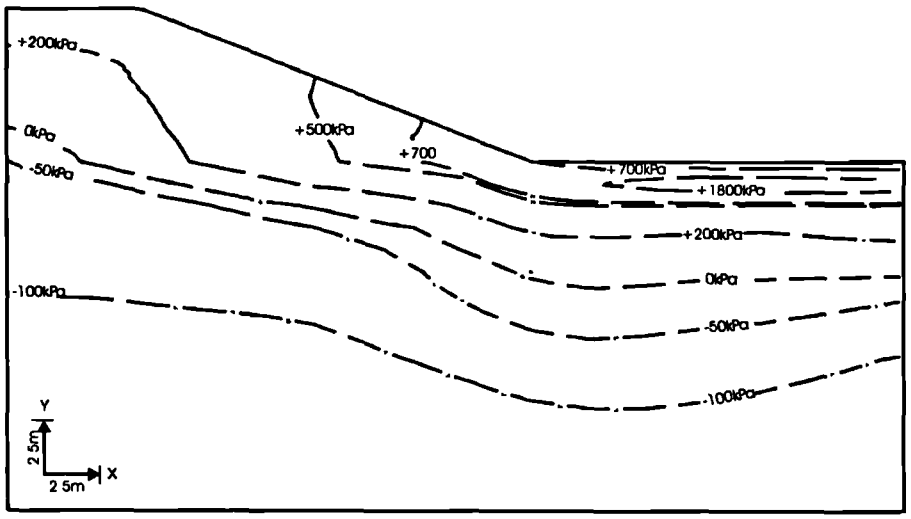

(a) Maximum root depth = 2m

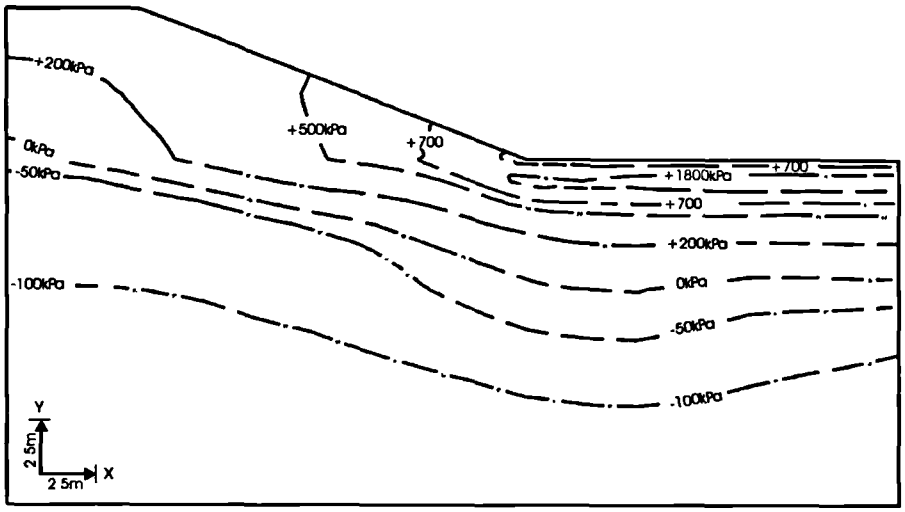

(b) Maximum root depth = 2.5m

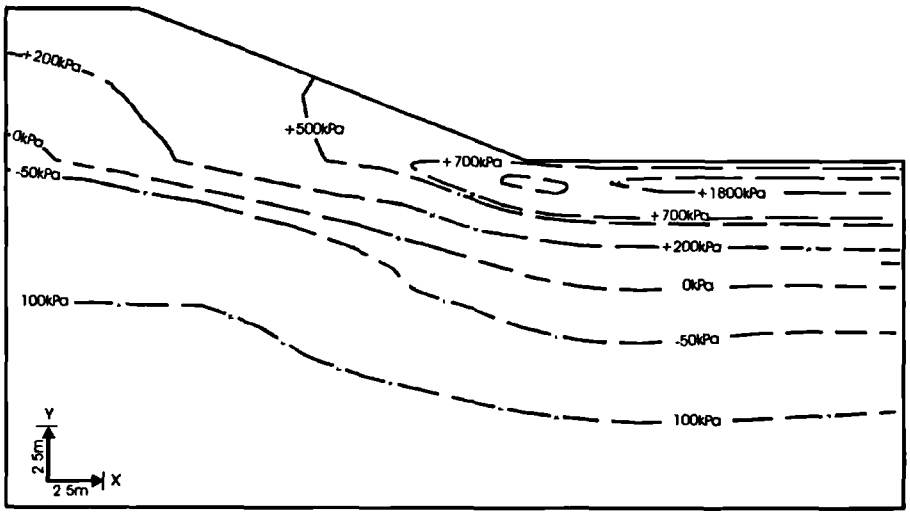

(c) Maximum root depth = 3m

Figure 7.2 Contours of accumulated pore water pressure predicted by r_{max} of 2m, 2.5m and 3m at the end of the first summer (Aug yr1).

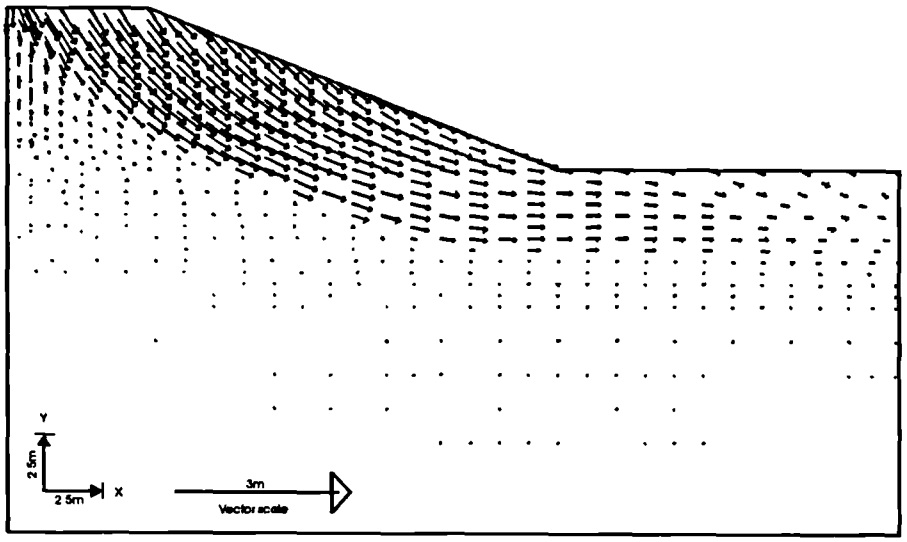

(a) Maximum root depth = 2m

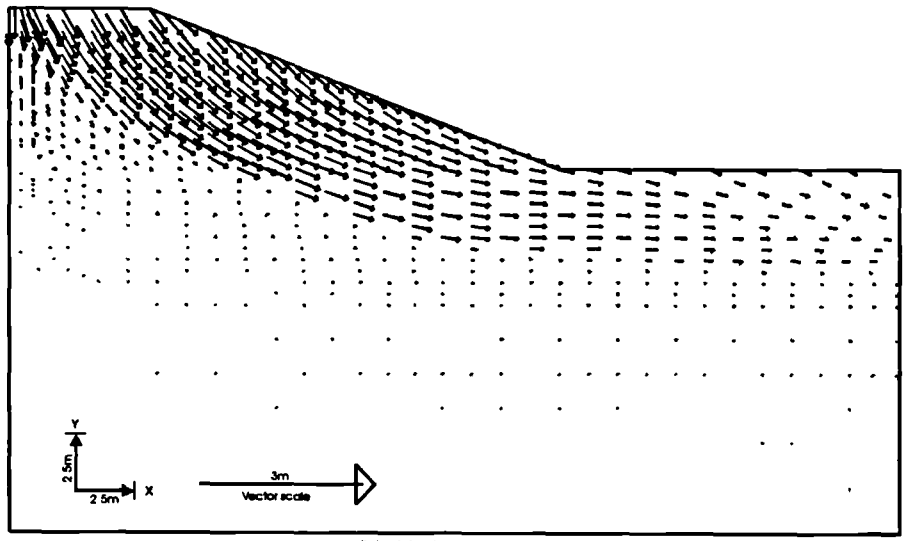

(b) Maximum root depth = 2.5m

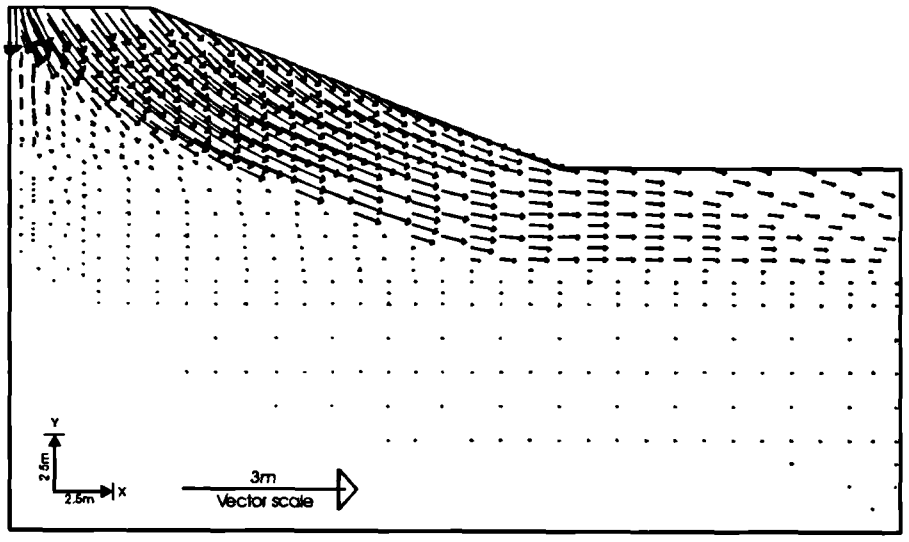

(c) Maximum root depth = 3m

Figure 7.3 Vectors of sub-accumulated movements predicted by r_{max} of 2m, 2.5m & 3m during the first summer (Mar-Aug yr1)

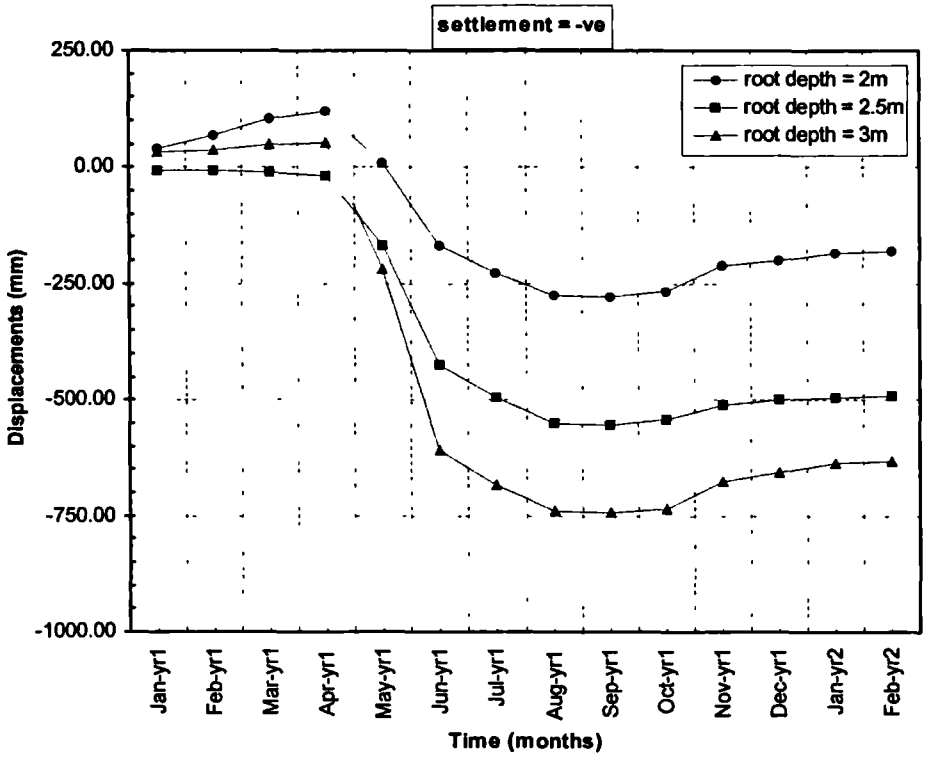

Figure 7.4a Sub-accumulated vertical movements at the crest centreline predicted for r_{max} of 2m, 2.5m & 3m.

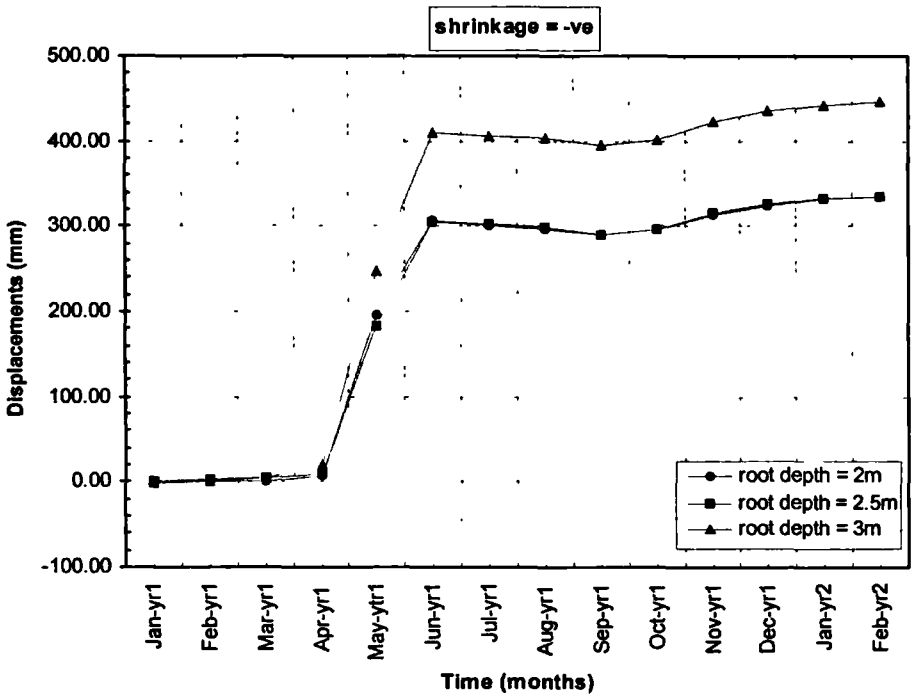

Figure 7.4b Sub-accumulated horizontal movements at ground level of mid-slope predicted for r_{max} of 2m, 2.5m & 3m.

At the inception of the RWUM, the pore water pressure profile indicates increasingly compressive pore water pressures with depth from approximately 1m depth below ground level. This means that for the large r_{max}, the lower nodes are at higher compressive pore water pressures when evapotranspiration commences. During the initial stages of the analysis, these lower nodes operate at relatively higher values of α, compared to the upper nodes. For large r_{max}, there are more nodes operating with high α values compared to small r_{max}. Therefore even though the potential evapotranspiration is the same for all 3 cases, it is expected that in a given time, comparatively more actual evapotranspiration will occur in the analysis involving large r_{max}, whence higher suctions would be expected.

Figure 7.3 shows the vectors of sub-accumulated movements during the period Mar-Aug yr 1, (the first summer cycle). The majority of the movements occur in the zone where most of the pore water pressure changes occur. From Figure 7.3, the maximum vertical movements at the crest centreline are 300mm, 450mm and 700mm for r_{max} values of 2m, 2.5m and 3m, respectively. The magnitude of movements is considered to be much larger than would occur in a prototype embankment (McGinnity *et al*, 1998 and ICON, 2001). This is considered to be a result of the large pore water pressure changes which are occurring in a relatively short period, at the onset of summer. Under field conditions, the growth of vegetation is a gradual process over several seasons. The plant roots will be initially shallow and evapotranspiration rates will also be small for young vegetation. As the vegetation grows its roots will deepen and the evapotranspiration rate also increases. The pore water pressure changes (and the associated movements) under field conditions will therefore be more incremental than has been assumed in these analyses.

An analysis to investigate the pore water pressure regime and ground stresses assuming gradual growth of vegetation was executed and the results are reported at the end of this section. The pattern of vectors in Figure 7.3 also reveals that although the overall direction of the sub-accumulated movements is downward, the vectors have a significant horizontal component. This is indicative of outward slope movements. The reason for the development of outward horizontal movements in the slope during drying out is a result of the development of plasticity, as shall be expatiated latter with reference to Figure 7.5.

Figure 7.4a shows the monthly sub-accumulated vertical movements at the crest centreline during application of the RWUM. The figure clearly reveals that the RWUM begins to have a significant influence on the movements from April onward, which matches the development of soil moisture deficit shown in Figure 5.13. The magnitude of movements is shown to be

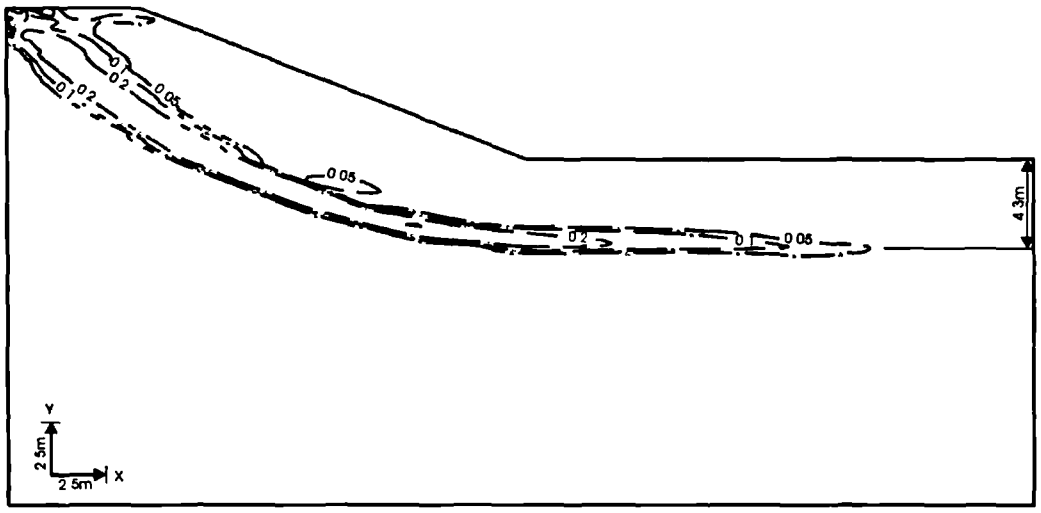

(a) Maximum root depth = 2m

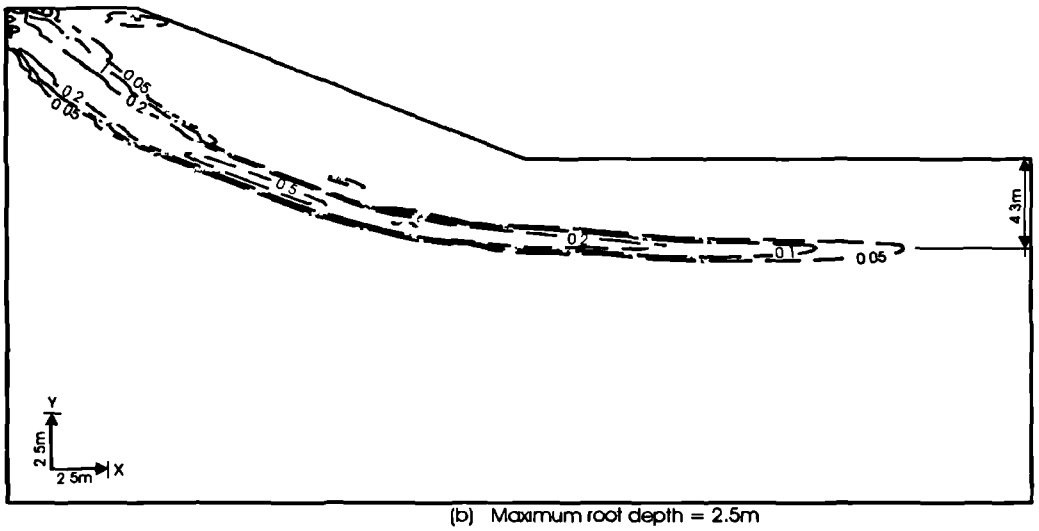

(b) Maximum root depth = 2.5m

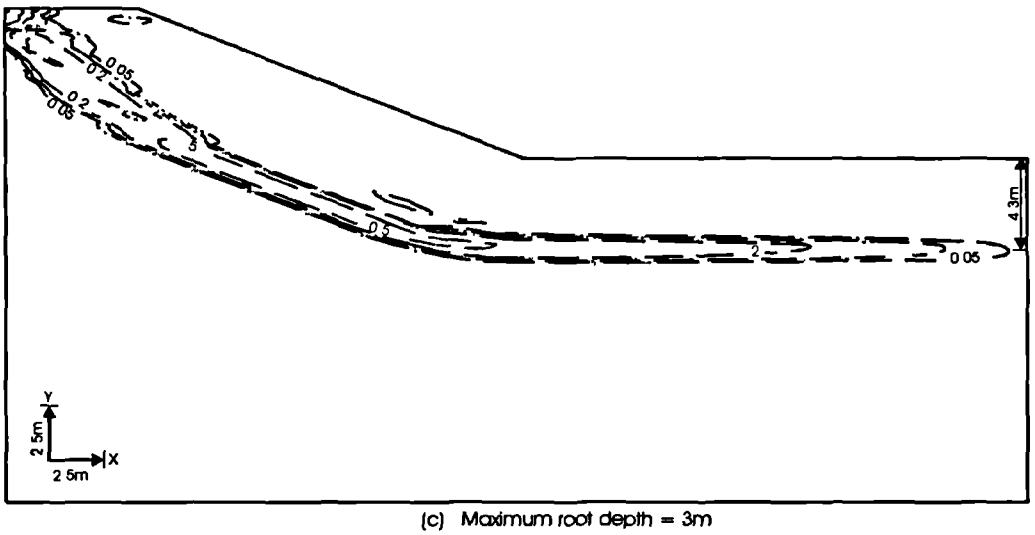

(c) Maximum root depth = 3m

Figure 7.5 Contours of sub-accumulated plastic strains predicted by r_{max} of 2m, 2.5m & 3m (Jan-Aug yr1)

dependent on the magnitude of r_{max}, with the general trend indicating that the larger the r_{max}, the larger the vertical movements eg. at the end of August, the settlements predicted at crest centreline since invokation of the RWUM are 275mm, 555mm and 740mm for r_{max} values of 2m, 2.5m and 3m, respectively.

The majority of the vertical movements occur within a relatively short period (May and June) when the rate of potential evapotranspiration begins to increase. This is considered to be a direct response to the large pore water pressure changes compared to those existing at the inception of the RWUM and the large stress changes arising thereof.

Figure 7.4b depicts the monthly sub-accumulated horizontal movements at ground level of mid-slope during yr 1. It is interesting to note that the magnitude of movements for r_{max} of 2m and 2.5m are virtually the same while the predictions by the r_{max} of 3m are 30% higher. Once more, the pattern confirms that the majority of the movements occur during May and June, as previously observed for vertical movements (Figure 7.4a). It can also be seen that very little horizontal movement occurs during the first 4 months. In addition, the pattern closely mirrors that of the sub-accumulated vertical movements at the crest (Figure 7.4a). The majority of the movements occur during the months of May and June, albeit there is no difference in prediction for r_{max} values of 2m and 2.5m.

The plasticity associated with the first summer is shown in Figure 7.5. This figure depicts the sub-accumulated plastic strains (absolute values) that occur from the period January to August of year 1. Further investigation established that over 90% of the plasticity occurred during the months of May and June. It can be seen that although the location of the plastic zone is not significantly influenced by r_{max}, the degree of plasticity varies depending on r_{max}. The figure reveals that the extent of the plastic zone (as demarcated by the 0.05 plastic strain contour) increases as r_{max} increases. In addition, the strain level within the plastic zone increases as r_{max} increases eg. the maximum strain level induced in the embankment with an r_{max} of 2m is 0.20 (20%) (Figure 7.5a), compared to 0.5 (50%) in the analyses with r_{max} of 2.5m and 3m. It can also be seen that in the latter two analyses, the plastic zone demarcated by the 0.5 plasticity contour is larger for an r_{max} of 3m.

The formation of this deep seated plastic zone is considered to be governed by the overall depth to which evapotranspiration induces stress changes in the ground. This is corroborated by Figure 7.6 which depicts the contours of minor principal total stress, σ_3. The overall pattern of

contours predicted by the three r_{max} is the same and reveals that the depth at which σ_3 changes from compressive to tensile (contour 0kPa), coincides with the elevation at which the plastic zone is located. However, it is not surprising that the location of this zone is approximately the same for the 3 cases since the values of potential evapotranspiration used in the RWUM are equal.

7.3.4 Behaviour during winter (yr 1)

Figure 7.7 shows contours of accumulated pore water pressures at the end of the first winter cycle (February yr 2). The pattern within the clay fill is similar for all the three r_{max}. The main difference lies in the maximum pore water pressures predicted at shallow depth of the foundation in the zone remote from the toe of the embankment. In this locality, maximum pore water pressures of 900kPa are predicted in the analysis involving an r_{max} of 2m whereas the predictions for r_{max} equal to 2.5m and 3m are in excess of 1200kPa.

Overall, suctions of 50kPa are predicted in the centre of the embankment, which indicates that pore water pressures did not fully recover during the winter. A shallow zone averaging (1-2m depth below ground level) with suctions less than 50kPa is predicted within the embankment. The magnitude of suctions predicted in the embankment is reasonable. However, it is noteworthy that the accuracy of the prediction may not be a true reflection of the meteorological input data. This is attributed to the inability of the constitutive model to reproduce desiccation cracking and its influence on the mass permeability of the clay fill and foundation. The latter is corroborated by the prediction of large suctions just below ground level in the zone remote from the embankment. This inadequacy and its impact on pore water pressure predictions was discussed in more detail in Chapter 5.

Figure 7.8 shows the pore water pressure changes that occur during the first winter (September yr 1 to February yr 2). During winter, the potential evapotranspiration rate significantly reduces and is accompanied by increased precipitation rates. The process results in recharge of compressive pore water pressures, as portrayed in Figure 7.8. Compressive pore water pressures changes in excess of 600kPa are predicted within the slope of the embankment for all three r_{max} values. It is also noteworthy that the RWUM predicts tensile pore water pressure changes over a significant depth of the foundation during winter. This is a result of the redistribution of the preceding end of summer suctions.

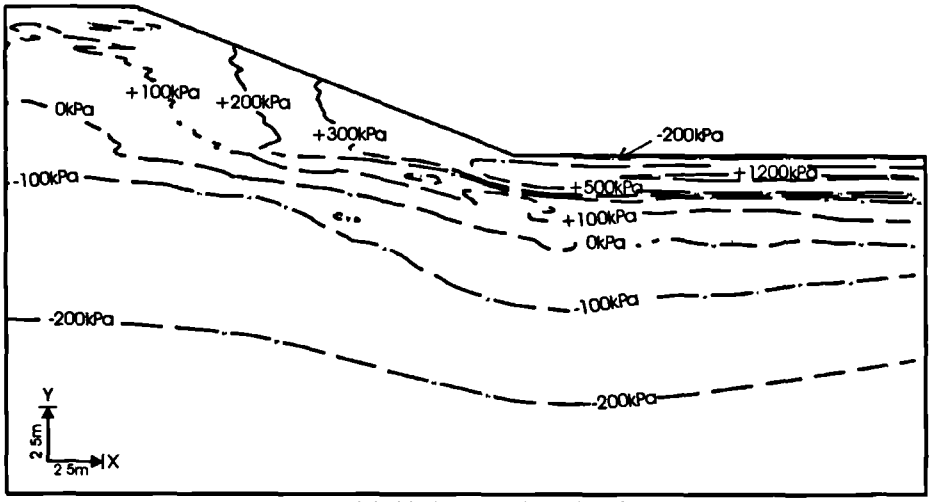

(a) Maximum root depth = 2m

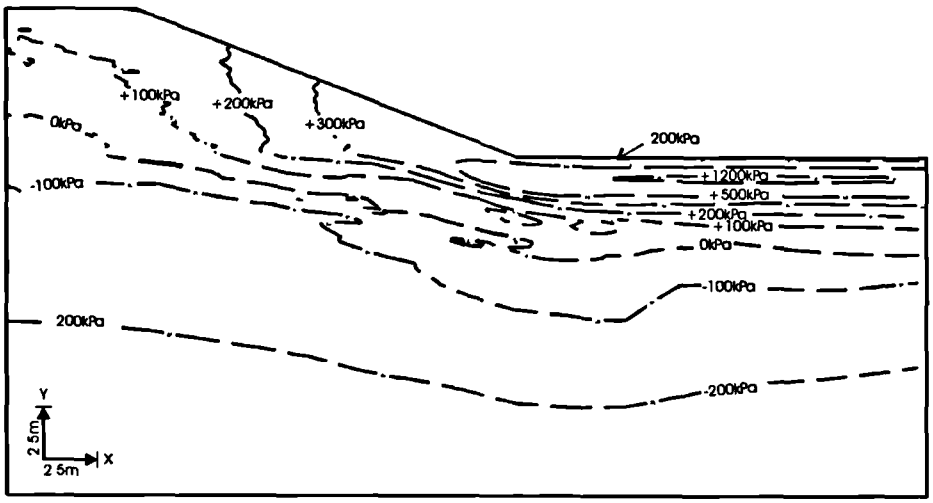

(b) Maximum root depth = 2.5m

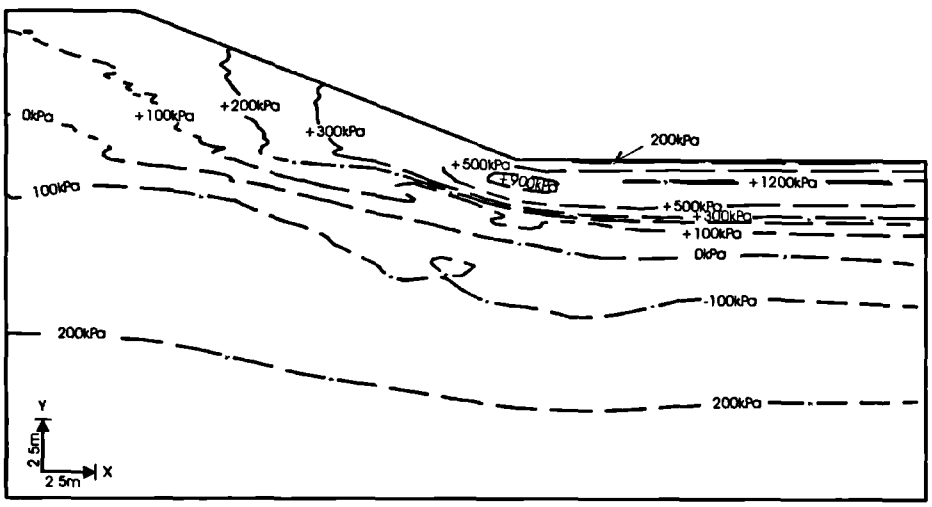

(c) Maximum root depth = 3m

Figure 7.6 Contours of accumulated minimum principal total stress (σ_3) predicted by r_{max} of 2m, 2.5m & 3m at the end of the first summer (Aug yr1).

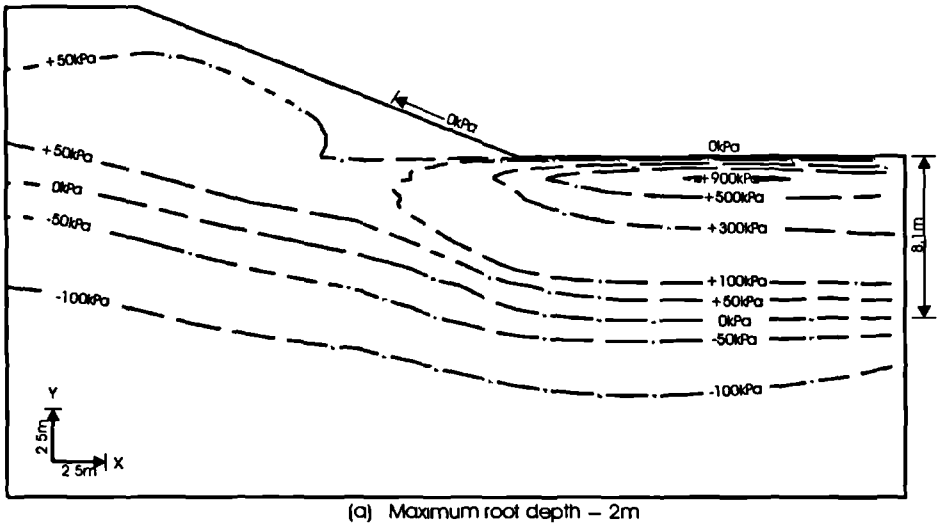

(a) Maximum root depth – 2m

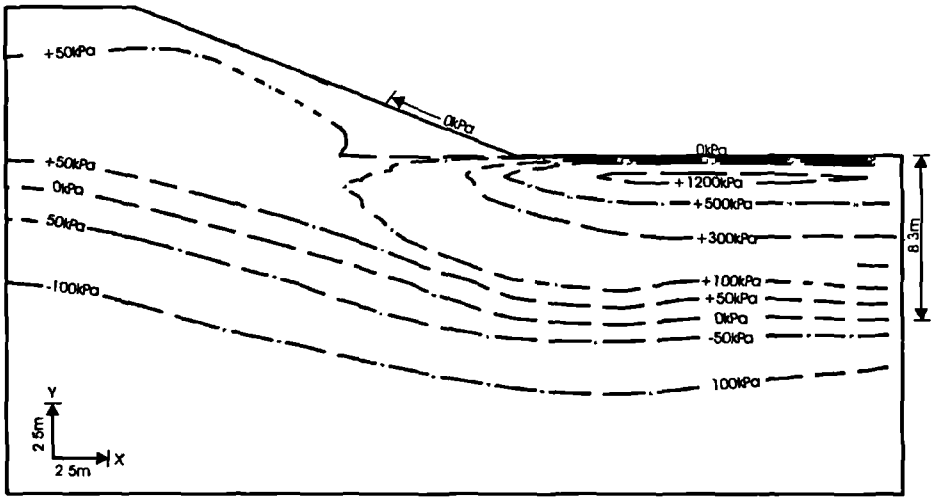

(b) Maximum root depth = 2.5m

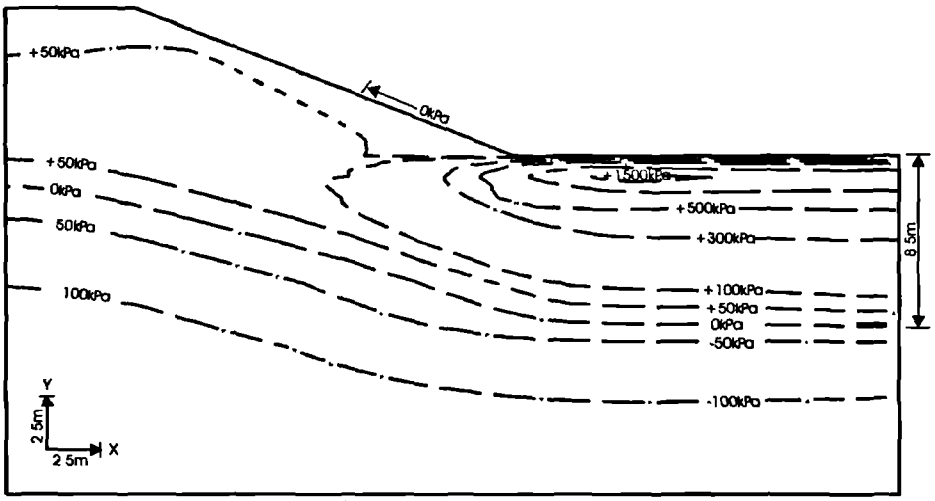

(c) Maximum root depth = 3m

Figure 7.7 Contours of accumulated pore water pressure predicted by r_{max} of 2m, 2.5m and 3m at the end of the first winter (Feb yr2).

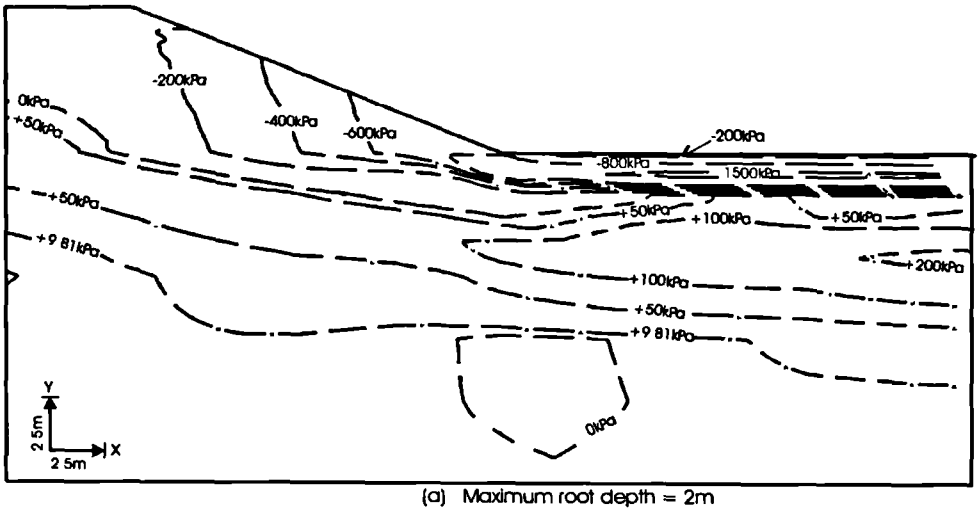

(a) Maximum root depth = 2m

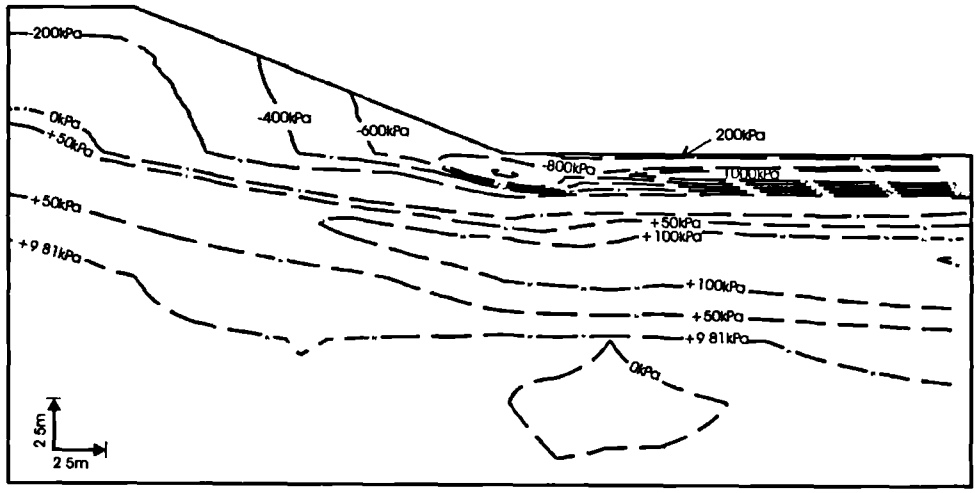

(b) Maximum root depth = 2.5m

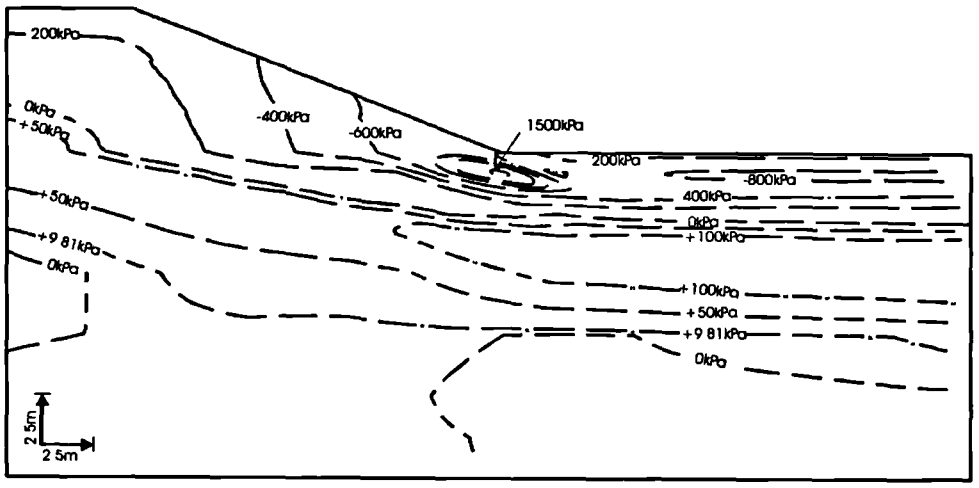

(c) Maximum root depth = 3m

Figure 7.8 Contours of sub-accumulated pore water pressure predicted by r_{max} of 2m, 2.5m & 3m during the first winter (Sept yr1-Feb yr2).

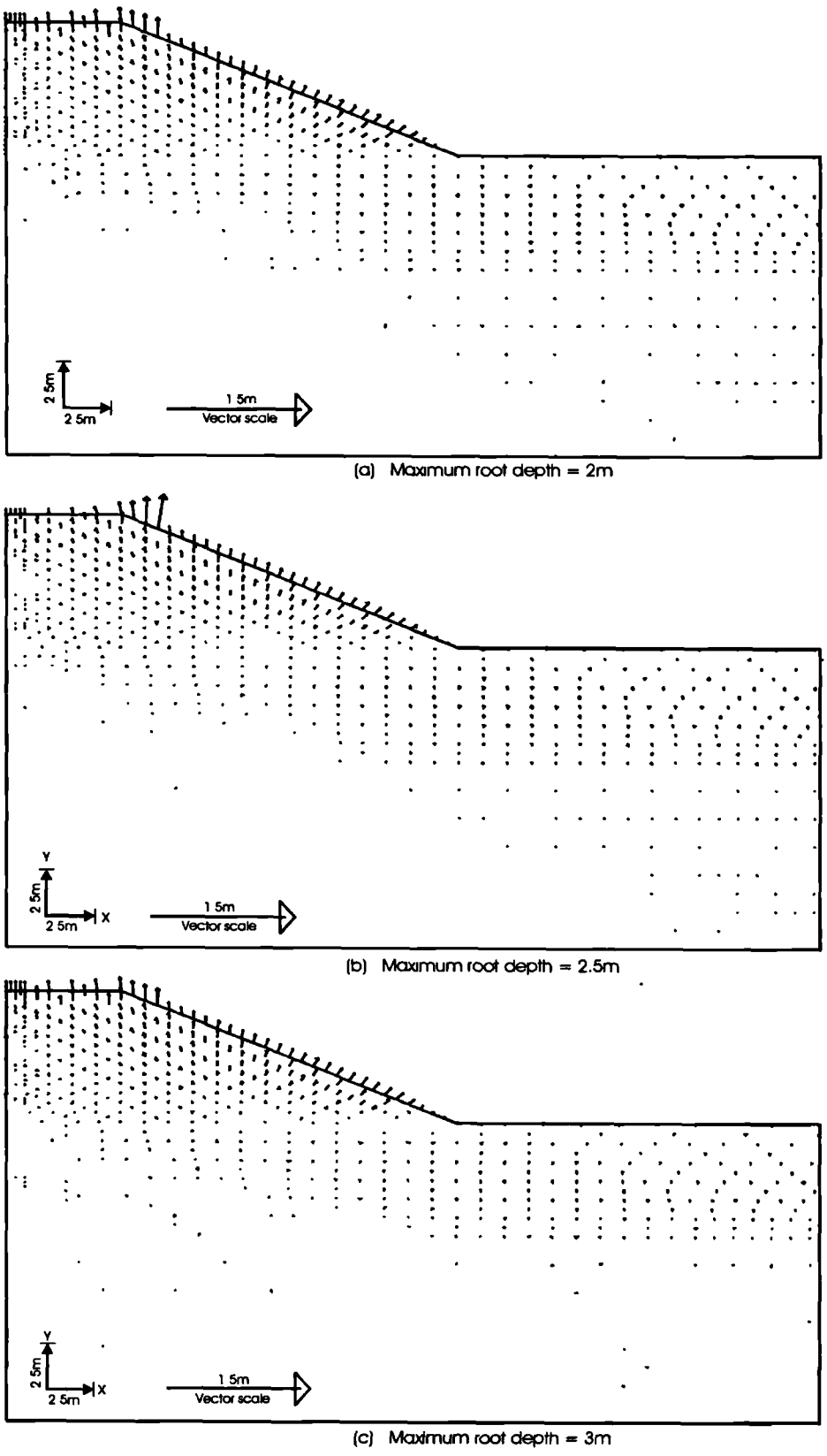

Figure 7.9 Vectors of sub-accumulated movements predicted by r_{max} of 2m, 2.5m & 3m during the first winter (Sept yr1 - Feb yr2)

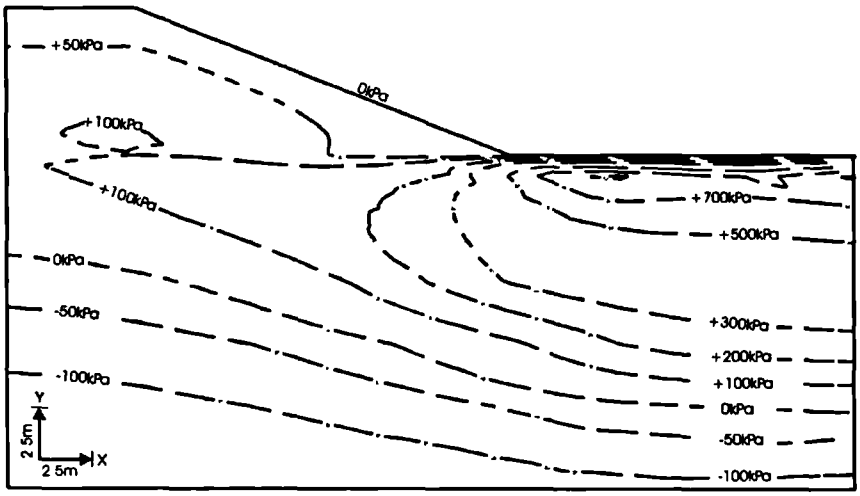

(a) Maximum root depth = 2m

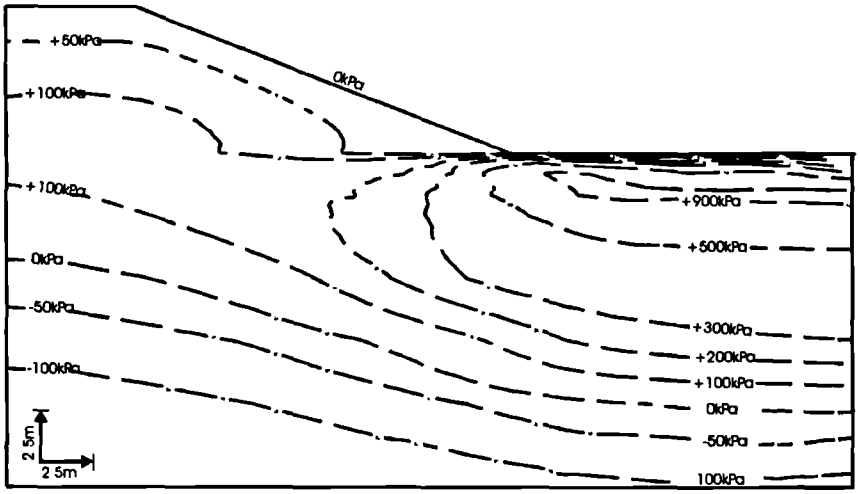

(b) Maximum root depth = 2 5m

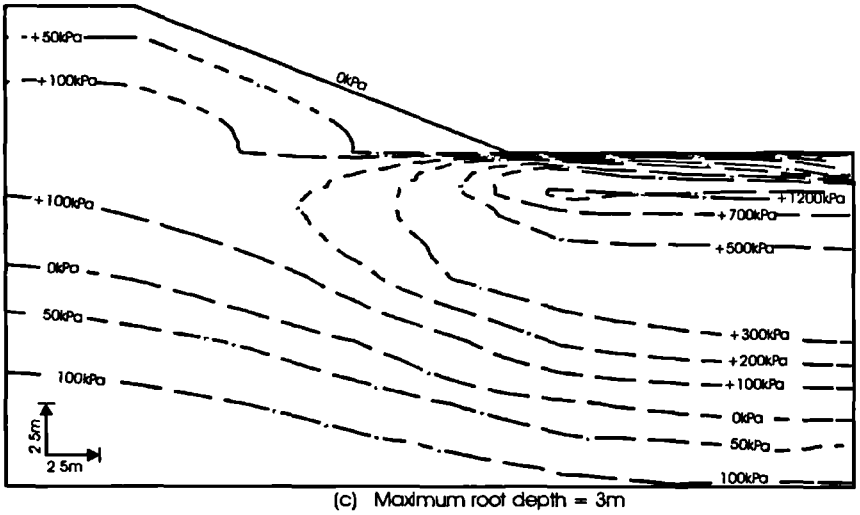

(c) Maximum root depth = 3m

Figure 7.10 Contours of accumulated pore water pressure predicted by r_{max} of 2m, 2.5m & 3m at the end of the 5 winter (Feb yr5).

Figure 7.9 shows the sub-accumulated vectors of movement during winter (ie. sub-accumulated from September yr 1 to February yr 2). The overall pattern of movement indicates swelling of the embankment. There is little difference in the pattern of vectors within the slope of the embankment predicted by the three r_{max}. This suggests that vegetation plays a minor role during winter and the embankment behaviour is dominated by the amount of precipitation which is inducing compressive pore water pressure recovery. It is worth reiterating that during winter, relatively little evapotranspiration takes place because most of the deciduous trees have no foliage.

The sub-accumulated vertical movements during winter yr 1 at the crest centreline are shown in Figure 7.4a. Because movement during winter is not very dependent on the magnitude of r_{max}, the difference in movements identified at the end of the preceding summer continue throughout the winter period. The figure indicates swelling of 100mm (September yr 1 to February yr 2) in the predictions by r_{max} of 2m and 3m. The corresponding prediction for a r_{max} of 2.5m is 60mm, which is significantly less. The lower magnitude of movements in the latter analysis suggests that under the given meteorological data, the r_{max} of 2.5m is effecting the most efficient control of seasonal pore water pressure changes.

Figure 7.4b shows the sub-accumulated horizontal movements at mid-slope (ground level) during winter yr 1 (September yr 1 to February yr 2). During this period, the mid-slope of the embankment with r_{max} of 2m and 2.5m moves outwards by 45mm while that with an r_{max} of 3m moves by 50mm. The larger movements in the latter embankment are a result of the comparatively larger compressive pore water pressure changes during winter, in response to larger suctions that developed during the preceding summer.

7.3.5 Behaviour during the first 5 yrs of cyling

The analyses were extended for 4 years to compare the trends in behaviour using the three r_{max} values. The period was considered adequate because the aim of this particular study was to investigate the influence of r_{max} on embankment behaviour before the development of a failure mechanism.

Figure 7.10 shows the distribution of pore water pressures at the end of winter (February yr 6) of the 5th cycle. Whilst acknowledging the limitations of the constitutive model to reproduce the development of desiccation cracks and its influence on ground movements and permeability, valid qualitative comparisons can nevertheless still be made because the only variant in the

analyses is r_{max}. From Figure 7.10, it can be seen that the main differences in pore water pressure predictions occur in the centre of the embankment as indicated by the size of the zone demarcated by the +100kPa suction contour. The smallest zone occurs in the analysis involving an r_{max} of 2m (Figure 7.10a) and gradually increases in size with r_{max} (Figures 7.10 b and c).

At shallow depth (typically less than 2-2.5m) within the embankment slope and crest, the predictions using the three values of r_{max} shows a pore water pressure pattern similar for all the three cases. However, there are some differences in pore water pressure predictions within this shallow zone. The relationship between the degree of desiccation and r_{max} is opposite to that identified above at the centre of the embankment. This is evidenced by location of the +50kPa contour in relation to ground surface. This contour gradually shifts towards ground surface as r_{max} increases. This pore water pressure pattern shows that all other things being equal, shallow rooted vegetation induces higher suctions at shallow depth compared to deeper roots.

The pore water pressure predictions in the foundation are also dependent on r_{max} eg. the +100kPa suction contour is located at 8.8m, 9.8m and 10m beneath the embankment toe for r_{max} values of 2m, 2.5m and 3m, respectively. Overall, the zone of desiccation in the foundation has enlarged during the 4 years from end of winter conditions after 1 year (Figure 7.7).

Figure 7.11 shows the accumulated pore water pressure predictions along a vertical profile at the mid-slope of the embankment after yr 3 and yr 5. It is encouraging to note that in general, the pattern of pore water pressure distribution within the embankment closely matches the meteorological input data eg. at ground level where the influence of rainfall on pore water pressure changes is greatest, the suctions predicted at the end of summer (August) after 3 and 5 years shown in Figure 7.11 are approximately 650kPa and 460kPa, respectively. The corresponding total rainfall for the preceding 8 months (January to August yr 3 and January to August yr 5) is 235mm and 285mm, respectively (plotted in Figure 5.13). The latter year received more rainfall during the period January to August; which is reflected by the lower suctions predicted at ground level in Figure 7.11.

Figure 7.12 shows the vectors of sub-accumulated movements during the four years of cycling (end of winter cycle 1 to end of winter cycle 5). The overall direction of the vectors indicates settlement of the embankment, with no discernible differences among the three r_{max} values.

Although there has been some horizontal slope movement there is no indication of the development of a potential failure at this stage, which is reasonable. The vectors also suggest global settlement of the upper horizon of the foundation. This however is a direct consequence of the deepening zone of desiccation identified in the predictions for accumulated pore water pressures (eg. Figure 7.10) and may not be a correct prediction, for reasons previously discussed.

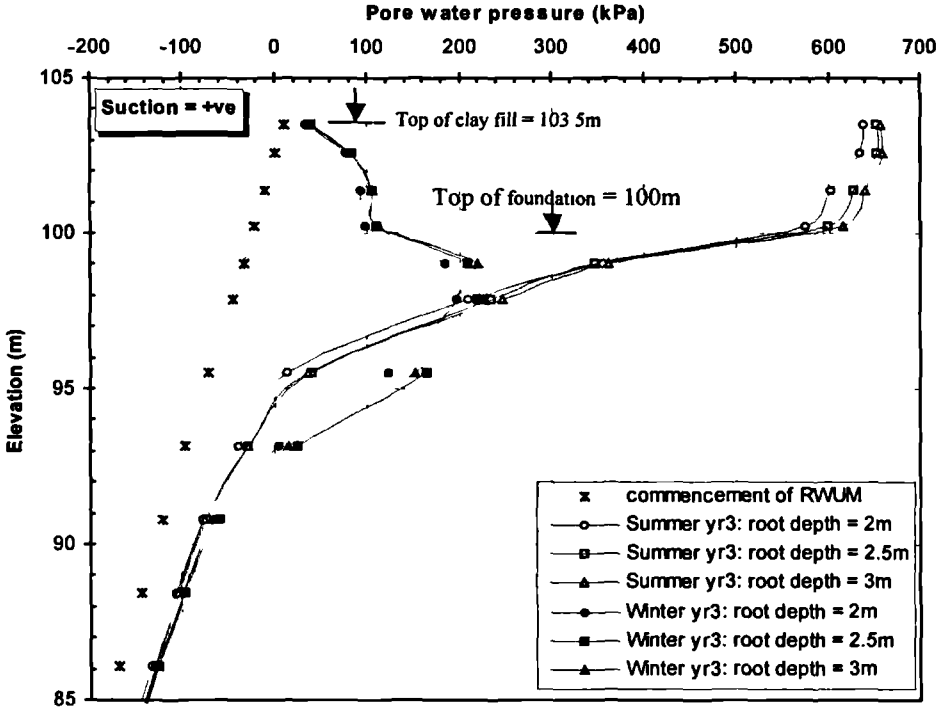

Figure 7.11a Predictions of accumulated pore water pressure at mid-slope of the embankment for maximum root depths of 2m, 2.5m & 3m after 3yrs.

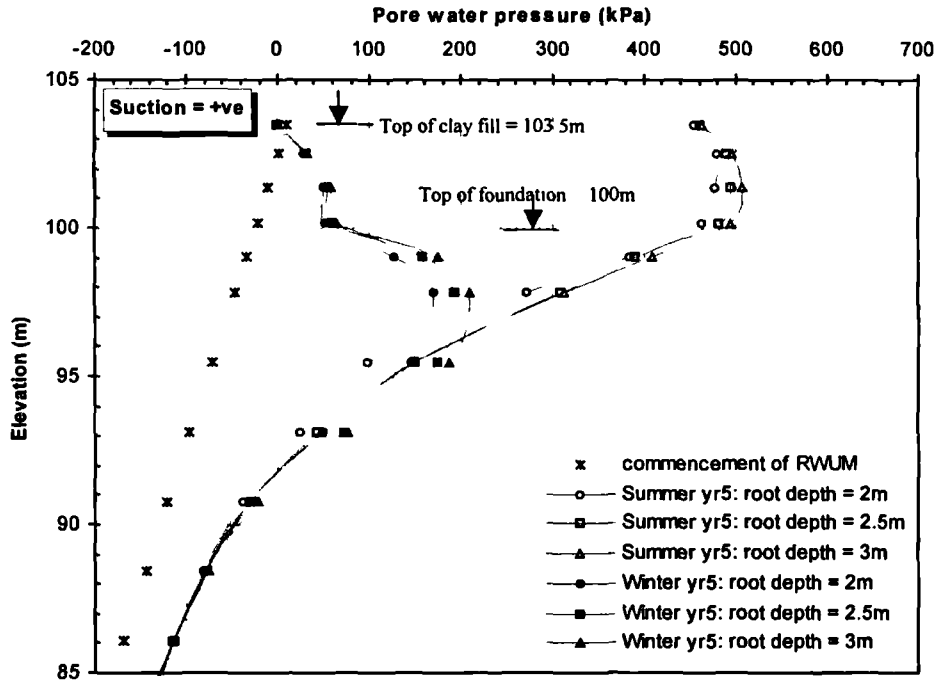

Figure 7.11b Predictions of accumulated pore water pressure at mid-slope of the embankment for r_{max} of 2m, 2.5m & 3m after 5yrs.

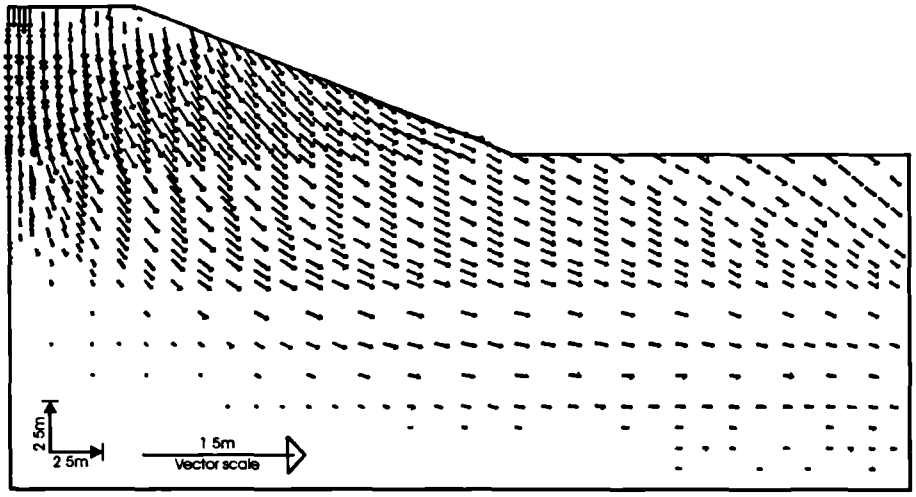

(a) Maximum root depth = 2m

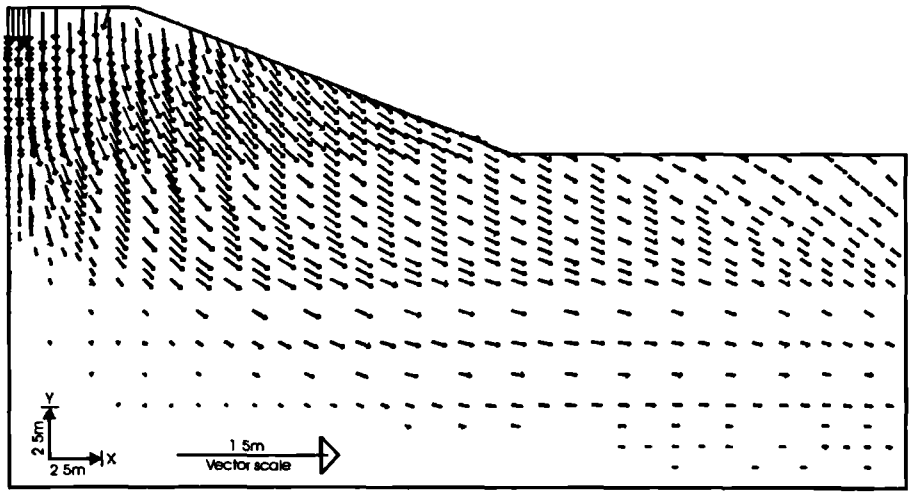

(b) Maximum root depth = 2.5m

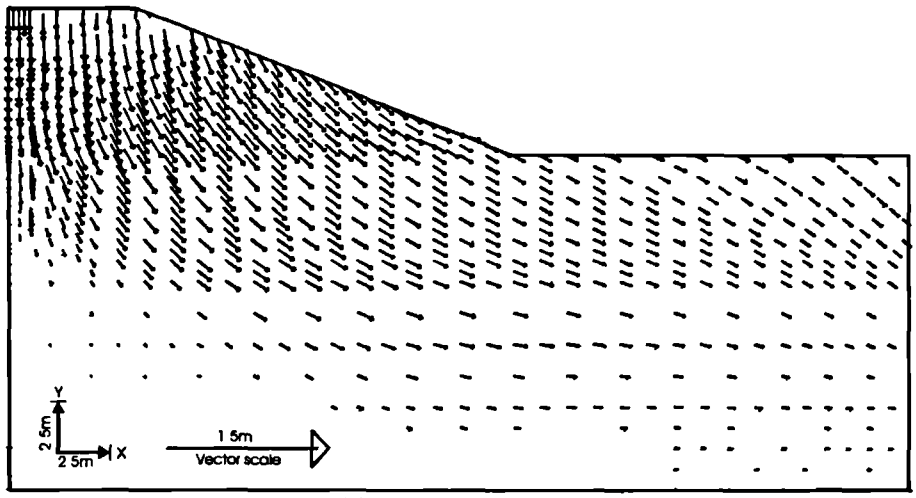

(c) Maximum root depth = 3m

Figure 7.12 Vectors of sub-accumulated movements predicted for r_{max} of 2m, 2.5m & 3m during the period Mar yr1 - Feb yr 6.

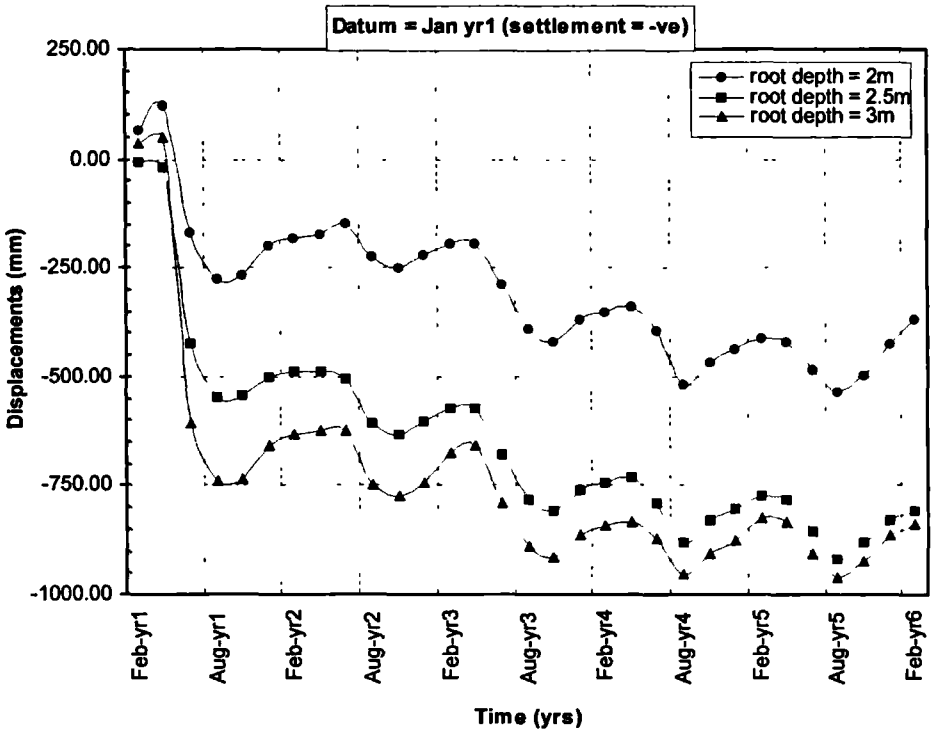

Figure 7.13a Sub-accumulated vertical movements at the crest centreline predicted for r_{max} of 2m, 2.5m & 3m during the first 5yrs of cycling (datum = Jan yr1).

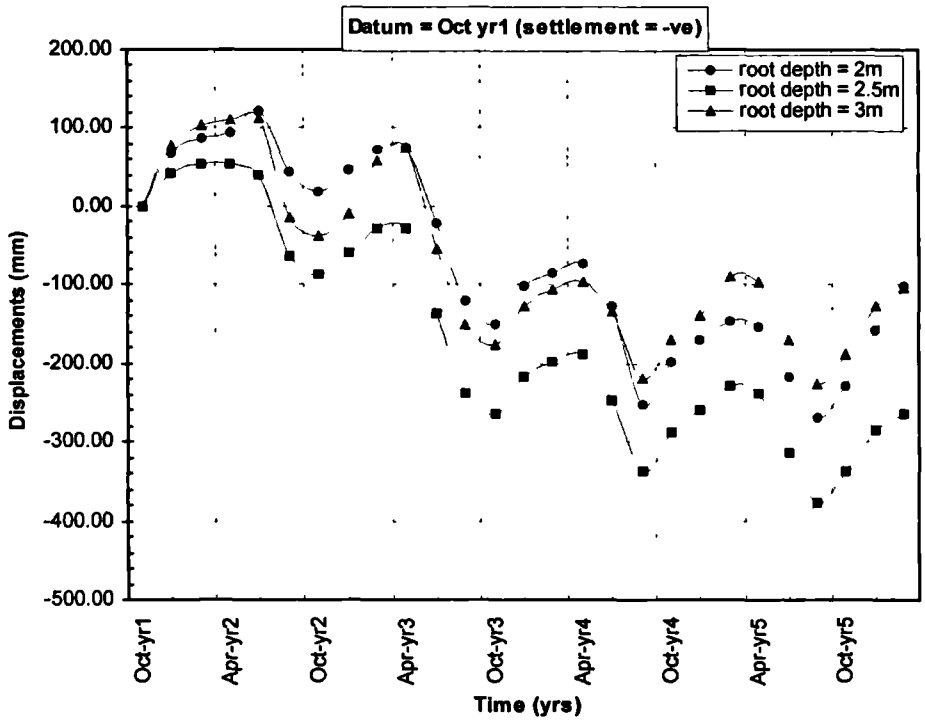

Figure 7.13b Sub-accumulated vertical movements at the crest centreline predicted for r_{max} of 2m, 2.5m & 3m during the first 5yrs of cycling (datum = Oct yr1).

The vertical movements occurring at the centreline of the crest during the 5 cycles are shown in Figure 7.13. Figure 7.13a depicts the sub-accumulated movements from January yr 1 when the RWUM is first applied whilst Figure 7.13b depicts the sub-accumulated movements assuming datum to be October yr 1 (end of the first summer). The latter has been chosen in an attempt to facilitate interpretation of the data by eliminating the effects of large pore water pressure changes associated with invokation of the RWUM ie. to discount the large movements during the first 8months (January to September of yr 1).

The pattern of crest movements in Figure 7.13a portrays a relationship between the magnitude of crest settlements and r_{max} ie. the larger the r_{max}, the larger the movements. The figure also reveals that at the end of 5 cycles, the predicted crest settlements using an r_{max} of 2.5m and 3m are approximately of the same order of magnitude whereas the predictions using an r_{max} of 2m are significantly less. There is evidence that with time, the differences in predictions diminish, notwithstanding that extreme events such as a drought would accentuate the differences in predictions among the three values of r_{max}.

It is also noteworthy that the movements associated with the first 8months of application of the RWUM constitute a large component of the overall settlements. During the 5cycles modelled here, the percentage of the movements occurring from January to September yr 1 as a fraction of the movements occurring from January yr 1 to September yr 5 are 50%, 60% and 75% for r_{max} values of 2m, 2.5m and 3m, respectively. In prototype embankments, the establishment and growth of vegetation is a gradual process, therefore the magnitude of movements during the early stages of vegetation establishment would be expected to be significantly less than is predicted here.

As expected, the displacements predicted using October yr 1 as datum and shown in Figure 7.13b are different to those in Figure 7.13a, where datum is January yr 1. Figure 7.13b shows that after the first summer, the largest settlements occur in the embankment with an r_{max} of 2.5m. In addition, Figure 7.13b shows that the settlements predicted using an r_{max} of 3m are initially larger than those predicted by an r_{max} of 2m up to the middle of year 4. After that period, the r_{max} of 2m predicts larger settlements compared to predictions by an r_{max} of 3m.

The seasonal cyclic movements in Figure 7.13b are summarised in Table 7. 3. The values have been obtained by scaling off the relative movements between peaks and troughs in the figure, to determine the magnitudes of swelling and shrinkage.

The largest of the seasonal movements predicted by the three r_{max} have been identified by an asterisk in Table 7.3. It can be seen that statistically, the predictions by an r_{max} of 3m yield the largest movements each season compared to r_{max} of 2m and 2.5m. This to some extent corroborates field evidence which indicates large seasonal movements in embankments with dense vegetation. Under these conditions the depths of roots are likely to be deeper with a larger zone of influence.

Table 7.3 Predicted seasonal vertical movements at the crest (mm)

Year	Winter			Summer		
	$r_{max} = 2m$	$r_{max} = 2.5m$	$r_{max} = 3m$	$r_{max} = 2m$	$r_{max} = 2.5m$	$r_{max} = 3m$
1	125*	55	120	-100	-140	-155*
2	60	70	115*	-230	-240	-250*
3	80	80	80	-180*	-150	-120
4	110	110	130*	-120	-150*	-140
5	165*	110	120	-	-	-
Number of times seasonal movements are largest (*): $r_{max} = 2m$ (3) $r_{max} = 2.5m$ (1) $r_{max} = 3m$ (4) Number of times seasonal movements are equal for all 3 r_{max} (= 1 , in winter of yr 3)						

From Table 7.3, it is also interesting to note that overall, the analysis using an r_{max} of 2.5m generates the least seasonal movements. It is considered that in this analysis, the ground water regime established for the meteorological data input induces the least seasonal pore water pressure changes. This behaviour supports the theory that well designed vegetation management can be effective to control seasonal cyclic movements in embankments. Under such conditions, an optimum water balance is achieved between precipitation and evapotranspiration.

As can be seen from Table 7.3, the number of times the largest seasonal movements are predicted by an r_{max} of 2m (3 times) is only slightly less compared to the number of times the largest seasonal movements are predicted by an r_{max} of 3m (4 times). It is considered that in this case, the zone of influence of the roots for an r_{max} of 2m is shallow hence the embankment is experiencing larger pore water pressure changes as a result of inadequate control of groundwater.

It is also noteworthy that the magnitude of the summer movements in Table 7.3 are significantly larger than the winter movements. This indicates that a significant proportion of the shrinkage movements do not recover during swelling and this process results in settlement of the embankment.

Figures 7.14a and b show the sub-accumulated horizontal movements at ground level of the mid-slope assuming the datum to be January yr 1 and October yr 1, respectively. The latter figure excludes movements associated with the formation of a plastic zone during the first summer. It can be seen from Figure 7.14a that the overall pattern suggests little difference in predictions by the three r_{max}. Again it can be seen that the difference in predictions gradually reduces during the 5 year period analysed.

The pattern of horizontal movements portrayed in Figure 7.14 suggests that in the early stages of application of the RWUM, the magnitude of movements are strongly influenced by r_{max}, with the largest r_{max} inducing the largest seasonal movements. It is considered that during the initial phases of application of the RWUM, the pore water pressure changes induced by the three r_{max} (albeit with identical meteorological data) are more dependent on the magnitude of r_{max}. After a few cycles, the embankment enters a phase during which the seasonal cyclic pore water pressure changes induced by the three r_{max} are approximately of the same order of magnitude, year on year (assuming no extreme climatic event). Once this state is attained, the pore water pressure changes become less dependent on the magnitude of r_{max}, hence the diminishing difference in predictions of ground movements. A similar pattern was displayed in Figure 7.13b.

The gradual reduction in seasonal movements is more clearly shown in Figure 7.15 where annual movements at the crest centreline (Figure 7.15a) and at ground level at the mid-slope during the 5 years (Figure 7.15b) are plotted. In the figures, the movements have been computed assuming each cycle to span the period September to August. (NB. For year 1, the period only spans from January to August). Although the annual movements diminish, the seasonal cyclic movements have been shown to be strongly influenced by r_{max} (Figures 7.13a and b and Table 7.3). In the long term scenario, it is the latter type of movements which initiate and propagate a progressive failure mechanism in brittle clay fills as shall be shown below.

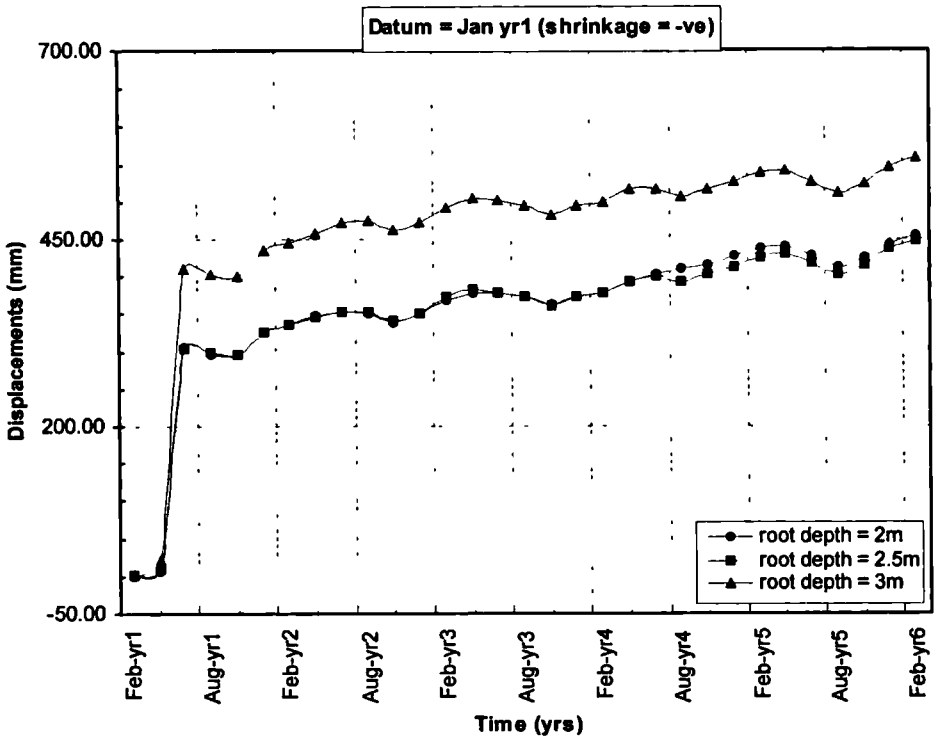

Figure 7.14a Sub-accumulated horizontal movements at ground level of mid-slope predicted for r_{max} of 2m, 2.5m & 3m during the first 5yrs of cycling (*datum = Jan yr1*).

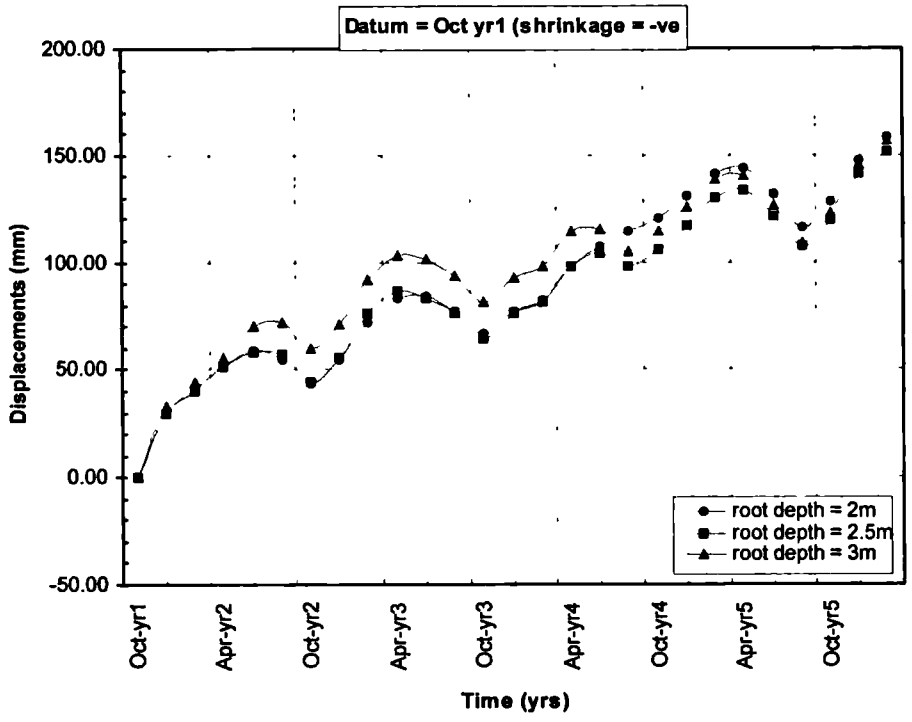

Figure 7.14b Sub-accumulated horizontal movements at ground level of mid-slope predicted for r_{max} of 2m, 2.5m & 3m during the first 5yrs of cycling (*datum = Oct yr1*).

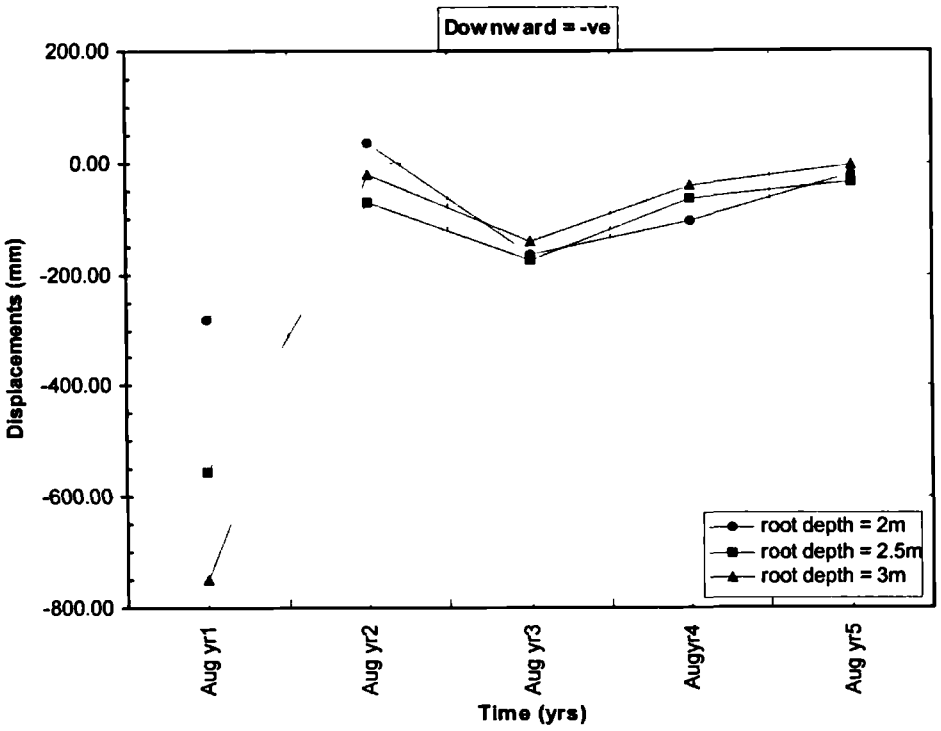

Figure 7.15a Annual sub-accumulated vertical movements at the crest centreline predicted for r_{max} of 2m, 2.5m & 3m.

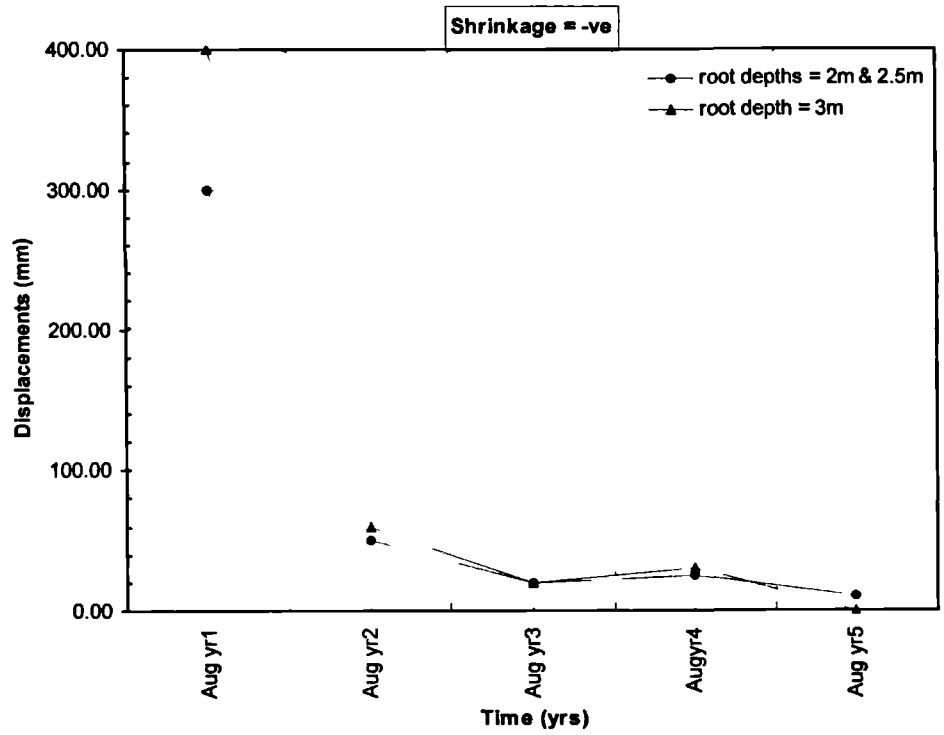

Figure 7.15 Annual sub-accumulated horizontal movements at ground level of mid-slope predicted for r_{max} of 2m, 2.5m & 3m.

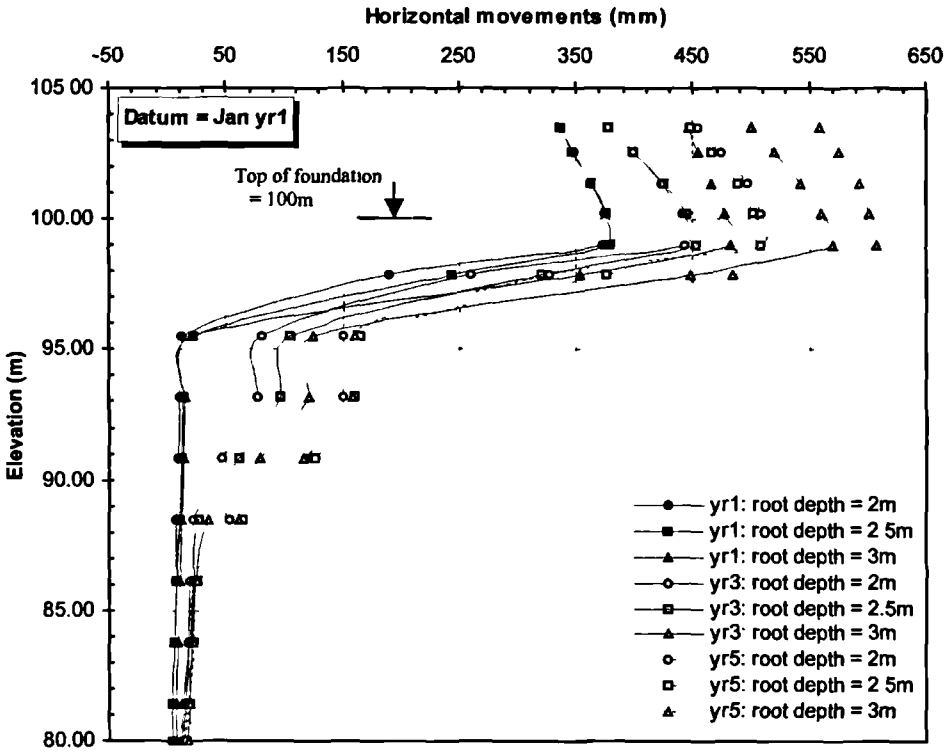

Figure 7.16a Sub-accumulated horizontal movements at mid-slope predicted at the end of winter (Feb) for r_{max} of 2m, 2.5m & 3m during the first 5yrs of cycling (*datum Jan yr1*).

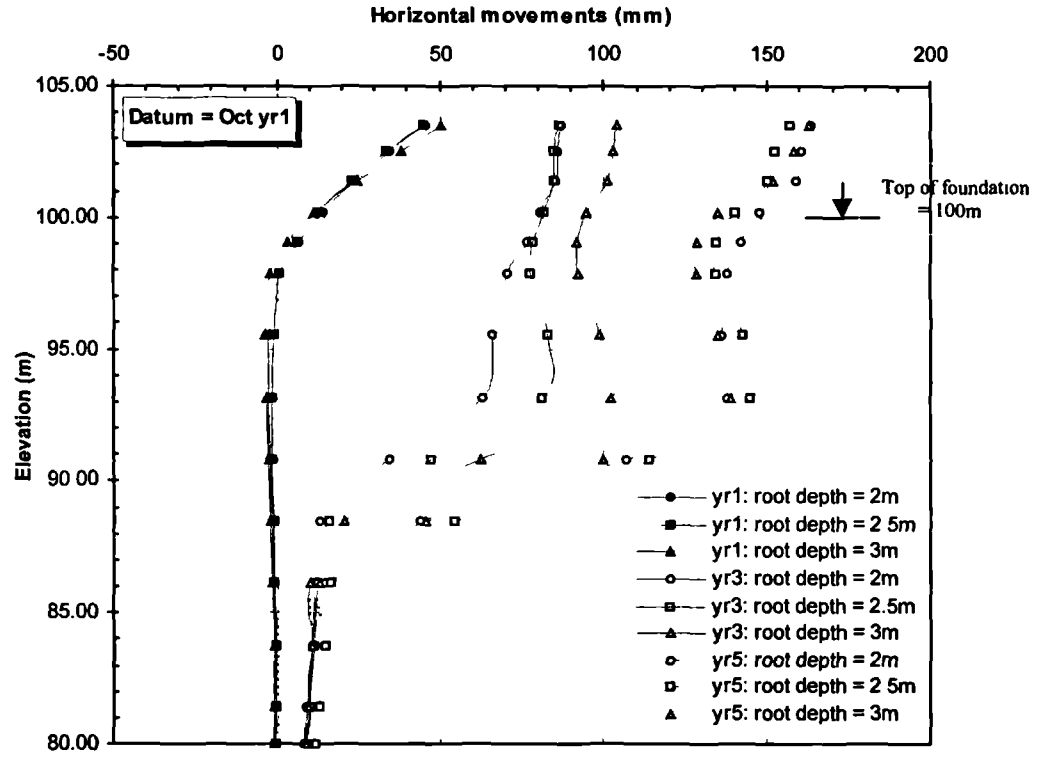

Figure 7.16b Sub-accumulated horizontal movements at mid-slope predicted at the end of winter (Feb) for r_{max} of 2m, 2.5m & 3m during the first 5yrs of cycling (*datum = Oct yr1*).

The horizontal movements occurring along a vertical profile at mid-slope are shown in Figure 7.16a. In this figure, the movements at the end of the 1st, 3rd and 5th winter cycles are shown. Overall, the pattern corroborates that portrayed in Figure 7.14 (ie. approximately the same order of magnitude of horizontal movements for r_{max} 2m and 2.5m). However, it can also be seen that the maximum movements occur in the upper 2m of the foundation, eg. 380mm at the end of the first year in the analysis involving r_{max} of 2m and 2.5m.

Again, in order to eliminate the effects of movements associated with the imposition of the RWUM (first 8months) the sub-accumulated horizontal movements assuming October yr 1 as datum are shown in Figure 7.16b. The figure reveals that during the first winter, the majority of the movements occur in the clay fill, with maximum movements occurring at ground level (ie. 45mm for r_{max} of 2m & 2.5m and 50mm in the embankment with an r_{max} of 3m. The movement in the foundation is significantly less (10mm) at the end of the first winter.

With increasing cycles, Figure 7.16b reveals two distinct patterns of movement. The first can be identified within the clayfill and is characterised by maximum movements at ground level whose magnitude reduces with depth. Within the clay fill, the maximum movements at the end of the 1st and 3rd winters occur in the embankment with an r_{max} of 3m whereas at the end of the 5th winter, the maximum horizontal movements occur in the embankment with an r_{max} of 2m. A possible explanation is that during the first few cycles, the embankment with an r_{max} of 3m experiences relatively larger swelling movements in response to the relatively larger degree of desiccation which occurs during summer (see Figure 7.11). With time, the embankment develops permanent desiccation with suctions of a magnitude high enough so as to make the embankment not swell by a large degree during winter (eg. Figure 7.10). In the embankment with an r_{max} of 2m, when a seasonal pore water pressure regime has been established, the degree of desiccation is relatively less (Figure 7.12), which leads to relatively larger swelling during precipitation.

The second pattern of movement can be identified in the foundation where it can be seen that the maximum horizontal movements are occurring at 6m depth below the top of the foundation. This pattern is considered to result from redistribution of suctions developed during the preceding summers eg. there is evidence that the depth over which horizontal movements occur gradually deepens with time.

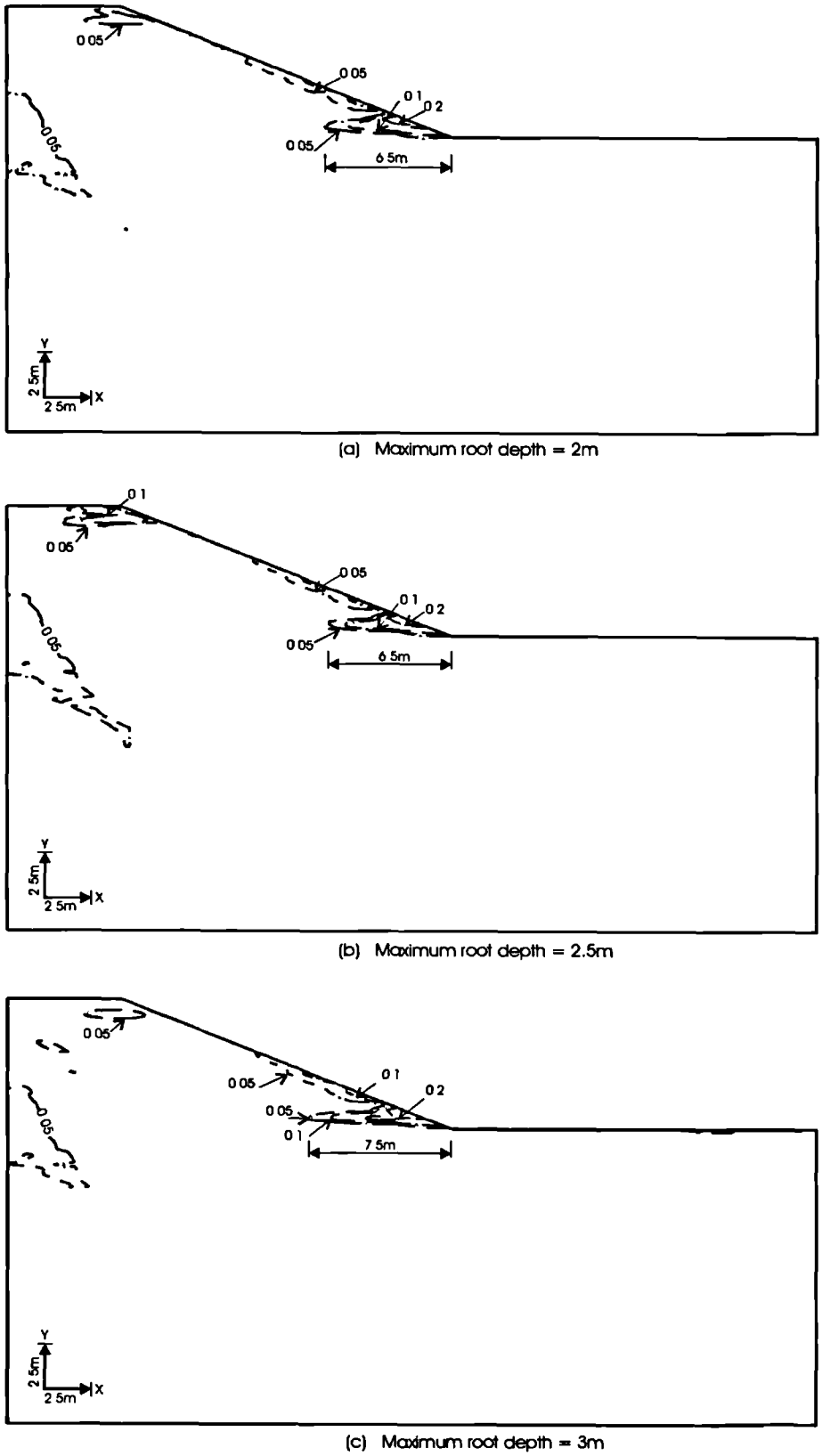

Figure 7.17 Contours of sub-accumulated deviatoric plastic strains predicted for r_{max} of 2m, 2.5m and 3m during the period Mar yr2 - Feb yr6.

Although redistribution of suctions does occur in the field, it is considered unlikely to be associated with horizontal movements of such a magnitude as depicted in Figure 7.16. This is likely to be a result of the inability of the constitutive model to accurately reproduce strain reversals during alternate wetting and drying. Also, the crack permeability model used in these analyses (with a $\frac{k_f}{k_i}$ ratio of 10) enhances permeability in the zones where σ_3 is greater than zero, to model the increase in permeability induced by desiccation cracks. The depth of the desiccated zone predicted by the model may be greater than what can be achieved in the field. Redistribution of suctions may thus be occurring to inappropriately greater depths.

Figure 7.17 depicts the amount of plastic strains that occur during the 4 years (March yr 2 to February yr 6). The plasticity during this period is characterised by the development of a potential slip surface at the toe of the embankment. No further plasticity occurs in the plastic zone that developed during the first summer (Figure 7.5). The figure shows that the degree of plasticity is the same for the analyses involving r_{max} of 2m and 2.5m whereas in the analysis involving an r_{max} of 3m, more plasticity has occurred. This is indicated by the 0.5% plasticity contour which has advanced 6.5m into the embankment for r_{max} of 2m and 2.5m, increasing to 7.5m in the analysis with r_{max} of 3m.

7.4 Influence of clay fill stiffness

7.4.1 Introduction

Application of vegetation and rainfall boundary conditions induces pore water pressure changes within the ground. The pore water pressure changes can either be positive or negative, depending on the relative magnitude between evapotranspiration and rainfall. Changes in pore water pressures in turn induce changes in the effective stress. The change in effective stress is the primary cause of soil deformation.

The manner in which a soil deforms in response to changes in effective stress can be described through a constitutive model. A key parameter of any such model is the Young's modulus, which relates the changes in strains to the changes in stress. In their studies on railway embankments involving seasonal cyclic pore water pressure changes, Kovacevic *et al* (2001) concluded that the stiffness of the clay fill did not significantly influence the overall behaviour of the embankment.

In this study, the influence of stiffness of the clayfill on the behaviour of a typical railway embankment was also investigated using the RWUM to simulate evapotranspiration. The overall objective was to verify/check the findings by Kovacevic *et al* (2001) regarding the influence of the clay fill stiffness.

7.4.2 Numerical modelling

The mesh, soil properties and numerical modelling were as described in Section 7.2. In these analyses, only the stiffness of the clay fill was altered. An r_{max} of 2.5m was used with clayfill stiffness values shown in Table 7.4. During construction of the embankment and the 5 year consolidation period prior to application of the RWUM, the stiffness of the clay fill was kept constant for both analyses and assigned values for case 1 in Table 7.4 ie. the stiffness in run 2 was invoked at the inception of the RWUM (increment 20).

Table 7.4 Soil stiffness used in analyses

Parameter	Ash fill	London Clay fill	In situ London Clay
Stiffness (kPa) RUN 1	1000 (linear elastic)	$E = 1500\left[\frac{100+p'}{100}\right]$ (during construction- min=2000) $E = 5000\left[\frac{100+p'}{100}\right]$ (after construction - min=5000) ***(referred to as stiff clay fill)***	$E = 2500\left[\frac{100+p'}{100}\right]$ (during construction- min=5000) $E = 10000\left[\frac{100+p'}{100}\right]$ (after construction - min=5000)
Stiffness (kPa) RUN 2	-ditto-	$E = 1500\left[\frac{100+p'}{100}\right]$ (during construction - min=2000) $E = 2500\left[\frac{100+p'}{100}\right]$ (after construction - min=2500) ***(referred to as soft clay fill)***	-ditto-

7.4.3 Behaviour during the first 5 yrs of cycling

The stiffness model used is dependent on p'. In general, p' increases during summer when the clay fill dries out and develops suctions. Contours of the tangent Young's Modulus at the end of

the first summer are shown in Figure 7.18, for the two runs. It can be seen that the tangent moduli within the stiffer embankment range between 10000-30000kPa, as opposed to 5000-10000kPa in the softer clay fill.

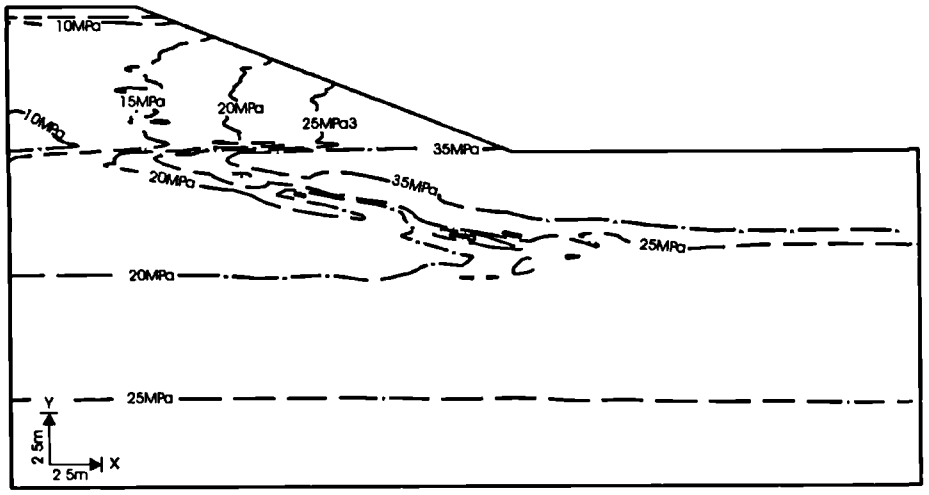

(a) Stiff clay fill

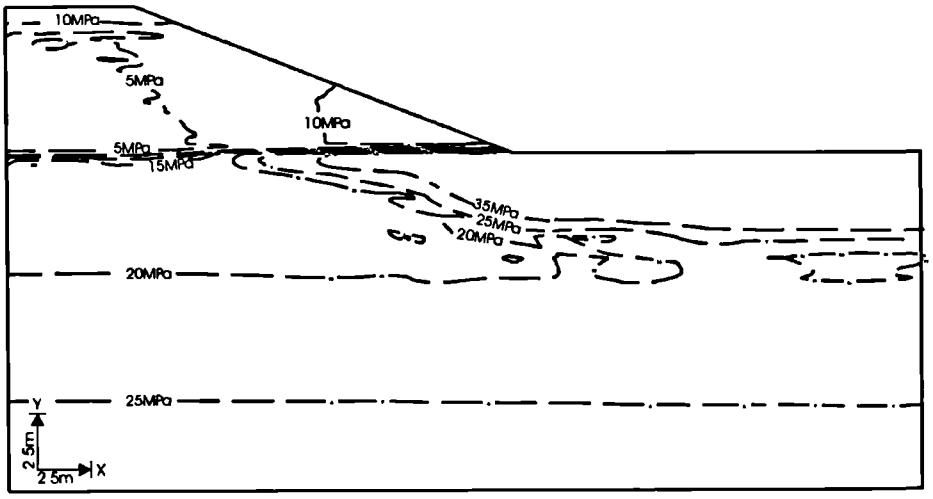

(b) Soft clay fill

Figure 7.18 Contours of effective tangent Young's modulus predicted in soft and stiff clay fill embankments at the end of the first summer (Aug yr1).

Figure 7.19a shows the accumulated pore water pressures at the end of the first summer (August yr 1) while Figure 7.19b depicts the accumulated pore water pressures at the end of the first winter (February yr 2), for the soft clay fill. The corresponding plots for the stiffer clay fill are shown in Figure 7.2b and 7.7b, respectively, for comparison. At the end of the first summer, the suctions in the softer clay fill range between 0-700kPa (Figure 7.19a) compared to 0-900kPa in the stiffer clay fill (Figure 7.2b). It can also be seen from Figure 7.19a that the zone with

compressive pore water pressures (0-50kPa) is significantly larger in the softer clay fill than in the stiffer clay fill. In addition, it can be seen from Figure 7.19b that at the end of the first winter, there still exists a zone with compressive pore water pressures at the centre of the softer embankment unlike in the stiff embankment where the whole clay fill is in tension.

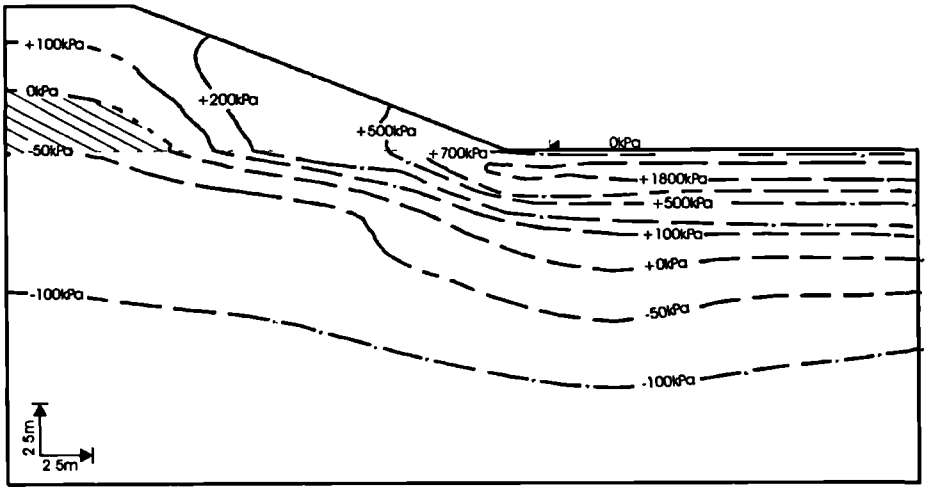

(a) Soft clay fill - end of first summer (Aug yr1)

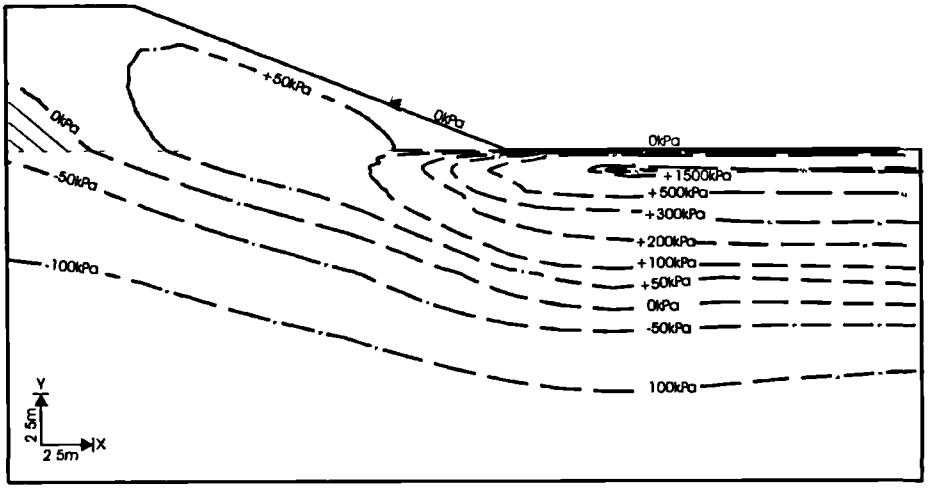

(b) Soft clay fill - end of first winter (Feb yr2)

Figure 7.19 Contours of accumulated pore water pressure predicted for the soft clay fill at the end of the first summer (Aug yr1) and first winter (Feb yr2).

The pore water pressures along a vertical profile at the mid-slope of the embankment are shown in Figure 7.20a, and b after 3 and 5 years, respectively. The pore water pressure pattern shows higher end of summer suctions within the embankment and foundation involving stiffer clay fill. A similar pattern is portrayed in the foundation for end of winter conditions. However, within the embankment, the pattern is reversed and shows higher suctions being predicted in the

analysis with the softer clay fill. As a result, comparatively larger pore water pressure changes occur in the stiffer embankment.

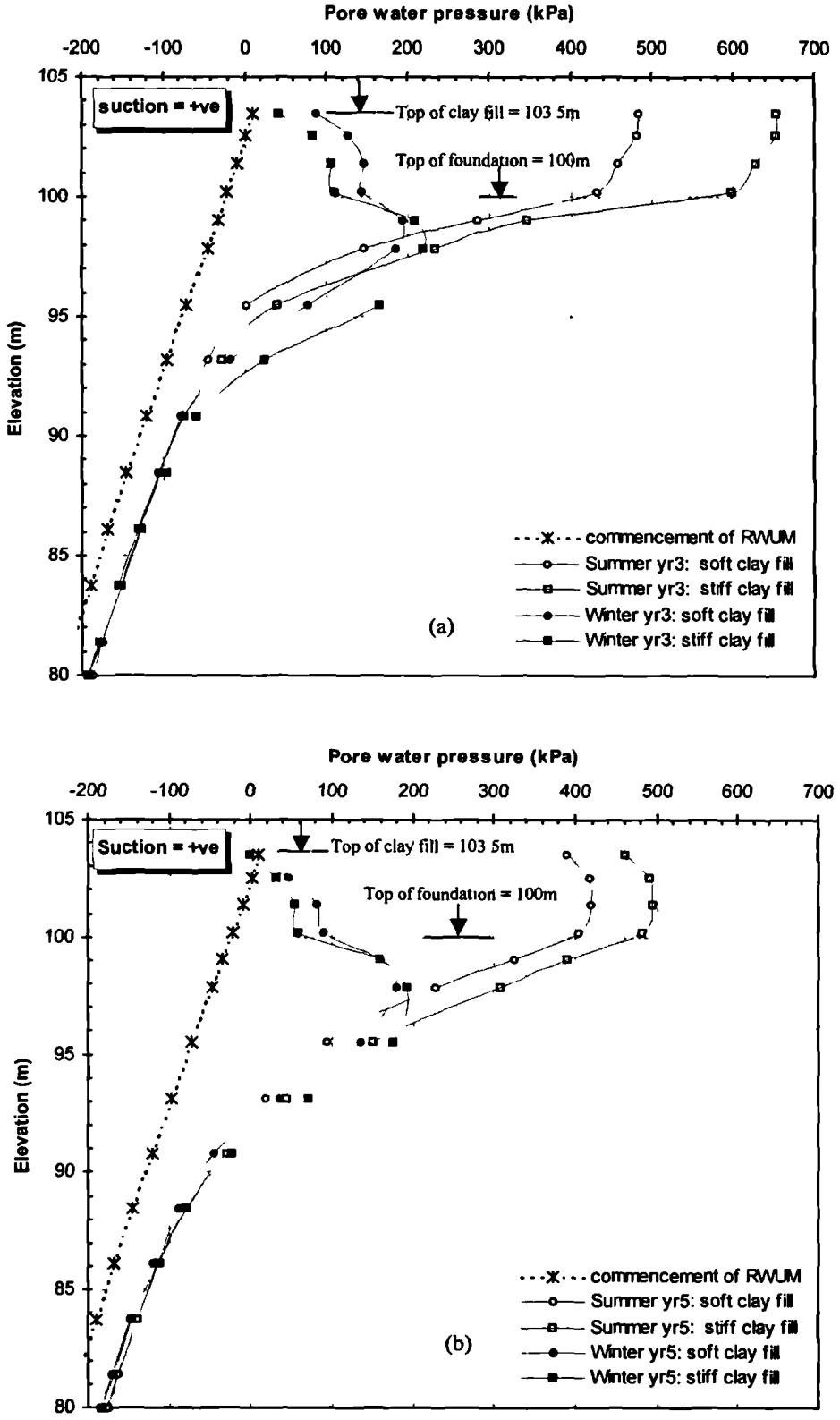

Figure 7.20 Predictions of accumulated pore water pressure at mid-slope for soft and stiff clay fills.

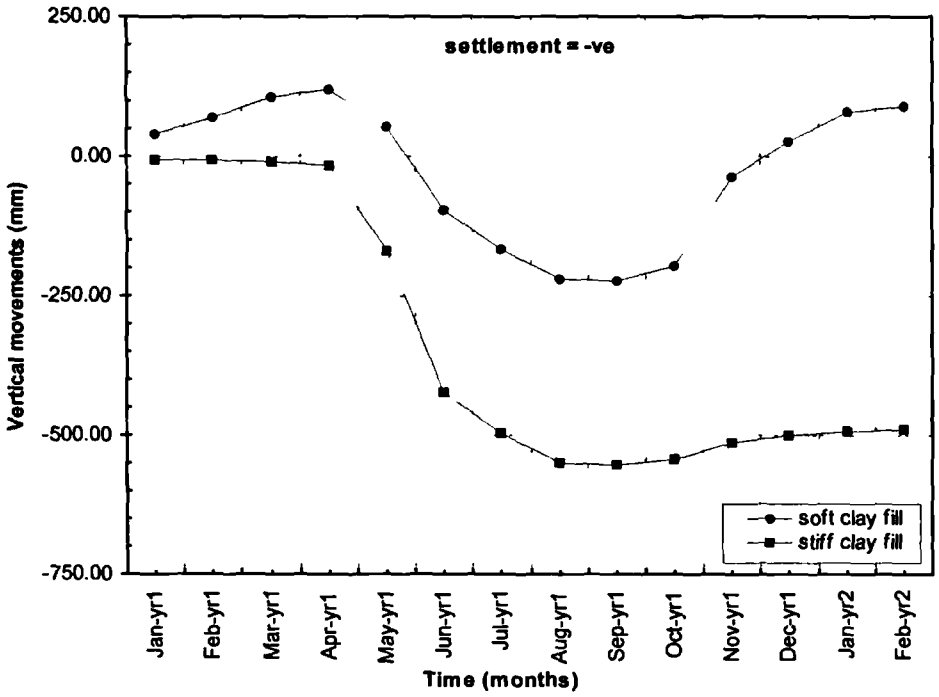

Figure 7.21a Predictions of sub-accumulated vertical movements at crest centreline in soft and stiff embankments.

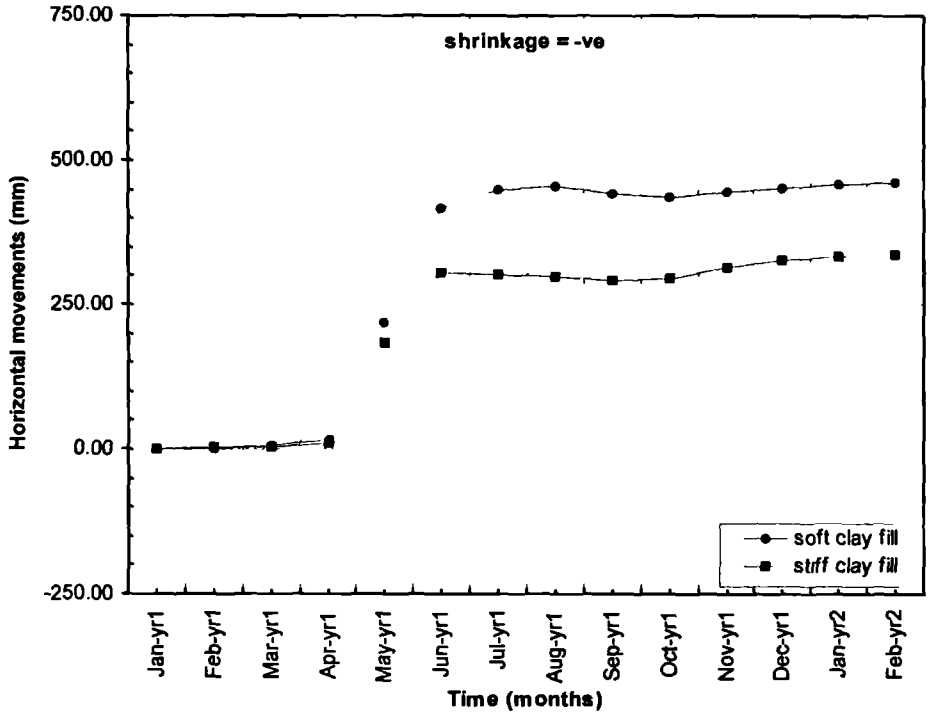

Figure 7.21b Predictions of sub-accumulated horizontal movements at mid-slope in soft and stiff embankments.

Figure 7.21a shows the sub-accumulated vertical movements at the crest centreline during the first 12 months of application of the RWUM. The movements have been sub-accumulated from the beginning of January yr 1. The figure reveals the differences in the pattern of movements predicted by the two clay fills. The figure shows little vertical movements during the first 4 months (January to April) in the stiff clay fill embankment. This is followed by large settlements during the early part of the summer season (April to August), as previously identified. At the end of summer (August), a settlement of 550mm is predicted at the crest centreline.

Behaviour in the softer embankment exhibits a different pattern. During the early period January to April yr 1, heave of up to 120mm is predicted at the crest centreline, followed by large settlements during summer (350mm). At the end of August, the total vertical movements predicted since invokation of the RWUM are 220mm in the softer embankment compared to 550mm in the stiffer embankment.

Although heave is predicted in both embankments during the first winter (September yr 1 to February yr 2), only 50mm is predicted in the stiffer embankment compared to 320mm in the softer embankment. At the end of the 12 months (February yr 2), a net settlement of 500mm is predicted at the crest centreline in the stiffer embankment as opposed to a net heave of 100mm in the softer embankment.

Figure 7.21b shows the horizontal movements at mid-slope (ground level) for the same period. The movements are sub-accumulated from January yr 1. As expected, the horizontal movements in the softer embankment are larger at the end of the 12months. It is also noteworthy that as for vertical movements, the majority of the movements occur at the onset of the dry period (May and June). The horizontal movements during these two months are 420mm (soft embankment) and 300mm (stiff embankment) compared to 460mm and 340mm, respectively at the end of 12 months.

The deformation pattern of the embankment during the early stages of application of the WRUM is therefore significantly different, as confirmed in Figure 7.21c where the vertical movements along the crest width are plotted. This latter figure reveals that in the stiffer embankment, overall settlement along the crest is approximately of the same order of magnitude; notwithstanding that the central section settles slightly more than the crest edge. In contrast, the pattern of movement in the soft embankment is characterised by large settlement of the crest edge relative to the central section of the crest.

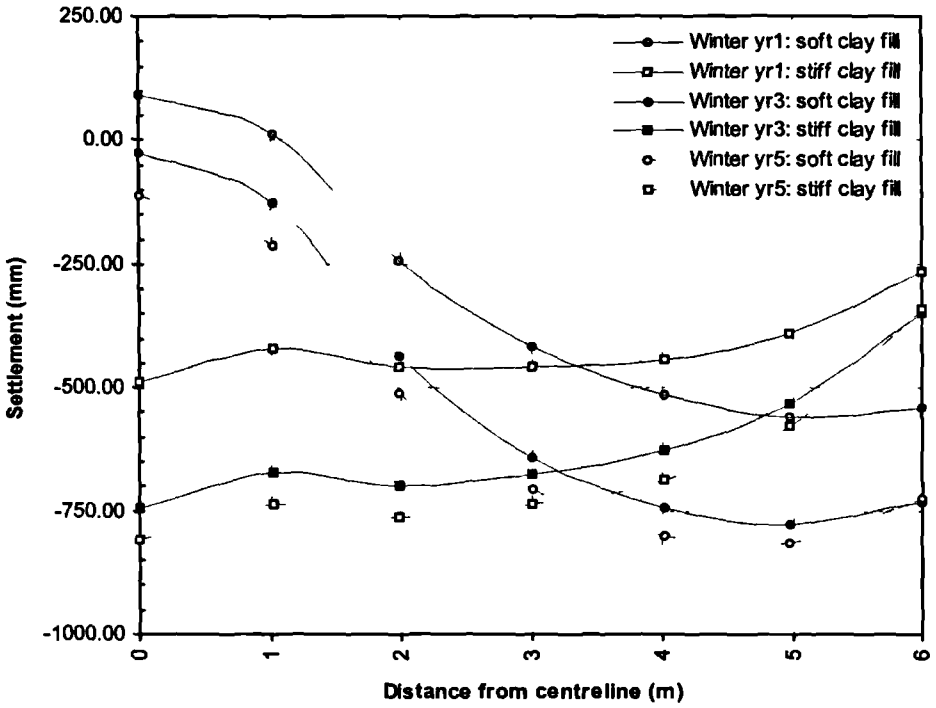

Figure 7.21c Predictions of sub-accumulated vertical movements along the crest width in soft and stiff embankments.

The sub-accumulated movements occurring during the first summer (March to August yr 1) and the first winter (September yr 1 to February yr 2) for the softer embankment are shown in Figures 7.22a and b, respectively. The corresponding figures for the stiffer embankment are Figures 7.3b and 7.9b. During summer, although the overall pattern of movements is similar, the magnitude of the vectors in the softer clay fill is larger. A similar trend exists during the first winter.

Figure 7.23 shows contours of sub-accumulated plastic strains during the first 12 months when the RWUM is operational. Plastic strains indicate the degree to which strains are developing within the clay fill, therefore comparisons can be made between the two clay fills. The figure shows that in both cases, a deep seated zone of plasticity has developed. However, the degree of plasticity is different eg. the zone encompassed by the 0.5 (50%) contour (residual strength) is larger in the softer clay fill compared to that existing in the stiffer clay fill. The higher plasticity portrayed in the softer embankment mirrors the pattern of horizontal movements shown in Figure 7.21.

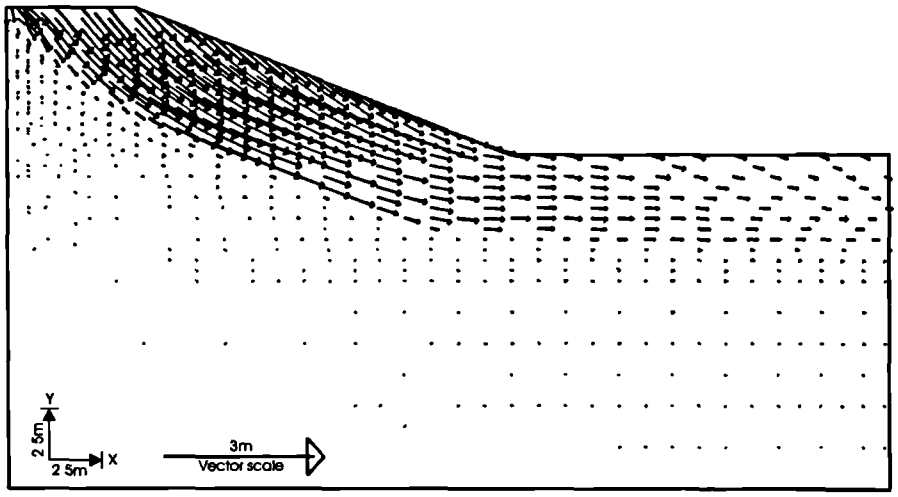

(a) Soft clay fill (Jan yr1 - Oct yr1)

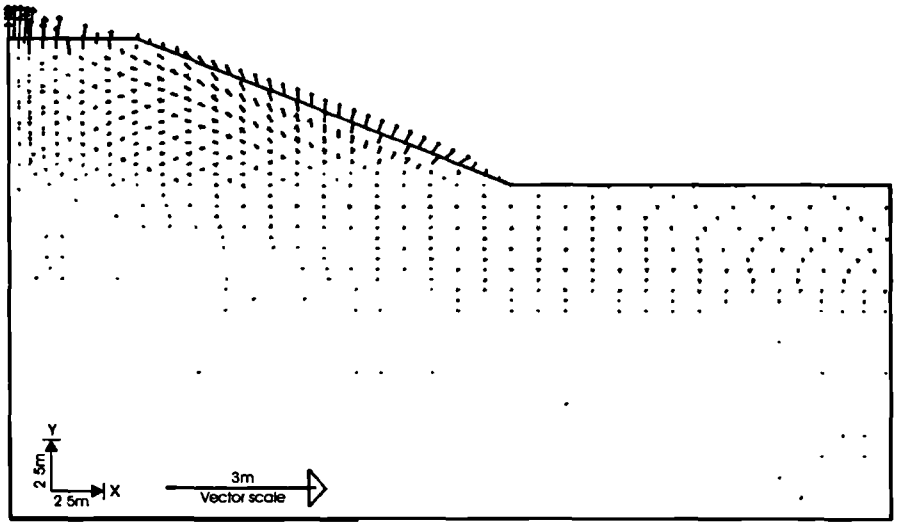

(b) Soft clay fill (Oct yr1 - Feb yr2)

Figure 7.22 Vectors of sub-accumulated movements predicted for soft clay fill embankment during the period Aug yr1 - Feb yr2.

The analysis was extended for 4 years to identify the medium term trends. Figure 7.24a shows the sub-accumulated vectors of movements during the 4 years (March yr 2 to February yr 6), for the soft embankment while plastic strains for the same period are shown in Figure 7.24b. The corresponding plot for the stiff clay fill are shown in Figure 7.14b and Figure 7.17b, respectively. The overall pattern depicted is very similar and suggests that during the 4 years, the behaviour of the embankment is not strongly influenced by the stiffness of the clay fill unlike the behaviour observed earlier ie. during the period January yr 1 to February yr 2.

Figure 7.25a shows the sub-accumulated horizontal movements at mid-slope (ground level) since inception of the RWUM (January yr 1). A similar figure with movements sub-

accumulated from June yr 2 is shown in Figure 7.25b, which portrays the long term trends since the plot eliminates the initial movements associated with invokation of the RWUM. The overall pattern suggests that after the first 12 months during which behaviour is significantly different in the two clay fills, the pattern of horizontal movements becomes similar. It is also noteworthy however that Figure 7.25b suggests that some differences in the magnitude of movements are identifiable during the summer months (up to 20mm). During winter, the predictions are almost of the same order. Overall, when consideration is made of the type of boundary value problem, the 20mm difference in movement is small.

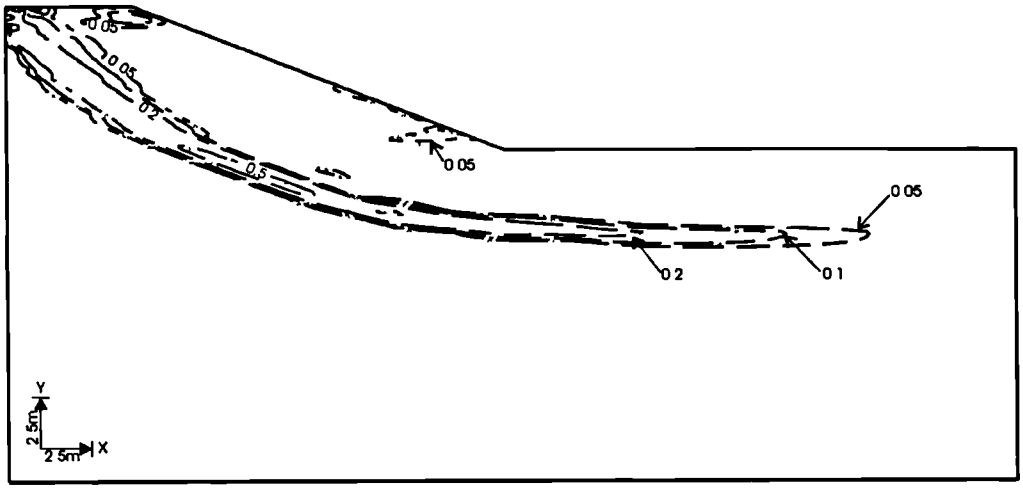

(a) Stiff clay fill

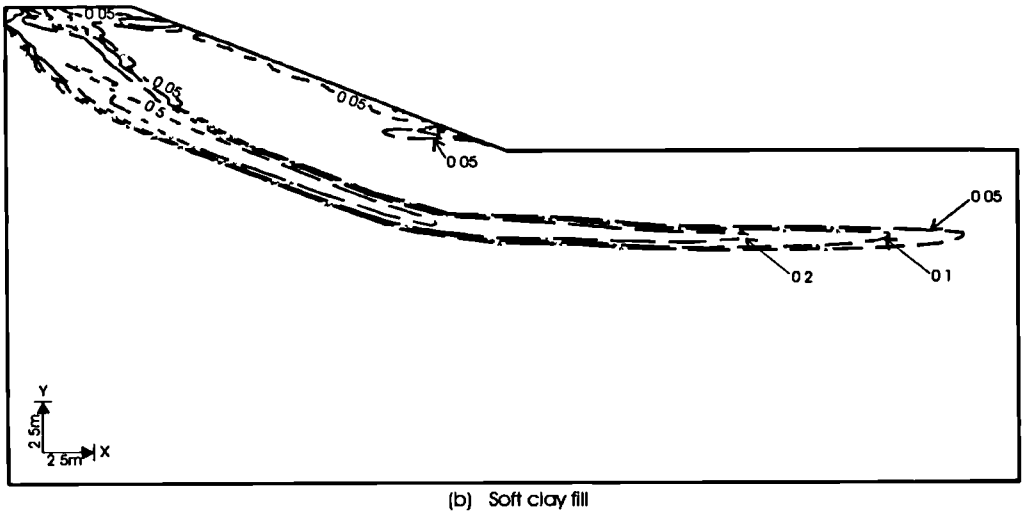

(b) Soft clay fill

Figure 7.23 Contours of sub-accumulated deviatoric plastic strains predicted for soft and stiff embankments during the period Jan yr1 - Feb yr2.

The small differences in the magnitude of movements are further exhibited in Figure 7.26 which depicts sub-accumulated horizontal movements along a vertical profile at mid-slope of the

embankment. Figure 7.26a (datum Jan yr 1) portrays all the movements since inception of the RWUM (Jan yr 1) while for comparison purposes, the movements associated with application of the RWUM are excluded in Figure 7.26b (datum June yr 2). There is indirect evidence from Figure 7.26b that the horizontal movements per cycle in the softer embankment are marginally higher than those occurring in the stiffer embankment eg. at the base of the embankment, the predictions of sub-accumulated horizontal displacements after 3 years are 40mm (stiff embankment) and 55mm (soft embankment), which is a 15mm difference. After 5 years, the predictions are 80mm (stiff embankment) and 100mm (soft embankment), which is a 20mm difference.

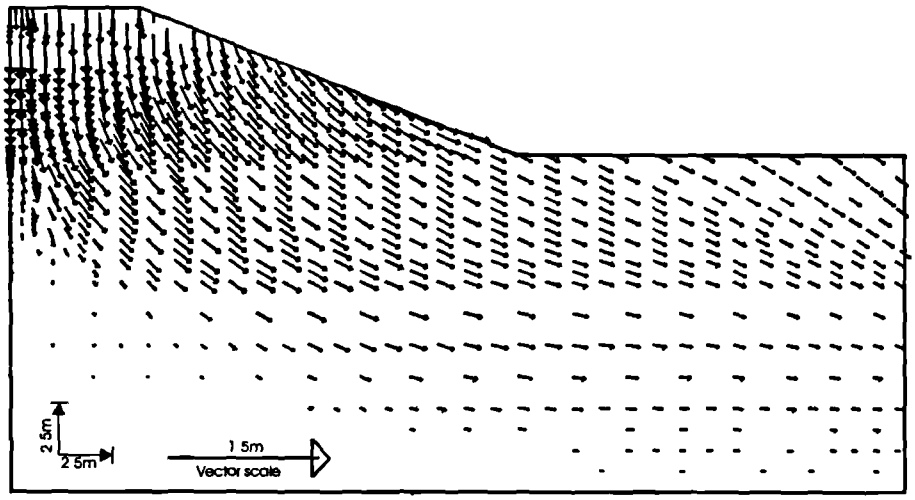

a Vectors of sub-accumulated displacements for soft clay fill embankment (Feb yr2 - Feb yr6).

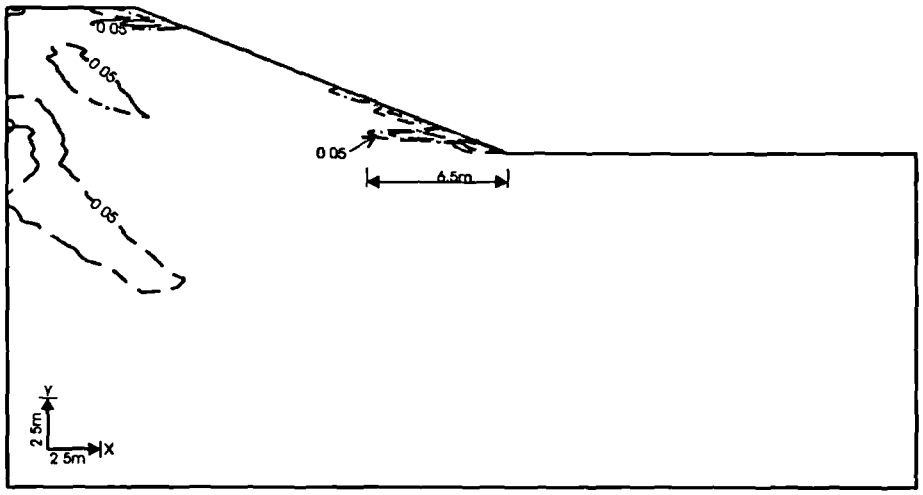

b Contours of sub-accumulated plastic strain for soft clay fill embankment (Feb yr2 - Feb yr6).

Figure 7.24 Vectors of sub-accumulated movements and contours of sub-accumulated deviatoric plastic strains predicted in soft embankment.

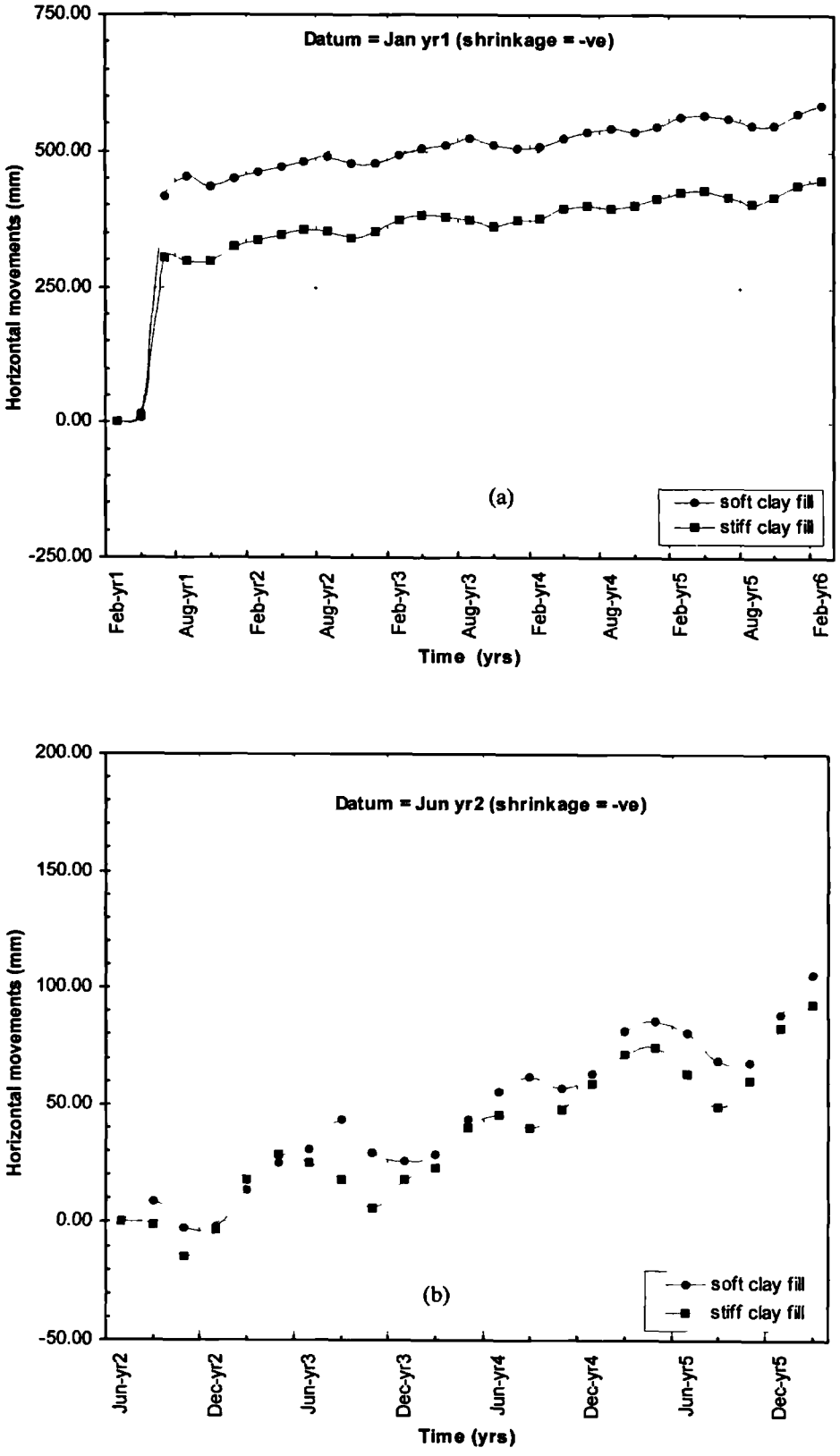

Figure 7.25 Sub-accumulated horizontal movements at ground level of mid-slope predicted in soft and stiff clay fill embankments during the first 5yrs.

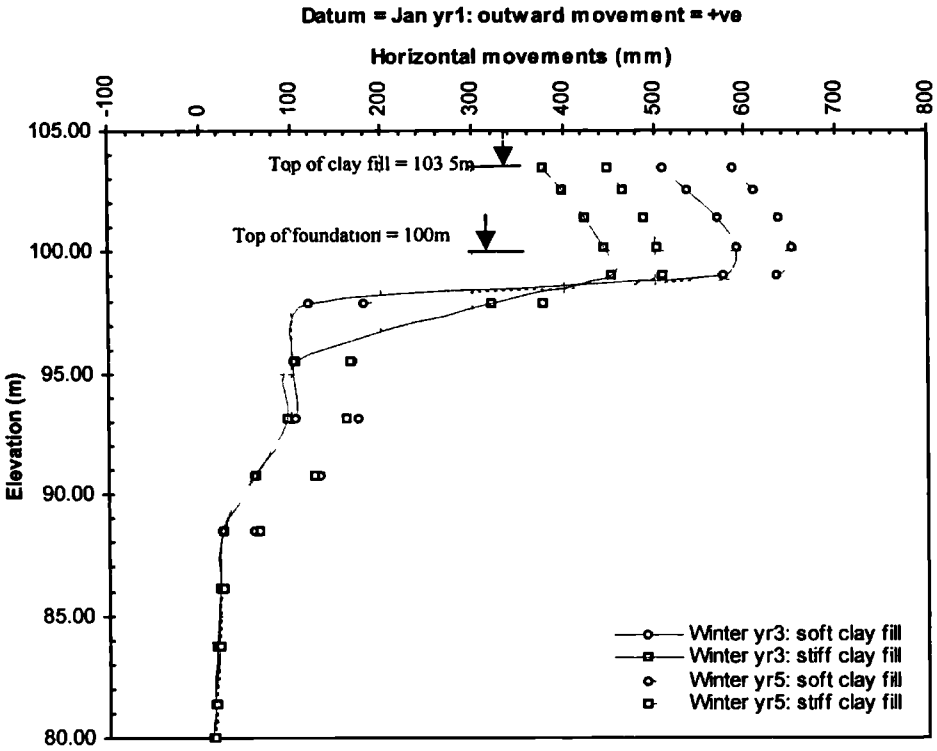

Figure 7.26a Sub-accumulated horizontal movements at mid-slope predicted in soft and stiff clay fill embankments during the first 5yrs (*datum Jan yr1*).

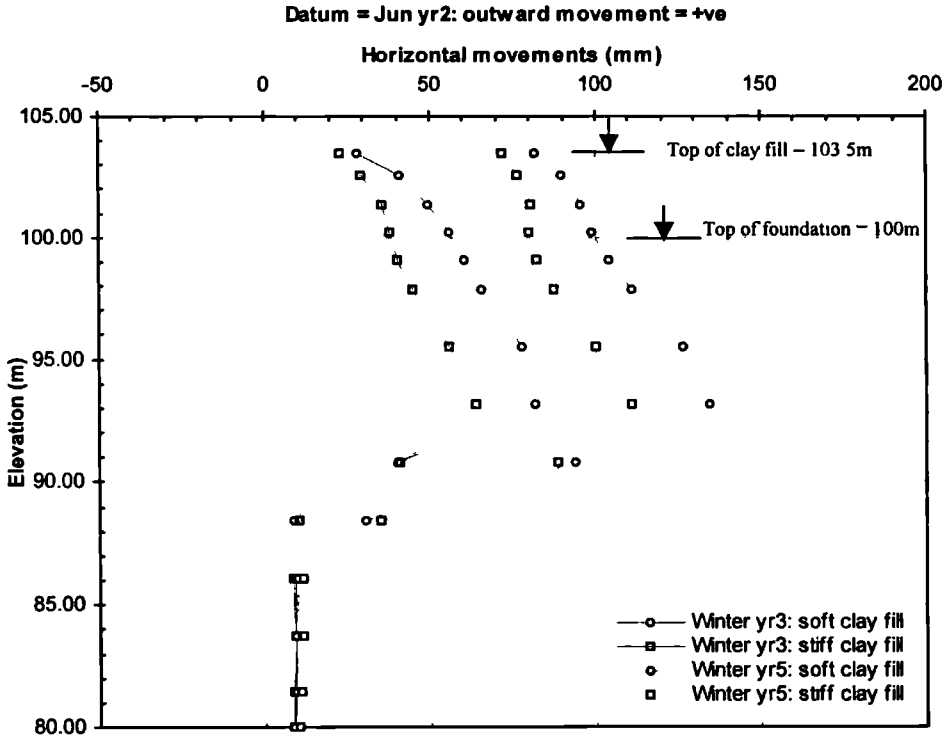

Figure 7.26b Sub-accumulated horizontal movements at mid-slope predicted in soft and stiff clay fill embankments during the first 5yrs (*datum – Jun*

The behaviour identified above indicates that stiffness is only playing a significant influence on embankment behaviour during the initial period soon after application of the RWUM. This initial phase is associated with large pore water pressure changes. After a few months when a cyclic pore water pressure pattern has been established, there is evidence that the overall pattern of movements is not siginificantly influenced by the magnitude of the clay fill stiffness. However the soft embankment exhibits marginally larger seasonal cyclic movements compared to the stiff embankment. It is considered that the differences in the magnitude of seasonal movements predicted by the two clay fills are not large enough to exhibit significant differences in the development and propagation of a progressive failure mechanism in the long term.

7.5 Influence of permeability increase due to desiccation cracking

7.5.1 Introduction

The influence of desiccation cracks on the mass permeability of a soil was discussed in greater detail in Section 2.5.7 of Chapter 2. This increase is primarily governed by the crack width and spacing. The mass permeability of a cracked ground can be several orders of magnitude higher than the mass permeability of the intact material (see Table 2.1 in Chapter 2). Desiccation cracks facilitate ingress of water into the soil and this accelerates the recharge of ground water during precipitation.

Under field conditions, desiccation primarily results from egress of water through evapotranspiration and recharge mainly results from precipitation. Underground water flow also plays a part in the interaction process, however, this may contribute to egress or ingress of water, depending on geological conditions.

The analyses to be presented in this section were carried out to assess the influence of permeability increase caused by desiccation cracking on the overall behaviour of a typical old railway embankment. Similar analyses undertaken for level ground where presented in Section 5.5.5 of Chapter 5 where the development of the vegetation boundary condition was discussed.

7.5.2 Numerical modelling

The mesh, boundary conditions and numerical modelling were as described in Section 7.2. The mass permeability of the clay fill and London Clay foundation were assumed to be $1\times10^{-9}e^{-0.003p'}m/\sec$ and $2\times10^{-10}e^{-0.0075p'}m/\sec$, respectively (see Table 7.1). Desiccation

cracking was assumed to commence when σ_3 exceeded zero and the ground was assumed to be fully cracked when σ_3 was equal to 100kPa (see Figure 5.24). Over this stress range, the permeability was assumed to increase according to a logarithmic law.

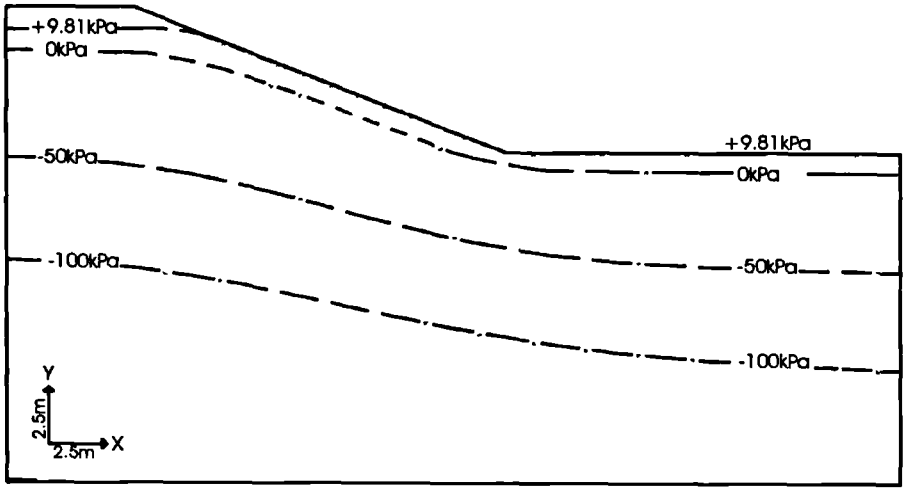

(a) Contours of accumulated pore water pressure at inception of vegetation boundary condition (Jan yr1) for k_f/k_i ratio = 100.

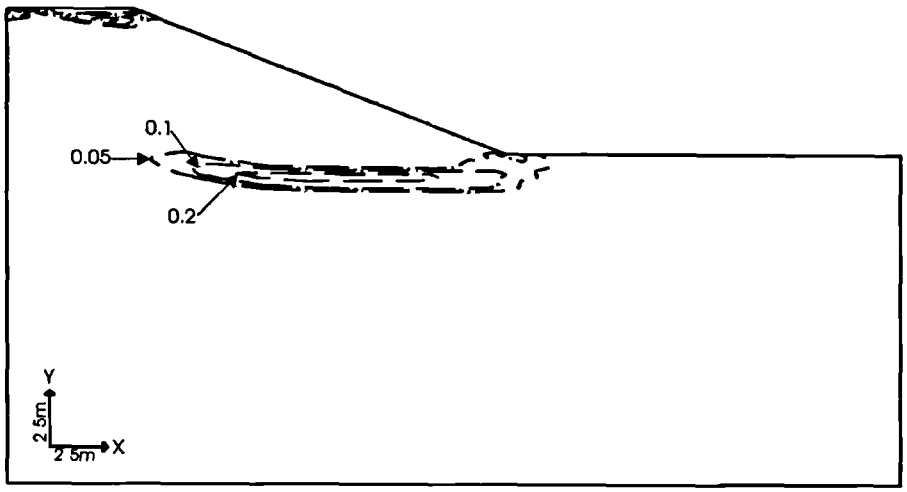

(b) Contours of accumulated deviatoric plastic strains at inception of vegetation boundary condition (Jan yr1) for k_f/k_i ratio = 100.

Figure 7.27 Contours of accumulated pore water pressure and deviatoric plastic strains at the inception of the vegetation boundary condition for k_f/k_i ratio = 100 (Jan yr1).

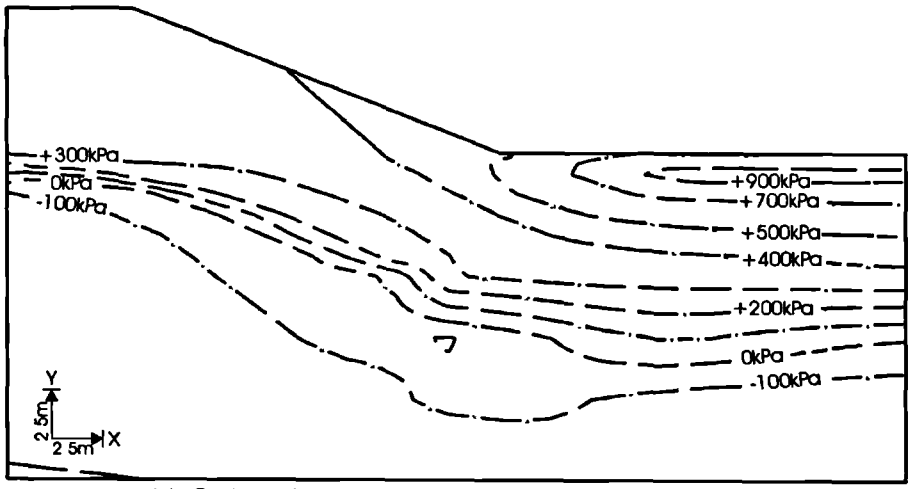

(a) Contours of accmulated pore water pressure in Aug yr1 for k_f/k_i = 100

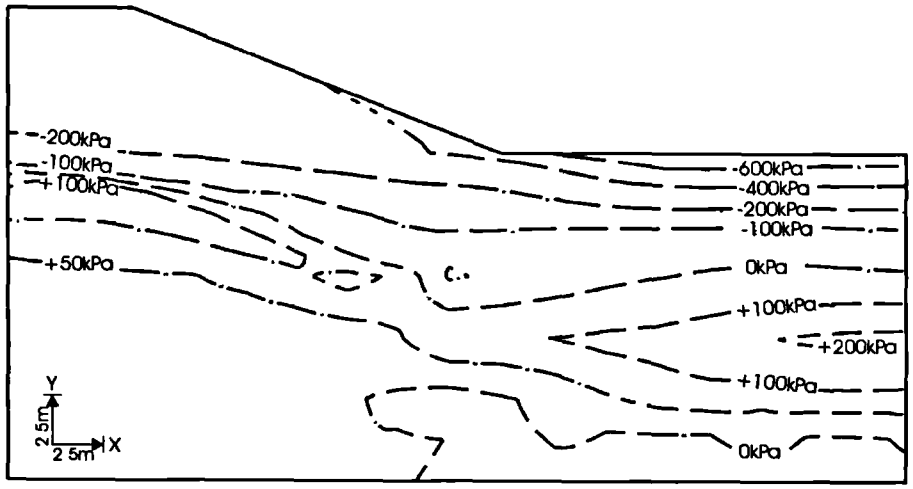

(b) Contours of sub-accumulated pore water pressures (Sept yr1 - Feb yr2) for k_f/k_i = 100.

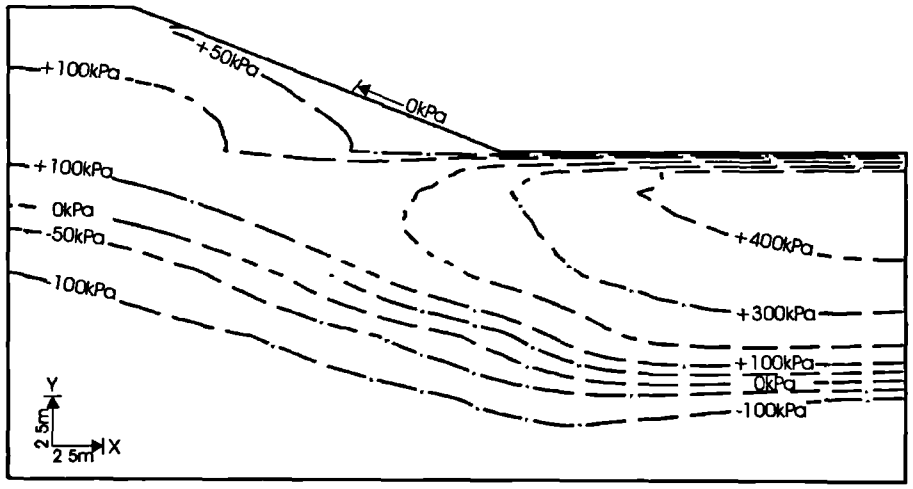

(c) Contours of accumulated pore water pressures for k_f/k_i = 100 (Feb yr2)

Figure 7.28 Pore water pressure distribution predicted for k_f/k_i = 100 during the period Aug yr1 to Feb yr2.

Two analyses were carried out in which the permeability ratio of the cracked to intact material ($\frac{k_f}{k_i}$ ratio) over the 0-100kPa σ_3 stress range was assumed to be 10 in the first analysis and 100 in the second analysis. The $\frac{k_f}{k_i}$ ratios were applied at the commencement of embankment construction. As discussed in Section 7.2, the embankment was allowed to consolidate/swell for 5 years soon after construction before inception of the RWUM. The distribution of pore water pressures and degree of plasticity at the end of the 5 yr swelling period are shown in Figure 7.1 (for a $\frac{k_f}{k_i}$ ratio of 10) and Figure 7.27 (for a $\frac{k_f}{k_i}$ ratio of 100). The higher degree of plasticity in the latter analysis is considered to be concomitant with the relatively larger pore water pressure changes which occur involving a $\frac{k_f}{k_i}$ ratio of 100 as opposed to the lower $\frac{k_f}{k_i}$ ratio of 10.

7.5.3 Behaviour during the first 5 yrs of cycling

Figure 7.28a shows the contours of accumulated pore water pressures at the end of the first summer (August year 1) for a $\frac{k_f}{k_i}$ ratio of 100 while Figure 7.2b shows similar plots for a $\frac{k_f}{k_i}$ ratio of 10. A comparison of Figures 7.28a and 7.2b shows lower suctions in the embankment with a $\frac{k_f}{k_i}$ ratio of 100 (ie. less than 500kPa) as opposed to 700kPa in the embankment with a $\frac{k_f}{k_i}$ ratio of 10; which is reasonable. Similar behaviour is noticeable at shallow depth in the zone remote from the toe of the embankment. Overall, the contour pattern typically shows pore water pressure changes over a larger depth in the embankment with the higher $\frac{k_f}{k_i}$ ratio. The latter behaviour is attributed to redistribution of suctions in all the zones where the minimum total stress, σ_3, has exceeded 0kPa, which is the trigger value for the smeared crack model to be invoked. In effect, the larger $\frac{k_f}{k_i}$ ratio results in pore water pressure changes over a wider region because the larger permeability involved allows more water to be abstracted, to meet the evapotranspiration demand.

Figure 7.28b shows the contours of pore water pressure changes that occur during the first winter (September yr 1 to February yr 2) in the embankment with a $\frac{k_f}{k_i}$ ratio of 100. The pattern for a $\frac{k_f}{k_i}$ ratio of 10 is shown in Figure 7.8b, for comparison. As previously noted, the compressive pore water pressure changes during winter (pore water pressure recovery) are dominated by the amount of precipitation rather than by the magnitude of potential evapotranspiration, during that period. Maximum pore water pressure changes of greater than -400kPa and -600kPa are predicted for $\frac{k_f}{k_i}$ ratios of 100 and 10, respectively. The largest change in the clay fill is -400kPa compared to in excess of -600kPa in the embankment with a $\frac{k_f}{k_i}$ ratio of 10. It is considered that the pattern of the relative differences in the magnitude of pore water pressure recovery mirrors the pattern of the maximum suctions that occurred in the preceding summer season.

The accumulated pore water pressures at the end of the first winter are shown in Figure 7.28c for a $\frac{k_f}{k_i}$ ratio of 100 while Figure 7.7b shows the plot for a $\frac{k_f}{k_i}$ ratio of 10. It can be seen that in the area remote from the embankment, the pore water pressure predictions for a $\frac{k_f}{k_i}$ ratio of 10 yield higher suctions compared to the analysis using a $\frac{k_f}{k_i}$ ratio of 100. These are 1200kPa and 400kPa for $\frac{k_f}{k_i}$ ratios of 10 and 100, respectively. In this area the ground was modelled as horizontal therefore lower suctions would be expected at the end of winter.

Within the embankment, the analysis with a $\frac{k_f}{k_i}$ ratio of 10 predicts suctions of 50kPa in the majority of the embankment whilst suctions of up to 100kPa are predicted in the analysis with a $\frac{k_f}{k_i}$ ratio of 100. In addition, there is evidence that pore water pressures are recovering more at shallow depth in the analysis with a higher $\frac{k_f}{k_i}$ ratio, notwithstanding that the larger $\frac{k_f}{k_i}$ ratio is also predicting significant redistribution of suctions at depth and resulting in the development of a desiccated zone beneath the embankment. At this stage, the $\frac{k_f}{k_i}$ ratio of 10 is considered to be yielding pore water pressure predictions which are closer to field observations compared to the

$\frac{k_f}{k_i}$ ratio of 100. Current field monitoring data (eg. ICON, 1999c) in LUL embankments suggests significant pore water pressure recovery in the embankments at the end of winter, with no evidence of desiccation at depths greater than 5m during summer. The results of pore water pressure monitoring during the period January 1996 to March 1997 on the four embankments reported in ICON (1999c) indicated maximum summer suctions of 70kPa. However, more recent studies (ICON, 2001) and Ridley and Dineen (2003) suggest that average maximum summer suctions in old railway embankments under tree cover are significantly higher than the 70kPa reported in ICON (1999c).

The pattern of pore water pressure changes depicted in Figure 7.8b and Figure 7.28b also indicates larger changes in the analysis involving a $\frac{k_f}{k_i}$ ratio of 10, which is reasonable. It is considered that in a "wet" climate such as that which prevails in the UK, the greater recharge of pore water pressure associated with increasing values of $\frac{k_f}{k_i}$ ratios yields lower seasonal cyclic pore water pressure changes. This would induce less plasticity per seasonal cycle within the embankments, compared to a situation involving larger cyclic pore water pressure changes. Similar behaviour was observed in Chapter 4, where analyses were carried out using the ICON pore water pressure profiles for winter and summer. Therefore it could be argued that the enhanced flows that occur in response to a permeability increase following desiccation cracking may constitute a beneficial effect on the long term stability of embankments.

Another important observation to note in Figures 7.8c and 7.28c is the pattern and influence of the redistribution of suctions predicted as the $\frac{k_f}{k_i}$ ratio increases eg. it can be seen that significantly larger pore water pressure changes are predicted at 2m below foundation level in the analysis with a $\frac{k_f}{k_i}$ of 100 compared to a $\frac{k_f}{k_i}$ of 10. Similar behaviour was depicted in the column analyses discussed in Chapter 5. It was noted during the analyses that in the long term, the desiccated zone predicted at depth by the smeared crack model begins to dominate the behaviour of the embankment by curtailing pore water pressure recharge. This in turn inhibits development of a progressive failure mechanism, and such a response is considered to be at variance with observed field behaviour.

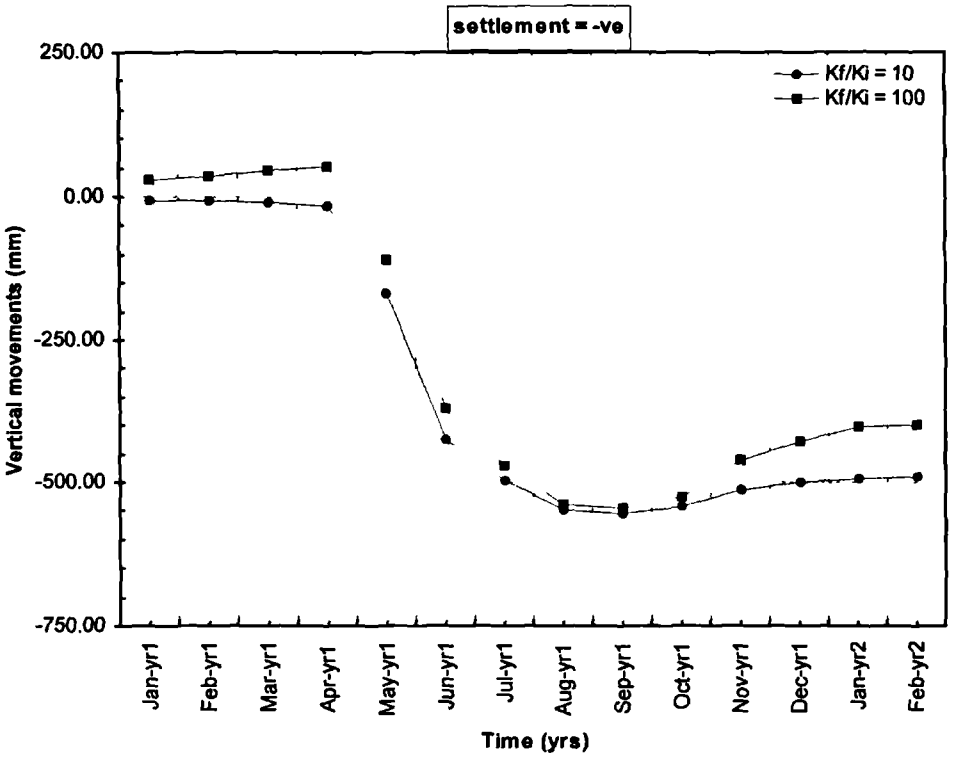

Figure 7.29a Predictions of vertical movements at the crest centreline for $\frac{k_f}{k_i}$ ratios of 10 & 100 during yr 1.

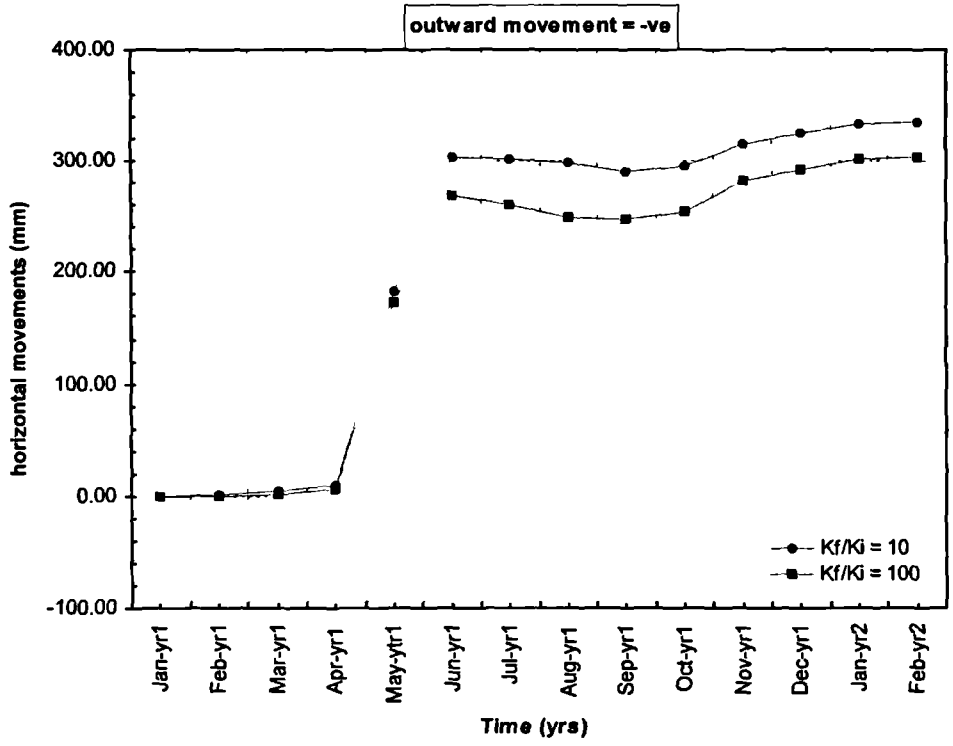

Figure 7.29b Predictions of horizontal movements at mid-slope for $\frac{k_f}{k_i}$ ratios of 10 & 100 during yr 1 .

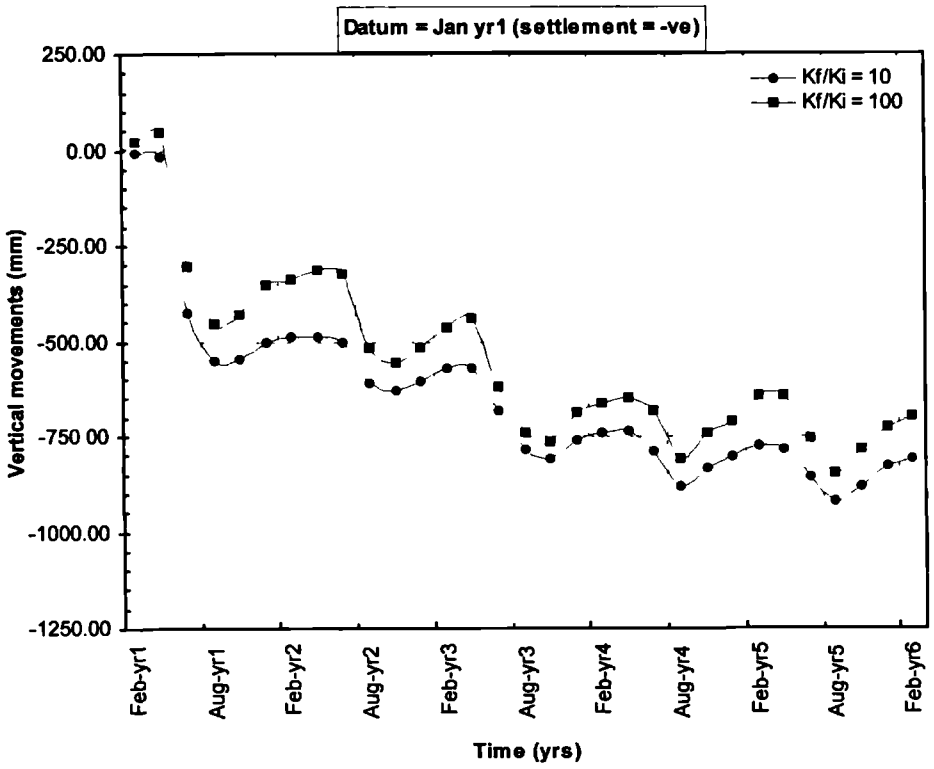

Figure 7.30a Predictions of vertical movements at the crest centreline for $\frac{k_f}{k_i}$ ratios of 10 & 100 during the first 5yrs of cycling (datum = Jan yr 1).

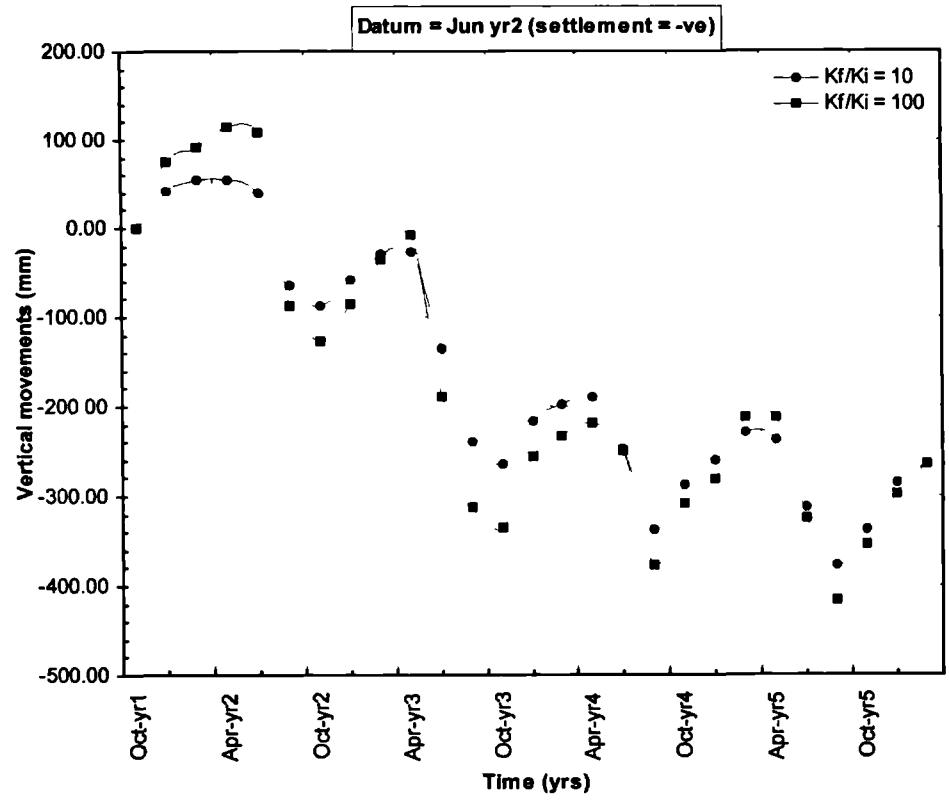

Figure 7.30b Predictions of vertical movements at the crest centreline for $\frac{k_f}{k_i}$ ratios of 10 & 100 during the first 5yrs of cycling (datum = Jun yr 2).

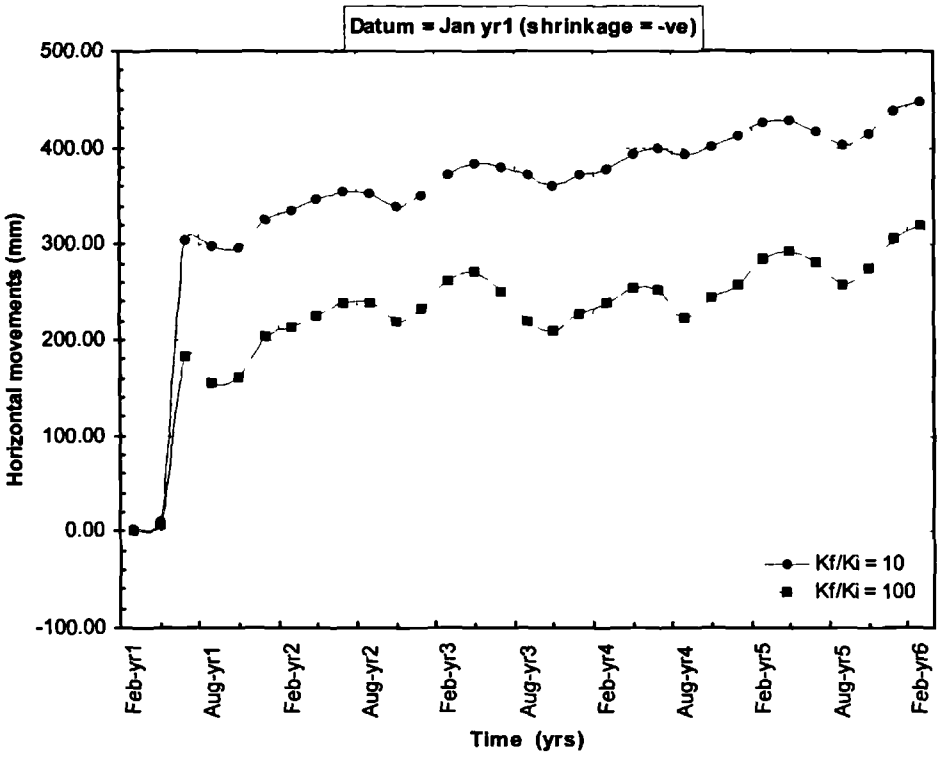

Figure 7.31a Predictions of horizontal movements at ground level of mid-slope for $\frac{k_f}{k_i}$ ratios of 10 & 100 during the first 5yrs of cycling (datum = Jan yr1).

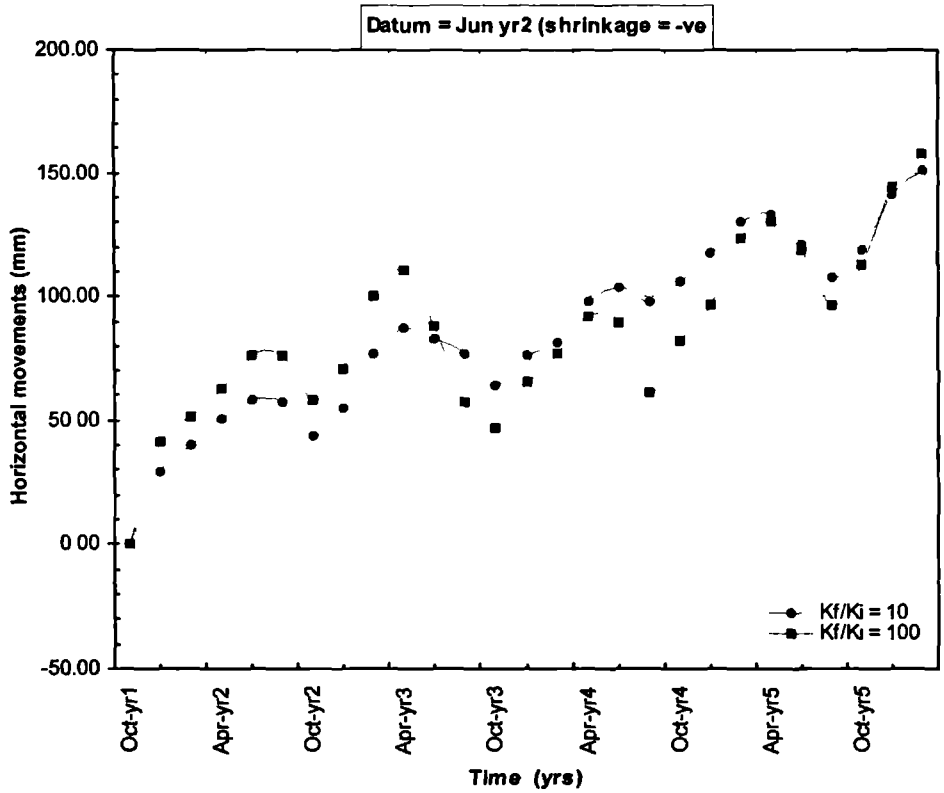

Figure 7.31b Predictions of horizontal movements at ground level of mid-slope for $\frac{k_f}{k_i}$ ratios of 10 & 100 during the first 5yrs of cycling (datum = Jun yr2).

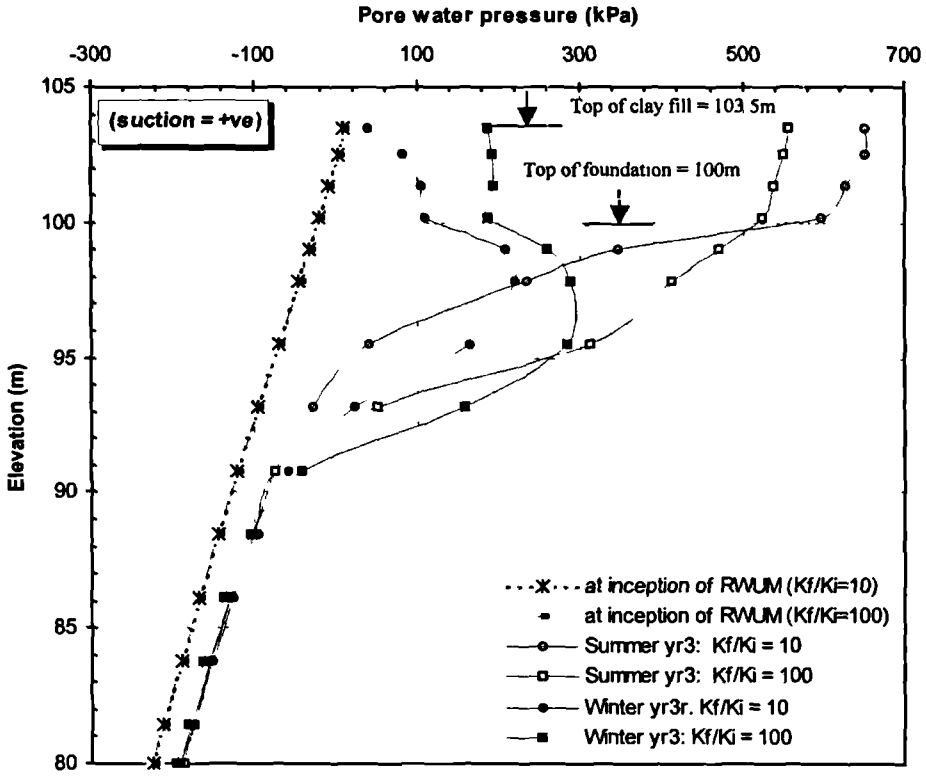

Figure 7.32a Accumulated pore water distribution at mid-slope for $\frac{k_f}{k_i}$ ratios of 10 & 100 after 3yrs and 5yrs.

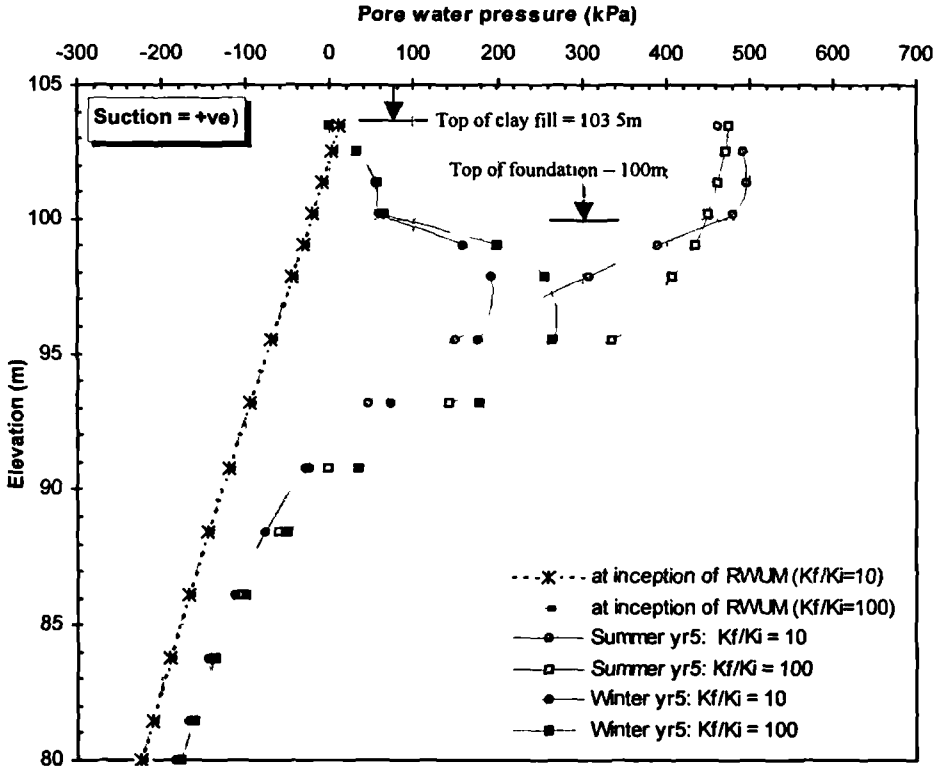

Figure 7.32b Accumulated pore water distribution at mid-slope for $\frac{k_f}{k_i}$ ratios of 10 & 100 after 3yrs and 5yrs.

Figure 7.29a shows the sub-accumulated vertical movements during the first year at the crest centreline and portrays the differences in prediction by the two $\frac{k_f}{k_i}$ ratios. During the wet months, the heave that occurs in the embankment with a $\frac{k_f}{k_i}$ ratio of 100 is significantly larger than that occurring in the embankment with a $\frac{k_f}{k_i}$ ratio of 10, which is reasonable eg. at the end of April yr 1, heave of 50mm is predicted by the higher ratio whereas settlement of 15mm is predicted by the lower ratio. However, despite these early differences, the sub-accumulated movements at the end of the first summer (August yr 1) are equal; the latter behaviour reinforcing the view that behaviour during winter is primarily dominated by the magnitude of precipitation.

The horizontal movements at mid-slope (ground level) are show in Figure 7.29b. Once again as previously observed, large movements associated with the development of a deep seated zone occur during May and June as drying occurs. The magnitude of movements during these two months is approximately 90% of the total movements at the end of 12 months. The larger movements occur in the embankment with a lower $\frac{k_f}{k_i}$ ratio. This is considered to be reasonable because this embankment experiences larger suctions during summer (compare Figure 7.28a with Figure 7.2b). It is considered that the development of relatively larger plastic strains in the clay fill with a lower $\frac{k_f}{k_i}$ ratio is being manifested in the larger horizontal movements depicted in Figure 7.29b.

Figure 7.30a shows the vertical movements at the crest centreline during the first 5 years (since inception of the RWUM) while Figure 7.30b depicts the movements, assuming October yr 1 to be datum. The figures reveal that the pattern identified during the first year (Figure 7.29a) is continued during the remainder of the period ie. larger heave and shrinkage movements predicted in the analysis with a $\frac{k_f}{k_i}$ ratio of 100 compared to a $\frac{k_f}{k_i}$ ratio of 10. Similar behaviour is depicted in the horizontal movements at ground level at the mid-slope (Figure 7.31). The pattern is made clearer in Table 7.5 which summarises the vertical movements at the crest centreline. The values in Table 7.5 have been computed from Figure 7.30a and assuming summer to span from March to September and winter from October to February.

Table 7.5 Predicted seasonal vertical movements at crest centreline (mm)

Year	Winter		Summer	
	$\frac{k_f}{k_i}=10$	$\frac{k_f}{k_i}=100$	$\frac{k_f}{k_i}=10$	$\frac{k_f}{k_i}=100$
	-	-	-540	-475
1	60	120	-140	-210
2	55	95	-230	-295
3	60	100	-105	-125
4	95	145	-125	-175
5	95	125	-	-

Results of monitoring on LUL embankments have shown peak seasonal movements of 40-50mm on unremediated embankments (McGinnity *et al*, 1998). Again it is noteworthy that the predictions using a $\frac{k_f}{k_i}$ ratio of 10 are closer to field behaviour than those made by a higher $\frac{k_f}{k_i}$ ratio.

The author considers that field behaviour involving high $\frac{k_f}{k_i}$ ratios would result in enhanced recharge of water at shallow depth where the majority of desiccation cracks develop. Recharge of water at shallow depth provides a ready supply of water to meet the evapotranspiration demand and thus limit water abstraction at depth. The desiccated profile does not therefore continue to increase with time. It is therefore considered that the redistribution of suctions to deeper horizons within the foundation is inducing unduly high desiccation (and the associated seasonal cyclic movements). This view is reinforced by the pattern of pore water pressure after 3 yrs and 5 yrs depicted in Figure 7.32 from which it can be seen that the depth of desiccation predicted by a $\frac{k_f}{k_i}$ ratio of 100 is larger compared to a $\frac{k_f}{k_i}$ ratio of 10. In addition, the magnitude of suctions is also larger eg. after 5 years, maximum suctions of 190kPa and 260kPa are predicted by $\frac{k_f}{k_i}$ ratios of 10 and 100, respectively (see Figure 7.32b).

In theory, the embankment which experiences larger seasonal cyclic movements develops a progressive failure mechanism at a faster rate than that which experiences cyclic movements of a lower magnitude. For this type of embankment, the development of a progressive failure mechanism takes many years to develop and therefore the differences in prediction of plasticity between the two $\frac{k_f}{k_i}$ ratios is unlikely to be identifiable in the 5 years modelled here. The pore

water pressure predictions in Figure 7.32 suggest that larger seasonal pore water pressure changes are occurring in the clay fill with a $\frac{k_f}{k_i}$ ratio of 10. This embankment would therefore be expected to fail earlier, in the long term. This is borne testimony to by Figure 7.33 which shows a 5m long zone of a potential slip surface (as defined by the 0.05 plastic strain contour) in the embankment with a $\frac{k_f}{k_i}$ ratio of 100 compared to 6.5m (Figure 7.17b) for a $\frac{k_f}{k_i}$ ratio of 10.

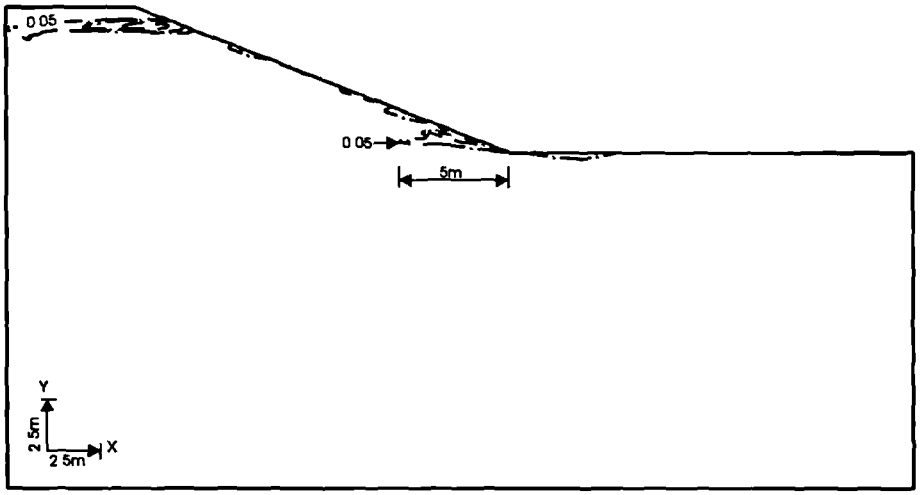

Figure 7.33 Contours of sub-accumulated deviatoric plastic strains for k_f/k_i = 100 during the first summer (Sept yr1 - Feb yr6).

Once again it is worth reiterating the fact that in the field, the degree of fracturing and width of the cracks varies tremendously both spatially and with time, in response to the water balance. Modelling such behaviour requires more sophistication than has been assumed in the smeared crack model developed in this study. Nevertheless, the analyses that have been presented here are diagnostic and illuminatory, in so far as understanding the influence of cracks on embankment behaviour is concerned.

7.6 Influence of mass permeability of the clay fill

7.6.1 Introduction

The influence of mass permeability of the clay fill on embankment behaviour was investigated in Chapter 4 using the state-of-the-art method used in industry to simulate winter and summer pore water pressures. In the analyses reported in Chapter 4, homogeneous permeabilitites of $1\times10^{-9}\,m/\sec$, $1\times10^{-8}\,m/\sec$ and $1\times10^{-7}\,m/\sec$ for the clay fill were used. As discussed in

Chapter 4, the method currently used in industry is simplistic; the major drawback being that the pore water pressures contrived to simulate observed desiccation profiles may not be consistent with the meteorological data. A major advantage of RWUMs over current industry methods is the ability to use actual meteorological data as input into the analysis and allow pore water pressures to be predicted rather than prescribed.

In this section, the influence of mass permeability of the clay fill on the behaviour of a typical railway embankment was investigated using the RWUM. This investigation is of interest to identify differences in the response of vegetated embankments of similar geometry, stratigraphy, within the same locality (and hence same meteorological conditions) but with significantly different values of mass permeability. Under such conditions, water flow in response to evapotranspiration demand will be different.

7.6.2 Numerical modelling

The mesh, boundary conditions and numerical modelling were as described in Section 7.2. The permeability of ash and London Clay foundation were assigned values shown in Table 7.1. Three analysis were executed using clay fill permeabilities of $1\times10^{-9}e^{-0.003p'}m/\sec$, $1\times10^{-8}e^{-0.003p'}m/\sec$ and $1\times10^{-7}e^{-0.003p'}m/\sec$. In all the analyses, a $\frac{k_f}{k_i}$ ratio of 10 was used with the p' dependent permeability model. The permeability was specified at the beginning of embankment construction, in order to eliminate the influence of pore water pressure changes and movements associated with changes in the magnitude of the permeability, prior to application of the RWUM. As in previous sections, the discussion will focus on the behaviour of the embankment during application of the RWUM.

7.6.3 Behaviour during summer (yr 1)

The accumulated pore water pressures and plastic strains at the end of 5 years of consolidation/swelling period (which marks the invokation of the RWUM) are shown in Figure 7.1 for the clay fill with a permeability of $1\times10^{-9}e^{-0.003p'}m/\sec$. Those for clay fill permeabilities of $1\times10^{-8}e^{-0.003p'}m/\sec$ and $1\times10^{-7}e^{-0.003p'}m/\sec$ were found to be very similar and are therefore not presented. The plot for accumulated plastic strains (Figure 7.1) indicates that the plasticity is virtually zero at this stage of the analysis.

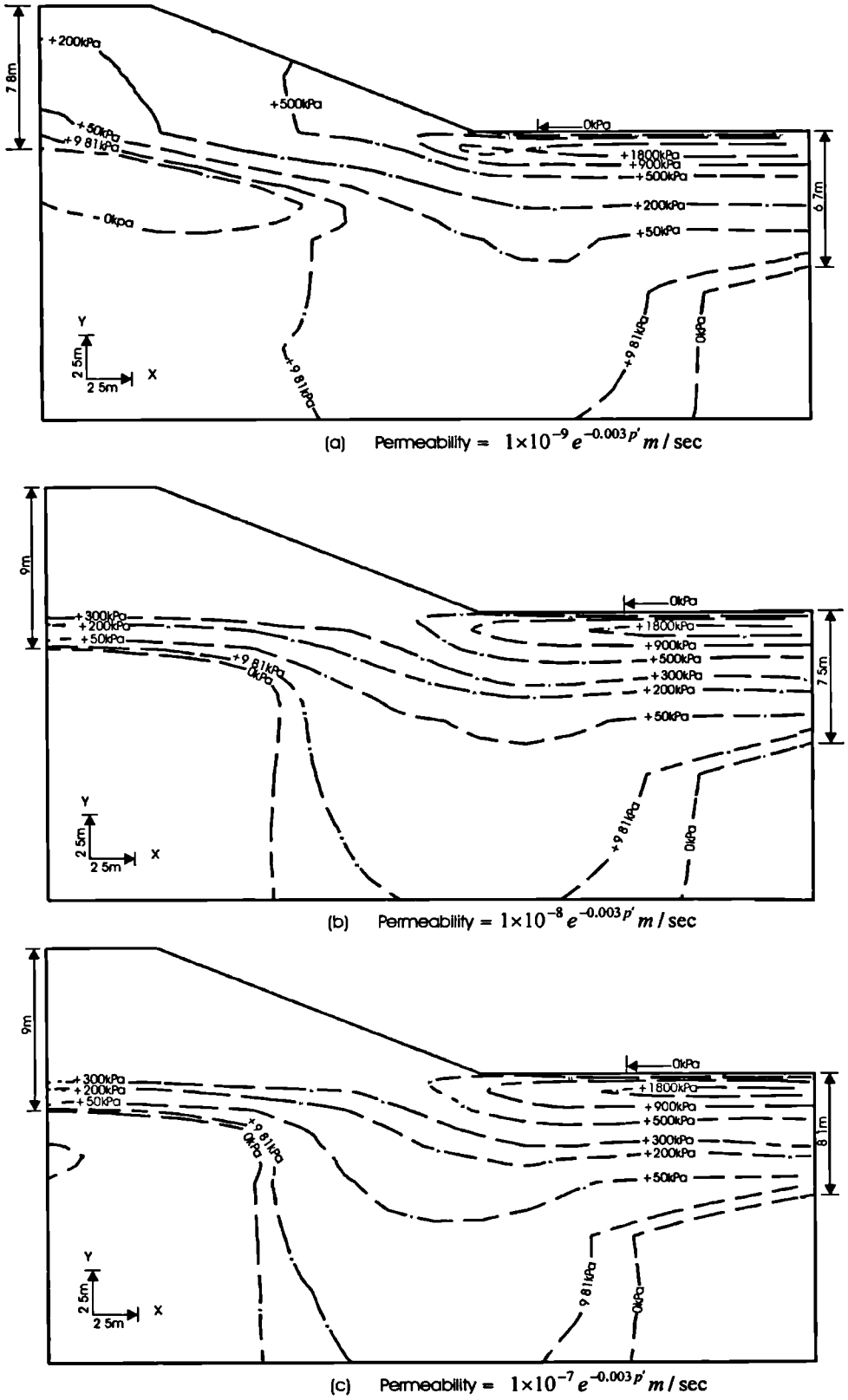

Figure 7.34 Contours of sub-accumulated pore water pressures predicted by 3 permeabilities during the first summer Mar yr1 - Aug yr1.

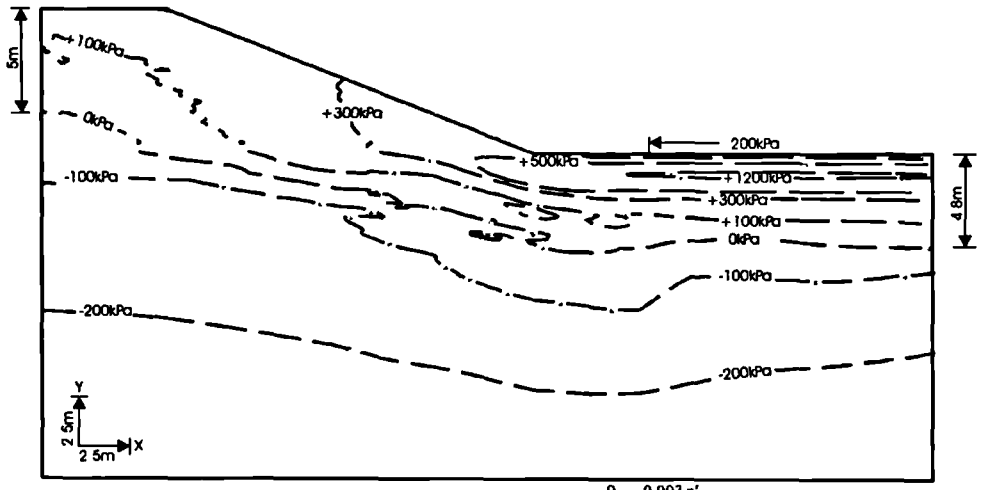

(a) Permeability = $1\times10^{-9}e^{-0.003p'}$ m / sec

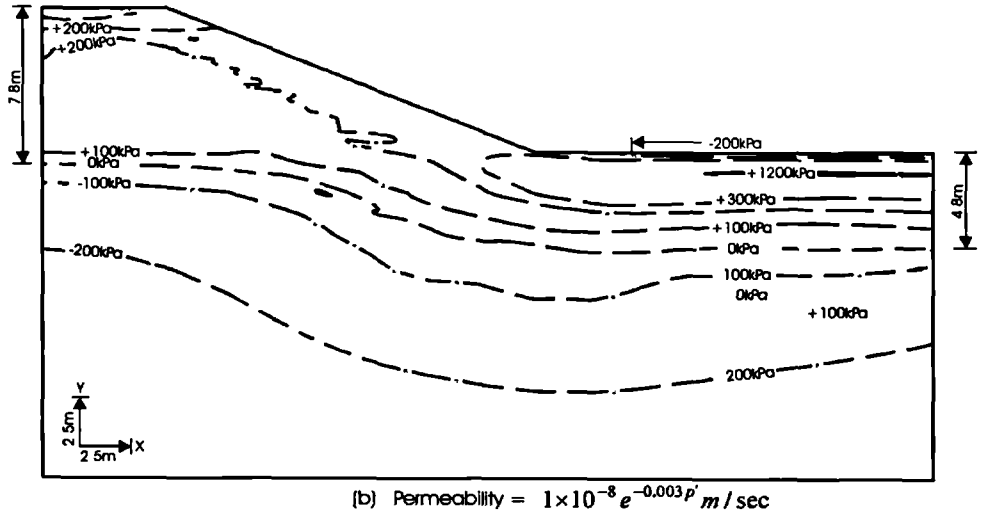

(b) Permeability = $1\times10^{-8}e^{-0.003p'}$ m / sec

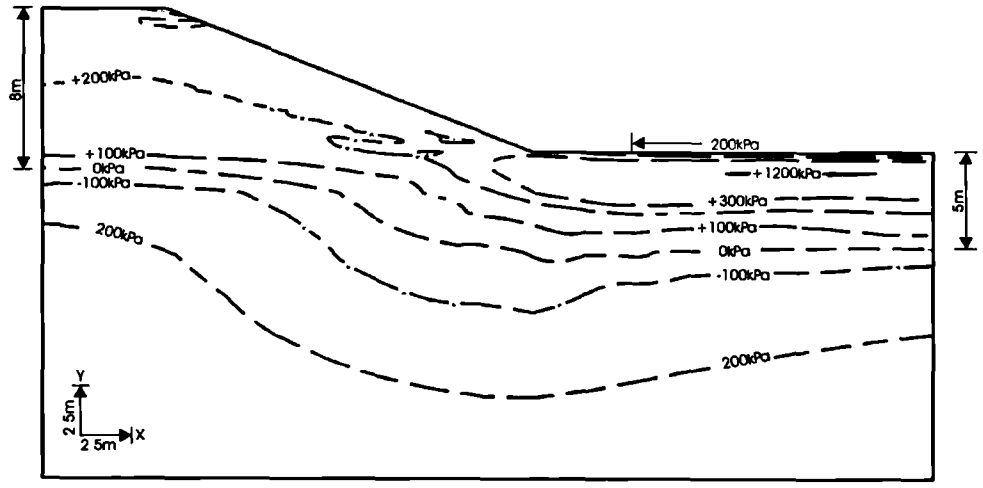

(c) Permeability = $1\times10^{-7}e^{-0.003p'}$ m / sec

Figure 7.35 Contours of accumulated minimum total principal stress, σ_3, predicted by 3 permeabilities at the end of the first summer (Aug yr1).

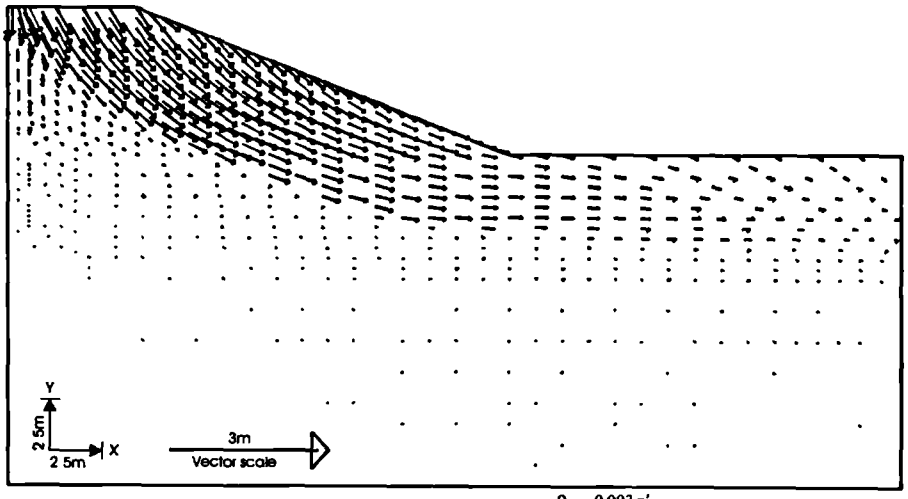

(a) Permeability = $1\times10^{-9}e^{-0.003p'}$ m / sec

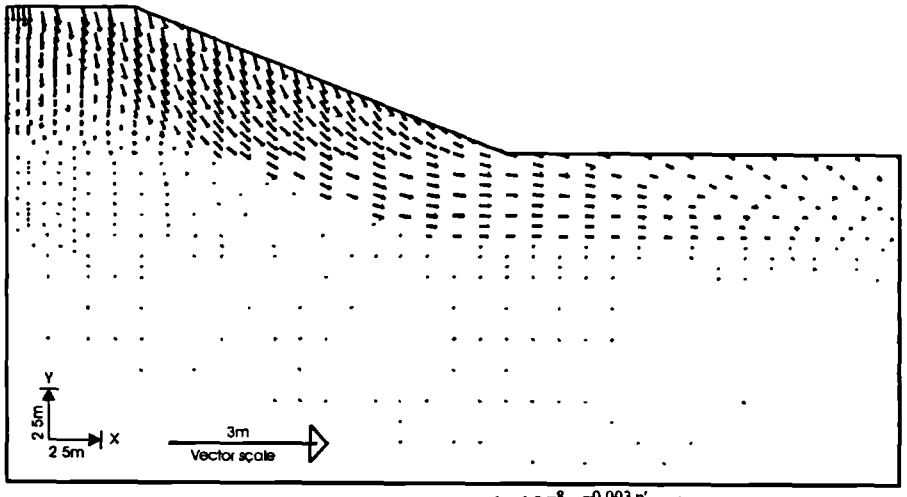

(b) Permeability = $1\times10^{-8}e^{-0.003p'}$ m / sec

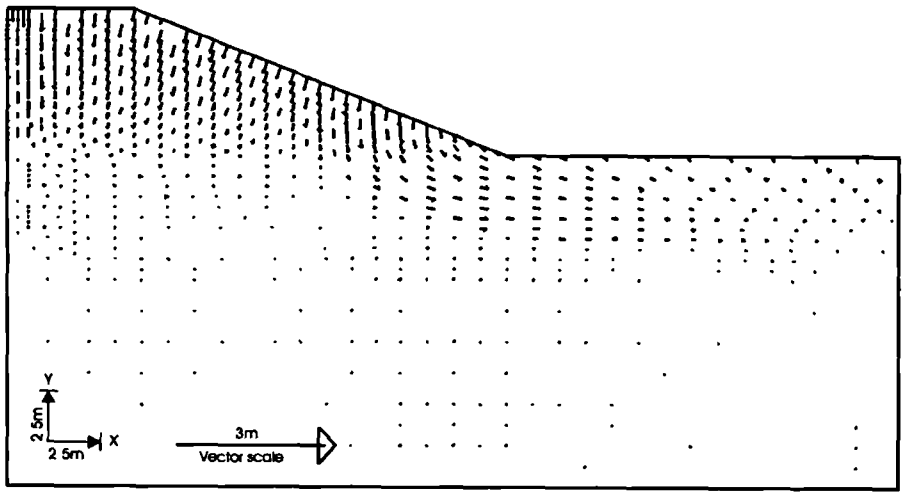

(c) Permeability = $1\times10^{-7}e^{-0.003p'}$ m / sec

Figure 7-36 Vectors of sub-accumulated displacements predicted by 3 permeabilities during the first summer (Mar yr1 - Aug yr1).

Figure 7.34 shows the predictions of pore water pressure changes within the embankment during the first summer (March to August of year 1). It can be seen that the predictions by the permeabilities of $1\times10^{-8}e^{-0.003p'}m/\sec$ and $1\times10^{-7}e^{-0.003p'}m/\sec$ are very similar (maximum suctions in the embankment of 300kPa-500kPa). In contrast, the prediction by a permeability of $1\times10^{-9}e^{-0.003p'}m/\sec$ indicates a wider range of suctions (25-900kPa) within the clay fill. This is attributed to the fact that a low permeability involves low flow rates which results in relatively higher moisture depletion in a asmaller zone, to meet the evapotranspiration demand, compared to more permeable clay fills. It is considered that in this latter situation, the actual evapotranspiration per given time is lower, compared to clay fill permeabilites of $1\times10^{-8}e^{-0.003p'}m/\sec$ and $1\times10^{-7}e^{-0.003p'}m/\sec$. The overall pattern of pore water pressure changes predicted in the foundation indicates an increasing depth of desiccation with permeability.

Figure 7.35 shows the contours of the minimum principal total stress, σ_3 at the end of Aug yr 1 (NB. The crack model is also in operation with a $\frac{k_f}{k_i}$ ratio of 10). The distribution of σ_3 gives an approximate indication of the depth at which tensile total stresses are predicted. Once again, the figure confirms the similarities in predictions between permeabilities of $1\times10^{-8}e^{-0.003p'}m/\sec$ and $1\times10^{-7}e^{-0.003p'}m/\sec$. The predictions show tensile stresses in the whole embankment at the end of the first summer whereas predictions by a permeability of $1\times10^{-9}e^{-0.003p'}m/\sec$ yield a compressive zone beneath the centre of the embankment, albeit small in extent. The figure confirms that stress changes are occurring to a shallower depth in the latter clay fill, compared to the former two more permeable clay fills.

However, it is worth mentioning that the predictions in Figure 7.35 may not be a true reflection of the overall depth to which tensile total stresses can develop, because of the limitations of the constitutive model used in the analyses. This limitation is likely to result in over-prediction of ground movements because the model allows higher mean effective stresses to be mobilised in the desiccated zone, than could be sustained in the field.

The vectors of movements during the first summer (March -August yr 1) are shown in Figure 7.36. The pattern of vectors clearly shows the differences in predictions among the three permeabilities. Figure 7.36a depicts the vectors for the lowest permeability ($1\times10^{-9}e^{-0.003p'}m/\sec$) which indicate significant horizontal movements of the slope. This pattern is consistent with the one identified in previous analyses (Sections 7.3 to 7.6) and is characterised by the development of a deep seated zone of plasticity where σ_3 changes from

positive to negative. This behaviour is muted as the clay fill permeability increases (Figures 7.36b and 7.36c). The pattern in the most permeable clay fill ($1\times10^{-7}e^{-0.003p'}m/\sec$) indicates overall inward movements suggestive of shrinkage, with very little indication of outward horizontal movements in the slope.

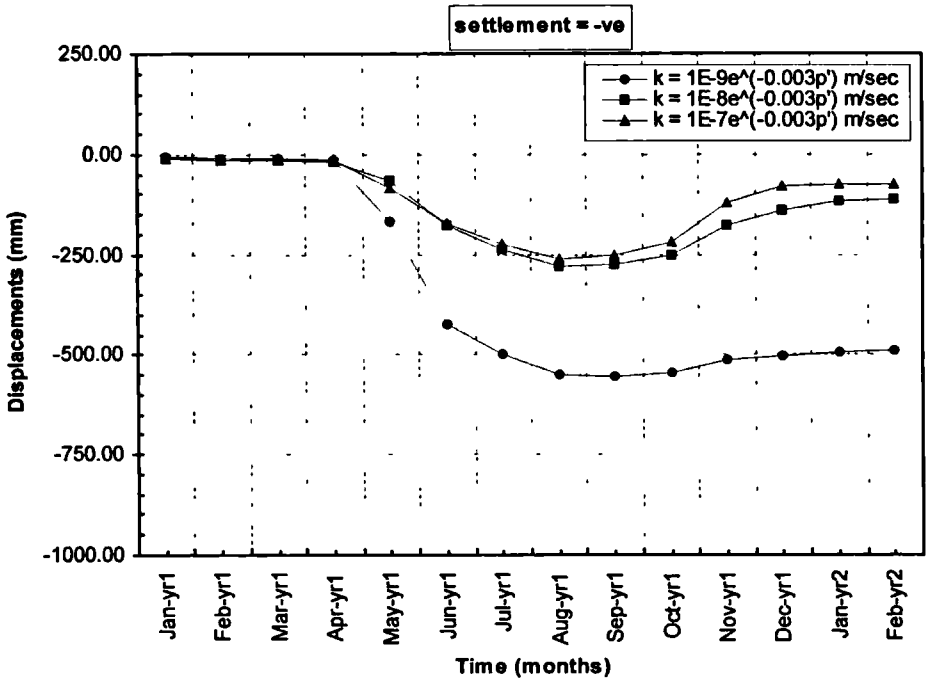

Figure 7.37a Influence of mass permeability of the clay fill on sub-accumulated vertical movements at the crest centreline (Jan yr 1 - Feb yr 2).

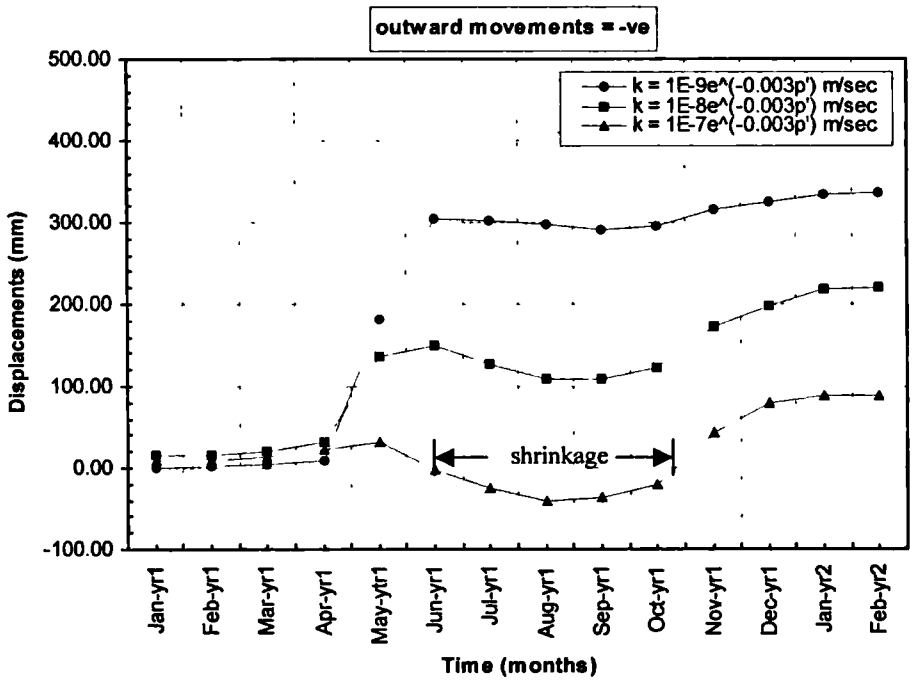

Figure 7.37b Influence of mass permeability of the clay fill on sub-accumulated horizontal movements at GL of mid-slope (Jan yr 1 - Feb yr 2).

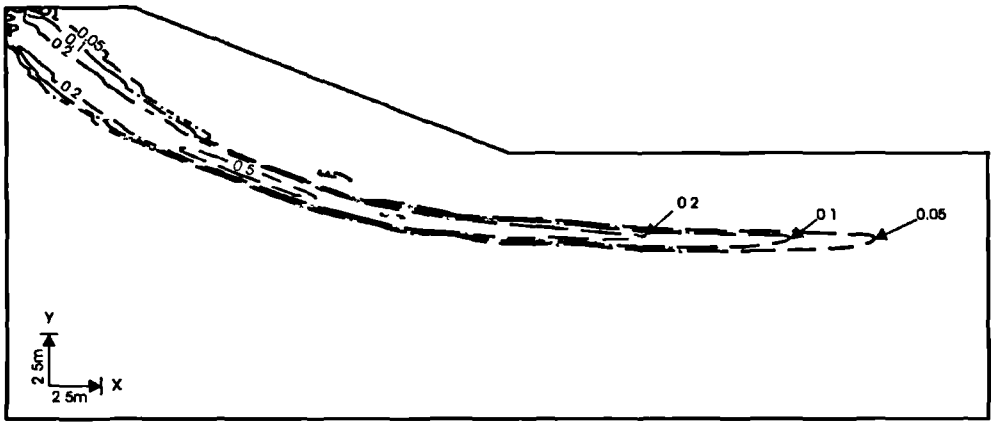

(a) Permeability = $1\times10^{-9}e^{-0.003p'}m/sec$

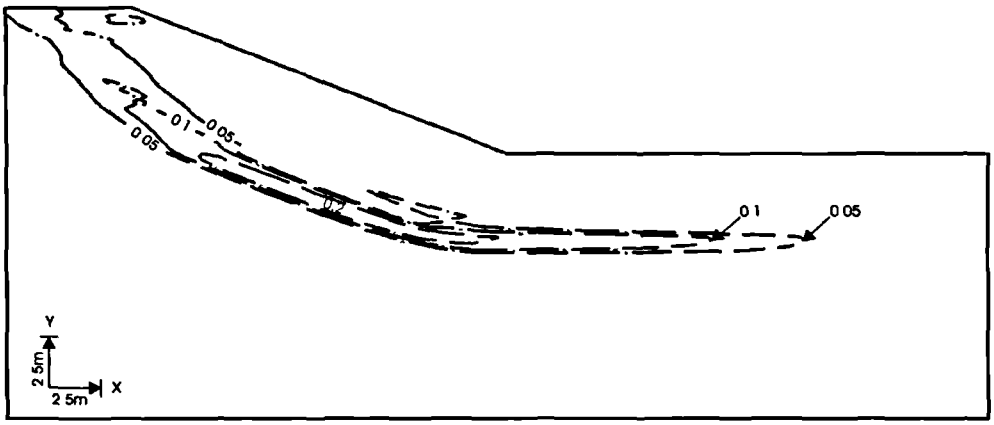

(b) Permeability = $1\times10^{-8}e^{-0.003p'}m/sec$

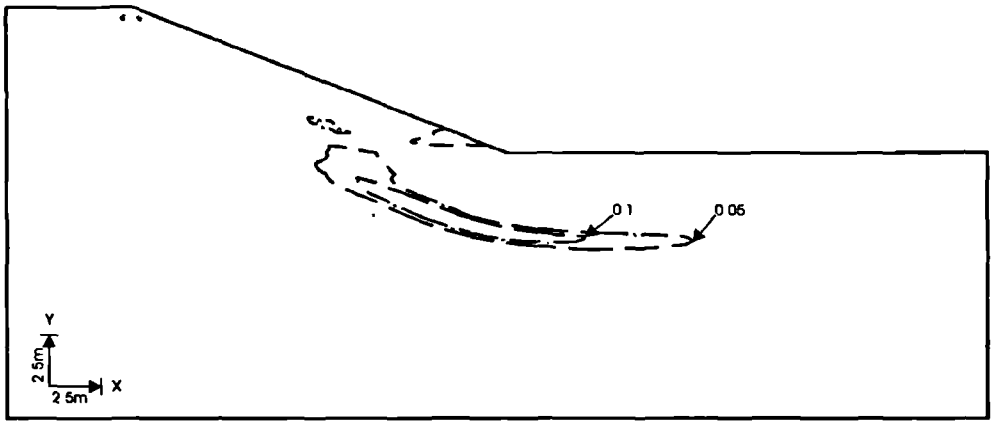

(c) Permeability = $1\times10^{-7}e^{-0.003p'}m/sec$

Figure 7.38 Contours of sub-accumulated deviatoric plastic strains predicted by 3 permeabilitites during the first summer (Mar yr1 - Aug yr1).

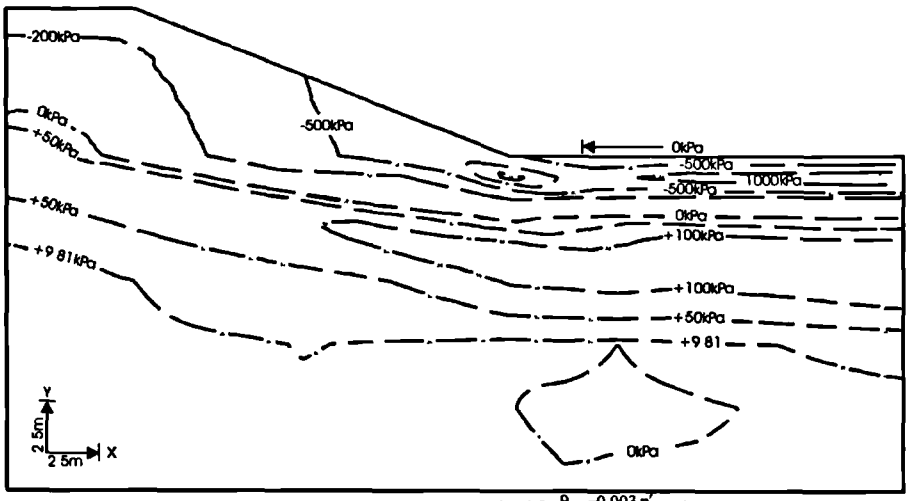

(a) Permeability = $1\times10^{9}e^{-0.003p'}m/\text{sec}$

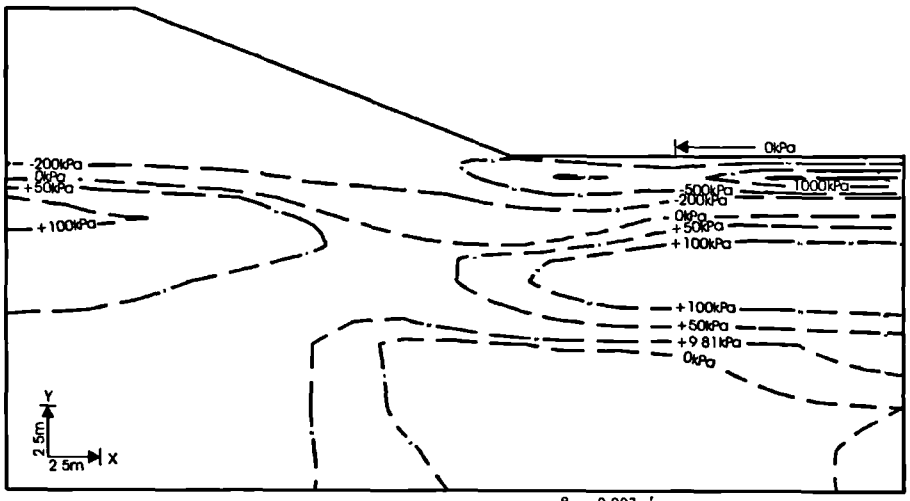

(b) Permeability = $1\times10^{-8}e^{-0.003p'}m/\text{sec}$

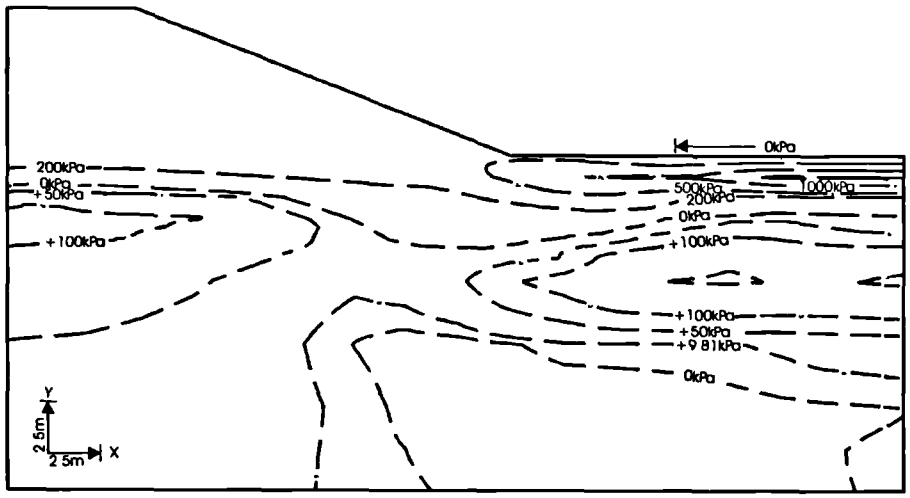

(c) Permeability = $1\times10^{-7}e^{-0.003p'}m/\text{sec}$

Figure 7.39 Contours of sub-accumulated pore water pressure predicted by 3 permeabilities during the first winter (Oct yr1 - Feb yr2).

The pattern of movement identified above is further confirmed in Figure 7.37a where the sub-accumulated vertical movements at crest centreline are plotted and Figure 7.37b which depicts the sub-accumulated horizontal movements at mid-slope (ground level). The crest centreline settles by the same magnitude for permeabilities of $1\times10^{-8}e^{-0.003p'}m/\sec$ and $1\times10^{-7}e^{-0.003p'}m/\sec$ and the overall magnitude of settlement is less compared to predictions by the $1\times10^{-9}e^{-0.003p'}m/\sec$ clay fill. At the end of August yr 1, the vertical movements predicted are 225mm in the two more permeable clay embankments compared to 550mm in the least permeable embankment. The horizontal movements predicted at the end of August yr 1 are 40mm (inward) in the $1\times10^{-7}e^{-0.003p'}m/\sec$ clay fill, 110mm (outward) in the $1\times10^{-8}e^{-0.003p'}m/\sec$ clay fill and 300mm (outward) in the $1\times10^{-9}e^{-0.003p'}m/\sec$ clay fill.

Figure 7.38 shows the contours of sub-accumulated plastic strains during the period March to August yr 1. The clay fill with the least permeability is clearly experiencing larger plasticity as a result of the large stress changes occurring at shallower depth compared to the more permeable clay fills. The deep seated plastic zone does not daylight at the toe but instead runs parallel at approximately 4m depth below the top of the foundation in the section near the embankment. Investigation of this plastic zone revealed accumulated plastic strains at residual strength over a part of the plastic zone.

In comparison, the more permeable clay fills ($1\times10^{-8}e^{-0.003p'}m/\sec$ and $1\times10^{-7}e^{-0.003p'}m/\sec$) allow abstraction of water over a larger zone to meet the specified potential evapotranspiration rate, in a given time. This results in relatively lower stress changes (and corresponding strain changes) per given depth, within the zone of influence of the RWUM. This modelling aspect is considered to be a demonstration of the superiority of the RWUM in reproducing field behaviour over modelling techniques currently used in industry.

7.6.4 Behaviour during winter (yr 1)

Figure 7.39 shows the contours of pore water pressure changes during winter (September yr 1 to February yr 2) for the 3 permeabilities. The pore water pressures within the embankment almost fully recover (cf. Figure 7.34) in the clay fills with permeabilities of $1\times10^{-8}e^{-0.003p'}m/\sec$ and $1\times10^{-7}e^{-0.003p'}m/\sec$. However, within the foundation the redistribution of suctions to lower horizons continues during winter, as previously observed in Sections 7.3 to 7.4. The overall depth of pore water pressure changes within the foundation is shown to be permeability dependent. This is predicted to 11m in the $1\times10^{-9}e^{-0.003p'}m/\sec$ permeability clay fill and drastically increases to in excess of 16m in the more permeable clay

fills ($1\times10^{-8}e^{-0.003p'}m/\sec$ and $1\times10^{-7}e^{-0.003p'}m/\sec$). As previously discussed, the depth of pore water pressure change in the foundation is considered to be excessive.

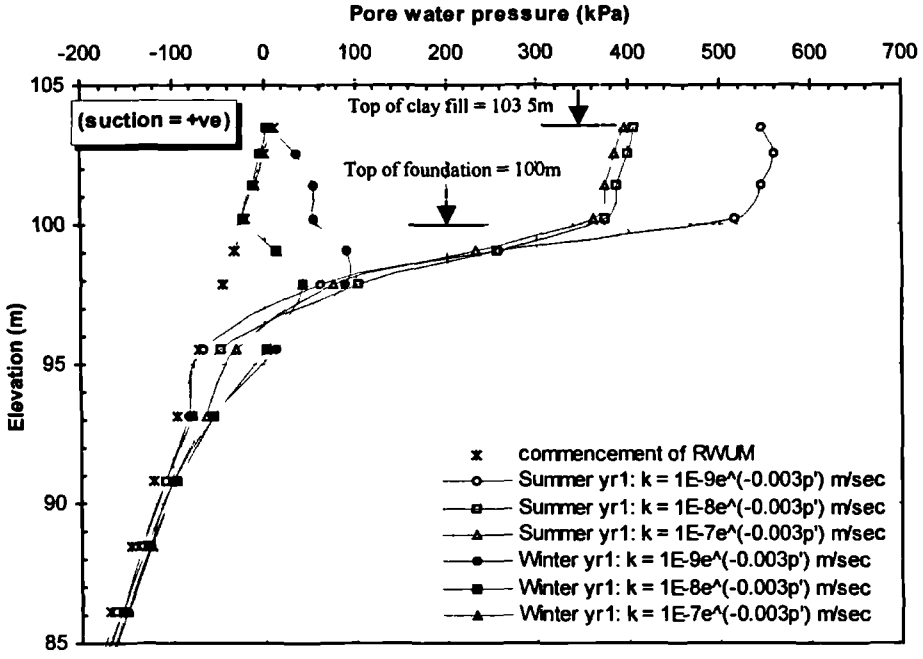

Figure 7.40 Influence of mass permeability of the clay fill on accumulated pore water pressure at mid-slope after 1yr.

In Figure 7.40, the predictions of accumulated pore water pressure at the end of the first winter for clay fill permeabilities of $1\times10^{-8}e^{-0.003p'}m/\sec$ and $1\times10^{-7}e^{-0.003p'}m/\sec$ are approximately of the same order at this location. The figure shows that pore water pressures in the clay fill recover to their initial values at the end of the first winter. However, the predictions for the permeability of $1\times10^{-9}e^{-0.003p'}m/\sec$ reveal that at the end of winter, there still exist suctions of up to 60kPa within the clay fill. The pattern during summer confirms the earlier observation that higher suctions are being predicted in the clay fill with a permeability of $1\times10^{-9}e^{-0.003p'}m/\sec$. For all the 3 permeabilities, desiccation is predicted in the foundation during both summer and winter.

The pore water pressure pattern revealed in Figure 7.40 is corroborated by Figure 7.41 which shows the contours of accumulated pore water pressures in the embankment and the foundation at the end of the first winter. It can be seen that in the two more permeable clay fills (Figures 7.41b and c), the pore water pressure in the lower third of the embankment is 0kPa, with suctions of up to 25kPa in the upper horizon. In the $1\times10^{-9}e^{-0.003p'}m/\sec$ clay fill, a large zone of material with a suction of 50kPa exists at the centre of the embankment.

The plasticity (absolute values) that occurs during the first winter (August yr 1 to February yr 2) as the pore water pressures recover and the embankment swells are shown in Figure 7.42. The contours do not include the plasticity prior to the application of the RWUM. The figure shows that the least plasticity occurs in the embankment with the lowest permeability (Figure 7.42a). Maximum plastic strains of 0.05 (5%) are predicted at the toe of the embankment over a zone 3.8m long. The corresponding predictions for permeabilities of $1\times10^{-8}e^{-0.003p'}m/\sec$ (Figure 7.42b) and $1\times10^{-7}e^{-0.003p'}m/\sec$ (Figure 7.42c) are 5.8m and 7m. The degree of plasticity during winter increases as permeability increases, in line with the larger pore water pressure recovery associated with the higher permeability.

The vertical movements which occur during the first winter at the crest centreline are shown in Figure 7.37a. Maximum vertical movements of 50mm, 170mm, and 185mm are predicted by clay fill permeabilities of $1\times10^{-9}e^{-0.003p'}m/\sec$, $1\times10^{-8}e^{-0.003p'}m/\sec$ and $1\times10^{-7}e^{-0.003p'}m/\sec$, respectively. This once more portrays the dependency of movement on permeability, during winter. The pattern is also mirrored in the magnitude of horizontal movements that occur at mid-slope (Figure 7.37b). In the latter figure, the predicted horizontal movements are 40mm, 110mm and 130mm for permeabilities of $1\times10^{-9}e^{-0.003p'}m/\sec$, $1\times10^{-8}e^{-0.003p'}m/\sec$ and $1\times10^{-7}e^{-0.003p'}m/\sec$, respectively.

7.6.5 Behaviour during the first 5 yrs of cycling

The RWUM was applied for a further 4 years to establish the trends in predictions by the three permeabilities.

Figure 7.43 shows the accumulated pore water pressures at the end of the fifth winter (February yr 6). Although there has been an increase in tensile pore water pressures in the foundation for all three permeabilities, it is encouraging to note that the overall pore water pressure distribution in the embankment has not changed in the more permeable clay fills ($1\times10^{-8}e^{-0.003p'}m/\sec$ and $1\times10^{-7}e^{-0.003p'}m/\sec$). This is evidenced by the size of the zone with zero pore water pressure (0kPa contour). In fact, the size of this zone is larger than that which existed at the end of the first winter (Figure 7.41). The maximum suctions for these two cases are still 25kPa at shallow depth. In general, the predictions are primarily governed by the magnitude of the input monthly MORECS data, and by the current pore water pressures in the ground.

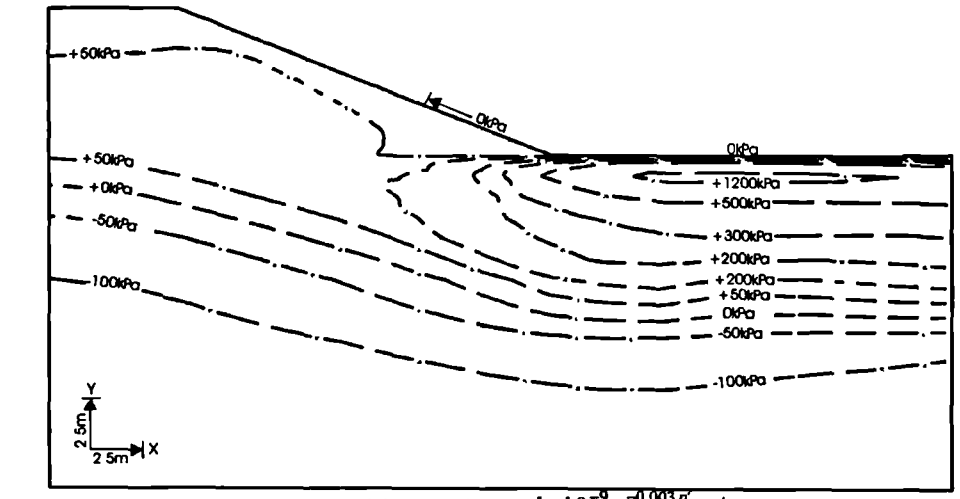

(a) Permeability = $1\times10^{-9}e^{-0.003p'}$ m / sec

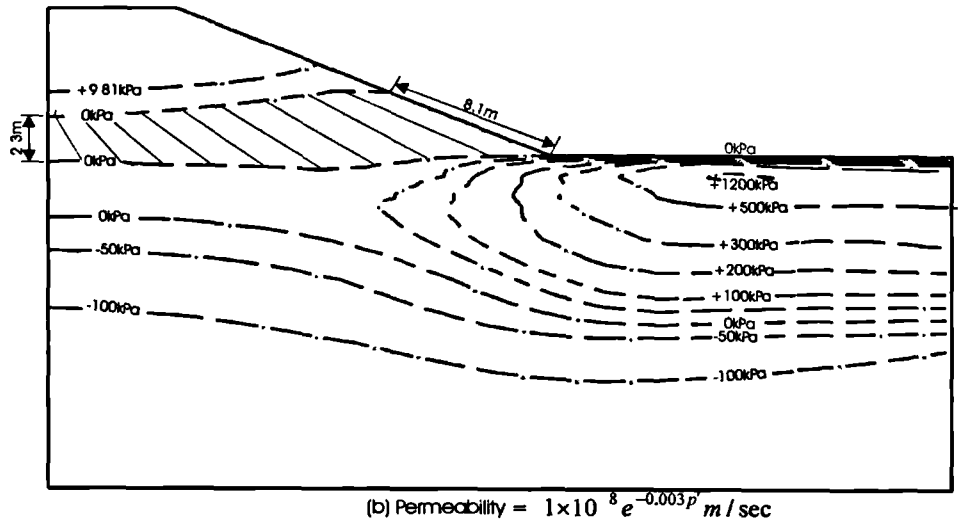

(b) Permeability = $1\times10^{8}e^{-0.003p'}$ m / sec

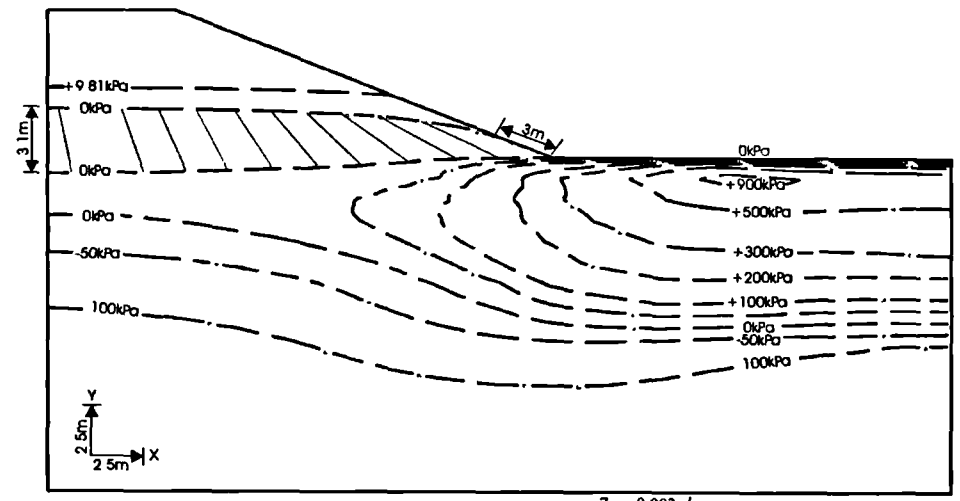

(c) Permeability = $1\times10^{-7}e^{-0.003p'}$ m / sec

Figure 7.41 Contours of accumulated pore water pressure predicted by 3 permeabilities at the end of the first winter(Feb yr2).

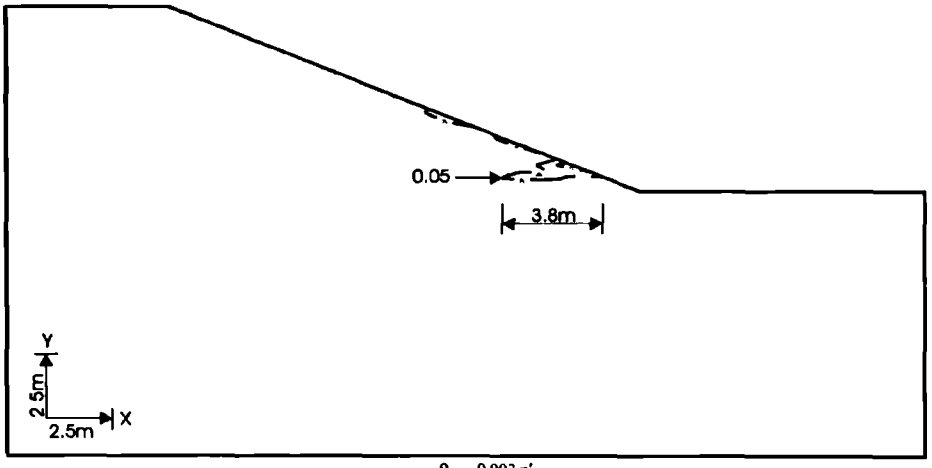

(a) Permeability = $1\times10^{-9}e^{-0.003p'}$ m / sec

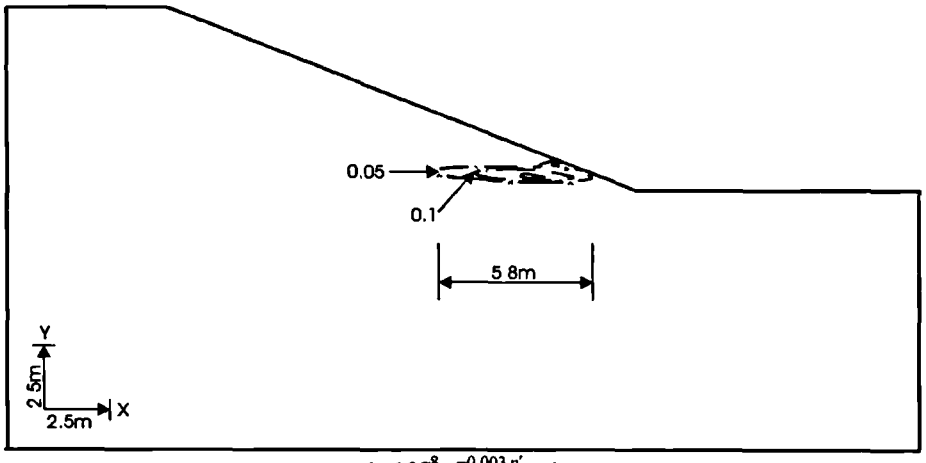

(b) Permeability = $1\times10^{-8}e^{-0.003p'}$ m / sec

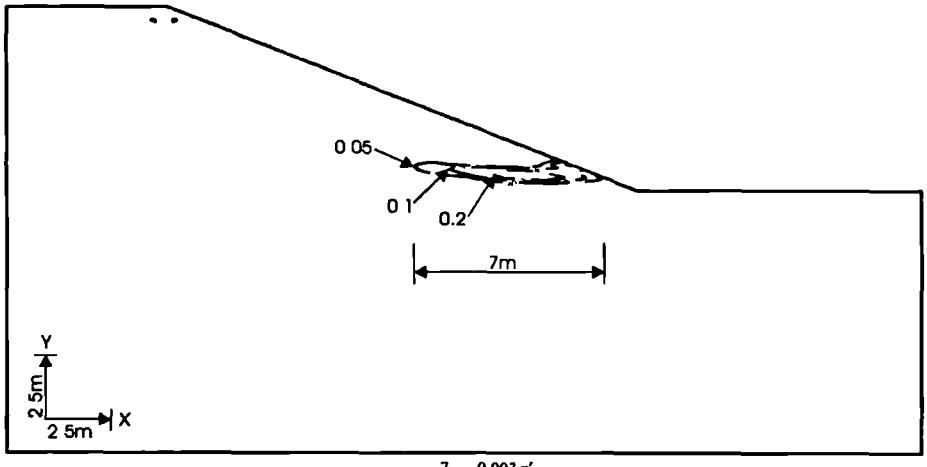

(c) Permeability = $1\times10^{-7}e^{-0.003p'}$ m / sec

Figure 7.42 Contours of sub-accumulated deviatoric plastic strains predicted by 3 permeabilities (Oct yr1 - Feb yr2).

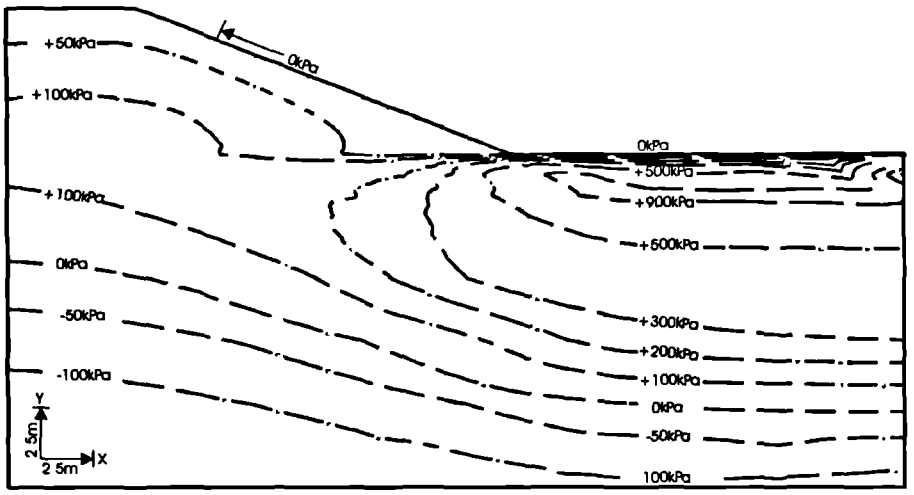

(a) Permeability = $1\times10^{-9}e^{-0.003p'}\,m/\text{sec}$

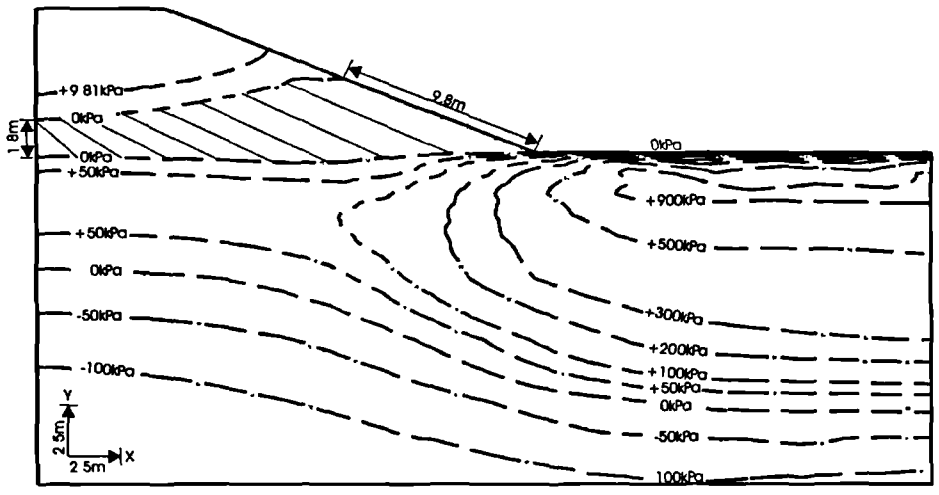

(b) Permeability = $1\times10^{-8}e^{-0.003p'}\,m/\text{sec}$

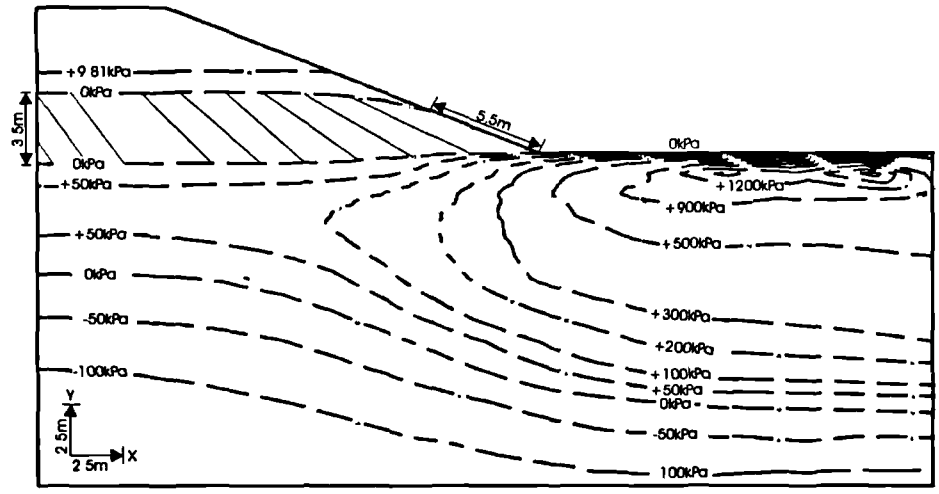

(c) Permeability = $1\times10^{-7}e^{-0.003p'}\,m/\text{sec}$

Figure 7.43 Contours of accumulated pore water pressure predicted by 3 permeabilities at the end of the 5 winter (Feb yr6).

The behaviour in the clayfill with a permeability of $1\times10^{-9}e^{-0.003p'}m/\sec$ is different to the other two. The predictions show a significant increase in the magnitude of maximum suctions in the embankment (100kPa at the end of the 5th winter as opposed to 50kPa at the end of the first winter). The longterm predictions for the embankment would therefore be likely to be unrealistic. Similar behaviour is occurring in the foundation. The pore water pressure predictions in the clay fills with permeabilities of $1\times10^{-8}e^{-0.003p'}m/\sec$ and $1\times10^{-7}e^{-0.003p'}m/\sec$ are not being significantly affected by the limitations of the RWUM to more accurately predict the recharge of pore water pressures. The mass permeability for the latter cases is believed to be high enough for pore water pressure changes to satisfy the evapotranspiration demand, with a $\frac{k_f}{k_j}$ ratio of 10.

Figure 7.44 shows the pore water pressure distribution along a vertical profile at mid-slope after 3 and 5 years. The figure shows end of summer and end of winter values. Again, the figure highlights the difference in pore water pressure response predicted for the embankment and foundation, similar to what was observed in yr 1 (Figure 7.39) ie. higher suctions predicted for the permeability of $1\times10^{-9}e^{-0.003p'}m/\sec$ compared to permeabilities of $1\times10^{-8}e^{-0.003p'}m/\sec$ and $1\times10^{-7}e^{-0.003p'}m/\sec$. It is also encouraging to note that the response in the end of winter values of pore water pressure matches the meteorological data (Figure 5.13) ie. yr 3 is "drier" than yr 5. This ability to simulate the effects of varying annual meteorological is another powerful facet of the RWUM, unlike current methods which involve application of the same pore water pressure boundary condition for each season, year on year.

Figure 7.45 depicts the plasticity that occurs during the 4 year period March yr 2 to February yr 6. As expected, the figure reinforces the previous observation that the degree of plasticity increases as permeability increases. The length of the plastic zone that develops during this period is 5.8m, 8.8m and 9.5m for clay fill permeabilities of $1\times10^{-9}e^{-0.003p'}m/\sec$, $1\times10^{-8}e^{-0.003p'}m/\sec$ and $1\times10^{-7}e^{-0.003p'}m/\sec$, respectively. In the latter two predictions the maximum plastic strains induced are 0.5 (50%) compared to a maximum of 0.2 (20%) in the clay fill with a permeability of $1\times10^{-9}e^{-0.003p'}m/\sec$. It is also considered that although the largest seasonal pore water pressure changes occur in the analysis with a permeability of $1\times10^{-9}e^{-0.003p'}m/\sec$, the associated end of winter suctions are on average higher and result in a stiffer clayfill (see Figure 7.40 & Figure 7.44c). The high stiffness in turn diminishes the magnitude of strains arising from the seasonal pore water pressure changes.

The trend identified in Figure 7.45 is corroborated by the vectors of movement for this period shown in Figure 7.46. The latter figure clearly shows the significant horizontal movements that have occurred in the clay fill with permeabilities of $1\times10^{-8}e^{-0.003p'}m/\sec$ and $1\times10^{-7}e^{-0.003p'}m/\sec$; with larger movements being predicted in the latter. In comparison, movement in the clay fill with a permeability of $1\times10^{-9}e^{-0.003p'}m/\sec$ is overall downward with very little horizontal movement in the slope of the embankment.

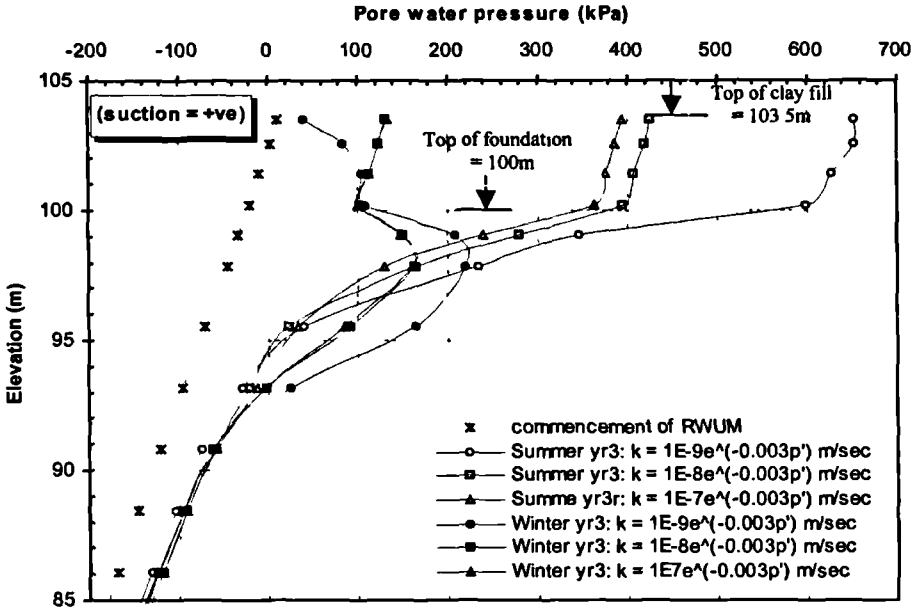

Figure 7.44a Influence of mass permeability of the clay fill on accumulated pore water pressure at mid-slope after 3yrs.

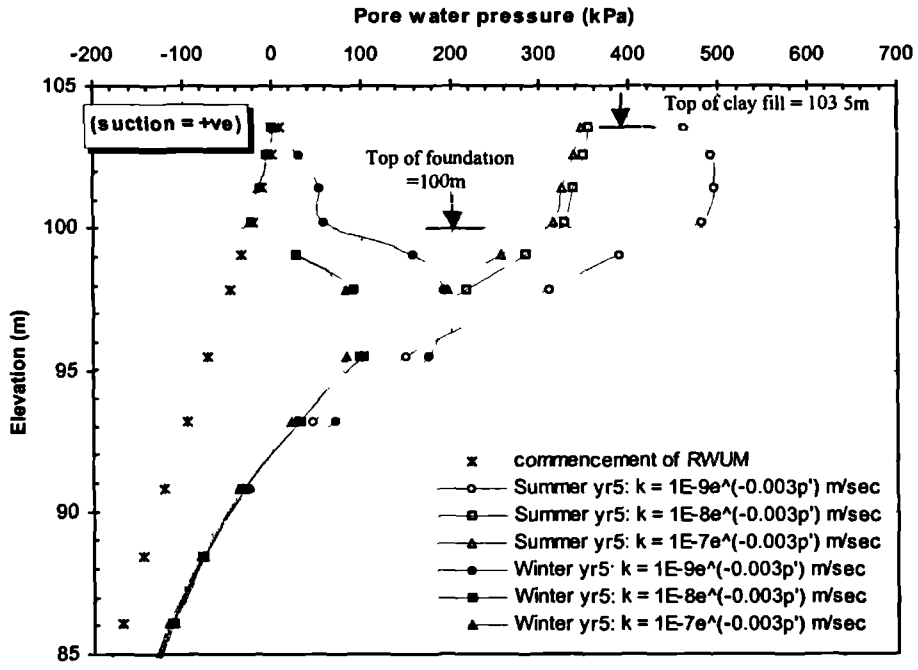

Figure 7.44b Influence of mass permeability of the clay fill on accumulated pore water pressure at mid-slope after 5yrs.

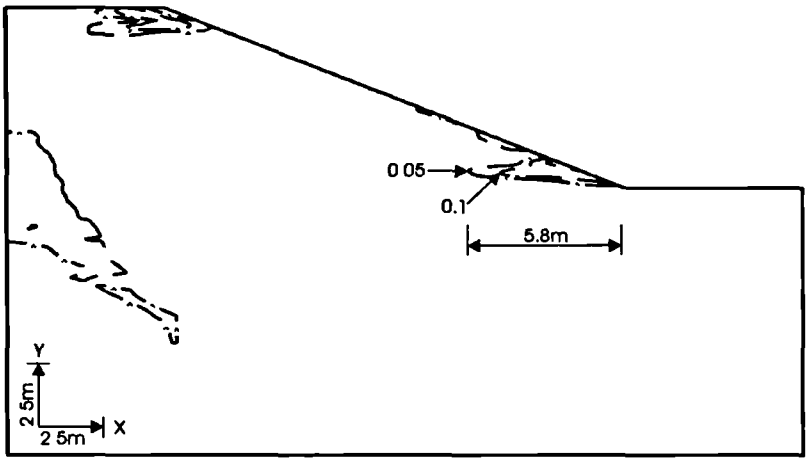

(a) Permeability = $1\times10^{-9}e^{-0.003p'}m/sec$

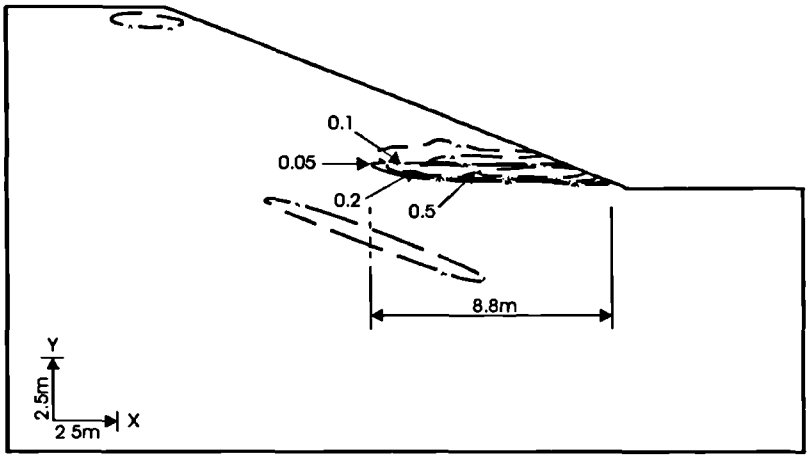

(b) Permeability = $1\times10^{-8}e^{-0.003p'}m/sec$

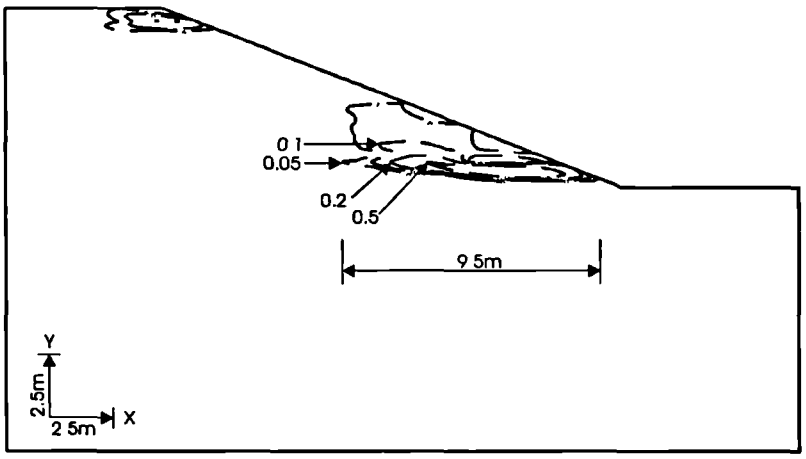

(c) Permeability = $1\times10^{-7}e^{-0.003p'}m/sec$

Figure 7.45 Contours of sub-accumulated deviatoric plastic strains predicted by 3 permeabilities (Feb yr2 - Feb yr6).

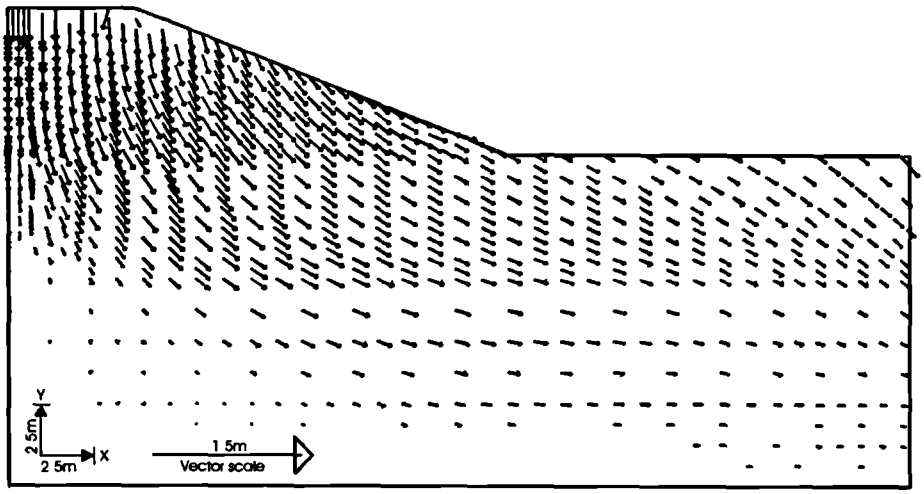

(a) Permeability = $1\times10^{-9}e^{-0.003p'}$ m / sec

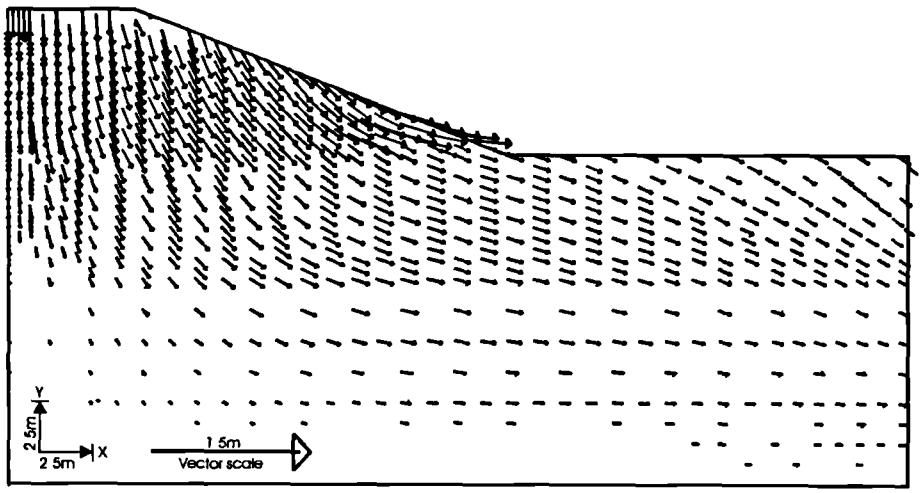

(b) Permeability = $1\times10^{-8}e^{-0.003p'}$ m / sec

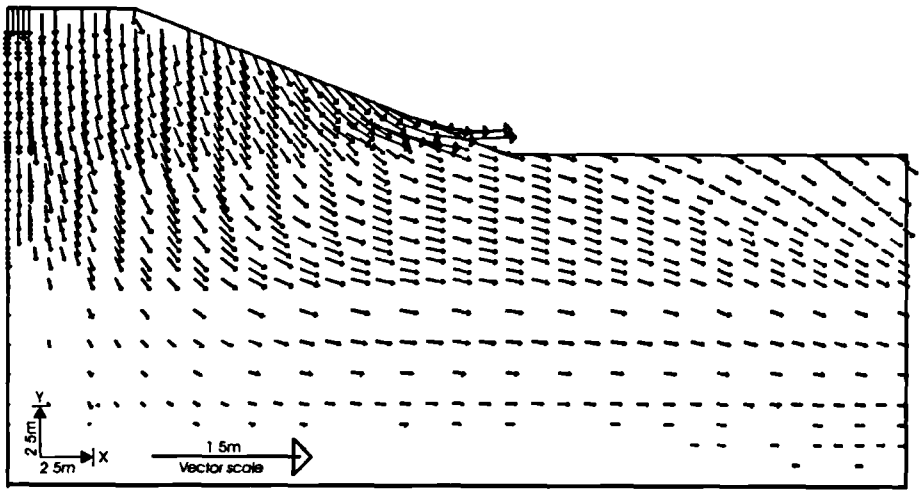

(c) Permeability = $1\times10^{-7}e^{-0.003p'}$ m / sec

Figure 7.46 Vectors of sub-accumulated displacements predicted by 3 permeabilities during the period Feb yr2 - Feb yr6.

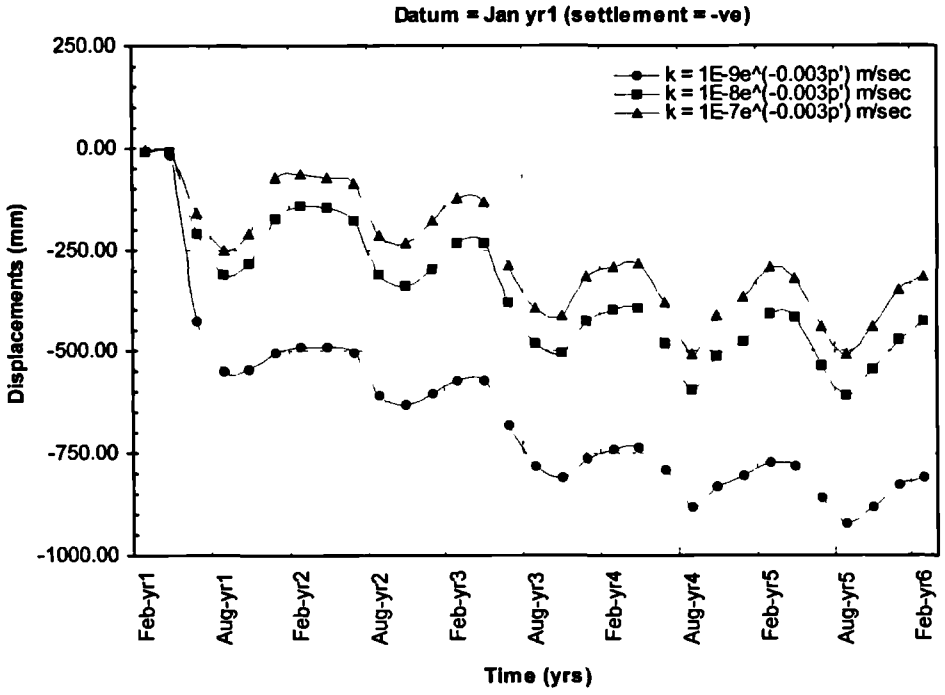

Figure 7.47a Influence of mass permeability of the clay fill on sub-accumulated vertical movements at the crest centreline (Janyr1-Febyr6):- *datum = Jan yr1*.

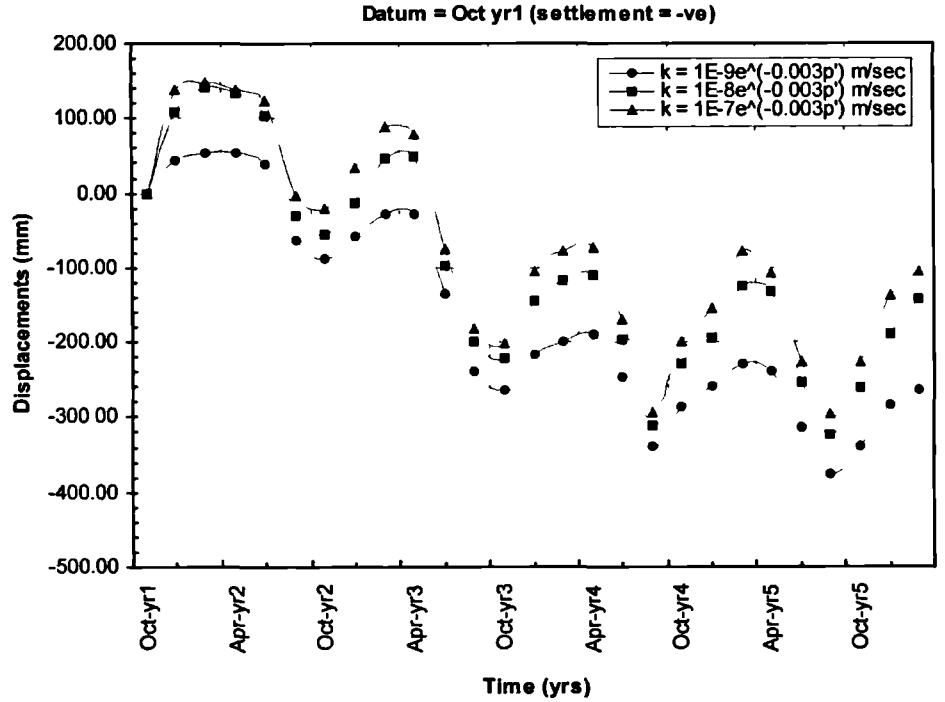

Figure 7.47b Influence of mass permeability of the clay fill on sub-accumulated vertical movements at the crest centreline (Janyr1-Febyr6):- *datum = Oct yr1*.

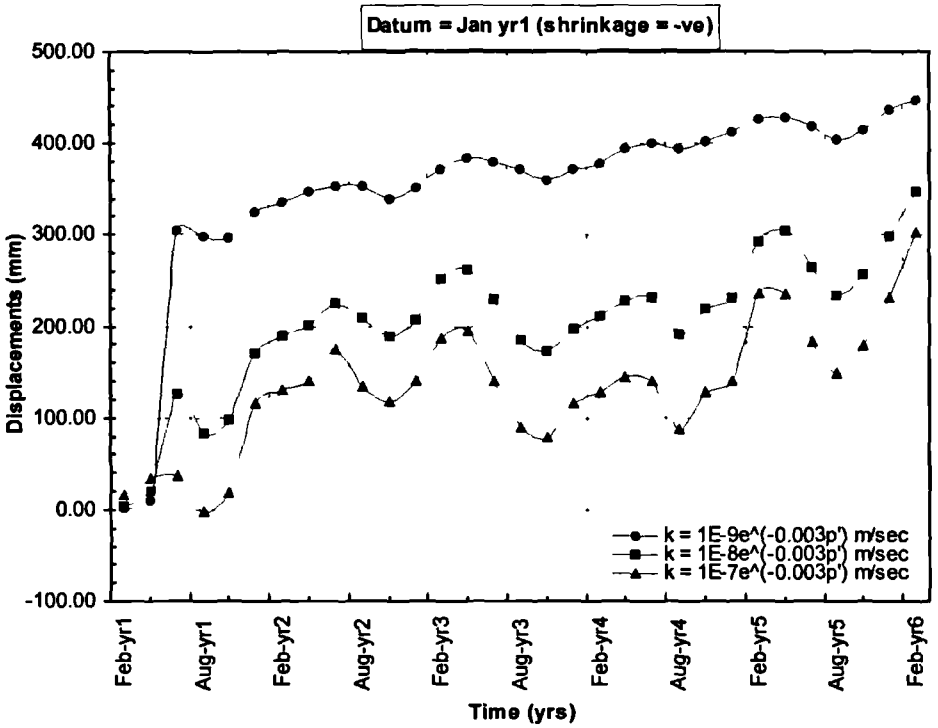

Figure 7.48a Influence of mass permeability of the clay fill on sub-accumulated horizontal movements at GL of mid-slope (Jan yr1-Feb yr6):- *datum = Jan yr1.*

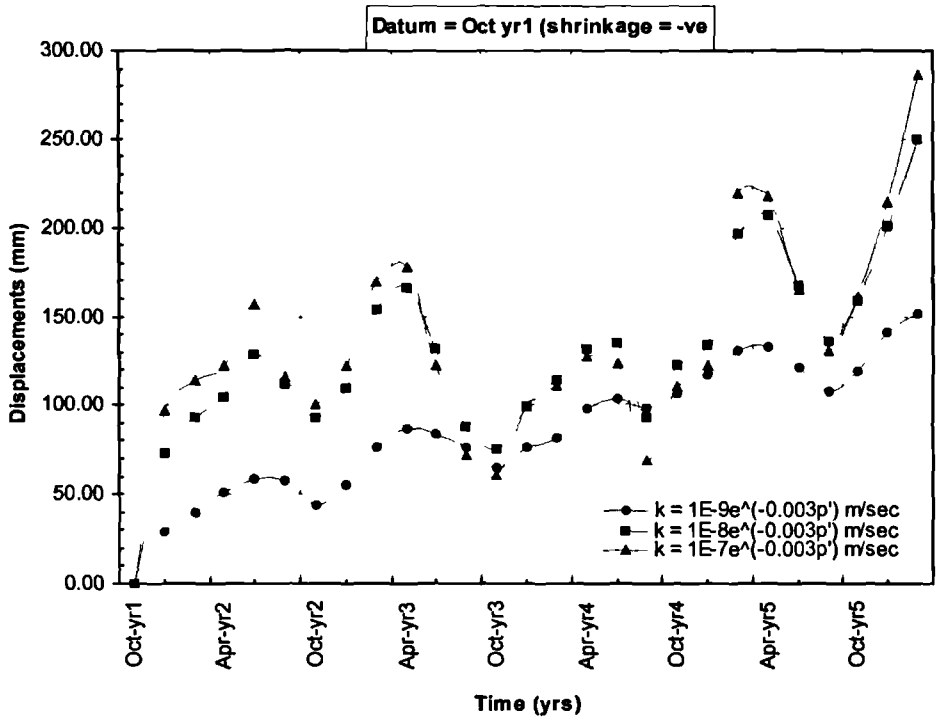

Figure 7.48b Influence of mass permeability of the clay fill on sub-accumulated horizontal movements at GL of mid-slope (Jan yr1-Feb yr6):- *datum = Oct yr1.*

Figure 7.47 shows the vertical movements at the crest centreline during the 5 year application of the RWUM. In Figure 7.47a the datum has been assumed to be January yr 1 to coincide with the inception of the RWUM whilst in Figure 7.47b, the datum has been taken to be Oct yr 1, in order to eliminate the effects of large pore water pressure changes associated with the initial application of the RWUM. Both figures portray a similarity in the pattern of vertical movements predicted by permeabilities of $1\times10^{-8}e^{-0.003p'}m/\sec$ and $1\times10^{-7}e^{-0.003p'}m/\sec$. The vertical movements predicted in the first year (Figure 7.47a) are only 50% of the magnitude predicted using a permeability of $1\times10^{-9}e^{-0.003p'}m/\sec$.

A similar pattern is shown in the horizontal movements (Figure 7.48) where the sub-accumulated horizontal movements at mid-slope (ground level) are plotted. Although lateral outward movement occurs in the clay fill of intermediate permeability ($1\times10^{-8}e^{-0.003p'}m/\sec$), the magnitude of movements during the first year is only 50% of that predicted using a permeability of $1\times10^{-9}e^{-0.003p'}m/\sec$.

A closer examination of the seasonal movements (Figures 7.47b and 7.48b) reveals their strong dependency on the magnitude of permeability. It can be seen that overall, the trend suggests increasing seasonal movements as permeability increases. The seasonal horizontal movements shown in Figure 7.48b are summarised in Table 7.6. The values have been derived by considering the maximum swelling and shrinkage during each annual cycle, with no reference to specific months/time scales. Such an approach enables direct comparisons among the three permeabilities to be made.

The pattern of movements shown in Table 7.6 further affirms that the magnitude of seasonal movements increases as permeability increases.

Table 7.6 Predicted seasonal horizontal movements (mm)

Year	Winter			Summer		
	$1\times10^{-9}e^{-0.003p'}m/\sec$	$1\times10^{-8}e^{-0.003p'}m/\sec$	$1\times10^{-7}e^{-0.003p'}m/\sec$	$1\times10^{-9}e^{-0.003p'}m/\sec$	$1\times10^{-8}e^{-0.003p'}m/\sec$	$1\times10^{-7}e^{-0.003p'}m/\sec$
1	60	140	150	-	-	-
2	40	80	75	-15	-30	-55
3	40	100	70	-20	-90	-120
4	35	125	150	-5	-45	-60
5	40	120	155	-25	-75	-95
-ve = shrinkage, +ve = swelling						

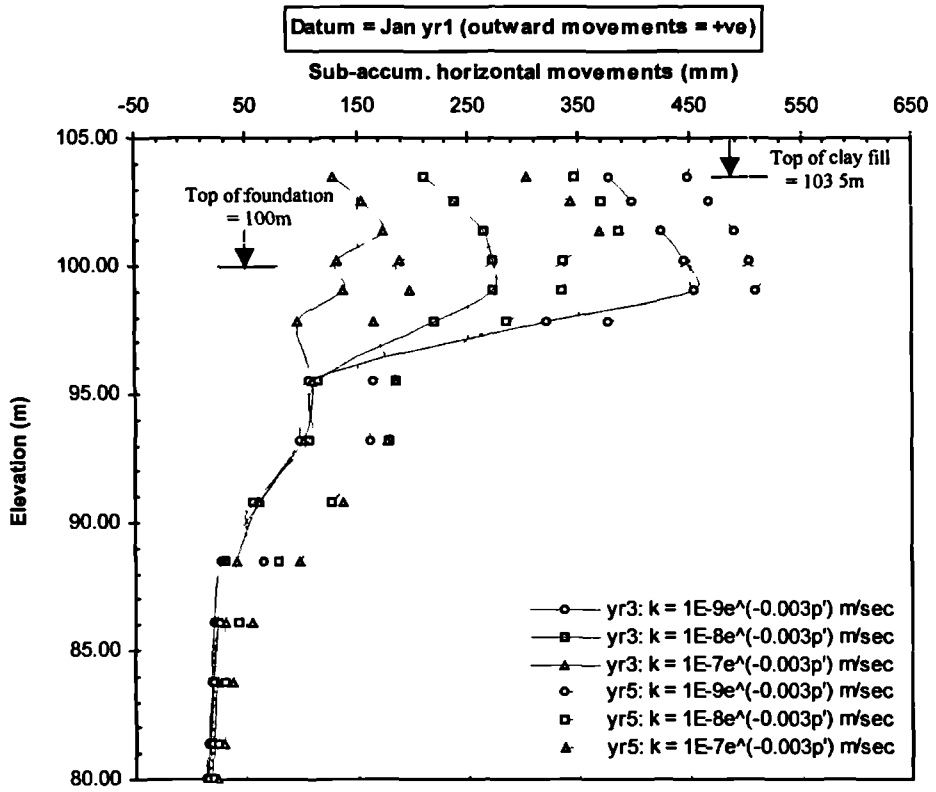

Figure 7.49a Influence of mass permeability of the clay fill on sub-accumulated horizontal movements along a vertical profile at mid-slope:- *datum Jan yr1*.

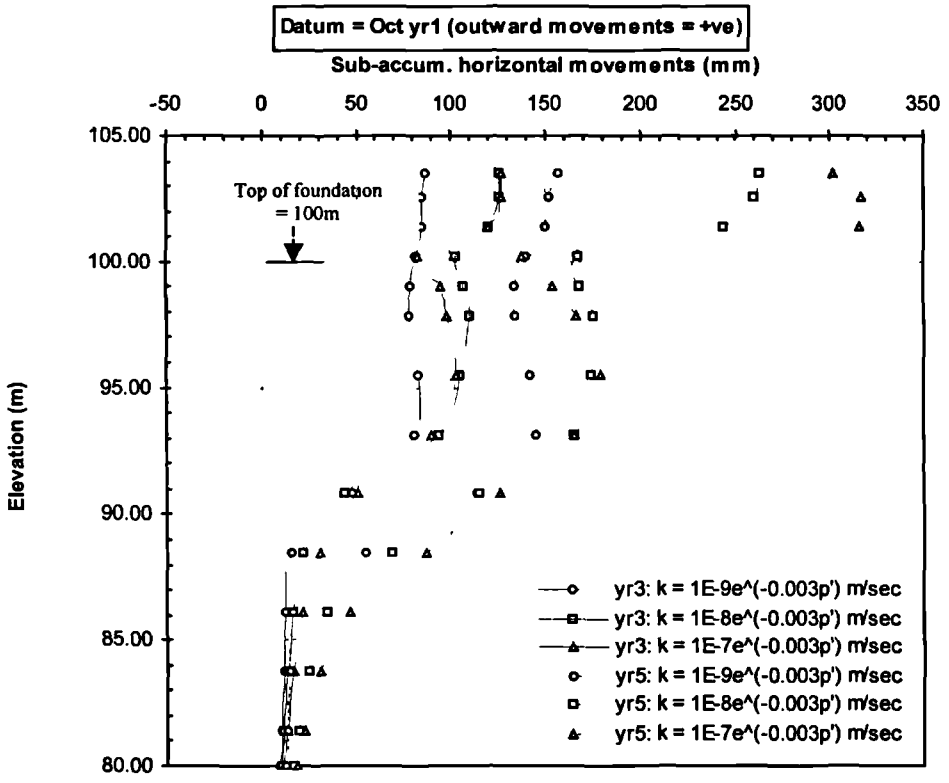

Figure 7.49b Influence of mass permeability of the clay fill on sub-accumulated horizontal movements along a vertical profile at mid-slope:- *datum Oct yr1*.

Figure 7.49 shows the sub-accumulated horizontal movements along a vertical profile at the mid-slope of the embankment. Once more, the plots have been presented for two datums (Jan yr 1 and Oct yr 1) for reasons previously mentioned. The latter plot (Figure 7.49b) further confirms that the most permeability embankment is experiencing the largest horizontal movements with time and would thus be expected to fail first, in the long term. The maximum movements (sub-accumulated from Oct yr 1) are 160mm, 265mm and 320mm for permeabilities of $1\times10^{-9}e^{-0.003p'}m/\sec$, $1\times10^{-8}e^{-0.003p'}m/\sec$ and $1\times10^{-7}e^{-0.003p'}m/\sec$, respectively. The figure also reveals that although some horizontal movements are predicted in the upper horizons of the foundation, there is a marked difference in the magnitude of the movements in the two more permeable clay fills at the clay fill/foundation interface. This is corroborated by Figures 7.46 and 7.50 which depicts the vectors of sub-accumulated movements and contours of sub-accumulated plastic deviatoric strains, respectively, during the period October yr 1 to February yr 6.

It can also be seen from Figure 7.50 that no further plasticity develops in the deep seated plastic zone that formed at the beginning of the first summer. This indicates that the behaviour of the embankment from the first summer onward is driven by the potential rupture surface that is developing in the slope of the embankment. The extent of the plastic zone increases with permeability, as shown in the figure.

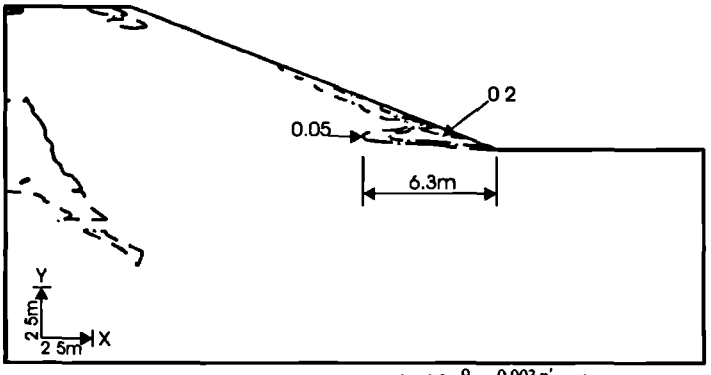

(a) Permeability = $1\times10^{-9}e^{-0.003p'}m/\sec$

Figure 7.50a Contours of sub-accumulated deviatoric plastic strains predicted by 3 permeabilities (Sep yr1 - Feb yr6).

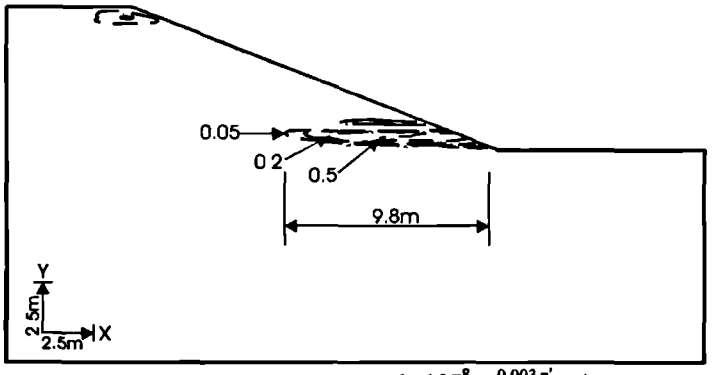

(b) Permeability = $1\times10^{-8}e^{-0.003p'}m/\sec$

Figure 7.50b Contours of sub-accumulated deviatoric plastic strains predicted by 3 permeabilities (Sep yr1 - Feb yr6).

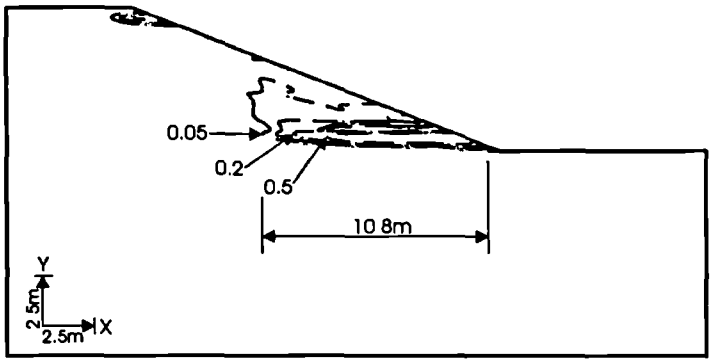

(c) Permeability = $1\times10^{-7}e^{-0.003p'}m/sec$

Figure 7.50c Contours of sub-accumulated deviatoric plastic strains predicted by 3 permeabilities (Sep yr1 - Feb yr6).

7.7 Predictions assuming gradual root growth

All the studies presented above have showed the development of a deep seated plastic/shear zone during the early part of the first summer. The location of this zone appears to coincide with the depth at which σ_3 changes from positive to negative.

The development of this deep seated zone of plasticity is believed to be a true representation of field behaviour but the rate at which it develops and its ultimate extent is thought to be dependent on the magnitude of the potential evapotranspiration and magnitude of the maximum root depth, r_{max}. In the analyses presented above, each month was modelled using 12 increments and a single value of r_{max} was used. It was therefore surmised that the large stress changes arising from evapotranspiration at the onset of the first summer could be eliminated if gradual root development coupled with incremental application of evapotranspiration rates were modelled. Such an approach is a closer approximation to actual field behaviour but involves extra computing time.

A number of analyses were executed in which the magnitudes of r_{max} and potential evapotranspiration rates were applied incrementally to mimic vegetation growth. The numerical modelling procedure prior to application of the WRUM was as described in Section 7.2 ie. a 5 yr swelling/consolidation period was allowed for after embankment construction, prior to the application of the WRUM. A permeability of $1\times10^{-9}e^{-0.003p'}m/sec$ was used. The analyses revealed that the extent and degree of plasticity of the deep seated zone reduced as the number of sub-steps to model r_{max} and potential evapotranspiration increased. In addition, it's formation was delayed. In the analyses presented below, the magnitudes of r_{max} and potential evapotranspiration (PE) computed by MORECS given in Table 7.7 were applied during the first year.

Table 7.7 Predicted seasonal movements during the first 12 months (mm)

Month	J	F	M	A	M	J	J	A	S	O	N	D
% of PE	8.3	16.7	25	33.3	41.7	50	58.3	66.7	75	83.3	91.7	100
r_{max} (m)	0.04	0.08	0.13	0.17	0.21	0.25	0.29	0.33	0.38	0.42	0.46	0.50

At the end of the first year, the full magnitude of PE (from MORECS) was applied and r_{max} was increased incrementally as follows: 1m during yr 2, 1.5 during yr 3, 2m during yr 4 and 2.5 during yr 5 and thereafter.

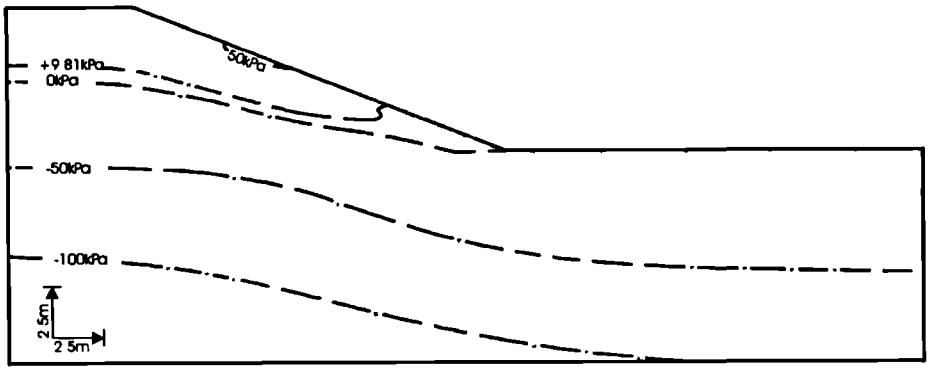

Figure 7.51a Contours of accumulated pore water pressure (Oct yr1) assuming gradual root growth..

Figure 7.51a shows the contours of accumulated pore water pressures in Oct yr 1. The pattern of contours clearly reveals the huge difference in predictions from the previous analyses which predicted suctions of up to 900kPa in the slope (eg. Figure 7.2b). Pore water pressures are still compressive in the foundation and a large section of the embankment. Maximum suctions of 50kPa are predicted in a small section of the slope.

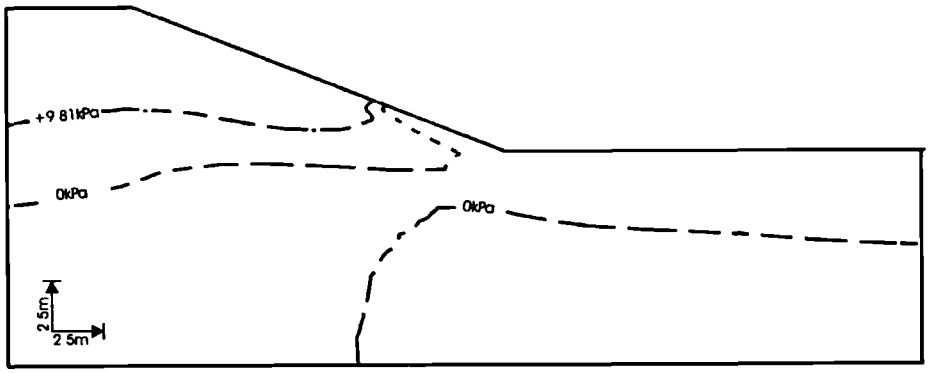

7.51b Contours of sub-accumulated pore water pressure (Jan yr1 - Oct yr1) assuming gradual root growth.

Pore water pressure changes during the period January to October yr 1 are shown in Figure 7.51b. The figure reveals that during that period, tensile pore water pressure changes ranging

from 0 to 50kPa are predicted in the embankment, with very little change in the foundation. In contrast, in the previous analysis where the full PE was used with an r_{max} of 2.5m during the first year (Figure 7.34a), large tensile pore water pressures of up to 500kPa were predicted in the clay fill, the magnitude of which increased in the foundation.

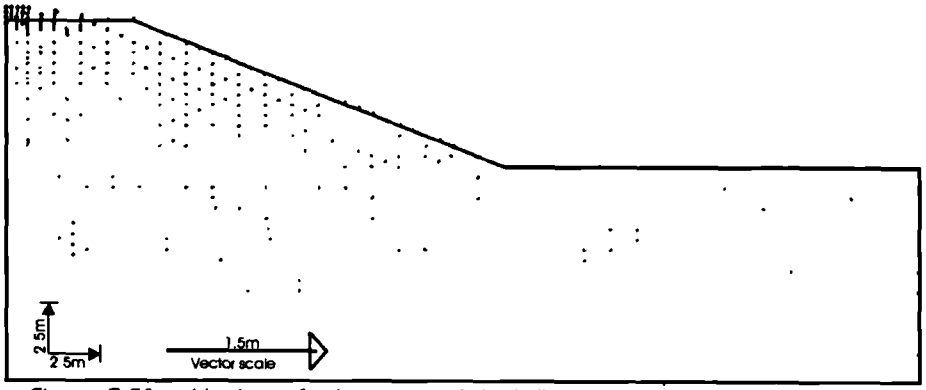

Figure 7.51c Vectors of sub-accumulated displacements (Jan yr1 - Oct yr1) assuming gradual root growth..

Figure 7.51c shows the sub-accumulated vectors of movements that are predicted during the period January to October yr 1 as a result of the pore water pressure changes shown in Figure 7.51b. Very little movement is predicted during this period unlike the earlier predictions which indicated large movements associated with the development of the deep seated zone (Figure 7.3b).

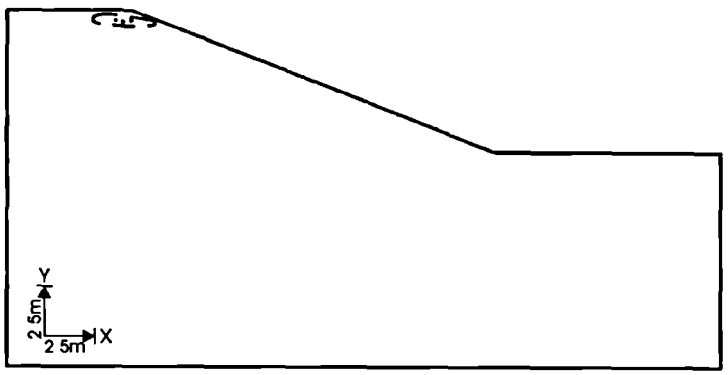

Figure 7.52a Contours of deviatoric plastic strain predicted assuming gradual root growth (Jan yr 1- Feb yr 2).

The analysis was extended over a 10 yr period and the degree of plasticity examined at selected periods of interest. The periods were (i) Jan yr1 to Feb yr2 (ii) Feb yr 2 to Feb yr 5 and (iii) Feb yr 5 to Feb yr 10. The plasticity occurring during those periods are shown in Figure 7.52. It is interesting to note that virtually no plasticity occurs during the first year (Figure 7.52a) whereas all the previous studies indicated a deep seated plastic zone developing during the first summer (eg. Figure 7.5). The deep seated zone then develops during the second period (Feb yr

2 to Feb yr 5) as seen in Figure 7.52b. No further plasticity occurs in the deep seated zone after 5 yrs (Figure 7.52c).

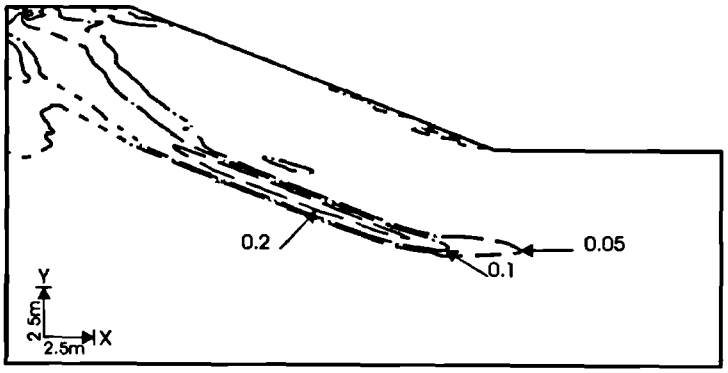

Figure 7.52b Contours of deviatoric plastic strain predicted assuming gradual root growth (Feb yr 2- Feb yr 5).

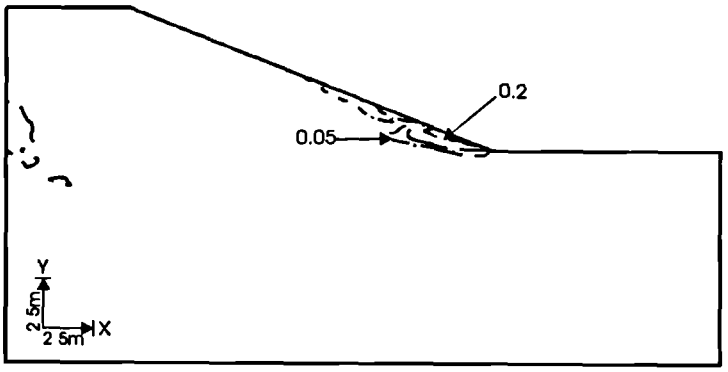

Figure 7.52c Contours of deviatoric plastic strain predicted assuming gradual root growth (Feb yr 5 - Feb yr 10).

Summary

The analyses have shown that the coded RWUM is capable of reproducing the observed seasonal pattern of pore water pressure changes observed in old railway embankments. In the analyses, a 5 year consolidation/swelling period was assumed during which the influence of vegetation was assumed to be negligible. The influence of evaporation was taken into account by specifying a surface pore water pressure boundary condition of 10kPa suction, during the 5 year consolidation/swelling period. The RWUM was then applied at the end of the consolidation period to mimic evapotranspiration.

The results have demonstrated that the RWUM is capable of reproducing the development of a desiccated profile during summer, followed by a reduction in the magnitude of the suctions during winter as pore water pressure recovery occurs. The ability to track the pattern of

meteorological data enables more accurate predictions of embankment behaviour to be made. This is not possible using the current industry methodologies.

In all the analyses reported here, the RWUM was applied in January (which is a wet month) at the end of a 5 year swelling/consolidation period. The rate of evapotranspiration during the period January to April is relatively small and the predictions have indicated little movement occurring in the embankment, which is reasonable.

The analyses have shown that at the onset of summer (May & June) when evapotranspiration rapidly increases, large tensile pore water pressures develop in the embankment and foundation. This is accompanied by the development of a deep seated plastic zone, the location of which coincides with the depth at which σ_3 changes from positive to negative. The location of this zone does not differ significantly for all the analyses and is considered to be primarily governed by the depth to which stress changes occur in response to the applied meteorological data. The degree of plasticity of this deep seated zone does not increase after the first summer.

Analyses were later executed to further understand the reasons for the development of the deep seated plastic zone by modelling incremental root growth and evapotranspiration rates. The analyses demonstrated that if the magnitudes of r_{max} and potential evapotranspiration are applied incrementally, to simulate vegetation growth, the magnitude of pore water pressure and stress changes within the ground correspondingly diminish and the deep seated zone of plasticity takes longer to develop. In addition, the extent of the plastic zone also reduced. This latter prediction is considered to be more reflective of true field behaviour.

Sensitivity/parametric studies have been executed to investigate the influence of r_{max}, clay fill stiffness, increase of permeability due to desiccation cracking and initial permeability of the clayfill. All the analyses have indicated that the largest movements occur in the initial stages of application of the RWUM when pore water pressure changes are large. Once the pore water pressure regime attains an annual cyclical pattern, the overall magnitude of annual movements thereafter reduces. However, sharp changes in ground response will occur in the event of extreme events such as an above normal precipitation or drought. The RWUM is capable of tracking the influence of such events whereas current methods cannot. This once again makes the new approach a more efficacious methodology of analysing the stability of such types of earthworks.

The analyses to investigate the influence of r_{max} have indicated that pore water pressure changes occur to a greater depth for larger magnitudes of r_{max}, which is reasonable. In the

analyses, the greatest pore water pressure changes and movements occurred during the first summer when the RWUM was first applied. It is considered that in prototype embankments, these changes would occur over a longer period but the overall trend would still be expected to indicate increasing magnitude of movements as r_{max} increases. However, although the predictions of pore water pressure changes have indicated increasing depth of pore water pressure changes as r_{max} increases, the analyses have indicated that maximum suctions during summer are generated in the embankment with an r_{max} of 2m. This suggests that although a shorter r_{max} induces pore water pressure changes to a shallower depth compared to a larger r_{max}, the magnitude of suctions that occur for shallow r_{max} are larger than those induced by larger r_{max}. Current methods do not take account of differing values of r_{max}, but instead take an "average" pore water pressure profile deemed to be applicable for all types of vegetation, regardless of root depth. The ability to study the influence of r_{max} comprises another major step forward in modelling and investigating the influence of vegetation on embankments.

The analyses have shown that the pattern of pore water pressure recovery during winter is primarily governed by the magnitude of rainfall. The overall pattern suggests that the magnitude of swelling increases as r_{max} increases, mirroring the pattern of desiccation. This results in large seasonal pore water pressure changes for embankments with large r_{max}. An analysis of the frequency with which the largest movements are predicted by r_{max} of 2m, 2.5m and 3m showed that an r_{max} of 2.5m had the highest frequency during which the predicted seasonal movements were lowest. This would confirm field evidence which suggests that good vegetation management can achieve an optimum balance between rainfall and evapotranspiration whereas shallow rooted vegetation or deep rooted vegetation may, under certain meteorological conditions, accentuate the seasonal movements in embankments (McGinnity *et al*, 1998). The aspect has not been previously successfully investigated because current methods are incapable of modelling the influence of r_{max} on pore water pressure changes.

The results have also indicated that the largest differences in predictions of pore water pressure changes and movements among the three r_{max} occur during the early years. Once an annual cycle of pore water pressure pattern is established, the differences in prediction reduce. However, the pattern of movements may change significantly for different values of r_{max} if extreme events such as drought occur. The RWUM is capable of assessing the effects of such events; which makes it a more powerful tool when making predictions, unlike current methods.

Analyses were carried out to study the influence of stiffness of the clay fill on embankment behaviour. Two stiffness values were investigated, the first of which was double the value used in the second analysis. The stiffer clay fill predicted larger tensile pore water pressures during the first summer but less tensile pore water pressures at the end of winter compared to the softer clay fill. In general, the differences in predictions were much larger for end of the first summer conditions compared to the end of the first winter.

During the first 12 months, the overall deformation pattern of the embankments was significantly different. Settlement in the stiffer embankment was overall uniform across the crest, notwithstanding that the centre settled more than the crest edge. In the softer clay fill, the settlement profile of the crest was typified by large settlement of the crest edge; with comparatively less settlement occurring at the centre of the crest.

However, the analyses revealed that the differences in the pattern of movements diminished after the first 12 months, albeit there was some evidence that the annual movements in the softer embankment were marginally larger than those in the stiffer clay fill. Although the pore water pressure predictions after 1 year were different among the two stiffnesses, the magnitude of difference did not appear to have a significant influence on the overall pattern of the progressive failure mechanism. Kovacevic *et al* (2001) investigated similar type of embankments and also concluded that stiffness did not have a significant influence on the propagation of a progressive failure mechanism.

It is also noteworthy that the significant difference in the predictions for pore water pressures and movements identified during the 12 months are more likely to arise from the large pore water pressure changes associated with invokation of the RWUM. It is considered that these differences would be smaller if gradual root development were more rigorously modelled.

In the analyses to investigate the influence of desiccation cracks on the mass permeability of the clay fill, $\frac{k_f}{k_i}$ ratios of 10 and 100 were used. It was observed that at shallow depth, larger magnitudes of pore water pressure recovery were achieved in the analyses involving a $\frac{k_f}{k_i}$ ratio of 100, which is reasonable. The predictions of end of winter pore water pressures on level ground indicated suctions, in both analyses. In general, the predictions of pore water pressures and movements by the two $\frac{k_f}{k_i}$ ratios were different. The $\frac{k_f}{k_i}$ ratio of 10 predicted larger suctions in summer and lower suctions in winter in the embankment compared to predictions

using a $\frac{k_f}{k_i}$ ratio of 100. The $\frac{k_f}{k_i}$ ratio of 10 predicted larger seasonal pore water pressure changes, which in the long term is expected to induce larger plasticity in a potential slip surface, per given time. This was confirmed in the pattern of horizontal movements of the slope.

It was also observed that use of the crack model causes redistribution of the preceding end of summer suctions to deeper horizons. The degree of redistribution of the suctions increases with the $\frac{k_f}{k_i}$ ratio. The degree of redistribution occurred to depths which are greater than current observations on natural ground (Crilly and Driscoll, 2000) and in LUL embankments (ICON 2001). Moreover, the redistribution of suctions causes the desiccated zone to gradually increase with time (in depth and magnitude of suctions), which in the long term significantly inhibits the propagation of a progressive failure mechanism. This ultimately leads to wrong predictions of seasonal vertical movements as summer settlements are overpredicted; owing to the larger degree of desiccation that occurs.

Finally, sensitivity analyses to investigate the influence of the clay fill permeability on embankment behaviour were executed using clay fill permeabilities of $1\times10^{-9}e^{-0.003p'}m/\sec$, $1\times10^{-8}e^{-0.003p'}m/\sec$ and $1\times10^{-7}e^{-0.003p'}m/\sec$. The results revealed similar predictions of pore water pressure changes and movements by permeabilities of $1\times10^{-8}e^{-0.003p'}m/\sec$ and $1\times10^{-7}e^{-0.003p'}m/\sec$ whereas the predictions using a permeability of $1\times10^{-9}e^{-0.003p'}m/\sec$ were significantly different.

In general, maximum summer suctions were predicted in the analysis with a permeability of $1\times10^{-9}e^{-0.003p'}m/\sec$. This is considered to be reasonable because the value of potential evapotranpiration was the same in all the 3 cases. It is considered that in the least permeable clay fill, comparatively more water is extracted per given layer to meet the evapotranspitation demand because water cannot be readily drawn from deeper strata. The results have shown that at the end of winter, significant suctions still exist in the least permeable clay fill ($1\times10^{-9}e^{-0.003p'}m/\sec$) unlike in more permeable clay fills ($1\times10^{-8}e^{-0.003p'}m/\sec$ and $1\times10^{-7}e^{-0.003p'}m/\sec$) where evidence suggests pore water pressure recovery to their initial values (pre-RWUM) during some years. The end of winter suctions in the least permeable clay fill result in a stiffer clay fill (stiffness is p' dependent) compared to the more permeable clay fills, which results in smaller swelling movements during winter.

Overall, there is evidence that the magnitude of seasonal cyclic pore water pressure (and the associated movements) increases with the magnitude of permeability. During summer, the

greater depths of pore water pressure changes associated with the more permeable clay fills results in larger shrinkage movements compared to the low permeable clay fill. A similar process occurs during recharge, in winter. The more permeable clay fills are able to imbibe more water, and consequently, larger swelling movements occur. The overall pattern of movements involves larger vertical and horizontal movements as permeability increases. In addition, the large seasonal movements associated with the more permeable clay fills induce more plasticity along a potential slip surface. The rate at which the potential shear surface advances increases with permeability.

The overall pattern of horizontal movements in the embankment with a permeability of $1\times10^{-9}e^{-0.003p'}m/\sec$ indicated gradually diminishing magnitudes of movements. This is attributed to the gradual build-up of suctions in both the clay fill and foundation of this embankment. Although the magnitude of suctions also increased with time in the embankments with permeabilities of $1\times10^{-8}e^{-0.003p'}m/\sec$ and $1\times10^{-7}e^{-0.003p'}m/\sec$, the magnitude of increase in the clay fill was small and did not appear to significantly affect the propagation of the potential slip surface. This is likely to be a result of the pore water pressures recovery that occurred during winter, within these more permeable embankments.

The crack permeability model as currently coded is able to mimic the increase in permeability due to desiccation cracking, at shallow depth. The behaviour at shallow depth is reasonable and the model enhances modelling features. However, because the model works on the assumption that desiccation cracks form wherever σ_3 exceeds a prescribed threshold value, suctions are being predicted by the model to depths which are much greater than are observed in the field. The author believes that at depth, where desiccation exists, behaviour is likely to be typified by low permeability (because of high p' suction) and an absence of desiccation cracks whereas at shallow depth, desiccation cracks can develop and lead to an increase in permeability. The stress regime which results in the formation of desiccation is believed to be much more complex than has been modelled here in the smeared crack permeability model.

Chapter 8

CONCLUSIONS AND SUGGESTIONS FOR FURTHER RESEARCH

8.1 Introduction

This thesis has explored a number of facets concerning pore water pressure changes induced by vegetation and their influence on the ground with special emphasis on the behaviour of typical UK old railway embankments constructed in stiff clay fill.

A significant number of old railway embankments are over 100 years old and were constructed prior to the discovery of scientific knowledge about compaction. Construction was undertaken using end-tipping and side-tipping methods. In clay fill embankments, the relatively uncontrolled manner in which the material was placed resulted in granular inclusions of variable grading and random spatial distribution. The mass permeability of most of these embankments is therefore expected to vary significantly, within short distances. Although some laboratory permeability tests have been carried out on some intact clay fill samples, representative values of the mass permeability can only be determined using field tests. Consequently, in the first section of this thesis, the influence of mass permeability on the stability of a typical UK old railway embankment has been explored.

The mass permeability of the ground controls the rate of water flow, which in turn governs the volume changes of the ground. Where vegetation exists, the magnitude of the water flow (and soil volume change) is also dictated by the transpiration demand. Previous research in UK old railway embankments eg. Kovacevic *et al* (2001) and Russell *et al* (2000) indicated that the strains induced as a result of the seasonal pore water pressure changes can generate a progressive failure mechanism, in the long term. However, the influence of permeability on the magnitude of the strains generated during seasonal pore water pressure changes has previously not been investigated. This aspect has been investigated in the first section of this thesis.

The second section of the thesis describes a nonlinear root water uptake model (RWUM) which mimics root water uptake by vegetation and has been coded in the Imperial College Finite Element Program (ICFEP). This new development marks a step forward from the current industry approach in which pore water pressure changes induced by vegetation are simplified into two profiles - governing winter and summer profiles. The RWUM uses potential evapotranspiration as input data to predict the pore water pressure changes; rather than for the user to prescribe them during an analysis using values that have been contrived from field observations. The contrived pore water pressure values are unlikely to be valid for embankments in locations with a different micro or macro climate. The performance of the RWUM has been investigated for varying maximum root depths, permeability, soil suctions and meteorological data. The RWUM has also been used to predict vertical ground movements in London Clay at BRE's field test site at Chattenden, in Kent. The predictions by the RWUM have been compared with field measurements made by BRE.

In the third section of the thesis, the behaviour of a typical UK old railway embankment was investigated using the RWUM. The investigations focused on the influence of maximum root depths and permeability and stiffness of the clay fill, to identify the embankment behaviour prior to collapse. The initiation and propagation of a progressive failure mechanism is demonstrated, as seasonal pore water pressure changes are modelled using the RWUM.

This chapter summarises the main conclusions drawn from this thesis and also identifies areas for further research.

8.2 Conclusions

8.2.1 Influence of permeability on stability of vegetated clay fill embankments

The influence of permeability was investigated in Chapter 4 using clay fill permeabilities of $1\times10^{-9} m/\sec$, $1\times10^{-8} m/\sec$ and $1\times10^{-7} m/\sec$. The embankment was assumed to be 7m high, comprising 6m of London Clay fill, a 1m deep ash mantle and 1 in 2.5 side slopes. A 1 month construction period was modelled to simulate the relatively "quick" construction period associated with end-tipping techniques. The clay fill was assumed to have a suction of 50kPa during placement. A 5 year post construction period was assumed during which consolidation/swelling to a 10kPa surface boundary was allowed; to simulate vegetation growth prior to application of seasonal pore water pressure changes. The seasonal pore water pressure changes were modelled using the current industry methodology, described in Chapter 4.

The results have confirmed that the degree of pore water pressure dissipation that occurs increases with the magnitude of permeability. Behaviour during the 5 year swelling/consolidation period is also strongly influenced by the magnitude of permeability. The results indicate that at the end of the 5 year swelling/consolidation period, full dissipation of suctions occurs in the clay fills with permeabilities of $1\times10^{-8}\,m/\sec$ and $1\times10^{-7}\,m/\sec$, whereas the predictions using a permeability of $1\times10^{-9}\,m/\sec$ indicates suctions within the clay fill. This pattern is repeated during cycling ie. pore water pressures fully dissipate in the more permeable clay fills ($1\times10^{-8}\,m/\sec$ and $1\times10^{-7}\,m/\sec$).

Upon invokation of the first few cycles, the stress paths in $t'-s'$ space near the toe and at the midslope along a potential shear surface indicate a reduction in the magnitude of shear stress, t', and an increase in average stress, s' for all three permeabilities. The degree of reduction diminishes as the permeability increases. It is also shown that during the early phases of cycling, (to mimic seasonal pore water pressure changes during winter and summer), the stress path moves away from the failure envelope. This response indicates the stabilising influence of vegetation in the short to medium term. The results also indicate that the reduction in shear stress arising from the introduction of vegetation is relatively small in the most permeable clay fill ($1\times10^{-7}\,m/\sec$). The stabilising effects of transpiration in this latter embankment are therefore small and overall behaviour is dictated by the build-up of strains induced by the seasonal pore water pressure changes.

The pattern of pore water pressure predictions reveals some important historical aspects of these embankments. Where construction resulted in low mass permeabilities, relatively high suctions existed at the end of construction, compared to more permeable clay fills. Once vegetation established itself, desiccation induced by transpiration would have curtailed the magnitude of post-construction swelling. These predictions suggest that the embankments with very low permeabilities are likely to have maintained suctions for many years after construction. This may explain why a number of the embankments have stood for more than 100 years without failing, despite having undergone several cycles of seasonal pore water pressure changes. The mass permeability of the clay fill and the length of time before vegetation begins to significantly control pore water pressures clearly govern the stability/instability of these embankments in the short to medium term.

It is nevertheless important to point out the fact that in the field, the pore water pressure regime is much more complex than has been assumed in these analyses. Not only is the pore water pressure regime quasi-stable, extreme events such as drought or unusually "wet" seasons have a significant influence on the rate and magnitude at which a desiccated profile enlarges or diminishes. To correctly reproduce such features and their influence on embankments requires more sophisticated methods which are capable of tracking the meteorological data, eg. the RWUM described in Chapter 5.

During cycling, it has been revealed that the magnitude of the seasonal cyclic movements increase with the magnitude of permeability. These seasonal movements induce strains, whose magnitude monotonically increases with the number of cycles and gradually trigger a strain softening progressive failure mechanism. The differences in embankment stability predicted by the three permeabilities are clearly demonstrated by the results which indicate collapse after 15 cycles ($1\times10^{-7}\,m/\sec$), after 40 cycles ($1\times10^{-8}\,m/\sec$) and no failure but significant outward slope movements in the clay fill with a permeability of $1\times10^{-9}\,m/\sec$ after 180 years. All the analyses predict a deep-seated slip surface at the base of the embankment. The slip surface commences at the toe and advances into the slope of the embankment. It is also worth reiterating that the majority of the old railway embankments have stood for over 100 years. It could be argued that their mass permeability is low and likely to be close to $1\times10^{-9}\,m/\sec$.

It is also interesting to note that predictions of slope movements in the two more permeable clay fills $1\times10^{-7}\,m/\sec$ and $1\times10^{-8}\,m/\sec$ indicate continuously increasing outward movements as soon as cycling commences. However, the behaviour in the least permeable clay fill ($1\times10^{-9}\,m/\sec$) is different. It is epitomised by overall shrinkage, as consolidation dominates the behaviour. The shrinkage movements decrease in magnitude with time. After approximately 50 years, the shrinkage movements are virtually insignificant. This is followed by a further 20 year period during which the embankment slope hardly moves. After approximately 70 years of cycling the magnitude of the outward slope movements begin to increase again and are accompanied by the propagation of a potential slip surface at the toe.

The behaviour of the latter embankment highlights an important aspect regarding numerical analysis of these embankments. In order to accurately model the behaviour of type of embankments and predict future performance, it is necessary that the cycling history be accurately modelled, in order to establish the correct strain levels. Accurate determination of current plasticity in turn leads

to accurate predictions of future performance, otherwise there is a risk that an embankment is prematurely classified as stable during the design period.

8.2.2 Numerical modelling of evapotranspiration using a RWUM

The literature review has established that although in general, vegetation enhances slope stability through pore water pressure reduction, the shrinkage and swelling cycles triggered by seasonal pore water pressure changes can induce plastic strains. With time, the magnitude of the accumulated plastic strains can be large enough to initiate and propagate strain softening in brittle clays, resulting in the development of a progressive failure mechanism. This process is exacerbated by vegetation in climatic regions epitomised by wet and dry seasons eg. SE England, in UK.

In order to be able to quantify the magnitude of strain changes that are induced by the vegetation requires correct modelling of the water abstracted by the roots. This aspect has been researched in soil science and agronomy and several models have been proposed. A model amenable to modelling vegetation encountered in civil/engineering was adopted and has been coded and tested in ICFEP (Chapter 5). The model assumes a nonlinear distribution of root water uptake over the root zone. Computation of the magnitude of root water uptake takes account of the in situ pore water pressures, as these govern the water uptake capabilities of the roots. Meteorological data comprising potential evapotranspiration is used as input data; from which the RWUM computes the actual evapotranspiration. Rainfall data is input in a separate module (which already existed within ICFEP prior to this research). In the UK, rainfall and potential evapotranspiration data are routinely computed by the Meteorological Office using the Meteorological Office Rainfall and Evaporation System (MORECS).

Investigations have been carried out to determine the maximum element size that can be used with the RWUM, without compromising the accuracy. It has been found that this can be achieved if a maximum element thickness equal to the maximum root depth is used.

The RWUM has been used to predict pore water pressure changes and vertical ground movements on an idealised 1m wide by 105m deep soil column. The predictions of pore water pressure changes and ground movements match the pattern of rainfall and potential evapotranspiration ie. swelling is predicted during months with low evapotranspiration and or/ high rainfall, whilst shrinkage is predicted during periods of high evapotranspiration and/or low rainfall.

The influence of the maximum root depth has been studied using maximum root depths (r_{max}) of 2m, 2.5m and 3m. The results indicate two patterns of pore water pressure changes. At shallow depth (typically less than 2m), the magnitude of suctions increases as r_{max} reduces. This behaviour is expected because shallower roots have to extract more water to meet the specified potential evapotranspiration demand, per given time. The pattern at deeper horizons is different and is typified by larger suctions being predicted as r_{max} increases. Overall, the magnitude of vertical movements increases as r_{max} increases.

However, it is noteworthy that in the field, the response of roots to water demand is slightly different to the assumptions made above. In general, plants have a capacity to extend their roots in the quest for water; preferring to extend their roots to zones of high water potential rather than draw water against increasing soil suctions. Moreover, there is evidence that plants close their stomata when transpiration needs outstrip the rate of root water uptake. Therefore, the overall behaviour is much more complex than has been modelled; notwithstanding that the studies in this thesis constitute a significant step forward in modelling root water uptake and its effects on the ground.

An investigation to assess the magnitude of soil suctions at which root water uptake begins to significantly reduce (magnitude of S3 in α function) has been undertaken. The magnitude of S3 is thought to be species dependent but is yet to be fully investigated for non-agricultural vegetation. In the literature, values of S3 ranging from 50kPa to 200kPa have been cited, although it is also acknowledged that in some cases the magnitude can be much larger eg. drought resistant species.

In this research, S3 values of 50kPa, 100kPa, 200kPa and 400kPa have been investigated. Little difference in predictions of pore water pressure changes and movements is shown for S3 magnitudes of 50kPa and 100kPa. However, as the magnitude of S3 increases beyond 100kPa, the differences in predictions have been shown to increase. The overall pattern shows larger pore water pressure changes as S3 increases beyond 100kPa. This is logical and implies that under a given evapotranspiration demand vegetation capable of tolerating higher suctions is able to extract more water from the ground, in a given time. This may partly explain the differences in soil movements associated with different tree species.

A comparison of predictions by different permeability models has also been carried out using homogeneous, inhomogeneous and a p' dependent model. The results have demonstrated that the p' dependent model inhibits the ingress of precipitation as a result of the low permeabilities that are predicted by the model when suctions increase. However, at deeper horizons it has been shown that the homogeneous and inhomogeneous permeability models predict large pore water pressure

changes compared to the p' dependent model. This is a result of the inability of the homogeneous and inhomogeneous models to reproduce field behaviour which depicts a reduction in the magnitude of permeability with depth. This latter aspect is more closely mimicked by the p' dependent model.

Pore water pressure predictions by all three permeability models yield a desiccated profile which gradually increases in depth and magnitude of suctions, with time. This prediction is at variance with observed field behaviour and is attributed to the inability of the current permeability models to correctly reproduce the increase in permeability, when desiccation cracks develop. Real field behaviour has shown that desiccation cracks occur in clays. The cracks effectively constitute pathways through which recharge of water is facilitated during precipitation. In the field, this results in a significant reduction in the magnitude of suctions, rather than a gradual increase in the degree of desiccation with time, as currently predicted by the permeability models. Therefore the current permeability models in ICFEP needed further development to take account of cracks; in order to improve predictions by the RWUM.

A smeared crack permeability model has been developed to mimic the increase in permeability that occurs in cracked ground ie. the initiation and propagation of individual cracks is not modelled but instead, the increase in permeability predicted is smeared over a domain of the mesh. Isotropic conditions are assumed in the model, ie. the direction of cracking is not considered. In the model, cracking is assumed to occur when a specified value of the minimum total principal stress, σ_3, is exceeded. The user defines the magnitudes of σ_3 at which crack initiation commences and is fully developed, as well as the ratio by which the permeability increases between the two stress levels (σ_3). Values of 0kPa and 100kPa, respectively, were used in most of the analyses reported in this thesis. The magnitude of permeability is assumed to increase from an initial value, k_i (uncracked ground) to a final value k_f (fully cracked ground) according to a logarithmic law. Ratios of 10, 100 and 1000 were investigated.

Predictions using the new crack model have demonstrated its capability to reduce suctions at shallow depth; which constitutes a significant advancement in modelling permeability in cracked ground. Since the model is largely dependent on σ_3 only, the increase in permeability is effected wherever the trigger values are exceeded, regardless of depth. This results in "cracked ground" being predicted at depths which the author believes are greater than field values. Prediction of cracked ground at depth leads to predictions of higher permeabilities redistribution of suctions by the crack model. The results have shown that the degree of redistribution increases with the $\frac{k_f}{k_i}$ ratio. The stress regime that governs crack formation is complex and is likely to include more than

one parameter (σ_3). This subject is currently not well researched and understood by geotechnical engineers. However, the author believes that the crack model in its current form has the fundamental principles for modelling crack behaviour but requires further modifications to enable it to correctly predict the maximum depth of cracked ground.

The parametric studies on the performance of the RWUM have revealed that a number of parameters affect the predictions of pore water pressure changes (and vertical movements) ie. r_{max}, meteorological data, permeability and magnitude of S3. Therefore careful selection of the parameters is required in analyses, for accurate predictions to be obtained.

8.2.3 Prediction of ground movements using the RWUM

As part of the validation exercise for the newly developed RWUM, prediction of vertical ground movements and pore water pressures were made for BRE's field testing site at Chattenden, details of which are given in Chapter 6. A one-dimensional consolidation/swelling analysis was carried out on a 1m wide by 105m deep soil column. Potential evapotranspiration and the associated rainfall data for the period 1970-1995 were used as input into the vegetation and precipitation boundary conditions, respectively. The predictions of pore water pressures and ground movements were compared with BRE's field measurements during the period 1988-1995.

The predictions of pore water pressures by the RWUM at depths less than 5m are approximately equal to the field measurements for the two cases considered ie. September 1991 and 1995. In addition the predicted depth at which maximum suctions occur matches the field vales.

A comparison of ground movement predictions by the RWUM involving various magnitudes of S3, r_{max}, and the ratio of the unload/reload stiffness of the London Clay showed that these parameters have a small effect on predictions after 20 years of application of the RWUM. Overall, the predicted cyclic pattern of movements is similar to the field pattern. Nevertheless, the RWUM over-predicts heave at ground level during winter and over-predicts shrinkage during summer at 4m depth. This anomaly is considered to result from the inability of the constitutive model to reproduce the shrinkage and swelling characteristics of the London Clay as well as the inability of the permeability model to correctly simulate the permeability changes associated with cracked ground.

The predictions of heave following tree removal gave magnitudes of movements very close to field observations at ground level and 1m depths. However, the variation between predictions and field

observations increases at depth. This is attributed to the fact that prior to tree removal, the RWUM over-predicts the redistribution of suctions at depth hence relatively larger heave compared to the field situation is predicted following tree removal, as ground water recharge progresses. The pattern of movements also suggested that the rate at which the water-front advanced, as predicted by the RWUM, was much faster compared to actual field behaviour.

8.2.4 Numerical analysis of vegetated clay fill embankments using the RWUM

Following the successful implementation and testing of the RWUM in ICFEP on a soil column, the RWUM was used in Chapter 7 to analyse the behaviour of a typical vegetated railway embankment. The geometry of the embankment was identical to that described in Section 4.4.1 and the meteorological data from Chattenden was employed (detailed in Chapter 5).

The results indicated that the RWUM is capable of reproducing the pattern of seasonal cyclic movements observed in these embankments; albeit their magnitude is larger (2-4 times observed movements). The pattern of movements mirrors the profile of soil moisture deficit.

It has been shown that for a given set of meteorological data (rainfall and potential evapotranspiration), the RWUM predicts changes in σ_3 to a depth which is largely independent of the mass permeability of the clay fill, r_{max} and clay fill stiffness. The depth at which σ_3 changes from tension to compression demarcates a zone in which large strains occur. Similar behaviour was observed by Kovacevic (1994) during numerical analysis of road embankments. In his analyses, Kovacevic (1994) modelled the development of cracks over a shallow depth in the slope of an embankment by changing the magnitude of permeability during the course of the analysis. He noted the development of plasticity at the maximum depth of the assumed cracked zone and attributed its formation to the large strain changes induced by the large water flows, in response to the sudden increase in permeability. In this research, the development of the plastic zone has been investigated using gradually increasing potential evapotranspiration rates and maximum root depth, to model the establishment and development of vegetation. The analyses have revealed that although there is a delay in the formation of the plastic zone if an incremental approach is used to model the growth of vegetation, the plastic zone nevertheless still forms in the long term.

Sensitivity and parametric studies have been undertaken to investigate the influence of r_{max} and the stiffness and permeability of the clay fill. The studies have indicated that larger pore water pressure changes (and movements) occur during the first 1-2 years of the analyses; after which they reduce significantly in magnitude. This is attributed to the fact that the pore water pressure changes

induced by the RWUM during the initial period are significantly different to those at the end of construction. With time, the magnitude of the pore water pressure changes between consecutive months reduces. In prototype embankments, the development of vegetation is a much more gradual process than has been modelled in these studies. Therefore it is expected that overall, the effects of vegetation in the initial stages would be muted compared to the magnitudes predicted in these analyses. It is also noteworthy that a rigorous approach to the modelling of incremental growth of vegetation involves more computing resources; which can be significant, depending on the number of elements in the mesh.

The investigations to assess the influence of the maximum root depth were executed assuming three values of r_{max} ie. 2m, 2.5m and 3m. They have shown that during summer, the maximum suctions are predicted by r_{max} of 2.5m. The depth to which suctions develop increases as the maximum root depth increases. During winter, overall behaviour is dictated by the magnitude of rainfall, and this has been shown by the small difference in predictions by all three values of r_{max}.

The study has also indicated that the frequency with which the smallest seasonal cyclic movements are predicted occurs in the analysis with r_{max} of 2.5m. This suggests that for the modelled embankment and meteorological input data, a shallow maximum root depth (2m) and deeper root depth (3m) are inducing larger movements. This would confirm field evidence which suggests that vegetation management can achieve an optimum balance between rainfall and evapotranspiration whereas shallow rooted vegetation or deep rooted vegetation may, under certain meteorological conditions accentuate the seasonal movements in embankments.

The influence of clay fill stiffness on embankment behaviour has shown that the largest differences in pore water pressure changes and deformations occur during the first year. During this initial period, the embankment with a lower stiffness moves more than the stiffer one, which is reasonable. However, it could be argued that if an incremental approach were used to model vegetation growth, the differences between the two stiffneses would be significantly smaller than have been predicted. The predictions after the first year indicate minor differences in overall pore water pressure changes and movements. Therefore it can be concluded that the stiffness of the clay fill has little effect on overall behaviour of these embankments. Similar conclusions were reached by Kovacevic *et al* (2001) in which seasonal pore water pressure changes were modelled, using the simplified industry approach.

Investigations into the influence of mass permeability of the clay fill have been executed using permeabilities of $1\times10^{-9}e^{-0.003p'}m/\sec$, $1\times10^{-8}e^{-0.003p'}m/\sec$ and $1\times10^{-7}e^{-0.003p'}m/\sec$. They have

shown that the more permeable clay fills ($1\times10^{-8}e^{-0.003p'}m/\sec$ and $1\times10^{-7}e^{-0.003p'}m/\sec$) predict larger pore water pressure changes, as expected. During summer, more water is abstracted to meet the potential evapotranspiration demand; resulting in large shrinkage movements whereas during winter, the high permeability allows ingress of larger volumes of rainfall; which results in larger swelling movements. During winter, the predictions using permeabilities of $1\times10^{-8}e^{-0.003p'}m/\sec$ and $1\times10^{-7}e^{-0.003p'}m/\sec$ indicate recovery of pore water pressures to their long term values. The predictions using a permeability of $1\times10^{-9}e^{-0.003p'}m/\sec$ indicate suctions during both winter and summer. This pattern is similar to that identified in Chapter 4 and summarised in Section 8.2.1 where a simplified approach was used to model seasonal pore water pressure changes induced by vegetation.

The large seasonal movements associated with the more permeable clay fills induce larger plastic strains along the potential slip surface. The rate at which the potential shear surface advances increases with the magnitude of permeability. This would suggests that in the long term, the most permeable embankment would be expected to fail first. Again, this was shown to be the case in the analyses reported in Chapter 4, using a simplified method to model seasonal pore water pressure changes induced by vegetation.

The influence of the $\frac{k_f}{k_i}$ ratio was investigated using values of 10 and 100. The pattern of predictions were similar to those detailed in the column analyses (Chapter 5) and summarised in Section 8.2.2.

The crack permeability model as currently coded is able to mimic the increase in permeability due to desiccation cracking, at shallow depth. The predictions at shallow depth are reasonable and the model enhances modelling features. It is also worth reiterating that the model works on the assumption that desiccation cracks form wherever σ_3 exceeds a prescribed threshold value. Where desiccation exists at depth, behaviour is more likely to be typified by very low permeability (because of high p' suction) and an absence of cracks. In comparison, desiccation causes cracking of the ground at shallow depth and results in an increase in permeability. Therefore, the author considers that the crack permeability model is enhancing modelling capabilities at shallow depth but further modifications to the model are necessary to ensure that the model does not over-predict permeability at depth as this results in over-prediction of redistribution of the suctions.

The major positive facets of the RWUM in such type of boundary value problems are its ability to use meteorological data as input into the model, to predict pore water pressures in real time. Microclimatic influences can therefore be more accurately quantified which is currently not

possible using the industry methodology. Most importantly, the RWUM has been shown to be capable of predicting pore water pressure changes, movements and initiation and propagation of a potential slip surface for specific meteorological data. The behaviour of the embankment on a monthly basis has been quantified and behaviour at shorter time scales eg. weeks or days are possible when using the RWUM if the meteorological data is input appropriately. This capability again constitutes a significant improvement to current modelling methodologies which are much more simplistic.

Through using a RWUM, extreme events such as a drought can be modelled and their effects more accurately quantified. In addition, it is possible to study the behaviour of embankments in the same micro-climatological location with different vegetation because it is possible to accommodate such variations in a WRUM. Use of a RWUM enables types more informed design of instrumentation/monitoring systems and remedial works to be achieved. Moreover, long term predictions can be made for various climatological scenarios eg. the influence of climate change.

Although this thesis has not included the study of cut slopes, it is considered that RWUMs are equally applicable to study the influence of vegetation on the behaviour of such infrastructure.

8.3 Suggestions for further research

This research has demonstrated the applicability of root water uptake models to model evapotranspiration. The new approach offers advantages over current methods to model pore water pressure changes induced by vegetation. However, a number of avenues still need further research to enhance the modelling capabilities of this new method and these are outlined below.

8.3.1 Root water uptake models

Most of the root water uptake models have been developed and validated on agricultural crops. While each model differs from the next one in its methodology of distributing potential transpiration, in all the models (including the one used in this thesis), the actual water uptake in any discrete layer is not allowed to exceed the potential transpiration allocated to that layer. Such an assumption implies that should water abstraction in a particular layer diminish as a result of increasing suctions, compensation through increasing the water uptake from other wetter layers is forbidden. However, research has shown that when the upper layers are depleted of available water, a significant proportion of the transpiration can be met by uptake from deep, sparsely rooted soil layers. Modifications to root water uptake model are therefore continuously being made, in the

light of new research. Other recent developments include the extension of current 1D and 2D root water extraction functions to analyse 3D problems. This is important when root water uptake is varying spatially eg. sparse vegetation, it is most appropriate that a 3D approach be used to enable a more accurate quantification of spatial variability of the soil water regime. The following avenues of research are suggested:

- In the author's view, use of root water extraction functions offer an efficient and elegant method of modelling transpiration. However, their development requires an in depth understanding of plant physiology; a subject beyond the scope of most geotechnical engineers. Therefore, in order for geotechnical engineers to benefit from state-of-the-art knowledge regarding RWUMs requires literature reveiew of agro-forestry and other allied publications.

- The root water uptake model currently coded in ICFEP is capable of analysing one and two dimensional boundary value problems. Its capabilities would therefore be significantly enhanced if it were extended to analyse 3D problems.

- A key input parameter into any root water uptake model is the maximum root depth. Although ground investigations occasionally include a description of vegetation, this usually only includes a description of that part of the vegetation above the ground. It is suggested that investigations also encompass root morphology to enable predictions by RWUMs to be more accurate.

- The analyses executed in this thesis have indicated that the magnitude of the soil suction at which root water extraction is assumed to be significantly impeded (S3) can have an influence on the predictions, in some cases. Again, the author believes that it is necessary for geotechnical users of a RWUM to research this area in the relevant agro-forestry publications, to improve predictions.

8.3.2 Shrinkage and swelling behaviour

In this thesis, predictions of movements at large strains in London Clay have been made using a Mohr-Coulomb failure model with an elastic stiffness dependent on p'. The same model has been used in the analysis of embankments to determine the pre-peak behaviour. Progressive failure depends strongly on the magnitude of strains generated. The magnitude of strains generated during each shrinkage and swelling cycle are governed by the shrinkage and swelling moduli, respectively. There is little data on the swelling and shrinkage characteristics of stiff clays such as London Clay

involving repetitive cycles at the appropriate stress level, to simulate field conditions. The following studies would be invaluable:

- Laboratory studies to determine the shrinkage/swelling characteristics of stiff clay fills eg. London Clay at stress levels concomitant to those which prevail in vegetated embankments under normal seasonal pore water pressure changes would be useful.

- Development of a soil constitutive model capable of reproducing the stress-strain behaviour of stiff clays under repetitive large shrinkage/swelling cyles.

8.3.3 Influence of partial saturation

During drying cycles, a soil undergoes desiccation; which can render the soil partly saturated. The shrinkage/swelling behaviour of a partly saturated soil is significantly different to its behaviour when fully saturated. eg. its shear strength and permeability. Laboratory tests on the air entry value for London Clay at Chattenden gave values in excess of 3000kPa (Marinho, 1994). The magnitude of suctions predicted during the analyses was less than this value, therefore use of fully saturated soil mechanics for the clay appears valid.

However, for the ash at the top of the embankment, the magnitude of suctions generated would have warranted invokation of partly saturated soil mechanics. This is important since the ash (being a granular material) has a significant influence on the pore water regime by acting as a capillary break during drying (summer). The latter aspect has implications on pore water pressure regimes in old railway embankments where remedial measures have incorporated granular fill (mostly Type 6P/6N as described in the Specification of Highway Works (1992) on regraded slopes. The facets to model partly saturated soil behaviour in ICFEP were unavailable at the time the analyses for this thesis were undertaken. It is proposed that future research should include the following:

- Laboratory studies to determine the soil water characteristic curve and other pertinent parameters required in ICFEP to model partly saturated behaviour. The study could include the ash and Type 6P/6N granular material.

- Investigate the influence of the ash mantle and granular fill on embankment behaviour using partly saturated soil mechanics in numerical analyses.

8.3.4 Influence of desiccation cracks

The current research has highlighted the significant influence of desiccation cracks on volume changes and the mass pemeability of the clay. The volume change characteristics of the cracked soil are different to those when it's intact and these facets should be incorporated in a constitutive model if correct predictions are to be made. Moreover, it has been demonstrated in this thesis that the magnitude by which permeability increases when the ground cracks can have a large influence on the predictions of pore water pressures and ground movements. Unfortunately, the initiation and propagation of desiccation cracks has hitherto received little attention by researchers. This includes the manner in which ground stresses change in response to the water balance and the depth and rate at which the cracks open and close; all of which are important.

The state-of-the-art methodology of predicting vertical ground movements arising from desiccation involves use of an empirically determined "water shrinkage factor" and the predictions obtained are often inaccurate. In order to advance knowledge on this subject using numerical analysis requires the development of a model based on theoretical soil mechanics rather than empiricism. It is suggested that future understanding of this subject would be improved if the following areas were investigated:

- research on the stress regime governing the initiation and propagation of cracks using physical models
- development of theories based on fundamental soil mechanics. These could be supplemented with field based studies involving monitoring of meteorological data, pore water pressures, ground stresses, in situ permeability, crack development and vegetation studies at specific sites.

Knowledge from these studies could then be applied to the smeared crack model that has been developed and coded in ICFEP, to improve its accuracy in predictions.

8.3.5 Validation of root water uptake model

An attempt has been made to validate the root water uptake model used in this thesis. The predictions have revealed that a number of parameters can have an influence on the results. The most important of these are the assumption of the maximum root depth (r_{max}), permeability, and the suction at which root water uptake commences to be significantly curtailed (S3), notwithstanding that the studies for Chattenden site indicated that r_{max} and S3 do not have a significant influence. Predictions of vertical ground movements at Chattenden by the RWUM have yielded movement patterns which approximately match field observations, notwithstanding that overall, the RWUM

predicts larger seasonal movements. It is suggested that these analyses be repeated when further developments have been made to the permeability and constitutive models.

During the final phase of this research, the author became aware of a study carried out by the Transport Research Laboratory (discussed in Section 2.6.5 of Chapter 2). TRL's study involved monitoring the growth of vegetation, root morphology, pore water pressures and meteorological data on a carefully engineered 2m high by 34m long embankment. Invaluable information would be obtained if the following were carried out:

- Numerical modelling of TRL's embankment using the RWUM. The major advantages with this embankments are that its engineering, vegetation, pore water pressure regime and meteorological data are known. The existence of high quality data would facilitate a validation exercise.

- A similar exercise could also be undertaken on a prototype embankment eg. pore water pressures, movements and meteorological data have been continuously monitored on some selected embankments on the LUL network. Again numerical analyses using the RWUM on one or more of the prototype embankments would be invaluable to test the efficacy of the RWUM.

REFERENCES

Alonso, E. and Gens, A. (1994). "Elastoplastic model for unsaturated expansive soils". *Numerical Methods in Geotechnical Engineering*, Smith (ed), Balkema, Rotterdam.

Al-Tabbaa, A. and Wood, D.M. (1989). "An experimentally based 'bubble' model for clay". *Int. Conf. Num. Models Geomech.*, NUMOG III, Edt. Pietruszczak & Pande, Balkema, pp 91-99.

Anderson, M.G., Hubberd, M.G, and Kneale, P.E. (1982). "The influence of shrinkage cracks on pore water pressure within a clay embankment". *Quarterly Journal of Engineering Geology* Vol. 15, pp 9-14.

Anderson, M.G. and Kneale, P.E. (1980a). "Pore water pressure changes in a road embankment". *Journal of the Institution of Highway Engineers*, Vol. 5, pp 11-17.

Anderson, M.G. and Kneale, P.E. (1980b). "Pore water pressure and stability conditions on a motorway embankment. *Earth Surface Processes*, Vol. 5, pp 37-46.

Anderson, M.G. and Kneale, P.E. (1984). Discussion on the Fourth Geotechnique Symposium in Print "The influence of vegetation on the swelling and shrinking of clays". *Geotechnique* **34**, pp 150-151.

Anderson, M.G. (1979). "On the potential of radiography to aid studies of hillslope hydrology". *Earth Surface Processes,* Vol. 4, pp 77-83.

Ayres, D.J. (1994). "Hydrofracture grouting of landslips in cohesive soils". *Grouting in the Ground*. Thomas Telford, London.

Barbour, S.L. (1998). Nineteenth Canadian Geotechnical colloquium: The soil-water characteristic curve: a historical perspective. *Canadian Geotechnical Journal*, Vol, 35, pp 873-894.

Barker, D.H. (1995). "*Vegetation and slopes*". Stabilisation, protection and ecology. London. Published by Thomas Telford Ltd., London , UK.

Bathe, K.J. (1982). "Finite element procedures in engineering analysis", Prentice-Hall.

Belmans, C., Wesseling, J.G. and Feddes, R.A. (1983). "Simulation of the water balance of a cropped soil: SWATRE. *Journal of Hydrology*, Vol. 63, pp 271-286.

Biddle, P.G. (1993).). "Patterns of soil drying and moisture deficit in the vicinity of trees on clay soils". *Geotechnique* **33**, No.3, pp 107-126.

Biddle, P.G. (1998). "*Tree Root Damage to Buildings, Vol. 1: Causes, Diagnosis and Remedy*". Willowmead Publishing Ltd, UK.

Biot, M.A. (1941) "General theory of three-dimensional consolidation". *Jnl. Appl. Phys.*, Vol 12, pp 155-164.

Bishop, A.W. and Blight, G.E (1963). "Some aspects of effective stress in saturated and partly saturated soils". *Geotechnique* **13**, No.3, pp 177-197.

Bishop, A.W. and Garga, V.K. (1969). "Drained tension tests on London Clay". *Geotechnique* 19, No.2, pp 309-313.

Bishop, A.W. (1967), "Progressive failure - with special reference to the mechanism causing it", *Proceedings of the Geotechnical Conference.* Oslo, Vol.2, pp 142-150.

Bishop, A.W. (1971)a, "Shear strength parameters for undisturbed and remoulded soil specimens". *Proceedings of the Roscoe Memorial Symposium.*, pp 3-139.

Bishop, A.W. (1971)b, "The influence of progressive failure on the choice of the method of stability analysis", *Geotechnique*, Vol. 21, pp 168-172.

Bjerrum, L. (1967), "Progressive failure in slopes of overconsolidated plastic clays and clay shales", ASCE, *Journal of Soil Mechanics and Foundation Division*, Vol. 93, pp 3-49

Blight, G.E .(1965). "As study of effectrive stresses for volume change". *Moisture Equilibria & Moisture Changes in Soils Beneath Covered Areas*, Australia, pp 259-269.

Blight, G.E .(1967). "Horizontal stresses in stiff and fissured lacustrine clays". *4th Regional Conference for Africa on Soil Mechanics and foundation Engineering*, Cape Town, South Africa, pp 95-99.

Blight, G.E. (1971). "Cracks and fissures by shrinkage and swelling". *Proceedings of 5th Regional Conference for Africa*, Luanda, Angola, Vol. 1, pp 15-22.

Blight, G.E. (1997) 37th Rankine Lecture: "Interactions between the atmosphere and the Earth". *Geotechnique* 47, No.4 pp 715-766.

Booker, J.R. and Small, J.C. (1975). "An investigation of the stability of numerical solutions of Biot's equations of consolidation". *Int. Jnl. Solids Struct.*, Vol 11, pp 907-917.

Borja, R.I. (1991). "Cam clay plasticity,Part II: Implicit integration of constitutive equations based on nonlinear elastic stress prediction", *Comput. Mech. Appl. Mech. Eng.*, Vol. 88, pp 225-240.

Borja, R.I. and Lee, S.R. (1990). "Cam clay plasticity, Part I: Implicit integration of constitutive relations", *Comput. Mech. Appl. Mech. Eng.*, Vol. 78, pp 49-72.

Bracegirdle, A., Vaughan, P.R. and Hight, D.W. (1992). "Displacement prediction using rate effects on residual shear strength". *Proceedings of the 6th International Symposium on Landslides, Christchurch* 1, pp 343-347, Balkema, Rotterdam.

BS 8004 (1986). "*British standard code of practice for foundations*". Published by the British Standards Institution, London.

Bromhead, E.N. (1992). "*The stability of slopes*" Glasgow: Blackie Academic & Professional.

Bromhead, E.N. and Vaughan, P.R. (1980). "Solutions for seepage in soils with an effective stress dependent permeability". *Proceedings of conference on numerical methods for non-linear problems*, Vol 1, pp 567-578.

Bronswick, J.J. (1991). "Relation between vertical soil movements and water content changes in cracking clays". *Soil Science Society American Journal* 55, pp 1220-1226.

Bronswick, J.J. (1989). "Prediction of actual cracking and subsidence in clay soils". *Soil Science* 148 (2) pp 87 –93.

Bronswick, J.J. (1988). "Modelling of water balance, cracking and subsidence of clay soils". *Journal of Hydrology* 97, pp 199-212.

Brown, P.T. and Booker, J.R. (1985). "Finite element analysis of excavation". *Computers in Geotechnics*, Vol. 1, pp 207-220.

Burland, J.B. (1961). "The concept of effective stresses in partly saturated soils". MSc Thesis, University of Witwatersrand.

Burland, J.B., Longworth, T.I and Moore, J.F.A. (1977), "A study of ground movement and progressive failure caused by an excavation in Oxford clay", *Geotechnique*, Vol. 27, pp 557-591.

Burland, J.B. (1990). "On the compressibility of and shear strength of natural clays". *Geotechnique* **40**, No. 3, pp 329-378.

Burland, J.B, Rampelo, S., Georgiannou, V.N. and Calabresi, G. (1996). "A laboratory study of the strength of four stiff clays" *Geotechnique* **46**, No. 3, pp 491-514.

Calabresi, G. and Scarpelli, G. (1985). "Effects of swelling caused by unloading in overconsolidated clays". *Proceedings of the 11th International conference on Soil Mechanics and Foundation Engineering*, San Francisco Vol. 2, pp 411-414.

Canadell, J.R.B., Ehleringer, J.R., Mooney, H.A., Sala, O.E. and E.D. Schulze, and Schulze, E.D. (1996). "Maximum rooting depth of vegetation types at the global scale", *Oecologia*, Vol. 108, pp 583-595.

Carter, M. and Bently, S.P. (1991). "Correlations of soil properties". Petentech Press, pp 130.

Celia, M.A., Bouloutas, E.T., and Zarba, R.L. (1990). "A general mass conservative numerical solution for the unsaturated flow equation", *Water Resources Research* Vol. 26, pp 1483-1496.

Chandler, R.J. (1984). "Delayed failure and observed strengths of first-time slides in stiff clays: a review. *Proceedings of the 4th International Conference on Landslides*, Toronto 2, pp 19-25.

Chandler, R.J., Crilly, M.S. and Montgomery-Watson, G. (1992). "A low cost method of assessing clay desiccation for low-rise buildings". *Proceedings of Institution of Civil Engineers.* Civ. Eng. 92, pp 82-89.

Chandler, R.J. and Guitierrez, C.I. (1986). "The filter paper method for suction measurement". *Geotechnique* **36,** No.4, pp 593-598.

Kucharski, E.S, Chow, F.C., Price, G.P., Vaughan, P.R. and McGinnity, B.T. (2000). "Investigations into the stabilsation of ash using the calcite in situ precipitation systrem". *Proceedings of the international conference in GeoEng2000*, Melbourne.

CIRIA RP 296 (2000). "*Infrastructure embankments: Condition appraisal and remedial treatment*". Construction Industry and Information Association.

Cooper, M.R., Bromhead, E.N., Petley, D.J., and Grant D.I (1998). "The Selborne Cutting stability experiment". *Geotechnique* **48**, No.1, pp 83-101.

Coppin NJ and Richards IG (1990). "*Use of Vegetation in Civil Engineering*". Construction Industry and Research Information Association. Butterworths, London.

Cotecchia, F. and Chandler, R.J. (1997) "The influence of structure on the pre-failure behaviour of a natural clay". Geotechnique **47**, No.3, pp 523-544.

Cowan, I.R. (1965). "Transport of water in the soil-plant-atmosphere". *Journal of Applied Ecology*, Vol. 2, pp 221-239.

Crabb, G.I. and Atkinson, J.H. (1991), "Determination of soil strength parameters for the analysis of highway slope failures", *Proc. Int. Conf. Slope Stability Engineering*, Inst. Civ. Eng., London, pp 13-18.

Crilly, M.S. and Driscoll, R.M.C. (2000). "The behaviour of lightly loaded piles in swelling ground and implications for their design". *Proceedings of the Institution of Civil Engineers, Geotechnical Engineering*, Vol. 143, pp 3-16.

Crilly, M.S., Driscoll, R.M.C .and Chandler, R.J. (1992). "Seasonal ground and water movement observations from an expansive clay site in the UK". *Proceedings of 7th International Conference on Expansive Soils*, Dallas, Texas.

Croney, D. (1977). "The Design and Performance of Road Pavements". Department of Transport - Transport and Road Research Laboratory. Published by Her Majesty's Stationery Office.

Cutler, D.F., Gasson, P.E. and Farmer, M.C. (1990). "The wind-blown tree survey: analysis of results". *Arboriculture Journal* 14(3), pp 265-286.

Danielson, R.E. (1967). "Root systems in relation to irrigation". *Irrigation of Agricultural Lands*. Vol. 11. Hogan, R.M., Haise, H.R. and Edminster, T.W. (Eds). American Society of Agronomy, Madison, Wisconsin.

Day, R.A. and Potts, D.M. (1990). "Curved Mindlin beam and axi-symmetric shell elements - A new approach". *Int. Jnl. Num. Meth. Eng.*, Vol. 30, pp 1263-1274.

De Jong, R. and Cameron, D.R. (1979). "Computer simulation model for predicting soil water content profiles". *Soil Science Journal*, Vol. 128, pp 41-48.

De Mello, V.F.B. (1977). "Reflections on design decisions of practical significance to embankment dams. *Geotechnique* **27**, No.3, pp 279-356.

Department of Transport (1992). "Manual of contract documents for highway works / Specification for highway works. 7th edition, HMSO, UK.

Dixon, N. and Bromhead, E.N. (1991). "The mechanics of first time slides in the London clay cliff at the Isle of Sheppey", England. *Proceedings of the International Conference on Slope Stability Engineering : Developments and Applications* (ed. R.J. Chandler), Isle of Wight, pp 277-282.

Dounias, G.T. (1987). "*Progressive failure in embankment dams*". ,PhD thesis. Imperial College, University of London.

Driscoll, R. (1983). "The influence of vegetation on the swelling and shrinking clays soils in Britain". *Geotechnique* **33**, No. 2, pp 93-105.

Duncan, J.M. (1992), "Static stability and deformation analysis", Proc. Spec. Conf. Stability and Performance of Slopes and Embankments – II, *Geot. Eng. Div., ASCE*, Vol. 1, (Edt. Seed and Boulanger), pp 222-266.

Duncan, J.M. and Dunlop, P. (1969), "Slopes in stiff fissured clays and shales", *ASCE Journal of Soil Mechanics and Foundation Division*, Vol. 95 pp 467-492.

Duncan J.M. and Chang, C.Y. (1970), "Non-linear analysis of stress and strains in soils", *ASCE Journal of Soil Mechanics and Foundation Division*, Vol. 96, pp 1629-1653.

Dunlop, P. and Duncan, J.M. (1970), "Development of failure around excavated slopes", *ASCE Soil Mechanics and Foundation Division*, Vol. 96, pp 471-493.

Duncan, J.M. (1992) "State-of-the-art: static stability and deformation analysis". *ASCE Specialty Conference on Stability and Performance of slopes and Embankmnents II, San Francisco* Vol. 1, pp 222-266.

Esu, F. (1966). "Short-term stability of slopes in unweathered jointed clays". *Geotechnique* Vol. 16(4), pp 321-328.

Feddes, R.A. and Rijtema, P.E. (1972). "Water withdrawal by plant roots". *Journal of Hydrology*, Vol. 17, pp 33-59.

Feddes, R.A., Bresler, E., and Neuman, S.P. (1974). "Field test of a numerical model for water uptake by root systems". *Water Resources Research*, Vol. 10, No. 6, pp 1199-1206.

Feddes, R.A., Kowalik, P.J., Kolinka-Malinka and Zaradny, H. (1976). "Simulation of field water uptake by plants using a soil water dependent root extraction function". *Journal of Hydrology*, Vol. 31, pp 13-26.

Feddes, R.A., Kowalk, P.J. and Zaradny, H. (1978). "*Simulation of field water use and crop yield.* Halsted Press, John Wiley and Sons, New York.

Fourie A.B., Rowe, D. and Blight, G.E. (1999). "The effect of infiltration on the stability of the slopes of a dry ash dump". *Geotechnique* **49**, No.1, pp 1-13.

Fredlund, D.G. (2000). "The 1999 R.M. Hardy Memorial Lecture: The implementation of unsaturated soil mechanics into geotechnical engineering". *Canadian Geotechnical Journal*, Vol 37, pp 963-986.

Fredlund, D.G., Xing, A, and Huang, S. (1994). "Predicting the permeability function for unsaturated soil using the soil-water characteristic curve". *Canadian Geotechnical Journal*, Vol. 31, pp 533-546.

Fredlund,D.G. and Xing, A. (1994). "Equations for the soil-water characteristic curve". *Canadian Geotechnical Journal*, Vol. 31, pp 521-532.

Fredlund, D.G., Morgenstern, N.R., and Widger, R.A. (1978). "Shear strength of unsaturated soils". *Canadian Geotechnical Journal*, Vol.15, pp 313-321.

Fredlund, D.G. and Morgenstern, N.R. (1977). "Stress state variables for unsaturated soils". *Journal of the Geotechnical engineering Division*, ASCE, Vol. 103, No.GT5, pp 447-466.

Freeman, T.J., Burford, D and Crilly, M.S. (1991). "Seasonal foundation movements in London Clay". *Proceedings of the International Conference on Ground Movements and Structures*, Cardiff, 1991.

Gardner, W.R. (1958). "Some steady state solutions for the unsaturated moisture flow equation with application to evaporation from a water table". *Soil Science*, Vol. 85, No.4, pp 228-232.

Gardner, W.R. (1960). "Dynamic aspects of water availability to plants". *Soil Science*, Vol. 89, pp 63.

Gardner, W.R. (1964). "Relation of root distributiion to water uptake and availability". *Agronomy Journal*, Vol. 56, pp 35-41.

Gasson, P.E. and Cutler, D.F. (1990). "Tree root plate morphology". *Arboriculture Journal* (14(3), pp 193-264.

Gates, R.H. (1972), "Progressive failure model for clay shales", in "*Application of the finite element method in Geotechnical Engineering*", US Army Corps of Engineers, Waterways Experimental Station, pp 327-348.

Gens, A. and Alonso, E.E. (1992). A framework for the behaviour of unsaturated expansive clays. *Canadian Geotechnical Journal* Vol. 29, No. 6, pp 1013-1032.

Georgiannou, V.N. and Burland, J.B. (2001). "A laboratory study of post-rupture strength". Geotechnique **51**, No.8, pp 65-675.

Geotechnical Observations (2001). "Peak pore pressures measured in earth structures (winter 2000-2001)". GeO Report No. Jo1-007/A. *Unpublished report for London Underground Limited.*

Gray, D.H. (1995). "*Influence of vegetation on the stability of slopes*". In: Vegetation and slopes. Stabilisation, protection and ecology. Ed. D.H. Barker, pp 2-25. London. Published by Thomas Telford.

Green, S. and Clothier, B. (1999). "The root zone dynamics of water uptake by a mature apple tree". Plant Soil, Vol. 206, pp 61-77.

Greenway, D.R. (1987). Vegetation and slope stability. In "*Slope Stability*", Anderson, M.G. and Richards, K.S. eds. John Wiley & sons Ltd.

Haefeli, R. (1965), "Creep and progressive failure in snow, soil, rock and ice", *Proccedings of the 6th International Conference on Soil Mechanics and Foundation Engineering*, Montreal, Vol. 3, pp 134-148.

Hamza, M.M.A.F. (1976), "*The analysis of embankment dams by non-linear finite element method*", PhD thesis, Imperial College, University of London.

Hanks, R.J., Klute, A. and Bresler, E. (1969). "A numeric method for estimating infiltration, redistribution, drainage and evaporation of water from soil". *Water Resources Research* Vol. 5, No. 5, pp 1064-1069.

Hansbo, P., Larsson, R., Runesson, K. and Wiberg, N.E. (1985), "On the behaviour of natural slopes with emphasis on progressive failure", *Proceeding s of the 11th International conference on Soil mechanics and Foundation Engineering*, San Francisco, Vol. 2, pp 757-760.

Haverkamp, R., Vauclin, M., Tourma, J, Wierenga, P.J. and Vachaud, G. (1977). "A comparison of numerical simulation models for one dimensional infiltration". *Soil Science Society of America Journal*, Vol. 41, pp 285-294.

Hight, D.W. (1998). "Soil characterisation: the importance of structure anisotropy and natural variability". 38th Rankine Lecture, Geotechnique, in preparation.

Hillel,D., Talpaz, H. and Van Keulen, H. (1976), "A macroscopic model of water uptake by a non-uniform root system and of water and salt movement in the soil profile". *Soil Science* 121, pp 242-255.

Hillel, D., van Beek, C.G. and Talpaz, H. (1975). "A microscopic scale model of soil water uptake and salt movement to plant roots". *Soil Science*, 120, pp 385-399.

Hiller, D.M. and MacNeil, D.J. (2001). "*A review of the use of live willow poles for stabilising highway slopes*". TRL Report 508, Published by Highway Agency, Crowthorne, Berkshire, UK..

Hoogland, J.C., Feddes, R.A. and Belmans, C. (1981). "Root water uptake model depending on soil water pressure head and maximum extraction rate". *Acta Horticulture*, Vol. 119, pp 123-131.

Hough, M., Palmer, S., Weir, A., Lee, M. and Barrie, I. (1997). "*The Meteorological Office Rainfall and Evaporation Calculation System: MORECS Version 2.0 (1995)* ". An update to Hydrological Memorandum 45, Meteorological Office.

Huang, S.Y., Barbour, S.L., and Fredlund, D.G. (1998). "Development and verification of a coefficient of permeability function for a deformable, unsaturated soil". *Canadian Geotechnical Journal*, Vol. 35: pp 411-425.

Huck, M.G., Klepper, B. and Taylor, H.M. (1970). "Diurnal variations in root diameter". *Plant Physiology*, Vol. 45, pp 529-530.

ICON (1995). "Ash embankment investigation for London Underground Limited". Commission No. 8063. *Unpublished report for London Underground Limited.*

ICON (1999a). "*Ash embankment project E3.* Finite element analysis of typical LUL embankment at Canons Park including the effects of shrinkage and swelling. Report F". *Unpublished report for London Underground Limited.*

ICON (1999b). "*Ash embankment project E3.* Finite element analysis of an embankment with a tied-back wall. Report H". *Unpublished report for London Underground Limited.*

ICON (1999c). "*Ash embankment project E3.* Pore pressures and vegetation". *Unpublished report for London Underground Limited.*

ICON (2001). "Civil asset knowledge and planning project, Commission N0. CN19256, Vegetation study". *Unpublished report for London Underground Limited.*

Inoue, M., Simunek, J., Hopmans, J.W., and Clausnitzer, V. (1998). "In situ estimation of soil hydraulic functions using a multi-step soil-water extraction technique", *Water Resources Research*, Vol. 34, pp 1035-1050.

James, P.M. (1970). "*Time effects and progressive failure in clay slopes*", PhD thesis, University of London.

James, P.M. (1970). "The role of progressive failure in clay slopes". *Proceedings of 1st Australia & New Zealand Geomechanics Conference*, Melbourne, Vol.1, pp 344-348.

Jardine, R.J., Potts, D.M., Fourie, A.B. & Burland, J.B. (1986). "Studies of the influence of nonlinear stress-strain characteristics in soil-structure interaction. *Geotechnique* **36**, No. 3, pp 377-396.

Jarvis, N.J. (1989). "A simple empirical model of root water uptake". *Journal of Hydrology*, Vol. 107, pp 57-72.

Jennings, J.E.B. (1961). "A revised stress law for use in prediction of behaviour of unsaturated soils". *Conf. Pore Pressures and Suction in Soils*, ISMFE, London.

Karajeh, F.F. and Tanji, K.K. (1994). "Agro-forestry drainage management model II: field water flow". *Journal of Irrigation and Drainage Engineering*, ASCE 120(2) pp 382-396.

Kenny, T.C. and Lau, K.C. (1984). "Temporal changes of groundwater pressure in a natural slope of non-fissured clay". *Canadian Geotechnical Journal*, Vol. 21, No.1, pp 138-146.

Klepper, B. and Taylor, H.M. (1979). "Limitations to current models describing water uptake by plant root systems". In "The Soil-Root Interface". *Proceedings of an International Symposium held at Oxford*, England. Harley, J.L. and Russell, S.C. eds. Academic Press, New York.

Kondner, R.L. (1963), "Hyperbolic stress-strain response: cohesive soils", *ASCE Journal of Soil Mechanics and Foundation division*, Vol. 98, pp 653-665.

Konrad, J.M. and Ayad, R. (1997). "Desiccation of a sensitive clay: Field experimental observations". *Canadian Geotechnical Journal,* Vol. 34, No.6, pp 929-942.

Konrad, J.M. and Ayad, R. (1997). "An idealised framework for the analysis of cohesive soils undergoing desiccation". *Canadian Geotechnical journal*, Vol. 34, pp 477-488.

Kodikara, J.K., Barbour, S.L. and Fredlund, D.G. (1999). Discussion: "An idealised framework for the analysis of cohesive soils undergoing desiccation". Canadian Geotechnical Journal, Vol. 34, pp 1112-1114

Kodikara, J.K., Barbour, S.L. and Fredlund, D.G. (2000). "Desiccation cracking of soil layers". *Unsaturated Soils for Asia*. Rahardjo, Toll & Leong (eds). Published by Balkema.

Kovacevic, N. (1994). "*Numerical analyses of rockfill dams, cut slopes and road embankments*". PhD thesis. Imperial College, University of London.

Kovacevic, N, Potts, D.M. and Vaughan, P.R. (2001). "Progressive failure in clay embankments due to seasonal climate changes". *Proceedings of the15th International Conference in Soil Mechanics & Geotechnical Engineering*, Instanbul, Turkey, pp 2127-2130.

Kozlowski, T.T. (1982). " Water supply and tree growth". *Forestry Abstracts* 43(2) pp 57-95.

Kozlowski, T.T. (1971). "*Root growth – Chapter 5 of Growth and development of trees*". Academic Press, pp 196-305.

Kramer, P.J. and Boyer, J.S. (1995). "Water relations of plants and soils". Academic Press pp 495.

Kramer, P.J. (1969). "*Plant and Soil Water Relationships: A Modern Synthesis.*" McGraw-Hill, New York.

Kulhawy, F.H. and Duncan, J.M. (1972). "Stresses and movements in Oroville dam". ASCE J. Soil Mech. Found. Div., Vol 98, pp 653-665.

Lacerda, W.A. (1989). "Fatigue of residual soils due to cyclic pore pressure variation". *Proceedings of the 12th International conference on Soil mechanics and Foundation Engineering, Rio de Janeiro*, Vol. 5, pp 3085-3087.

Lacerda, W.A. (1997). "Stability of natural slopes along the tropical coast of Brazil". *Proceedings of the International Symposium on recent Developments in Soil and Pavement Mechanics, Rio de Janeiro*, pp 17-39.

Lacerda, W.A., Santos, O.F. Jr and Ehrlich, M. (1997). "The influence of piezometric level variations on the stability of residual soil slopes". *Proceedings of the 2nd Pan-American Symposium on Landslides*.

Lachenbruch, A.H. (1961). "Depth and spacing of tension cracks", *Journal of Geophysical Research*, Vol. 66, No. 12, pp 263-277.

Lade, P.V. (1977). "Elasto-plastic stress-strain theory for cohesionless soil with curved yield surfaces". *Int. Journal of Solids Structures*, Vol. 13, pp 1019-1035.

Lambe, T.W. and Whitman R.V. (1969). "*Soil mechanics*", SI version, New York: John Wiley.

Lauritzen, C.W. (1948). "Apparent specific volume and shrinkage characteristics of soil materials". *Soil Science*, Vol. 65, pp 155-179.

Lauritzen, C.W. and Stewart, A.J. (1941). "Soil volume changes and accompanying moisture and pore size relationships". *Proceedings of the Soil Science Society of America*, Vol. 6, pp 113-116.

Lemos, L.J.L. (1986), "*The effect of rate on residual strength of soil*" PhD thesis, Imperial College, University of London.

Leong, E.C. and Rahardjo, H. (1997). "Permeability functions for unsaturated soils". *Journal of Geotechnical and Geoenvironmental Engineering*, ASCE, 123 (12): pp 1106-1117.

Leroueil, S. (2001). "Natural slopes and cuts: movement and failure mechanisms" 39th Rankine Lecture, Geotechnique **51**, No.3, pp 197-243.

Leroueil, S. and Vaughan, P.R. (1990). "The general and congruent effects of structure in natural soils and weak rocks. *Geotechnique* 40, No.3, pp 1669-1678.

Leroueil, S., Guerriero, G., Picarelli, L. and Saihi, F. (1997). "Large deformation shear strength of two types of structured soils". *Proceedings of the international symposium on deformation and progressive failure in geomechanics, Nagoya*, pp 217-222, Pergamon.

Li, K.Y., Boisvert, J.B. and De Jong, R. (1999). "An exponential root-water-uptake-model". *Canadian Journal of Soil Science*, Vol. 79, pp 333-343.

Li, K.Y., Boisvert, J.B. and De Jong, R. (2000). "Comparison of root-water-uptake models". *Proceedings of 10th International Soil Conservation Organisation Conference,* May 23-28, 1999, Purdue University, West Lafayette, IN.

Lupini, J.F. (1980). "*The residual strength of soils*". PhD thesis, Imperial College, University of London.

Lupini, J.F., Skinner, A.E. and Vaughan, P.R. (1981). "The drained residual strength of cohesive soils". *Geotechnique* **31**, No.2, pp181-213.

MacNeil, D.J, Steele, D.P., McMahon, W., and Carder, D.R. (2001). "*Vegetation for slope stability*", TRL Report 515, Published by the Highway Agency, Crowthorne, Berkshire, UK.

Marinho, F.A.M. (1994). "Shrinkage behaviour of some plastic soils". PhD thesis. Imperial College, University of London.

Marriot, C.A., Hood, K., and Crabtree, J.R., MacNeil, D.J. (2001) "*Establishment of vegetation for slope stability*", TRL Report 506, Published by the Higway Agency, Crowthorne, Berkshire, UK.

Marsland, F., Ridley, A.M., Vaughan, P.R. and McGinnity, B.T. (1998). "Vegetation and its influence on the soil suction in clay slopes". *Proceedings of 2nd International Conference on Unsaturated Soil.* Beijing, China, pp 249-254.

Materechera, S.A., Dexter, A.R. and Alston, A.M.(1991). "Penetration of very strong soils by seedling roots of different plants species". *Plant and Soil* 135 pp 31-41.

Mathur, S. (1999). "Settlement of soil due to water uptake by plant roots. " *International Journal for Numerical and Analytical Methods in Geomechanics*, Vol. 23, pp 1349-1357.

Mattheck, C. (1990). "Why they grow, how they grow; the mechanics of trees". *Arboriculture Journal* 14(1) pp 1-17.

McCarthy, E.J., Flewelling, J.W. and Skaggs, S.W. (1992). "Hydrologic model for drained forest watershed". *Journal of Irrigation and Drainage Engineering*, ASCE 118(2).

McCombie, P.F. (1993). "The relative water demand of broad leaved trees – a new analysis of the Kew tree root survey". *Arboriculture Journal* 17(4) pp 359-374.

McGinnity, B.T., Rankin, W., Russell, D. (1998). "A systematic and cost-effective approach to inspecting, prioritising and upgrading London Underground's earth structures". The Value of Geotechnics in Construction. *ICE Conference Proceedings*. Thomas Telford, London.

McGinnity, B.T. and Russell, D. (1996). "Investigation of London Underground earth structures". *International Conference on Advancers in Site Investigation practice. ICE conference proceedings*. Thomas Telford, London.

McGinnity, B.T. and Gellatley, M.J. (1988). "Stabilisation of old railway embankments using lime". *British Lime Association Seminar, 1988. Lime Treatment for Roads, Railways, Buildings and Contaminated Land.*

Molz, F.J. and Remson, I. (1970). "Extraction term models of soil moisture use by transpiring plants". *Water Resources Research*, Vol. 6, pp 1346-1356.

Moore, R., Dennis Clark, W., Stern, K.R., and Vodopich, D. (1995). "Botany", Wm. C. Brown.

Morris, P.H., Graham, J. and Williams, D.J. (1992). "Cracking in drying soils". *Canadian Geotechnical Journal*, Vol. 29, pp 263-277.

Mott MacDonald (1999a). "Ground investigation of Central and Metropolitan Lines. Advanced laboratory testing interpretative report". Reference 45354/F&G/REP/350/B, *Unpublished report for London Underground Limited.*

Mott MacDonald (1999b). "Research Stage II: Assessment of Clay Fill, London Underground Limited". Reference 51683/F&G/REP/100/A, *Unpublished report for London Underground Limited.*

Mott MacDonald (1999c). "Research Stage II: Assessment of Embankments, London Underground Limited". Reference 51683/F&G/REP/200/A, *Unpublished report for London Underground Limited.*

Mualem, Y., (1976). "A new model for predicting the hydraulic conductivity of unsaturated porous media". *Water Resources Research*, Vol. 12, pp 513-522.

Muir Wood, D., Jendele, L., Chan, A.H.C. and Cooper, M.R. (1995). "Slope failure by pore pressure recharge: numerical analysis". *Proceedings of the 11th European Conference on Soil Mechanics and Foundation Engineering, Copenhagen* Vol 6, pp1-8.

Naylor, D.J. (1974). "Stresses in nearly incompressible materials by finite elements with application to the calculation of excess pore water pressure". *Int. Jnl. Num. Anal. Meth. Eng.*, Vol 8, pp 443-460.

Naylor, D.J. (1991). "Stress-strain laws and parameter values", *Advances in Rockfill Structures*, Edt. Maranha das Neves, pp 269-290.

Naylor, D.J. (1999). "On the use of the FEM for assessing the stability of cuts and fills". *Numerical models in Geomechanics*, NUMOG VII, Edt. Pietruszczak & Pande, pp 636-648.

Neuman, S.P., Feddes, R.A. and Bressler, E. (1975). "Finite element analysis of two dimensional flow in soil considering water uptake by roots", Vol. I, Theory, *Soil Science Society of America Journal*, Vol. 35, pp 224-230.

Ng C.W.W., Wang, B. and Tung, Y.K. (2001). "Three-dimensional numerical investigations of groundwater response in an unsaturated slope subjected to various rainfall patterns". *Canadian Geotechnical Journal*, Vol. 38, pp 1049-1062.

Nour el-Din, M.M., King, I.P. and Tanji, K.K. (1987). "Salinity management model II: 1 and 2D applications". *Journal of Irrigation and Drainage Engineering* , ASCE 113(4) pp 454-468.

Nyamah, J.U. and Black, T.A., (1977). "Rates and patterns of water uptake in a Douglas fir forest". *Soil Science Society of America Proceedings*, Vol. 41, pp 972-979.

Oberg, A.I., (1995). "Negative pore pressures - Seasonal variation and importance in slope stability analysis". *Proceedings of the 1st International Conference on Unsaturated soils, Paris*, Vol .2, pp 907-913.

Parry, L.N. (1992). "Desiccation, some examples measured in London Clay". *Proceedings of the 7th International Conference on Expansive Soils*, Dallas, Texas.

Peck, R.B., (1967). "Stability of natural slopes", *ASCE Journal of Soil Mechanics and Foundation Division*, pp 403-436.

Penman, H.L. (1948). "Natural evaporation from open water, bare soil and grass". *Proceedings of the Royal Society, London Series A*, Vol. 193, pp 120 145.

Prat, C.C., Ledesma, A. and Cabeza, L (2002). "Drying and cracking of soils: numerical modelling". *Numerical Models in Geomechanics* - NUMOG VIII, Pande & Pietruszczak (Eds), Lisse.

Perry, J. (1989). "A survey of slope condition on motorway earthworks in England and Wales". *Research Report RR199*, Crowthorne: TRL Limited.

Perry, J., McGinnity, B. T. and Russell, D. (1999). "Railway earth structures: their condition, management and effect on track quality". Railway Engineering 1999, *Second International Conference*, London, May 1999.

Potts, D.M. and Ganendra, D. (1994). "An evaluation of substepping and implicit stress point algorithms". *Comput. Meth. Appl. Mech. Eng.*, Vol. 119, pp 341-354.

Potts, D.M. and Gens, A. (1985). "A critical assessment of methods of correcting for drift from the yield surface in elasto-plastic finite element analysis", *Int. Jnl. Num. Anal. Meth. Geomech.*, Vol. 9, pp149-159.

Potts, D.M., Dounias, G.T. and Vaughan, P.R., (1990). "Finite element analysis of progressive failure of Carsington embankment". *Geotechnique* **40**, No.1, pp 79-101.

Potts, D.M., Kovacevic, N. and Vaughan, P.R., (1994). "*Progressive failure in motorway slopes of clay*". Contract report, Crowthorne: Transport Research Laboratory.

Potts, D.M., Kovacevic, N. and Vaughan, P.R., (1997). "*Delayed collapse of cut slopes in stiff clays*". *Geotechnique* **47** pp 953-982.

Potts, D.M. and Zdravkovic, L. (1999). "*Finite element analysis in geotechnical engineering: Theory*". Thomas Telford Publishing, London.

Potts, D.M. and Zdravkovic, L. (2001). "*Finite element analysis in geotechnical engineering: Applications*". Thomas Telford Publishing, London.

Potts, D. M. (2002) "Imperial College Finite element Program: *User's Manual*", Imperial College.

Prasad, R. (1988). "A linear root water uptake model". *Journal of Hydrology*, Vol. 99, pp 297-306.

Proebsting, E.L. (1943). "Root distribution of some deciduous fruit trees on California orchard". *Proceedings of the American Society of Horticultural Science*, Vol. 43, pp 1-4.

Puzrin, A.M. and Burland, J.B. (1998). "Nonlinear model of small strain behaviour of soils". Geotechnique, Vol. **48**, No.2, pp 217-233.

Raats, P.A.C. (1974). "Steady flows of water and salt in uniform soil profiles with plant roots", *Soil Science Society of America Journal*, Vol. 38, pp 717-722.

Reeve, M.J., Hall, D.G.M. and Bullock, P. (1980). "The effect of soil composition and environmental factors on the shrinkage of some clayey British soils". *Journal of Soil Science 31*, pp 429-442.

Reeve, M.J., and Hall, D.G.M. (1978). "Shrinkage in clayey subsoils of contrasting structure". *Journal of Soil Science* 29, pp 315-323.

Ridley, A.M. and Burland, J.B. (1995). "A pore water probe for the in situ measurement of a wide range of soil suctions". *Proceedings of International Conference on Advances in Site Investigation Practice*. Thomas Telford, London.

Ridley, A.M. and Dineen, K. (2003). Personal communication with author.

Roscoe, K.H., Schofield, A.N. and Wroth, C.P. (1958). "On the yielding of soils". *Geotechnique* **8**, No. 1, pp 22-53.

Roscoe, K.H. and Burland, J.B. (1968). "On the generalised stress-strain behaviour of 'wet' clay". *Proceedings of the Symposium on plasticity, Cambridge*, pp 535-610.

Russell, R.S. (1977). *"Plant root systems: Their function and interaction with the soil"*. McGraw-Hill Book Co. (UK) Ltd.

Russell, D., Ellis, E., O'Brien A., McGinnity, B. (2000). "Role of vegetation in the stability and serviceability of railway embankments". *1st International Conference on Railway Engineering*, London.

Santos, O.F., Lacerda, W.A.. and Ehrlich, M. (1997). "Triaxial tests with cyclic pore pressure variation for simulation of the seasonal variation of water level in slopes". *Proceedings of the international symposium on recent developments in soil and pavement mechanics*, Rio de Janeiro, pp 279-282.

Santos, O.F., Lacerda, W.A. and Ehrlich, M. (1996). Discussion of "Collapse of saturated due to reduction in confinement" by Anderson and Rriemer (1995). *ASCE, Journal of Geotechnical Engineering Division*, Vol. 122, No. 6, pp 505-506.

Schofield, A.N. and Wroth, C.P. (1968). *"Critical state soil mechanics"*. McGraw-Hill, London.

Shaw, E.M. (1994). *"Hydrology in practice"*. 3rd edition. Chapman & Hall, London, UK, pp 262-263.

Skempton, A.W. and Northey, R.D. (1952). "The sensitivities of clays". *Geotechnique* **3**, No. 1 pp 100-106.

Skempton, A.W. (1964), "Long term stability of clay slope", *Geotechnique*, Vol. 14, pp 77-101

Skempton,A.W. and Petley, D.J. (1967). "The strength along structural discontinuities in stiff clays", *Proceedings of Geotechnical Conference*, Oslo, Vol. 2, pp 29-46

Skempton, A.W., Schuster, R.L. and Petley, D.J. (1969). "Joints and fissures in the London Clay at Wraysbury and Edgware". *Geotechnique* **19**, No. 2, pp 205-217.

Skempton, A.W. (1985a). "Residual strength of clays in landslides, folded strata and the laboratory". Geotechnique **35**, No.1, pp 3-18.

Skempton, A.W. (1985b). "Geotechnical aspects of the Carsington dam failure", *Proceedings of the 11th International conference on soil mechanics and foundation engineering*, Vol. 2, pp29-46.

Skempton, A.W., and Coats, D.J. (1985) "*Carsington Dam failure*", Proceedings "*Failures in earthworks*", Institution of Civil Engineers, London, pp 203-220.

Skempton, A.W. (1996). "Embankments and cuttings on the early railway". *Construction History* Vol. 11 pp 33-49.

Skempton, A.W. (2000). Personal communication with author.

Skinner, A.E. (1975). "*The effect of high pore water pressures on the mechanical behaviour of sediments*". PhD thesis, Imperial college, University of London.

Sloan, S.W. (1987). "Substepping schemes for numerical integration of elasto-plastic stress-strain relationships". *Int. Jnl. Num. Meth. Eng.*, Vol. 24, pp 893-911.

Symons, I.F. (1978). "Performance of clay fills (General report). *Proc. Inst. Civil Eng. Conf. On Clay Fills*, London, pp 297-302.

Tempany, H.A. (1917). "The shrinkage of soils". *Journal of Agricultural Science*. Cambridge, Vol. 8, pp 312-333.

Terzaghi, K. (1936). "The stability of slopes of natural clay". *Proceedings of the 1st International conference on soil mechanics and foundation engineering*, Harvard, Vol.1, pp 161-164.

Terzaghi, K. and Peck, R.B. (1948). "*Soil Mechanics in engineering practice*". John Wiley and Sons, New York.

Taylor, D.W. (1948). "*Fundamentals of soil mechanics*". John Wiley and Sons New York.

Tick, T.E., Vaughan, P.R., and Lemos, L.J. (1996). "Fast shearing of pre-existing shear zones in soil". Geotechnique **46**, No.2, pp 197-233.

Tratch, D.J.; Wilson, G.W. and Fredlund, D.G. (1995). "An introduction to analytical modelling of plant transpiration for geotechnical engineers". *Proceedings of the 48th Canadian Geotechnical Conference*, Vol. 2, pp. 771-780.

Vanapalli, S.K.; Fredlund, D.G.; Pufahl, D.E. and Clifton, A.W. (1996). "Model for the prediction of shear strength with respect to soil suction". *Canadian Geotechnical Journal*, Vol 33(3); pp 379-392.

Van Genuchten, M.T. (1980). "A closed form equation for predicting the hydraulic conductivity of unsaturated soils", *Soil Science Society of America Journal*, Vol. 44, pp 892-898.

Van Genuchten, M.T. and Gupta, S.K. (1993). A reassessment of the crop tolerance response function, *Bulletin of the Indian Society of Soil Science*, Vol. 4, pp 730-737.

Vaughan, P.R. and Walbancke, H.J. (1975), "The stability of cut and fill slopes in boulder clay", *Proceedings of a Symposium on Engineering Behaviour of Glacial Materials*, Midlands Society of Soil mechanics and Foundation Engineering, Birmingham, pp 209-219.

Vaughan, P.R. (2000). Personal communication with author.

Vaughan, P.R. (1994) "Assumption, prediction and reality". 34th Rankine Lecture, *Geotechnique* **44 No.4** pp 573-609.

Vaughan, P.R. (1989). Non-linearity in seepage problems - theory and field observations. *De Mello Volume*, pp 501-516, Sao Paulo: Edgard Blucher.

Vaughan, P.R. and Hamza, M.M.A.F. (1977). "Clay embankments and foundations: monitoring stability by measuring deformations. Proceedings of the 9th international conference on Soil Mechanics, Tokyo, pp 37-48.

Vaughan, P.R., Hight, D.W., Sodha, V.G. and Walbancke, H.J. (1978). "Factors controlling the stability of clay fills in Britain. In *Clay fills*, pp 205-218. London: Institution of Civil Engineers.

Vrugt, J.A., van Wijk, M.T. , Hopmans, J.W. and Simunek, J. (2001) "One-, two- and three dimensional rot water uptake functions for transient modelling". *Water Resources Research Journal*, Vol. 37, No. 10, pp 2457-2470.

Walbancke, H.J. (1976). "*Pore pressures in clay embankments and cuttings*". PhD thesis. Imperial College, University of London.

Wallace, K.B. and Lytton, R.L. (1992). "Crack and block models for expansive clay soils: theoretical analysis". *Proceedings of 7th International Conference on Expansive Soils*, Dallas, Texas, Vol. 1.

Ward, W.H. (1953). "Soil movement and weather". *Proceedings of the 3rd International Conference on Soil Mechanics*. Zurich , Vol. 4, pp 477-482.

Waring, R.H. and Schlesinger, W.H. (1985). "*Forest Ecosystems : Concepts and Management.*" Academic Press, Orlando, FL.

Whisler, F.D., Klute, A. and Millington, R.J. (1968). "Analysis of steady state evapo-transpiration from a soil column". *Soil Science American Proceedings*, Vol. 32, pp 167-174.

Wilson, G.W., Fredlund, D.G. and Barbour, S.L. (1994). "Coupled soil-atmosphere modelling for soil evaporation". *Canadian Geotechnical Journal* **31**, No. 2, pp 151-161.

Wilson, G.W., Fredlund, D.G. and Barbour, S.L. (1997). "The effect of soil suction on evaporative fluxes from soil surfaces". *Canadian Geotechnical Journal*, Vol. 34, pp 145-155.

Whittle, A.J. (1993). "Evaluation of a constitutive model for overconsolidated clays". *Geotechnique*, **43**, No.2, pp 289-313.